SHORT PAPERS IN—

Analytical methods

Astrogeology

Economic geology

Estuarine hydrology

Geochronology

Geophysics

Glacial geology

Ground water

Isotope studies

Limnology

Mineralogy

Petrology

Quality of water

Remote sensing

Stratigraphy and paleontology

Structural geology

Surface water

Volcanology

GEOLOGICAL SURVEY RESEARCH 1972

Chapter C

GEOLOGICAL SURVEY PROFESSIONAL PAPER 800–C

GEOLOGICAL SURVEY RESEARCH 1972

Chapter C

GEOLOGICAL SURVEY PROFESSIONAL PAPER 800–C

Scientific notes and summaries of investigations in geology, hydrology, and related fields

UNITED STATES GOVERNMENT PRINTING OFFICE, WASHINGTON: 1972

UNITED STATES DEPARTMENT OF THE INTERIOR

ROGERS C. B. MORTON, Secretary

GEOLOGICAL SURVEY

V. E. McKelvey, Director

For sale by the Superintendent of Documents, U.S. Government Printing Office, Washington, D.C. 20402 - Price $3
Stock Number 2401-2178

CONTENTS

GEOLOGIC STUDIES

HYDROLOGIC STUDIES

INDEXES

GEOLOGICAL SURVEY RESEARCH 1972

This collection of 37 short papers is the second published chapter of "Geological Survey Research 1972." The papers report on scientific and economic results of current work by members of the Conservation, Geologic, and Water Resources Divisions of the U.S. Geological Survey.

Chapter A, to be published later in the year, will present a summary of significant results of work done in fiscal year 1972, together with lists of investigations in progress, cooperating agencies, and Geological Survey offices.

"Geological Survey Research 1972" is the thirteenth volume of the annual series Geological Survey Research. The twelve volumes already published are listed below, with their series designations.

Geological Survey Research	*Prof. Paper*
1960	400
1961	424
1962	450
1963	475
1964	501
1965	525
1966	550
1967	575
1968	600
1969	650
1970	700
1971	750

PARTIAL DRAINING AND CRUSTAL SUBSIDENCE OF ALAE LAVA LAKE, KILAUEA VOLCANO, HAWAII

By DONALD A. SWANSON and DONALD W. PETERSON,
Hawaiian Volcano Observatory

Abstract.—Eruptions of basaltic lava in 1969 filled Alae Crater with a complex lava lake, and subsequent overflows built the southeastern crater rim 24 m higher. The lake partly drained in August 1970, refilled during the next 3 months, and partly drained again in February and March 1971. The solidified crust of the lake subsided 13 m during the 1970 draining and 23 m during the 1971 draining. The volume of draining was about 10^6 m^3 during both events. The August 1970 draining took place when a lava tube, located 2–3 m above the base of the new lava overlying the crater rim, reopened accompanying rapid addition of lava beneath the crust of the lake. The February-March 1971 draining was more complicated; the pre-February lake crust sank into the molten lake because of the weight of new overlying flows. This subsidence displaced underlying molten lava upward and out of the lake through the outlet tube. The elevation of the base of the lake crust after both draining events was controlled in a crudely hydrostatic fashion by the elevation of the outlet tube.

Alae Crater, formerly a 165-m-deep pit crater on the east rift of Kilauea Volcano (fig. 1), underwent a complex sequence of filling, partial draining, and refilling during the 1969–71 Mauna Ulu eruption (Swanson and others, 1971; Swanson and others, 1972). Alae first filled to overflowing on October 10, 1969; subsequent additions of basaltic lava built the surface 24 m higher than the low point on the preeruption rim (fig. 2*A*). A plugged lava tube near the level of the old rim reopened in early August 1970 and quickly drained the upper part of the impounded lava lake, causing the crust to subside and creating an elliptical subsidence bowl that marked the site of the former crater (fig. 1*A*). Minor settling took place in November 1970 as the tube opened still further.

Mauna Ulu continued to feed lava into the crusted lake in Alae for the next few months; this supply was approximately balanced by outflow through the tube. During February 1971, a voluminous surface flow filled the August subsidence bowl to overflowing and built the surrounding levees 5 m higher, to about 29 m above the low point on the preeruption crater rim. The rate of inflow then declined, but a high rate of outflow through the tube continued for several days, again causing a partial draining of the lava lake and the development of a new subsidence bowl (fig. 1*B*). Rates of inflow and outflow once again balanced by early March 1971, by which time crustal subsidence was virtually complete. The crust continued to settle slightly over the next 2 to 3 months owing to mechanical lag effects.

The subsidence events of August 1970 and February–March 1971 each followed an episode of rapid addition of large volumes of lava to the lake. The final elevations of the base of the lake crust at the end of each subsidence were virtually identical and apparently were hydrostatically governed by the elevation of the outlet tube. This participation of the Alae reservoir in the active system of near-surface lava tubes (Swanson and others, 1971; Anderson and others, 1971; Swanson, 1972) is an important and unusual feature of the Mauna Ulu eruption. Analysis of the subsidence events is necessary for an understanding of the interrelations in this complex system.

Acknowledgments.—R. T. Okamura and J. B. Judd assisted in gathering data and in making field observations. The advice and comments of R. O. Castle and W. A. Duffield have helped clarify the presentation.

DESCRIPTION OF THE AUGUST 1970 DRAINING AND CRUSTAL SUBSIDENCE

Numerous lava flows erupting between February and October 1969 filled Alae Crater to overflowing; overflows continued through December 1969. The resulting crusted lava lake was about 190 m deep and was characterized by numerous highly complicated internal structures (Swanson and others, 1972). The low, southeast part of the crater's former rim was buried 24 m below the surface of the new flows (figs. 2*A* and 4), as determined by precise surveys. A concealed lava tube that had developed by roofing of a surface channel on October 20, 1969, extended about 2.5 km southeastward from the drowned southeastern rim of the crater. This tube, the floor of which was 2 to 3 m above the preeruption rim, channeled a small volume of lava out of the crater between October 20 and

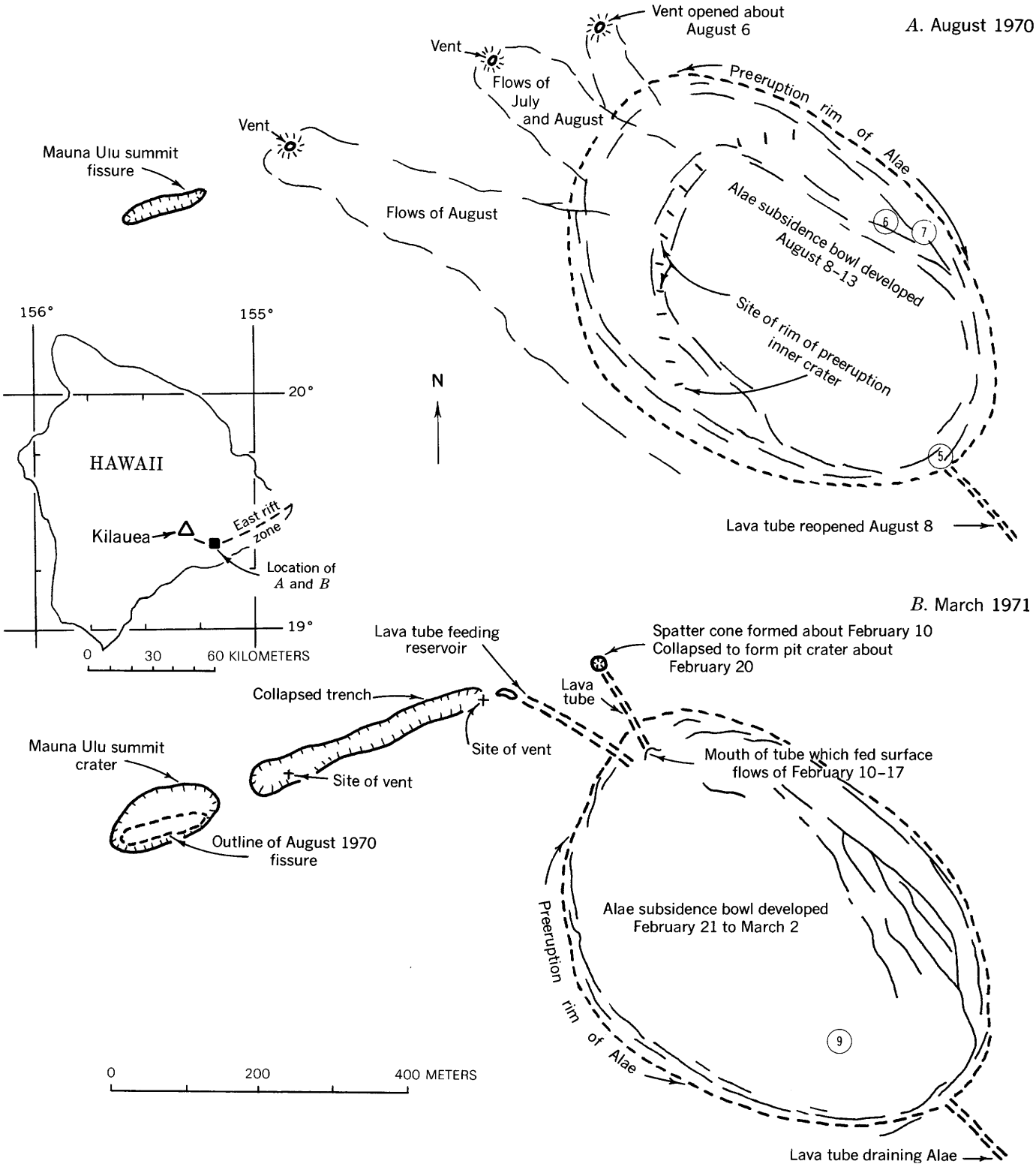

Figure 1.–Sketch maps of Mauna Ulu and Alae Crater. *A*, configuration in late August 1970; *B*, configuration in early March 1971. Inset shows location of area on Kilauea's east rift. Locality of photographs (figs. 5–7, and 9) indicated by circled numbers.

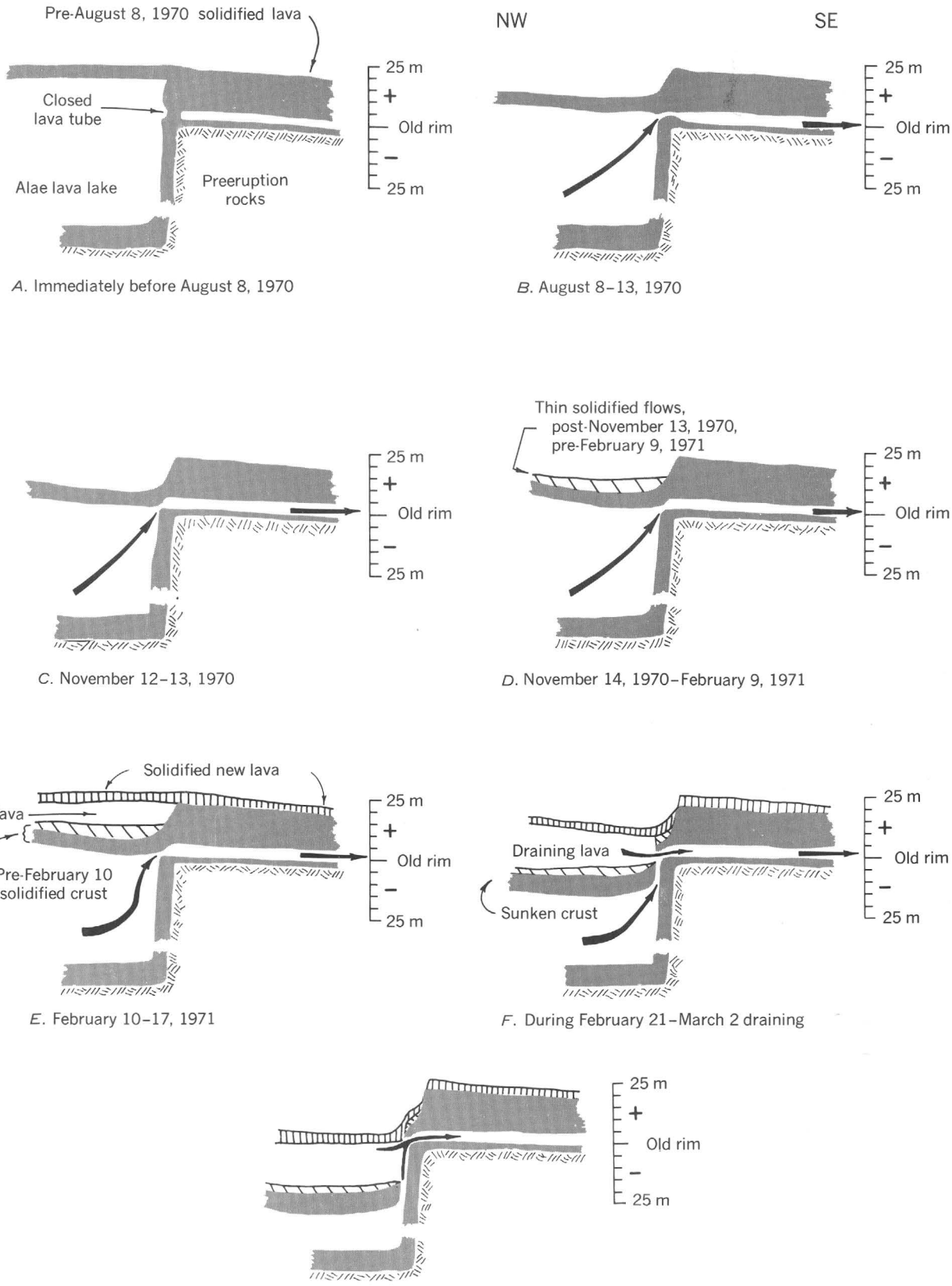

Figure 2.–Schematic cross sections of southeast part of filled Alae Crater, showing sequence of important events between August 1970 and May 1971. Heavy arrows indicate inferred movement of lava.

29, 1969. It subsequently closed, probably by collapse of its walls or blockage of its entrance (fig. 2*A*), and was inactive from October 1969 until August 1970.

Additional lava was added to Alae July 6–9, 13–15, 16–17, and 20–21, 1970, by small flows issuing from a vent 150 m northwest of the crater (fig. 1*A*); none of these flows completely covered the surface crust of the lava lake. Some lava may have been contributed to the molten interior of the lake through a subsurface tube during one or more of these episodes.

A new vent opened about 650 m east-northeast of the summit of Mauna Ulu sometime between August 4 and the early hours of August 7, probably on August 6 (fig. 1*A*). Lava quietly welled out of this vent, flowed in a surface river for 50–100 m, and then disappeared into a tube which carried the lava for several tens of meters before feeding it beneath the crust into the molten part of the lava lake in Alae Crater. Concurrently, other small flows advanced a short distance across the crater floor from the vent 150 m northwest of Alae (Greeley, 1971), and some of this lava may also have entered the molten lake beneath the surface crust. An increase of hydrostatic pressure within the lake accompanied the addition of new lava below the crust, and the crust was probably uplifted as a result. The increased fluid pressure in the lake eventually broke the barrier that sealed the lava tube of October 1969 (fig. 2*B*), and lava poured out of the lake through the tube and emerged about 2.5 km southeast of the crater as a surface flow. The flow was discovered about 0830, August 11, when it had advanced 2–3 km from the lower end of the feeder tube.

Draining of lava through the tube withdrew support for the overlying lake crust, and the crust consequently subsided. Subsidence began late on August 7 or, more likely, early on August 8 but did not become conspicuous until the afternoon of August 8 (Greeley, 1971). We estimated that the surface of the lake had subsided about 10 m when we visited Alae at 1030, August 11 (fig. 2*B*). This estimate is very close to the measured value obtained from later planetable mapping (fig. 3), suggesting that virtually all of the draining and most of the crustal subsidence had been completed by this time. Slight settling of the crust continued until August 13, however, owing perhaps to lag effects resulting from friction, tensile strength of the crust, and other complexities.

All of the subsidence features shown on the topographic and geologic map (fig. 3) were developed by August 11, but the map was not made until November. During this interval, flows that erupted from the vent north of the crater added about 2 m to the entire floor; thus the maximum subsidence in August was about 2 m more than is indicated by the topographic map (fig. 3)—that is, 13 m rather than the indicated 11 m (table 1). Some structures were covered or partly covered by the time the map was made, but their locations and general nature could be determined from aerial photographs taken on August 11. Molten lava flooded many of the structures during and shortly after the mapping, in places completed minutes before lava covered the area.

The August subsidence bowl was elliptical in plan view, conforming to the shape of the filled crater (fig. 1). Its northwestern limb, however, dipped much more gently than the southeastern limb (figs. 3 and 4), and the area of maximum subsidence was located only about 50 m from the entrance to the outlet tube (fig. 4). The constructional slope of the postsubsidence lava fan exaggerates this northwest-southeast asymmetry, but observations made on August 11, before the fan had formed, showed that most of the asymmetry was related to the subsidence itself. Most of the subsidence took place by differential sagging of the lake surface; cumulative vertical displacement along the bordering faults was less than 10 percent of the maximum subsidence amplitude of 13 m (table 1).

Table 1.—*Altitudes, in meters, at various times during the subsidence events*

[Datum is preeruption southeast rim of Alae Crater. Inferred altitude of base of crust refers to the lake crust near the outlet tube]

	Lowest point on lake surface	Altitude	Change in altitude	Inferred altitude of base of crust[1]
1.	Before August 1970 subsidence. Same as thickness of new flows above preeruption rim.	24		19
			-13	
2.	Immediately after August 1970 subsidence.	11		6
			+2	
3.	November 11, 1970, after 2 m of new lava had been added (fig. 3 portrays this time).	13		6
			-3	
4.	November 14, 1970, after November 12–13 settling.	10		3
			+8	
5.	February 9, 1971	18		3+
			+11	
6.	February 17, 1971	29		27
			-19	
7.	March 2, 1971	10		8
			-4	
8.	June 28, 1971 (after final settling).	6		4

[1] For the period through February 9, 1971, the lake crust is that present before the August 1970 subsidence. For the period after February 9, the lake crust is that formed during the interval February 9–17, 1971. See text for details.

Two crudely concentric sets of faults were recognized (figs. 3 and 4). The outer set was defined by small, nearly vertical cracks, generally less than 75 cm wide, that outlined the position of the buried rim of the crater. Most of these boundary faults had less than 5 cm vertical displacement, and many showed no vertical offset. The only substantial vertical displacement (1.3 m) on a fault of this set was at the southeast end of the subsidence bowl, directly above the location of the outlet tube (figs. 2*B*, 3, 4, and 5) and close to the area of maximum subsidence.

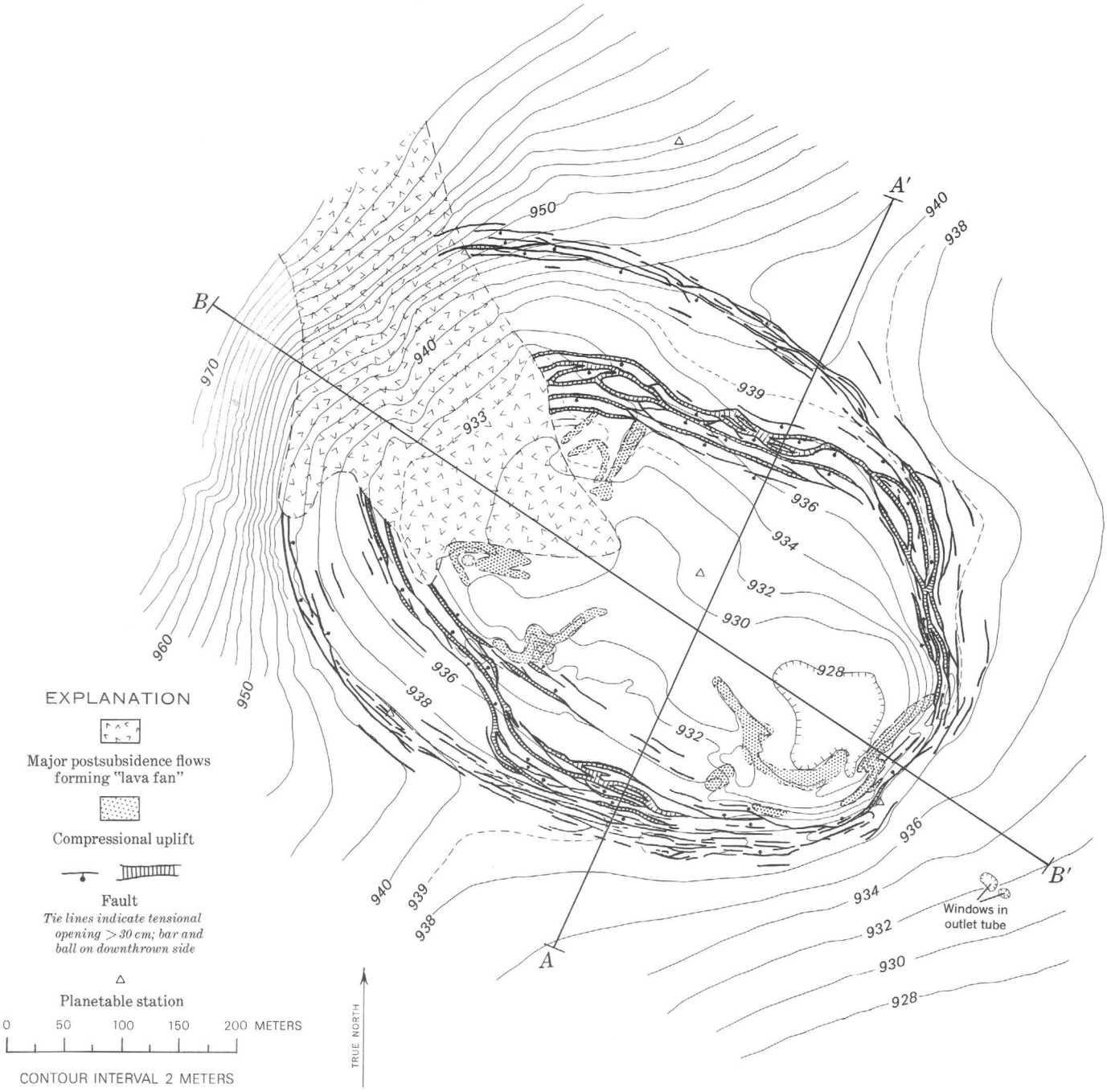

Figure 3.—Geologic map of subsidence bowl in Alae Crater, November 1970. Topography based on planetable mapping by D. W. Peterson, R. T. Okamura, J. B. Judd, and D. A. Swanson. Geology by D. A. Swanson and D. W. Peterson. Elevation in meters above sea level.

The inner set of faults (fig. 3) was defined by large, gaping cracks as much as 8 m wide and averaging 2–4 m. Almost all of these cracks penetrated the zone of partly molten material (plastic crust) between the crust and melt about 5 m below the surface, and viscous lava from this zone oozed upward and largely filled the cracks (figs. 4 and 6), suggesting that the lava was less dense than the overlying crust. Most of the faults probably bottomed out in this zone (fig. 4), and the tensional opening of the faults apparently took place as lava in this viscous layer slowly flowed toward the axis of subsidence, carrying the overlying crust with it.

Vertical displacement on most of the faults of the inner set was small, although offsets as large as 2 m occurred locally. The surfaces of crustal blocks bounded by large faults

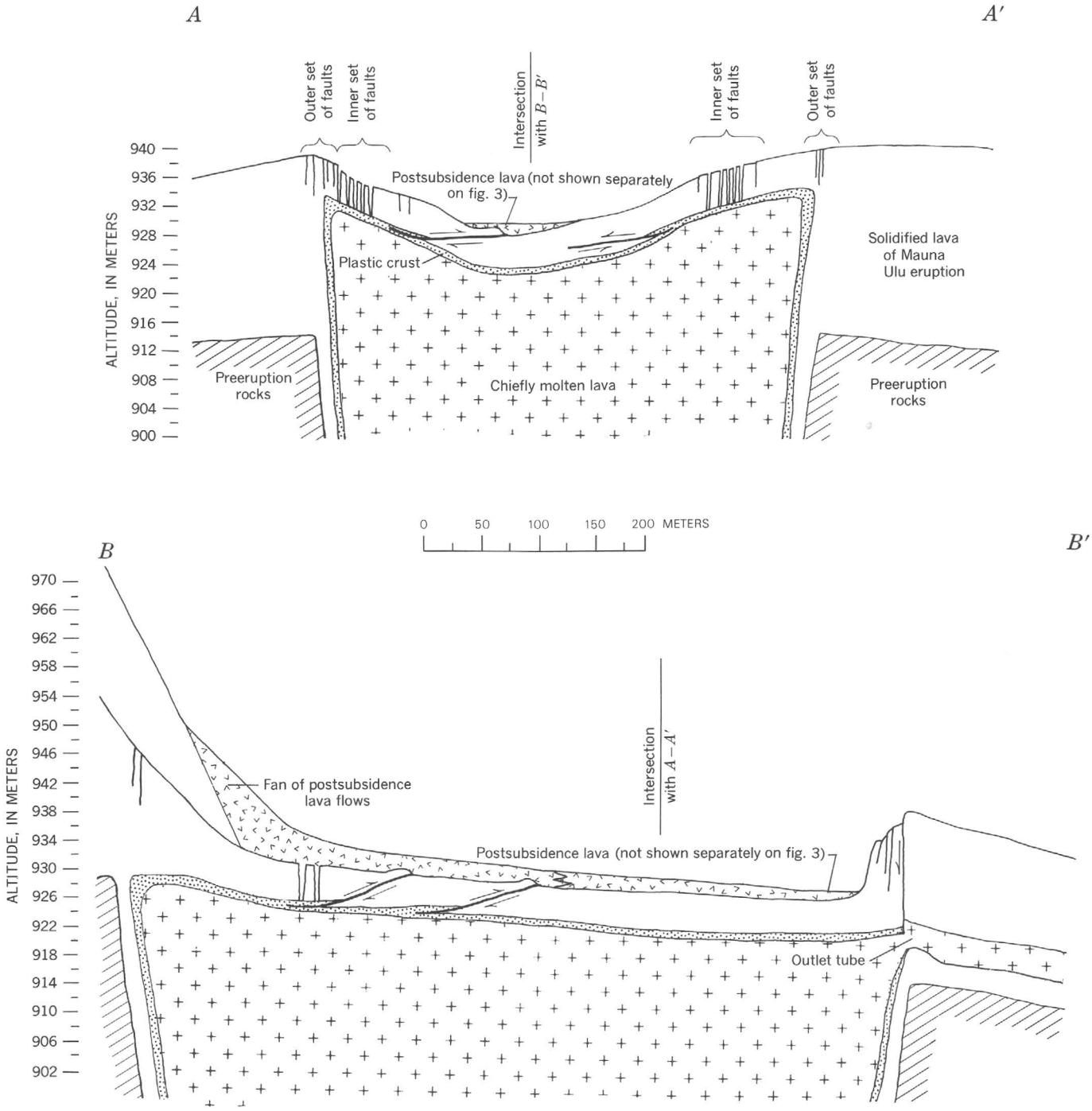

Figure 4.—Schematic cross sections of August 1970 subsidence depression along profile lines shown in figure 3. Lava that oozed upward into open cracks in inner set of faults is not shown. Relations near entrance to outlet tube are generalized; actually this area is jumbled in a highly complex manner owing to postsubsidence rock falls and slumps.

generally dipped inward at the prevailing gradient of the subsidence bowl, but a few were rotated such that dips were flattened or even directed outward. All faults were vertical at the surface.

The inner and outer sets of faults merged toward the southeast end of the crater but formed two separate zones elsewhere (fig. 3). The sets diverged at approximately the location of the buried rim of the inner pit in Alae Crater (fig. 1*A*), and some causal relation seems likely; in detail, however, the correspondence to the rim was far from perfect.

As the two sides of most cracks in both sets could be matched like pieces of a jigsaw puzzle, the azimuth and

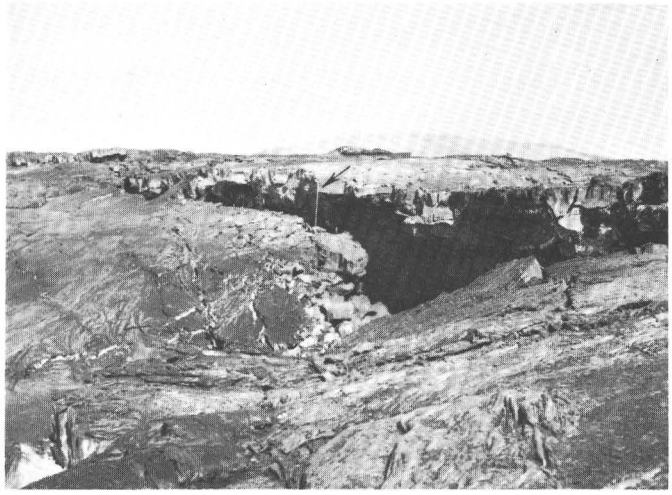

Figure 5.—Vertical displacement on master fault at southeast margin of August 1970 subsidence bowl. Leveling rod (arrow) is 1.5 m long. Note sharply defined trough, a local structure developed immediately adjacent to entrance to outlet tube (hidden in shadow). Photograph taken in mid-November 1970, when lava could be seen flowing in tube from a vantage point in trough. See figure 1 for location.

Figure 6.—Wide crack in inner fault set, east side of subsidence bowl, mid-November 1970. Filled by viscous lava (rough surfaced, dark rock) during August 1970 subsidence; later crustal settling (November 12–13, 1970) caused fault to reopen, cracking lava fill. Leveling rod 1.5 m long spans new crack. See figure 1 for location.

magnitude of the horizontal component of fault displacement could be easily measured (fig. 7). The azimuths of opening were locally quite variable, probably because of slight rotation of blocks or the guiding of stress by preexisting cooling joints; overall, however, they describe an axis of subsidence, not a point source (fig. 8), as do the vertical displacements (fig. 3).

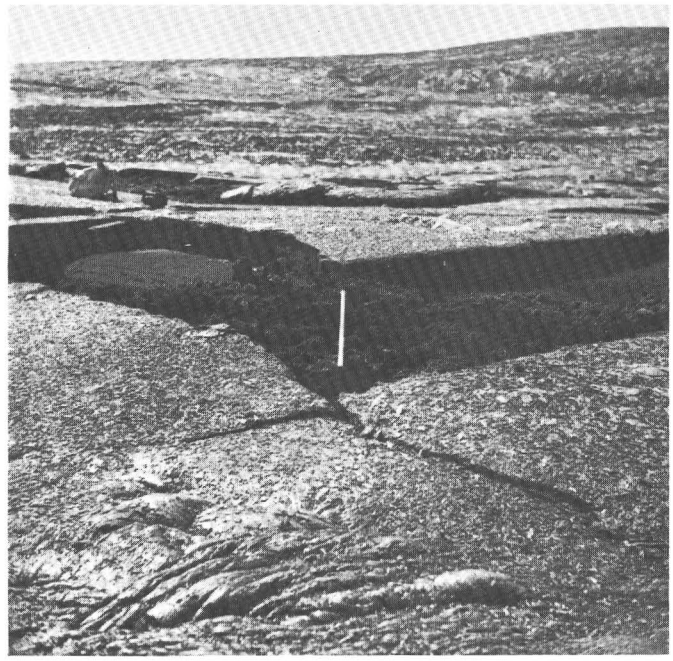

Figure 7.—Tension fault, east side of subsidence bowl, mid-November 1970. Opposite walls can be matched, indicating azimuth and amount of opening. Leveling rod is 1.5 m long. See figure 1 for location.

If minor elastic effects are disregarded, the total amount of extensional opening along a profile perpendicular to the subsidence contours indicates the amount of maximum basinward displacement of the crust within the fault zone (fig. 8). The measured displacement across the two fault zones was about 15 m on the northeastern flank of the subsided area, and about 14 m on the southwestern flank. Horizontal displacement was less than 1 m at the southeast end of the area, where vertical displacement greatly dominated, and was estimated from direct observations and photographs to be several meters at the northwest end, which was covered by new lava before measurements could be made.

The distribution of compressional ridges and domes that formed between the axis of subsidence and the inner set of tensional faults (fig. 8) defined quite closely the line of inflection between tensional and compressional stresses (Yerkes and Castle, 1969; Hamilton and Meehan, 1971, fig. 6). The compressional structures were rarely greater than 5 m high, and many were buried by younger lava before they could be mapped in detail; their approximate locations (fig. 8) are based on aerial photographs taken on August 11. No uplifts formed along the northeastern slope of the subsidence bowl. Elsewhere they were crudely concentric to the subsidence basin, except for the boxwork pattern developed by the northwestern structures. Many, if not all, of the uplifts probably formed by buckling at the toe of the upper plate of thrust faults (fig. 4), a process actually watched during the February 1971 subsidence (fig. 9*A*).

The magnitude of thrusting during the August 1970 subsidence can be easily calculated. The surface distance between

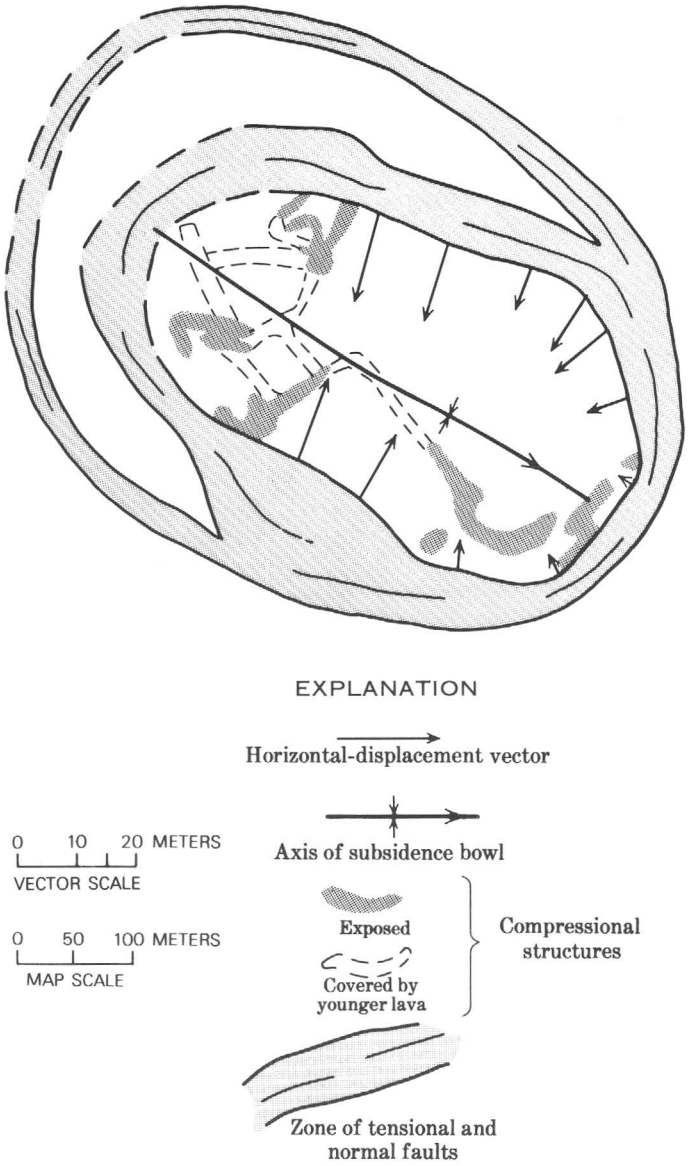

Figure 8.—Generalized structural map of August 1970 subsidence depression, showing horizontal displacement at line of inflection between tensional and compressional strain. Dashed lines indicate structures mapped from aerial photographs taken in mid-August and covered by new lava before geologic map (fig. 3) was made.

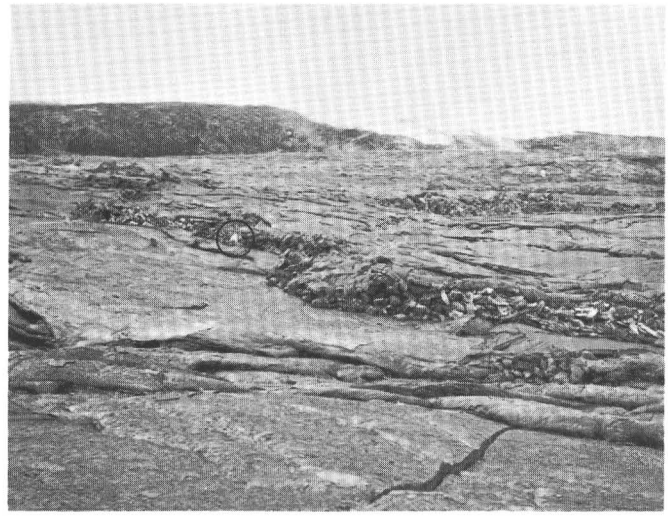

A

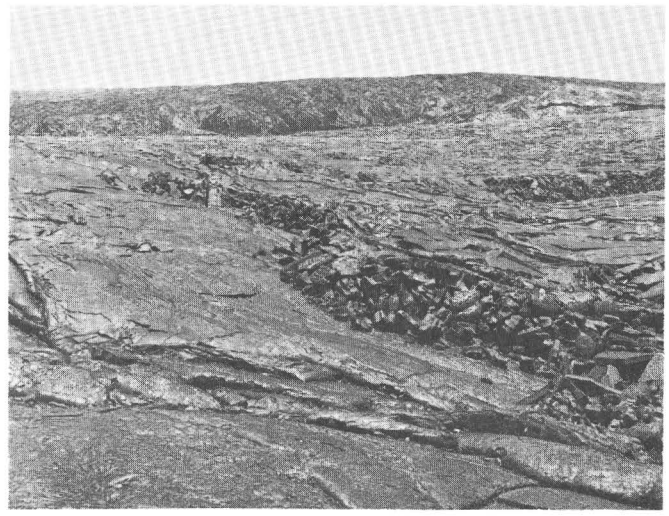

B

Figure 9.—Thrusting and subsidence of lake crust.

A. Actively forming compressional ridge at buckled toe of thrust fault, February 26, 1971. Thrust is moving 1.2 cm/hour toward crouching man (circled). Note how thrust has apparently advanced across what is now the axis of subsidence (near right edge of photograph). Cliff in background consists of 1969–71 lava flows that accreted on preeruption rim of crater, building rim several tens of meters higher. Thickest fume cloud in upper right issues from active inlet tube and hides part of slope of Mauna Ulu. See figure 1 for location.

B. Approximately same view as *A*, June 28, 1971. Note greatly steepened slopes of subsidence bowl, reflecting 6 m of subsidence after photograph *A* was taken and 4 m since March 2.

two points on opposite sides of the lake increased when subsidence occurred, as illustrated in figure 10*A*. If no thrusting is assumed, the difference between x_h (original distance) and x_s (distance after subsidence) should equal the total cumulative opening of the tensional faults (F) less the effect due to compressional buckling and uplift (P), giving $x_h = x_s - F + P$ (fig. 10*A*). However, measurements of the August fault openings and compressional structures (including the required correction for their partial burial) revealed an important discrepancy. A northeast-southwest profile of the actual subsidence bowl showed that $x_s - x_h = 3$ m. The value of P was determined to be a maximum of 13 m. The measured value of F totalled 29 m. According to the equation, however, $F = (x_s - x_h) + P = 3 + 13 = 16$ m. The tension faults had actually opened 13 m farther than they should have if they alone were to account for the increased surface distance across the subsided lake surface.

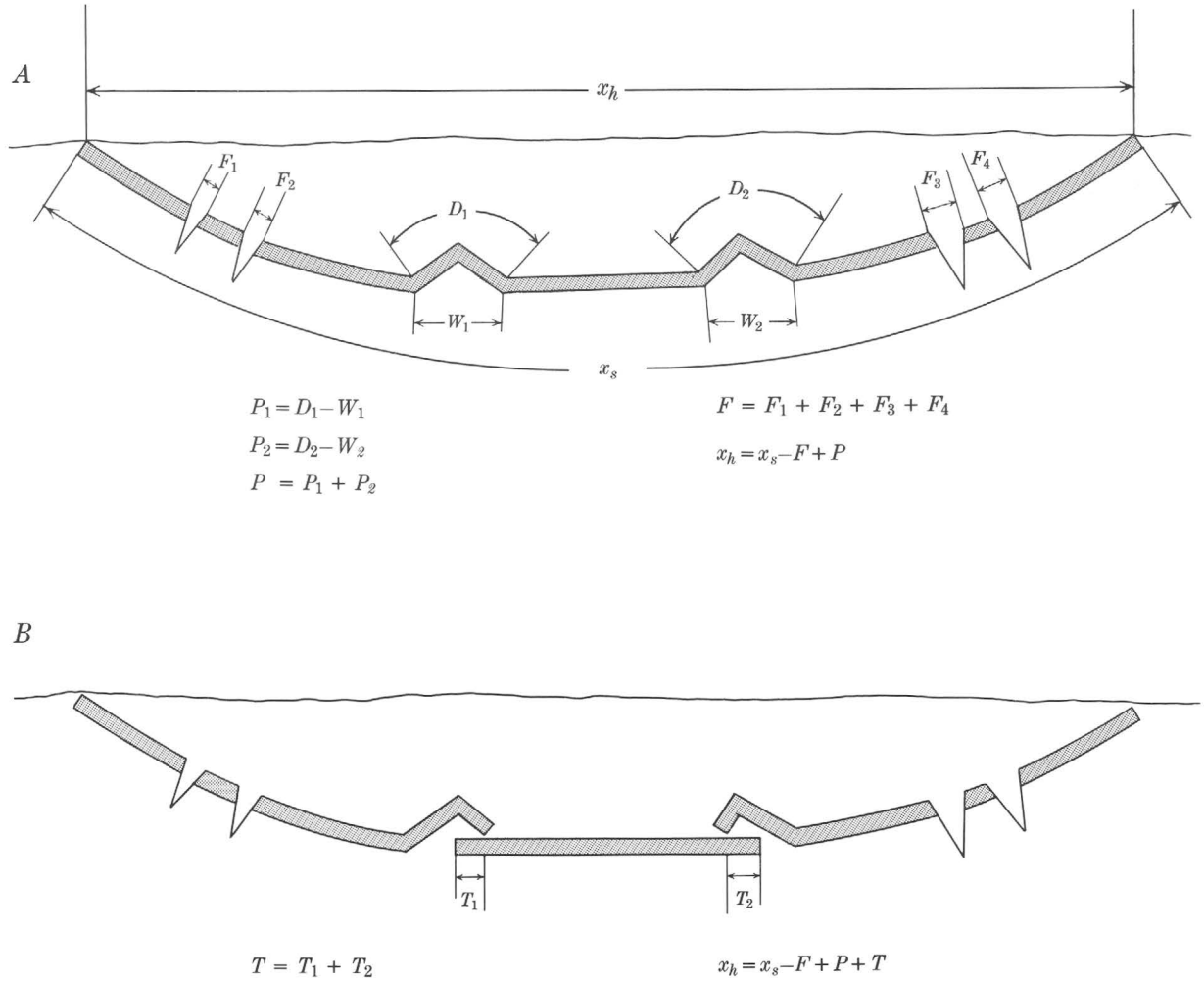

Figure 10.—Diagrams illustrating method of calculating magnitude of thrusting.
A. Relations between presubsidence surface distance across lake (x_h), postsubsidence distance (x_s), total tensional opening of faults (F), and effect of buckling of compressional uplifts (P). Elastic strain is neglected.
B. Similar to *A*, except that effect of thrust faults (T) is included.

The explanation for the discrepancy between predicted and observed surface deformation was discovered during the February 1971 subsidence, when plates of crust were observed being thrust over one another (fig. 9*A*), creating compressional structures of the type formed in August 1970. Hence the relation between x_h and x_s is properly expressed by the equation $x_h = x_s - F + P + T$, where T is the horizontal component of thrusting, as shown in figure 10*B*. According to this interpretation, displacement caused by thrusting amounted to about 13 m during the August subsidence. The thrusting probably took place at the base of the crust or in the layer of viscous, partly crystalline material underlying the crust, and the thrusting was doubtless caused by gravity acting on the sloping sides of the subsidence depression.

Renewed settling occurred during the night of November 12–13, and a partial resurvey revealed that the southeastern part of the depression had lowered about 3 m (fig. 2*C*; table 1). The topography shown in figure 3 is that existing prior to the settling. Several of the larger tensional faults along the east and southeast slope of the depression were reactivated during the settling. The total amount of new fault opening was slightly more than 1 m and was recognized by cracking of the solidified viscous lava fill in several of the August faults (fig. 6) and by pulling away of the inner wall of a large fault from its rooted, viscous lava fill. Lack of evidence for such processes before November 12 suggests little, if any, subsidence between August 13 and November 12.

MECHANISM OF THE AUGUST 1970 DRAINING AND CRUSTAL SUBSIDENCE

The subsidence was caused by a disparity in the rates of flowage of lava into and out of the lake. Direct observations indicate that inflow continued during the subsidence at an

estimated rate of about 1.3×10^4 m^3/hour. The average rate of outflow is roughly calculated to have been about 3.4×10^4 m^3/hour; this average rate assumes the rate of inflow cited above, a subsidence volume of 10^6 m^3 (determined by computer from the topographic map), and a duration of draining of 2 days (noon August 8–noon August 10). The calculated average rate of outflow is probably valid to a factor of 2 and is consistent with lower rate estimates for lava flowing in tubes at times when no draining is taking place (Hawaiian Volcano Observatory, unpub. data, 1970–71).

The preeruption southeast rim of Alae Crater was buried beneath about 24 m of new lava prior to the August draining (fig. 2*A*; table 1). The maximum amplitude of the August subsidence was 13 m; hence the floor of the subsidence bowl was about 11 m higher than the old southeast rim (fig. 2*B*). The thickness of the lava-lake crust which formed the floor of the subsidence depression can be estimated as follows. This crust began to form on October 20, 1969, and was probably about 3 m thick when it was uplifted several meters by subcrustal injection of lava on December 30, 1969 (Swanson and others, 1972), on the basis of the rate of crustal growth determined by Peck and others (1966) and Shaw and others (1968). Injection of the December 30 lava probably disturbed the thermal regime sufficiently to make calculation of subsequent crustal growth unreliable. An upper limiting value, if no thermal disturbance is assumed, gives a total, but unreasonably large, crustal thickness of about 7 m by August 1970. If a crustal thickness of 5 m is assumed, then the base of the crust after the August subsidence was about 6 m higher than the lowest point on the buried southeast rim (fig. 2*B*; table 1).

Observations of the October 20, 1969, surface channel that developed into the outlet tube show that the floor of this tube was 2 to 3 m above the low point on the preeruption southeast rim and 3 to 4 m lower than the base of the subsided crust of the lake (fig. 2*B*).

Knowledge of the relative elevations of the critical features is essential for an interpretation of the subsidence. Hydrostatic pressure in the lake increased sufficiently during the subcrustal addition of lava in early August to reopen the plugged, preexisting lava tube. Lava stored within the lake rapidly drained through the tube at an average rate of about 3.4×10^4 m^3/hour, about 2.5 times the rate of inflow. The upper surface of the molten lava lake (base of crust) consequently dropped to about the level of the top of the lava tube, which probably was several meters above the tube floor. Draining continued at a reduced rate until the outflow in the tube just balanced the inflow of about 1.3×10^4 m^3/hour, at which time the level of molten lava stabilized. The solid crust subsided as its support was withdrawn, and it became detached from the walls, but owing to mechanical lag effects slight amounts of local settling continued for several days beyond the time at which inflow balanced outflow.

The crustal settling of about 3 m on November 12–13 (fig. 2*C*; table 1) is consistent with this interpretation, if the entrance of the outlet tube in early August remained partly blocked to a height of about 3 m above its floor (fig. 2*B*). If this blockage had been removed in November, the lake would have drained and the crust would have settled until the equilibrium state was again reached (fig. 2*C*). An alternative explanation is that the crust settled in November to the level that the surface of molten lava had already reached during the August draining. This explanation implies that a tabular void about 3 m thick existed between the crust and lava surface during the August–November interval, and does not involve draining of excess lava from the lake in November. Either alternative is preferred to one of a relatively sudden decrease in rate of inflow on November 12, which is not indicated by either direct observations of the inflow tube or tilt and seismic records.

The final elevation of the liquid surface of the lava lake was controlled in a basically hydrostatic fashion by the elevation of the entrance to the outlet tube. But details of the subsidence show marked departure from ideal hydrostatic behavior. For example, the crust of the lake should have subsided pistonlike, with no differential settling, if the subsidence were purely hydrostatic. The complex structures on the crust indicate, in fact, considerable mechanical complication. Such structures (fig. 3) include the elongate asymmetric trough that parallels the dominant flow direction, the overall southward slope of the lake surface, and the depression near the exit tube.

Lava behaves more nearly like a Bingham than a Newtonian fluid (Shaw and others, 1968); hence, the laws of hydrostatic fluid behavior did not strictly apply as the lava traveled through the reservoir and drained through the outlet tube. Furthermore, the internal complexity of Alae lava lake (Swanson and others, 1972)–layers of melt sandwiched between partly melted layers of crust–indicates that the lake was not a simple pool of fluid. As a result, the circulation pattern of throughgoing lava in the lake was probably complicated. Lateral gradients in temperature and crystallinity governed local variations in viscosity which, in turn, influenced paths of most rapid flowage. In addition, the effective tensile strength of the crust itself probably was highly variable from place to place, owing to differences in thickness, vesicularity, and adhesion to the walls of the crater; thus the response of the crust to stress changes was nonuniform. Factors such as these must have played a significant part in producing the irregular surface of the downdropped crust throughout the entire subsidence event. Indeed, when all these complications are considered, it is remarkable that the draining and resulting crustal subsidence were as strongly hydrostatically controlled as they were.

DESCRIPTION OF THE FEBRUARY–MARCH 1971 DRAINING AND CRUSTAL SUBSIDENCE

Lava was more or less continually introduced into Alae Crater through the inlet tube and withdrawn through the

outlet tube for several months following the August 1970 subsidence, yet, with the exception of the November 12–13 event, no deformation affected the surface crust of the lava lake. Apparently a balance was struck between the rates of inflow and outflow, about 1.3×10^4 m^3/hour. Between November 1970 and early February 1971, thin surface flows from Mauna Ulu intermittently entered Alae Crater and eventually inundated the entire floor of the subsidence depression, covering the area of maximum subsidence with about 8 m of solidified lava (fig. 2*D*; table 1).

On February 10, 1971, a large volume of lava began to pour onto the lake surface from a tube fed by a fissure about 150 m north of the crater (fig. 1*B*), filling the remainder of the subsidence bowl (about 8×10^5 m^3 in volume) to overflowing within about a day (fig. 2*E*). Lava probably entered the molten lake beneath its surface crust as well, via the preexisting inlet tube. The surface activity continued until February 17, and accretion from overflow of the lake built the southeast rim about 5 m higher, to about 20 m above the preeruption rim (fig. 2*E*; table 1). A flight over the area on February 20 revealed that lava was pouring out of the crater through the outlet tube active since August 1970, but there was no noticeable subsidence of the lake crust. Strong fumes from the old inlet tube in Alae suggested that lava was still entering the lake beneath the surface.

The lake crust had already subsided a maximum of 8 m by February 23, when the crater was visited on the ground. We presume that the subsidence began somewhat earlier, probably on February 21. By February 26, the crust had lowered 17 m, and most of the surface structures related to the subsidence had already formed. Deformation was largely complete by March 2, when the subsidence bowl was about 19 m deep (table 1; fig. 2*F*). Slow settling of the crust continued over the next several months, amounting to an additional 4 m by June 28 (figs. 2*G* and 9*B*). Periodic observations between March 2 and June 28 suggest that the settling ended in May.

The structures produced by the February subsidence were generally similar to those of the August 1970 event, but details were different. The subsidence depression, defined by small faults along its circumference (figs. 11 and 12), was again elliptical in plan view. The southeast end was the deepest, and the northwest end showed barely any subsidence; as a result, the entire floor was inclined toward the southeast at an average gradient of about 1:25. The depression was also asymmetric in a northeast-southwest direction (fig. 12), so that the axis of greatest subsidence was located 20 to 30 m northeast of that formed in August. This asymmetry was reflected by the location of the major faults, which were much larger and more numerous along the northeast slope than anywhere else (figs. 11 and 12). These major faults differed from the otherwise similar August faults by their greater vertical displacements, which averaged 0.5 to 1 m, and by their shallower "roots", generally about 2 m beneath the surface (compare figs. 2*B* and 2*F*).

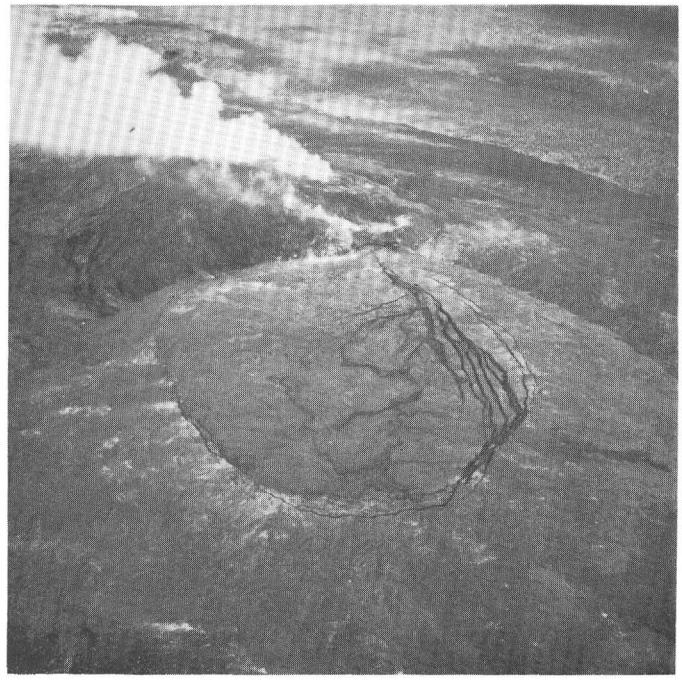

Figure 11.—View looking northwest over February–March 1971 subsidence bowl on March 1, 1971. Sinuous compressional ridges are concentrated near but mostly northeast of axis of subsidence. Tensional faults surround subsidence bowl and define buried rim of Alae Crater. Large faults, with vertical displacement of several tens of centimeters, occur within eastern part of bowl. Largest fume cloud issues from vent at east end of collapsed trench (fig. 1*B*) on flank of Mauna Ulu; smaller cloud near subsidence bowl comes from window in active inlet tube.

Many sinuous compressional ridges and irregular uplifts formed during the February 21–March 2 subsidence (figs. 9, 11, and 12). They tend to outline two crude lobes extending toward the southwest from the northeast flank (figs. 11 and 12). Most of the compressional structures were northeast of the axis of subsidence, as were the tension faults; this coexistence suggests that the compressional structures developed to help accommodate the extension along the northeast limb of the subsidence bowl.

Most of the compressional uplifts probably formed by buckling at the toes of actively moving thrust faults; one such uplift was actually observed in the process of formation on February 26. The upper plate of a thrust, marked by a ridge about 1 m high, advanced at a rate of 1.2 cm/hour over the lower plate (fig. 9*A*). The ridge was buckling and oversteepening as thrusting continued. Large blocks occasionally rolled off the oversteepened slope, only to be slowly pushed ahead or even overridden by the advancing upper plate. The upper plate advanced 3.3 m within the next 4 days (to March 2) but only 10 cm over the next 21 days; movement probably stopped shortly after March 2, although settling continued slowly for 2 months longer (fig. 9*B*). The plane of thrusting was largely within the semisolid, plastic layer immediately

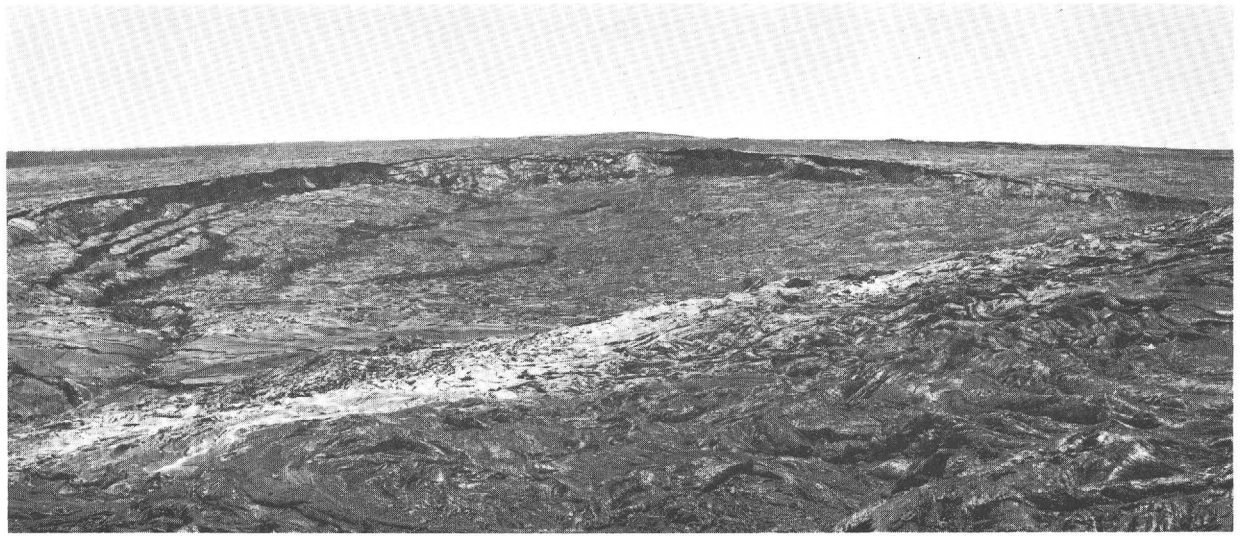

Figure 12.—View looking southeast over February–March 1971 subsidence bowl on June 28, 1971, from southeast flank of Mauna Ulu. Note asymmetry of depression, concentration of large faults on northeast flank, and two lobate compressional ridges near center of photograph. Maximum amplitude of subsidence, near southeast end of depression, is 23 m. Preeruption crater rim is buried 29 m beneath lava flows at southeast end of depression.

below the solid crust, although the toe of the thrust rode over the ground surface. In places, this plastic layer—deeply scored, striated, and crisscrossed by narrow tension cracks—could be seen through cracks in the upper plate. The thrust faults may have bounded large lobes of crust that slid basinward, as suggested by the pattern of compressional structures (figs. 11 and 12).

MECHANISM OF THE FEBRUARY–MARCH 1971 DRAINING AND CRUSTAL SUBSIDENCE

The basic process of draining and crustal subsidence was hydrostatically controlled and virtually the same during the February–March 1971 and August 1970 events: Net lava outflow through a tube exceeded inflow, causing the crust of the lake to subside to a final elevation governed by the outlet tube; the elevation of the base of the crust was the same after each event. The two events, however, were characterized by three significant differences: (1) Immediately prior to the 1971 subsidence, the upper part of the reservoir consisted of new lava whose surface crust was considerably thinner than the crust of the reservoir in early August. (2) The pre-February 10 crust was a solid layer sandwiched between two layers of molten lava above the elevation of the outlet tube; no such layer existed in August (compare figs. 2*A* and 2*E*). (3) This solid layer sank into the underlying lava, thus displacing an equal volume of lava upward and out through the outlet tube. Deductions on the behavior of the solid layer are important to understanding the mechanism of the February–March 1971 subsidence.

The pre-February 10 solid layer must have subsided a total of at least 13 to 16 m, after it was torn from the walls of the crater, to account for the final elevation of the surface of the lake, as determined in the following way. The thin flows added to the floor between November 13 and February 9 had a maximum solidified thickness of 8 m. If the solid layer had sunk just 8 m, however, it would have blocked the outlet tube (fig. 2*E*). Hence, it had to sink an additional 3 to 6 m, as shown in fig. 2*F*, to allow the overlying February 10–17 lava to drain. Finally, observations of the new crust that formed on the February 10–17 lava showed it to be about 2 m thick by the end of the event. Thus the submerged solid layer must have sunk at least as much as the total of these increments, or 13 to 16 m. This sinking implies that the crust had a specific gravity equal to or slightly higher than that of the liquid lava. As measured ranges of specific gravities of solidified basalt and glassy melt samples overlap (Hawaiian Volcano Observatory, unpub. data, 1971), this implication is reasonable, and the upward injection of lava into many of the tension cracks likewise suggests that the lava was less dense than the solid crust.

The solid layer consisted not only of the lake crust that had subsided in August, but also of the series of thin solidified flows, totaling about 10 m in thickness, that had been added between August and February 9 (figs. 2*D*, 2*E*, and table 1). When the lake refilled with the February 10–17 lava, this solid layer formed a barrier between the overlying new lava and the outlet tube (fig. 2*E*). During part of November and December 1970, a hole in the southeast wall of the subsidence bowl was open (fig. 5), and lava in the tube could be seen; this hole had been closed by slump debris when the February filling began, however. Thus we suspect that the barrier was complete in February and that little, if any, of the overlying lava drained immediately into the tube.

The timing and amount of sinking of the lake crust, and the overall behavior of the submerged solid layer during the subsidence, are interrelated. The basin refilled in about 20 hours, 1500 February 10 to 1100 February 11, and the added weight of the new lava, about 16×10^8 kg, on the underlying pre-February 10 solid layer must have greatly strained the fragile attachment of this layer to the solid walls. We do not know whether this attachment held until February 21, the day subsidence began and 4 days after surface inflow ceased, or whether it broke loose soon after the basin was filled or at some intermediate time. Regardless of the exact time, lava overlying this solid layer did not begin to drain through the outlet tube until February 21, indicating that the submerged solid layer remained an effective barrier for 4 days after surface inflow stopped.

If the solid layer had been detached during the surface inflow, it would have sunk whole or piecemeal as long as lava beneath it was able to escape through the outlet tube. However, the solid layer would have blocked the tube after it subsided 1 to 3 m, causing the system to become static. This metastable blockage could have existed indefinitely if the solid layer were of equal or only slightly higher specific gravity than the molten lava, or if the layer were hung up on the inward sloping walls of the crater.

For the period immediately preceding and including February 21, then, one of the following situations obtained:

1. The submerged solid layer blocked the outlet tube. In this situation, addition of lava from the inlet tube (which aerial observations suggest was still carrying lava) would have increased hydrostatic pressure in the lake beneath the solid layer, eventually breaking the layer and allowing communication between the outlet tube and the liquid lava on either side of the solid layer. The solid layer would then have sunk as lava drained out the tube.
2. The submerged solid layer remained attached to the walls above the level of the outlet, leaving the underlying liquid lava free to flow out the tube. In this situation, the hydrostatic pressure in the lake almost certainly would not have increased, because the inflow rate would have had to increase manyfold to exceed the capacity of the outlet tube. More likely, in fact, inflow dwindled after surface flowage stopped. In any case, the weight of overlying lava eventually caused the solid layer to tear away from the walls, allowing this lava to drain through the tube, the process being delayed until February 21 because of rate-related mechanical parameters, perhaps including some partial melting. The solid layer would have had to crack near the outlet tube for the underlying lava to be displaced upward and out the tube as the solid layer sank.

We cannot decide between these possibilities, nor can we state whether the solid layer sank piecemeal or as a whole. The general southeastward slope of the floor of the subsidence bowl suggests, however, that the solid layer was "hinged" and sank as a trap door, with maximum sinking adjacent to the outlet tube.

SUMMARY

1. The August 1970 partial draining of a lava lake in and above Alae Crater occurred when increased hydrostatic pressure accompanying renewed inflow forced a sealed, inactive tube to reopen. Outflow through the reopened tube was rapid, exceeding flow into the reservoir by a factor of about 2.5, and the crust of the lake subsided. When the crust lowered to a level governed by the elevation of the tube, the rate of outflow decreased; net draining ceased when the outflow balanced the inflow. Local crustal settling continued for several more days because of mechanical lag effects.

2. Peripheral tensional faults and central compressional ridges were developed by basinward sliding of blocks and lobes of solid crust over the partly molten, semisolid substratum under the influence of gravity. The amounts of tensional and compressional deformation were balanced if the extension of the surface due to subsidence is considered.

3. A small episode of crustal settling took place November 12–13, probably as a result of further opening of the outlet tube or lowering of the crust to the top of the molten lake; no accompanying reduction in inflow rate was recognized.

4. The August subsidence bowl was refilled in February 1971, and the subsequent draining and crustal subsidence were hydrostatically controlled and basically analogous to the August event. Shallower faults developed during the February subsidence owing to the thinner crust. Additional complexities in the reservoir plumbing system were created by the sinking of the pre-February crust and consequent displacement of an equal volume of underlying molten lava. Most crustal subsidence was complete within 2 weeks, but slight settling continued for 2 to 3 months as the crust slowly adjusted mechanically.

5. The observed relations between draining of molten lava, subsidence of the surface crust, and rates of inflow and outflow help confirm and refine the active role that the Alae lava reservoir played in the shallow conduit system feeding flows that descended the south flank of Kilauea from August 1970 to May 1971.

A new chapter was added to Alae's history in early 1972. Lava from a new eruption at Mauna Ulu first reached the 1971 subsidence bowl on February 7, and by February 12 the bowl was filled. Lava spilled over the southeast rim and fed a surface flow, but no lava entered the outlet tube that had drained Alae in 1970 and 1971. The flow into Alae ended about February 16, and the crust subsided only 1 to 2 m, probably solely because of cooling. Lack of lava in the outlet tube and lack of significant subsidence together support the conclusion that tube activity and crustal subsidence are directly related.

REFERENCES

Anderson, L. A., Jackson, D. B., and Frischknecht, F. C., 1971, Kilauea Volcano—Detection of shallow magma bodies using the VLF and ELF induction methods: Am. Geophys. Union Trans., v. 52, no. 4, p. 383.

Greeley, Ronald, 1971, Observations of actively forming lava tubes and associated structures, Hawaii: Modern Geology, v. 2, p. 207–223.

Hamilton, D. H., and Meehan, R. L., 1971, Ground rupture in the Baldwin Hills: Science, v. 172, no. 3981, p. 333–344.

Peck, D. L., Wright, T. L., and Moore, J. G., 1966, Crystallization of tholeiitic basalt in Alae lava lake, Hawaii: Bull. Volcanol., v. 29, p. 629–656.

Shaw, H. R., Wright, T. L., Peck, D. L., and Okamura, R. T., 1968, The viscosity of basaltic magma: An analysis of field measurements in Makaopuhi lava lake, Hawaii: Am. Jour. Sci., v. 266, p. 225–264.

Swanson, D. A., 1972, Pahoehoe flows from the 1969–71 Mauna Ulu eruption, Kilauea Volcano, Hawaii: Geol. Soc. America Bull. [Inpress]

Swanson, D. A., Duffield, W. A., Jackson, D. B., and Peterson, D. W., 1972, The complex filling of Alae Crater, Kilauea Volcano, Hawaii: Bull. Volcanol. [In press]

Swanson, D. A., Jackson, D. B., Duffield, W. A., and Peterson, D. W., 1971, Mauna Ulu eruption, Kilauea Volcano: Geotimes, v. 16, no. 5, p. 12–16.

Yerkes, R. F., and Castle, R. O., 1969, Surface deformation associated with oil and gas field operations in the United States: Assoc. Internat. D'Hydrologie Scientifique, Extrait de la Pub. 88, Colloque de Tokyo, 1969, p. 55–66.

FLUID-INCLUSION STUDIES OF SOME GOLD DEPOSITS IN NEVADA

By J. THOMAS NASH, Menlo Park, Calif.

Abstract.—Fluid inclusions were studied in samples from nine gold-producing districts in Nevada. The ore fluids are characterized by low salinities, commonly below 2.1 wt percent NaCl equivalent. These salinities are less than those of most base-metal deposits but still higher than those of hot-spring systems, which provide an excellent model for the gold deposits. Fluid-inclusion homogenization temperatures range from 200° to 330°C for the gold-adularia veins; this large range suggests that temperature is not a prime factor in the formation of these deposits. Disseminated fine-gold deposits at Carlin, Cortez, and Gold Acres appear to have formed at about 200°C from solutions of about 6 percent salinity. Fluid density and pressure played major roles in the genesis of these deposits and are considered to be useful parameters in conceptual exploration models.

Fluid inclusions have been studied in vein samples from nine gold-producing districts in Nevada in order to learn the chemical and physical nature of the ore-forming fluids and to outline some systematic similarities and differences between these deposits. The ore deposits studied fall into two groups, according to geologic occurrence: (1) vein deposits of gold with quartz and adularia in structurally simple fissures, and (2) disseminated gold deposits in complexly deformed and altered carbonate rocks. The geology of many of these gold districts is discussed by Roberts and others (1971). Although sampling in most districts was limited to mine dumps, these studies nevertheless permit a fair reconstruction of part of the geochemical system.

Samples were examined megascopically for paragenetic relations, and fluid inclusions were studied in conventional thin sections or in doubly polished thinned plates. Some inclusions were studied on a freezing stage similar to Roedder's (1962) to obtain a measure of fluid salinity by the depression-of-freezing-point technique and then tested on the heating stage. The methods and assumptions of these techniques have been discussed elsewhere (Roedder, 1967a; Nash and Theodore, 1971).

GOLD-QUARTZ-ADULARIA VEINS

Examples of the classic gold-quartz-adularia veins have been studied from the Tenmile, Round Mountain, Manhattan, Jefferson, and Aurora districts of Nevada (fig. 1). These veins are typically open and vuggy, and the well-formed quartz crystals contain excellent fluid inclusions. A series of samples, collected in the Tenmile district, will be described in detail, then briefly compared with examples from other districts. The vein-gold deposits at Copper Canyon (Nash and Theodore, 1971), which are similar mineralogically except that they do not contain adularia, are included for comparison.

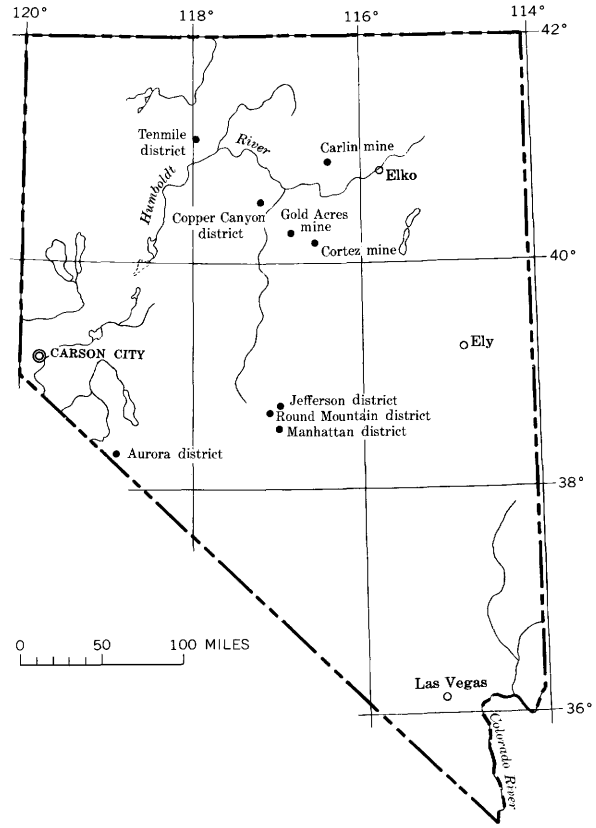

Figure 1.—Index map of Nevada, showing location of deposits studied.

U.S. GEOL. SURVEY PROF. PAPER 800-C, PAGES C15–C19

Tenmile district

Gold deposits in the Tenmile district (fig. 1) occur in phyllitic rocks of the Triassic Raspberry Formation (Ferguson and others, 1951). Small stocks of Tertiary granodiorite intrude the Raspberry, and in places the ore seems to be related to dikes of "diorite" porphyry. The veins appear to have been complexly sheared and are discontinuous. From field observations in trenches and from samples on mine dumps, it was possible to determine that the paragenetic sequence was similar throughout the district and consists of early massive milky quartz, grading into euhedral glassy amethystine quartz, followed by clear euhedral quartz before and intergrown with adularia, and finally, drusy quartz. Free gold occurs in the amethystine to clear-quartz stage and possibly overlaps the adularia stage. Minor amounts of pyrite occur in the early quartz and on adularia. No appreciable wallrock alteration was observed. Late calcite associated with manganese oxide occurs in the northern fringe of the district, and in these deposits, no adularia was seen.

Measurements of the temperature at which the two-phase (liquid + vapor) fluid inclusions in quartz homogenize to a single liquid phase give approximate temperatures of formation for that particular stage of mineralization (table 1). In the Tenmile district, temperatures ranged from 330° to 135°C.

Table 1.—*Fluid inclusion data from gold-producing deposits, Tenmile district, Nevada*

[All sample localities are in R. 36 E., T. 36 N.; N.d., not determined]

	Sample No.	Homogenization temperature (°C)	Salinity (wt percent NaCl)
Tenmile or Taylor mine (SE¼ sec. 22):			
Later clear quartz	N70	245	7.3
Reo mine area (shaft, SW¼ sec. 22):			
Quartz, pre-adularia, gold?	N71a	270	1.7
Quartz, post-adularia	N71b	250	1.7
Reo mine area (trench, NW¼ sec. 22):			
Quartz, pre-adularia, gold	N72	305	2.0
Quartz, pre-adularia	N14	295	1.0
Reo mine area (trench, NE¼ sec. 22):			
Quartz, late?	N73	245	6.4
Unnamed mine (adit, SW¼ sec. 22):			
Quartz, pre-adularia, gold?	N74	308	2.1
Golden Amethyst mine (trench, NE¼ sec. 28):			
Amethystine quartz; gold	N75B	302	2.1
Amethystine quartz; gold	N13	295	1.2
Clear quartz, visible gold	N15	330	1.8
Late quartz, post-adularia	N75C	248	1.6
Mitzie mine (adit, sec. 9):			
Clear quartz, overlain by calcite	N76	265	N.d.
Mullinix mine (shaft, sec. 5):			
Clear early quartz; gold?	N77A	300	1.0
Amethystine quartz; gold?	N77B	285	1.0
Amethystine quartz	N12	265	.9
Late rhomb calcite	N77C	135	.4

The late calcite plus manganese oxide stage formed at distinctly cooler temperatures and presumably is not related to the gold mineralization. Where several stages could be examined from a single sample, the conditions of gold mineralization can be bracketed rather closely. The range of homogenization temperatures for the gold stage is 270° to 330°C, or an average of about 300°C. The homogenization temperatures are minimum temperatures of formation, and a correction for pressure must be added to them. This correction would be about +10°C for 1 mile of hydrostatic head and would be larger for greater depths or lithostatic conditions. A correction of +10°C to no more than 25°C seems appropriate for this setting, bringing the actual temperature range of gold mineralization to about 285° to 340°C±15°C.

Fluid inclusions from the Tenmile district give three types of geochemical information about ore-forming fluids through (1) daughter minerals, (2) first-melting characteristics, and (3) the freezing point of the fluids. Many inclusions contain a lathlike, birefringent daughter mineral with inclined extinction whose optical properties suggest chlorite or dawsonite (Sillitoe and Sawkins, 1971). If these mineralogic interpretations are correct, these daughter minerals provide evidence for the presence of aluminum, iron, and magnesium, or sodium, aluminum, and carbonate in the fluids. When cooled to -35°C, these fluid inclusions have a clear, slightly granular appearance, indicating partial melting. This very low temperature of first melting suggests the presence of calcium in the solution, in addition to sodium and potassium (Roedder, 1971). The temperature at which the last ice crystal in an inclusion remains in equilibrium with the solution is equivalent to the freezing point of the solution. The freezing-point, or freezing-point-depression, determination is best expressed in terms of NaCl content that would produce an equivalent depression. Sodium and chlorine are typically the major ions in fluid inclusions; thus the system, NaCl–H_2O, is a reasonable approximation. Determinations of depression of freezing point range from -0.2° to -4.4°C and are equivalent to 0.4 to 7.3 wt percent NaCl (table 1). Values for the gold stage of metallization in this district are in a narrow range from 1.0 to 2.1 wt percent NaCl, which is very low by comparison to most metal deposits.

The gold mineralization is associated with quartz and adularia, and even if the gold occurs without adularia, the fluids probably were close to or in the adularia stability field. Experimental work indicates that at 300°C the ratio of K^+ to H^+ would be about $10^{3.4}$ (Meyer and Hemley, 1967), which is considerably more alkaline than other common fluids producing, for example, argillic alteration. The indicated pH is nevertheless about 1 unit more acidic than neutrality at this temperature.

Other gold-quartz-adularia veins

Fluid inclusions in veins comparable to those of the Tenmile district (table 2) indicate that these veins likewise formed from

Table 2.—*Fluid inclusion data from some gold-adularia deposits in Nevada*

[N.d., not determined]

District	Mineral[1]	Sample No.	Homogenization temperature (°C)	Salinity (wt percent NaCl)
Jefferson	Q	41	255	0.8
Round Mountain	Q	39	260	.2–1.4
	Q	69	250	.2–1.0
Aurora	Q	130	255	.5
	Q	131	255	1.7
	Q	133	227	N.d.
	Q	134	245	.2
Manhattan	F	52	220	.6
	C	53	205	.5
	F	54	210	.6
	C	56	222	.4–1.9
	F	57g	200	.5
	F	57w	215	.8
	Q	57	235	.8
	C	67	233	.3
Copper Canyon	Q	31	299	4.9
	Q	35	330	8.0
	Q	37	230	2.1
	Q	41	305	1.8–33
	Q	48	302	.3–9.4
	Q	50	225	4.0
	Q	84	292	12.2
	Q	95	265	9.3
	Q	100	250	1.8

[1] Q = quartz, F = fluorite, C = calcite.

solutions of very low salinity. However, note that there is a great range of temperatures represented by the several districts, but within each district the temperature range is rather small (for the small number of samples examined). The common occurrence of salinities of less than 2.1 wt percent NaCl is a parameter that these deposits seem to have in common, a parameter that apparently is independent of temperature. In some samples, the salinities are higher, and in others, salinity varies greatly within single crystals, which has been interpreted to reflect boiling (Nash and Theodore, 1971, p. 395). Boiling does not seem to be characteristic of these deposits, because the fluid-inclusion phase proportions and compositions generally are very consistent within a sample.

DISSEMINATED DEPOSITS

The open pit at Gold Acres (fig. 1) yielded some quartz veins suitable for study, and four samples contained inclusions large enough for freezing tests. Attempts to study the fine-gold deposits at Carlin and Cortez have been frustrated by very fine grained material with small fluid inclusions. In all of these deposits, the age relationship of quartz and its contained fluid inclusions to gold has been difficult to establish and is not known with any certainty.

The fluid-inclusion studies at Gold Acres were fairly successful; seven samples of vein quartz, some with coexisting sulfides, were examined on the heating stage. The range of homogenization temperatures in six was from 160° to 185°C; inclusions in one other sample homogenized at 265°C, and they may represent a separate stage of mineralization or could be anomalous. Visual estimates on six other vein samples suggested homogenization temperatures near 175°C. Freezing-stage determinations on four samples ranged from 5.4 to 7.3 wt percent NaCl, with no apparent temperature correlation.

Silicified limestone and small quartz veinlets in the Carlin and Cortez deposits contain abundant fluid inclusions, but all are less than 10 microns, and none are suitable for the freezing stage. Observation at about X 1,000 permits easy recognition of the inclusions; they consistently have low vapor fractions near 5 volume percent, but within many samples, there is variation from about 3 to 10 volume percent, probably the result of changes after trapping. No daughter minerals have been noted, but liquid CO_2 is present in several samples from the Carlin mine. Judging from the vapor fractions, I infer that the inclusions would homogenize at 175±25°C. With provision for a pressure correction, 200°C would seem to be a reasonable estimate of the temperature of formation at Carlin and Cortez.

DISCUSSION

These gold deposits all have similar relatively low salinity fluids. However, from one district to another, there are rather large differences in apparent temperature of formation. The disseminated fine-gold deposits seem to have formed at lower temperatures than the gold-adularia veins. In order to elucidate the nature of these deposits, they will be compared with some other types of metal deposits studied by the same fluid-inclusion techniques, and with hot springs.

Paired heating- and freezing-stage data from fluid inclusions (fig. 2) point out a broad range of ore-fluid salinities and temperatures observed in several types of metal deposits having different geologic settings. Note that fluid-inclusion data for Gold Acres and gold-adularia vein deposits fall into a distinctive area of figure 2 because of their low salinities. If the salinities observed in samples from Gold Acres are typical of the disseminated gold deposits, then the fluids in that type of deposit do not quite overlap those of the gold-adularia veins. The differences in salinities between the two types of gold deposits is not great and is not considered as instructive as the differences relative to the base-metal deposits.

Fluid density, which has both chemical and physical influence, is an appropriate parameter for characterizing ore fluids. Fluid densities in ancient systems may be determined only from measurements on fluid inclusions. On figure 2, densities for the system NaCl–H_2O (Haas, 1970) are shown as an approximation of the more complex natural fluids, with the assumption that homogenization temperatures are not much different from formation temperatures and that the volatile content was low. With the grid on figure 2, the density of any fluid inclusion can be estimated from its salinity and homogenization temperature. In terms of density, the gold-adularia vein-forming fluids, as well as those from Gold Acres, fall into distinct areas of the figure. The rather large spread in densities from the gold-adularia deposits ($\rho \approx 0.87$ to 0.70 g/cc) reflects

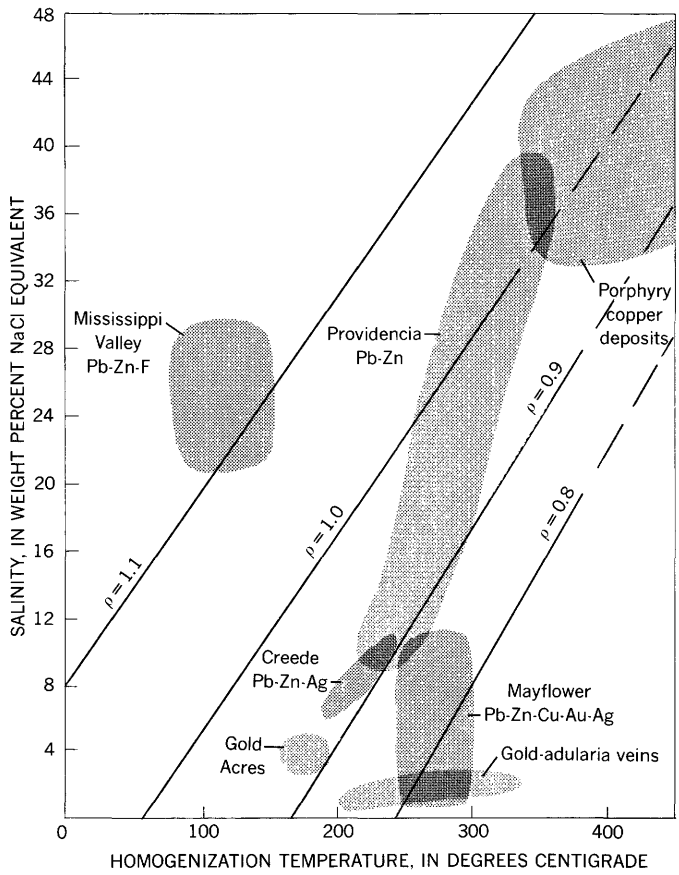

Figure 2.—Fluid-inclusion homogenization temperature and salinity data for some gold and base-metal deposits. Diagonal grid shows fluid densities (ρ), in grams per cubic centimeter, from the system $NaCl-H_2O$ (Haas, 1970). Data for Gold Acres mine and the gold-adularia deposits are from this study. Data for base-metal deposits are generalized from the following sources: Mississippi Valley type deposits (Roedder, 1967b); Creede, Colo., OH vein (Roedder, 1965; Nash, unpub. data); Mayflower mine, Utah (Nash, 1972); Providencia district, Mexico (Sawkins, 1964); porphyry copper deposits (Nash and Theodore, 1971; Roedder, 1971; Nash, unpub. data).

the large temperature range observed for those deposits. These very low densities seem to be characteristic of an environment in which near-surface waters circulate in open fractures. The densities inferred from the Gold Acres data are somewhat higher than for the gold-adularia veins. A contrasting environment characterized by high-density fluids of the type observed in porphyry copper deposits (fig. 2) may be common in and adjacent to intrusive rocks of the Basin and Range province, whether or not they are mineralized (Zirkel, 1876; J. T. Nash, unpub. data). These postmagmatic fluids in intrusive rocks owe their high densities to salinities commonly in the range 30 to 50 wt percent. Because of the density difference, the dilute low-density fluids of the gold-adularia deposits, and possibly the disseminated deposits, may be reasonably inferred to have floated above the hotter postmagmatic fluids in intrusive rocks. Fluid density thus is believed to be a possible tool in exploration: if, in mapping fluid-inclusion types and corresponding densities, one can demonstrate lateral or vertical zonation, these zones may suggest targets for finding ore associated with low-density (epithermal gold?) or high-density fluids (disseminated copper or molybdenum?).

Selection of exploration targets on the basis of temperature is not recommended because other physical and chemical parameters seem more important in the mineralizing process. The observed wide range from 200° to 330°C in homogenization temperatures in different districts having comparable mineralogic systems suggests that temperature is not of prime importance in gold deposition. Contrary to some inferences about temperatures (Helgeson and Garrels, 1968; Roberts and others, 1971), I recognize no special or optimum temperatures of formation. Chemical parameters, such as oxygen and sulfur fugacity, are important (Barnes and Czamanske, 1967), as are chemical interactions with wallrocks (Meyer and Hemley, 1967). Furthermore, relatively small changes in pressure may be very important at shallow depths because of the effect of pressure on carbon dioxide solubility and boiling, both of which strongly influence pH and chemical reactions. Although these fluid-inclusion observations do not document changes in carbon dioxide pressures, that mechanism may well explain the precipitation of adularia in this environment (Ellis, 1967; Meyer and Hemley, 1967).

The physical properties and possibilities of fluid zonation outlined above can be supplemented by geochemical reasoning on the behavior of gold during hydrothermal transport. Gold forms very stable complexes with either sulfide or chloride ligands (Barnes and Czamanske, 1967; Helgeson and Garrels, 1968; Weissberg, 1970) and can be expected to be deposited after most other metals. The mechanisms of increasing pH or decreasing temperature should lead to deposition from either of these gold complexes; oxidation promotes deposition from gold-sulfide complexes, whereas reduction breaks up gold-chloride complexes. There is much debate about which gold complex is relevant in nature. Salinity determinations indicate that chloride concentrations are far in excess of likely ore-metal concentrations, thus permitting formation of chloride complexes. Fluid-inclusion data cannot answer questions of sulfide-ion activity, but in gold deposits, sufficient sulfide minerals seem to be present to provide evidence for gold transport as a sulfide complex. Regardless of these details, it is significant that either transport model implies gold deposition after most other metals and a spatial zonation that agrees well with the observed zonation of fluids.

The salinities of the gold-depositing fluids approach those of hot springs (Ellis, 1967; White, 1967), although many of the salinities determined here are higher. Other types of metal-depositing fluids typically are orders of magnitude more saline than are those in hot springs. Unfortunately, we do not know enough about the chemistry of these inclusion fluids to make further comparisons. The present observations are qualitatively similar to the recent observations of silver and gold that are

being deposited from hot-spring precipitates (Weissberg, 1969), although most of the gold-adularia deposits appear to contain smaller quantities of sulfides than do those reported by Weissberg. It is interesting to note also that the maximum temperature observed in these deposits agrees with a similar limit for modern hot springs (D. E. White, oral commun., 1970; Ellis, 1967). The physical and chemical processes in hot springs thus provide an excellent model for these gold deposits.

REFERENCES

Barnes, H. L., and Czamanske, G. K., 1967, Solubilities and transport of ore minerals, *in* Barnes, H. L., ed., Geochemistry of hydrothermal ore deposits: New York, Holt, Rinehart, and Winston, Inc., p. 334–381.

Ellis, A. J., 1967, The chemistry of some explored geothermal systems, *in* Barnes, H. L., ed., Geochemistry of hydrothermal ore deposits: New York, Holt, Rinehart, and Winston, Inc., p. 465–514.

Ferguson, H. G., Muller, S. W., and Roberts, R. J., 1951, Geology of the Winnemucca quadrangle, Nevada: U.S. Geol. Survey Geol. Quad. Map GQ-11.

Haas, J. L., 1970, An equation for the density of vapor-saturated NaCl–H_2O solutions from 25° to 325°C: Am. Jour. Sci., v. 269, p. 489–493.

Helgeson, H. C., and Garrels, R. M., 1968, Hydrothermal transport and deposition of gold: Econ. Geology, v. 63, p. 622–635.

Meyer, Charles, and Hemley, J. J., 1967, Wall rock alteration, *in* Barnes, H. L., ed., Geochemistry of hydrothermal ore deposits: New York, Holt, Rinehart, and Winston, Inc., p. 166–235.

Nash, J. T., 1972, Geochemical studies in the Park City district, Utah–Pt. 1, Ore fluids in the Mayflower mine: Econ. Geology, v. 67 [In press].

Nash, J. T., and Theodore, T. G., 1971, Ore fluids in a porphyry copper deposit at Copper Canyon, Nevada: Econ. Geology, v. 66, p. 385–399.

Roberts, R. J., Radtke, A. S., and Coats, R. R., 1971, Gold-bearing deposits in north-central Nevada and southwestern Idaho, *with a section on* Periods of plutonism in north-central Nevada, by M. L. Silberman and E. H. McKee: Econ. Geology, v. 66, p. 14–33.

Roedder, Edwin, 1962, Studies of fluid inclusions–Pt. 1, Low temperature application of a dual-purpose freezing and heating stage: Econ. Geology, v. 57, no. 7, p. 1045–1061.

——1965, Evidence from fluid inclusions as to the nature of the ore-forming fluids, *in* Symposium–Problems of postmagmatic ore deposition with special reference to the geochemistry of ore veins, Prague, 1963, v. 2: Prague, Geol. Survey of Czechoslovakia, p. 375–384.

——1967a, Fluid inclusions as samples of ore fluids, *in* Barnes, H. L., ed., Geochemistry of hydrothermal ore deposits: New York, Holt, Rinehart, and Winston, Inc., p. 515–574.

——1967b, Environment of deposition of stratiform (Mississippi Valley type) ore deposits, from studies of fluid inclusions, *in* Brown, J. S., ed., Genesis of stratiform lead-zinc-barite-fluorite deposits in carbonate rocks: Econ. Geology, Mon. 3, p. 349–361.

——1971, Fluid inclusion studies on the porphyry-type ore deposits at Bingham, Utah, Butte, Montana, and Climax, Colorado: Econ. Geology, v. 66, p. 98–120.

Sawkins, F. J., 1964, Lead-zinc ore deposition in the light of fluid inclusion studies, Providence mine, Zacatecas, Mexico: Econ. Geology, v. 59, p. 883–9191.

Sillitoe, R. H., and Sawkins, F. J., 1971, Geologic, mineralogic, and fluid inclusion studies relating to the origin of copper-bearing tourmaline breccia pipes, Chile: Econ. Geology, v. 66, p. 1028–1041.

Weissberg, B. G., 1969, Gold-silver ore-grade precipitates from New Zealand thermal waters: Econ. Geology, v. 64, p. 95–108.

——1970, Solubility of gold in hydrothermal alkaline sulfide solutions: Econ. Geology, v. 65, p. 551–556.

White, D. E., 1967, Mercury and base-metal deposits with associated thermal and mineral waters, *in* Barnes, H. L., ed., Geochemistry of hydrothermal ore deposits: New York, Holt, Rinehart, and Winston, Inc., p. 575–631.

Zirkel, Ferdinand, 1876, Microscopical petrography: U.S. Geol. Explor. 40th Parallel (King), v. 6, 297 p., 12 pls.

PETROGRAPHIC EVIDENCE OF VOLUME INCREASE RELATED TO SERPENTINIZATION, UNION BAY, ALASKA

By ALLEN L. CLARK and WILLIAM R. GREENWOOD,
Menlo Park, Calif., Jiddah, Saudi Arabia

Work supported in part by National Aeronautics and Space Administration

Abstract.—Petrographic studies of samples from the dunite core of the ultramafic complex at Union Bay in southeastern Alaska reveal several features that indicate volume expansion was associated with serpentinization. These features include kink bands offset along transecting serpentine veinlets, rotated fragments of larger olivine grains enclosed by serpentine, expanded chromite grains cut by serpentine-filled fractures, and radially fractured diopside grains adjacent to preferentially serpentinized olivine grains.

The question of which remains constant during serpentinization of ultramafic rocks—volume or composition—has been debated by Turner and Verhoogen (1960, p. 316–321) and Thayer (1966), who believe that serpentinization is an equal volume process accompanied by the loss of MgO and SiO_2, and by Shteinberg (1960), Hess and Otalora (1964), Green (1964), and Hostetler and others (1966), who contend that serpentinization involves volume increase with constant composition except for hydration. Beeson and Jackson (1969) maintain that under certain conditions both volume and composition may remain constant. This paper presents petrographic evidence that has a bearing on the problem.

GENERAL GEOLOGY

The ultramafic complex at Union Bay, southeastern Alaska, approximately 35 miles north-northwest of Ketchikan, is one of 35 or more ultramafic bodies that crop out along the 350-mile-long Alaskan panhandle (fig. 1) (See Clark and Greenwood, 1972, p. C157–C160, this chapter).

Previous studies on the complex at Union Bay resulted in a number of brief descriptions by Buddington and Chapin (1929), Kennedy and Walton (1946), and Walton (1951), and a detailed report by Ruckmick and Noble (1959). A review of the zoned ultramafic occurrences of southeastern Alaska by Taylor (1967) includes a sketch map and a brief description of the complex at Union Bay.

Ruckmick and Noble (1959, p. 981) describe the complex as follows:

> A body of gabbro, approximately circular in plan and about 6 miles in diameter, intrudes folded sedimentary rocks of probably Triassic and Cretaceous age. A moderately low grade of regional metamorphism in the sedimentary rocks is increased to almandite-zone grade adjacent to the gabbroic contact. Intrusive into the gabbro is a remarkable ultramafic complex which comprises a vertical pipe approximately 1 mile in diameter, to which is attached a lopolithic offshoot approximately 5 miles long and 3 miles wide. The ultramafic units range through hornblende pyroxenite, pyroxenite, olivine pyroxenite, periodotite, and dunite, and both the pipe and the lopolith show a well-developed concentric zoning with dunite in the center and pyroxenite or hornblende pyroxenite on the periphery. Magnetite is a primary constituent of the pyroxenite unit.

The present study focused on the dunite core, which is exposed over an area of approximately 1 square mile in the eastern part of the complex (fig. 2).

Extrapolated from unaltered parts, the primary original composition of dunite from the core was 95 to 98 percent olivine in an equigranular aggregate of equant to subhedral grains. Ruckmick and Noble (1959, p. 1003) report a narrow range of composition from Fo_{90} to Fo_{93}. Most of the olivine grains show a wavy or undulatory extinction, and indication of strain. The olivine is commonly "kink" banded, indicating inhomogeneous translation gliding (Orowan, 1942; Hess and Barrett, 1949).

Diopside constitutes the remaining 2 to 5 percent of the unaltered dunite from the core; it occurs primarily as scattered anhedral grains interstitial to the olivine.

The dunite core is locally strongly serpentinized. According to Ruckmick and Noble (1959, p. 1003), "In a typical specimen of partially serpentinized dunite, only 5–10 percent of the olivine has been altered to bowlingite, antigorite, chrysotile and secondary magnetite along fractures." During the present study, mineral separates from the serpentinized dunite were studied by X-ray diffraction techniques described

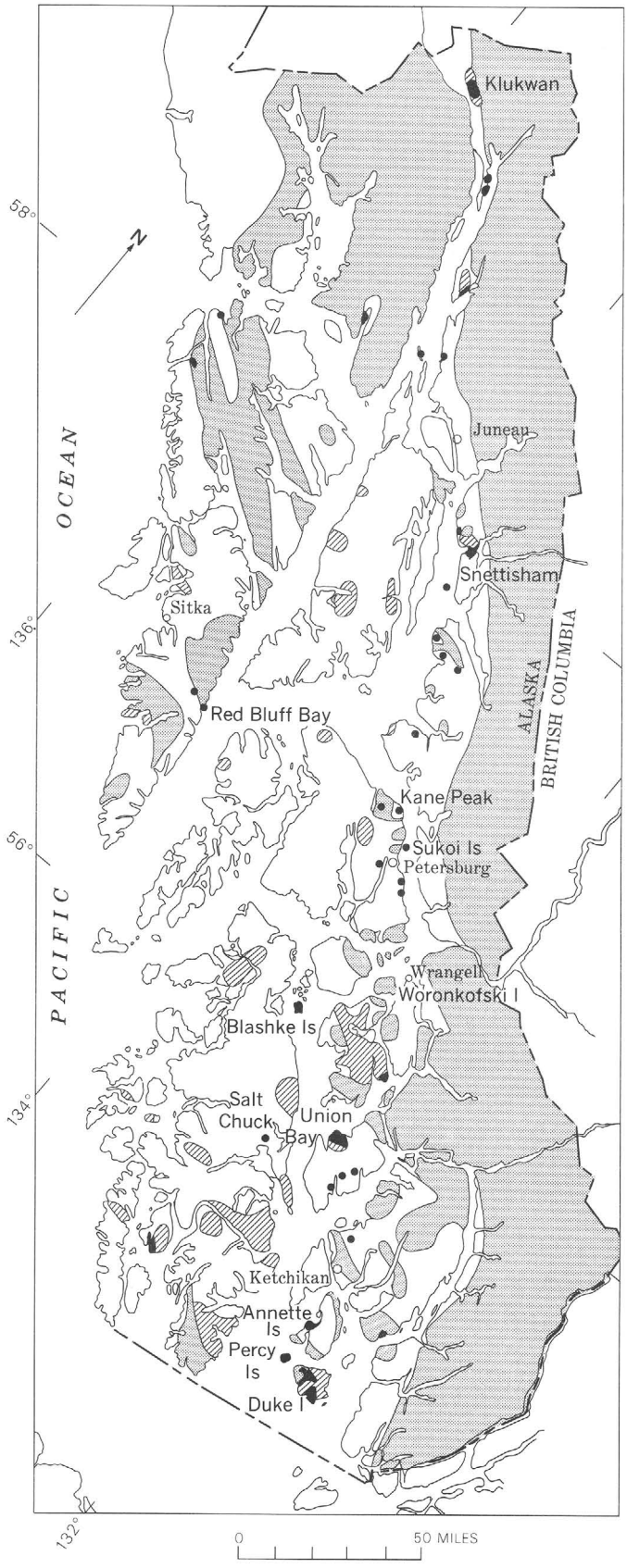

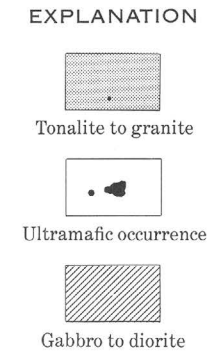

Figure 1.—Distribution of ultramafic complexes in southeastern Alaska, after Buddington and Chapin (1929).

by Page and Coleman (1967). These studies show the serpentine minerals to be lizardite and clinochrysotile with variable amounts of associated brucite. No antigorite was found. The significance of these determinations is discussed in the following section.

Modal analyses of strongly serpentinized parts of the dunite core show that locally the rocks are serpentinites containing 40 to 50 percent serpentine and 40 to 50 percent strongly serpentinized olivine and minor unserpentinized diopside.

Magnetite and chromite occur throughout the core, primarily as disseminated subhedral to euhedral fine grains. Locally, chromite forms pods ranging from 2 to 6 inches in long dimension and ½ inch to 4 inches in short dimension. Chromite also occurs as discontinuous, locally complexly folded stringers.

CHEMICAL AND MINERALOGICAL EVIDENCE OF VOLUME INCREASE

Chemical and mineralogical studies indicate that serpentinization of the dunite core of the complex at Union Bay resulted in volume increase.

Coleman (1971, p. 907–908) showed that if silica is not added or magnesia subtracted during serpentinization, then a dunite can be converted to serpentine by addition of water only according to the reaction

$$2\,MgSiO_4 + 3\,H_2O \rightleftharpoons Mg_3Si_2O_5(OH)_4 + Mg(OH)_2\,.$$

olivine (dunite) added — serpentine — brucite

The presence of lizardite, clinochrysotile, and brucite, identified by X-ray diffraction, therefore substantiates that serpentinization progressed as shown in the above formula. Brucite indicates that the excess magnesia from the formation of serpentine was not lost. The presence of lizardite and clinochrysotile indicates that the serpentine formed by chemical reaction of water with olivine rather than by metamorphic

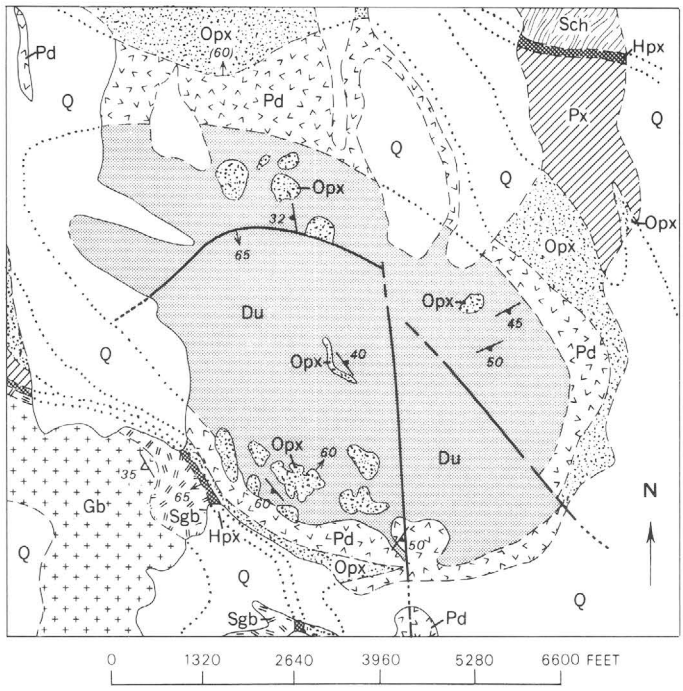

EXPLANATION

INTRUSIVE ROCKS

Du — Dunite, < 10 percent pyroxene

Pd — Peridotite, 40-90 percent olivine

Opx — Olivine pyroxenite, 10-40 percent olivine

Px — Pyroxenite, < 10 percent olivine

Hpx — Hornblende pyroxenite

Gb — Gabbro

Sgb — Saussuritized gabbro

METAMORPHIC ROCKS

Sch — Schist

SEDIMENTARY ROCKS

Q — Quaternary undifferentiated

STRUCTURE SYMBOLS

60 — Contact, showing dip. *Dashed where poorly exposed, approximately located; dotted where covered*

65 — Fault, showing dip. *Dashed where inferred; dotted where concealed*

40 — Mineral banding in intrusive rocks

35 — Foliation in intrusive rocks

Figure 2.—Geologic map of the dunite core and other rocks, ultramafic complex at Union Bay, southeastern Alaska. Modified from Ruckmick and Noble (1959).

processes that would be expected to yield antigorite (Coleman, 1971, p. 906–907).

According to Coleman (1971, p. 908), "The average MgO/SiO_2 ratio for dunites is ≈1.23 and if serpentinization of a dunite is accomplished only by addition of water, this ratio should remain constant." For the brucite-bearing massive serpentinite derived from dunites, the MgO/SiO_2 value has been found to be ≈1.23 (Thompson, 1968; Coleman and Keith, 1972). Calculated MgO/SiO_2 values for serpentinized and unserpentinized dunites from the dunite core (Ruckmick and Noble, 1959, p. 984–985, table 1, samples 183a and 231) and analyses by the authors yield a range of 1.18 to 1.24. Samples studied contained from 0 to 35 percent modal serpentine. The mineralogy, that is, the presence of lizardite, clinochrysotile, and brucite, and the chemistry as represented by MgO/SiO_2 values ≈1.23, clearly demonstrate that serpentinization of the dunite core involved only the addition of water.

Because serpentine minerals contain from 12 to 13.5 weight percent water, there must be resultant increase in volume related to the formation of serpentine.

Volume-factor analyses (fv) following the equation developed by Gresens (1967) yield values of fv = 1.196 and fv = 1.165 based on samples that contain 0 to 10 percent modal serpentine, with specific gravities of 3.3 and 2.85, respectively, and MgO/SiO_2 values for the dunite of 1.19 and for the resultant serpentinite of 1.22. These values are taken to represent average serpentinized dunite of the core and show that volume expansion of 16 to 20 percent must have taken place to maintain the same MgO/SiO_2 values in the serpentinite as in the dunite.

The data therefore show that the dunite core has undergone volume expansion of 16 to 20 percent resulting from the addition of water and the resultant formation of serpentine without addition of silica or removal of magnesia.

PETROGRAPHIC EVIDENCE RELATING TO THE PROBLEM OF VOLUME INCREASE DURING SERPENTINIZATION

The proponents of volume expansion during serpentinization have suggested various amounts of expansion. Hess (1955, p. 403) suggested a 25-percent increase in volume in serpentinized dunites; Hostetler and others (1966) argued that a volume increase of 35 to 40 percent is probably common in rocks that originally contained only pyroxene, and Engin and Hirst (1970, p. 292) calculated a volume increase of 39 percent in the harzburgites of the Andrezlik-Zimparalik peridotite body of Turkey. Thayer (1966, p. 695) calculated that volume increases of 35 to 40 percent, the general range proposed by other workers, would result in an equivalent linear expansion of 11 to 12 percent and should be readily detectable in rocks under suitable conditions.

The dunite core of the ultramafic complex at Union Bay is locally strongly sheared and serpentinized (fig. 3). Thin-section studies reveal an apparent disruption of internal features: kink bands are offset along transecting serpentine veinlets, rotated fragments of larger olivine grains are enclosed by serpentine, expanded chromite grains are cut by serpentine-filled fractures, and radially fractured diopside grains are adjacent to preferentially serpentinized olivine grains related to volume

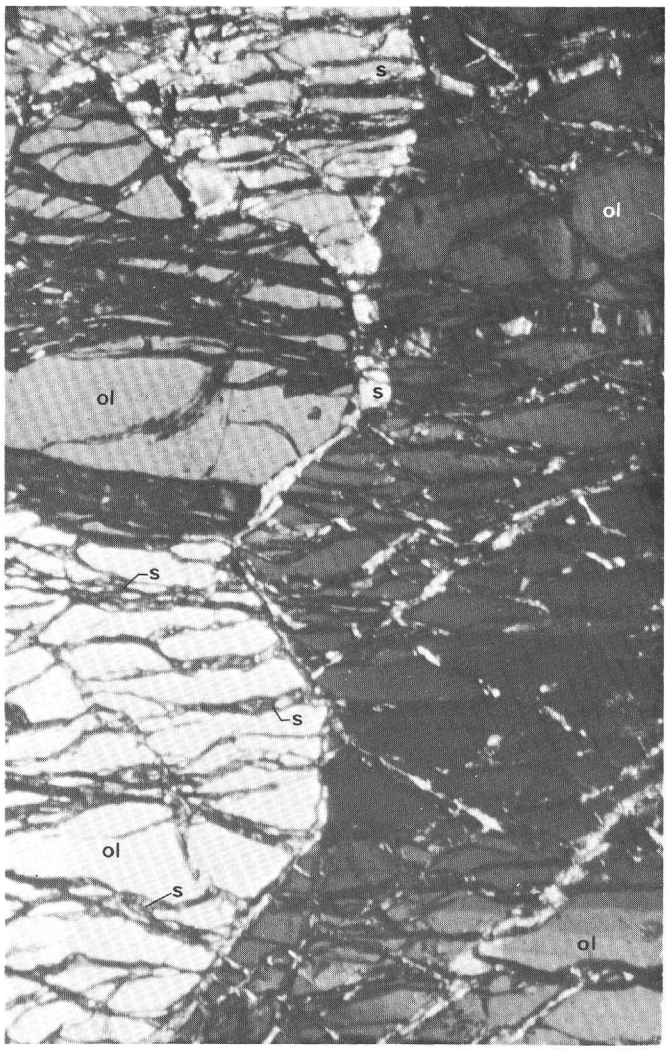

Figure 3.—Strongly sheared and serpentinized dunite. Serpentine veinlets form complex anastomosing network. ol, olivine; s, serpentine.

increase of approximately the amount (16–20 percent) calculated.

Offset of kink bands

Olivine grains in the dunite core characteristically have well-developed kink bands (figs. 4 and 5). The general nature and origin of such kink bands are duscussed by Raleigh (1968). Those in the ultramafic complex at Union Bay are being studied by W. R. Greenwood and others in work in progress.

At Union Bay, serpentine veinlets that crosscut kink bands in the olivine characteristically displace the bands. The significance of this displacement was discussed by Raleigh 1963, p. 63), who stated:

> Exsolution lamellae of clinopyroxene, which persist through serpentinized parts of the grains, are offset by zones of serpentine which intersect the lamellae at angles of less than 90 degrees. The offsets in every case are in the sense which would be produced by expansion in the serpentine band normal to its boundaries. In the same grains, the traces of lamellae are not offset by zones of serpentine trending perpendicular to the lamellae. The lamellae within the serpentinized zone are commonly pulled apart slightly along their length. These relationships can only be explained by expansion within the zone of serpentine approximately normal to its boundaries***.
>
> The boundaries of extinction bands in olivine grains are also offset in the proper sense (like offsets on reverse faults) where they are intersected at less than 90 degrees by bands of serpentine.

Figure 4 shows serpentine veinlets that cut nearly at right angles across the kink bands with no apparent offset of the bands of the individual parts of the olivine grain. Figure 5 shows a veinlet transecting a kink band at an oblique angle, causing a lateral shift in the band.

Figure 5 clearly indicates that linear expansion associated with volume increase during the development of the crosscutting serpentine veinlets has resulted in offset of the kink bands. The authors are aware that shearing and fine-scale fractures and faults could cause the features observed. How-

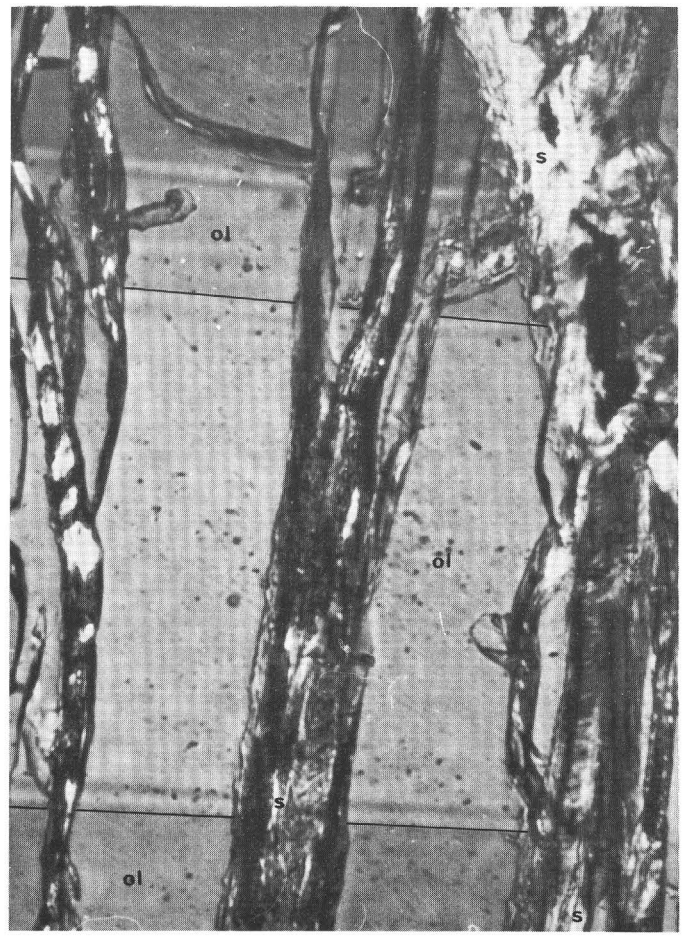

Figure 4.—Strongly kink banded olivine grain, with kinks developed parallel to (100) cut by serpentine veinlets. ol, olivine; s, serpentine.

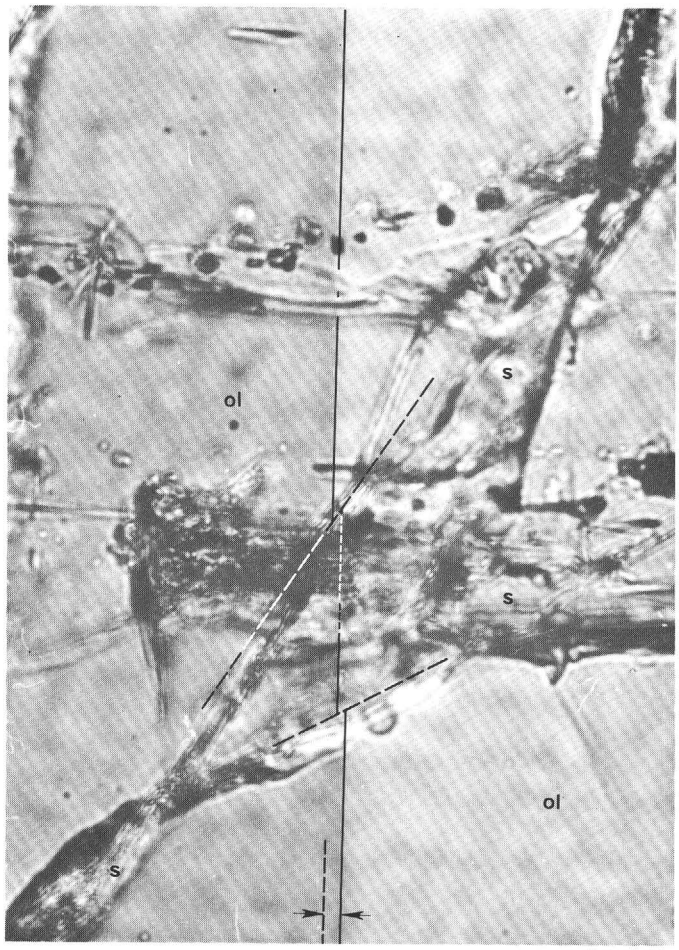

Figure 5.—Olivine grain with kink band parallel to (100) offset by serpentine veinlet (dashed lines) crossing kink band at oblique angle. Arrows show total offset. ol, olivine; s, serpentine.

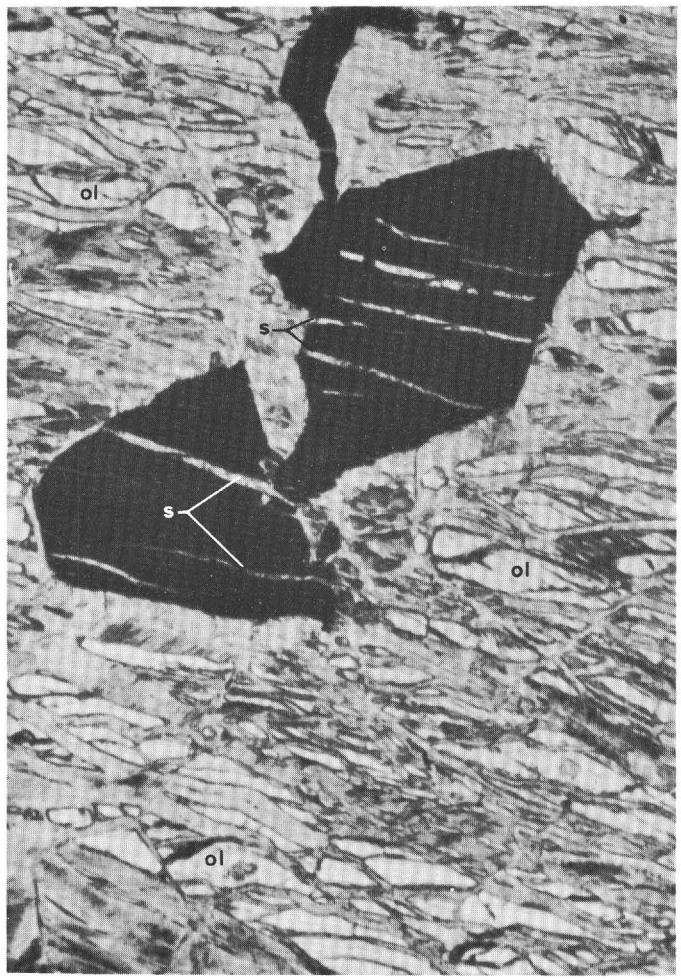

Figure 6.—Chromite grains cut by serpentine veinlets; individual grain fragments are slightly rotated and entire grain expanded. ol, olivine; s, serpentine.

ever, the parallelism across serpentine veinlets that cross the kink bands at 90 degrees and the offset along serpentine veinlets that cross at an acute angle strongly suggest that the serpentine veinlets caused the internal disruptions. It is also conceivable that minor shearing and fracturing may accompany the volume increase, resulting in rotation and disruption of individual isolated parts of the same olivine grains. In addition, it will be shown later that calculated offsets are of the magnitude expected, if they are the result of volume expansion during serpentinization.

Volume expansion of chromite grains

Euhedral to subhedral grains of chromite and magnetite are common within the dunite of the ultramafic complex at Union Bay. Many are cut by veinlets of serpentine and appear to have undergone volume expansion related to the growth of the veinlets (figs. 6 and 7).

In most of the chromite grains, the walls on either side of the serpentine veinlets are matched, so the grain simply spread apart as the veinlet grew. The separation of the various parts of individual grains appears to be entirely the result of growth of the veinlets, because replacement of chromite by serpentine is unknown within the complex at Union Bay.

Volume expansion associated with preferential serpentinization of olivine

Within the dunite core, olivine grains normally are preferentially serpentinized with respect to adjacent grains of diopside. At the contact of the grains of olivine and diopside, a radial fracture pattern is developed in the diopside. Ruckmick and Noble noted that the same phenomenon developed where interstitial areas of diopside enclose partly serpentinized grains of olivine (1959, p. 1001, pl. 3, fig. 3).

Similar radial structures have been described in feldspars surrounding serpentinized olivine grains and considered as strong evidence of volume increase during serpentinization (Smith, 1958). On a larger scale, Mossman (1970, p. 3756)

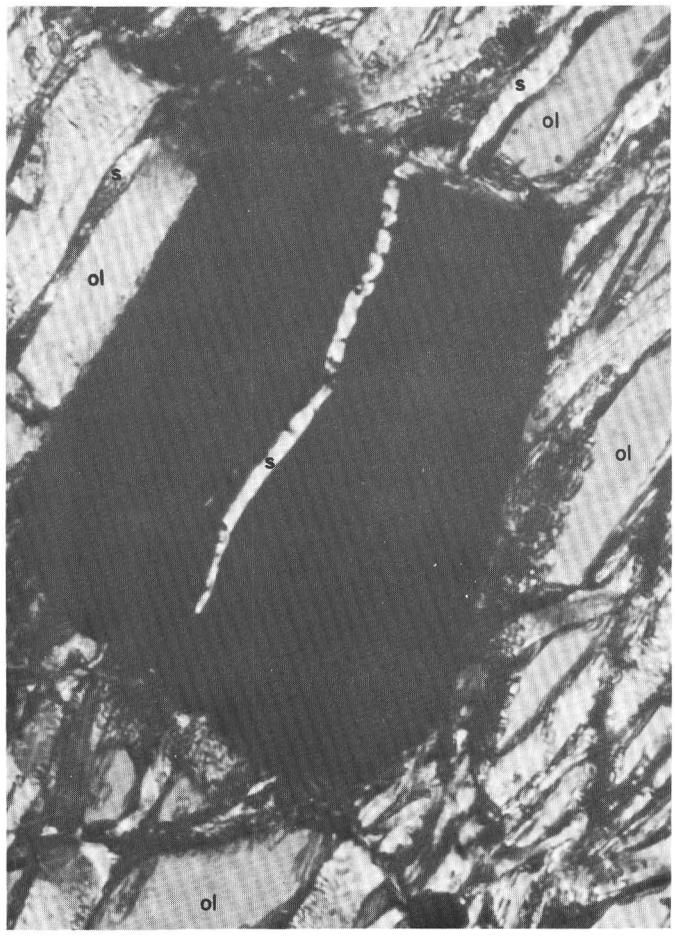

Figure 7.—Chromite grain cut by serpentine veinlet. Note matching opposed walls along veinlet indicating separation and expansion of grain. ol, olivine; s, serpentine.

described similar radial structures associated with serpentinized dunite blocks in wehrlite. A similar phenomenon was described by Ruckmick and Noble (1959, p. 1001), who stated:

> In many places in the structural peridotite where dunitic material exhibits a rounded, convex contact against the olivine pyroxenite, radial fracture patterns occur in pyroxene-rich rock adjacent to the contact. This feature is especially obvious where small bodies of dunitic rock show a circular cross section. The nature of this secondary (post-solidification) fracture pattern indicates either that the olivine has increased in volume or that the pyroxene has decreased in volume. Because the coefficient of expansion with temperature is greater for olivine than for diopside ***, the fractures were probably not caused by differential contraction as the intrusion cooled. All the dunitic rocks associated with this feature contain approximately 10 percent or more of serpentine minerals, and possibly the fractures were caused by relative expansion of the dunitic material during serpentinization of the olivine.

Ruckmick and Noble's contention that the fractures were not produced as the intrusion cooled is substantiated by the absence of high-temperature antigorite and the presence of low-temperature lizardite and clinochrysotile (Coleman, 1971, p. 901).

It is especially noteworthy that within the complex at Union Bay, volume expansion associated with preferential serpentinization occurs at both microscopic and macroscopic scales, which supports Thayer's contention (1966, p. 696) that major disruptions should be associated with serpentinization.

CALCULATIONS OF LINEAR EXPANSION ASSOCIATED WITH VOLUME INCREASE

Detailed measurements on individual olivine grains, showing offset of kink bands along serpentine veinlets, were made using the technique described by Raleigh (1963, p. 63–69). (See figure 8.) According to Raleigh, the volume increase in the bands of serpentine can be calculated by assuming that

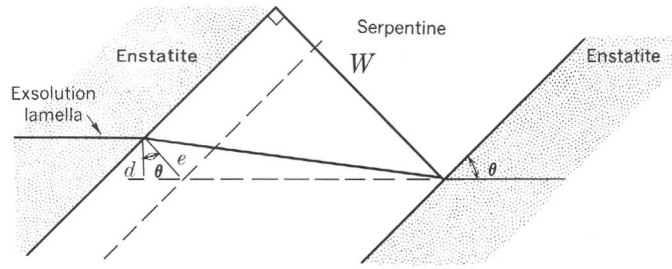

Figure 8.—Diagram showing offset, d, of exsolution lamella by expansion of amount, e, in band of serpentine (of width W) transecting a grain of enstatite (after Raleigh, 1963, p. 65–66).

expansion took place only in a direction normal to the boundaries of the bands. This assumption is verified by observations on lamellae that persist through bands of serpentine lying normal to the lamellae; the lamellae within the bands show no displacement parallel to the margins of the band. Referring to figure 8, the linear expansion, e, normal to the boundary is given by

$$e = \frac{d}{\cos \theta}$$

where d is the amount of offset of the lamella and θ is the acute angle between the lamella and the boundary of the band. The fraction of volume increase, $\frac{\Delta V}{V}$, is then

$$\frac{\Delta V}{V} = \frac{e}{W - e},$$

where W is the thickness of the band.

Six grains were studied and $\frac{\Delta V}{V}$ calculated for each. The values calculated ranged from 10 to 34 percent and averaged 22 percent. The range is attributable to variations in amount

of modal serpentine, 5 to 18 percent, and difficulty in accurately measuring the band widths.

Volume expansion of chromite grains was measured by enlarging photographs of serpentine-bearing chromite grains, computing the present volume, then cutting out the serpentine veinlets from the photographs, fitting the grains back to their original configuration, and recalculating the volume. The difference between the two volume calculations then represented the volume increase, which ranged from 8 to 29 percent for the four grains measured. The wide range probability stems from our inability to make a three-dimensional calculation on an individual grain.

Although the range in percentage of volume increase calculated by these methods is fairly large, the averages are very close to the 16 to 20 percent calculated by Gresens' (1967) technique.

CONCLUSIONS

Mineralogical and chemical studies of dunite samples from the core of the ultramafic complex at Union Bay show that serpentinization took place without addition of silica or removal of magnesia. The volume increase to be expected was calculated as ranging from 16 to 20 percent. Measurements of the actual amount of volume increase associated with offset kink bands and serpentinization of individual chromite grains are approximately the same as the theoretically calculated amounts.

Petrographic studies show that serpentinization of the dunite core of the complex at Union Bay caused internal disruption of structural elements. Kink bands are offset by transecting veinlets of serpentine, chromite grains have expanded owing to development of serpentine veinlets, and differential serpentinization of olivine grains has produced radial fractures in adjacent diopside grains. Both the small- and large-scale structural disruptions are best explained by volume increase during serpentinization of the dunite core.

The mineralogical, chemical, and petrographic studies show that serpentinization of the dunite core was a constant-composition process resulting in volume increase of approximately 16 to 20 percent.

REFERENCES

Beeson, M. H., and Jackson, E. D., 1969, Chemical composition of altered chromites from the Stillwater Complex, Montana: Am. Mineralogist, v. 54, p. 1084–1100.

Buddington, A. F., and Chapin, Theodore, 1929, Geology and mineral deposits of southeastern Alaska: U.S. Geol. Survey Bull. 800, 389 p.

Clark, A. L., and Greenwood, W. R., 1972, Geochemistry and distribution of platinum-group metals in mafic to ultramafic complexes of southern and southeastern Alaska, *in* Geological Survey Research 1972: U.S. Geol. Survey Prof. Paper 800-C, p. C157–C160.

Coleman, R. G., 1971, Petrologic and geophysical nature of serpentinites: Geol. Soc. America Bull., v. 82, p. 897–918.

Coleman, R. G., and Keith, T. E. C., 1971, A chemical study of serpentinization–Burro Mountain, California: Jour. Petrology, v. 12, pt. 2, p. 311–328.

Engin, T., and Hirst, D. M., 1970, Serpentinization of harzburgites from the Alpine Peridotite belt of southwest Turkey: Chem. Geology, v. 6, p. 281–295.

Green, D. H., 1964, The petrogenesis of the high-temperature peridotite intrusion in the Lizard area (Cornwall): Jour. Petrology, v. 5, p. 134–188.

Gresens, R. L., 1967, Composition-volume relationships of metasomatism: Chem. Geology, v. 2, p. 47–65.

Hess, H. H., 1955, Serpentinites, orogeny and epiorogency, *in* A. Poldervaart, ed., Crust of the Earth: Geol. Soc. America Spec. Paper 62, p. 391–408.

Hess, H. H., and Otalora, G., 1964, Mineralogical and chemical composition of the Mayaguez serpentine cores: Natl. Acad. Sci.–Natl. Research Council Pub. 1188, p. 152–168.

Hess, J. B., and Barrett, C. S., 1949, Structure and nature of kink bands in zinc: Am. Inst. Mining Metall. Eng. Trans., v. 185, p. 599–606.

Hostetler, P. B., Coleman, R. G., Mumpton, F. A., and Evans, B. W., 1966, Brucite in Alpine serpentinites: Am. Mineralogist, v. 51, p. 75–98.

Kennedy, G. C., and Walton, M. S., 1946, Geology and associated mineral deposits of some ultramafic bodies in southeastern Alaska: U.S. Geol. Survey Bull. 947-D, p. 65–84.

Mossman, D. J., 1970, Fracture phenomena in and around serpentinized dunite in ultrabasic rocks from the Green Hills Complex, New Zealand: Geol. Soc. America Bull., v. 81, p. 3753–3756.

Orowan, E., 1942, A type of plastic deformation new in metals: Nature, v. 149, p. 643.

Page, N. J, and Coleman, R. G., 1967, Serpentine-mineral analyses and physical properties, *in* Geological Survey Research 1967: U.S. Geol. Survey Prof. Paper 575-B, p. B103–B107.

Raleigh, C. B., 1963, Fabrics of naturally and experimentally deformed olivine: Univ. California at Los Angeles, unpub. Ph. D. thesis 215 p.

——1968, Mechanisms of plastic deformation of olivine: Jour. Geophys. Research, v. 73, p. 5391–5406.

Ruckmick, J. C., and Noble, J. A., 1959, Origin of the ultramafic complex at Union Bay, southeastern Alaska: Geol. Soc. America Bull., v. 70, p. 981–1018.

Shteinberg, D. S., 1960, New data concerning the serpentinization of dunites and peridotites of the Urals: Internat. Geol. Cong., 21st, Doklady Sovet Geol., Probl. 13, p. 250–260 [Russian, with English summ.].

Smith, C. H., 1958, Bay of Islands igneous complex, western Newfoundland: Canada Geol. Survey Mem. 290, 132 p.

Taylor, H. P., Jr., 1967, The zoned ultramafic complexes of southeastern Alaska, *in* P. J. Wylie, ed., Ultramafics and related rocks: New York, John Wiley and Sons, p. 96–118.

Thayer, T. P., 1966, Serpentinization considered as a constant-volume metasomatic process: Am. Mineralogist, v. 51, p. 685–710.

Thompson, R. B., 1968, Serpentinization accompanied by volume changes: Pacific Geology [Japan], pt. 1, p. 167–174.

Turner, F. J., and Verhoogen, J., 1960, Igneous and metamorphic petrology, 2d ed.: New York, McGraw-Hill, 602 p.

Walton, M. S., 1951, The Blashke Islands ultrabasic complex: Columbia Univ., New York, unpub. Ph. D. thesis, 266 p.

GRAIN-SIZE VARIATIONS WITHIN AN OLIVINE CUMULATE, STILLWATER COMPLEX, MONTANA

By NORMAN J PAGE, RICHARD SHIMEK, and CLAUDE HUFFMAN, JR.,
Menlo Park, Calif.

Abstract.—Abrupt changes in olivine grain size are found within the 348 feet of olivine cumulate of cyclic unit 2 in the upper part of the Nye Creek basin in the Stillwater Complex, Montana. These olivine size changes correlate with variations in chromite grain size, proportions of cumulus and postcumulus minerals, composition of olivine, and concentrations of Cr, Ti, V, Mn, S, Ni, Cu, and Co. The variations are ascribed to oscillation of physical conditions and composition, or both, within the magma batch that formed the olivine cumulate of cyclic unit 2.

Cyclic units, repetitions of cumulus minerals, in the Ultramafic zone of the Stillwater Complex of Precambrian age were introduced in the petrologic studies of Jackson (1961, 1963, 1967, 1968, 1969, 1970, 1971); at least 15 cyclic units are recognized in the Peridotite member of the Ultramafic zone. The repetitious nature of the cumulus mineral layers is well illustrated by Jackson's columnar sections of the Peridotite member in the West Benbow and Mountain View areas (1968, fig. 6, p. 1506). Normal, complete cyclic units in the Peridotite member invariably contain the same sequence of cumulus phases: olivine, olivine + bronzite, and bronzite. Any cyclic unit that lacks an olivine-bronzite or bronzite layer or both, for example, cyclic units 1 or 10 in the West Benbow area (fig. 1), is called beheaded (Jackson, 1970, p. 390–401). Where an olivine cumulate overlies another olivine cumulate in a beheaded cycle, the contact between the cycles is "recognized by a sharp change in grain size of the cumulus olivine * * *" (Jackson, 1970, p. 399–401). To explain cyclic units, Jackson (1961, p. 96–99) proposed that crystals accumulated from batches of basaltic magma, one batch per cycle, brought into the zone of crystallization near the floor by variable-depth convection.

Recent investigations have included 1:12,000–scale mapping of the complex on the northern flank of the Beartooth Mountains in southwestern Montana (Jones and others, 1960; Page and Nokleberg, 1970) and the examination of the platinum-group metals and mineralogy of sulfides (Page and Jackson, 1967; Page and others, 1969; Page, 1971a, b). During the latter studies, geologic and mineralogic relations were established that suggested the need for a more detailed understanding of the cyclic unit. One of these relations is the disparity between the thicknesses of the olivine cumulates of normal (32–95 feet) and beheaded (180–350 feet) cyclic units.

This study focuses on the olivine cumulate from cyclic unit 2, which contains the B-chromitite zone (Jackson, 1963, 1968), as it was believed to represent a one-phase cumulate in a complete cyclic unit. Core was obtained from a drill hole[1] in the upper part of the Nye Creek Basin, an area between the West Benbow and Mountain View areas. The hole was collared below the Peridotite member and drilled up section through its lower part. The general stratigraphic position of a section of the core, its internal stratigraphy, and its correlation with the columnar sections of Jackson (1968), are shown on figure 1. Drilling footages are used for the core because the exact dip of the section is unknown. The nearest measured strike and dip of the layering in the Peridotite member is N. 78° W., and 80° S., respectively, which indicate that core footages may be decreased by 26 percent to obtain true thicknesses.

Acknowledgments.—We are grateful to the Anaconda Co. for making the drill core available for study and for cooperating fully with the project. Discussions with geologists of the company were of great benefit, as were the critical reviews of A. B. Ford and Howard Wilshire. L. B. Riley, L. B. Bresden, and Joseph Haffty analyzed one chromitite for Pt, Pd, and Rh; Warren J. Nokleberg assisted during the early logging of the core.

TECHNIQUES

The split half of a 2-inch-diameter core, obtained by sawing the original core, was examined visually and logged; a part of the log is shown on figure 1. Samples 2 to 5 inches long (the

[1]Drilling was angled 50° from the horizontal and headed N. 30° E. Coordinates of the hole, N. 499,010, E. 1,917,015 (in feet) are those obtained from the Montana (south) rectangular grid which appears on the Mount Wood 15-minute quadrangle and in Page and Nokleberg (1970).

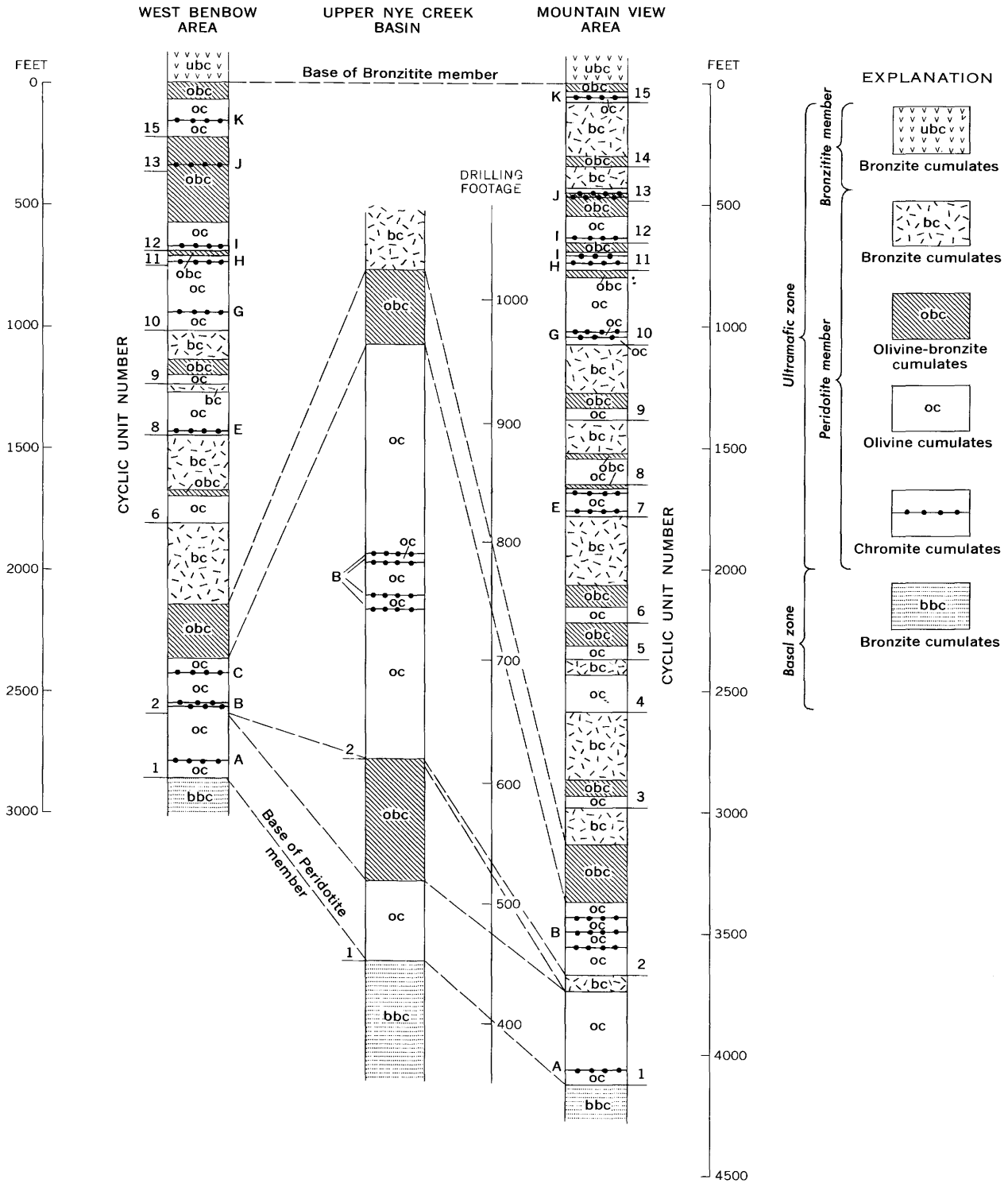

Figure 1.—Correlation of columnar sections of parts of the Peridotite member from West Benbow, upper part of the Nye Creek basin (vertically expanded section), and Mountain View areas. West Benbow and Mountain View areas modified from Jackson (1968).

majority were 3–4 in. long) were selected from the 348-foot section of olivine cumulate at intervals of approximately 5 feet, then rehalved by sawing. One-half of this was crushed to pass a 32-mesh screen and split for minor-element analysis; the remaining half was saved for polished and unpolished thin sections, slab staining, mineral separations, and density measurements. The information from these 2- to 5-inch samples is assumed to be representative of the 348 feet of olivine cumulate.

Grain sizes of olivine and chromite were generally measured

in thin section with a micrometer ocular. Maximum and minimum apparent diameters of every grain available in each thin section, that is, between 50 and 100 grains, were averaged to give grain size. Corrections were not applied to the measurement of grain diameters in thin sections because the results are used for a comparative purpose within a single study (see Jackson, 1961, p. 21, for further discussion). Modal data are based on point counting of 1,000 points in polished thin sections. Compositions of olivine were determined by using the X-ray method of Jackson (1960) developed specifically for Stillwater olivines; the precision of the measurements ranges from ±0.05 to ±1.2 mole percent $Mg/(Mg+Fe^{+2})$ and averages ±0.31 percent.

Chemical analyses for trace elements were done in the analytical laboratories of the U.S. Geological Survey as follows: total S was determined by I. C. Frost by the combustion-iodametric titration method (precision about ±0.01 percent); Co, by Wayne Mountjoy by atomic absorption (value reported has a precision of about ±5 percent of the amount present); Cr, by V. E. Shaw, J. A. Thomas, and Claude Huffman, Jr., by spectrophotometry and atomic absorption (average value reported has a precision of about ±400 ppm Cr); Cu, Mn, and Ni, by J. A. Thomas and Claude Huffman, Jr., by atomic absorption; Ti, by J. P. Cahill and Claude Huffman, Jr., by spectrophotometry (precision about ±5 percent of the amount present); and V, colorimetrically by W. D. Goss.

TEXTURE OF THE OLIVINE CUMULATE

Two types of primary minerals, distinguished on the basis of shape and mutual grain relations, occur in the olivine cumulate. In one type, mineral grains are commonly euhedral, always occur as individual grains, and if elongate, tend to lie in the plane of the layering. In the other, mineral grains are anhedral and fill the space between the individual euhedral grains. The first type consists of the cumulate minerals, olivine and chromite; the second type of the postcumulus minerals, plagioclase, orthopyroxene, clinopyroxene, brown hornblende, and biotite. The sulfide minerals occur both as inclusions in the cumulus minerals and as interstitial space fillings. They are considered to be cumulates, although the observed minerals did not accumulate in their present form but probably as immiscible sulfide liquid droplets (Page 1971a, b).

Most of the rocks used in this study are partly altered—olivine and orthopyroxene altering to serpentine (lizardite+chrysotile) and magnetite, chromite on margins to ferrichromite and magnetite (Beeson and Jackson, 1969), and plagioclase to carbonate and clay minerals. The degree of serpentinization ranges from 7 to 80 percent, most rocks averaging around 40 percent. The alteration appears to preserve the original texture and for the purpose of this paper can be ignored.

Grain size

Olivine.—Average apparent grain sizes range from 0.92 to 7 mm for olivine and 0.12 to 0.22 mm for chromite (fig. 2*B*). These values are within the ranges reported by Jackson (1961, p. 21) for the whole complex and are comparable to his range of grain sizes, 1.5 to 2.4 mm for olivine and 0.20 mm for chromite, for cyclic unit 2 of the Mountain View area (Jackson, 1961, fig. 19, p. 22). Ratios of average apparent length to width range from 1:0.52 to 1:0.64 and average 1:0.60—values similar to those reported by Jackson (1961, p. 42).

Grain size of olivine tends to decrease upward through the whole olivine cumulate (fig. 2*B*) to about the middle of the section and then to increase toward the top. Abrupt changes in grain size are superimposed on this trend. Each vertical grain-size change consists of a gradual decrease in the grain size of olivine upward, followed abruptly by a significantly coarser grain olivine cumulate. These abrupt vertical changes suggest or mark six definite and two possible breaks or repeats within the olivine cumulate of cyclic unit 2, numbered sequentially from the base in figure 2*A*. To be consistent with Jackson's terminology (1967, p. 22) the units will be called size-graded units.

Chromite.—Although chromite is a minor cumulus constituent in these rocks, its grain size was measured over a small interval (fig. 2*C*). Vertical changes in the grain size occur abruptly, as in olivine. Moreover, changes in the grain size of chromite correspond directly to those of olivine, the change consisting of a gradual decrease in size upward to an abrupt break that is followed by coarse-grained chromite. Because statistical considerations of the grain sizes of olivine and chromite show a high degree of correlation, the grain size of chromite in the rest of the samples was not measured. For the 17 samples listed by Jackson (1961, table 3, p. 34) and the seven samples from this report, the calculated product moment correlation coefficient is +0.926 at greater than the 99.9 percent confidence interval. From this high degree of correlation, it is expected that the increases and decreases in grain size shown by olivine through the upper Nye creek basin section would be the same for chromite.

Grain-size distributions and sorting

The size distributions and sorting characteristics of olivine in individual samples, in olivine size-graded units, and in the whole cumulate section were examined by separating average grain diameters into 1/2 Udden size grades, plotting cumulate frequency curves, and graphically obtaining quartile sorting coefficients. The size distributions and sorting coefficients are comparable to those recorded by Jackson (1961, p. 20–37). Quartile sorting coefficients for the olivine size-graded units range from 1.22 to 1.45, well sorted; the average sorting coefficient for all the measured olivine grains in the section is

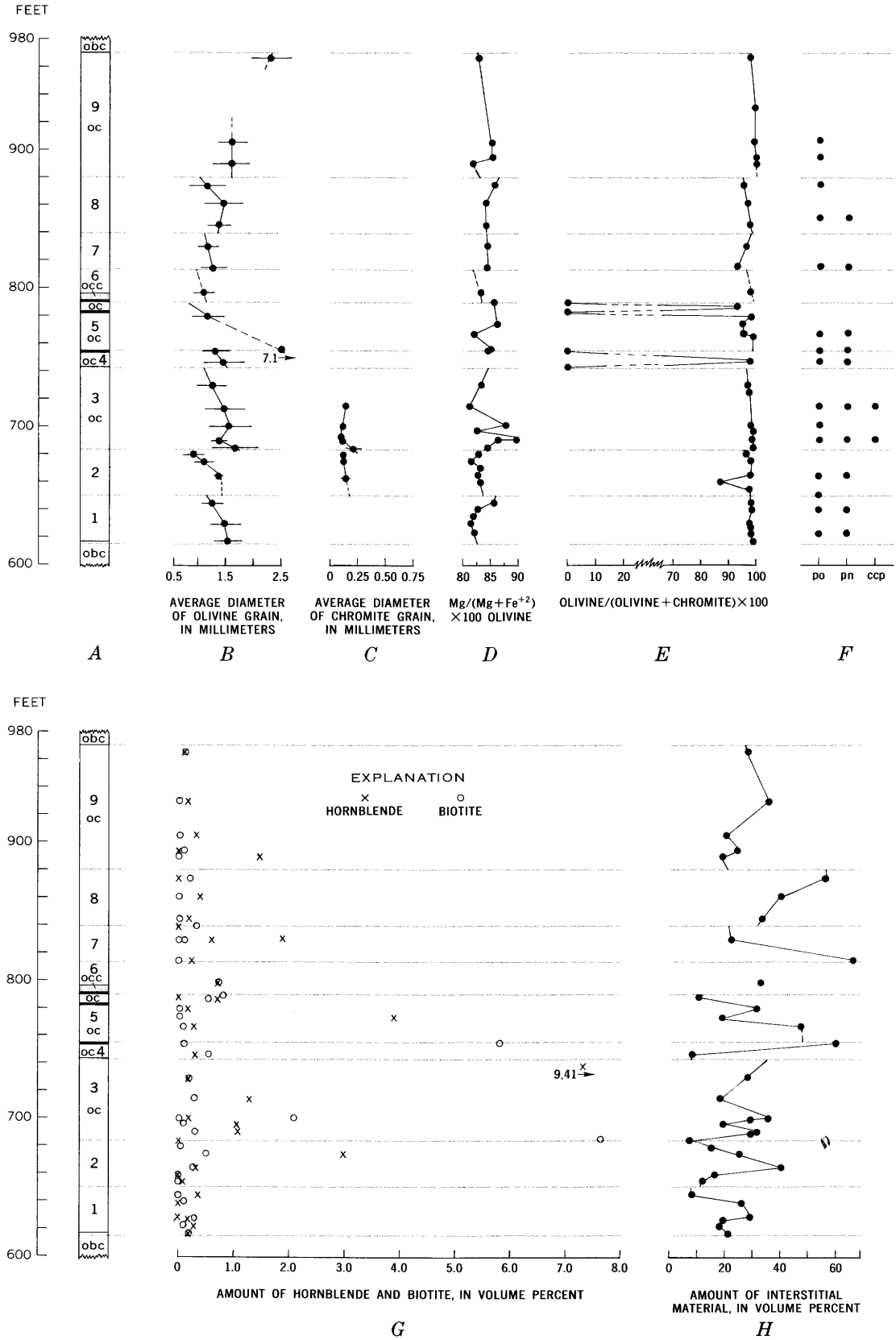
FEET
980
900
800
700
600
obc
9
oc
8
7
6
occ
oc
5
oc
oc 4
3
oc
2
1
obc
7.1
0.5 1.5 2.5
AVERAGE DIAMETER OF OLIVINE GRAIN, IN MILLIMETERS
A
B
0 0.25 0.50 0.75
AVERAGE DIAMETER OF CHROMITE GRAIN, IN MILLIMETERS
C
80 85 90
Mg/(Mg+Fe+2) ×100 OLIVINE
D
0 10 20 70 80 90 100
OLIVINE/(OLIVINE+CHROMITE)×100
E
po pn ccp
F
FEET
980
900
800
700
600
EXPLANATION
HORNBLENDE
BIOTITE
9.41
0 1.0 2.0 3.0 4.0 5.0 6.0 7.0 8.0
AMOUNT OF HORNBLENDE AND BIOTITE, IN VOLUME PERCENT
G
0 20 40 60
AMOUNT OF INTERSTITIAL MATERIAL, IN VOLUME PERCENT
H

Figure 2.

1.34. Chromite, where measured, shows good sorting characteristics, although it has a much finer average grain size.

MINERALOGY

The olivine cumulate examined is typical, as shown by the modal data of the 41 individual samples. The ranges and average volume percentages of minerals are given in table 1, together with Jackson's average mode (1961, table 1, col. 4). The only significant difference between the two averages is in the proportions of postcumulus minerals. The olivine cumulates of cyclic unit 2 contain larger amounts of plagioclase and clinopyroxene than Jackson's average. Jackson (1968, p. 1501 and 1503) notes that elsewhere in the complex, the olivine cumulate of cyclic unit 2 is enriched in postcumulus clinopyroxene.

Table 1.—*Summary of modal data, in volume percent, of the olivine cumulate core samples of cyclic unit 2 in the Stillwater Complex, Montana*

Minerals	Range of modes	Average of modes	
		This report (41 samples)	E. D. Jackson[1] (22 samples)
Cumulates:			
Olivine	32–92	70.9	70.4
Chromite	[2]0–10.9	1.7	2.0
		72.6	72.4
Postcumulates:			
Plagioclase	0–33.8	11.1	7.0
Orthopyroxene	0–49.8	6.0	17.6
Clinopyroxene	0–37.0	9.0	2.8
Hornblende	0–9.4	.7	–
Biotite	0–7.7	.5	.2
		27.3	27.6

[1]From Jackson (1961, table 1, col. 4).
[2]Sample 660 is appropriately labeled an olivine-chromite cumulate. None of the other samples contain more than 4.8 percent chromite.

Cumulus minerals

Olivine.—The $Mg/(Mg+Fe^{+2})\times100$ content of olivine ranges from 81.6±0.6 to 89.8±0.8 and averages 84.0 (fig. 2*D*) in the olivine cumulate. This variation supports Jackson's statement (1970, p. 401) that cumulus minerals change composition vertically within cyclic units and also demonstrates that olivine can vary widely in composition within a single cumulate unit. Jackson (1970, table 2, p. 401) reported a $Mg/(Mg+Fe^{+2})\times100$ ratio of 82.0 percent for a sample from the base of cyclic unit 2 in the Mountain View area, which corresponds with our value of 82.1 for the base of the olivine cumulate from upper Nye Creek basin (fig. 1). The variation of olivine composition with stratigraphic position is a sequence of complex fluctuations in $Mg/(Mg+Fe^{+2})$ ratio. The general trend for each olivine size-graded unit is one of slight increases in the $Mg/(Mg+Fe^{+2})$ ratio in olivine, which seemingly is opposite to the iron enrichment expected upward in the section, but nevertheless is in accord with Jackson's observations (1963, 1970) that iron enrichment in the Peridotite member does not begin until cyclic unit 11. The unexpected iron depletion is explained by Jackson (1963, 1970) as a failure of the Stillwater magma to reach crystallization conditions of complete equilibrium until later in the Peridotite member.

Chromite.—The chromite was not analyzed, but the total $Fe/(Fe^{+2}+Fe^{+3})$ probably falls between 5.59 and 6.03 cations per unit cell, on the basis of Jackson's study (1963, p. 50) of chromitite zones in the Stillwater Complex. The $Fe^{+3}/(Fe^{+2}+Fe^{+3})$ probably is near 0.288 cations per unit cell. Jackson (1969) has also shown that the cation fractions of Mg and Fe^{+2} in chromite are related to the proportions of the two minerals in the cumulate layers. Although his study was done for the G and H chromitite zone, similar relations probably exist for the B chromitite, and therefore the variations in composition of chromite with stratigraphic position should be similar in trend and magnitude relative to the olivine, as in Jackson's study.

Except for four thin layers of olivine-free chromite cumulate, the ratio olivine: olivine+chromite changes gradually but slightly (fig. 2*E*).

Sulfide minerals.— Pyrrhotite, pentlandite, and chalcopyrite are the only sulfide minerals identified (fig. 2*F*); they occur as grains of less than 200 microns, either as inclusions in cumulus phases or as irregular grains associated with the postcumulus material. Pyrrhotite is most abundant, pentlandite next, and chalcopyrite was observed in only two polished thin sections. A complete textural description of these types of occurrence of sulfide minerals is contained in Page (1971a). The chromite cumulate at 789.5 was analyzed[1] for Pt, Pd, and Rh in triplicate, with the following results: Pt 0.73, 0.67, 0.63 ppm; Pd 4.25, 3.39, 3.96 ppm; and Rh 0.27, 0.21, 0.24 ppm. Page, Riley, and Haffty (1969, 1971) discuss the occurrence of platinum metals in more detail; a comparison of results

Figure 2.—Properties of cumulus and postcumulus minerals correlated with stratigraphic position. *A*, Columnar section of olivine cumulate, cyclic unit 2, upper part of the Nye Creek basin, with size-graded units numbered. occ, olivine-chromite cumulate; oc, olivine cumulate; obc, olivine-bronzite cumulate; heavy lines, chromite cumulates. *B*, Olivine grain size. *C*, Chromite grain size. *D*, $Mg/(Mg+Fe^{+2})\times100$ ratio for olivine. *E*, Olivine/(olivine + chromite)×100. *F*, Presence of pyrrhotite (po), pentlandite (pn), and chalcopyrite (ccp) represented by a dot. *G*, Modal percentage of hornblende and biotite. *H*, Modal percentage of interstitial material.

[1]Method from Haffty and Riley (1968). Analysts: L. B. Riley, L. B. Bresden, and Joseph Haffty.

demonstrates that the concentrations of platinum group metals determined are typical of the B chromitite zone. No platinum-group minerals have been identified in the chromite cumulate of this zone or the cyclic unit 2 section from the upper Nye Creek basin.

Postcumulus minerals

None of the postcumulus minerals in this section have been chemically analyzed. Flat-stage microscopic study suggests that the plagioclase ranges from An_{75} to An_{46} and averages about 65 percent anorthite; values of An_{60} to An_{80} were reported by Hess (1960, p. 60) for the Ultramafic zone. The orthopyroxene is a bronzite with a composition between En_{75} and En_{90}. The clinopyroxene is probably similar to the two augite determinations of Hess (1949, p. 646, 647), who suggests that the augite has nearly a constant composition.

Amphibole has been reported by Hess (1960, p. 72) in two specimens of the Norite zone; he believed the amphibole to be primary. Other described amphiboles in the complex are secondary and are believed to be associated with serpentinization or other alteration processes (for example, Hess, 1960, p. 54). To our knowledge, the brown hornblende occurring as postcumulus material in the Peridotite member has not been described previously. It occurs as interstitial material molded around cumulus minerals, especially chromite. Its modal distribution (fig. 2*G*) is irregular, but it occurs in greatest abundance near the abrupt changes in the grain size of olivine. The modal distribution of biotite (fig. 2*G*) is irregular, but like the brown hornblende, its maximum abundances coincide with olivine grain size breaks in the section. Further descriptions of the occurrence of biotite are given by Jackson (1961, p. 66–69, 71–73).

Jackson (1961, p. 88–89), in discussing the origin and meaning of the postcumulus minerals (interprecipitate material), pointed out the limitations in obtaining significant measurements of the modal proportions of the postcumulus material. The major limitation is the extreme range of grain sizes of the interstitial material, which makes it difficult to obtain reproducible measurements of the postcumulus minerals. Therefore, apparent modal quantities of each mineral for individual samples have a highly irregular variation with respect to stratigraphic position.

Over the whole section of the olivine cumulate, the volume of interstitial material varies widely, but within most of the size-graded units it tends to increase from the bottom to the top (fig. 2*H*). The average arithmetic normalized proportions of plagioclase, orthopyroxene, and clinopyroxene were calculated for each group of samples within olivine size-graded units (fig. 3). Proportions of minerals appear to differ for each size-graded unit and, in general, each unit appears to be distinct.

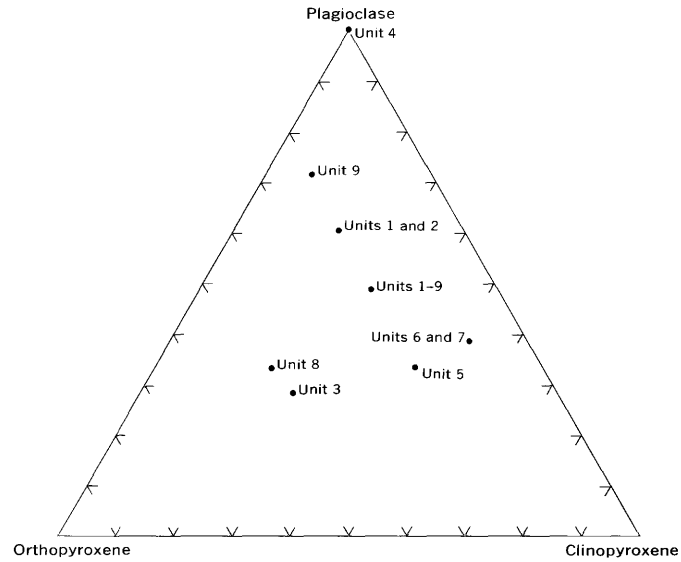

Figure 3.—Triangular diagram showing volume of the interstitial minerals—plagioclase, clinopyroxene, and orthopyroxene—for the olivine cumulate. Unit numbers refer to size-graded units shown in figure 2.

TRACE-ELEMENT VARIATION WITHIN THE OLIVINE CUMULATE

A limited number of elements was chosen for study. The elements Cr, Ti, V, and Mn were selected because they should reflect the variations in oxide minerals; S, Ni, Cu, and Co were selected in order to examine variations in the sulfide mineralogy. The analytical data are plotted in figure 4, with the olivine size-graded units superimposed for reference.

The variation in Cr concentration with stratigraphic position is mainly a function of the amount of chromite, for the product moment correlation coefficient between Cr and modal chromite is +0.994 at greater than the 99.75 level of confidence. Some of the variation is probably caused by changes in the composition of chromite. Although the overall changes with position are large and fluctuate widely, within each olivine size-graded unit the variation has a repetitious pattern. The Cr concentration is low to moderate at the base of most of the size-graded units, increases to maximum value toward the top of the individual units, where it changes abruptly to a lower concentration, and then the pattern is repeated. Some of the maximum values correspond to chromite cumulates.

The distributions of Ti and V in the olivine cumulates are more irregular, and within size-graded units they exhibit both increasing and decreasing trends from bottom to top of the units. The concentrations of Ti and V correlate with the concentration of Cr at greater than the 99.75 confidence limit with +0.943 and +0.968 product moment correlation coefficients, respectively, indicating that Ti and V are closely related to the amount of chromite present. Ilmenite was identified in

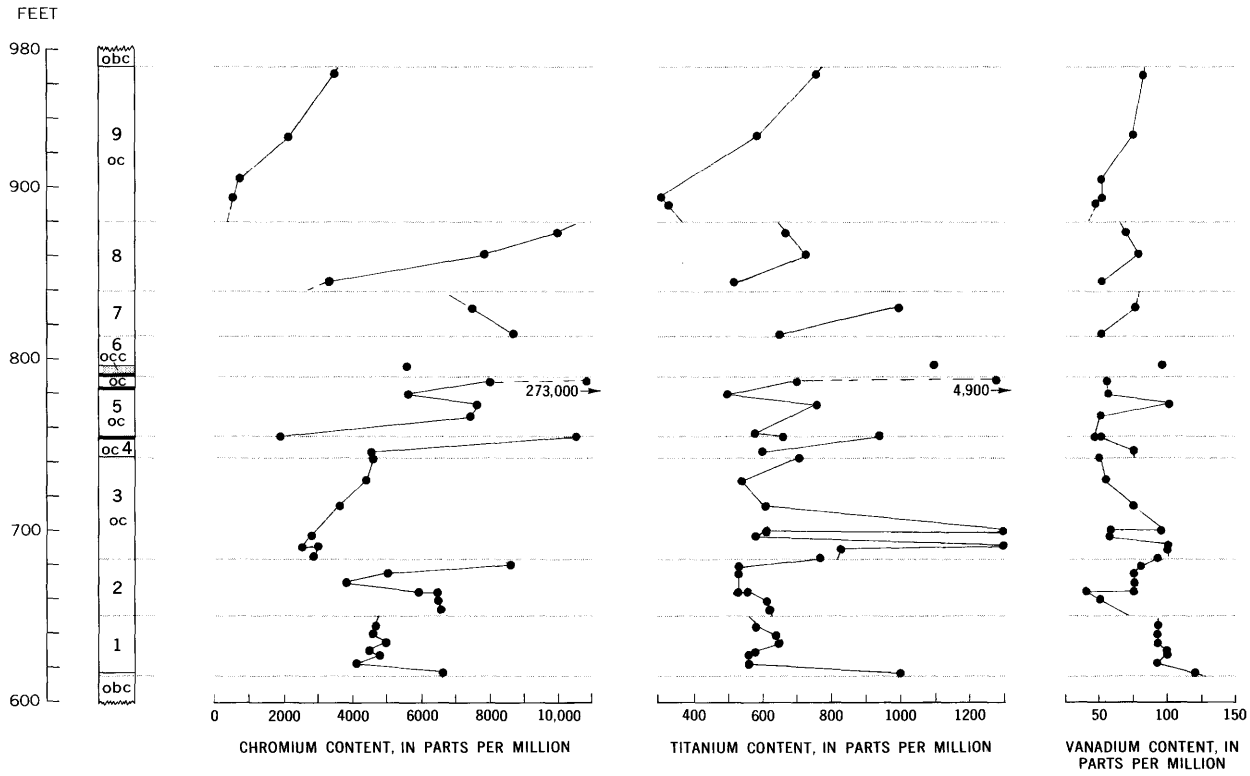

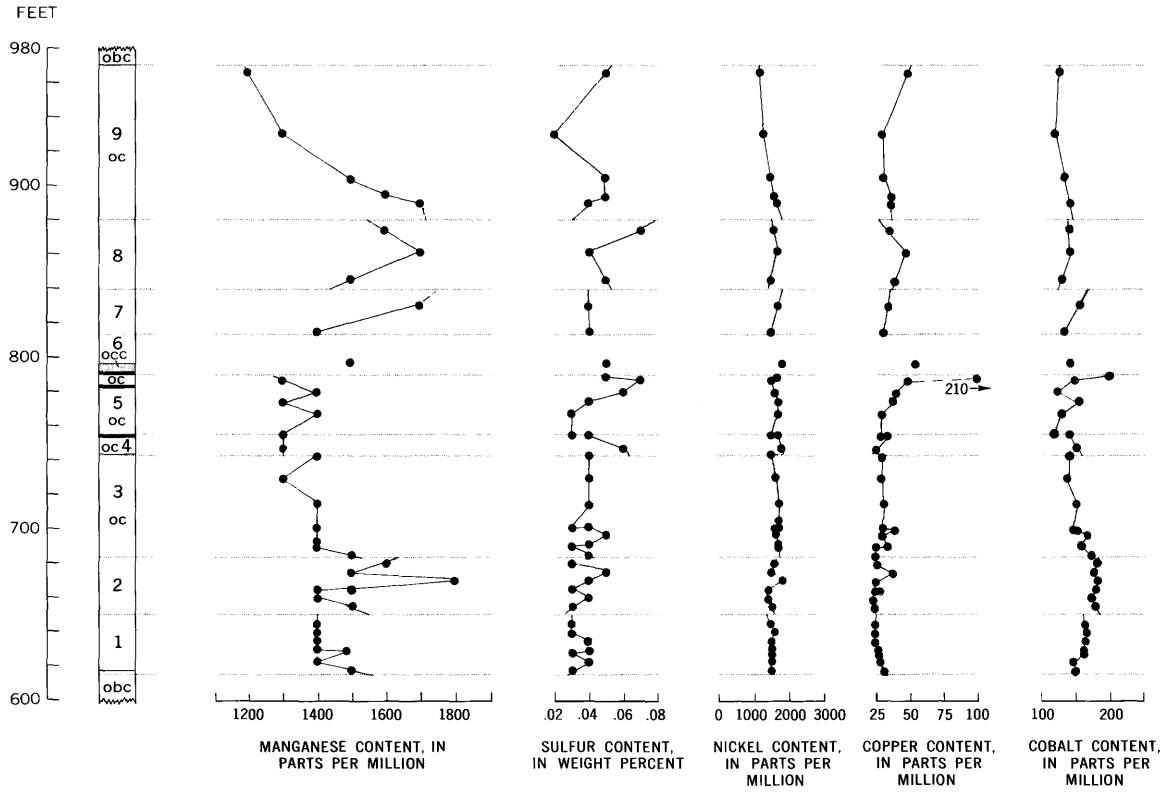

Figure 4.—Trace-element variation with stratigraphic position in the olivine cumulate. Refer to *A* in figure 2 for explanation of symbols in column.

four or five samples, rutile possibly in one sample associated with cumulus chromite. Some of the higher Ti concentrations reflect the presence of ilmenite.

The concentration of Mn fluctuates with stratigraphic position, but decreases with height in the majority of the size-graded units. Distribution of Mn is similar to the distribution of postcumulus interstitial material and does not correlate with the Cr concentration. Manganese is probably substituting in the clinopyroxenes and orthopyroxenes.

Although the sulfide minerals occur in minor amounts, their distribution is reflected by the analyses of S, Ni, Cu, and Co. From top to bottom of the olivine cumulate, S has a fairly constant concentration except at the top of most of the size-graded units, where S increases to a maximum very abruptly. No significant correlation between S and Cr concentrations was found. The concentration of Ni, Cu, and Co is fairly constant through the section, except for the maxima at the top of most of the size-graded units. Because all three metal elements have maximum concentrations in olivine size-graded units that correlate with S maxima, they are present in part as sulfides in addition to being in solid solution in the silicate and oxide minerals.

Nickel is known to occur in olivine, and if a large proportion is in the olivine, other relations could be masked. Irvine and Smith (1967, p. 47) used the variation in concentration of Ni, which they ascribe to solid solution in the olivine, in olivine cumulates of the Muskox intrusion to separate several cyclic units in otherwise homogeneous dunite. Within these cyclic units, the Ni concentration decreases from bottom to top, unlike the Ni concentration in the size-graded units of the olivine cumulate of cyclic unit 2. Within the lower part of the Peridotite member, at least, Ni does not appear to be distributed as in the Muskox intrusion except that it can be used to mark some grain-size breaks in the olivine cumulate.

TEXTURAL, MINERALOGIC, AND CHEMICAL VARIATIONS

Parameters that show abrupt changes at the same stratigraphic positions are: grain size of olivine and chromite cumulates, olivine compositions, olivine/olivine + chromite ratios, volume of postcumulus interprecipitate material, proportions of postcumulus minerals, and concentrations of Cr, Ti, V, Mn, S, Cu, Ni, and Co as shown by figures 2–4. Some properties that change abruptly vary by a relatively large amount, others by lesser amounts. In addition, each of the properties shows repetition of its trends at least six, possibly eight, separate times within one major olivine cumulate.

Grain-size variations probably were caused by changes in the supply of olivine and chromitite in the magma or by a decreasing growth or increasing nucleation rate for both olivine and chromite with stratigraphic position. Both olivine and chromite, when considered separately, show size-graded units (fig. 2*B*, *C*) that could be explained by the coarser particles settling more rapidly than the finer particles under the influence of gravity. But as Jackson (1961, 1971) has demonstrated in other parts of the Ultramafic zone, when the grain sizes of associated chromite and olivine from the same rock are compared by calculation of relative settling velocities, there is no hydraulic equivalence between olivine and chromite. And through this section there are no structures suggestive of current sorting. Therefore, mechanical sorting or gravity settling will not account for the size-graded units. All the other properties of cumulate minerals considered in this report are controlled by the composition and physical condition of magma. Only the volume of postcumulus interprecipitate material could be a function of mechanical processes.

The currently accepted model for the formation of cyclic units in the Stillwater Complex postulates sudden refreshment of magma by variable-depth convection (Jackson, 1961) and a subsequent crystallization of cumulate minerals near the floor of the complex. In this model there are two possible explanations for the abrupt variations described here: (1) each size-graded unit, except for unit 9, represents a beheaded cyclic unit, and (2) the size-graded units represent an oscillatory or cyclic process within the refreshed magma. In order to develop a mechanism defining the volume of magma required to produce a particular volume of rock, the cumulate units that most likely came from the same volume of magma must be defined, and one must decide between explanations 1 and 2.

Examples of evidence against the beheading process are furnished by Jackson (1970, p. 396), who states that the variation in olivine composition within single olivine cumulate units is commonly within 0.01 $Mg/(Mg+Fe^{+2})$ and that the olivine cumulates of cyclic units 9 and 15 in the Mountain View area appear not to have grain-size breaks within them. However, Jackson's samples may have been too far apart to define possible breaks. Despite this evidence, cyclic unit 10 is shown on the geologic map of the Mountain View area (Peoples and others, 1954) as containing four separate olivine cumulates separated by three thin, discontinuous bronzite cumulates. This suggests that cyclic unit 10 could be considered as consisting of four beheaded cyclic units. Jackson's more detailed study (1969) of the G and H chromitite zones demonstrates that within a cyclic unit there are oscillatory processes controlled either by small-scale changes in physical conditions of the magma or by slight compositional changes in the magma layer precipitating the cumulus phases. Page's study (1971a, b) of sulfide minerals within the chromitite zones supports the small-scale oscillation model.

For the olivine cumulate of cyclic unit 2 in upper Nye Creek basin, the clinopyroxene enrichment of the postcumulus material of each size-graded unit suggests an overall homogeneity for the parent magma batch. Because the clinopyroxene enrichment has been found elsewhere and only in cumulates of cyclic unit 2, the process forming the unit is not a local one. If the enrichment involves beheading, one must

conclude that the overall variable-depth convection process was able to derive eight very similar bulk magma compositions. Although grain size alone could be taken as evidence of beheaded units, the nature of the postcumulus materials suggests that we are examining the oscillatory process within a single batch of magma. The available evidence, therefore, supports the model of small-scale variation within one magma batch rather than separate batches, as required by the beheading process.

If variation took place in a single batch of magma, physical conditions or composition of the magma near the floor must have varied or oscillated differently than in the rest of the magma batch. Small changes in temperature or magma density caused by precipitation are possible causes of small-scale convection near the floor, which could then turn a magma batch into a small-scale version of Jackson's variable-depth convection model (1961). Yet such a model is not entirely satisfying in view of the great lateral distribution of thin layers noted elsewhere in the Stillwater Complex.

REFERENCES

Beeson, M. H., and Jackson, E. D., 1969, Chemical composition of altered chromites from the Stillwater Complex, Montana: Am. Mineralogist, v. 54, nos. 7–8, p. 1084–1100.

Haffty, Joseph, and Riley, L. B., 1968, Determination of palladium, platinum, and rhodium in geologic materials by fire-assay and emission spectrography: Talanta, v. 15, p. 111–117.

Hess, H. H., 1949, Chemical composition and optical properties of common clinopyroxenes, Pt. I: Am. Mineralogist, v. 34, nos. 9–10, p. 621–666.

——1960, The Stillwater igneous complex, Montana, a quantitative mineralogical study: Geol. Soc. America Mem. 80, 230 p.

Irvine, T. N., and Smith, C. H., 1967, The ultramafic rocks of the Muskox intrusion, Northwest Territories, Canada, *in* Wyllie, P. J., ed., Ultramafic and related rocks: New York and London, John Wiley and Sons, p. 38–49.

Jackson, E. D., 1960, X-ray determinative curve for natural olivine of composition Fo_{80-90} :Art. 197 *in* U.S. Geol. Survey Prof. Paper 400-B, p. B432–B434.

——1961, Primary textures and mineral associations in the Ultramafic zone of the Stillwater complex, Montana: U.S. Geol. Survey Prof. Paper 358, 106 p.

——1963, Stratigraphic and lateral variation of chromite composition in the Stillwater Complex: Mineralog. Soc. America Spec. Paper 1, p. 46–54.

——1967, Ultramafic cumulates in the Stillwater, Great Dyke, and Bushveld intrusions, *in* Wyllie, P. J., ed., Ultramafic and related rocks: New York and London, John Wiley and Sons, p. 20–38.

——1968, The chromite deposits of the Stillwater Complex, Montana, *in* Ridge, J. D., ed., Ore deposits of the United States 1933–1965: New York, Am. Inst. Mining, Metall., and Petroleum Engineers, p. 1496–1510.

——1969, Chemical variation in coexisting chromite and olivine in chromitite zones of the Stillwater Complex, *in* Wilson, H. D. B., ed., Magmatic ore deposits: Econ. Geology Mon. 4, p. 41–71.

——1970, The cyclic unit in layered intrusions–A comparison of repetitive stratigraphy in the ultramafic parts of the Stillwater, Muskox, Great Dyke, and Bushveld Complexes, *in* Visser, D. J. L., and von Gruenewaldt, G., eds., Symposium on the Bushveld igneous complex and other layered instrusions, Pretoria, July 7–14, 1969: Geol. Soc. South Africa Spec. Pub. 1, p. 391–424.

——1971, The origin of ultramafic rocks by cumulus processes: Fortschr. Mineralogie, v. 48, no. 1, p. 128–174.

Jones, W. R., Peoples, J. W., and Howland, A. L., 1960, Igneous and tectonic structures of the Stillwater Complex, Montana: U.S. Geol. Survey Bull. 1071-H, p. 281–340.

Page, N. J, 1971a, Sulfide minerals in the G and H chromitite zones of the Stillwater Complex, Montana: U.S. Geol. Survey Prof. Paper 694, 20 p.

——1971b, Comments on the role of oxygen fugacity in the formation of immiscible sulfide liquids in the H chromitite zone of the Stillwater Complex, Montana: Econ. Geology, v. 66, p. 607–610.

Page, N. J, and Jackson, E. D., 1967, Preliminary report on sulfide and platinum-group minerals in the chromitites of the Stillwater Complex, Montana, *in* Geological Survey Research, 1967: U.S. Geol. Survey Prof. Paper 575-D, p. D123–D126.

Page, N. J, and Nokleberg, W. J., 1970, Preliminary geologic map of the Stillwater Complex Montana: U.S. Geol. Survey open-file report, scale 1:12,000.

Page, N. J, Riley, L. B., and Haffty, Joseph, 1969, Platinum, palladium and rhodium analyses of ultramafic and mafic rocks from the Stillwater Complex, Montana: U.S. Geol. Survey Circ. 624, 12 p.

——1971, Lateral and vertical variation of platinum, palladium, and rhodium in the Stillwater Complex, Montana: Geol. Soc. America Abs. with Programs, v. 3, no. 6, p. 401.

Peoples, J. W., Howland, A. L., Jones, W. R., and Flint, Delos, 1954, Geologic map, sections, and map of underground workings of the Mountain View Lake area, Stillwater County, Montana: U.S. Geol. Survey open-file report.

PETROGRAPHIC EVIDENCE FOR VOLCANIC ORIGIN OF PART OF THE PORTERS CREEK CLAY, JACKSON PURCHASE REGION, WESTERN KENTUCKY

By JOHN D. SIMS, Menlo Park, Calif.

Work done in cooperation with the Kentucky Geological Survey

Abstract.—The occurrence of fresh glass shards in the Porters Creek Clay in Kentucky points strongly to the volcanic origin of at least part of the material in this formation. The occurrence of heulandite, "disordered cristobalite," and large quantities of biotite, and the fact that the smectite clays are dominated by montmorillonite, are corroborating evidence of volcanic origin. If one assumes in-place formation of the diagenetic mineral assemblages, the major chemical reaction responsible for formation of the clay was as follows: glass + H_2O + CO_2 = montmorillonite + cristobalite + zeolite + cations. The nonvolcanogenic components, kaolinite, illite, detrital quartz, and feldspar, are mainly weathering products of rocks of surrounding landmasses.

The Porters Creek Clay, of Paleocene age, crops out in the eastern and northern parts of the Jackson Purchase region, Kentucky (fig. 1). Its relation to the overall stratigraphy of the rocks of the Mississippi embayment has been described in detail (Stearns and Armstrong, 1955; Stearns, 1957; Murray, 1961). Mineralogical studies have dealt mainly with clay minerals (Pryor and Glass, 1961), heavy minerals (Hunter, 1968), or clay mineral–zeolite diagenetic assemblages (Reynolds, 1970), but there is no summary of the complete mineralogy of the Porters Creek Clay.

Although volcanic glass shards were identified in the Porters Creek Clay of southeastern Missouri by Allen (1935), little information was available concerning the cristobalite and heulandite in this formation other than that provided by Reynolds (1970). Glass shards, cristobalite, and heulandite provide evidence of an origin at variance with previous interpretations. This report describes the mineralogy, with emphasis on the diagenetic assemblage, and focuses on evidence for a volcanic origin.

GENERAL APPEARANCE AND STRATIGRAPHIC RELATIONS

The Porters Creek Clay is a distinctive unit of dark, generally massive, conchoidally fracturing mudstone; locally, however, it contains interbedded glauconitic micaceous quartz arenites. In most outcrops in Kentucky, the Porters Creek has a generally homogeneous texture, owing to the effects of extensive burrowing. The effects of burrowing are best seen where lighter, more sand- or silt-rich material has filled the voids. Where sand- or coarse silt-rich burrow fillings are absent, weathering of the mudstone yields a mottled effect in the otherwise dark massive rock to reveal the evidence of burrowing. The existing stratigraphic information, in addition to the mapped distribution, forms a framework in which the mineralogic data can be evaluated and the genesis of the formation interpreted.

The Porters Creek Clay crops out parallel to the margin of the Mississippi embayment and is present in the subsurface for a considerable distance downdip from outcrops. It conformably overlies and is intimately related to the Clayton Formation, also of Paleocene age (fig. 2). In Kentucky, the Clayton overlies unconformably rocks assigned to the McNairy Sand of Cretaceous age. However, these rocks are not differentiated in the Jackson Purchase region because of lithologic similarity of the two units. The Owl Creek Formation, commonly underlying the Clayton in much of the Mississippi embayment, is not positively identified in Kentucky but is present in Illinois and Missouri.

All the aforementioned units were formed during the transgressive-regressive movements of the Cretaceous-Tertiary seas. The lower part of the McNairy is transgressive (T_1) and is, in part, a nearshore facies of the Selma Group to the south (fig. 3). The upper part of the McNairy Sand and the Clayton Formation record the regressive phase of the sea in the Late Cretaceous (R_1) and transgressive phase of early Paleocene time (T_2). The R_1 phase of the McNairy Sand corresponds to the prograding clastic wedge illustrated by Pryor (1960). The major part of the Porters Creek Clay represents the maximum transgression in the middle Paleocene. Sand in the upper Porters Creek Clay, the "Paleocene sand" of Stearns (1957),

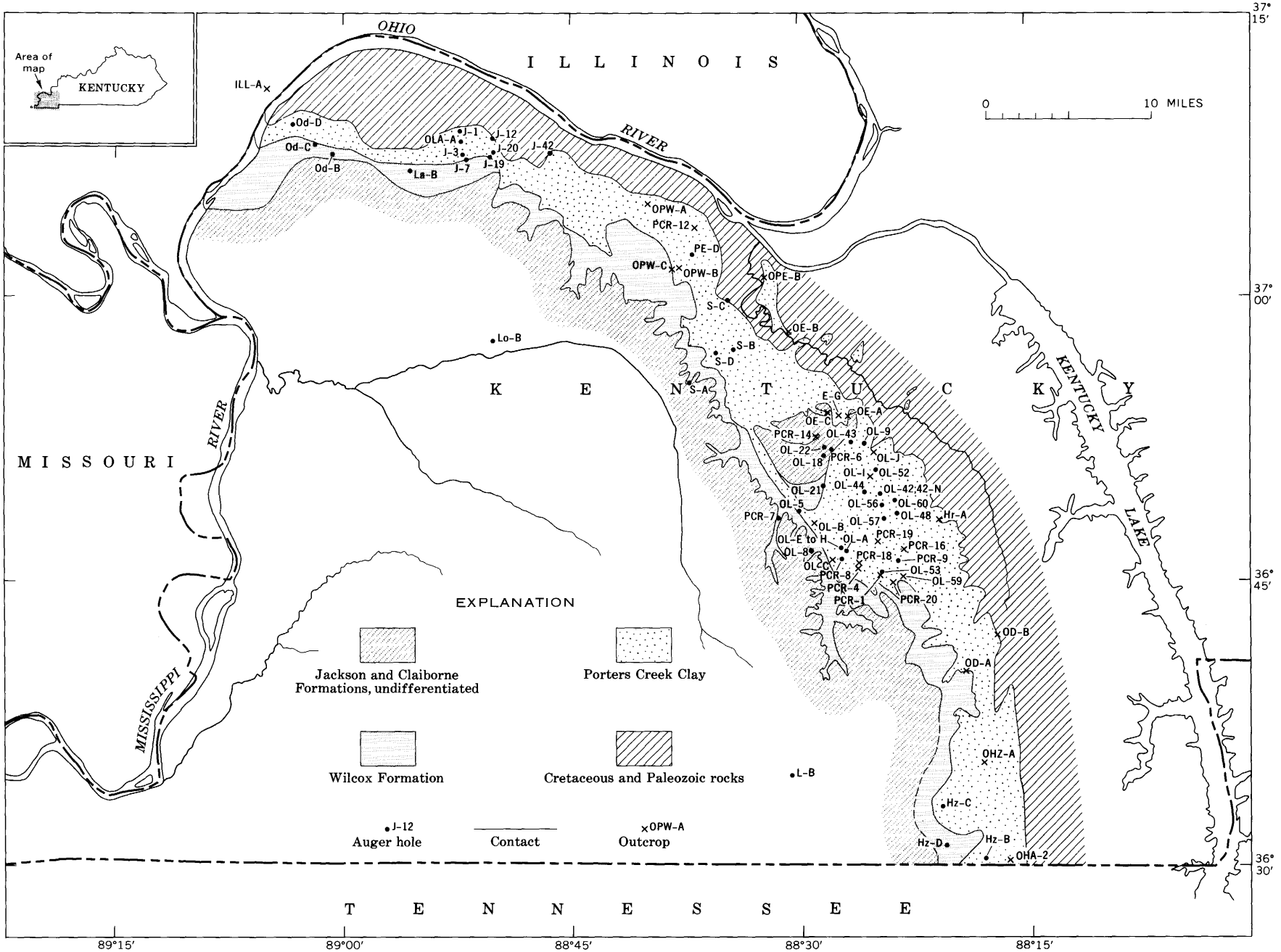

Figure 1.—Geologic map showing sample localities of Porters Creek Clay and adjacent rocks in the Jackson Purchase region, Kentucky.

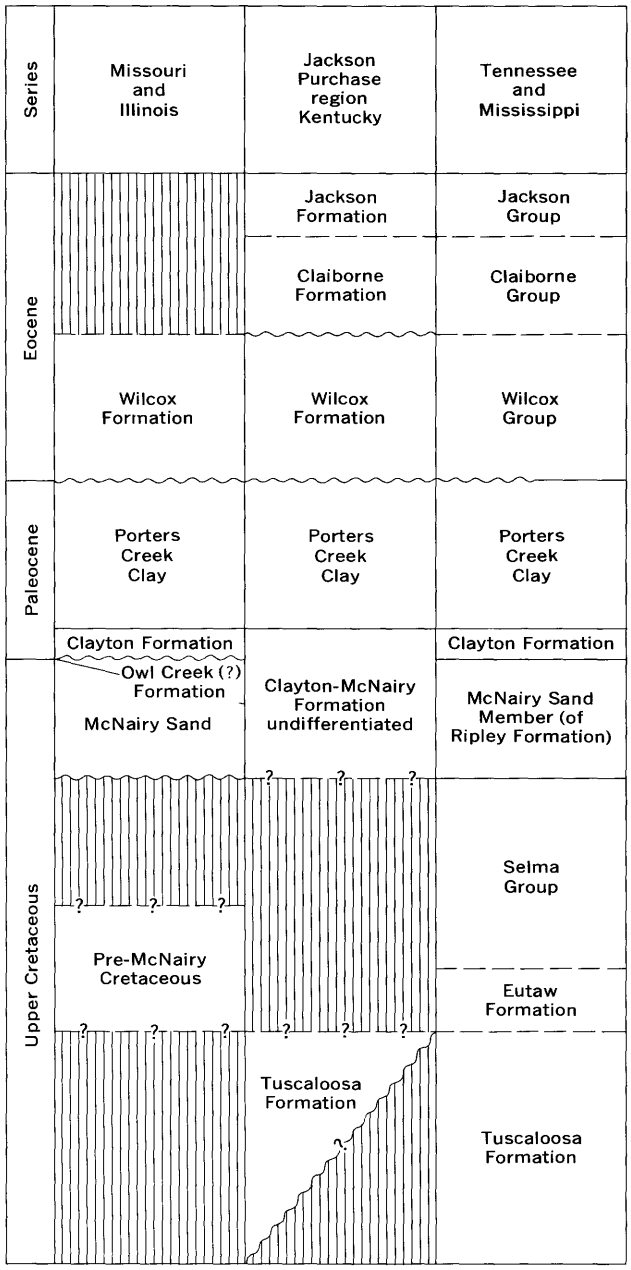

Figure 2.–Stratigraphic relations of Upper Cretaceous and lower Tertiary rocks of the northern Mississippi embayment.

represents the regressive phase (R_2) in the late Paleocene (fig. 3). Paleocurrent indicators have not been found in the Porters Creek; however, Stearns' (1957) lithofacies map suggests that sediments could have been transported from the east and northeast (fig. 4).

ANALYTICAL METHODS

Mineralogical data in table 1 were obtained by quantitative X-ray analyses of nonoriented material for bulk analyses and oriented settle slides for clay-mineral analyses as used by Schultz (1964). Supplementary data obtained from thin sections are limited to the more arenaceous parts of the formation, because much of the Porters Creek is extremely fine grained and contains large amounts of organic material.

The analytical methods of Schultz (1964), including the diffraction factors presented in his Pierre Shale study for the quantification of the X-ray diffraction data, are used because considerable X-ray analysis was completed on the Porters Creek samples by H. A. Tourtelot and R. P. Christian, U.S. Geological Survey, previous to the present study.

Accuracy of the determinations varies for each mineral with respect to its X-ray reflecting properties. In general, the order of decreasing accuracies is quartz, gypsum, feldspars, dolomite, calcite, heulandite, disordered cristobalite, and clay minerals. The range in sums of minerals present is 60–103 percent, indicating that the X-ray diffraction characteristics of some minerals in the Porters Creek Clay differ from those of the mineral standards used by Schultz (1964) in studying the Pierre Shale.

MINERALOGY

The Porters Creek Clay is composed chiefly of silica minerals and clay. The silica minerals are quartz and a mineral of the type referred to by Schultz (1964) as "disordered cristobalite." The clay minerals, in order of relative abundance, are montmorillonite, kaolinite, mixed-layer clay minerals, illite, and chlorite (table 1). Opaline silica is not generally present (H. A. Tourtelot, written commun., 1966).

Silica as quartz is present in all the 116 analyzed samples in amounts ranging from 5 to 50 percent, with a mean of 21 percent. Silica as "disordered cristobalite" is present in most samples and ranges from 2 to 35 percent, with a mean of 10 percent in all samples.

The distribution of cristobalite varies stratigraphically. The lower part of the Porters Creek contains 10 to 35 percent, the upper part 0 to 12 percent (table 1). Cristobalite is not commonly observed in thin sections because it is evidently dispersed as a fine-grained low-birefringent matrix cement. The large amounts of clay minerals, in addition to abundant organic material, tend to mask out any details of petrofabric in the fine-grained mudstones.

Heulandite makes up less than 10 percent of 9 of 116 samples and is identified by its 10° 2θ peak in bulk X-ray diffractograms. Clinoptilolite has a similar diffraction pattern. However, heating tests in conjunction with diffraction studies led Reynolds (1970) to identify heulandite as the sole zeolite mineral in the Porters Creek Clay in Alabama, so the zeolite phase in the Jackson Purchase region is considered to be heulandite. The heulandite in these samples is not regularly associated with cristobalite or glass shards (table 1). It is more abundant in the fine-grained rocks, probably as a dispersed interstitial mineral and therefore is not seen in thin sections.

Total clay content of the samples studied ranges from 13 to 84 percent with a mean value of 54 percent. The clay-mineral

Table 1.—*Quantitative X-ray analysis data for the Porters Creek Clay in the Jackson Purchase region, Kentucky*

[Stratigraphic position, where shown, refers to approximate time-stratigraphic assignment based on palynological evidence using methods described by Schultz (1964). Precision of determinations generally within 10 percent. Sample localities

Sample No. and stratigraphic position		Whole-rock analyses, in percent										Clay-mineral fraction, in percent					Remarks	
		Quartz	Heulandite	Dolomite	Calcite	K-feldspar	Plagioclase	Gypsum	Cristobalite	Total clay minerals	Total	Kaolinite	Illite	Chlorite	Montmorillonite	Mixed-layer clay minerals	Analyst (See headnote)	+, micaceous (includes muscovite and biotite) W, weathered sample
Hz-B1	lower ..	15	...	...	2	...	...	2	2	76	97	28	3	...	30	39	C	+
B2	do. ...	17	...	...	1	2	...	1	15	64	100	24	7	...	36	33	C	
C1	do. ...	16	...	...	...	...	...	1	...	84	101	35	4	...	23	38	C	+
C2	middle?.	7	...	...	...	...	...	2	13	74	97	16	9	...	39	36	C	
C3	upper ..	14	...	...	...	2	...	2	11	71	100	23	5	...	30	42	C	+
D1	lower ..	13	...	1	...	1	...	2	...	72	89	18	10	...	36	36	C	+
D2	middle .	8	...	...	...	...	1	4	16	71	100	16	9	...	32	43	C	
D3	upper ..	32	...	...	1	...	...	...	4	63	100	33	19	...	11	37	C	
S-A	do. ...	18	...	1	1	...	...	...	2	80	102	48	6	...	14	32	C	+
B	.....	17	7	1	2	...	...	...	12	58	97	13	2	...	36	49	C	
C	lower ..	47	1	...	...	...	...	2	...	45	95	35	5	...	27	33	C	
D	upper ..	30	...	...	...	...	2	...	...	40	72	28	13	...	13	46	C	
Od-B	.....	35	...	...	...	...	...	...	...	64	99	30	13	...	14	43	C	
C	.....	10	...	...	...	...	...	...	16	64	90	16	12	...	40	32	C	
D	.....	12	9	...	3	...	...	...	4	72	100	6	10	...	52	32	C	+
E-G	lower ..	12	1	...	...	2	...	2	...	77	94	55	8	...	12	25	C	
La-B	... ...	20	...	...	1	...	...	...	...	77	98	37	17	...	26	20	C	
L-B	middle..	42	4	...	...	...	...	...	4	50	100	36	15	...	22	27	C	
Lo-B1	lower ..	17	3	...	9	...	...	...	...	71	100	13	7	...	34	46	C	
B2	upper ..	25	...	...	...	2	...	...	...	71	98	19	10	...	37	34	C	
B3	middle..	22	6	...	...	...	...	...	9	63	100	11	11	...	44	34	C	
PE-D	.....	8	...	...	...	3	...	...	15	74	100	17	13	...	37	33	C	
OHA-2	.....	30	...	...	...	...	...	...	...	70	100	70	16	...	2	12	C	
OL-A	upper ..	26	...	1	1	...	2	...	...	59	89	69	23	...	...	8	T	W
B	do. ...	30	...	...	...	...	2	...	...	55	87	65	26	...	...	9	T	W
C	do. ...	20	...	...	...	...	...	...	...	50	100	65	20	...	...	5	T	Marcasite, 30 percent.
OD-A	do. ...	26	...	...	...	...	...	...	...	70	96	53	8	...	37	2	C	
OE-C	do. ...	21	...	...	...	...	...	...	15	50	86	32	...	...	...	68	C	
OPW-C	do. ...	12	...	...	...	...	...	...	7	60	81	28	8	...	42	22	C	
ILL-A	lower ..	8	...	...	...	...	...	...	...	77	85	N.d.	N.d.	N.d.	N.d.	N.d.	T	
OD-B	do. ...	5	...	...	...	...	...	...	35	65	105	10	21	...	50	19	C	
OE-A	do. ...	13	...	...	...	...	...	...	22	51	92	38	19	...	36	7	C	Average of three samples.
B	do. ...	7	...	...	...	...	...	...	25	75	107	19	23	...	13	44	C	Pyrite, 5 percent.
OPW-A	do. ...	6	...	...	...	...	...	...	28	67	101	12	5	...	39	45	C	Average of two samples.
B	do. ...	50	...	...	...	...	...	...	9	30	89	8	17	...	50	25	C	
OL-E	do. ...	12	...	...	...	...	1	...	7	65	86	22	11	...	42	25	C	
F	do. ...	14	...	...	...	...	...	...	7	52	73	14	14	...	55	17	C	
G	do. ...	6	...	...	...	...	...	...	16	65	87	16	13	...	53	18	C	
H	do. ...	35	6	...	...	...	...	...	7	35	83	...	13	...	37	50	C	
I	do. ...	7	...	...	...	...	...	...	18	65	90	23	6	...	46	25	C	
J	do. ...	7	...	...	...	...	...	...	16	77	100	28	7	...	38	27	C	
Hr-A	do. ...	8	...	...	...	...	...	...	25	67	100	44	14	...	22	20	C	
OHZ-A	middle..	12	...	...	...	...	...	...	25	60	97	32	20	...	29	19	C	
OLA-A	lower ..	7	...	...	...	...	...	...	21	50	78	12	7	...	56	25	C	
OPE-B	.....	20	...	...	...	...	...	...	5	55	55	6	34	...	21	34	C	Abundant iron.
PCR-1b	.....	22	...	...	...	...	...	...	12	48	82	N.d.	N.d.	N.d.	N.d.	N.d.	S	
PCR-6-1	.....	30	...	...	5	...	...	...	4	64	103	62	30	...	3	4	S	
3b	.....	21	...	...	...	25	...	...	3	51	100	21	20	...	25	34	S	
5	.....	54	...	...	...	26	...	...	2	13	95	39	23	...	12	26	S	
7a	.....	37	...	...	...	...	...	...	...	26	63	23	40	...	14	23	S	
9a	.....	40	...	...	...	8	...	...	2	26	76	25	20	3	34	34	S	
11b	.....	36	...	...	...	...	...	...	17	45	98	28	20	3	29	21	S	
13	.....	25	...	...	8	1	3	...	9	51	98	19	15	...	42	23	S	
PCR-7-9a	.....	46	...	...	...	17	...	...	...	38	101	69	13	12	6	...	S	
9d	.....	28	...	...	...	1	...	...	...	38	67	52	39	3	4	2	S	
10b	.....	22	...	...	...	...	...	...	...	64	86	33	16	12	25	14	S	
11	.....	23	...	...	...	...	...	...	4	58	85	19	23	16	17	25	S	
13	.....	22	...	...	...	23	...	...	...	38	83	36	26	6	13	18	S	
15	.....	23	...	...	...	5	...	...	...	38	66	15	23	16	19	26	S	
17	.....	25	...	...	...	5	...	...	...	45	75	24	20	6	18	31	S	
19a	.....	20	...	...	...	22	...	...	...	32	74	16	34	5	20	25	S	
19b	.....	22	...	...	...	8	27	...	2	26	85	23	23	...	10	44	S	
21	.....	16	...	...	...	...	...	...	7	51	74	23	30	4	21	22	S	

Table 1.—*Quantitative X-ray analysis data for the Porters Creek Clay in the Jackson Purchase region, Kentucky*—Continued

(R. H. Tschudy, written communs., 1964–68), X-ray analyses by R. P. Christian (C), H. A. Tourtelot (T), and J. D. Sims (S), are shown on figure 1. N.d., not determined; leaders (. . .), not detected, assumed zero]

Sample No. and stratigraphic position	Whole-rock analyses, in percent										Clay-mineral fraction, in percent					Remarks	
	Quartz	Heulandite	Dolomite	Calcite	K-feldspar	Plagioclase	Gypsum	Cristobalite	Total clay minerals	Total	Kaolinite	Illite	Chlorite	Montmorillonite	Mixed-layer clay minerals	Analyst (See headnote)	+, micaceous (includes muscovite and biotite) W, weathered sample
PCR-8-1	28	...	...	...	...	...	...	12	60	100	54	21	...	19	6	S	
3	14	...	...	...	...	...	...	10	51	75	32	19	...	20	29	S	
5	18	...	...	...	5	3	...	11	60	99	12	25	2	15	46	S	
7	15	...	...	...	4	...	...	16	65	100	31	18	...	29	16	S	
11	8	...	...	...	...	...	...	2	58	68	31	17	...	28	15	S	
13	7	...	...	...	...	...	...	20	70	97	34	16	3	14	33	S	
15	10	...	...	...	4	3	...	19	64	100	21	19	5	29	25	S	
17	9	...	...	...	...	...	...	21	64	94	21	16	...	23	40	S	
19	20	...	...	...	...	...	...	22	77	119	23	10	...	22	45	S	
20	10	...	...	...	5	...	...	22	64	101	19	17	5	29	30	S	
PCR-9-6	24	...	...	...	9	...	...	4	32	69	55	19	...	10	16	S	
7	20	...	...	...	4	...	...	14	62	100	24	29	...	1	46	S	
9	25	...	...	...	5	...	...	15	55	100	33	12	...	14	41	S	
11	10	...	...	...	...	...	...	14	45	69	29	18	...	19	34	S	
13	17	...	...	...	...	...	...	13	70	100	34	13	...	18	35	S	
15b	14	...	...	...	...	3	...	14	38	69	35	21	...	22	22	S	
16	31	...	...	...	6	5	...	7	16	65	32	23	...	13	32	S	+
PCR-12c	40	...	...	...	...	...	...	10	50	100	N.d.	N.d.	N.d.	N.d.	N.d.	S	
14	40	...	...	...	...	...	...	3	64	108	N.d.	N.d.	N.d.	N.d.	N.d.	S	
18	57	...	...	...	7	...	...	4	32	100	12	55	...	3	30	S	Wilcox Formation.
19	51	...	...	...	2	13	...	7	25	100	70	20	...	8	2	S	
20	53	...	...	...	8	...	...	...	32	100	N.d.	N.d.	N.d.	N.d.	N.d	S	Mica, 7 percent.
J-1	21	...	...	...	...	1	...	...	40	62	9	14	1	57	19	S	
3	36	...	...	...	...	...	...	6	32	74	15	11	...	12	62	S	
7	5	...	...	...	2	...	...	...	60	67	20	13	...	67	...	S	
J-12-1	24	2	...	...	1	3	...	2	53	91	10	15	...	49	24	S	Siderite, 6 percent.
2	10	...	...	...	...	6	...	18	56	90	15	28	5	11	41	S	
3	7	...	...	...	...	...	...	20	64	91	4	18	1	27	50	S	
J-19-1	7	...	...	5	...	2	...	3	48	65	30	8	2	40	22	S	
2	32	...	...	...	...	...	...	...	64	95	18	4	...	32	43	S	
3	32	...	...	...	12	12	...	6	16	78	20	18	1	32	31	S	
4	6	...	...	...	1	2	...	22	65	96	20	12	...	61	6	S	
5	6	...	...	...	...	...	...	27	64	97	17	12	...	4	26	S	
6	7	...	...	...	1	1	...	24	64	97	14	11	...	38	36	S	
J-20	8	...	...	...	...	...	...	25	67	100	7	11	1	54	28	S	
J-42	10	1	...	...	...	1	...	2	64	78	18	21	...	17	44	S	
OL-J-1	40	...	...	...	1	2	...	4	32	79	70	12	7	1	10	S	
OL-5	8	...	...	3	...	7	...	16	56	90	29	40	...	28	3	S	
8	40	...	...	...	...	2	...	3	48	93	71	17	...	...	11	S	
9	15	...	...	...	1	...	...	8	56	80	23	20	...	26	32	S	
18	28	...	...	3	2	1	...	10	56	100	32	34	...	6	28	S	
21	26	...	...	...	...	...	...	2	32	60	35	22	...	20	23	S	
22	26	...	...	...	2	...	...	4	40	66	19	12	...	46	24	S	
42	10	...	...	...	1	...	...	28	64	103	30	28	...	11	31	S	
42-N	38	...	...	...	...	...	...	...	64	102	65	22	...	...	13	S	
43	5	...	...	...	...	...	...	18	48	71	30	18	...	40	13	S	
44	6	...	...	...	...	...	...	28	64	98	33	27	...	21	19	S	
48	7	...	...	...	...	...	...	28	64	99	32	23	...	19	26	S	
52	24	...	...	3	1	1	...	8	32	84	38	31	...	25	6	S	Mica, 15 percent.
53	40	...	...	...	...	...	...	3	16	59	38	23	...	29	10	S	
56	5	...	...	...	...	10	...	17	60	92	35	12	...	23	29	S	
57	11	...	...	...	1	1	...	23	64	100	33	22	...	45	...	S	
59	15	...	...	...	...	6	...	13	64	98	19	16	...	19	44	S	
60	6	...	...	...	...	...	...	28	64	98	26	22	...	21	31	S	
Statistical parameters (zero values excluded)																	
Mean value	20.6	4.0	1	3.2	6.0	4.3	2	12.6	55.0	...	29.0	17.4	5.0	26.8	27.7		
Sample variance	165.4	8.2	0	6.5	49.1	31.8	.7	70.9	250.0	...	266.6	78.8	21.0	220.9	178.3		
Standard deviation	12.9	2.9	0	2.5	7.0	5.6	.9	8.4	15.8	...	16.3	8.9	4.6	14.9	13.4		
Number of samples in which mineral was reported.	117	10	4	15	40	27	9	89	117	...	111	111	22	106	109		
Statistical parameters for total population (zero values included)																	
Mean value	20.6	.34	.03	.41	2.04	1.10	.17	9.6	55.0	...	28.8	17.3	1.06	25.4	26.9		
Sample variance	...	1.9	.03	.41	24.5	10.8	.2	83.2	250.0	...	271.8	80.8	8.6	245.8	193.7		
Standard deviation	12.9	1.4	.18	1.9	5.0	3.2	.4	9.1	15.8	...	16.5	9.0	2.9	15.7	13.9		
Total number of samples.	117	117	117	117	117	117	117	117	117	...	112	112	112	112	112		

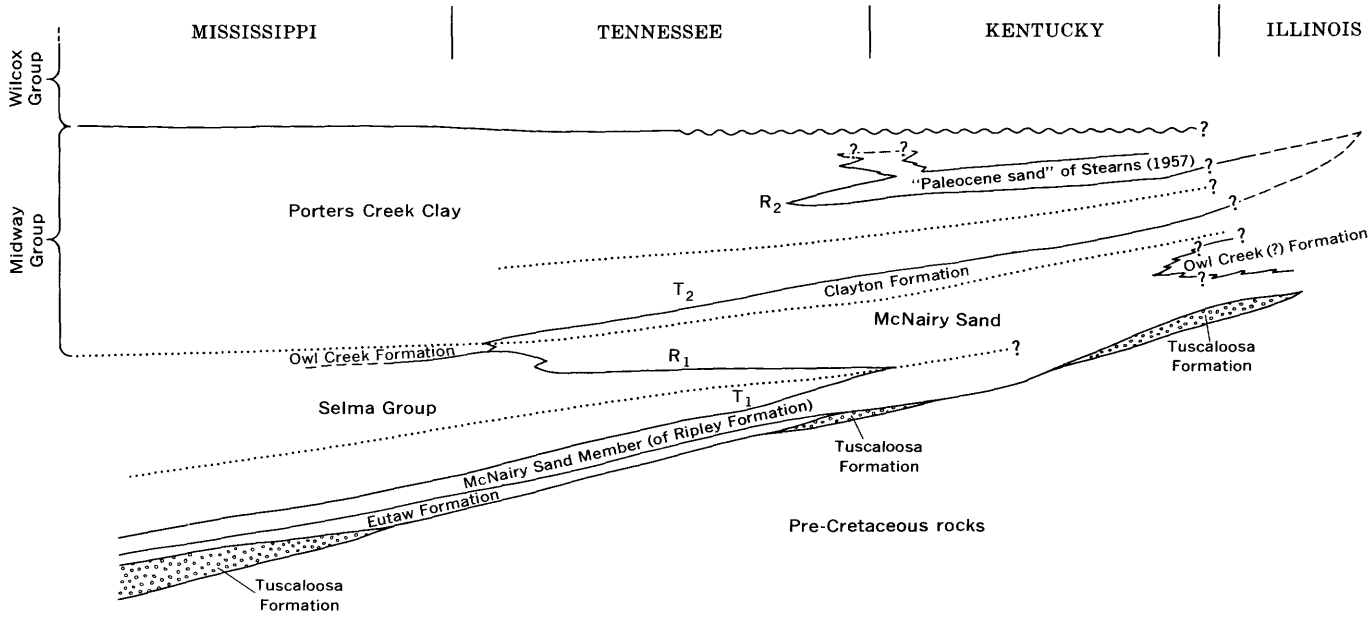

Figure 3.—Schematic stratigraphic reconstruction of Upper Cretaceous–lower Tertiary rocks showing transgressions (T) and regressions (R) and general facies relations (modified from Stearns, 1957).

suite is composed dominantly of montmorillonitic smectite, kaolinite, illite, and mixed-layer clay minerals. Montmorillonitic smectite is generally the most abundant clay mineral (table 1), but in some samples kaolinite or mixed-layer clay minerals may be dominant. The mixed-layer clay minerals are commonly composed mostly of montmorillonitic layers.

In the classification of the smectite group minerals, distinctions are made on structural and chemical criteria and location of the net structural charge. The distinction of importance is the location of the structural charge in the dioctahedral 2:1 smectite minerals, beidellite and montmorillonite. According to Schultz (1969), the net structural charge of beidellite is mainly due to the substitution of Al^{3+} for Si^{4+} in the tetrahedral sheet of the smectite, and that of montmorillonite, mainly to Mg^{2+} for Al^{3+} substitution in the octahedral sheet.

The Li^+ test of Greene-Kelly (1953) was used on selected clay-mineral fractions of the Porters Creek Clay to distinguish between montmorillonite, whose structural charge is dominantly in the octahedral sheet, and beidellite, whose structural charge is dominantly in the tetrahedral sheet in smectites (Grim, 1968, p. 86; Ross and Hendricks, 1945). Table 2 illustrates the results. The range for 18:9.6 A peak ratios for montmorillonites and beidellites is 0–50 percent and >50 percent, respectively (Schultz, 1969). The range in percentage reexpansion of the 18:9.6 A peak ratios has been arbitrarily divided into three classes of montmorillonite-beidellite smectites: <30 percent reexpansion = montmorillonite dominant, 30–60 percent reexpansion = montmorillonite-beidellite, and >60 percent reexpansion = beidellite dominant. On this basis all but one of the smectites tested, of the Porters Creek samples, are classified as dominantly montmorillonitic.

Table 2.—*Results of* Li^+ *test of Greene-Kelly*

Sample	Smectite diffractogram (001) peak heights		Percentage reexpansion	Smectite type (M, montmorillonite; B, beidellite)
	Li^+ at 200°C	Glycerated		
J-1.....	33	23	30	M
3.....	11	11	0	M, dominant.
7.....	21	13.5	45	M-B
J-19-1 ...	38	16	40	Do.
2 ...	50	23	65	B, dominant.
3 ...	26	19	25	M, dominant.
4 ...	14	9	35	Do.
6 ...	20	18	10	Do.
J-20.....	20	14	30	Do.
42.....	11	11	0	Do.
OL-8	12	12	0	Do.
18 ...	8	8	0	Do.
22 ...	22	18	20	Do.
42-N .	16	16	0	Do.
43 ...	11.5	8.5	25	Do.
52 ...	7	7	20	Do.
53 ...	15	8	45	M-B
56 ...	12	12	0	M, dominant.
60 ...	11	11	0	Do.
OL-J-1 ...	5	5	0	Do.

Biotite has a variety of forms and may be grouped generally as follows: (1) unaltered detrital grains (fig. 5*A*); (2) expanded (and hydrated?) grains (fig. 5*B*); and (3) chloritized(?) grains (fig. 5*C*). Chloritization(?) of biotite results in a reduction of the original pleochroism and of birefringence. The birefringence in altered grains decreases regularly from the unaltered core toward the margin of a grain. Most of the decrease in pleochroism and birefringence takes place in a thin zone at the edge of a grain. Some grains appear to assume a vermicular habit as chloritization(?) and hydration progress, especially in

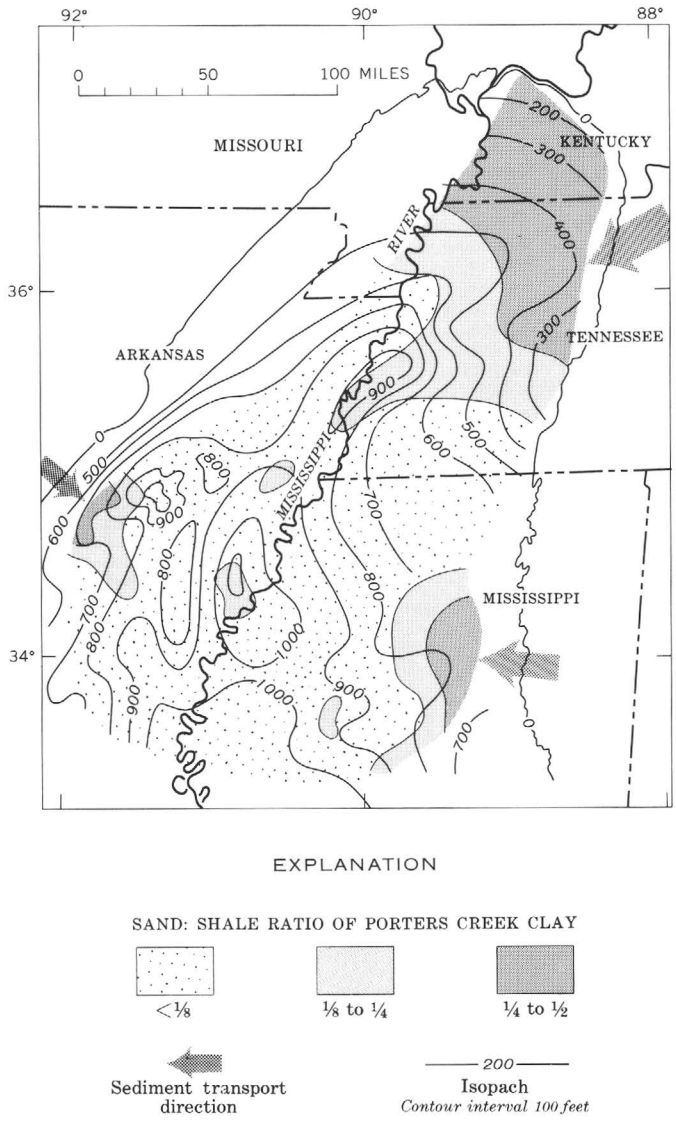

Figure 4.—Isopach and lithofacies map for Midway Group (Clayton Formation and Porters Creek Clay), showing approximate direction of sediment transport. Size of arrow is approximately proportional to amount of sediment influx (modified from Stearns and Armstrong, 1955).

samples taken near the contact of the overlying Wilcox Formation (fig. 6).

Muscovite is detrital and is common in many samples but absent in others (table 1). Many of the grains are expanded into a fan shape at the edges (fig. 7). No alteration of birefringence is noted, and thus the expanded edges may be due to physical rather than chemical processes.

Glauconite is common in the coarser materials and occurs as two types: (1) rounded mottled bright-green grains, and (2) olive-green to brownish grains with good cleavage (fig. 8). Cleavage in the second type suggests that this is an alteration product of biotite. A fecal origin is assumed for glauconites of the first type.

ORIGIN OF THE PORTERS CREEK CLAY

Several lines of evidence are used here to illustrate the volcanic origin of the bulk of the minerals in the Porters Creek. Most of the original material has been altered to a diagenetic mineral assemblage of montmorillonite, cristobalite, and heulandite. These minerals are associated with some primary volcanic debris, and themselves yield some information about their precursor materials.

The glass shards in the Porters Creek are primary evidence of volcanism. Their fine grain size (avg ≈40 μm) indicates considerable transport but cannot be related to a specific distance. Glass shards have been reported previously in the Porters Creek Clay of southeastern Missouri (Allen, 1935), but no refractive index was reported.

Glass shards are found in only one thin section (PCR-16), where some shards are fresh and some partly devitrified (fig. 9). Other thin sections yield grains that resemble completely altered shards, but positive identification is impossible. The shards appear typical of those associated with silicic to intermediate volcanic materials; they range from trilete to blade shaped, and most are bounded by concave surfaces. The refractive index, n = 1.55 to 1.546, was determined for several of the fresher shards separated by elutriation in water. Silica contents corresponding to this range of refractive indices are ≈53.5 to ≈55.25 percent, respectively (Moorhouse, 1959, p. 203). These silica contents agree favorably with published or inferred silica contents of presumed Cretaceous volcanic rocks in the Mississippi embayment but are lower than those of shards in Eocene and Oligocene volcaniclastic rocks in the Mississippi embayment (Monroe, 1954; Murray, 1961; Ross and others, 1929). If the shards are partly hydrated and the refractive indices too high, these silica contents can only be considered as minimums.

Heulandite is associated in some samples with "disordered" cristobalite and abundant montmorillonite. Zeolites are commonly found in altered volcanic sediments in a variety of environments (Hay, 1966; Deffeyes, 1959; Nayudu, 1964; Bonatti, 1963; Iijima and Utada, 1966; Reynolds, 1970). Hay (1966) and Deffeyes (1959) have described a variety of zeolitic diagenetic mineral assemblages associated with volcaniclastic material. Thus, the presence of zeolites, cristobalite, and montmorillonitic smectite in the Porters Creek strongly suggests in-place alteration of volcaniclastic material in an environment similar to that described by Reynolds (1970).

Cristobalite is more commonly associated with smectites in the Porters Creek than with heulandite and smectites together. The common occurrence of cristobalite in bentonites and other occurrences of smectites derived by the alteration of volcanic material was reported by Gruner (1940). Gruner also reported about 25 percent cristobalite in a sample of Porters Creek Clay near Olmstead, Ill., and from 40 to 50 percent in a sample from near Ardeola, Mo. Cristobalite in the Porters Creek is associated with altered glass shards in Missouri (Allen, 1935) and fresh to slightly altered glass in Kentucky. No glass

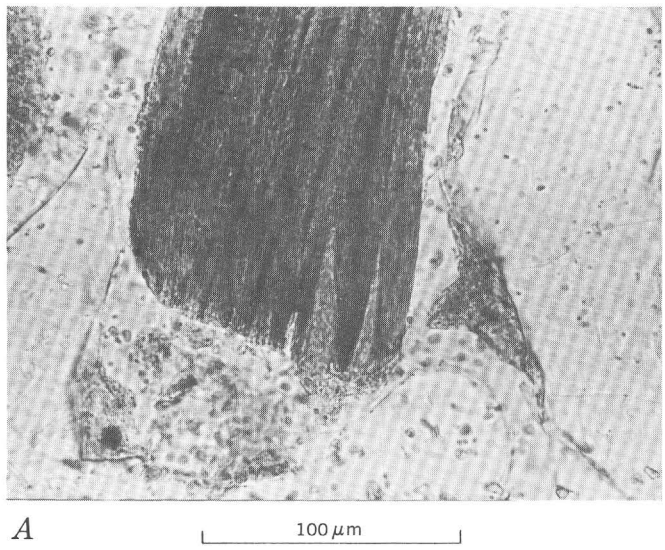

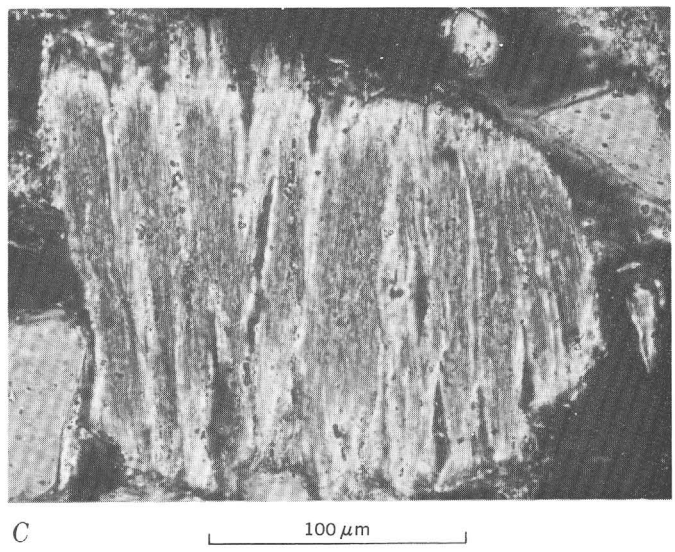

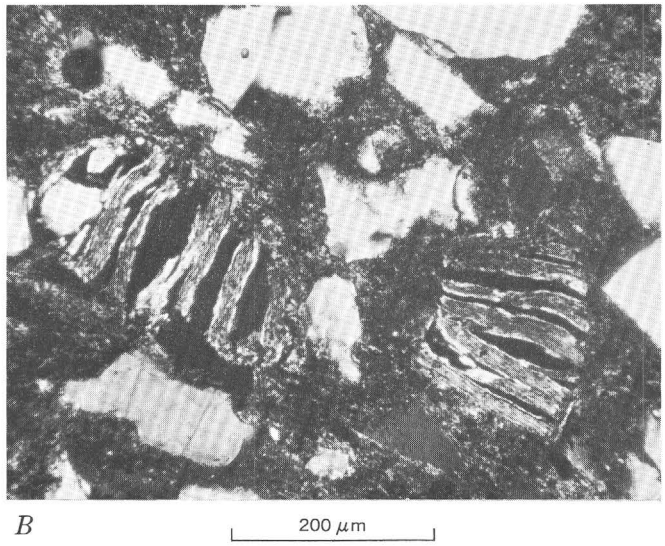

Figure 5.—Photomicrographs of biotite grains in the Porters Creek Clay (sample PCR-12). *A*, Generally unaltered detrital biotite; wedge-shaped cleavage filling may be matrix or incipient alteration; plane-polarized light. *B*, Expanded and hydrated(?) biotite; polarizers crossed, *C*, Chloritized(?) biotite; birefringence changes marked within single grains—first-order yellow and orange on rim and along cleavage planes, higher order colors on the interior; polarizers crossed.

shards have been reported in the Illinois occurrence of the Porters Creek. Reynolds (1970) reported no cristobalite in the Porters Creek of Alabama.

Bentonites have not been identified in Porters Creek Clay in the Jackson Purchase region but have been reported from it in Mississippi in Tippah County (Conant, 1941, p. 34, 65–66), Union County (Conant, 1942, p. 62), and in Chickasaw, Webster, Oktibbeha, and Pontotoc Counties (Ross and others, 1929). Bentonites of Paleocene age are also known in northern Mexico (Murray, 1961, p. 372). Episodes of ash accumulation followed by extensive bioturbation in the Porters Creek sediments would tend to obliterate ash beds, or bentonites, if formed.

Montmorillonitic smectites are generally associated with the alteration of volcanic materials, whereas beidellitic smectites are not. Table 2 illustrates the dominantly montmorillonitic nature of smectites of the Porters Creek Clay. Biotite commonly occurs in bentonites (Slaughter and Earley, 1965). Grim (1968, p. 567) considered biotite, among other minerals, as "characteristic of igneous material" and believed that it "may provide evidence for the origin from ash." Some of the biotite in these rocks has been altered to glauconite and still retains its original cleavage (fig. 8). Allen (1935) described similar glauconite in the Porters Creek Clay of Missouri; however, the possibility of fecal origin of some of these grains cannot be completely overlooked. Tripplehorn (1961) described, among other types of glauconite, grains identified as alterations of books of mica, and concluded that the origin of glauconite depends on the type of material present. Hallam and Sellwood (1968) considered biotite in the Nutfield fuller's earth too unstable to have been a "normal detrital mineral" and too chloritized to be authigenic. They favored a volcanic origin.

The association of glauconite with volcanogenic deposits,

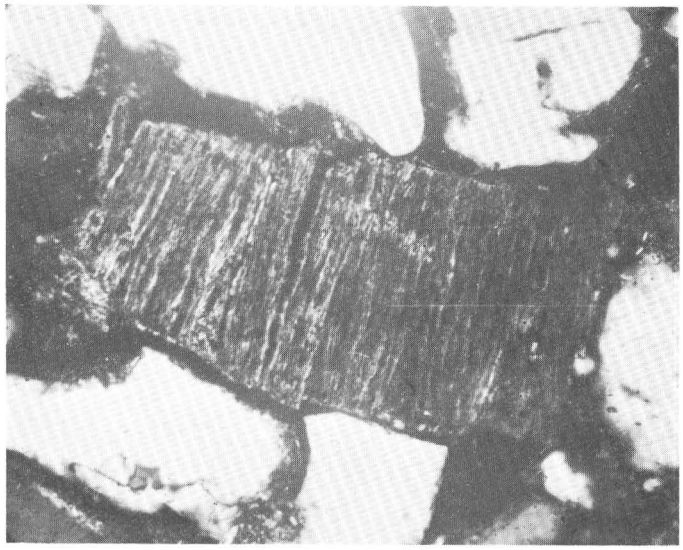

Figure 6.—Vermicular habit of chloritized biotite in sample PCR-4a. This specimen is from a few feet below the contact of the Porters Creek Clay with the overlying sands of the Wilcox Formation. Polarizers crossed.

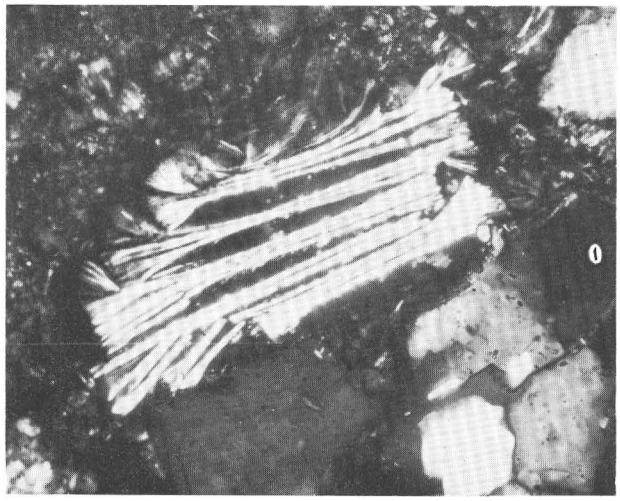

Figure 7.—Detrital muscovite from Porters Creek Clay with expanded (hydrated?) edges, Polarizers crossed. This sample (PCR-4a) is from within a few feet of the Wilcox Formation contact.

particularly bentonites, in the Gulf Coastal Plain is discussed briefly by Grim (1968, p. 569). The fuller's earth in Mississippi is also associated with glauconite (Bay, 1935, p. 32, 37). Glauconite formation is commonly considered (for example, Grim, 1968) to be associated with environments rich in organic material and a low sedimentation rate. Thus, episodic ash falls occurring in this type of environment, generally descriptive of the Porters Creek, would give rise to the association of volcanogenic deposits and glauconite.

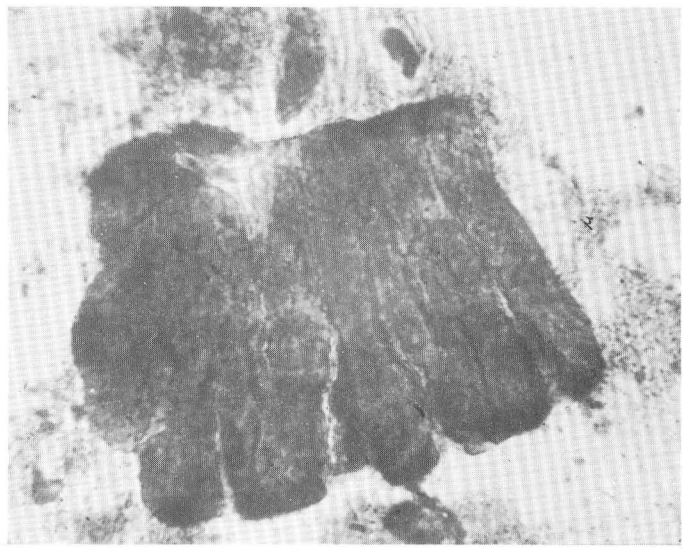

Figure 8.—Glauconite grain showing good cleavage. Precursor grain is considered to be biotite. This grain is probably similar to some described by Allen (1935). Sample PCR-4a; plane-polarized light.

The conclusion that the Porters Creek Clay is composed of a mineral assemblage largely attributable to volcanic activity is, nevertheless, at variance with published works on the upper Mississippi embayment. Pryor (1960), Pryor and Glass (1961), and Potter and Pryor (1961) suggested that the sediments in the upper Mississippi embayment were composed of detritus derived from the Blue Ridge and Piedmont Plateau region of the Appalachians. Pryor and Glass (1961) characterized the clay-mineral composition of the Cretaceous-Tertiary rocks of the upper Mississippi embayment as conforming approximately to salinity regimes in the Mississippi embayment seas of that time, resulting in three clay-mineral-facies environments. However, they interpreted the genesis of the Cretaceous-Paleocene rocks of the upper Mississippi embayment area without completely taking into consideration (1) the presence of volcaniclastic material in the Cretaceous-Tertiary rocks of the Gulf Coast, (2) the lack of major quantities of smectites in the source area suggested by them, (3) the presence of minerals such as "disordered cristobalite," montmorillonitic smectites, zeolites, and biotite; and (4) the presence of glass shards.

The clay-mineral suite available from rocks of the Blue Ridge and Piedmont Plateau region consists predominantly of illite and chlorite (Weaver, 1958). Furthermore, the Ohio, Cumberland, Tennessee, Duck, and Clinch Rivers, which drain an area similar to the eastern source area postulated by Pryor and Glass (1961), today carry a clay-mineral assemblage dominantly composed of kaolinite (10–20 percent) and illite (65–75 percent) (Holmes and Hearn, 1942). Smectites of all types in the present-day Ohio River sediments range between

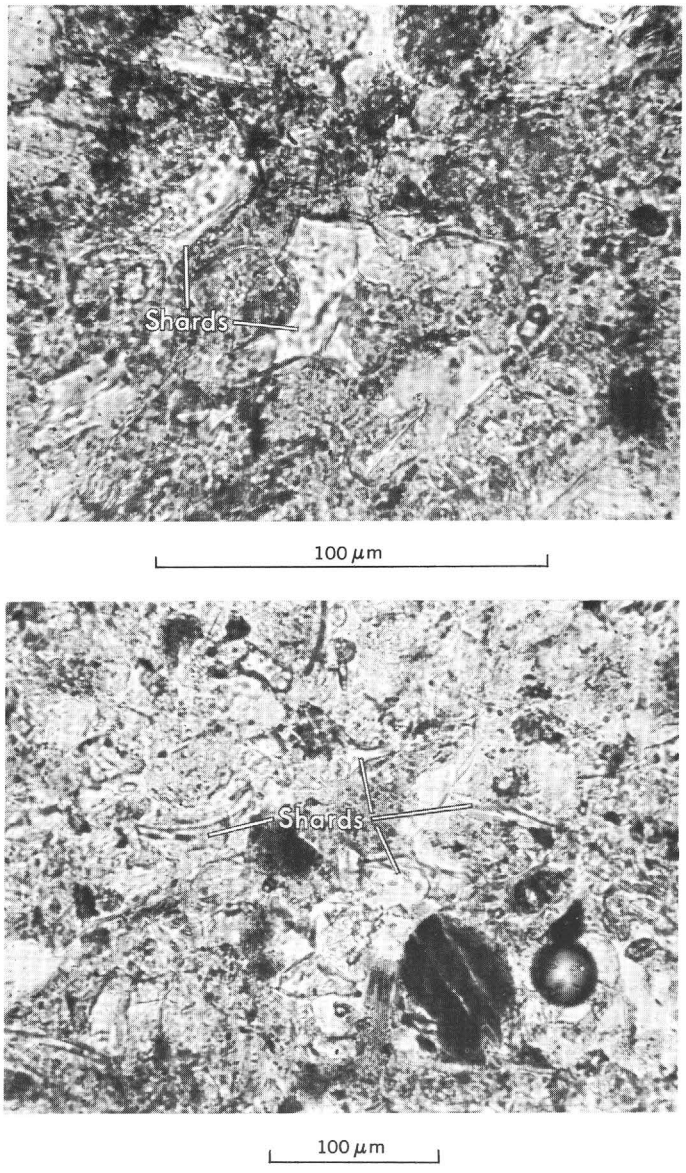

Figure 9.—Glass shards from the Porters Creek Clay. Sample PCR-16; plane-polarized light.

mixed-layer and fully expandable smectites or between montmorillonitic and beidellitic smectites. Climatic conditions in the Paleocene were, however, unlike present climates, being warmer and wetter and probably approximating subtropical to warm temperate (Tschudy, oral commun., 1971). Such climatic conditions in the Paleocene would favor the formation of silicic clay minerals in source areas. Thus, the work of Pryor and Glass did not resolve the problem of the source of montmorillonitic smectites deposited in the upper Mississippi embayment.

The only units in the Cretaceous-Tertiary sequence of the Mississippi embayment that are dominantly kaolinitic are the Tuscaloosa, Coffee, McNairy, and the Eocene undifferentiated (Wilcox and Claiborne Formations). These formations have fluviatile components or are completely fluviatile.

The Cretaceous rocks underlying the Porters Creek are, for the most part, composed of a kaolinite-illite clay-mineral assemblage, much as would be expected if a terrane of Paleozoic and crystalline rocks had undergone extensive subaerial erosion (Weaver, 1958) and the detritus had been deposited in the Mississippi embayment.

SOURCE OF VOLCANIC DETRITUS

No conclusive evidence exists regarding the source of the volcanic material in the Porters Creek Clay. Ross (1955) suggested widespread and volumetrically important volcanic activity during the Tertiary in the Gulf Coastal Plain. Nearby volcanic centers were suggested for the lower Tertiary rocks containing diagenetic mineral assemblages of volcanic origin in Alabama (Reynolds, 1970). A search for Paleocene volcanic centers in the Gulf Coast yields only the tentative identification of the Jackson dome at Jackson, Miss., the Sabine uplift of northwestern Louisiana and northeastern Texas, and the Monroe uplift of northeastern Louisiana, southeastern Arkansas, and western Mississippi (fig. 10). However, firm evidence for Paleocene volcanism on the uplifts shown on figure 10 is lacking.

DIAGENETIC MECHANISM

The Eh-pH conditions of the diagenetic environment may be estimated from a consideration of certain mineral components of the rocks with respect to the diagram of Krumbein and Garrels (1952). Glauconite, diagenetic silica, and organic matter are abundant in the samples studied. Carbonate has also been reported by Lamar and Sutton (1930). These observations suggest an estimated Eh of −0.1 and pH of 7.8 for the Paleocene sea. The probable diagenetic environment may be described more precisely by examining data for equilibrium mineral assemblages in sea water (fig. 11). The principal reaction in the diagenetic modification of the sediments of the Porters Creek may be expressed generally as glass + H_2O + CO_2 = montmorillonite + cristobalite + zeolite + cations.

The principal diagenetic minerals in the Porters Creek Clay are "disordered cristobalite," heulandite, and montmorillonite. If they were derived from a glass of relatively low silica content, as is indicated by the volcanic rock types present in the Jackson dome, there is a likelihood of a high calcium content. The equilibrium mineral relationships of the system CaO-Al_2O_3-SiO_2-H_2O at 25°C and 1 atm (fig. 11) (Sims, 1968; and unpub. data) suggest that the diagenetic mineral assemblage of montmorillonite, heulandite, and "disordered cristobalite" in the Porters Creek Clay does not represent an equilibrium assemblage in average sea water. However, sea-water chemistry may not be representative of pore-water chemistry during diagenesis. If one assumes that the diagenetic mineral assemblage of montmorillonite, heulandite, and "disordered cristobalite" is an equilibrium assemblage, the pore-water composition in contact with these minerals (fig. 11)

Figure 10.—Volcanic centers in the Mississippi embayment, their relationship to major structural features, and distance from the Jackson Purchase region (near intersection of circles).

would have $\log a_{Ca^{+2}}/a^2_{H^+} = 14$, $\log a_{H_4SiO_4} = -3.3$.

Heulandite is not present in all samples, so that the assumed diagenetic environment would tend to be at $9 < \log a_{Ca^{+2}}/a^2_{H^+} < 14$ along the Ca-montmorillonite-amorphous silica boundary (fig. 11), or perhaps within the Ca-montmorillonite field with cristobalite present metastably (Reynolds, 1970, p. 837).

CONCLUSIONS

It is obvious that a simplistic approach to sedimentological problems in the Porters Creek Clay in the upper Mississippi embayment does not adequately explain the various facts. Clay-mineral and associated mineral suites cannot be derived in the fashion of Pryor and Glass (1961). Volcaniclastic material was undoubtedly added and probably formed the bulk of the detritus deposited in the Paleocene seas. This conclusion is based on:

(1) the presence of glass shards in Kentucky and Missouri,
(2) the montmorillonitic nature of the smectite clays,
(3) the large quantities of altered volcaniclastic material in equivalent rocks in Mississippi (Ross and others, 1929; Conant, 1941, 1942), Alabama (Reynolds, 1970), Missouri (Allen, 1935), and Illinois (Grim, 1933),
(4) the presence of, at places, large quantities of cristobalite,
(5) the presence of large quantities of biotite and biotite alteration products in the Porters Creek Clay of Kentucky, Missouri, and Illinois, and
(6) the presence of heulandite in some samples.

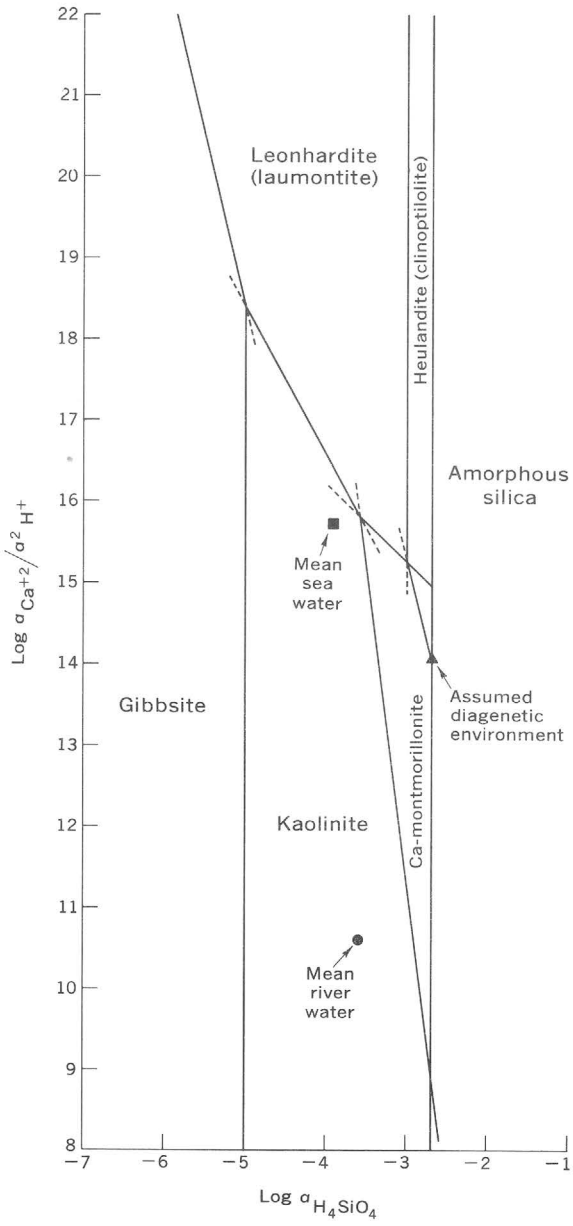

Figure 11.—Activity diagram for the system $CaO-Al_2O_3-SiO_2-H_2O$. Mean sea-water and river-water compositions are presented as reference points. See text for discussion of assumed diagenetic environment. Leonhardite contains one-half less molecule per formula weight H_2O than laumontite and can be regarded as the same mineral. Heulandite was chosen as an analog for clinoptilolite because thermodynamic data for clinoptilolite are lacking, and they occupy approximately the same stability field.

REFERENCES

Allen, V. T., 1934, Petrography and origin of fuller's (bleaching) earth of southeastern, Missouri: Econ. Geology, v. 29, no. 6, p. 590–598.

Bay, H. X., 1935, A preliminary investigation of the bleaching clays of Mississippi: Mississippi Geol. Survey Bull. 29, 62 p.

Bonatti, Enrico, 1963, Zeolites in Pacific pelagic sediments: New York Acad. Sci. Trans., ser. 2, v. 25, no. 8, p. 938–948.

Conant, L. C., 1941, Tippah County mineral resources: Mississippi Geol. Survey Bull. 42, 228 p.

—— 1942, Union County mineral resources: Mississippi Geol. Survey Bull. 45, 158 p.

Deffeyes, K. S., 1959, Zeolites in sedimentary rocks: Jour. Sed. Petrology, v. 29, no. 4, p. 602–609.

Greene-Kelly, R., 1953, Identification of montmorillonoids: Jour. Soil Sci., v. 4, p. 233–236.

Grim, R. E., 1933, Petrography of the fuller's earth deposits, Olmstead, Illinois, with a brief study of some non-Illinois earths: Econ. Geology, v. 28, no. 4, p. 344–363.

—— 1968, Clay mineralogy, 2d ed.: New York, McGraw-Hill, Book Co. 596 p.

Gruner, J. W., 1940, Abundance and significance of cristobalite in bentonite and fuller's earths: Econ. Geology, v. 35, no. 7, p. 867–875.

Hallam, A., and Sellwood, B. W. 1968, Origin of fuller's earth in the Mesozoic of southern England: Nature, v. 220, no. 5173, p. 1193–1195.

Hay, R. L., 1966, Zeolites and zeolitic reactions in sedimentary rocks: Geol. Soc. America Spec. Paper 85, 130 p.

Holmes, R. S., and Hearn, W. E., 1942, Chemical and physical properties of some of the important alluvial soils of the Mississippi drainage basin: U.S. Dept. Agriculture Tech. Bull. 833, 81 p.

Hunter, R. E., 1968, Heavy minerals of the Cretaceous and Tertiary sands of extreme southern Illinois: Illinois State Geol. Survey Circ. 428, 22 p.

Iijima, Azuma, and Utada, Minoru, 1966, Zeolites in sedimentary rocks, with reference to the depositional environments and zonal distribution: Sedimentology, v. 7, no. 4, p. 327–357.

Krumbein, W. C., and Garrels, R. M., 1952, Origin and classification of chemical sediments in terms of pH and oxidation-reduction potentials: Jour. Geology, v. 60, no. 1, p. 1–33.

Lamar, J. E., and Sutton, A. M., 1930, Cretaceous and Tertiary sediments of Kentucky, Illinois, and Missouri: Am. Assoc. Petroleum Geologists Bull., v. 14, no. 7, p. 845–866.

Monroe, W. H., 1954, Geology of the Jackson area, Mississippi: U.S. Geol. Survey Bull. 986, 133 p.

Moorhouse, W. W., 1959, The study of rocks in thin section: New York, Harper & Bros., 514 p.

Murray, G. E., 1961, Geology of the Atlantic and Gulf coastal province of North America: New York, Harper & Bros., 692 p.

Nayudu, Y. R., 1964, Palagonite tuffs (hyaloclastites) and the products of post-eruptive processes: Bull. Volcanol., v. 27, p. 391–409.

Potter, P. E., and Pryor, W. A., 1961, Dispersal centers of Paleozoic and later clastics of the Upper Mississippi Valley and adjacent areas: Geol. Soc. America Bull., v. 72, no. 8, p. 1195–1250.

Pryor, W. A., 1960, Cretaceous sedimentation in upper Mississippi embayment: Am. Assoc. Petroleum Geologists Bull., v. 44, no. 9, p. 1473–1504.

Pryor, W. A., and Glass, H. D., 1961, Cretaceous-Tertiary clay mineralogy of the upper Mississippi embayment: Jour. Sed. Petrology, v. 31, no. 1, p. 38–51.

Reynolds, W. R., 1970, Mineralogy and stratigraphy of lower Tertiary clays and claystones of Alabama: Jour. Sed. Petrology, v. 40, no. 3, p. 829–837.

Ross, C. S., 1955, Provenience of pyroclastic materials: Geol. Soc. America Bull., v. 66, no. 4, p. 427–434.

Ross, C. S., and Hendricks, S. B., 1945, Minerals of the montmorillonite group, their origin and relation to soils and clays: U.S. Geol. Survey Prof. Paper 205-B, p. 23–79.

Ross, C. S., Miser, H. D., and Stephenson, L. W., 1929, Water-laid volcanic rocks of early Upper Cretaceous age in southwestern Arkansas, southeastern Oklahoma, and northeastern Texas: U.S. Geol. Survey Prof. Paper 154-F, p. 175–202.

Schultz, L. G., 1964, Quantitative interpretation of mineralogical composition from X-ray and chemical data for the Pierre Shale: U.S. Geol. Survey Prof. Paper 391-C, 31 p.

—— 1969, Lithium and potassium absorption, dehydroxylation temperature, and structural water content of aluminous smectites: Clays and Clay Minerals, v. 17, no. 3, p. 115–150.

Sims, J. D., 1968, Thermodynamic model for zeolitic diagenesis in the Livingston Group, northern Crazy Mountains, Montana [abs.]: Geol. Soc. America Spec. Paper 121, p. 636–637.

Slaughter, M., and Earley, J. W., 1965, Mineralogy and geological significance of the Mowry bentonites, Wyoming: Geol. Soc. America Spec. Paper 83, 95 p.

Stearns, R. G., 1957, Cretaceous, Paleocene, and lower Eocene geologic history of the northern Mississippi embayment: Geol. Soc. America Bull., v. 68, no. 9, p. 1077–1100.

Stearns, R. G., and Armstrong, C. A., 1955, Post-Paleozoic stratigraphy of western Tennessee and adjacent portions of the upper Mississippi embayment: Tennessee Div. Geology, Rept. Inv. 2, 29 p.

Tripplehorn, D. M., 1961, The petrology of glauconite: Urbana, Ill., Univ. Illinois, unpub. Ph. D. thesis, 125 p.

Weaver, C. E., 1958, Geologic interpretation of argillaceous sediments. Part I, Origin and significance of clay minerals in sedimentary rocks: Am. Assoc. Petroleum Geologists Bull., v. 42, no. 2, p. 254–271.

GEOLOGIC RELATIONS AND X-RAY CRYSTALLOGRAPHY OF WAVELLITE FROM JACKSON COUNTY, WISCONSIN, AND THEIR GEOLOGIC IMPLICATIONS

By HARRY KLEMIC and MARY E. MROSE, Washington, D.C.

Abstract.—The occurrence of wavellite [$Al_3(PO_4)_2(OH)_3 \cdot 5H_2O$] as thin botryoidal crusts and small spherical masses in the Eau Claire Sandstone of Late Cambrian age near Black River Falls, Wis., is reported here. Single-crystal and X-ray powder diffraction studies of this wavellite leads to correction of powder diffraction data cited in the literature. The Wisconsin wavellite is orthorhombic, space group *Pcmn*; a=9.624 A, b=17.338 A, and c=6.986 A(all ±0.001 A). The strongest indexed X-ray powder lines are: 0.20, 8.670 A (100); 110, 8.415 A (100); 240, 3.220 A (60); 101, 5.654 (50); 012, 3.424 A (42); 200, 4.812 A (25); 161, 2.573 A (25); and 440, 2.105 A (21). The mineral is believed to be the product of leaching of phosphatic marine clastic sedimentary rocks. Spectrographic analysis of phosphatic shell materials from the Eau Claire Sandstone found rare earths in minor amounts and some possibly radiogenic lead; this could indicate that Upper Cambrian sandstones exposed in west-central Wisconsin were a possible source of radiogenic lead in the upper Mississippi Valley zinc-lead district. Greater concentrations of phosphatic materials may exist in the Upper Cambrian sandstones in the study area.

Wavellite [$Al_3(PO_4)_2(OH)_3 \cdot 5H_2O$] occurs in the Eau Claire Sandstone and in the upper part of the Mount Simon Sandstone, of Late Cambrian age, in the Black River Falls quadrangle, Jackson County, Wis. The mineral locality at which the wavellite was first noted in this area and where the wavellite described in this report was obtained is near lat 44°21′45″ N., long 90°50′45″ W., at the north edge of sec. 27, T. 22 N., R. 4 W., about 4 miles north of the north edge of the city of Black River Falls (fig. 1). The wavellite is in loose pieces in debris weathered from friable sandstone exposed on the east side of West Snow Creek Road on a low bank which is clear of vegetation for a vertical distance of about 6 feet and a length of more than 25 feet.

A long curving multispurred ridge a short distance to the north rises more than 200 feet above the site. Roadcuts exposing the Eau Claire Sandstone on the flanks of the ridge were examined and wavellite was found in additional places about 0.8 mile to the northeast along East Snow Creek Road in sec. 23, T. 22 N., R. 4 W., and about 2.5 miles to the north, near the center of sec. 10, T. 22 N., R. 4 W. Although overlying formations have been reported to contain the phosphatic material collophane, wavellite has not previously been described from this region.

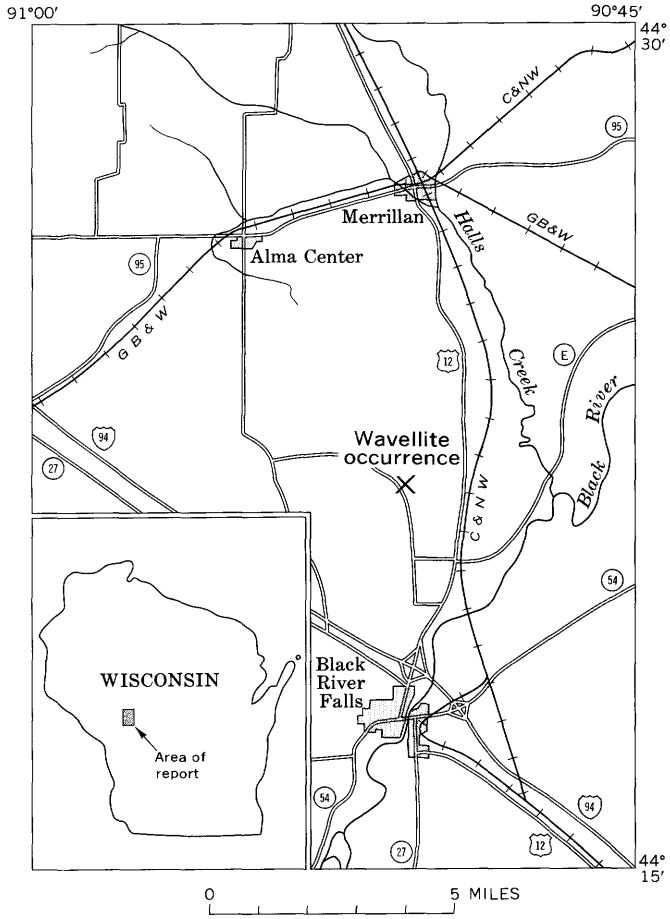

Figure 1.—Index map showing location of wavellite occurrence in Jackson County, Wis.

GEOLOGIC SETTING

The Elk Mound Group and part of the Tunnel City Group, both of Ostrom (1966) and of Late Cambrian age, form a

U.S. GEOL. SURVEY PROF. PAPER 800-C, PAGES C53-C62

400-foot-thick sequence of flat-lying Paleozoic clastic sedimentary rocks overlying the igneous and metamorphic Precambrian basement rocks in Jackson County, Wis. This part of the Paleozoic section has been described by Ostrom (1966) and Ostrom, Davis, and Cline (1970) as consisting of lithotopes that represent different and distinct marine shelf sediment zones. The stratigraphic section includes, in ascending order, the Mount Simon Sandstone, the Eau Claire Sandstone, and the Wonewoc Formation of the Elk Mound Group, and the Lone Rock Formation of the Tunnel City Group. These units are described on figure 2.

OCCURRENCE OF PHOSPHATIC MATERIAL

In the Black River Falls area, the lowest observed occurrence of abundant fragments of phosphatic fossil brachiopod shells is in the Eau Claire Sandstone in crossbedded layers and in thin horizontal layers. The fossils are in relatively flat lying beds which crop out about 200 feet stratigraphically above the base of the Mount Simon Sandstone which is exposed to the east along Black River. Wavellite occurs in the same stratigraphic position and is present along fractures that extend below the fossiliferous beds. Phosphatic brachiopod shells also occur in sandstone beds interlayered with thin- to medium-bedded, crossbedded argillaceous, glauconitic, and micaceous sandstone, and with thin-bedded siltstone and shale in the Lone Rock Formation about 200 feet higher in the stratigraphic section. Phosphatic material is also present in the uppermost Cambrian formations in areas to the south and west. Potter and Pryor (1961) stated that the Franconia and Trempealeau Formations contain collophane pseudomorphs and fragments of fossil debris that may constitute several percent of some samples.

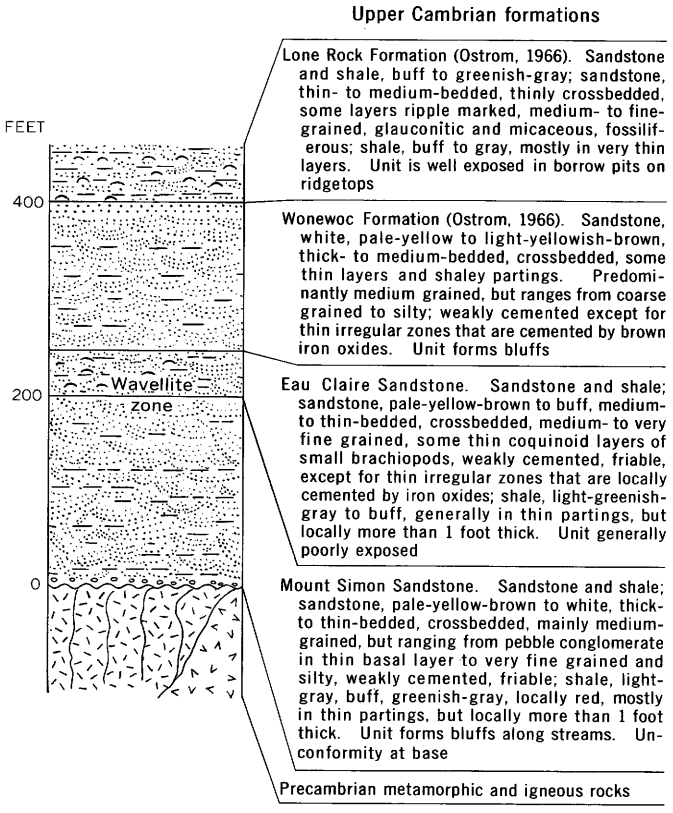

Figure 2.—Generalized stratigraphic section of Paleozoic sedimentary rocks near Black River Falls, Jackson County, Wis., showing the approximate position of the wavellite occurrence.

The local fossiliferous beds also contain molds of brachiopods and trilobites, indicating that organic materials were leached from the rocks after lithification. Some of the phosphatic brachiopods in the Eau Claire Sandstone have been partially dissolved in their present position, as indicated by molds of the dissolved parts. The small brachiopod shells remaining either were originally richly phosphatic or were preferentially phosphatized and therefore were less soluble than the calcareous material in other fossils which have been thoroughly leached from sandstone beds.

Solution of the parts of the quartz grains adjacent to the phosphatic shell material has resulted in the formation of flat or slightly concave faces on the sides of the quartz grains adjacent to the fossils. Other quartz grains in the rock have slightly etched surfaces but retain their rounded to subrounded forms. This reaction probably occurred during compaction and lithification of the sandstone, for individual grains of sand between closely spaced fossil shells have flat surfaces at each contact with shell material, although the remainder of the grain is well rounded. This modification of grain shape in the quartz sand and empty molds of fossils indicates that the rock has been subject to leaching by permeating waters.

Radioactivity measurements were made at outcrops of the Cambrian sandstone and on hand specimens to check for the presence of uranium in the phosphatic material. The background radioactivity at outcrops of thick-bedded medium-grained quartz sandstone of the Wonewoc Formation is relatively low. Radioactivity of shale, shaly sandstone, and coquinoid sandstone at the wavellite locality on West Snow Creek Road was found to be two to three times higher than that of the thick-bedded sandstone but was not exceptionally high in comparison with that of shaly rocks in general. Quantitative measurements of the radioactivity were not made.

Hand specimens containing wavellite and others containing concentrations of phosphatic fossil shells were not noticeably radioactive, as measured using a portable scintillation counter. Uranium in the phosphate-rich rock either was negligible or has largely been removed by leaching.

MINERALOGY

The secondary mineral, wavellite, and the primary mineral, carbonate-fluorapatite, of which the fossil shells are composed and which is the probable source of the phosphorus in the

wavellite, are described in some detail in this section; other constituents of the rocks have not been studied in detail.

Wavellite

Physical and optical properties

The wavellite is in clear to cloudy or milky-white crusts about 0.5 cm thick and consists of layers formed by coalescing radial growths on sandstone surfaces. Flat sides of the layers are adjacent to the sandstone, and the opposite sides of the layers have botryoidal surfaces on which there are pale-yellow-brown stains. Botryoidal masses extending between layered crusts, as shown in figure 3, indicate growth into open or solution-filled space. Within adjoining parts of the sandstone, wavellite occurs as a cement filling the pore spaces and as disseminated small (0.5-cm diameter) nodules enclosing sand grains. The botryoidal masses have a radiating internal structure, and most bulbous parts have a growth center either at the surface of the sandstone or within 1 or 2 mm of the surface, so that the botryoidal parts include clusters of nearly spherical to hemispherical shape.

Specific gravity of a wavellite sample from Wisconsin, weighing about 100 mg, was measured by Ellen Lillie, of the U.S. Geological Survey, using a 1-ml pycnometer and toluene as a solvent; specific gravity was found to be 2.30. The specific gravity of wavellite from Florida was reported by Altschuler Jaffe, and Cuttitta (1956, p. 499) to be between 2.30 and 2.33; that of wavellite from other localities described in the literature is as high as 2.36. The low specific gravity of the Wisconsin wavellite may be caused by voids enclosed during growth of the radiating mineral. The hardness was estimated to be about 4.

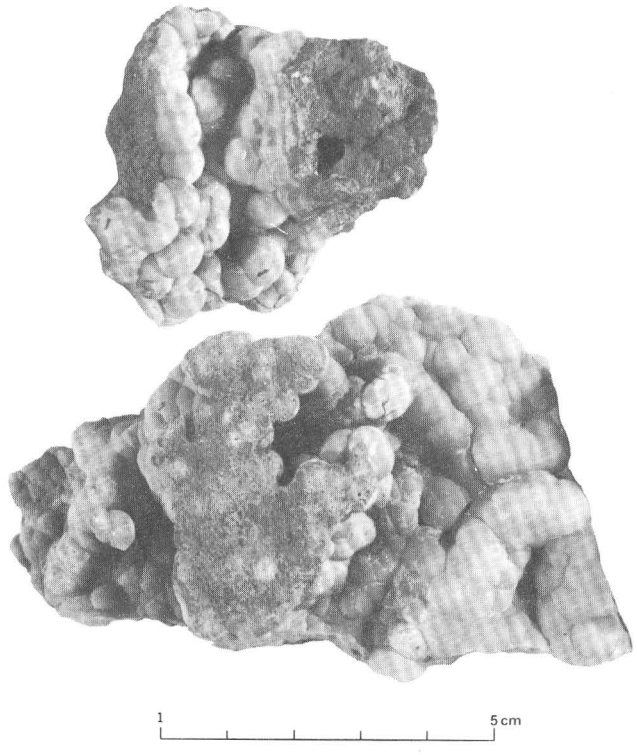

Figure 3.—Botryoidal wavellite from Jackson County, Wis.

The wavellite from Jackson County, Wis., is colorless and nonpleochroic in transmitted light and is biaxial positive (+) with moderately large $2V$ and $r>v$, perceptible; α=1.525±0.002, β=1.535±0.002, γ=1.551±0.002 (Na, at 25°C); Z = c (elongation). The indices of refraction were determined with sodium light, and the index oils were checked on an Abbe refractometer at the time the measurements were made. The optical observations for the wavellite from Wisconsin are in close agreement with those reported in the literature for wavellite from the following localities: Dug Hill, Ark.; Bohemia, Czechoslovakia; Llallagua, Bolivia; Hellertown, Pa.; and Seixeira, Portugal.

Single crystal X-ray data

An X-ray diffractometer trace made of the wavellite from Jackson County, using Cu$K\alpha$ radiation, clearly showed two very large distinct closely spaced peaks within the 8.0–9.0 A range of spacings. Because these findings differed from the X-ray data on wavellite that were used for comparison, more detailed X-ray studies were made of this material.

Single-crystal precession photographs were obtained from a carefully selected equant fragment of the wavellite from Wisconsin; both zirconium-filtered molybdenum radiation (λMo$K\alpha$=0.71069 A) and nickel-filtered copper radiation (λCu$K\alpha$=1.5418 A) were used. Diffraction data established orthorhombic symmetry; systematic absences are compatible with two possible space groups, $Pcmn$ and $Pc2n$, confirming the observations of Araki and Zoltai (1968) and Gordon (1950). The recent crystal-structure determination of wavellite (Araki and Zoltai, 1968) established $Pcmn$ as the correct space group.

Unit-cell parameters obtained from the precession photographs were used to initiate a least-squares analysis of the powder diffraction data of the Wisconsin wavellite; the refined cell constants thus obtained are listed in table 1. Indexed powder data based on these cell constants are tabulated in table 2. Miller indices assigned to the powder data for the wavellite were fixed by relating the observed intensities of the lines on the measured powder film to single-crystal intensity values of the respective reflections noted on the precession photographs.

X-ray powder diffraction data

X-ray patterns of wavellite from Wisconsin were taken in Debye-Scherrer powder cameras (diameter 114.59 mm) using both Ni-filtered copper radiation (λCu$K\alpha$=1.5418 A) and Mn-filtered iron radiation (λFe$K\alpha$=1.9373 A). The line resolu-

Table 1.—*Comparison of crystallographic data for wavellite,* $Al_3(PO_4)_2(OH)_3 \cdot 5H_2O$

Parameters	Data source and locality of specimen			
	Present study	Araki and Zoltai (1968)	Gordon (1950)[1]	Breskovska and Ivchinova (1961–1962)
	Jackson County, Wis.	Montgomery County, Ark.	Llallagua, Bolivia	Madjarovo, Bulgaria
Space group	*Pcmn*	*Pcmn*	*Pcmn*	*Pnma*
Unit-cell dimensions:				
a (A)	9.624±0.001	9.621±0.002	9.62	9.61
b (A)	17.338±0.001	17.363±0.004	17.34	17.34
c (A)	6.986±0.001	6.994±0.003	6.99	6.98
a : b : c	0.555:1:0.403	[2]0.554:1:0.403	[2]0.555:1:0.403	[2]0.544:1:0.403
Volume (A^3)	1165.7	[2]1168.3	[2]1166.0	[2]1163.1
Z	4	4	4	.....
Specific gravity:				
Calculated	[4]2.347	[2]2.342	[2]2.346	[2]2.352
Measured	[4]2.30	.....	2.36	2.33

Parameters	Data source and locality of specimen			
	Smelkova and others (1966)[1]	Svyazhin (1968)	Fu (1966)	Bouška and others (1969)
	Belkin deposit, Kemerovo, U.S.S.R.	Sysert region, Urals, U.S.S.R.	.....	Kolodĕje nad Lužnicí-Hosty, southern Bohemia, Czechoslovakia
Space group	.....	.....	$Pc2_1n$	*Pcmn*
Unit-cell dimensions:				
a (A)	9.76	9.76	9.57	9.592
b (A)	17.18	17.02±0.06	17.3	17.33
c (A)	7.00	6.82±0.03	6.98	7.008
a : b : c	[2]0.568:1:0.407	[2]0.573:1:0.401	[2]0.553:1:0.403	0.553:1:0.404
Volume (A^3)	[2]1173.7	[2]1132.9	[2]1155.6	[2]1164.9
Z	.....	.....	4	.....
Specitic gravity:				
Calculated	[2]2.330	[2]2.415	[2]2.367; [3]2.471	[2]2.349
Measured	2.35	2.38	.....	2.35

[1] Converted from kX units by the present authors.
[2] Calculated by the present authors.
[3] Calculated by the present authors for the structural formula, $Al_3(PO_4)_2(OH)_3 \cdot 6H_2O$, as given by Fu (1966).
[4] Determined by the pycnometer method.

tion on films taken in iron radiation was superior to that on films taken in copper radiation. Therefore, X-ray powder diffraction data (table 2) were determined from measurements of a film taken in iron radiation in a camera fitted with a Wilson adapter, so as to permit use of the Straumanis technique in film measurement. Comparison of the X-ray powder diffraction data for wavellite from Wisconsin was made with those cited in 11 references in the literature (Am. Soc. Testing Materials card no. 2-0075; Bouška and others, 1969; Breskovska and Ivchinova, 1961–1962; Kaemmel, 1961; Mäkelä, 1969; Mikheev, 1957, p. 631; Neves, 1960; Smelkova and others, 1966; Sumin, 1953; Svyazhin, 1968; Zanin and others, 1970). None recorded more than one line between 8.0 A and 9.0 A.

Powder patterns of wavellite in the standard reference film library at the U.S. Geological Survey, all taken in Cu$K\alpha$ radiation and representing seven localities (Dug Hill, Ark.; Graz, Austria; Llallagua, Bolivia; Vohidraty, Madagascar; East Waterford, Juniata County, Pa.; Mineral Ridge, near Woodstock, Va.; and Berkeley Springs, W.Va.), were carefully examined. Only under magnification (using a binocular 2.3× loupe magnifer) did each of these films show two very strong distinct though closely spaced lines in the region 8.0–9.0 A. Because the original spindles were available for further study, X-ray powder diffraction patterns of wavellite from the above-listed localities were taken in filtered Fe$K\alpha$ radiation; each distinctly showed resolution of the (020) and (110) interplanar spacings.

Semiquantitative spectrographic analyses

In order to confirm that the X-ray data did not represent either mixtures of two compositional phases of wavellite or more than one mineral, handpicked samples of clear and milky-white wavellite from Wisconsin were analyzed spectrographically. The results are shown in table 3.

The spectrographic analyses indicate that the samples of clear and milky-white wavellite from Wisconsin contain the major constituents of wavellite, namely phosphorus and

Table 2.—*Comparison of X-ray powder diffraction data for wavellite,* $Al_3(PO_4)_2(OH)_3 \cdot 5H_2O$

[Orthorhombic, *Pcmn*: *a*=9.624 A, *b*=17.338 A, *c*=6.986 A (all ±0.001 A)]

hkl	Present study: Black River Falls quadrangle, Jackson County, Wis.				Mäkelä (1969): Kittilä, Finland		Bouška and others (1969): Kolodĕje nad Lužnicí-Hosty, southern Bohemia, Czechoslovakia	
	Calculated[1]	Observed[2]			Observed[3]		Observed[4]	
	d_{hkl} (angstroms)	d_{hkl} (angstroms)	*I*	Single crystal *I*	d_{hkl} (angstroms)	*I*	d_{hkl} (angstroms)	*I*
020	8.669	8.670	100	vs	.....	.....	8.6	10
110	8.415	8.415	100	vs	8.41	10	.....	.....
101	5.654	5.654	50	vs	5.64	7	5.66	6
111	5.375	5.375	15	mw	5.37	3	5.37	4
130	4.955	4.954	13	mw	4.98	2	4.95_5	3
200	4.812	4.812	25	vs	4.84	3	4.79_5	5
121	4.736	.....	.....	w	.....		.....	.....
040	4.335	4.335	3	mw	.....	.....	4.34	1
220	4.207	.....	.....	vw	.....	.....	.....	.....
131	4.041	4.042	9	mw	4.04	3	4.05	3D
201	3.963	3.963	9	m	.....	.....	3.95	1
211	3.863	3.864	4	mw	.....	.....	3.86	<1
221	3.604	.....	.....	a	.....	.....	.....	.....
002	3.493	.....	.....	vw	.....	.....	.....	.....
141	3.440	.....	.....	w	.....	.....	.....	.....
012	3.424	3.424	42	vs	3.44	8	3.44	8
102	3.283	.....	.....	w	.....	.....	.....	.....
231	3.268	.....	.....	w	.....	.....	.....	.....
150	3.262	.....	.....	a	.....	.....	.....	.....
022	3.240	.....	.....	a	.....	.....	.....	.....
112	3.226	.....	.....	w	.....	.....	.....	.....
240	3.221	3.220	60	vs	3.21	8	3.24	8
310	3.155	3.155	9	mw	.....	.....	3.14	1
122	3.071	3.070	13	ms	3.06	3	3.08	3
032	2.989	.....	.....	mw	.....	.....	.....	.....
151	2.956	2.956	6	mw	2.95	4	2.958	3D
241	2.925	2.925	9	mw	.....	.....	.....	.....
301	2.915	.....	.....	vw	.....	.....	.....	.....
060	2.890	2.890	4	w	.....	.....	.....	.....
311	2.875	.....	.....	vw	.....	.....	.....	.....
132	2.855	.....	.....	vvw	.....	.....	.....	.....
202	2.827	.....	.....	vw	.....	.....	.....	.....
330	2.805	2.805	18	vs	2.79	4	2.805	4
212	2.790	.....	.....	vw	.....	.....	.....	.....
321	2.763	.....	.....	vw	.....	.....	.....	.....
042	2.720	.....	.....	vw	.....	.....	.....	.....
222	2.688	.....	.....	a	.....	.....	.....	.....
142	2.617	.....	.....	w	.....	.....	.....	.....
251	2.610	2.607	8	mw	.....	.....	.....	.....
331	2.603	.....	.....	mw	.....	.....	.....	.....
161	2.573	2.573	25	vs	2.57	7	2.591	7
232	2.539	2.539	6	mw	.....	.....	2.535	1
260	2.477	2.475	1	mw	.....	.....	2.479	1
052	2.461	.....	.....	w	.....	.....	.....	.....
341	2.419	.....	.....	w	.....	.....	2.417	1
400	2.406	2.406	3	m	.....	.....	.....	.....
170	2.399	.....	.....	vw	.....	.....	.....	.....
152	2.384	.....	.....	vvw	.....	.....	.....	.....
242	2.368	.....	.....	a	.....	.....	.....	.....
302	2.363	2.363	9	vs	2.36	4	2.372	3
350	2.355	.....	.....	a	.....	.....	.....	.....
312	2.341	.....	.....	a	.....	.....	.....	.....
261	2.335	.....	.....	vvw	.....	.....	.....	.....
420	2.318	.....	.....	vvw	.....	.....	.....	.....
322	2.280	.....	.....	vvw	.....	.....	.....	.....
401	2.275	2.275	11	vs	2.26	4	2.280	3
171	2.269	.....	.....	vvw	.....	.....	.....	.....
103	2.263	.....	.....	vvw	.....	.....	.....	.....
411	2.256	.....	.....	a	.....	.....	.....	.....
113	2.244	.....	.....	vvw	.....	.....	.....	.....
351	2.232	2.233	4	mw	.....	.....	2.248	1

Table 2.—*Comparison of X-ray powder diffraction data for wavellite,* $Al_3(PO_4)_2(OH)_3 \cdot 5H_2O$—Continued

[Orthorhombic, *Pcmn*: *a*=9.624 A, *b*=17.338 A, *c*=6.986 A (all ±0.001 A)]

hkl	Present study: Black River Falls quadrangle, Jackson County, Wis.				Mäkelä (1969): Kittilä, Finland		Bouška and others (1969): Koloděje nad Lužnicí-Hosty, southern Bohemia, Czechoslovakia	
	Calculated[1]	Observed[2]			Observed[3]		Observed[4]	
	d_{hkl} (angstroms)	d_{hkl} (angstroms)	*I*	Single crystal *I*	d_{hkl} (angstroms)	*I*	d_{hkl} (angstroms)	*I*
062	2.227	2.228	4	mw	.....	.....	.....	.....
421	2.200	2.198	3	mw	2.19	2	2.201	1D
252	2.191	.....	.....	vw	.....	.....	.....	.....
123	2.190	2.191	3	mw	.....	.....	.....	.....
332	2.187	.....	.....	a	.....	.....	.....	.....
162	2.169	.....	.....	vw	.....	.....	.....	.....
080	2.167	2.167	3	mw	.....	.....	2.160	6
431	2.117	.....	.....	vw	.....	.....	.....	.....
133	2.107	.....	.....	mw	.....	.....	.....	.....
440	2.104	2.105	21	vs	.....	.....	.....	.....
271	2.100	.....	.....	w	.....	.....	.....	.....
203	2.096	2.095	21	vs	2.09	7	.....	.....
213	2.081	2.081	2	mw	.....	.....	.....	.....
342	2.075	.....	.....	a	.....	.....	.....	.....
361	2.052	2.052	3	m	.....	.....	.....	.....
223	2.037	2.039	4	m	2.04	2	2.048	2
181	2.024	.....	.....	w	.....	.....	.....	.....
262	2.021	.....	.....	vvw	.....	.....	.....	.....
072	2.020	2.022	1	mw	.....	.....	.....	.....
441	2.014	.....	.....	vw	.....	.....	.....	.....
143	2.006	.....	.....	a	.....	.....	.....	.....
280	1.976	1.976	13	vs	.....	.....	.....	.....
370	1.961	1.960	13	vs	1.960	6	{1.984 / 1.964}	5VD
190	1.889	1.889	3	mw	1.889	2	1.898	2
362	1.829	1.829	3	mw	1.824	2	1.837	1
521	1.815	1.814	3	mw	.....	.....	1.820	1
333	1.792	1.792	2	mw	.....	.....	.....	.....
531	1.767	1.767	1	mw	.....	.....	.....	.....
004	1.747	1.746	6	s	1.751	3	1.756	3
		1.721	8	.....	.....	.....	1.724	4D
		1.719	2	.....	.....	.....	.....	.....
		1.707	2	.....	1.710	5	.....	.....
		1.671	6	.....	1.670	4	1.678	3
		.....	.....	.....	1.647	1	1.649	1
		1.608	8	.....	1.607	3	1.612	3
		1.592	6	.....	.....	.....	1.601	2
		1.571	8	.....	.....	.....	1.578	2
		1.554	8	.....	1.560	2	1.564	2
		1.535	8	.....	1.540	4	1.540	3
		1.519	4	.....	1.518	2	1.529	1
		1.483	3	.....	1.485	4	1.487	2
		1.467	3	.....	.....	.....	1.475	<1
		1.456	9	.....	1.450	6	1.459	5
		1.445	1	.....	.....	.....	.....	.....
		1.412	6	.....	1.410	4	1.417	3
		1.398	3	.....	1.397	2	1.405	1
		1.381	5	.....	1.376	2	1.387	1
							1.369	<1
		1.345	6	.....	1.343	5	1.350	5
		1.321	2	.....	.....	.....	1.324	<1
		1.307	1	.....	1.310	1	1.316	<1
		1.279	2	.....	.....	.....	1.284	<1
		1.266	2	.....	1.266	2	1.269	2
		1.252	4	.....	1.250	3	1.252	2
		1.247	2	.....	.....	.....	.....	.....
		1.238	2	.....	1.230	1	1.237	<1
		Plus additional lines with $I \leqslant 4$.			Plus eight additional lines with $I \leqslant 4$.		Plus 37 additional lines with $I \leqslant 3$.	

Table 3.—*Semiquantitative spectrographic analyses of wavellite from Jackson County, Wis.*

[Analyst: Joseph L. Harris, U.S. Geol. Survey]

Percentage range of elements	Field and Laboratory No. HK-BOT-1 (clear) W175034	HK-BOT-2 (milky white) W175035
Greater than 10	P, Al	P, Al
0.02 – 0.03	Fe	Fe, Si
0.01 – 0.015	Si, Na, V	Mg, Na, V
0.005 – 0.007	Mg, Ca	Ca
0.001 – 0.0015	Mn, Be, Cu	Mn, Ba, Be
0.0005 – 0.0007	Ba	Cu

Looked for but not found in either sample: Ag, As, Au, B, Bi, Cd, Ce, Co, Cr, Eu, Ga, Ge, Hf, In, K, Li, Mo, Nb, Ni, Pb, Pd, Pt, Re, Sb, Sc, Sn, Sr, Ta, Te, Th, Ti, Tl, U, W, Y, Zn, and Zr. Other elements were not looked for.

aluminum, and only minor amounts of other elements. There is no significant difference in the amounts of minor elements present in the two samples. No chemical analyses were made of the wavellite.

Carbonate-fluorapatite

Carbonate-fluorapatite is the major, and perhaps the only, mineral constituent of small (0.5–1.0 cm) milky-white brachiopod fossil shells and shell fragments which are locally abundant in the Eau Claire Sandstone and some overlying units. The shell assemblages include almost complete specimens having detailed surface markings, in addition to more abundant shell fragments showing considerable loss of material by solution or by abrasion. X-ray analyses were made of white brachiopod shells from the upper part of the Eau Claire Sandstone collected from localities several miles apart. The measured interplanar spacings and relative intensities are listed in table 4; these established their identity as carbonate-fluorapatite.

On the basis of the relationship of the angular difference in degrees 2θ between the (004) and (410) peaks (near 50.6° and 53.1°, respectively) and the CO_2 content of apatite, as described by Gulbrandsen (1970), the apatite is calculated to contain about 1 to 2.3 percent CO_2.

Table 4.—*X-ray d-spacings for apatite from fossil brachiopod shells from two localities in Jackson County, Wis.*

Sample OA3-18-1		Sample HK-SM-SW	
d	*I/I*	*d*	*I/I*
.....	...	8.19	5
4.04	8	4.05	5
3.86	5	3.86	5
3.439	35	3.45	45
3.16	10	3.17	15
.....	...	3.07	15
2.79	100	2.81	100
2.70	45	2.70	50
2.621	25	2.629	20
2.51	5	2.51	5
[1]2.248	...	[1]2.248	...
2.06	5	2.14	5
1.933	20	1.937	20
1.88	15	1.88	15
1.836	25	1.837	30
1.79	10	1.79	12
.....	...	1.77	10
1.76	10	1.76	10
1.746	10	1.74	10
1.72	15	1.72	10
.....	...	1.63	5
.....	...	1.54	10

[1] Coincides with peak from quartz standard.

Table 5.—*Semiquantitative spectrographic analysis of concentrated phosphatic fossil shell material from the lower part of the Eau Claire Sandstone, Jackson County, Wis.*

[Analysis of sample OA3-18-1 (lab No. W175532) by J. L. Harris, U.S. Geol. Survey]

Percent	Elements	Percent	Elements
10 or greater	P, Ca, Fe	0.03	Ba, Gd
7	Si	0.015	Zr, Sm, Dy
2	Al	0.01	Eu
0.5	F	0.007	Cu, Yb
0.3	Na, Ce	0.005	V
0.2	Sr	0.003	Sc
0.15	La, Y, Nd	0.002	Cr
0.1	Mg, Mn	0.001	Be
0.05	Ti, Pb	0.0003	Ga

Note:
Pr—not reported because of interference.
Ag—detected but below limit of determination.
As, Au, B, Bi, Cd, Co, Er, Ge, Hf, Ho, In, K, Li, Lu, Mo, Nb, Ni, Pd, Pt, Re, Sb, Sn, Ta, Tb, Te, Th, Tl, Tm, U, W, and Zn—not detected, or at limit of detection.

A concentrate of fossil shell material from the Eau Claire Sandstone was analyzed spectrographically for comparison with phosphatic material from other deposits. The results are listed in table 5. An X-ray analysis of part of this material showed that the only major peaks obtained were those of apatite, but minor amounts of quartz and other impurities are present, as indicated by the spectrographic analysis. The presence of more than 10 percent iron indicates that the concentrate of fossil shell material also contained some excess of iron over that likely to be in the structure of apatite. The rare-earth element total of more than 0.5 percent is probably in the apatite.

Footnotes for table 2:

[1] All possible calculated *hkl* listed for $d_{hkl} \geq 2.000$ A; calculated $d_{hkl} \leq 1.999$ and ≥ 1.745 listed only for those measured.

[2] Camera diameter, 114.59 mm; Mn-filtered Fe radiation ($\lambda FeK\alpha$= 1.9373 A). Measurements from Wilson type pattern with CaF_2 as internal standard; corrected for film expansion. Lower limit measurable for 2θ, approximately 7° (16 A). Intensities estimated visually by direct comparison with a calibrated intensity film strip. Single-crystal intensities estimated from precession patterns with various exposure times: vs = very strong, s = strong, ms = medium strong, m = medium, mw = medium weak, w = weak, vw = very weak, vvw = very very weak, and a = absent.

[3] Camera diameter, 114.6 mm. Ni-filtered Cu radiation ($\lambda CuK\alpha$= 1.5418 A). Intensities estimated visually.

[4] Camera diameter, 114.6 mm. Ni-filtered Cu radiation ($\lambda CuK\alpha$= 1.5418 A). Straumanis method. Intensities estimated visually. D = diffuse; VD = very diffuse.

COMPARISON OF THESE DEPOSITS WITH OTHER WAVELLITE OR PHOSPHATE DEPOSITS IN MARINE SEDIMENTARY ROCKS

The possible significance of a mineral occurrence as a guide to geologic conditions that have existed in an area is more easily understood if comparisons are made with similar occurrences described in the geologic literature. Phosphate deposits in marine sedimentary rocks that have features comparable to some found in the thin phosphatic zones in the Black River Falls area include those in the Bone Valley Formation, of Pliocene age, in Florida (Altschuler and others, 1956); in the Phosphoria Formation, of Permian age, in Idaho and other Western States (McKelvey and Carswell, 1956); in the Ridgeley Sandstone and Shriver Chert, of Devonian age, in Pennsylvania (Carter, 1969); and in the Maquoketa Shale, of Ordovician age, in Iowa (Brown, 1966).

Wavellite has been reported at two of these deposits—in the Bone Valley Formation in Florida, and in the Shriver Chert in Pennsylvania. In the deposits in Florida, wavellite and crandallite [$CaAl_3(PO_4)_2(OH)_5 \cdot H_2O$] are considered to have formed as secondary minerals from leached fluorapatite, largely in the upper part of the phosphatic zone. In contrast, in the Eau Claire and Mount Simon Sandstones, in Wisconsin, wavellite is in the lower part of the phosphatic zone as is the wavellite occurrence in the Shriver Chert in Pennsylvania. The position of the wavellite with respect to the phosphatic source zone in each locality is related to the probable direction of movement of ground water through the phosphatic zone toward the water table. Because the wavellite is a secondary mineral, it may also occur in other stratigraphic horizons related to the position of perched water tables above shaly strata or to paleowater tables within the permeable sandstones. A specimen of wavellite having the form of dripstone found in this area is evidence that at least some of the wavellite formed above the water table.

The phosphate deposits in the Maquoketa Shale in Iowa (Brown, 1966) are the nearest geographically and stratigraphically to the wavellite-bearing rocks of the Black River Falls area in Wisconsin. In the Maquoketa Shale, phosphatic material of the approximate composition of carbonate-fluorapatite has replaced various types of marine invertebrate fossils and part of a dolomitic layer of rock. The deposit is more representative of a concentration by replacement than a leached remnant of a phosphatic zone. Because the Maquoketa Shale is overlain and underlain by carbonate beds and is therefore in a calcium-rich environment, it is unlikely that wavellite, a calcium-deficient mineral, should be present in the Maquoketa, and none has been found.

Another feature common to phosphate deposits in marine sedimentary rocks is the presence of uranium and rare-earth elements in the phosphorites. The phosphate deposits in the Bone Valley Formation in Florida and in the Phosphoria Formation in the Western States are known to contain fluorapatite and to have associated uranium and rare-earth elements. The uranium content of the deposits in the Ridgeley Sandstone in Pennsylvania, in the Maquoketa Shale in Iowa, and in the Eau Claire Sandstone in Wisconsin, as estimated on the basis of radioactivity measurements, is relatively low.

Uranium is more abundant in the aluminum phosphate zone in the leached part of the Bone Valley Formation than in the relatively unleached apatite-rich lower zone (Altschuler and others, 1956), but the highly weathered parts of the phosphate beds in the Phosphoria Formation contain less uranium than their unweathered equivalents (McKelvey and Carswell, 1956). This may also be attributable to the differences in the position of the water table relative to the position of the phosphatic zones. Uranium in the apatite in the Black River Falls area, if present originally but largely removed by leaching, has not been concentrated with the wavellite. Uranium that was adsorbed to surfaces would be more readily contacted by permeating waters and therefore would be leached more readily than the uranium that had been taken into the mineral lattice as a replacement for calcium. The radioactive decay of uranium in these sites would leave radiogenic lead in the lattice. Therefore, much of the lead (about 0.05 percent) detected by spectrographic analysis of the fossil-shell concentrate from the Black River Falls area (table 5) may be radiogenic lead. The ratios of lead isotopes in the apatite would be dependent upon the amounts of common lead and of uranium and thorium that were originally included in the apatite.

Rare earths are present in the phosphate-rich rock at each of the localities mentioned. The percentage of rare earths in a sample of the concentrate of phosphatic shell material from the Black River Falls area (nearly 0.8 percent) is considerably higher than the amount (nearly 0.05 percent) reported to be present in three samples of apatite from the Bone Valley Formation in Florida (Altschuler and others, 1967); it is somewhat higher than the average percentage (less than about 0.2 percent) in nine samples of phosphorite of comparable composition from the Phosphoria Formation in Idaho and Wyoming (Gere and others, 1966, table 1). Although some part of the total rare earths in samples from each of these deposits may be in accessory minerals that tend to be concentrated with the apatite, most of the amount in the sample from this area is probably in apatite or in some phosphate mineral derived from the phosphatic shell material.

In the reactive system in which phosphorus was leached from the phosphatic shell material and transported and deposited to form wavellite, the rare earths, uranium, thorium, and radiogenic lead would also be leached from the same material. They would be transported and deposited along the route of movement of the solutions. The wavellite does not contain rare earths. A possible locus of concentration of the transported rare earths is in replacement-type concentrations of phosphates such as those in the Maquoketa Shale.

CONCLUSIONS AND HYPOTHESES

The general characteristics of the host rock and the physical form of the wavellite in the Black River Falls area indicate that the wavellite was deposited as a secondary mineral. Apatitic fossil shells and decomposing grains of feldspar and other aluminum-bearing silicates in the sandstone are the probable sources of phosphorus and aluminum, the main constituents of the wavellite. These elements were probably leached from the rock by ground water, carried in solution through the porous and permeable sandstone, and deposited as wavellite in openings along bedding planes and joints. The solutions bearing phosphorus probably moved downward or laterally from fossiliferous beds to the site of deposition of the wavellite, because the wavellite locality is near the base of a ridge of permeable sandstone beds that rises about 200 feet a short distance to the north, and because the underlying sandstone is mostly devoid of any significant amount of phosphatic fossil material in comparison with the amounts present in the overlying beds.

Although uranium was not detected in the spectrographic analysis of the concentrate of phosphatic shell material and we do not know the isotopic composition of the lead in the sample, we suggest that the phosphatic material in the Upper Cambrian sandstones may contain uranium and associated radiogenic lead like the association of uranium with phosphate deposits of the Bone Valley Formation in Florida and in the Phosphoria Formation of the Western United States. The extensive blanket of fossiliferous Upper Cambrian sandstones on the flanks of the present Wisconsin dome of Precambrian rocks has been uplifted, dissected, and exposed to leaching by ground water. Uranium and its daughter product, radiogenic lead, may have been leached from the phosphates, taken into solution into the ground water, and carried southward down the dip of the beds.

Galena in the zinc-lead deposits in southwestern Wisconsin is known to contain anomalous amounts of radiogenic lead (Heyl and others, 1966), and the ratio of radiogenic lead to common lead appears to be greatest in the northeastern part of the district. In discussing the possible sources of this radiogenic lead, Heyl and others (1966, p. 942–947) have considered several systems, including the possibility that an anomalous J-type (radiogenic) hydrothermal lead may have arisen in the northeastern part of the district and migrated southwestward. We suggest that radiogenic lead from uranium associated with these phosphatic marine sedimentary rocks of Late Cambrian age and perhaps others of Ordovician age on the western and southwestern flank of the Wisconsin dome may have been carried by ground water to blend with indigenous lead in solutions from which galena was deposited in the upper Mississippi Valley zinc-lead district.

If we attribute the radiogenic lead in the upper Mississippi Valley zinc-lead district to a source in the leached phosphatic marine sedimentary rocks to the northeast in Wisconsin, a related hypothesis is needed to explain the probable cycle of uranium in the leaching solutions and ground water. The ratio of uranium to daughter-product lead in the phosphatic rocks would have been large. The observation that highly weathered phosphatic beds contain less uranium than their unweathered equivalents has been mentioned. The Upper Cambrian sandstones have apparently been leached of much of their uranium, at least in the surficial zone of weathering. The questions arise whether this uranium may have been deposited in disseminated form throughout a large volume of the same aquifers through which it was transported or whether it was deposited somewhere in concentrations that may be of economic interest. Uranium was not deposited with the radiogenic lead in the zinc-lead district, and the phosphate deposits in the Maquoketa Shale in Iowa (Brown, 1966) do not contain appreciable amounts of uranium.

The presence of layers of coquinoid phosphatic material in the sandstones indicates that some of the geologic conditions necessary for the development of phosphate deposits were existent in this region in Late Cambrian time. The possibility that a larger concentration of phosphatic material exists in this region might be tested by further geologic studies of the paleogeography of the Upper Cambrian marine sedimentary rocks and by a search in areas where these rocks can be sampled.

REFERENCES

Altschuler, Z. S., Jaffe, E. B., and Cuttita, Frank, 1956, The aluminum phosphate zone of the Bone Valley Formation and its uranium deposits, *in* Page, L. R., and others, compilers, Contributions to the geology of uranium and thorium by the United States Geological Survey and Atomic Energy Commission for the United Nations International Conference on Peaceful Uses of Atomic Energy, Geneva, Switzerland, 1955: U.S. Geol. Survey Prof. Paper 300, p. 495–504.

Altschuler, Z. S., Berman, Sol, and Cuttita, Frank, 1967, Rare earths in phosphorites–Geochemistry and potential recovery, *in* Geological Survey Research 1967: U.S. Geol. Survey Prof. Paper 575-B, p. B1–B9.

Araki, Takaharu, and Zoltai, Tibor, 1968, The crystal structure of wavellite: Zeit. Kristallographie, v. 127, no. 1-4, p. 21–33.

Bouška, Vladimir, Povondra, Pavel, and Tichý, Ladislav, 1969, Variscite and vanadian wavellite from Kolodĕje nad Lužnicí-Hosty (southern Bohemia): Acta Univ. Carolinae, Geologica, no. 1, p. 13–24.

Breskovska, V. V., and Ivchinova, L., 1961–1962, [Wavellite from the Madjarovo polymetallic deposits]: Sofia Univ. Godishnik, v. 56, p. 275–284 [In Russian].

Brown, C. E., 1966, Phosphate deposits in the basal beds of the Maquoketa Shale near Dubuque, Iowa, *in* Geological Survey Research 1966: U.S. Geol. Survey Prof. Paper 550-B, p. B152–B158.

Carter, W. D., 1969, The W. L. Newman phosphate mine, Juniata County, Pennsylvania: Pennsylvania Geol. Survey, 4th ser., Inf. Circ. 64, 16 p.

Fu, P'ing-Ch'iu, 1966, Crystal structure of wavellite: Sci. Geol. Sinica, no. 2, p. 116–135 (through Mineralog. Abs., v. 19, p. 181, 1968).

Gere, W. C., Schell, E. M., and Moore, K. P., 1966, Stratigraphic sections and phosphate analyses of Permian rocks in the Teton

Range and parts of the Snake River and Gros Ventre Ranges, Idaho and Wyoming: U.S. Geol. Survey open-file report, 71 p., map.

Gordon, S. G., 1950, Crystallographic data on wavellite from Llallagua, Bolivia and on cacoxenite from Hellertown, Pennsylvania [abs.]: Am. Mineralogist, v. 35, no. 1-2, p. 132.

Gulbrandsen, R. A., 1970, Relation of carbon dioxide content of apatite of the Phosphoria Formation to regional facies, *in* Geological Survey Research 1970: U.S. Geol. Survey Prof. Paper 700-B, p. B9–B13.

Heyl, A. V., Delevaux, M. H., Zartman, R. E., and Brock, M. R., 1966, Isotopic study of galenas from the upper Mississippi Valley, the Illinois-Kentucky, and some Appalachian Valley mineral districts: Econ. Geology, v. 61, no. 5, p. 933–961.

Kaemmel, Thomas, 1961, Geologie, Petrographie und Geochemie der Zinnlagerstatte "Tannenberg" (Vogtland): Geologie, no. 30, p. 1–105.

Mäkelä, Kaarlo, 1969, Wavellite from Kittilä, Finnish Lapland: Geol. Soc. Finland Bull., no. 41, p. 193–197.

McKelvey, V. E., and Carswell, L. D., 1956, Uranium in the Phosphoria Formation, *in* Page, L. R., and others, compilers, Contributions to the geology of uranium and thorium by the United States Geological Survey and Atomic Energy Commission for the United Nations International Conference on Peaceful Uses of Atomic Energy, Geneva Switzerland, 1955: U.S. Geol. Survey Prof. Paper 300, p. 483–487.

Mikheev, V. I., 1957, Rentgenometricheskii opredelitel mineralov [X-ray determination of minerals]: Moscow, Gasudar. Nauch.–Tekh. Izd. Lit. Geol. i Okhrane Nedr, 868 p.

Neves, J. M. Correia, 1960, Pegmatitos com berilo, columbite-tantalite e fosfatos da Bendada (Sabugal, Guarda): Coimbra Univ. Mem. e Noticias, no. 50, p. 90–92.

Ostrom, M. E., 1966, Cambrian stratigraphy in western Wisconsin: Wisconsin Geol. and Nat. History Survey Inf. Circ. 7, 79 p.

Ostrom, M. E., Davis, R. A. Jr., and Cline, L. M., 1970, Field trip guidebook for Cambrian-Ordovician geology of western Wisconsin: Wisconsin Geol. and Nat. History Survey Inf. Circ. 11, 131 p.

Potter, P E., and Pryor, W. A., 1961, Dispersal centers of Paleozoic and later clastics of the upper Mississippi Valley and adjacent areas: Geol. Soc. America Bull., v. 72, no. 8, p. 1195–1250.

Smelkova, Yu. F., Smirnov, A. I., and Krasilnikova, N. A., 1966, [Wavellite from the Belkin deposit]: Vses. Mineralog. Obshchestvo, Zap., v. 95, p. 609–614 [In Russian].

Sumin, N. G., 1953, [On the question of the identity of fischerite and wavellite]: Akad. Nauk SSSR, Mineralog. Museya Trudy, v. 5, p. 146–152 [In Russian].

Svyazhin, N. V., 1968, Vavellit iz rayona Syserti na Urale [Wavellite from the Sysert region, Urals]: Vses. Mineralog. Obshchestvo, Zap., v. 97, no. 6, p. 712–714.

Zanin, Yu. N., Grigoryeva, T. N., Chileko, E. F., and Novozhilova, M. V., 1970, Alyumofosfatnyye mineraly Telekskogo mesto-rozhdeniya [Aluminophosphate minerals from the Telek deposit]: Vses. Mineralog. Obshchestvo, Zap., v. 99, no. 6, p. 752–756.

THALENITE AND ALLANITE DERIVED FROM YTTROFLUORITE IN THE WHITE CLOUD PEGMATITE, SOUTH PLATTE AREA, COLORADO

By JOHN W. ADAMS and WILLIAM N. SHARP, Denver, Colo.

Abstract.—Thalenite and allanite occur in veinlets in yttrofluorite in the White Cloud pegmatite, Colorado, and seem to have been formed by the metasomatic replacement of yttrofluorite by late-stage silicic fluids. A comparison of optical and physical data for yttrium-bearing fluorites from this and other deposits shows a nearly linear relationship between the yttrium content and the refractive index, specific gravity, and unit-cell size.

Two rare yttrium-bearing minerals, yttrofluorite and thalenite, were found in the fluorite-rich White Cloud pegmatite located in sec. 36, T. 7 S., R. 70 W., near the community of South Platte, Jefferson County, Colo., about 20 miles southwest of Denver. The occurrence was of particular interest in that it afforded an opportunity to make a comparative study of fluorite of varied rare-earth content and to investigate the origin of thalenite.

The rarity of thalenite in pegmatites, in which other rare-earth minerals may be abundant, suggests that it can form only under very unusual conditions, the primary condition being the general absence of certain elements with which yttrium will combine in preference to the formation of the simple silicate. In the deposit studied the conditions were met by the metasomatic replacement of yttrofluorite by silicic fluids. This reaction produced not only thalenite but also the cerium-rich silicate, allanite.

Thalenite has been previously reported from only two other localities in North America—a pegmatite near Kingman, Ariz. (Pabst and Woodhouse, 1964), and the Snowflake pegmatite in Teller County, Colo. (Adams and others, 1962).

THE WHITE CLOUD PEGMATITE

The White Cloud pegmatite, which was mined first for feldspar and later for quartz, seems to be fairly typical of many well-zoned fluorine-rich bodies that occur in an area of about 10 square miles in the northeast edge of the Pikes Peak batholith. The geologic setting, zonation, and mineralogy of many of these pegmatites were described by Haynes (1965), who reported the occurrence of the following rare-earth minerals at the White Cloud: allanite, doverite, fergusonite, gadolinite, yttrofluorite, and cerfluorite. The mineral cerfluorite is a rare-earth-bearing fluorite analogous to yttrofluorite, but in which cerium-group elements predominate. Haynes also noted an "unidentified orange-red yttrium mineral with bastnaesite structure."

The zonal relationships at the White Cloud pegmatite are shown in figure 1. Thalenite and yttrofluorite occur just outside the quartz core of the pegmatite, in a quartz-perthite-fluorite zone which is well developed on the north side of the core at the deposit.

THALENITE

Thalenite was found in an undisturbed remnant of the quartz-perthite-fluorite zone in the southeast end of the opencut. Here it occurs abundantly in dark-colored replace-

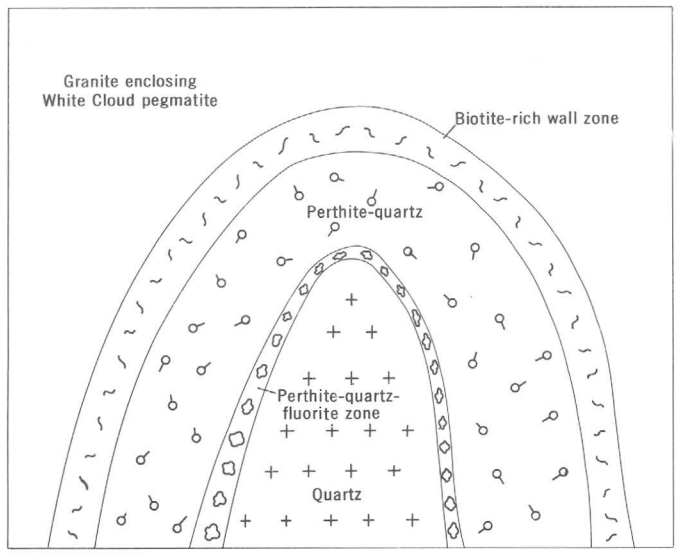

Figure 1.—Diagrammatic sketch of zonal relations at the White Cloud pegmatite, Colorado.

U.S. GEOL. SURVEY PROF. PAPER 800-C, PAGES C63-C69

ment veinlets that dissect pinkish-brown yttrofluorite to produce the coarse sea-island texture shown in figure 2. In addition to containing thalenite, the veinlets are made up of allanite and colorless fluorite, with minor amounts of zircon, muscovite, quartz, thorite, and gadolinite.

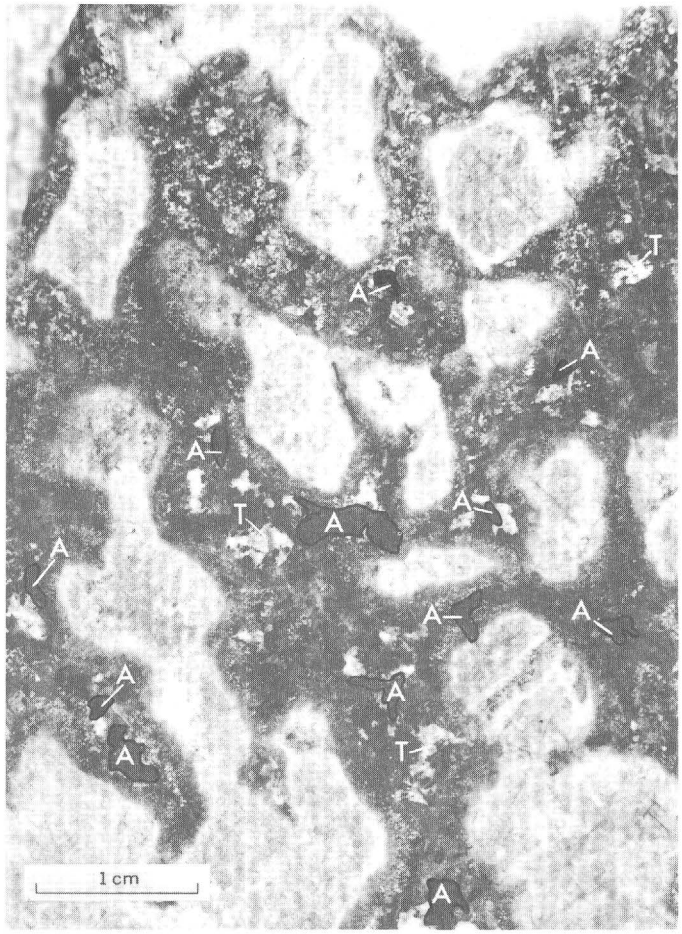

Figure 2.—Photograph of yttrofluorite-thalenite rock showing conspicuous sea-island replacement texture. White islands of yttrofluorite are surrounded by dark vein material of fluorite, white splotches of thalenite (T), and dark allanite (A).

The thalenite occurs chiefly as anhedral grains that commonly are less than 0.1 mm, and rarely exceed 3 mm, in maximum dimension. These grains may be colorless and clear, or white, dull, and cloudy. Clear grains are almost indistinguishable from quartz in hand specimens but show characteristic absorption lines when examined with a microspectroscope (Adams, 1965). In thin section, the clear thalenite grains are highly anisotropic, whereas the dull, cloudy grains are virtually isotropic. Both types, however, give good X-ray patterns without heating, which suggests that the apparently isotropic grains probably are microcrystalline rather than metamict. The typical appearance of thalenite in thin section is shown in figure 3.

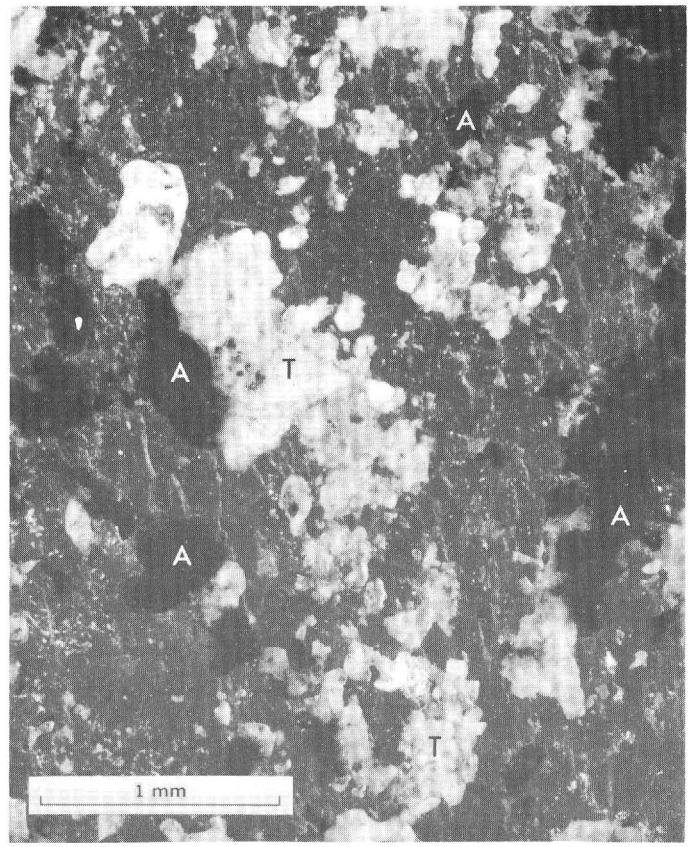

Figure 3.—Photomicrograph showing detail of the dark vein material with thalenite (T) and allanite (A) in gray fluorite matrix.

An X-ray fluorescence analysis of the thalenite is given in table 1, and the distribution of the lanthanide elements, in atomic percent, is depicted in figure 4, which shows that ytterbium is the most abundant lanthanide. The lanthanide distribution in this thalenite is very similar to that found in the thalenite from the Snowflake pegmatite in Colorado, but some thalenites have been reported in which gadolinium or erbium is dominant.

Table 1.—*X-ray fluorescence analysis, in percent, of thalenite from the White Cloud pegmatite*

[Analysis by J. S. Wahlberg]

La_2O_3	0.3	Yb_2O_3	5.7
Ce_2O_3	.5	Lu_2O_3	<.9
Pr_2O_3	.2	Y_2O_3	44
Nd_2O_3	1.1	Sc_2O_3	<.1
Sm_2O_3	.8	Ti_2O_3	<.05
Eu_2O_3	<.2	CaO	2.0
Gd_2O_3	1.7	K_2O	<.1
Tb_2O_3	<.2	Al_2O_3	2.0
Dy_2O_3	4.3	U_3O_8	<.8
Ho_2O_3	1.2	ThO_2	<.7
Er_2O_3	3.5	Fe_2O_3	.2
Tm_2O_3	<.7		

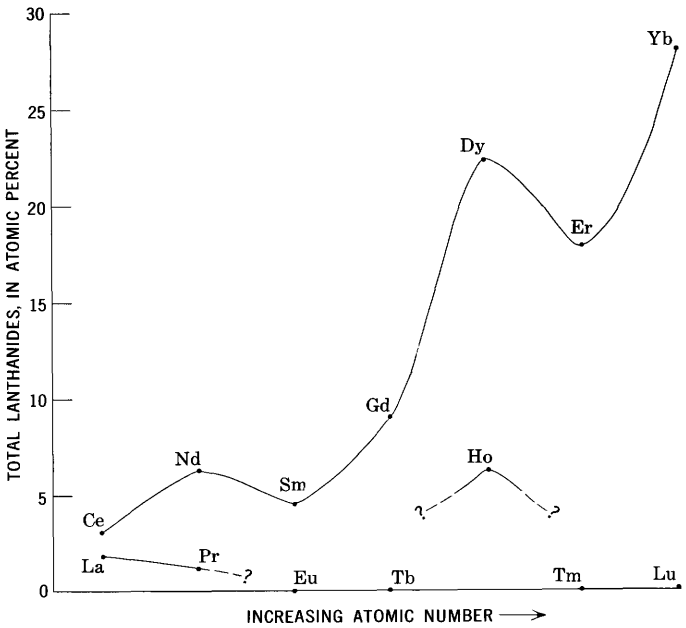

Figure 4.—Distribution of lanthanide elements in thalenite. Values for Eu, Tb, Tm, and Lu below limits of detection by X-ray fluorescence method.

OTHER MINERALS IN THE VEINLETS

Allanite is closely associated with thalenite and may occur as irregular grains (fig. 3) or as well-formed crystals as much as 5 mm long. A partial analysis of the allanite, by X-ray fluorescence, is shown in table 2.

Gadolinite is less abundant than allanite and where present appears to have grown preferentially on allanite, which it may enclose.

Other silicates include a yellow-green muscovite, metamict zircon, and a honey-yellow isotropic mineral (n=1.70) that is apparently metamict thorite. The thorite, after heating for 1 hour in air at 1,000°C, gives an X-ray pattern that is dominantly that of ThO_2 with weaker lines of thorite.

Clear, normally colorless fluorite makes up most of the veinlets and encloses all other minerals; this fluorite where in contact with thorite is colored deep purple by radiation damage.

Table 2.—*Partial analysis, in percent, of allanite from the White Cloud pegmatite*

[Analysis, by X-ray fluorescence method, by J. S. Wahlberg]

La_2O_3	4.7	Er_2O_3	<0.4
Ce_2O_3	10.0	Tm_2O_3	<.7
Pr_2O_3	1.6	Yb_2O_3	<.3
Nd_2O_3	7.5	Lu_2O_3	<.9
Sm_2O_3	1.3	Y_2O_3	2.0
Eu_2O_3	<.2	Sc_2O_3	.1
Gd_2O_3	.9	CaO	8.9
Tb_2O_3	<.2	Al_2O_3	15.0
Dy_2O_3	.4	Fe_2O_3	14.0
Ho_2O_3	<.2		

FLUORITE AND YTTROFLUORITE

Most of the rare earths in the pegmatite are probably contained in fluorite which ranges in composition from nearly pure CaF_2 to material which contains at least 25 percent total rare-earth oxides and which can properly be called yttrofluorite.

The greater part of the fluorite is a pale, greenish-yellow variety which occurs in anhedral masses as much as several feet across and which contains about 3 percent yttrium and 6.4 percent lanthanides, chiefly cerium-group elements. This fluorite, which is represented by our sample A-70-3 (table 3), is probably the material described by Haynes (1965) as "yttrofluorite," but which will be referred to here as yttrian fluorite. The physical properties of the yttrian fluorite are given in table 3, and its rare-earth content is shown in table 4.

The yttrian fluorite contains numerous inclusions, largely in the 5μ to 10μ range, that are arranged parallel to the growth planes of the fluorite. To identify these inclusions, the fluorite was dissolved in boiling $AlCl_3$ solution and the suspended material was collected on a 5μ Millipore filter. X-ray diffraction patterns of the retained material gave the strong lines of both bastnaesite and fluocerite (CeF_3), with bastnaesite the

Table 3.—*Summary data on fluorite from the White Cloud pegmatite*

[Explanation of symbols: n, refractive index; a_0, unit-cell dimension, in angstroms; Σ_{Ln}, total lanthanides; Σ_{RE}, total rare earths]

Sample	n	a_0	Specific gravity	Analytical data (percent) Y	Σ_{Ln}	Σ_{RE}	Description and remarks
JA-70-2 and A-67-14.	1.434–1.436	5.46	3.210	0.5	1.71	2.21	Fluorite, green. Occurs at margins of pale-yellow yttrian fluorite. Margin of core.
A-70-3.....	1.438	5.47	3.29	3.00	6.45	9.45	Yttrian fluorite, pale-greenish-yellow. Occurs as large masses at margin of core.
A-70-5.....	1.463–1.464	5.51	3.698	11.42	12.07	23.49	Yttrofluorite, brown.
A-67-10.....	1.434–1.46	5.47, 5.49, 5.51	3.646	11.81	10.33	22.14	Fluorite, pinkish-brown; partly replaced yttrofluorite; associated with thalenite and allanite.

Table 4.—*Analytical data on yttrian fluorite from the White Cloud pegmatite*

[Rare earths determined by spectrographic analysis by N. M. Conklin. Total carbon determined by I. C. Frost]

Rare earth	Weight percent	Atomic percent lanthanides
La	1.00	16.4
Ce	1.50	24.4
Nd	1.50	23.7
Pr	.30	4.8
Sm	.30	4.6
Eu	.02	.2
Gd	.70	10.3
Tb	.05	.7
Dy	.50	7.1
Ho	.07	.9
Er	.15	2.0
Tm	.03	.5
Yb	.30	3.9
Lu	.03	.5
Y	3.00	...
Total carbon	.14	

dominant phase. To exclude the possibility that fluocerite was synthesized during the treatment of the yttrian fluorite, a sample was ground to −120 mesh size and centrifuged with methylene iodide. Material from the lowest part of the funnel was X-rayed and showed peaks characteristic of fluocerite as well as those of bastnaesite and fluorite. Fluocerite has also been reported intergrown with yttrofluorite and bastnaesite in a Norwegian pegmatite (Sverdrup, 1968, p. 247).

The percentage of bastnaesite and fluocerite present in the yttrian fluorite is difficult to determine. Visual estimates suggest that the inclusions make up 15–20 percent of the field area in thin sections, but this percentage may be quite misleading inasmuch as the inclusions appear to be extremely thin discoidal plates and thus represent a much smaller volume than suggested by their areal distribution. This deduction is supported by the total carbon content of the yttrian fluorite (0.14 percent), which permits only 2.5 percent bastnaesite. It is also more in keeping with a 1-percent value for total inclusions recovered on the Millipore filter, although in this process there were undoubtedly losses of ultrafine material.

With such speculative data as to the total amount of inclusions and the relative proportions of constituent bastnaesite and fluocerite it is of course impractical to adjust the analyses to represent the actual rare earths present in the fluorite lattice. The effect of a small amount of bastnaesite would, however, be appreciable. For example, if the 2.5 percent bastnaesite permitted by the carbon content were actually present it would represent about 0.8 percent cerium, which is nearly half of the total amount found in the sample. As both bastnaesite and fluocerite are cerium-selective minerals their effect on the yttrium and yttrium-group lanthanides will be negligible, but the values reported for the cerium-group lanthanides will certainly be higher than what is actually contained in the fluorite lattice.

The large yttrian fluorite masses are commonly rimmed by a sharply defined band of clear green fluorite a few inches wide. This fluorite, which is represented by our samples JA-70-2 and A-67-14, is relatively low in rare earths (table 3) and probably formed late in the sequence when the still-fluid part of the pegmatite had been largely depleted in these elements. Inclusions are virtually absent, so the rare earths may be assumed to be all contained in the CaF_2 structure. The physical properties of the green fluorite (table 3) are close to those of pure fluorite.

Fluorite that can properly be called yttrofluorite seems to be rare in the deposit as now exposed and is limited to a small area in the southeast end of the opencut. Much of the yttrofluorite has been wholly or partly replaced by thalenite and other minerals, and only one specimen was found that contained small areas of virtually unaltered yttrofluorite. This specimen is a coarse intergrowth of light-brown yttrofluorite, plagioclase, and a little microcline all transected by a few very narrow veinlets of quartz. Where these veinlets intersect yttrofluorite they widen and are composed of the dark-colored assemblage that characterizes the thalenite-bearing rock shown in figure 2, but on a microscale. The sample probably represents material only weakly affected by the silicic fluids, and the yttrofluorite it contains is mostly unaltered. The optical and physical properties of this yttrofluorite (A-70-5) are shown in table 3. The analytical data and distribution of the rare earths are shown in table 5 and figure 5.

Inclusions in the yttrofluorite, unlike those in the yttrian fluorite, are not arranged parallel to growth planes, but are localized in irregular patches and bands. X-ray patterns of Millipore-filter residues showed predominantly bastnaesite, with some hematite and thalenite. The thalenite was undoubtedly derived from the replacement veinlets cutting the

Table 5.—*Analytical data on yttrofluorite from the White Cloud pegmatite*

[Rare earths determined by J. S. Wahlberg by $Li_2B_4O_7$ fusion method. Total carbon determined by I. C. Frost. Optical and physical properties shown in table 3, sample A-70-5]

Rare earth	Weight percent as oxides	Weight percent as elements	Atomic percent lanthanides
La_2O_3	1.9	1.6	14.5
Ce_2O_3	3.2	2.7	24.1
Pr_2O_3	.5	.4	3.8
Nd_2O_3	2.0	1.7	14.7
Sm_2O_3	1.0	.9	7.0
Eu_2O_3	.4	.3	2.8
Gd_2O_3	1.3	1.1	8.9
Tb_2O_3	.3	.3	2.0
Dy_2O_3	1.2	1.0	8.0
Ho_2O_3	.2	.2	1.2
Er_2O_3	1.0	.9	6.6
Tm_2O_3	.1	.1	.6
Yb_2O_3	.9	.8	5.7
Lu_2O_3	<.1	<.1	....
Y_2O_3	12.9	10.1	....
Total carbon		.77	

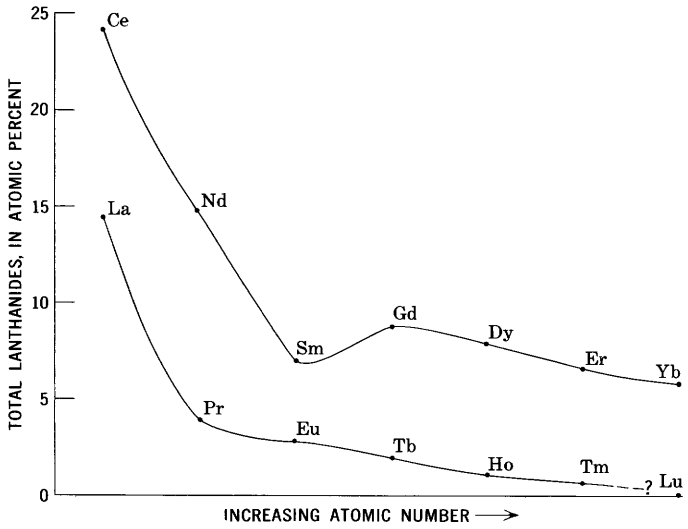

Figure 5.—Distribution of lanthanide elements in yttrofluorite. Value for Lu below limit of detection by spectrographic method.

rock, and should not be present in the yttrofluorite used for analysis, because the sample (A-70-5) was prepared from fragments that appeared to be free of the dark material.

The yttrofluorite contained 0.77 percent total carbon. This relatively large carbon content can be ascribed partly to bastnaesite and partly to calcite or some other readily soluble carbonate which is also present as shown by minute centers of effervescence, especially along fractures, that appear when the surface of the yttrofluorite-bearing rock is moistened with dilute acid. Calcite is readily soluble in $AlCl_3$ solution and hence would not appear in the Millipore-filter residues.

COMPARISON OF PHYSICAL PROPERTIES

The three types of rare-earth-bearing fluorite represented in our samples offered an opportunity to compare certain physical properties in fluorites of widely different yttrium contents. Measurements were made of refractive index, specific gravity, and unit-cell dimension (table 3); the unit-cell measurements were made by X-ray diffractometer using halite as an internal standard. The results, which are shown in figure 6, indicate that these three parameters all increase with increase in yttrium content.

For comparison, the reported data for two fluorites from Norway (Sverdrup, 1968) and one from the Ukraine (Gurov and others, 1971) are also shown on the graphs and, like the White Cloud fluorites, they are plotted in relation to their yttrium content. The descriptions and analyses (in percent) for these samples are as follows:

No. (fig. 6)	*Description*	RE_2O_3	Y	Ce
4	Yttrofluorite, Eivolden, Norway.	22.10	11.01	1.24
5	Cerfluorite, Hundholmen, Norway.	40.23	5.11	11.97
6	Cerium-rich fluorite, Ukraine.	6.9	.92	1.9

The lines drawn on the graphs are plotted by the least-squares regression method using our data for the White Cloud

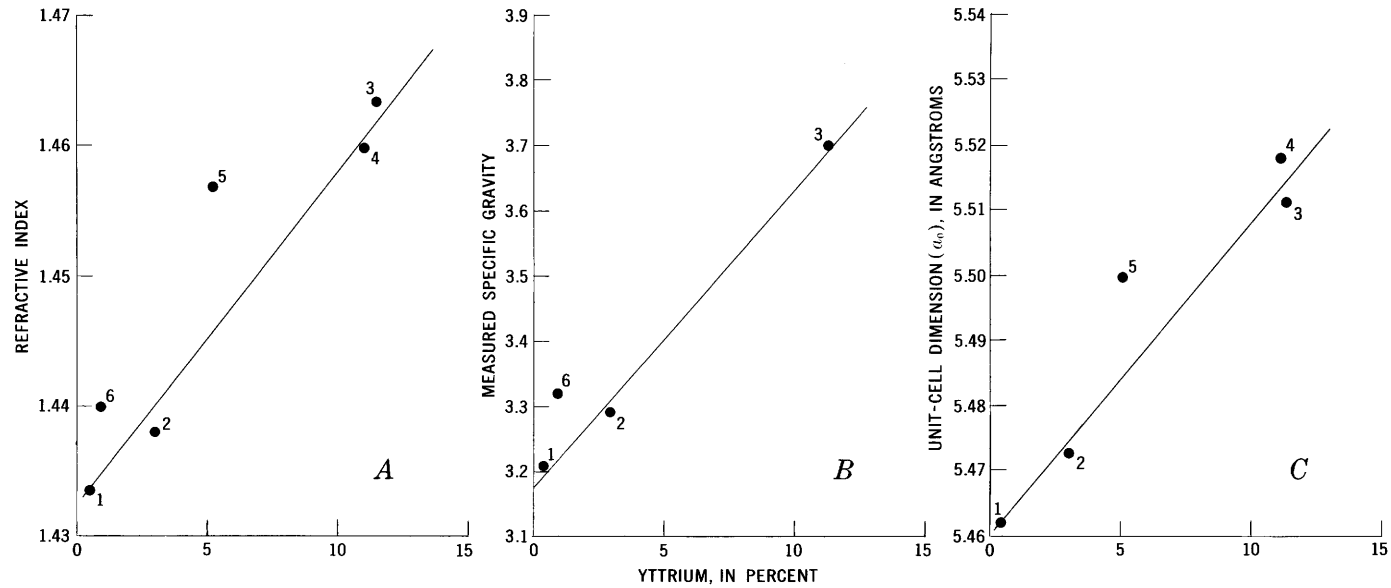

Figure 6.—Plots of the physical properties of fluorites in relation to their yttrium contents. *A*, refractive index; *B*, measured specific gravity; *C*, unit-cell dimension. Samples: 1, green fluorite; 2, yttrian fluorite; and 3, yttrofluorite, all three from White Cloud pegmatite, Colorado; 4, yttrofluorite; and 5, cerfluorite, both from Norway; 6, cerium-rich fluorite from Ukraine.

fluorites, Sverdrup's data for the Eivolden yttrofluorite, and data for pure CaF_2. The data for the two cerium-rich samples (5 and 6) were not included in the least-squares calculations, because these samples did not contain yttrium as the dominant rare earth.

Studies of crystalline solutions of CaF_2 and rare-earth fluorides, which included fluorides of yttrium and of the lanthanide elements Pr, Sm, Gd, Ho, and Yb, disclosed that the refractive index, density, and cell dimensions of the synthetic fluorites increased linearly, or nearly so, with increases in rare-earth content (Short and Roy, 1963; Roy and Roy, 1964). The individual rare earths, however, vary in their effects on these parameters, the variation being related roughly to their ionic radius and atomic weight.

The ionic radius of the lanthanides becomes progressively smaller from lanthanum to lutetium; therefore the unit-cell dimensions of a compound such as LuF_3 will be smaller than those of LaF_3. Yttrium has an ionic radius close to that of dysprosium and holmium; therefore the cell dimensions of YF_3 will be smaller than those of LaF_3 but larger than those of LuF_3.

The progressive increase in atomic weight of the lanthanides from lanthanum to lutetium results in increased density (or specific gravity) values for isostructural compounds containing these cations. Because the atomic weight of yttrium is well below that of any of the lanthanides, those compounds containing an yttrium cation will show the lowest density of all.

The control of the refractive indices of a crystalline material is related to several factors that affect the concentration of electrons in the space between the atoms of the crystal (Povarennykh, 1964); these factors are ionic radii, the type of bonding, valency relations, and density. In a series of synthetic rare-earth borates studied by Levin (1964) a general decrease was found in mean refractive index from $LaBO_3$ to $LuBO_3$, and YBO_3 had a mean index lower than that of any of the lanthanide borates. Similarly, the refractive index of the CaF_2-YF_3 crystalline solutions is lower than that of any of the synthetic fluorites containing the same mole percent of any of the lanthanide fluorides (Roy and Roy, 1964).

That yttrium compounds show a lower refractive index than comparable lanthanide compounds seems anomalous inasmuch as the specific refractive energy values reported for yttrium are considerably higher than those determined for the lanthanides (Jaffe, 1956; Levin, 1964). However, when the refractive index is calculated by the Dale-Gladstone rule formula, $(n-1)/d = K$, the higher specific refractive energy of yttrium is more than counteracted by the lower density of the compound, and the resulting refractive index will be lower.

In natural fluorites either yttrium or cerium will expectably be found to be greatly in excess of the other rare-earth elements even though all or nearly all of the group may be present. Of these two elements, yttrium is more commonly dominant; in fact, Fleischer (1969) noted that yttrium predominated over the total lanthanides in two-thirds of the 44 fluorites for which complete rare-earth analyses were available. We can therefore conclude that to the extent that the properties of fluorite are controlled by the rare-earth content the major effects will be produced by either yttrium or cerium. When properties are plotted as a function of the predominant element, some departure from linearity will be expectable, owing to the individual effects of the other ions present in the structure.

ORIGIN OF THE THALENITE

Yttrofluorite is the host rock for the thalenite-bearing veinlets, which we believe were formed by invasion of the yttrofluorite by residual late-stage silicic fluids. This metasomatism apparently was very local and was effected by a small pocket of fluid lying along the upper part of the pegmatite core. This fluid mobilized the components of the yttrofluorite, including the rare earths which recombined with silica to form thalenite and allanite. The calcium from the yttrofluorite was partly utilized by the allanite, but it was mostly recombined with fluorine as the fluid became depleted in silicon, thus producing the clear fluorite groundmass that makes up much of the veinlets. Some corrosion of the newly formed silicates probably took place at that time.

The evidence for the development of thalenite and allanite by this metasomatic process lies chiefly in the textural relations indicating replacement of the yttrofluorite. Such relations include the control of replacement along cleavage directions, incompletely replaced islands of yttrofluorite (fig. 2), and the development of swarms of minute thalenite crystals along the margins of the yttrofluorite islands.

A metasomatic origin is further supported by some analytical data which strongly suggest that the process operated as a closed system. In order to determine what changes, if any, took place in the rare-earth assemblage during the replacement process, a sample of the veined yttrofluorite was crushed and hand picked to separate the fragments into two fractions, one the material of the veinlets and the other the relict yttrofluorite. The results of partial X-ray fluorescence analyses of the two fractions and their rare-earth distribution patterns are shown on figure 7. Regardless of the rather crude nature of the sampling, the analyses show a remarkable similarity in both the total content and the distribution of the rare earths. The calcium content also is virtually unchanged. Aluminum and iron both are more abundant in the veinlets than in the relict yttrofluorite and presumably were introduced. Some addition of zirconium and beryllium was necessary to form the zircon and the gadolinite.

At the White Cloud pegmatite the development of thalenite was favored by localized conditions in which silicon was available to the relative exclusion of those elements with which yttrium commonly combines. The absence of both xenotime and the multiple oxide minerals from the assemblage

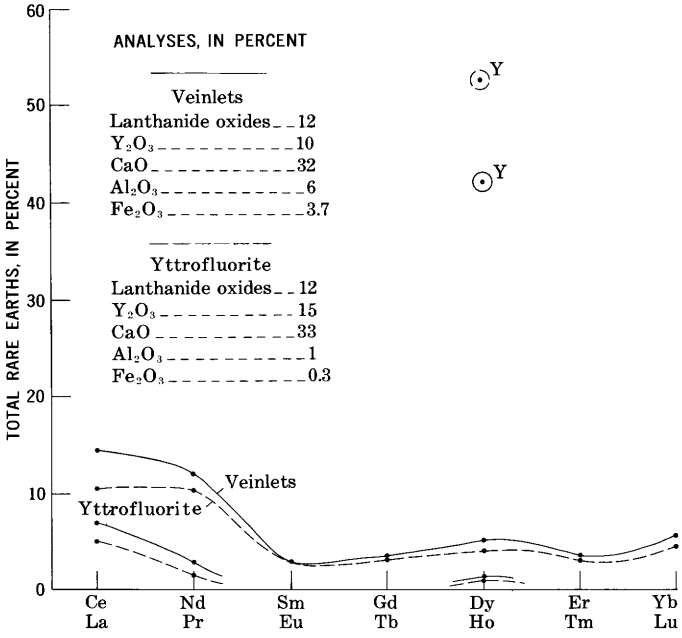

Figure 7.—Plot of rare-earth element distribution, and a partial analysis of relict (island) yttrofluorite and of dark material of veinlets. Based on X-ray fluorescence analysis by J. S. Wahlberg.

in the veinlets suggests that phosphorus, niobium, and titanium were not present in the system, and the very minor amount of gadolinite that formed indicates that beryllium was in such low concentration as to be readily depleted.

REFERENCES

Adams, J. W., 1965, The visible region absorption spectra of rare-earth minerals: Am. Mineralogist, v. 50, nos. 3–4, p. 356–366.

Adams, J. W., Hildebrand, F. A., and Havens, R. G., 1962, Thalenite from Teller County, Colorado: Art. 121 *in* U.S. Geol. Survey Prof. Paper 450-D, p. D6–D8.

Fleischer, Michael, 1969, The lanthanide elements in fluorite: Indian Mineralogist, v. 10, p. 36–39 [1971].

Gurov, E. P., Gurova, E. P., and Marchenko, E. Ya., 1971, First find of high-cerium fluorite in the Ukraine [in Russian]: Akad. Nauk Ukrayin. RSR Dopovidi, Ser. B, v. 33, no. 4, p. 297–299; English abstract in Chem. Abs., v. 75, no. 8, item 51318, 1971.

Haynes, C. V., Jr., 1965, Genesis of the White Cloud and related pegmatites, South Platte area, Jefferson County, Colorado: Geol. Soc. America Bull., v. 76, no. 4, p. 441–462.

Jaffe, H. W., 1956, Application of the rule of Gladstone and Dale to minerals: Am. Mineralogist, v. 41, nos. 9–10, p. 757–777.

Levin, E. M., 1964, Refractivities of rare-earth oxides, *in* Vorres, K. S., ed., Rare-earth research II: New York, Gordon and Breach, p. 339–350.

Pabst, A., and Woodhouse, C. D., 1964, Thalenite from near Kingman, Arizona [abs.]: Geol. Soc. America Spec. Paper 82, p. 269.

Povarennykh, A. S., 1964, The relationship between refractive index and the fine structure of minerals, *in* Aspects of theoretical mineralogy in the U.S.S.R.: New York, The McMillan Co., p. 472–487.

Roy, D. M., and Roy, Rustum, 1964, Controlled massively defective crystalline solutions with the fluorite structure: Jour. Electrochem. Soc., v. 111, no. 4, p. 421–429.

Short, James, and Roy, Rustum, 1963, Confirmation of defect character in calcium fluoride-yttrium fluoride crystalline solutions: Jour. Phys. Chemistry, v. 67, p. 1860–1861.

Sverdrup, T. L., 1968, Contributions to the mineralogy of Norway, No. 37, Yttrofluorite-yttrocerite-cerfluorite in Norwegian pegmatites: Norsk Geol. Tidsskr., v. 48, no. 4, p. 245–252.

LATE TERTIARY STRUCTURAL DEVELOPMENT AT ELK HILLS OIL FIELD, KERN COUNTY, CALIFORNIA

By J. C. MAHER, R. D. CARTER, and R. J. LANTZ, Menlo Park, Calif.

Abstract.—Structure at Elk Hills consists of two broad-topped anticlines arranged en echelon and trending generally southeastward. The eastern anticline is cut by a system of normal faults. At the close of Reef Ridge time, the western anticline was slightly higher than the eastern one, but at the close of deposition of the Tupman Shale Member of the Etchegoin Formation the eastern anticline was the higher. Significant uplift took place in the Temblor Range during Carman time, tilting the western anticline eastward and raising the eastern anticline considerably. During the deposition of the San Joaquin Formation, both anticlines rose about equally, but regional tilting continued to affect the western one more. In Tulare time, two grabenlike troughs formed over the eastern anticline, probably by elongation southeastward along a glide surface at the top of the Reef Ridge Shale. Rough calculations indicate that at the top of the Tupman Shale Member the elongation was about 4 percent and at the Carman horizon, about 1,500 feet above, was about 6 percent. These calculations suggest that the master fault, or fault zone, along the glide surface at the top of the Reef Ridge Shale extends eastward beyond Elk Hills. Normal faults in the Etchegoin Formation in North Coles Levee oil field fit into this pattern.

The Elk Hills oil field, which constitutes a major part of Naval Petroleum Reserve No. 1, is located about 20 miles southwest of Bakersfield in the southern San Joaquin Valley of California (fig. 1). It extends over part of a large anticlinal structure whose surface expression is a line of hills about 20 miles long and as much as 7 miles wide. The ultimately recoverable oil reserves are presently estimated to be about 1.3 billion barrels (Elk Hills Eng. Comm., 1957 a, b) of which less than 300 million barrels have been produced. The U.S. Government owns about 80 percent of the reserves, which are administered by the U.S. Navy; the remainder is owned by Standard Oil Co. of California. Most of the reserves of oil and gas are included in a unit-plan contract between the Navy, acting for the Federal Government, and Standard Oil. At the request of the Navy's Office of Naval Petroleum and Oil Shale Reserves, the U.S. Geological Survey has undertaken a comprehensive geologic study of Naval Petroleum Reserve No. 1. The diagrams and discussion presented in this report are a part of this study and are published with the approval of the Navy.

This report reconstructs and contrasts the structural development of the two en echelon anticlines that make up the Elk Hills anticlinal structure. It discusses the differential effects of compressive forces creating the anticlinal traps, of regional tilting modifying the structural closure, and of surficial tensional stresses creating a system of normal faults that merge downward with a master fault, or fault zone, subparallel to the top of the Reef Ridge Shale. The compressive forces and regional tilting are important to understanding the time and distribution of petroleum accumulations. The tensional stresses are significant because they establish a pattern of

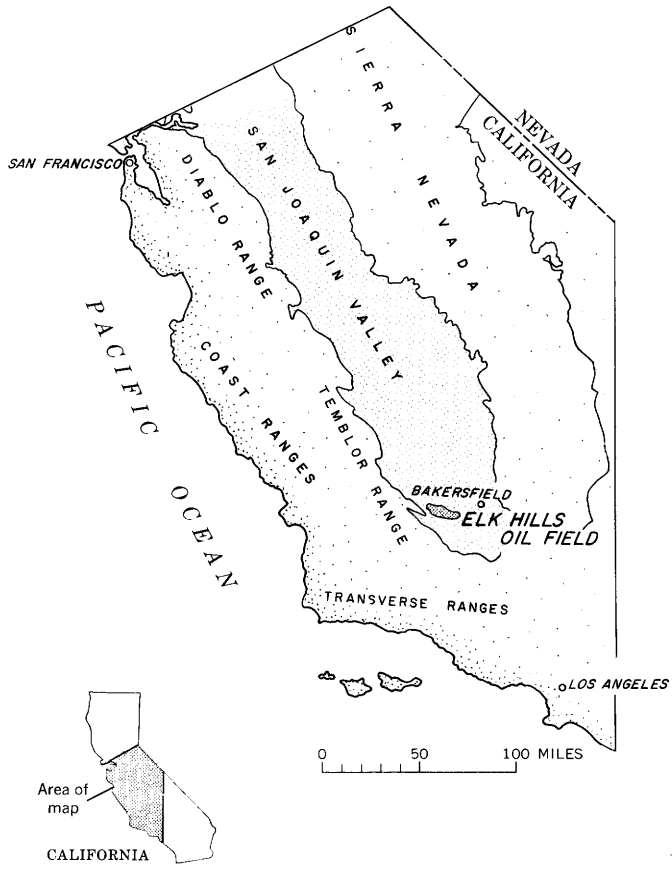

Figure 1.—Location of Elk Hills oil field in the San Joaquin Valley, Calif.

U.S. GEOL. SURVEY PROF. PAPER 800-C, PAGES C71-C78

faulting in the Pliocene rocks that may extend beyond Elk Hills or may be repeated at other places under similar structural conditions. This pattern has not been reported previously in the literature on Elk Hills and vicinity.

The stratigraphic data used for interpretations in this report have been derived from lithologic studies of 22 wells, paleontologic studies of 35 wells, and electric-log correlations of about 900 closely spaced wells. Stratigraphic reference sections were established in three Naval Reserve wells for which relatively complete sets of cores and samples have been preserved (Berryman, 1972; W. L. Adkison, unpub. data). The cores and samples of these wells were examined under a binocular microscope and logged in detail with reference to the corresponding electric logs. The fossils from the cores and samples were identified and age assignments made by R. S. Beck and James Burrow. Correlations were extended from the reference sections by means of a network of 21 interlocking electric-log cross sections. Thereafter, the electric logs of wells between the lines of cross section were correlated, and structure and thickness maps were prepared. Only a small part of these data can be shown in the accompanying diagrams.

Acknowledgments.—The writers are pleased to acknowledge the helpful discussions and suggestions of R. W. Kopf and Béla Csejtey, Jr., in regard to the postulated master fault at Elk Hills and the occurrence of similar faults in other areas.

REGIONAL SETTING

The San Joaquin Valley is an asymmetrical structural trough containing Mesozoic, Tertiary, and Quaternary sedimentary rocks. The principal axis lies considerably west of the center of the basin. The southern part of the San Joaquin Valley, in which the Elk Hills oil field is located, is bounded on the east by the Sierra Nevada, on the west by the Temblor Range, and on the south by the San Emigdio and Tehachapi Mountains (fig. 2). The gently dipping sedimentary rocks on the broad eastern flank reflect the subsurface extension of the westward-tilted Sierra Nevada fault block. The gentle westward dip of the eastern flank, and of the southeastern end of the basin as well, is interrupted by scattered normal faults and domal uplifts. The sedimentary rocks of the western flank and southwestern end of the basin, in contrast, are steeply dipping, sharply folded, and broken by reverse, thrust, and strike-slip faults. The structural pattern of the western flank has been determined by the development of the adjacent Temblor Range. The Temblor Range is composed of a series of anticlinal folds that diverge from the southerly trending Coast Range and plunge southeastward into the valley. One of these folds, the Elk Hills anticlinal structure, forms a line of hills that extends eastward from the Temblor Range through the Northeast McKittrick, Railroad Gap, and Elk Hills oil fields (fig. 2). The hills terminate in low stream-cut bluffs near the Kern River between the Elk Hills and North Coles Levee oil fields.

STRATIGRAPHIC SEQUENCE

In the development of the Elk Hills oil field, more than 1,000 wells have been drilled to oil and gas reservoirs in the upper part of the Monterey Shale of Miocene age and in the Etchegoin and San Joaquin Formations of Pliocene age. Fewer than 10 wells have been drilled through the Monterey Shale, and consequently geologic data on the older rocks are insufficient at this time for an interpretation of the early structural history. The stratigraphic units that can be used to outline the late Tertiary structural history of the Elk Hills oil field and the approximate range of thickness, in feet, for each unit in the vicinity are as follows:

Pliocene and Pleistocene Series:
- Tulare Formation, 600–2,000 feet.

Pliocene Series:
- San Joaquin Formation (includes Scalez horizon near base), 1,150–2,000 feet.
- Etchegoin Formation, 1,700–3,400 feet.
  - Carman Sandstone Member,[1] 900–2,000 feet.
  - Tupman Shale Member,[2] 700–1,400 feet.

Miocene Series:
- Reef Ridge Shale, 200–1,300 feet.
- Monterey Shale (includes Elk Hills Shale Member,[3] 1,800–3,300 feet thick, at top), 2,100–4,100 feet.

[1] New name that includes the Calitroleum, Gusher, Wilhelm, and Mulinia sands of local usage (Berryman, 1972).

[2] New name that includes the Olig sand of local usage where present, and the Buliminella silt of local usage (Berryman, 1972).

[3] New name for dominantly siliceous shale sequence above the McDonald shale of local usage (W. L. Adkison, unpub. data).

STRUCTURE

The Tulare Formation exposed at Elk Hills has been folded into a large anticlinal structure that has about 400 feet of closure (Woodring and others, 1932, pl. 1). This feature consists of two en echelon anticlines with broad tops and steep flanks. The western fold is a relatively simple fold that trends southeastward and has a separate closure of about 150 feet. The eastern anticline, whose axis curves from a southeastward direction to slightly north of east, has about 50 feet of separate closure. The surface rocks above the eastern anticline are cut by four normal faults that dip at angles of 55° to 66° and have relative displacements of 35 to 160 feet but have no topographic expression (Woodring and others, 1932, pl. 1). No faults have been observed in the surface rocks of the western anticline.

The structure at a depth of 2,000 to 3,500 feet on the Scalez horizon, a fossil and electric-log marker in the lower part of the San Joaquin Formation, is similar to that of the surface

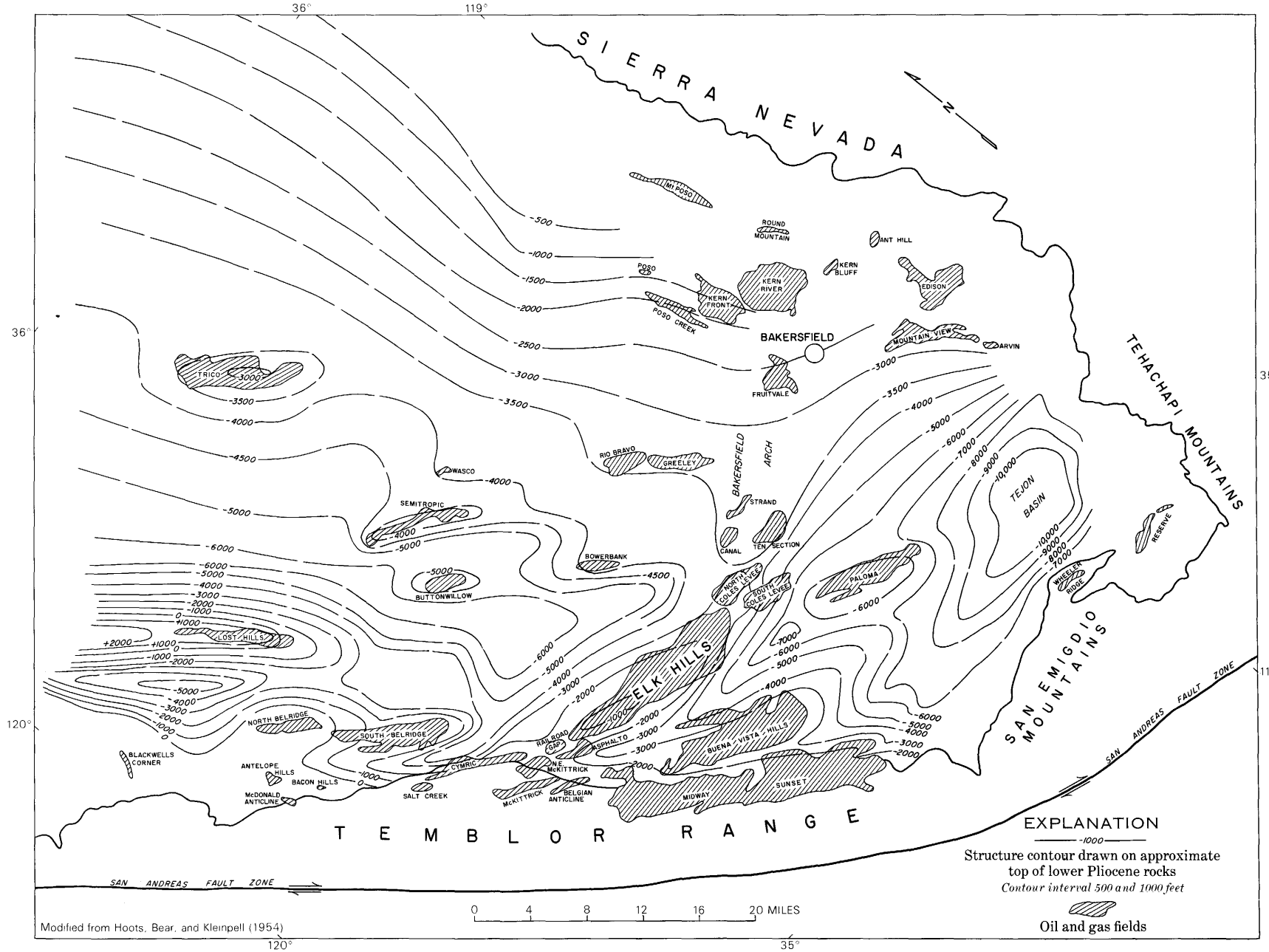

Figure 2.—Regional structure in relation to oil and gas fields of southern San Joaquin Valley, Calif.

rocks, except that the structural closure is about twice as much and many more normal faults are evident. These normal faults dip as much as 50° to 55° and have known vertical displacements of 35 to 340 feet. Four of the subsurface faults have been traced by the writers to those mapped by Woodring, Roundy, and Farnsworth (1932, pl. 1) in the surface rocks. Other subsurface faults probably reach the surface also but are not evident because of their lack of topographic expression and the scarcity of marker beds in the monotonous succession of similar lithologies making up the exposed Tulare Formation.

The structure at a depth of 4,500 to 8,000 feet on the top of the Elk Hills Shale Member is dominated by the two anticlinal folds noted in younger rocks. At this depth the folding is more pronounced; the western anticline has about 600 feet of closure and the eastern one about 2,300 feet. Faulting is minor; one normal fault has about 40 feet of throw on the southwestern flank of the western anticline, and two normal faults have 280 and 120 feet of throw on the west and east ends of the eastern anticline. The easternmost fault with 120 feet of throw cuts partly across the long nose that extends toward North Coles Levee oil field.

LATE TERTIARY STRUCTURAL HISTORY

The history of the Elk Hills anticlinal structure before middle Miocene time is obscure because only a few wells have penetrated rocks older than the Monterey Shale. Dipmeter surveys in some wells recorded steep dips in the older rocks, which may indicate more complex structural conditions at depth. The development of the Elk Hills structure since Reef Ridge time can be reconstructed, roughly and in part, by assuming that the top of a geologic unit represents approximate sea level at the close of deposition of that unit. This reconstruction, of course, does not take into account the depth of water, the effect of initial slope of deposition, and the possible wave-base erosion. However, the approximation is sufficient for useful comparisons of the structure during different intervals of geologic time. Such approximations have been used to reconstruct the history of structural development along line $A-E'$ (fig. 3), as shown on figure 4. This line of section extends from Railroad Gap eastward to the eastern nose of the eastern anticline. It does not cross the highest and lowest points of each anticline, so maximum structural closures cannot be measured from the section.

The structural diagrams in figure 4 show that two anticlinal folds have persisted on the Elk Hills anticlinal structure from Miocene time to the present. The low point of the median syncline separating the two folds along section $A-E'$ is near point C.

At the close of Reef Ridge time (fig. 4*A*), the western anticline appears to have been slightly higher structurally than the eastern anticline. The regional tilt was about 4° to 5° eastward. Movement on a normal fault on the west flank of the eastern anticline may have occurred just prior to deposition of the Tupman Shale Member of the Etchegoin Formation, and the resulting scarp may have been high enough above wave base to have undergone some erosion. On the other hand, the fault may have occurred in Tupman time and may be too obscure to be found in the soft shale of the Tupman. During Reef Ridge time, the seas deposited 200 to 1,300 feet of clay and silt with some silica and carbonate in the Elk Hills area.

During deposition of the Tupman Shale Member (fig. 4*B*), the eastern anticline grew more than the western one, and at the close the eastern one stood slightly higher structurally. Concurrently, shallowing seas deposited as much as 1,400 feet of clay and silt across the area.

During deposition of the Carman Sandstone Member (fig. 4*C*), appreciable uplift took place in the Temblor Range, which produced a regional tilt of about 9° eastward. As a result, the apparent height of the eastern anticline, as measured on the top of the Reef Ridge Shale, increased markedly compared to that of the western anticline. Shallow seas swept large volumes of sand and silt across the area; more than 1,900 feet of fine- to medium-grained siliceous clastic material was deposited along the line of section.

During the deposition of the San Joaquin Formation (fig. 4*D*), both anticlines rose a few hundred feet. Regional tilting to the east continued at a slower rate. Shallow seas deposited as much as 2,000 feet of clay, silt, and fine sand across the area.

During late Pliocene, Pleistocene, and Holocene time (fig. 4*E*), both anticlines continued to rise slowly, and concurrently, 600 to 2,000 feet of sand and gravel was deposited in the area. The regional tilt of the western anticline was reduced. Surficial tensional stresses caused extensive normal faults that cut obliquely across the axis of the eastern anticline and resulted in grabenlike troughs in the post-Miocene rocks. As viewed from the south, the blocks within the troughs appear to have been rotated vertically in a clockwise direction.

The grabenlike troughs appear to have been formed by elongation southeastward in the upper several thousand feet of beds. The troughs are bounded at their base by a glide surface along the top of the Reef Ridge Shale, a formation which, being partly siliceous in composition, is considerably harder and stronger than the overlying nonsiliceous Tupman Shale Member. The long master fault, or fault zone, that is postulated subparallel to the bedding at the top of the Reef Ridge Shale joins a fault that is known to curve upward near the crest of the eastern anticline and to approach the land surface about a mile west of the crest. This fault pattern compares closely with results of the experiments with models by Cloos (1968, fig. 16), in which one side of the model was pulled away from a stationary side.

The postulation of a master fault subparallel to the bedding planes is supported by a comparison of the total heave of the faults at two stratigraphic horizons—the top of the Carman Sandstone Member and the top of the underlying Tupman

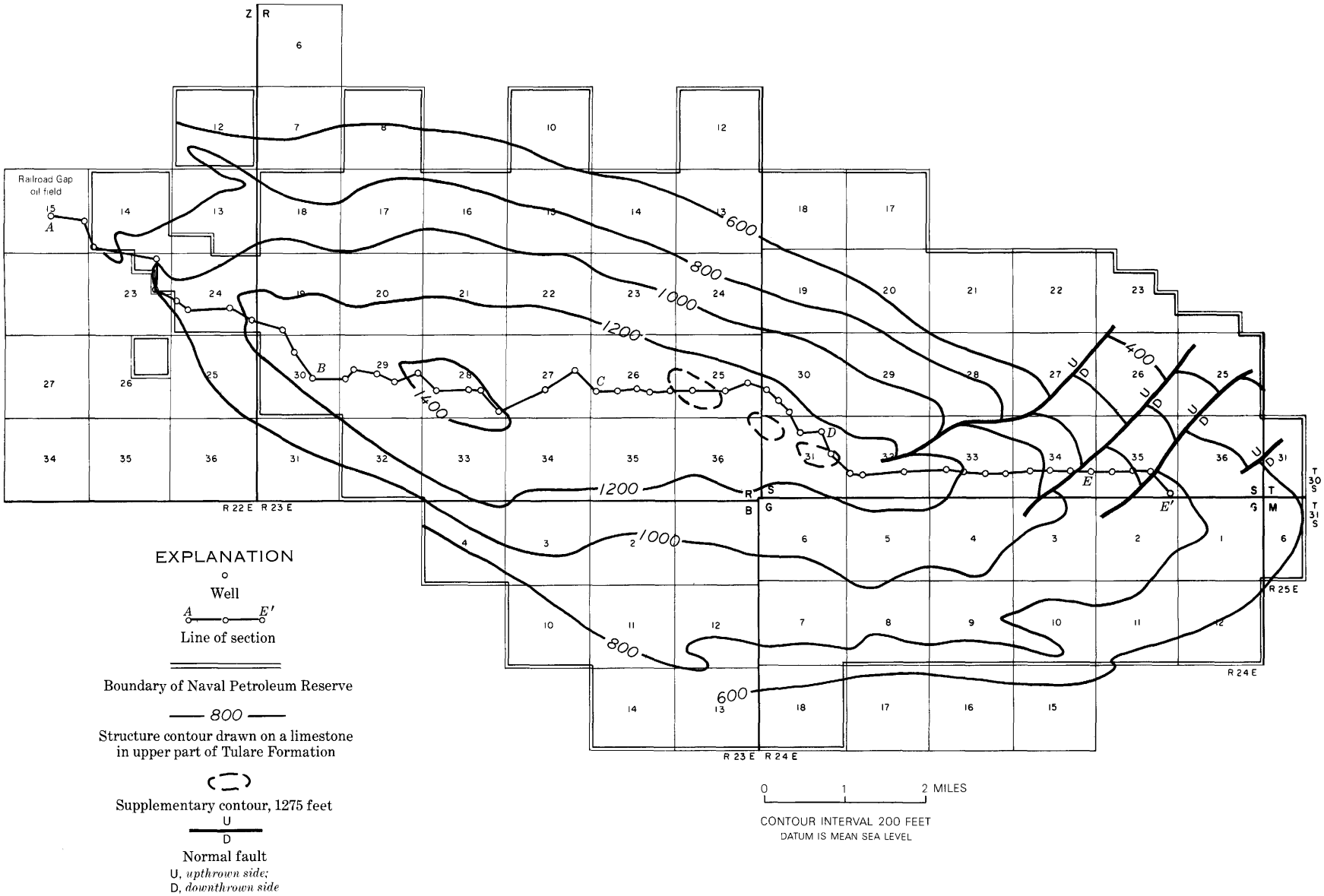

Figure 3.—Line of structural section A–E' in relation to surface structure, Elk Hills oil field, Kern County, Calif.

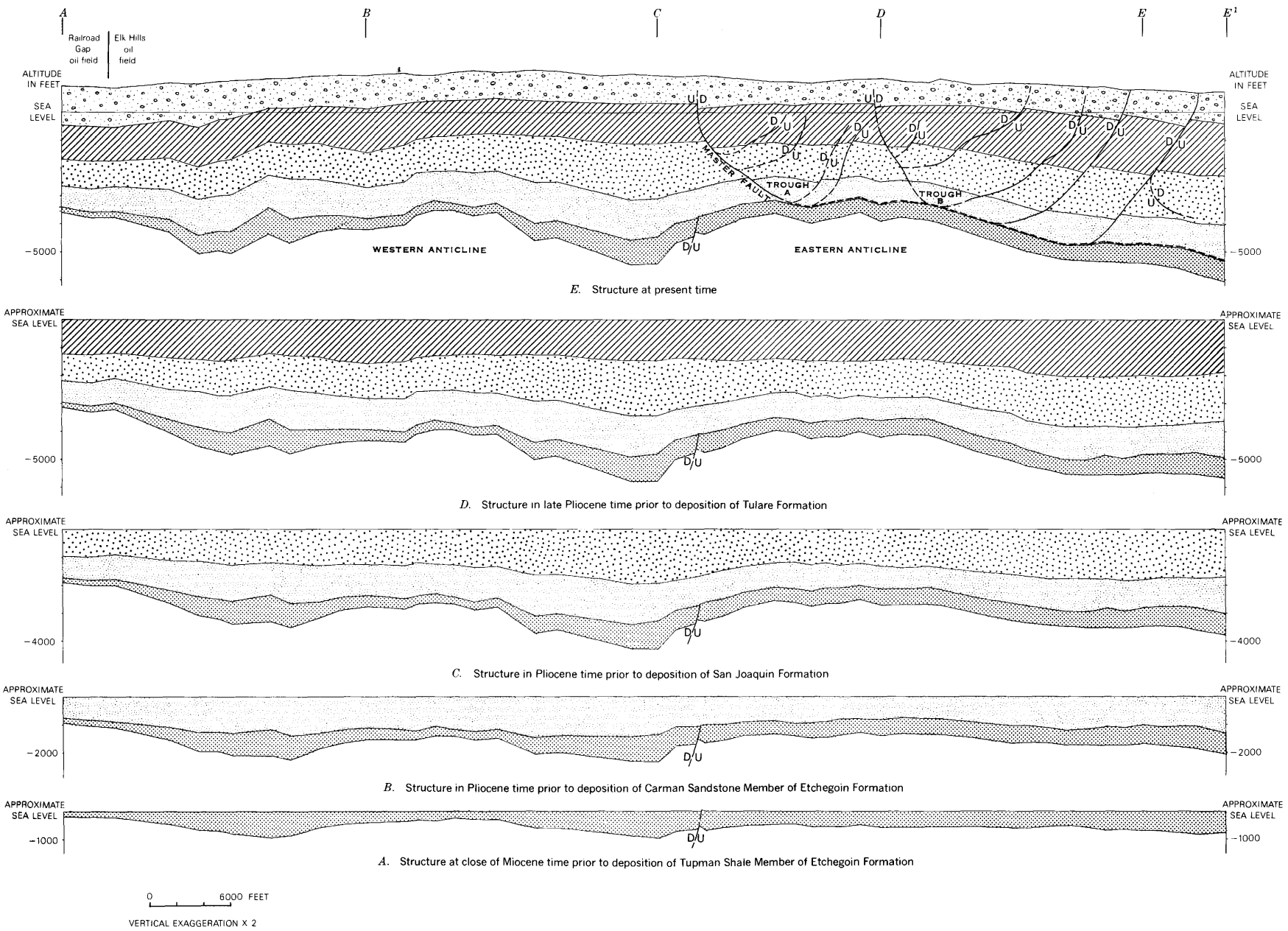

Figure 4.–Structural development along section A–E' from Railroad Gap oil field to eastern Elk Hills, Kern County, Calif.

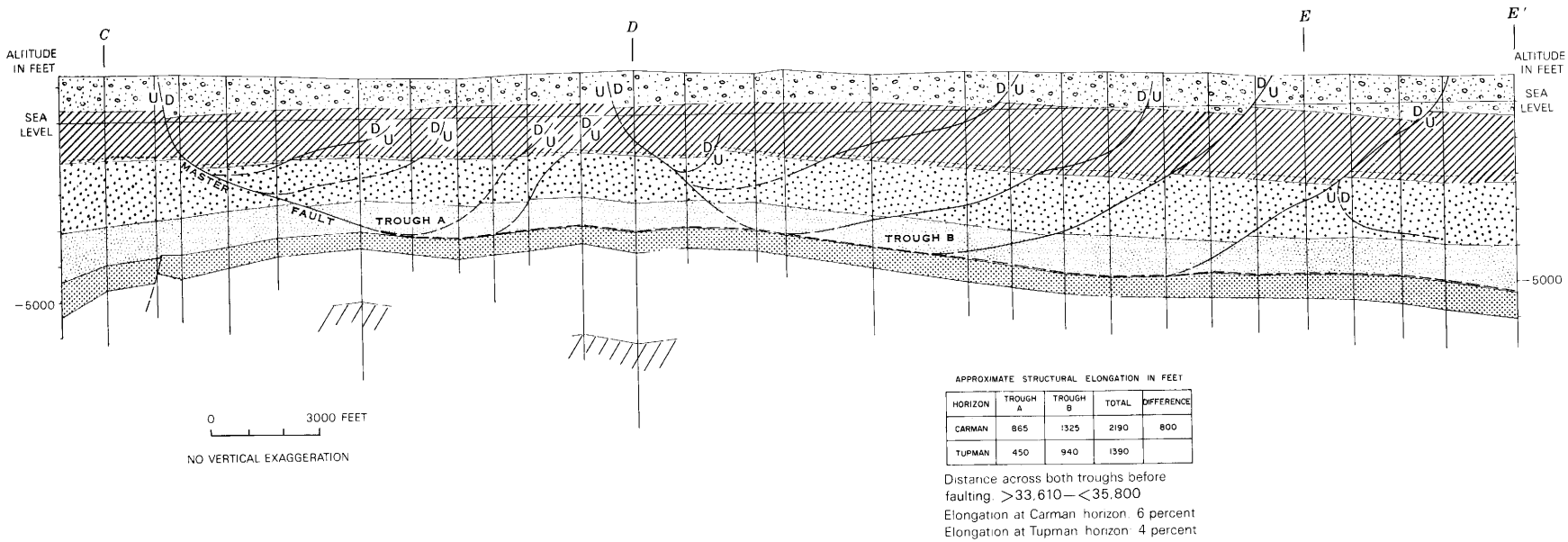

APPROXIMATE STRUCTURAL ELONGATION IN FEET

HORIZON	TROUGH A	TROUGH B	TOTAL	DIFFERENCE
CARMAN	865	1325	2190	800
TUPMAN	450	940	1390	

Distance across both troughs before faulting: >33,610—<35,800
Elongation at Carman horizon: 6 percent
Elongation at Tupman horizon: 4 percent

EXPLANATION

Pleistocene and Pliocene Series

Tulare Formation

Pliocene Series

San Joaquin Formation

Carman Sandstone Member of Etchegoin Formation

Tupman Shale Member of Etchegoin Formation

Miocene Series

Reef Ridge Shale

Monterey Shale (Elk Hills Member at top)

Temblor Formation

U / D — — —

Major normal fault

Solid where missing interval could be identified on electric log. Dashed where interpreted. D, *downthrown side;* U, *upthrown side*

Figure 5.—Fault system of the eastern anticline, Elk Hills, Kern County, Calif.

Shale Member. This comparison can be made most readily on a structural section drawn with equal horizontal and vertical scales as shown by figure 5. The measurements of heave in the plane of section $A-E'$ are only relative because the structure section $A-E'$ is not perpendicular to the fault traces. However, these relative measurements can be used to compare the elongation of the two horizons. If the structural troughs were rigidly bound, the total heave within the grabens would be the same at the top of both the Carman Sandstone and Tupman Shale Members. However, the Carman horizon appears to be elongated by 2,190 feet across troughs A and B and the deeper Tupman horizon elongated only 1,390 feet – a difference of 800 feet in the present distance of 35,800 feet across both troughs. If it is assumed that the rocks at the surface have moved less than the rocks at the Carman horizon because the heave of the faults decreases upward as the throw increases, the original distance before the troughs formed was between 33,610 feet and 35,800 feet. A rough calculation shows that the Carman horizon has been elongated about 6 percent and the Tupman horizon about 4 percent. The difference of 800 feet or 2 percent in the elongations of these horizons indicates that the structural troughs have sides that have expanded to allow more stretch in their upper strata than in their lower strata. This expansion can happen only by displacement along a bedding surface. The restriction of all but one fault to Pliocene and younger rocks, the projection of their curving fault planes, and the lithologic contrast between the hard, partly siliceous rocks of the Reef Ridge Shale and the overlying softer rocks point to the top of the Reef Ridge Shale as the probable glide surface for the master fault.

Structural sections across North Coles Levee oil field immediately east of Elk Hills (Hardoin, 1962, pls. 4 and 5) suggest that this fault system may be present there. The San Joaquin and Tulare Formations are not shown on the sections, but the Etchegoin Formation is cut by several normal faults, whose planes dip and flatten southeastward. If these fault planes were projected, they would approach the horizontal near the top of the Reef Ridge Shale.

The origin of the fault system on the eastern anticline seems most easily explained by the slipping-plane hypothesis of Quarles (1953), but the forces that caused the movement cannot be identified with certainty without more regional geological information. Gravity-sliding southeastward down the steep north flank of the Tejon basin is one possibility. However, the lack of similar faulting in the post-Miocene rocks of South Coles Levee oil field, as shown by Dosch (1962, pls. 4, 5, and 6), casts some doubt on this possibility because South Coles Levee oil field is located along the steepest part of the north flank of the Tejon basin. Another possibility seems to be tensional forces related to movement of the San Andreas fault in relation to the Bakersfield arch.

REFERENCES

Berryman, W. M., 1972, Lithologic characteristics of Pliocene rocks cored at Elk Hills, Kern County, California: U.S. Geol. Survey Bull. 1332-D. [In press]

Cloos, Ernst, 1968, Experimental analysis of Gulf Coast fracture patterns: Am. Assoc. Petroleum Geologists Bull., v. 52, no. 3, p. 428–429.

Dosch, M. W., 1962, South Coles Levee oil field: California Oil Fields–Summary of Operations, v. 48, no. 2, p. 63–72.

Elk Hills Engineering Committee, 1957a, Shallow oil zone, second revision dated May 1, 1957, of estimated recoverable oil and percentage participations as of November 20, 1942, *in* Unit operation – Naval Petroleum Reserve No. 1 (Elk Hills), Kern County, California: Bakersfield, Calif., Elk Hills Eng. Comm., 35 p.

—— 1957b, Stevens Zone, estimated recoverable oil and second revision of percentage participations as of November 20, 1942, *in* Unit operation – Naval Petroleum Reserve No. 1 (Elk Hills), Kern County, California: Bakersfield, Calif., Elk Hills Eng. Comm., 42 p.

Hardoin, J. L., 1962, North Coles Levee oil field: California Oil Fields–Summary of Operations, v. 48, no. 2, p. 53–61.

Hoots, H. W., Bear, T. L., and Kleinpell, W. D., 1954, Geological summary of the San Joaquin Valley, California *in* Geology of southern California: California Div. Mines Bull. 170, v. 1., p. 113–129.

Quarles, Miller, Jr., 1953, Salt-ridge hypothesis on origin of Texas gulf coast type of faulting: Am. Assoc. Petroleum Geologists Bull., v. 37, no. 3, p. 498–500.

Woodring, W. P., Roundy, P. V., and Farnsworth, H. R., 1932, Geology and oil resources of the Elk Hills, California: U.S. Geol. Survey Bull. 835, 82 p.

THRUST FAULTS, ANNETTE-GRAVINA AREA, SOUTHEASTERN ALASKA

By HENRY C. BERG, Menlo Park, Calif.

Abstract.—Thrust faults recently mapped on Annette and Gravina Islands, near Ketchikan, represent the first documented large-scale thrusting in southeastern Alaska. The thrusts displace bedded rocks as young as late Mesozoic and are offset by high-angle faults, probably mainly of middle Tertiary age. The largest zone of thrusting, on western Annette Island, juxtaposes geologically and physiographically dissimilar terranes, truncating a metamorphic aureole on one terrane by at least 5 miles. A thrust on southern Gravina Island emplaces slightly deformed Paleozoic rocks over intensely deformed Mesozoic rocks; its net slip may be as much as a mile. In places, intersections of this thrust with high-angle faults are marked by zones of hydrothermally altered rocks containing sparse copper minerals and barite. Large-scale thrust faults now are being recognized in many other places in southeastern Alaska. This recognition is leading to reinterpretations of the region's structural and tectonic history that favor mobilistic hypotheses of major tectonic dislocation and continental fragmentation.

The first low-angle thrust faults with large displacements to be documented in southeastern Alaska have been mapped on Annette and Gravina Islands (herein also called Annette-Gravina area) near Ketchikan (fig. 1). The main thrusts are, by their gentle dips and net slips of a mile or more, distinct from the numerous high-angle reverse faults and from the few other, less well-documented thrust faults mapped elsewhere in southeastern Alaska (Lathram and others, 1959, 1965; Loney and others, 1963a, b; Loney, 1964; Muffler, 1967). The thrusts are offset by presumably younger high-angle normal and strike-slip faults.

The thrusts originated in a Late Jurassic–middle Tertiary interval. In the Annette-Gravina area, they displace rocks as young as Late Jurassic and are cut by high-angle faults that are inferred correlatives of middle Tertiary faults known elsewhere in southeastern Alaska (Ovenshine and Brew, 1972). A more definitive interval of post-Early Cretaceous–pre-middle Tertiary time is suggested by recent mapping on Etolin Island, 65 miles northwest of Ketchikan, where beds as young as Albian probably were involved in the deformation that produced the thrusting in the Annette-Gravina area (Berg, unpub. data).

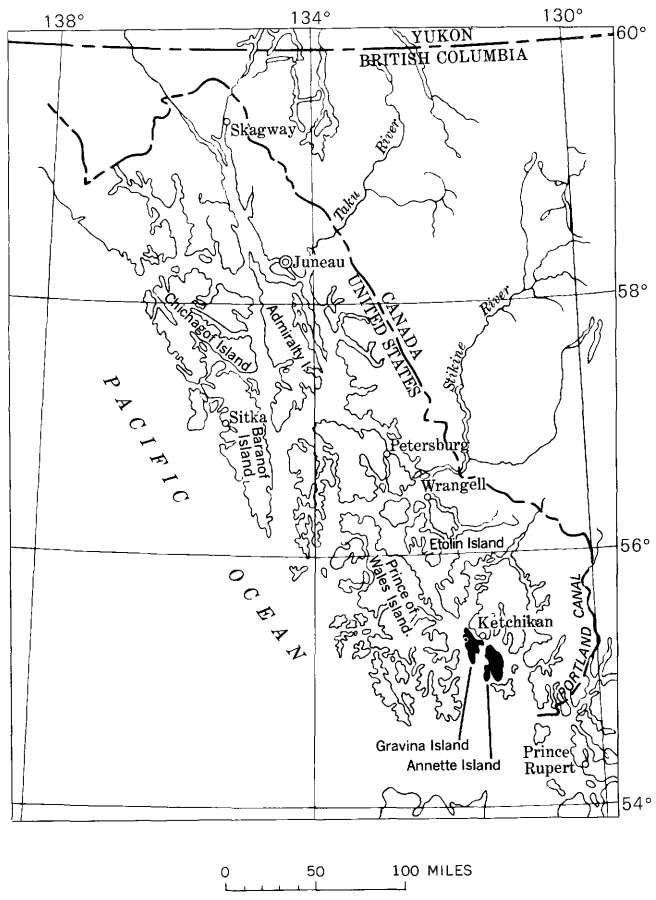

Figure 1.—Index map of southeastern Alaska, showing location of Annette and Gravina Islands.

ANNETTE ISLAND

Several thrust faults, including a main thrust zone with an estimated minimum net slip of 5 miles, occur on Annette Island, about 20 miles south of Ketchikan (fig. 2). The first such large-scale thrust mapped in southeastern Alaska, the main zone was first inferred from the occurrence of deep, water-bearing, permeable zones on Metlakatla Peninsula (Marcher, 1969), then documented by detailed geologic mapping (Berg, 1970, 1972; U.S. Geol. Survey, 1970). In addition to the main zone on western Annette Island, several other thrust faults have been mapped; their magnitude and

U.S. GEOL. SURVEY PROF. PAPER 800-C, PAGES C79-C83

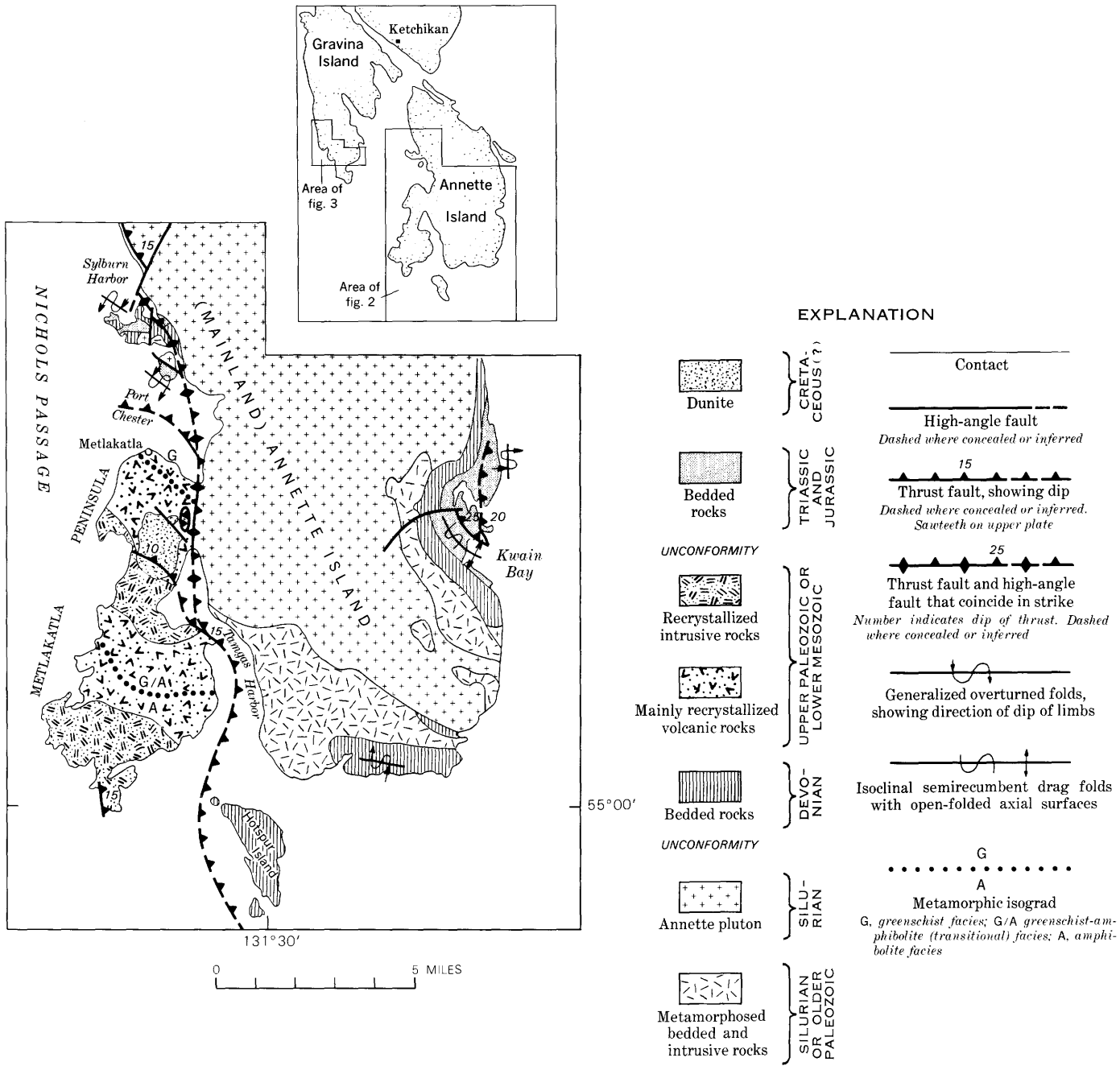

Figure 2.–Generalized geologic map of part of Annette Island, Alaska.

extent are less well known. All of the thrusts are disrupted by high-angle faults that in some places offset them and in others coincide with their strike (fig. 2).

Annette Island consists of two geologically distinct terranes that differ markedly in physiography, lithology, and type and grade of metamorphism (Berg, 1972)–mainland Annette Island and Metlakatla Peninsula, a large southwestern appendage of the island. Hotspur Island, just off the south coast of Annette Island, is included in the mainland Annette terrane.

Mainland Annette is mountainous (maximum elevation, 3,591 feet) and is underlain by a diverse suite of bedded and intrusive rocks ranging in age from Silurian or older Paleozoic to Middle or Late Jurassic. Except for the Annette pluton, whose core is brecciated but not schistose, the rocks commonly are foliated and characterized by greenschist facies and lower grade regional metamorphism.

Metlakatla Peninsula, a muskeg-covered lowland (maximum elevation, 540 feet), is underlain mostly by recrystallized volcanic and intrusive rocks of indefinite, but probably mainly late Paleozoic or early Mesozoic, age (Berg, 1972; revised in Berg, 1973) and by a small dunite body of Cretaceous(?) age. Most of the rocks are phyllitic to gneissic, but many lack

pronounced foliation. Metamorphism grades from greenschist facies on the north to amphibolite facies on the south.

The main thrust zone is a complex network of low- and high-angle faults that mainly separates Metlakatla Peninsula from the rest of Annette Island. In general, it strikes sinuously northward and dips eastward at an angle of 15° or less. Several strands that strike westward dip gently northward. Where the low-dipping faults coincide in strike with high-angle faults, the thrust surfaces commonly are rotated and dragged into much steeper attitudes and therefore are difficult to distinguish from the normally steep high-angle faults. Bedrock along the trace of the main zone, which in places may be as much as a mile wide, is intensely sheared, with numerous closely spaced graphitic and micaceous slip surfaces. Typically, the shear zones contain ellipsoidal blocks of relatively unsheared rock several tens of feet in maximum dimension. Differential erosion of the sheared rocks in the main zone has produced the three harbors on western Annette Island—Sylburn Harbor, Port Chester, and Tamgas Harbor. It is possible, in fact, that the flat, low-lying Metlakatla Peninsula was formed by a combination of glacial and marine planation along low-dipping shear surfaces contiguous to the main thrust zone.

The estimated net slip of the main thrust zone is based on the truncation of a metamorphic aureole on Metlakatla Peninsula. The aureole, produced by metamorphism that postdates a late Paleozoic or early Mesozoic pluton on the south end of the peninsula, grades from amphibolite facies on the south to biotite (and locally chlorite) zone greenschist facies on the north (fig. 2), indicating a width of at least 6 miles. The aureole has not been recognized in the Devonian and older Paleozoic rocks on mainland Annette Island and Hotspur Island. The metamorphic isograds trend west to northwest and terminate abruptly on the east against chlorite-zone greenschist facies rocks on mainland Annette and still lower grade (prehnite-pumpellyite metagraywacke facies?) rocks on Hotspur Island. That none of these older rocks were affected by the metamorphism on Metlakatla Peninsula indicates that they were beyond the 6-mile aureole at the time of that metamorphism. The present one-mile minimum between amphibolite on southern Metlakatla Peninsula and the low-grade rocks on Hotspur Island suggests a displacement of at least 5 miles on the main thrust zone.

Two other conspicuous thrust faults on Annette Island are exposed in the Kwain Bay area (fig. 2). The bedded rocks near these gently eastward dipping faults are intensely deformed, presumably largely by drag in conjunction with the thrusting, but the net slip cannot be measured because the thrusts juxtapose rocks of roughly the same age and lithology. The complex structures in the bedded rocks, which include isoclinal recumbent folds with warped axial surfaces, suggest that the cumulative displacement on these thrusts may be appreciable.

SOUTHERN GRAVINA ISLAND

A major thrust fault, indicated by anomalous stratigraphy and structure, is exposed over a 10-square-mile area near the south end of Gravina Island (fig. 3). This fault, which dips gently northward, thrusts slightly deformed Paleozoic rocks over intensely deformed Mesozoic rocks and is offset by high-angle faults.

The bedded rocks on southern Gravina Island comprise three unconformable sequences. The oldest consists of diverse greenschist-to-amphibolite facies metamorphosed bedded and intrusive rocks. It is assigned an age of Silurian or older Paleozoic because it is intruded by apophyses of the Annette pluton, a radiometrically dated Silurian stock that crops out mainly on Annette Island (Berg, 1972, 1973). The next younger sequence comprises weakly metamorphosed volcanic and sedimentary rocks. Its assigned age, based on scant, poorly preserved upper Silurian(?) and Devonian(?) fossils in the sedimentary rocks, is middle Paleozoic. The most significant unit in this sequence is the Puppets Formation (Berg, 1973), a conspicuous 400-foot-thick unit of metarhyolite whose anomalous outcrop pattern first led to the recognition of thrusting on southern Gravina Island. The youngest sequence includes sedimentary and mafic volcanic rocks, generally only slightly deformed and recrystallized, whose age, based on locally abundant fossils, ranges from Late Triassic to Late Jurassic.

The best exposures of the thrust fault are at Nehenta Bay, where horizontal and gently dipping metarhyolite of the Puppets Formation overlies complexly deformed Upper Triassic slate, limestone, and conglomerate. The contact is exposed on the north shore of the bay, where it dips gently to moderately northeastward. It ranges from a sharply delineated single surface with little gouge to a zone perhaps several tens of feet thick containing slices of country rock separated by graphite- and mica-coated slip surfaces. In other parts of the Nehenta Bay area, intersections of this fault with high-angle faults are marked by zones of intensely hydrothermally altered rocks that contain sporadically distributed copper minerals and barite.

The complex structures in the Triassic beds below the thrust include composite small folds and intersecting lineations and are attributed mainly to drag associated with the thrusting. Except for coastal exposures, mapping of these lower-plate rocks is hindered by poor outcrops and limited areal extent, but the available evidence suggests that the intensity of the deformation diminishes with increasing distance from the thrust.

The only other place where a thrust fault intersects the coastline of southern Gravina Island, and is thus fairly well exposed, is about 3½ miles north of Nehenta Bay. Although the fault there dips gently northeastward, it juxtaposes rocks of roughly the same age and lithology and can only be inferred to correlate with the main thrust at Nehenta Bay.

On the heavily forested ridges northeast of Nehenta Bay, the trace of the thrust is marked by an apparently intermittent, gently northward-dipping zone of intense brecciation and

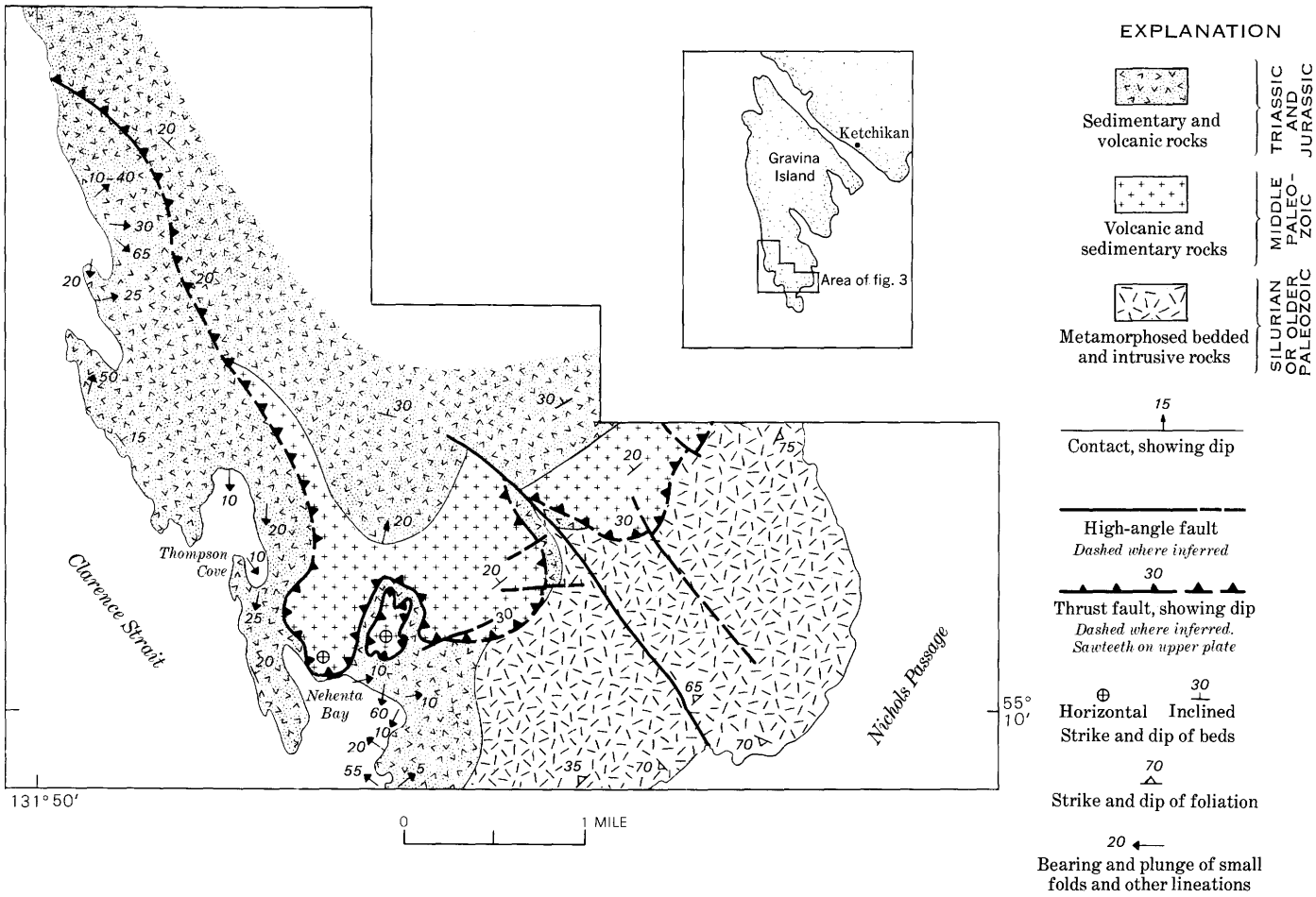

Figure 3.—Generalized geologic map of southern Gravina Island, Alaska.

hydrothermal alteration. Individual outcrops of altered fault breccia are as much as 10 feet in maximum dimension, but the thickness of the zone is unknown because exposures are poor. Areal mapping suggests that the fault thrusts Puppets metarhyolite over Silurian and older Paleozoic rocks in some places and over Upper Triassic rocks in others, but outcrops are too scattered to fully document thrusting at any single locality.

The displacement on the thrust fault on southern Gravina Island is uncertain. Its approximate stratigraphic throw, based on estimated thickness of beds faulted out by the thrust in the Nehenta Bay area, is 2,000 feet. The net slip, or total displacement, cannot be determined from the local geology, but a diagrammatic cross section of the regional geology of southwestern Gravina Island (Berg, 1973) indicates that it may be as much as a mile.

SUMMARY AND CONCLUSIONS

Late Mesozoic or Tertiary thrust faults with maximum estimated net slips of 5 miles or more—large displacements heretofore not recognized on the scattering of low-angle faults mapped elsewhere in southeastern Alaska— have been documented by detailed geologic mapping in the Annette-Gravina area near Ketchikan.

The similarity of the geology of Annette and Gravina Islands to that of many other parts of southeastern Alaska strongly suggests that thrust faults may be commonplace; but whereas reconnaissance geologic maps published to date record numerous high-angle normal, strike-slip, and reverse faults, they show only one or two low-angle faults, none with documented large-scale displacement.

Recent U.S. Geological Survey mapping in southern southeastern Alaska (A. L. Clark, A. T. Ovenshine, and H. C. Berg, unpub. data; G. D. Eberlein, and Michael Churkin, Jr., unpub. data) has revealed several major thrusts. In addition, juxtaposed dissimilar terranes and other anomalous features shown on existing geologic maps of other parts of southeastern Alaska probaly are at least partly due to major thrusting.

Recognition of this major thrusting is leading to new interpretations of southeastern Alaska's structural and tectonic history—interpretations that support such mobilistic hypotheses of large-scale tectonic dislocation and continental fragmen-

tation as those recently proposed by Monger and Ross (1971) and Jones, Irwin, and Ovenshine (1972).

REFERENCES

Berg, H. C., 1970, Paleozoic plutonism and contrasting metamorphic terranes, Annette Island, Alaska: Geol. Soc. America Abs. with Programs, v. 2, no. 2, p. 70.

——1972, Geologic map of Annette Island, Alaska: U.S. Geol. Survey Misc. Geol. Inv. Map I-684.

——1972, Geology of Gravina Island, Alaska: U.S. Geol. Survey Bull. 1373. [In press]

Brew, D. A., Loney, R. A., and Muffler, L. J. P., 1966, Tectonic history of southeastern Alaska, *in* A symposium on tectonic history and mineral deposits of the western cordillera in British Columbia and neighbouring parts of the United States: Canadian Inst. Mining and Metallurgy Spec. Vol. 8, p. 149–170.

Jones, D. L., Irwin, W. P., and Ovenshine, A. T., 1972, Southeastern Alaska—A displaced continental fragment?, *in* Geological Survey Research 1972: U.S. Geol. Survey Prof. Paper 800-B, p. B211–B217.

Lathram, E. H., Loney, R. A., Condon, W. H., and Berg, H. C., 1959, Progress map of the geology of the Juneau quadrangle, Alaska: U.S. Geol. Survey Misc. Geol. Inv. Map I-303, scale 1:250,000.

Lathram, E. H., Pomeroy, J. S., Berg, H. C., and Loney, R. A., 1965, Reconnaissance geology of Admiralty Island, Alaska: U.S. Geol. Survey Bull. 1181-R, 48 p.

Loney, R. A., 1964, Stratigraphy and petrography of the Pybus-Gambier area, Admiralty Island, Alaska: U.S. Geol. Survey Bull. 1178, 103 p.

Loney, R. A., Berg, H. C., Pomeroy, J. S., and Brew, D. A., 1963a, Reconnaissance geologic map of Chichagof Island and northwestern Baranof Island, Alaska: U.S. Geol. Survey Misc. Geol. Inv. Map I-388 (with text), scale 1:250,000.

Loney, R. A., Condon, W. H., and Dutro, J. T., Jr., 1963b, Geology of the Freshwater Bay area, Chichagof Island, Alaska: U.S. Geol. Survey Bull. 1108-C, 54 p.

Marcher, M. V., 1969, Ground-water reconnaissance of the Metlakatla Peninsula, Annette Island, Alaska: Geol. Soc. America Abs. with Programs for 1969, pt. 2, p. 20.

Monger, J. W. H., and Ross, C. A., 1971, Distribution of fusulinaceans in the western Canadian cordillera: Canadian Jour. of Earth Sciences, v. 8, no. 2, p. 259–278.

Muffler, L. J. P., 1967, Stratigraphy of the Keku Islets and neighboring parts of Kuiu and Kupreanof Islands, southeastern Alaska: U.S. Geol. Survey Bull. 1241-C, 52 p.

Ovenshine, A. T., and Brew, D. A., 1972, Separation and history of the Chatham Strait fault, southeast Alaska, North America: Internat. Geol. Cong., 24th, Montreal 1972, Proc. [In press]

U.S. Geological Survey, 1970, Lower Paleozoic pluton on Annette Island, *in* Geological Survey Research 1970: U.S. Geol. Survey Prof. Paper 700-A, p. A50.

TECTONIC IMPLICATIONS OF THE PRESENCE OF THE EDNA MOUNTAIN FORMATION IN NORTHERN ELKO COUNTY, NEVADA

By ROBERT R. COATS and MACKENZIE GORDON, JR.,
Menlo Park, Calif., Washington, D.C.

Prepared in cooperation with the Nevada Bureau of Mines

Abstract.—In the Divide Peak area of Elko County, Nevada, about 45 miles north of Elko, an erosional window in Tertiary volcanic rocks exposes Paleozoic rocks of two structural plates, separated by a major thrust that is structurally higher than the Roberts Mountains thrust. In the higher plate, clastic rocks of the Edna Mountain Formation of Permian (Phosphoria) age, that resemble those of the Antler Peak area, rest unconformably on and are involved in imbricate thrust relations with the Valmy Formation (Ordovician) of the western assemblage. In the lower plate, the Phosphoria Formation rests unconformably on the Valmy. Indirect evidence suggests that the thrusting occurred between early late Early Triassic, and the Middle or early Late Jurassic, probably nearer the earlier limit. The differences in sedimentary facies and faunas between the Phosphoria and Edna Mountain Formations of the Divide Peak area are attributed to major overthrusting. Unless autochthonous Edna Mountain Formation, of a facies similar to that of the Divide Peak area, can be found at some place between Antler Peak and Divide Peak, we think that this span of about 96 miles approximates the minimum horizontal dislocation.

In much of northern Nevada, outcrops of Paleozoic rocks were for a long time supposed to be confined mostly to the highlands, which are separated by immense expanses of Tertiary volcanic and sedimentary rocks. Exploration of the volcanic areas, however, has revealed many windows, some of considerable extent, in which the Paleozoic rocks are exposed. In some areas the Paleozoic rocks stand high topographically, as horsts, and many of these may never have been covered by Tertiary rocks, whereas in other areas, post-Tertiary faulting has permitted the stripping of the Tertiary cover and revealed the Paleozoic basement in windows. Information obtained from mapping in these horsts or windows may be vital in interpreting the Paleozoic and Mesozoic tectonic history, but because of the gaps resulting from areally limited and imperfect exposures, much of this interpretation must rest on inference rather than on observation. One window is in the Divide Peak area, 45 miles north of Elko, northern Elko County (fig. 1). The Divide triangulation station is on the south edge, near the southeast corner, of the Wild Horse

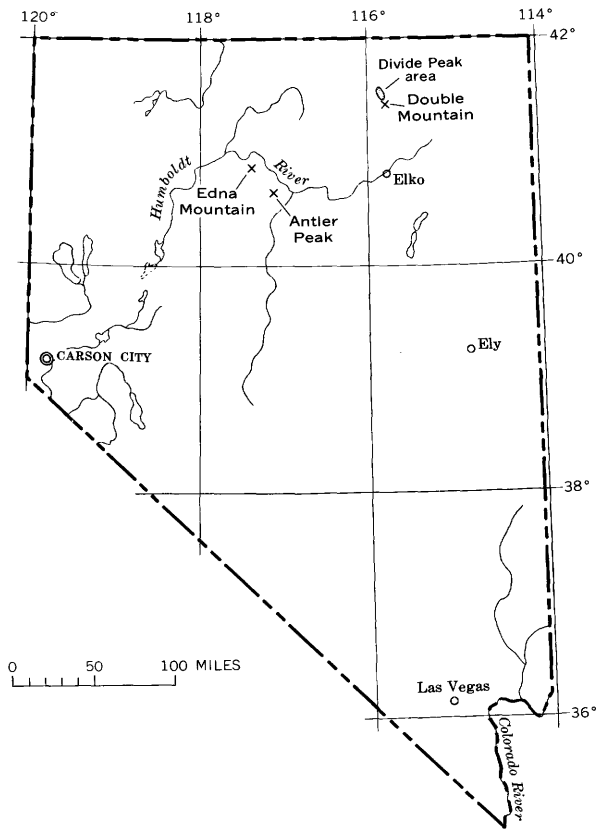

Figure 1.—Index map of Nevada, showing the locations of the Divide Peak area, Edna Mountain, and Antler Peak.

quadrangle. The Paleozoic rocks that are the principal subject of this paper are exposed both north and southeast of that point, in Tps. 41 and 42 N., R. 55 E. (Mount Diablo base line and meridian). The Paleozoic rocks belong to two sequences, in each of two blocks separated by a major thrust: the early Paleozoic western, or siliceous-volcanic sequence (Roberts and

U.S. GEOL. SURVEY PROF. PAPER 800-C, PAGES C85-C94

others, 1958; Silberling and Roberts, 1962), and the late Paleozoic, or western synorogenic sequence. The early Paleozoic rocks for which paleontologic data are available are part of the Valmy Formation of Ordovician age; others are of doubtful age, but the assignment of all to the western sequence is not in doubt. The late Paleozoic synorogenic rocks of the upper plate belong to the Edna Mountain Formation of Permian age, which lies in both depositional and thrust contact on the early Paleozoic rocks. The early Paleozoic rocks may also be thrust over the Edna Mountain Formation in some places; the thrust plate containing both sequences rests upon Paleozoic rocks of the western assemblage (Roberts and others, 1958; Silberling and Roberts, 1962) and upon the Phosphoria Formation, differing in facies and faunal content from the Edna Mountain Formation, though nearly of the same age.

EARLY PALEOZOIC ROCKS

Valmy Formation

The Valmy Formation in the type area (Roberts, 1951) has been subdivided into two members: the lower mainly of quartzite, dark-gray and greenish chert, gray to black siliceous shale, and some greenstone, the upper mainly of chert interbedded with dark shale and a little greenstone. The age of the Valmy is considered (Roberts and others, 1958, p. 2833; Silberling and Roberts, 1962, p. 12) to span the Ordovician Period.

The rocks of the Divide Peak area that have been identified as Valmy include white to light-tan or gray quartzite, chert, and calcarenite.

The most conspicuous lithic unit of the Valmy Formation is a quartzite which, because of its great resistance to erosion, forms the summit of the high ridge extending northward from Divide triangulation station. Small klippen or windows of the quartzite are found in the midst of exposures of Edna Mountain Formation in the lowlands west of the Divide ridge (fig. 2). The quartzite unit as mapped also includes a small amount of chert, shale, and calcarenite exposed on the southern nose of the ridge mentioned above. To the southeast, areas of low relief are underlain by poorly exposed chert and shale that have been mapped as part of the Valmy, but these have furnished no fossils.

The quartzite is typically gray and has a vitreous appearance on fracture, and in thin section displays a mosaic of quartz grains ranging in size from about 0.07 to 0.7 mm. The grains have simple, not digitate boundaries, and lack any signs of secondary enlargement. In a few places the quartzite is a quartz arenite in which similarly sized quartz grains still retain the high degree of sphericity they had at the time of deposition, and are cemented together by flamboyant quartz. Leaching of this and possibly other cements has left a rather porous arenite.

The calcarenite mentioned above has furnished the only fossil collections from the early Paleozoic rocks of this area. Two collections have been made: in 1964 (USGS 5455-C0), and in 1970 (USGS 7104-C0). Both collections yielded only conodonts, determined by John Huddle; the taxa determined in the smaller collection are also present, with others, in the larger subsequent collection. The Nevada (E. zone) coordinates of the site are E. 447,450, N. 2,457,400, scaled from the Wells 2° quadrangle. This point is about 800 feet S. 45° W. of Divide triangulation station on the south edge of the Wild Horse quadrangle. The fauna reported by Huddle is as follows:

	Number of specimens
Drepanodus robustus Hadding	
drepanodiform element	7
oistodiform element	7
Periodon aculeatus Hadding	
ozarkodiniform element	13
ligonodiform element	15
cordylodiform element	8
falodiform element	5
trichonodelliform element?	1
"Oistodus" multicorrugatus Harris	6
Scolopodus sp.	1

"This fauna is Middle Ordovician in age."

Greenstone and chert

In the southeastern part of the Divide Peak area, two fault slivers of rocks of different type, both lacking in fossils, are attributed to the western, or siliceous-volcanic assemblage. One of the slivers is a now chloritized and epidotized greenstone unit that locally is a calcareous peperitic breccia. This suggests that the breccia, probably of andesitic composition originally, was erupted into marine waters in which calcareous muds were accumulating. This unit is considered to be of Paleozoic age.

The other unit consists predominantly of black chert but includes minor amounts of pale-purplish and pale-greenish-gray shale. Its weathering yields few outcrops, and the surface is littered with a carpet of sharply angular inch-sized fragments of lustrous black chert, many with reentrant angles. The age of the chert is unknown. James Gilluly (oral commun., 1965) suggested that it might be correlatable with the Slaven Chert, of Devonian age, the type locality of which is in the northern Shoshone Range. The characteristics of the Slaven Chert, as described (Gilluly and Gates, 1965, p. 37), resemble closely those of the chert in this area, but the interbedded shale in the type area is described as dark colored, rather than varicolored. In nearby ranges, similar cherts have been found in fossiliferous Ordovician rocks of the western assemblage (Evans and Ketner, 1971).

PERMIAN ROCKS

Permian rocks of the Divide Peak area are referred to two formations, the Edna Mountain Formation and the Phosphoria Formation. These are approximately of the same age, but the lithologic facies differ, and the fossil assemblages also differ considerably. The Edna Mountain Formation rests in thrust

contact on the Phosphoria Formation in the southeastern part of the area.

Edna Mountain Formation

The type locality of the Edna Mountain Formation is in the Golconda quadrangle on the west slope of Edna Mountain, about 100 miles west-southwest of the Divide Peak area (Roberts, 1951; Ferguson and others, 1952). Lithologies in the study area generally resemble those in the type area. In the study area the rocks include minor well-indurated chert-quartz conglomerate and gray, buff-weathering sandstone and siltstone that contain a mold fauna. Some of the siltstone in the study area weathers to a highly characteristic pale-purplish red (5*RP* 6/2).

Almost all collections in our area are of a mold fauna in a buff-weathering sandstone or siltstone. Much of the sandstone is so massive that attitudes cannot be measured. The typical sandstone is a chert-quartz arenite, made up of angular fragments, that grades to a granule conglomerate. In some places as much as 5 percent of the fragments may be phyllite. Almost all the fragments are of rocks that are known to occur in the Valmy Formation. At station 1645 (E. 451,700, N. 2,447,500) the Edna Mountain rests unconformably on the Valmy. At this point the Edna Mountain is a poorly sorted granule to pebble sharpstone conglomerate of subangular fragments of brown-weathering porous quartzite. The quartzite consists of well-rounded quartz grains, partly cemented together by flamboyant quartz, leaving angular interstices now vacant, but apparently once filled with some iron-bearing mineral. The unconformable contact here dips 20° S. 15° E.

Phosphoria Formation

The rocks of the Divide Peak area that are attributed to the Phosphoria Formation of Permian age are almost entirely fine buff-weathering siltstones and massive light-gray limestone; a few beds are as much as 8 feet thick. The typical chert and phosphatic shale lithologies of the Phosphoria, which are present but a few miles to the north and south of the Divide Peak area, have not been recognized here, perhaps because of the restricted area of outcrop of the Phosphoria.

PERMIAN FAUNAS

The fossils of the Edna Mountain Formation are shown as the *Spiriferella* assemblage in table 1. This invertebrate fauna is made up predominantly of individuals of a spiriferoid brachiopod, *Spiriferella* sp. A, together with other less common brachiopods and a few mollusks. The fauna was recognized in 10 collections from eight stations and is typical of most of the Permian outcrops in this area. *Spiriferella* sp. A is also the dominant species in the type Edna Mountain Formation, where it is associated with *Hustedia* cf. *H. phosphoriensis* Branson. Some of the typical fossils of this assemblage are illustrated in figure 3.

The relatively close relationship of this assemblage to the predominantly molluscan fauna of the autochthonous *Cyrtorosta* assemblage, here referred to the Phosphoria Formation, is also indicated in table 1. Four species of brachiopods are common to the two assemblages: *Phrenophoria* sp. A, *Leiorhynchoidea*? sp., *Composita* cf. *C. mira* Girty, and *Hustedia* cf. *H. phosphoriensis* Branson.

The fossils from rocks referred to the Phosphoria Formation are shown as the *Cyrtorostra* assemblage in table 1. Occurrences of species common to it and the Edna Mountain Formation are listed under the *Spiriferella* assemblage. The *Cyrtorostra* assemblage, illustrated in figure 4, is restricted to the southeasternmost part of the Permian outcrop belt. The collection localities are listed in table 2. This is a fauna predominantly of mollusks associated with less abundant brachiopods. The most common species, *Cyrtorostra varicostata* Branson, is common also locally in the Franson and Ervay Members of the Park City Formation and the Tosi Chert Member of the Phosphoria Formation in western Wyoming and also occurs locally in the Rex Chert Member of the Phosphoria Formation in southeastern Idaho (Ciriacks, 1963, p. 58). The brachiopods identified here as cf. *Cancrinella phosphatica* (Girty) and *Rhynchopora* cf. *R. taylori* Girty have close affinities with species described from the Park City Formation (Girty, 1910). A pleurotomariacean snail, *Eirlysia* sp., (identified by E. L. Yochelson) is also common in this assemblage.

As discussed earlier in this article, the faunal assemblage of the Phosphoria and that of the Edna Mountain Formation are regarded as approximately the same age but are in fault contact, the Edna Mountain constituting an allochthonous formation in this area. The Phosphoria Formation rests unconformably upon the Valmy Formation.

The rocks containing the two assemblages are regarded as approximately contemporaneous. They are, however, separated by a thrust fault at the only locality where they are in juxtaposition, on a small hill 3 to 4 miles north-northwest of Double Mountain. The presence of the *Spiriferella* assemblage in the Divide Peak area is believed to be due to the incorporation of the Edna Mountain Formation in a thrust plate brought in from the west.

TERTIARY(?) AND TERTIARY ROCKS

On the extreme western edge of the mapped area, a small sliver of rocks, bounded on both sides by high-angle faults, is attributed to the Tertiary(?). These rocks are well-indurated, deeply iron stained roundstone conglomerates made up of clasts derived chiefly from the Valmy Formation. No fossils were found in them; they resemble the rocks described by Van Houten (1956, p. 2806) as eastern conglomerates, that rest on the Paleozoic rocks. Van Houten (1956, p. 2807) suggests that

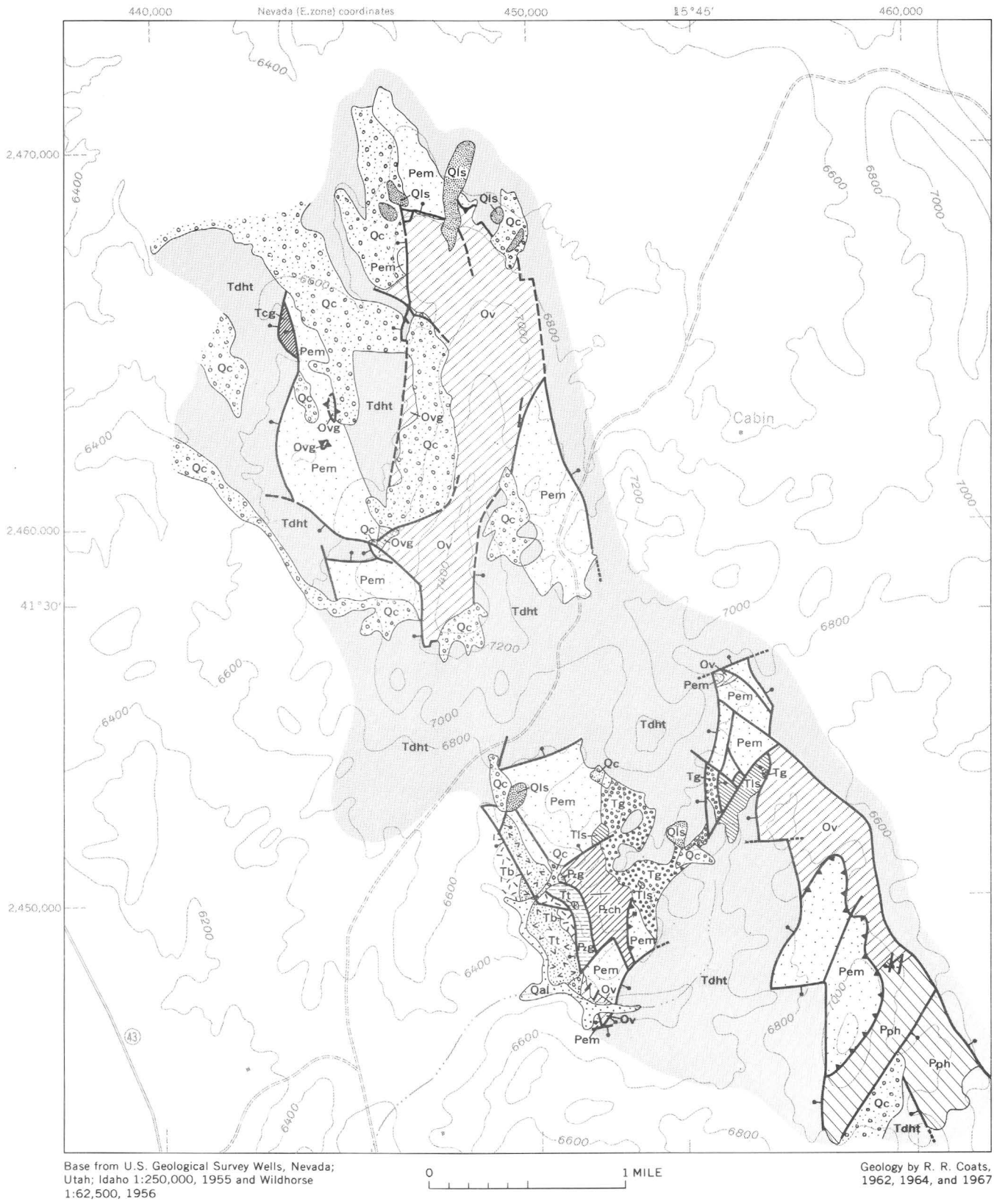

Figure 2.—Geologic map of the Divide Peak area, Elko County, Nev.

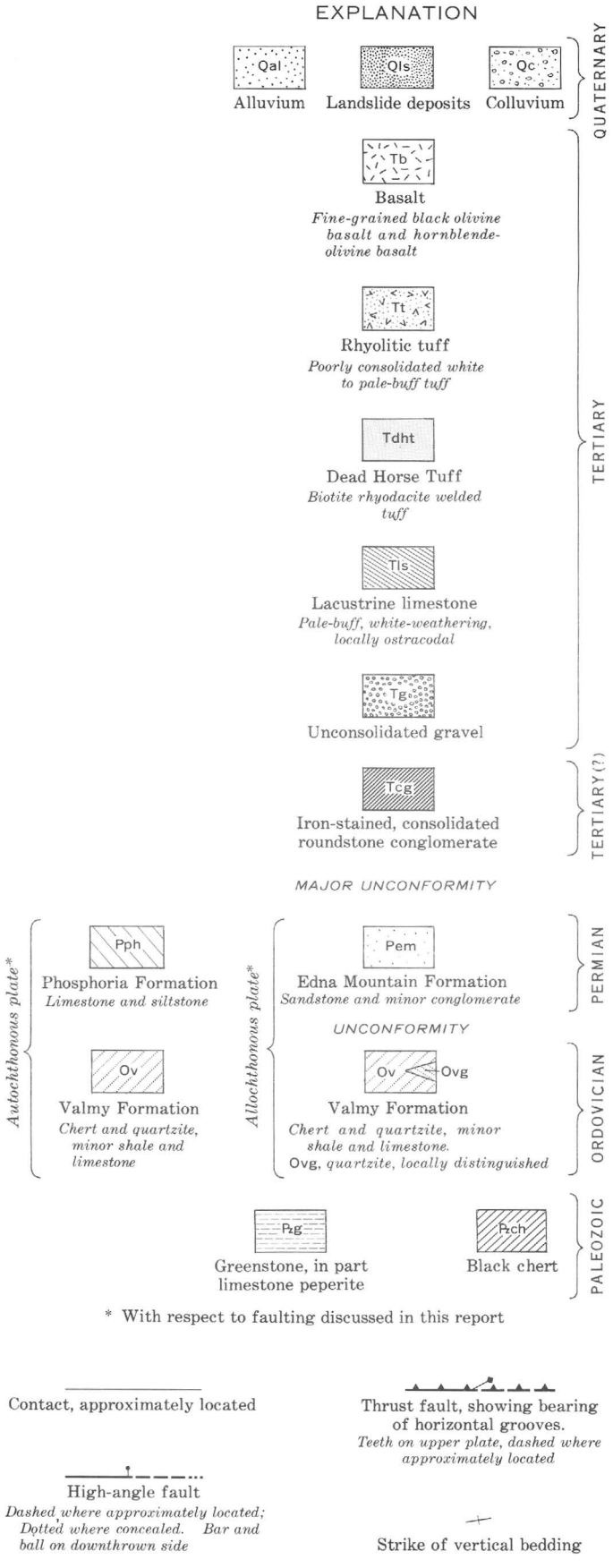

Figure 2.

these conglomerates in northwestern Utah and east-central Nevada may be equivalent to conglomerates in the Paleocene or lower Eocene Wasatch Formation of north-central Utah.

Near the middle of the mapped area, the Paleozoic rocks are obscured by a mantle of unconsolidated, poorly sorted angular gravel of fragments derived from the Paleozoic rocks. The thickness is uncertain because lack of outcrops prevents determination of the attitude, but it is probably less than 100 feet. In a few places the gravel is overlain by buff, white-weathering fine-grained ostracodal limestone, which may range in thickness from 2 feet to perhaps as much as 20 feet. The ostracodes are not of determinable age.

The most widespread of the Tertiary formations is a biotite rhyolite welded tuff which, at least locally, has scattered small grains of yellow andradite. Near the west margin of the area mapped, this tuff unit appears to interfinger with white lacustrine rhyolitic tuffs, now opalized in part, containing fragmentary leaves of grass and sedge. This unit is believed to be correlative with the Dead Horse Tuff (Coats, 1964, p. M7), for which a K-Ar age of 39.9 million years was determined (Axelrod, 1966, p. 500). Numerous high-angle faults, mostly north trending, cut the Dead Horse in this area, and the strata in many of the fault blocks display moderately steep dips.

On the southern flank of the area, the Dead Horse Tuff is overlapped by soft, poorly consolidated rhyolitic tuffs overlain by dense, black olivine basalt and hornblende-olivine basalt. The age of these rocks is unknown.

TECTONIC RELATIONS

The Valmy Formation and the undifferentiated western-assemblage Paleozoic rocks are allochthonous, wherever their relations have been determined in this region. The Edna Mountain Formation, as indicated above, is in depositional contact with the Valmy Formation; in most places, the contact is not well exposed, but at coordinates E. 451,700, N. 2,447,500 (Nevada, E. zone) the thin gently dipping basal conglomerate of the Edna Mountain rests with angular unconformity on the Valmy. In many places, however, the contact is a tectonic one; at E. 452,500, N. 2,499,700, the Edna Mountain rests on a fault surface on the undifferentiated Paleozoic chert. Here there is a well-developed horizontal mullion structure trending N. 55° E. Elsewhere the relations are equivocal. The ridge to the north of Divide triangulation station is capped by a plate of gray Valmy quartzite, apparently not more than 50 feet thick. The considerable horizontal extent of this plate suggests that it is nearly flat lying, but to the southwest of the triangulation station, fossiliferous Ordovician rocks trend nearly north and dip steeply, leading to the inference that the quartzite plate is thrust over the fossiliferous rocks. To the west of the high ridge of Divide Peak, in secs. 21 and 28, two isolated masses of Valmy are shown as windows. Both of these are quartzite, and numerous slickensided surfaces of diverse trend are present in

Table 1.—*Permian fossils from the Divide Peak area, Elko County, Nev.*

Fossils	Collection[1]													
	21583-PC	21584-PC	21585-PC	21593-PC	21594-PC	22820-PC	23216-PC	23778-PC	23779-PC	23780-PC	24513-PC	24514-PC	64NC133	64NC134
Spiriferella assemblage														
Corals:														
Horn coral, gen. and sp. indet.	...	...	X	...	X	X	...	...	...	...	...	...	...	...
Brachiopods:														
Orbiculoidea sp.	...	...	X	...	...	...	X	...	...	...	...	...	...	...
Sulcataria? sp. indet.	...	...	...	...	...	...	...	...	X	...	...	...	...	...
Strophalosia sp.	?	...	X	...	X	X	X	...	...	...	...	...	...	...
Productoid, gen. and sp. indet.	...	...	...	...	...	X	...	...	X	...	...	...	...	...
Phrenophoria sp. A.	X	X	X	X	X	X	...	...	...	X	X	X	...	...
Leiorhynchoidea? sp.	X	X	...	?	X	...	...	...	...	...	X	...	...	...
Rhynchopora? sp.	...	...	...	...	...	...	...	X	...	?	...	...	...	...
Cleiothyridina sp. indet.	...	...	X	...	X	...	X	...	...	...	...	...	...	...
Composita cf. *C. mira* Girty	...	X	...	X	...	X	X	...	X	...	...	...	...	...
Spiriferella sp. A	...	...	X	?	X	X	X	X	X	X	X	X	X	X
Xestotrema sp. indet.	...	...	...	...	...	...	...	X	...	...	...	...	...	...
Hustedia cf. *H. phosphoriensis* Branson	X	X	X	X	X	X	X	X	...	...	X	X	...	...
Beecheria sp. B.	...	...	...	...	...	...	...	X	...	X	...	...	...	...
Mollusks:														
Phestia sp. indet.	...	...	...	...	...	X	...	...	...	X	...	...	...	...
Parallelodon sp.	...	...	...	...	...	...	X	...	...	...	...	...	...	...
Aviculopinna? sp. indet.	...	...	...	...	...	...	...	...	...	X	...	...	...	...
Conocardium sp. indet.	...	...	...	...	...	...	...	...	...	X	...	...	...	...
Pleuronautilus (*Huanghoceras*) sp.	...	...	...	...	...	...	...	...	...	X	...	...	...	...
Cyrtorostra assemblage														
Bryozoans:														
Trepostome, small ramose form.	X	X	...	X	...	...	...	...	...	...	...	...	...	...
Echinoderms:														
Crinoid columnals	X	...	...	...	...	...	...	...	...	...	...	...	...	...
Brachiopods:														
cf. *Cancrinella phosphatica* (Girty)	X	X	...	X	...	...	...	...	...	...	...	...	...	...
Grandaurispina sp.	...	X	...	X	...	...	...	...	...	...	...	...	...	...
Rhynchopora cf. *R. taylori* (Girty)	...	X	...	X	...	...	...	...	...	...	...	X	...	...
Spiriferella? sp. B	X	X	...	X	...	...	...	...	...	...	...	...	...	...
Beecheria sp. A.	X	...	...	X	...	...	...	...	...	...	...	?	...	...
Mollusks:														
Nuculopsis sp. indet.	...	...	...	...	...	...	...	...	...	...	...	X	...	...
Streblochondria? cf. *S.*? *montpelierensis* (Girty)	X	X	...	X	...	...	...	...	...	...	...	...	...	...
Cyrtorostra varicostata Branson	X	X	...	X	...	...	...	...	...	...	...	...	...	...
Eirlysia sp.	X	X	...	X	...	...	...	...	...	?	...	X	...	...

[1]Five-figure numbers followed by "PC" are U.S. Geological Survey Upper Paleozoic collection numbers; numbers beginning 64NC are field specimen numbers assigned by R. R. Coats.

them; in the northern and larger window (if that is what it is) a continuous slickensided fault surface forms the upper surface of the quartzite over a considerable area. This fault surface is subcylindrical, the axis trends about N. 32° W., and the mullion structure on the surface plunges, on the southwest about 5° SW. and on the northeast, about 20° NE., passing through the horizontal on the crest of the convex-upward fault surface. Many minor, low-dipping slickensided fault surfaces are exposed in both Valmy and the Edna Mountain. The striations or mullions on these surfaces range in trend from N. 80° E. to S. 65° E. In addition to these low-angle faults, many steep faults with generally northerly trend cut the Valmy quartzite; although well-developed slickensides, with striations nearly down the dip, are observable in many of these, few of them can be traced far, and displacements are probably small.

Near the north end of the exposure of Valmy Formation, in the SW. cor. sec. 21, T. 42 N., R. 55 E., the Valmy is shown, on the map, as in thrust contact with the Edna Mountain Formation. This relation is inferred from the relative position and the map trend of the contact, as the actual contact surface is not exposed. Along a hill slope just to the north of the fossil locality at E. 450,450, N. 2,450,800, large blocks of pink quartzite are strewn upon the surface which is underlain by the Edna Mountain Formation. No topographically higher outcrop of the Valmy can now be found, but the former presence of a now totally removed klippe of Valmy, resting on the Edna Mountain near the top of the hill, seems the most likely explanation for the presence of the Valmy fragments here.

The Phosphoria Formation is autochthonous or parautochthonous in the Divide Peak area. The Valmy Formation on which it rests, in seeming depositional contact, must then be part of the upper plate of the Roberts Mountains thrust, or some other pre-Phosphoria thrust of regional extent.

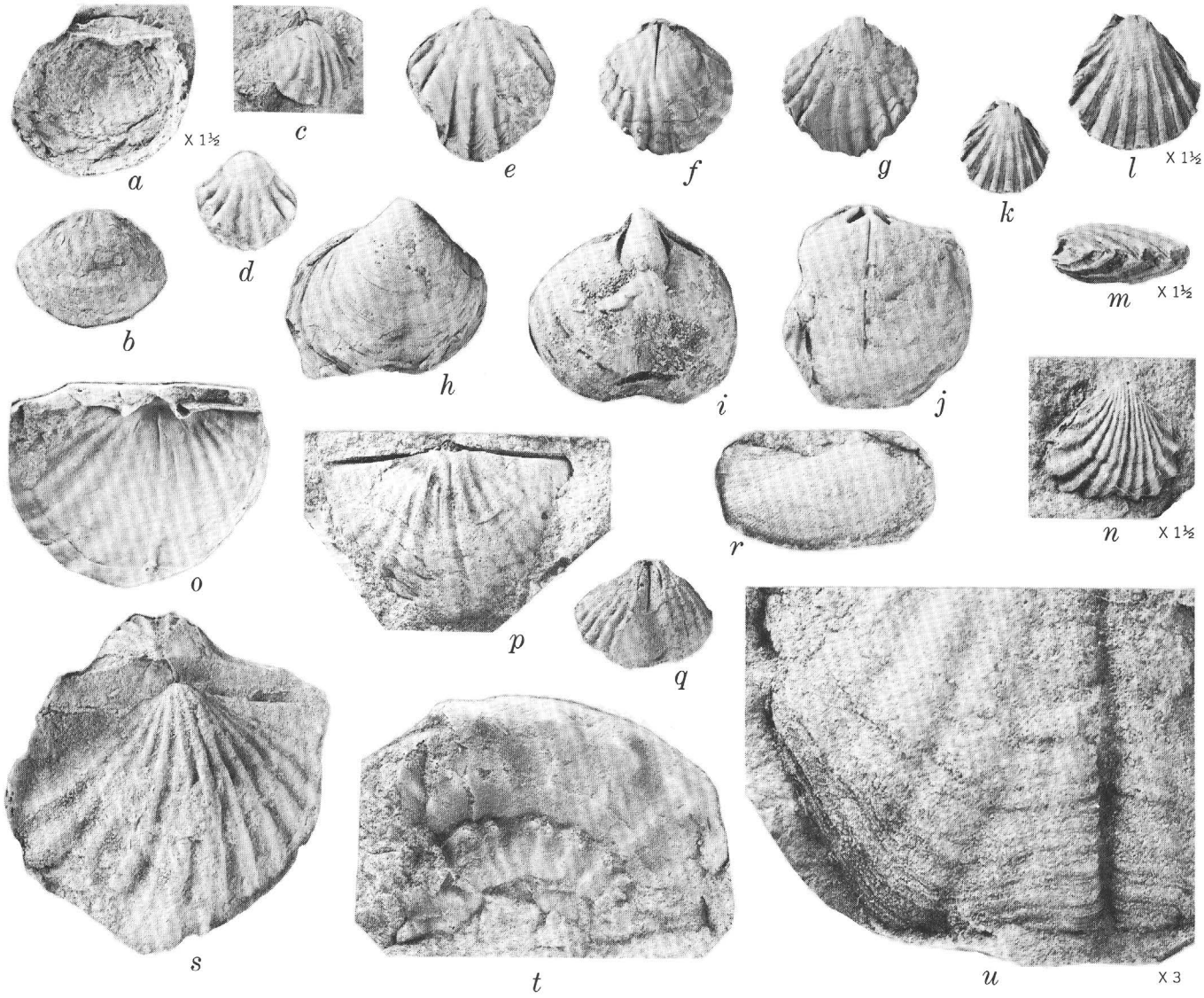

Figure 3.—Fossils of the *Spiriferella* assemblage from the Edna Mountain Formation in the Divide Peak area. Photographs natural size unless otherwise indicated.

a, b. Strophalosia sp. Enlarged brachial view of latex cast from USGS colln. 21594-PC and internal mold of pedicle valve from USGS colln. 24367-PC.

c, d. Phrenophoria sp. A. Slightly oblique view of brachial valve associated with *Strophalosia* of fig. *b*, and latex cast of pedicle valve from USGS colln. 22820-PC.

e–g. Leiorhynchoidea sp. Internal mold of pedicle valve from USGS colln. 24367-PC, and brachial and pedicle views of internal mold from same locality.

h–j. Composita cf. *C. mira* Girty. Pedicle view of latex cast, internal mold of pedicle valve, and incomplete internal mold of brachial valve; all from USGS colln. 22820-PC.

k–n. Hustedia cf. *H. phosphoriensis* Branson. Brachial view and enlarged brachial and side view of internal mold, also pedicle view of latex cast; both specimens from USGS colln. 22820-PC.

o, p, s, u. Spiriferella sp. A. Three brachial valves (*o, p, u*) from USGS colln. 22820-PC including interior view of latex cast, internal mold, and enlarged view of latex cast to show surface pustules; brachial view (*s*) of latex cast from USGS colln. 21585-PC.

q. Xestotrema sp. Internal mold of pedicle valve from USGS colln. 23778-PC.

r. Parallelodon sp. Latex cast of right valve from USGS colln. 23216-PC.

t. Pleuronautilus (*Huanghoceras*) sp. Latex cast of impression from USGS colln. 23780-PC.

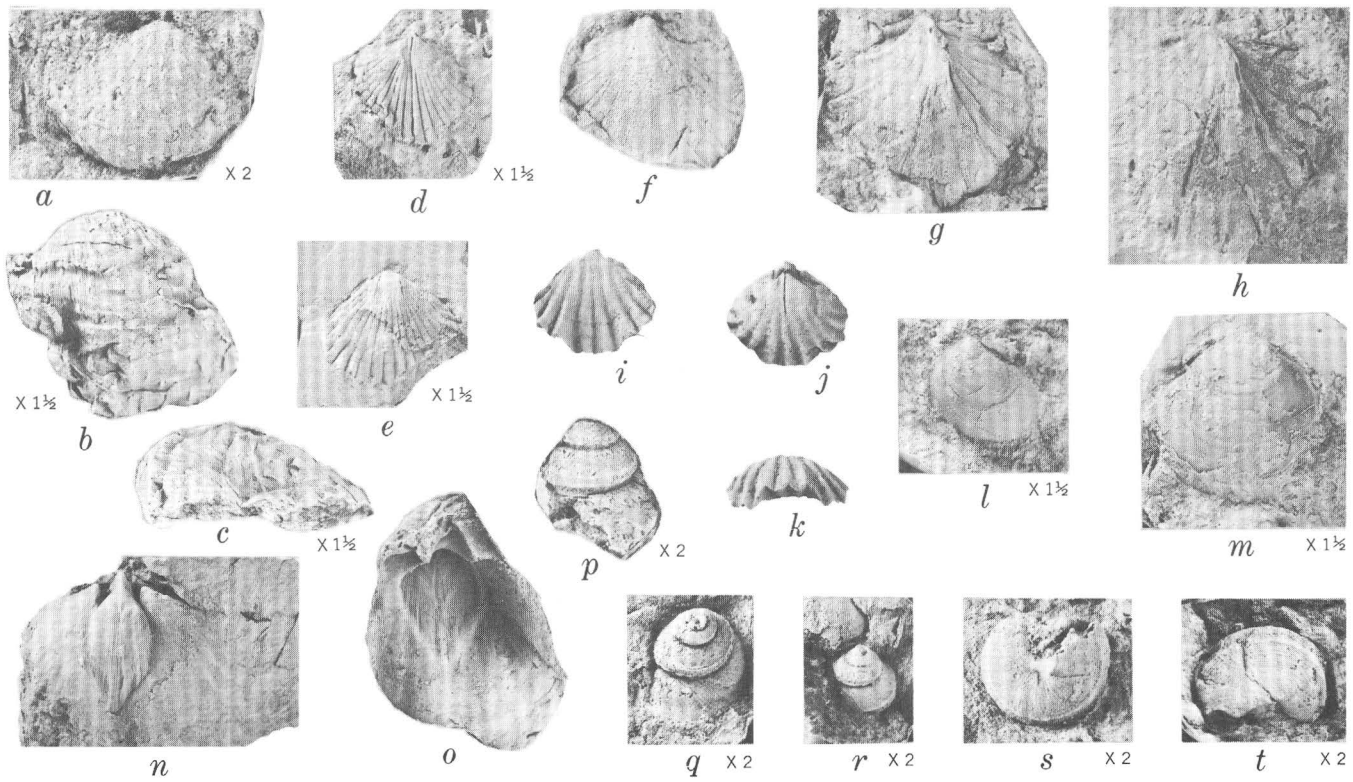

Figure 4.—Fossils of the *Cyrtorostra* assemblage from the Phosphoria Formation in the Divide Peak area. Photographs natural size unless otherwise indicated.

a. Grandaurispina sp. Enlarged view of latex cast of pedicle valve from USGS colln. 21584-PC.

b, c. cf. *Cancrinella phosphatica* Girty. Enlarged ventral and side views of pedicle valve from USGS colln. 21583-PC.

d, e. Rhynchopora cf. *R. taylori* Girty. Enlarged views of internal molds of brachial valve and pedicle valve, both from USGS colln. 21593-PC.

f–h. Cyrtorostra varicostata Branson. Latex cast of right valve and internal molds of two left valves from USGS colln. 21584-PC.

i–k. Phrenophoria sp. A. Ventral, dorsal, and anterior view of well-preserved internal mold from USGS colln. 21593-PC.

l, m. Streblochondria? cf. *S.*? *montpelierensis* Girty. Enlarged views of right and left valves from USGS colln. 21593-PC.

n, o. Spiriferella sp. B. Internal mold of pedicle valve and view of latex cast of pedicle valve, both from USGS colln. 21593-PC.

p–t. Eirlysia sp. Enlarged views of five latex casts showing surface of this little snail, all from USGS colln. 21593-PC.

The high-angle faults that cut both the Tertiary and Paleozoic rocks, and separate these units from one another, fall into two principal sets, one predominantly north trending, the other with a northwesterly trend. Both sets cut the older Tertiary rocks, but the faults that bound the younger tuffs and the basalt seem to be predominantly the northwest-trending set.

TECTONIC INFERENCES

The exposed and inferred structural relations of the Edna Mountain and Phosphoria Formations with the Valmy and other western assemblage Paleozoic rocks imply an imbricate relation for the western assemblage and the Permian rocks. Two possible explanations may be considered: either the Permian formations are nearly autochthonous in the Divide Peak region, and the imbricate thrusting has displaced them but little from their sites of deposition, or the Edna Mountain and the Valmy and other western assemblage Paleozoic rocks are all allochthonous, and make up part of a thrust sheet, resting on a plate containing the Valmy and Phosphoria. We favor the latter explanation for two reasons, both based on inferences from the facies relationships of the Edna Mountain of this area with other rocks of similar age. The lithology of the Edna Mountain differs markedly from that of the Phosphoria in the Divide Peak area as well as at sites a few miles to the north and south where the Phosphoria is dominantly dark shales, cherts, and limestones, phosphatic in part. On the other hand, the lithology of the Edna Mountain in the Divide Peak area differs significantly from that of the Edna Mountain on Edna Mountain, about 96 miles west-southwest. The type Edna Mountain Formation on Edna Mountain, in the Golconda quadrangle (Ferguson and others, 1952) is somewhat micaceous, whereas the sandstone of Edna

Table 2.—*Register of Permian fossil collection localities in the Divide Peak area*[1]

USGS colln. 21583-PC. Station 346. Projected position in SE¼ sec. 2, T. 41 N., R. 55 E. In a roadcut, 0.4 miles south from an obscure road junction. Coordinates E. 460,100, N. 2,447,600. Collected by R. R. Coats and Domingo Malicdem, 1961.

USGS colln. 21584-PC. Station 396. Coordinates E. 460,400, N. 2,446,700. About 300 feet east of road, at a point 2,000 feet south of obscure road junction. NW¼NW¼ sec. 12, T. 41 N., R. 55 E. Collected by R. R. Coats, Keith Howard, and Ralph Roberts, 1962.

USGS colln. 21585-PC. Station 397. Coordinates E. 450,550, N. 2,459,000. 100 feet west of road, just south of small gully, 3,000 feet northeast of Divide triangulation station, Wild Horse quadrangle. NE¼SW¼ sec. 27, T. 42 N., R. 55 E. Collected by R. R. Coats, Keith Howard, and Ralph Roberts, 1962.

USGS colln. 21593-PC. Station 346. See colln. 21583-PC above. Collected by R. R. Coats and Keith Howard, 1962.

USGS colln. 21594-PC. Station 368. Coordinates E. 457,400, N. 2,449,400. Collected by R. R. Coats, 1962.

USGS colln. 22820-PC. Station 397. See colln. 21585-PC above. Collected by R. R. Coats and Mackenzie Gordon, Jr., 1964.

USGS colln. 23216-PC. Station 1644. Coordinates E. 450,350, N. 2,450,800. Just south of mouth of shallow southeastward-trending gully, and near point where larger gully changes trend from west to south. NW¼NE¼ sec. 4, T. 41 N., R. 55 E.

USGS colln. 23778-PC. Station 951. Coordinates E. 444,050, N. 2,464,000, Wild Horse quadrangle. SW¼ sec. 21, T. 42 N., R. 55 E. Near prominent ledge of conglomerate, on brow of slope southwest of sharp bend in gulch. Collected by R. R. Coats, 1964.

USGS colln. 23779-PC. Station 962. Wells 2° sheet. Coordinates E. 449,900, N. 2,452,000. Near and on south side of ridge trending southwestward, 50 feet southeast of and below prominent ledge on brow of hill. Collected by R. R. Coats, 1964.

USGS colln. 23780-PC. Station 968. Coordinates E. 452,600, N. 2,449,800. Near center sec. 3, T. 41 N., R. 55 E.; top of 20-foot-high hill between two higher hills. Collected by R. R. Coats, 1964.

USGS colln. 24513-PC. Field No. 62NC12. Station 367. Coordinates E. 457,900, N. 2,450,300. Collected by R. R. Coats, 1962.

USGS colln. 24514-PC. Station H-2. Coordinates E. 460,450, N. 2,445,700. Crest of ridge, about 2,500 feet south of obscure road junction, and 900 feet east of roads NW¼ sec. 12, T. 41 N., R. 55 E. Collected by Keith Howard, 1962.

Field No. 64NC-133. Station 953. Coordinates E. 444,200, N. 2,462,750. Wild Horse quadrangle. NW¼NW¼ sec. 28, T. 42 N., R. 55 E. Collected by R. R. Coats, 1964.

Field No. 64NC134. Station 954. Wild Horse quadrangle. Coordinates E. 445,600, N. 2,458,200. SW¼SE¼ sec. 28, T. 42 N., R. 55 E., about ½ mile west of Divide triangulation station. Collected by R. R. Coats, 1964.

USGS colln. 24367-PC. West of where road traverses saddle, halfway between road and hilltop. NE¼ sec. 11, T. 41 N., R. 55 E. Five miles air line north-northeast of Double Mountain. Edna Mountain Formation. Collected by K. B. Ketner, 1969. (Not included in table 1.)

[1]Where possible, descriptions of the positions of fossil localities with respect to local features are included, but most geographic features in the study area are not named. Further locality information is given by use of the Nevada (E. zone) coordinate system, the positions given in feet. For the northwestern part of the map, positions have been plotted on the 1956 U.S. Geological Survey 1:62,500-scale map of the Wild Horse, Nev., quadrangle (southeast corner at 41°30′N., 115°45′ W.) from the aerial photographs on which the mapping was done. Coordinates in this part of figure 2 are thus scaled from a relatively good topographic map. In the southern and eastern parts of figure 2, which are derived from the 1955 1:250,000-scale map of the Wells quadrangle, precision of plotting of the collection localities is poorer. The coordinates of the collection localities given in this report are scaled with reference to the coordinate ticks appearing on figure 2; different coordinates may be assigned to the same localities when larger scale maps of this area are available and positions of the collection localities are replotted.

Mountain Formation in the Antler Peak quadrangle, about 20 miles farther southeast, consists predominantly of chert and quartz fragments, like the Edna Mountain Formation in the Divide Peak area. We therefore believe that the Edna Mountain Formation of the Divide Peak area is part of a single thrust plate of major extent with a horizontal displacement of at least 96 miles. The time of thrusting must be post-Edna Mountain. Some indirect evidence for the maximum age in this area is available. Clark (1957, p. 2205) has described an area of lower Triassic rocks in the vicinity of Coal Canyon, in the River Range, in T. 38 N., R. 56 E. Keith Ketner (written commun., 1967) collected from this area fossils placed by Norman Silberling (written commun., 1967) in the early, but not earliest, late Early Triassic. These rocks are characterized by limestone and shale with almost no conglomerate. It is arguable that the presence of a major thrust plate a short distance to the north at the time of deposition would have resulted in a much increased percentage of conglomerate.

The oldest pluton in the immediate area is the Gold Creek stock, at the northern edge of the Mount Velma quadrangle, about 18 miles to the north. McKee (written commun., 1970) determined an age of 152 m.y., by K-Ar methods, on biotite from this stock, which, because of lack of visible deformation, is thought to be postorogenic. This date, which corresponds to Middle or early Late Jurassic (Howarth, 1964), represents the extreme lower limit of the age of thrusting, but we prefer a Triassic age for the orogeny here described.

The thrusting here documented could be attributed to either of two orogenies, evidence for which has been recognized in this part of Nevada, or possibly even to a third, hitherto unrecognized orogeny, though we tend to reject this last alternative. The two orogenies previously recognized are the Sonoma orogeny (Silberling and Roberts, 1962, p. 36) and the Lewis orogeny (Gilluly and Gates, 1965, p. 123–125).

The Sonoma orogeny and its most conspicuous manifestation, the Golconda thrust, were considered by Silberling and Roberts (1962, p. 36) as of Late Permian, pre-Koipato age.

R. C. Speed has recently (Speed, 1971) traced the Golconda thrust southward for a distance of 270 miles. He believes that the Golconda thrust is no older than early Early Triassic and no younger than Early Triassic. This age assignment is compatible with the assignment of the thrusting in the Divide Peak area to the Sonoma orogeny.

It is possible also that the orogeny that has brought the Edna Mountain and associated rocks into this area correlates with the Lewis orogeny of Gilluly and Gates (1965, p. 123–125). They are unwilling to infer so great a distance of travel of the allochthonous upper Paleozoic rocks in the Shoshone Range as we have deduced in the Divide Peak area, preferring, apparently, the hypothesis of minor additional transport of rocks that had already been moved some distance by the Golconda thrust. The maximum age of the Lewis orogeny can be inferred in part from the youngest formation involved in it, the China Mountain(?) Formation, according to Gilluly and Gates. Nichols (1971, p. 171) has recently reported that the China Mountain(?) Formation of the Shoshone Range is more properly attributable to the Middle Triassic Panther Canyon Formation (largely Ladinian in age, according to Nichols), and accordingly, the Lewis orogeny must be post-Ladinian.

REFERENCES

Axelrod, D. I., 1966, Potassium-argon ages of some western Tertiary floras: Am. Jour. Sci., v. 264, p. 497–506.

Ciriacks, K. W., 1963, Permian and Eotriassic bivalves of the middle Rockies: Am. Museum Nat. History, Bull., v. 125, art. I, 100 p., 16 pls., 4 text figs., 25 tables.

Clark, D. L., 1957, Marine Triassic stratigraphy in eastern Great Basin: Am. Assoc. Petroleum Geologists Bull., v. 41, p. 2192–2222.

Coats, R. R., 1964, Geology of the Jarbidge quadrangle, Nevada-Idaho: U.S. Geol. Survey Bull. 1141-M, 24 p.

Evans, J. G., and Ketner, K. B., 1971, Geologic map of the Swales Mountain quadrangle and part of the Adobe Summit quadrangle, Elko County, Nevada: U.S. Geol. Survey Misc. Geol. Inv. Map I-667.

Ferguson, H. G., Roberts, R. J., and Muller, S. W., 1952, Geology of the Golconda quadrangle, Nevada: U.S. Geol. Survey Geol. Quad. Map GQ-15.

Gilluly, James, and Gates, Olcott, 1965, Tectonic and igneous geology of the northern Shoshone Range, Nevada, *with sections on* Gravity in Crescent Valley, *by* Donald Plouff, and Economic geology *by* Keith B. Ketner: U.S. Geol. Survey Prof. Paper 465, 153 p.

Girty, G. H., 1910, The fauna of the phosphate beds of the Park City Formation in Idaho, Wyoming, and Utah: U.S. Geol. Survey Bull. 436, 82 p., 7 pls.

Howarth, M. K., 1964, The Jurassic period, *in* The Phanerozoic timescale: a symposium: Geol. Soc. London, Quart. Jour., v. 120 S, p. 203–205.

Nichols, K. M., 1971, Overlap of the Golconda thrust by Triassic strata, north-central Nevada: Geol. Soc. America, Abs. with Programs, v. 3, no. 2, p. 171.

Roberts, R. J., 1951, Geology of the Antler Peak quadrangle: U.S. Geol. Survey Geol. Quad. Map GQ-10.

Roberts, R. J., Hotz, P. E., Gilluly, James, and Ferguson, H. G., 1958, Paleozoic rocks of north-central Nevada: Am. Assoc. Petroleum Geologists Bull., v. 42, no. 12, p. 2813–2857.

Silberling, N. J., and Roberts, R. J., 1962, Pre-Tertiary stratigraphy and structure of northwestern Nevada: Geol. Soc. America Spec. Paper 72, 53 p.

Speed, R. C., 1971, Golconda thrust, western Nevada–Regional extent: Geol. Soc. America, Abs. with Programs, v. 3, no. 2, p. 199–200.

Van Houten, F. B., 1956, Reconnaissance of Cenozoic sedimentary rocks of Nevada: Am. Assoc. Petroleum Geologists Bull., v. 40, no. 12, p. 2801–2825.

SIGNIFICANCE OF UPPER PALEOZOIC OCEANIC CRUST IN THE UPPER CHULITNA DISTRICT, WEST-CENTRAL ALASKA RANGE

By ALLEN L. CLARK, SANDRA H. B. CLARK; and CHARLES C. HAWLEY,
Menlo Park, Calif.; Anchorage, Alaska

Abstract.—An ophiolitic assemblage (ultramafic rocks, gabbro, chert, and basalt) in the Upper Chulitna district of the west-central Alaska Range is interpreted as fragmented upper Paleozoic oceanic crust incorporated into the continent. Permian through Mesozoic rocks overlying the ophiolitic assemblage record the development of an island arc followed by deposition of marine bedded rocks on continental crust. The Tertiary record indicates nonmarine deposition and intrusion of plutonic rocks. A similar history in the eastern Alaska Range shows parallel development and environmental changes.

Recent geologic investigations in the Upper Chulitna district of the west-central Alaska Range have revealed an ultramafic-mafic complex (ophiolite) that we interpret as upper Paleozoic oceanic crust. The purpose of this report is to describe this ophiolite sequence and the associated overlying strata and to speculate on their significance in the tectonic history of the Alaska Range.

The Upper Chulitna district is located on the southeast flank of the Alaska Range (fig. 1) about 130 miles north of Anchorage, Alaska, and 10 to 15 miles south of the Denali fault (figs. 1 and 2). The geology of the region has been previously studied by Capps (1919), Ross (1933), Wahrhaftig (1958), Wahrhaftig and Black (1958), Moxham, Eckhart, and Cobb (1959), Hawley and Clark (1968), Hawley and others (1969), and Hawley and Clark (1973a, b). In these earlier studies, the ultramafic-mafic rocks were interpreted as intrusive rocks of uncertain but probable Tertiary age.

The recognition of onland oceanic crust (ophiolite sequences) in many other places along the Pacific margin (Bailey and others, 1970; Richter and Jones, 1972) prompted us to reexamine the relationships in the Upper Chulitna district, where rocks of ophiolitic character were known to occur. As a result of this examination, the earlier concept of intrusive origin for the ultramafic-mafic sequence was rejected, and we now interpret these rocks as fragments of oceanic crust incorporated into the continent.

LITHOLOGIC UNITS

The rocks of the Upper Chulitna district (fig. 2) consist of an ophiolitic sequence overlain by a thick sequence of late Paleozoic to Tertiary volcaniclastic, volcanic, and sedimentary rocks of predominantly marine and subordinantly nonmarine deposition. Southeast of the ophiolitic sequence, a siliceous argillite unit of unknown age is exposed. The late Paleozoic to Tertiary bedded rocks are intruded by Tertiary(?) plutons.

Siliceous argillite

The siliceous argillite unit is composed primarily of siliceous argillite and silty argillite. Graywacke, impure quartzite, and sparse conglomerates are locally predominant.

The age of this group of rocks is unknown. Ross (1933, p. 294) correlated these rocks with rocks described by Moffit (1915, p. 24–27, 74) in the Broad Pass region that had been assigned a Devonian age by Kirk (*in* Moffit, 1915, p. 25). Because of extensive cover and large intervening distances, this correlation is highly speculative. Additional fieldwork and study will be necessary before the age of the unit is established. The contact between the siliceous argillite unit and the ophiolite sequence is interpreted as tectonic.

Ophiolitic assemblage

The ophiolitic assemblage consists of intermixed serpentinite, gabbro, basalt, and bedded chert. The serpentinite occurs as isolated bodies in a linear belt parallel to the Upper Chulitna fault zone (Hawley and Clark, 1973b) (fig. 2). The largest masses are up to 4 miles long and 100 to 5,000 feet wide; smaller masses occur locally throughout the belt. The serpentinite is black to greenish black and ranges from massive to strongly sheared. Locally, it is altered to a quartz carbonate rock. Thin-section study shows minor amounts of relict olivine and a bastite texture, suggesting that the original rock was a pyroxene-olivine ultramafic rock. The present rock is composed mainly of clinochrysotile and lizardite. Massive chromite was found in one locality.

Fine- to medium-grained basalt and gabbro form lenticular bodies intercalated with the serpentinite and also lenses and plugs on the flanks of the main belt of serpentinite. The

U.S. GEOL. SURVEY PROF. PAPER 800-C, PAGES C95-C101

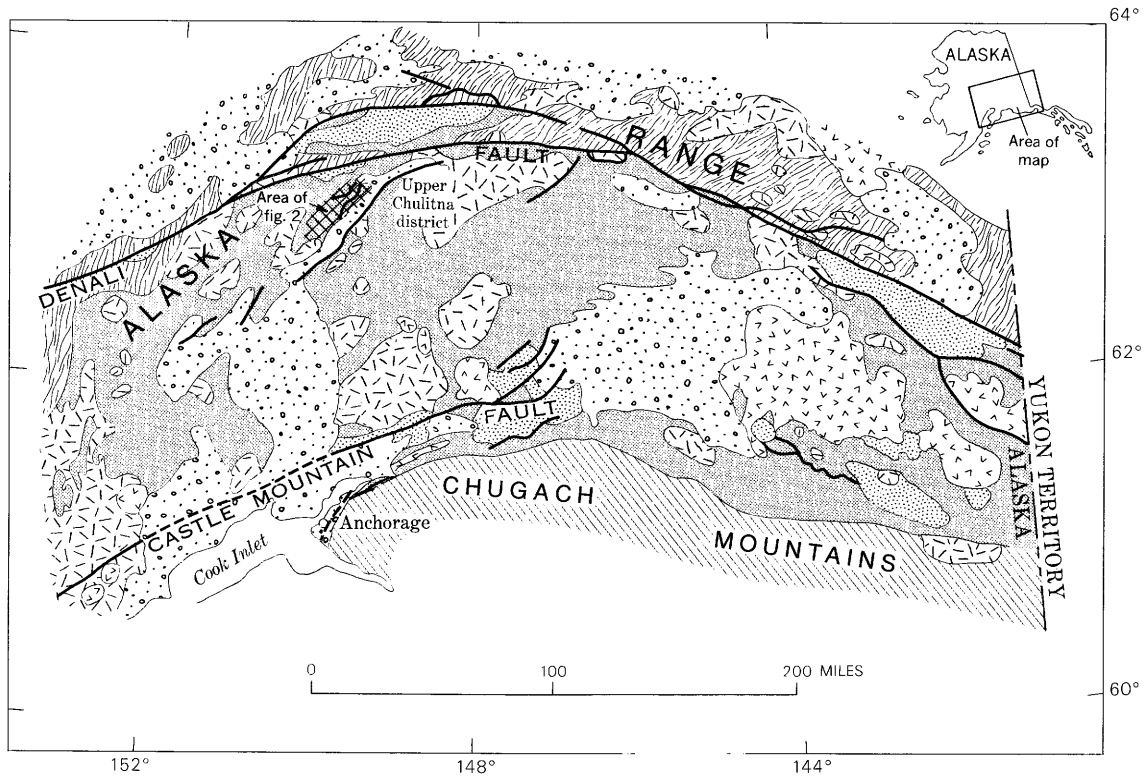

EXPLANATION

Tertiary nonmarine basinal deposits

Quaternary and Tertiary terrestrial volcanic rocks

Late Mesozoic deposits in basins on continental crust

Late Mesozoic eugeosynclinal deposits

Plutonic rocks, mostly Mesozoic to Tertiary

Late Paleozoic eugeosynclinal deposits and early Mesozoic deposits on continental crust

Middle Paleozoic and older cratonic rocks. Most are moderately to strongly metamorphosed

Contact

Fault
Dashed where concealed

Figure –Regional geologic setting of the Upper Chulitna district, Alaska. Modified from the tectonic map of North America (King, 1969).

gabbro and basalt are generally greenish black and massive. Thin-section study shows that they are composed of mainly plagioclase and pyroxene, both commonly altered, with interstitial serpentine minerals, possibly indicating the former presence of olivine. Plagioclase occurs as laths 1 to 5 mm long and 1 mm or less across. Mafic and opaque minerals fill the interstices.

The serpentinite, gabbro, and massive basalt are overlain by and locally intermixed with a sequence of approximately equal amounts of basaltic rocks, which locally show crude layering and pillow structures, and interlayered reddish-brown bedded chert and siliceous argillite. Irregular masses of red chert and carbonate are locally abundant in the basaltic layers.

The ophiolite sequence is assumed to be of Permian(?) age because it is immediately overlain by lenses of massive limestone containing Permian fossils that are described in the following section.

Volcaniclastic unit

Approximately 1,000 feet of red volcanic siltstone, sandstone, and conglomerate with interlayered limestone, tuff, sparse basalt, and, locally, quartz pebbles overlies and locally appears to grade into the ophiolitic sequence. The predominant constituents of this unit are red volcanic siltstone and conglomerate, which are interlayered on scales of a few inches to 10–20 feet. Locally, crystal tuff, massive tuff with sparse green siltstone interbeds, and volcanic conglomerate and breccia predominate. Although the conglomerate and breccia units vary widely in lithology, they are mainly volcanic pebble conglomerates with a tuffaceous matrix containing abundant crystal fragments.

Massive lenses of limestone occur near the base of the volcaniclastic sequence. These lenses contain abundant fossils, including bryzoans, crinoid columnals, pelecypods, brachiopods including *Waagenoconcha*, probably *Linoproductus*, and a large terebratuloid, *Dielasma* cf. *D. giganteum* Tschernyschew. The age of these fossils is most probably Permian, according to J. T. Dutro, Jr. (written commun., 1969).

A fossil collection from a limestone bed near the top of the volcaniclastic unit contains an abundant ammonoid fauna of Early Triassic age. The following forms were identified by N. J. Silberling (written commun., 1970):

Dieneroceras cf. *D. knechti* (Hyatt and Smith)
Euflemingites sp. indet.—immature specimen
Prosphingites cf. *P. slossi* Kummel and Steele
?Juvenites sp. indet.—immature specimen
Lanceolites bicarinatus Smith
Aspenites cf. *A. acutus* Hyatt and Smith
Arctoceras cf. *A. bloomstrangi* (Lindström)
Wyomingites sp. indet.

According to Silberling, this fauna is closely allied with the *Meekoceras gracilitatis* zone of the Western United States, as well as with the *Euflemingites romunderi* zone of northeastern British Columbia and arctic Canada and Alaska. Silberling and Tozer (1968) place these two zones in the lower Scythian Stage of the Early Triassic. This occurrence is the only Early Triassic fauna known from southern Alaska.

Limestone and basalt unit

The volcaniclastic unit is overlain by approximately 700 feet of calcareous siltstone, limestone, pillow basalt, and minor calcareous argillite. The lower part of this sequence is mainly fossiliferous limestone but locally contains volcaniclastic beds similar to those in the underlying unit. The middle part is mainly sandstone and siltstone, and the upper part is primarily massive limestone and pillow basalt. The limestone and pillow basalt sequence is locally at least 200 feet thick.

Fossils that are abundant in the limestone of the lower part are predominately pelecypods, gastropods, belemnites, ammonoids, and corals. R. W. Imlay (written commun., 1969) reported that the ammonite fragments are suggestive of a Triassic age. Ross (1933, p. 298–300) dated the limestones that contain corals as Early Triassic. The exact age of the limestone and pillow basalt in the upper part of the unit is unknown but is probably Late Triassic or Jurassic.

Argillite and graywacke unit

Overlying the limestone–pillow basalt unit are several thousand feet of fine- to coarse-grained detrital rocks. The unit's lowermost rocks are dark fine-grained argillites and cyclically interlayered graywacke and argillite. They are overlain by argillite, graywacke, and dark-matrix quartz argillite conglomerates that are lithologically similar to much of the lower Tertiary Cantwell Formation. Fossils collected from the lower argillite and graywacke include the pelecypod *Buchia sublaevis* (Imlay) of Early Cretaceous (Valangenian) age (D. L. Jones, written commun., 1968).

Plutonic rocks

The younger intrusive rocks are mainly diorite, quartz diorite, and granite that form small plugs and stocks without a dominant elongation direction. Geologic relations and recent potassium-argon dates obtained from a study now underway by M. A. Lanphere and B. L. Reed, U.S. Geological Survey (oral commun., 1971), indicate that the younger intrusive rocks are of early Tertiary age as proposed by Ross (1933, p. 305).

Nonmarine deposits

The youngest sedimentary rocks of the district are Oligocene (Hawley and Clark, 1973b). They are nonmarine, poorly consolidated arenaceous and carbonaceous rocks of the Costello Creek coal field. These rocks crop out in the extreme northeast part of the district and are either in unconformable

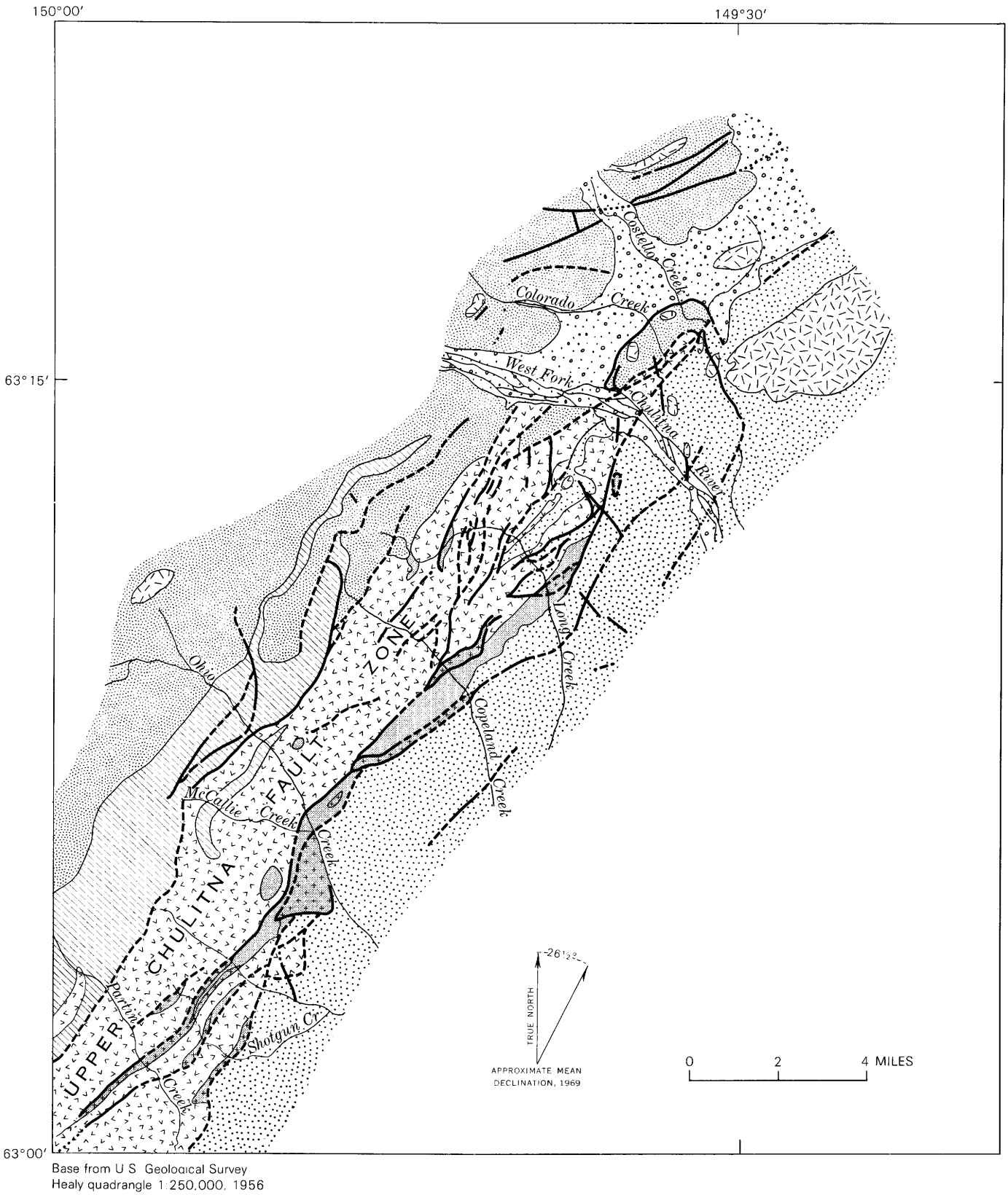

Base from U S Geological Survey
Healy quadrangle 1:250,000, 1956

Figure 2.

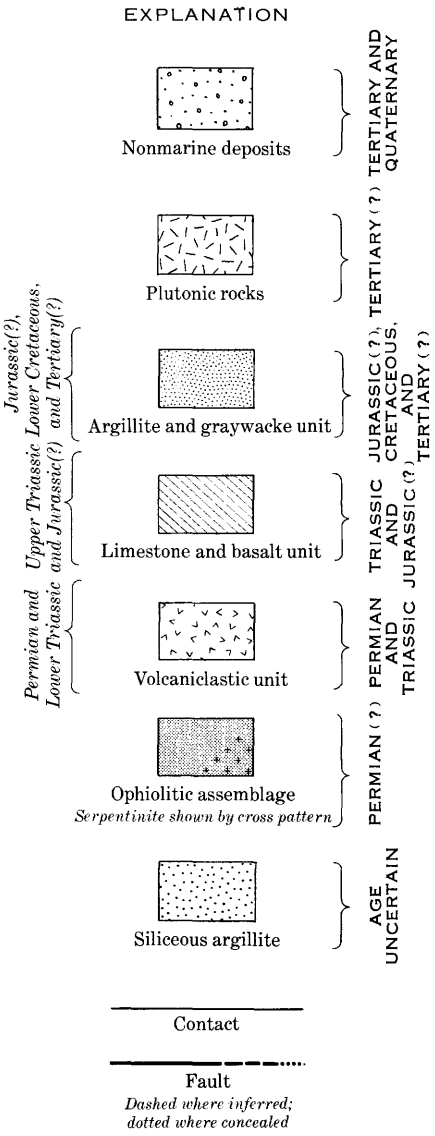

Figure 2.—Generalized geologic map of the Upper Chulitna district, Alaska. Modified from Hawley and others (1969).

or fault contact with the well-consolidated rocks of older units. The coal-bearing rocks appear to have formed in local swamps and are preserved in downwarped and downfaulted basins (Wahrhaftig, 1944).

STRUCTURE

The Upper Chulitna district is in the west-central Alaska Range south of the Denali fault, a major dextral strike-slip structure that separates the Alaska Range into two distinct geologic terranes (fig. 1). Cratonic, metamorphosed middle Paleozoic and older rocks are exposed north of the fault, whereas south of the fault the rocks are late Paleozoic and younger. The part of the Denali fault north of the Upper Chulitna district is composed of two strands, the McKinley strand on the south and the Hines Creek strand on the north. The eastern part of the Alaska Range is approximately parallel to the Denali fault (fig. 1). In the west-central Alaska Range, trends of the Denali fault and the structural trend of the Alaska Range diverge; the Alaska Range trends south-southwest toward the Alaska Peninsula, and the Denali fault trends southwest across the Kuskokwim River basin.

Rock units of the Upper Chulitna district trend approximately parallel to the trend of the Alaska Range and, although complexly folded and faulted, dip generally to the northwest, except for the southeast-dipping siliceous argillite and interlayered graywacke-argillite unit. Axial planes of asymmetric folds dip about 50° N. Major faults trend about N. 40°–50° E., approximately parallel to trends of folds and rock units and at an acute angle to the Denali fault.

INTERPRETATIONS AND COMPARISON WITH EASTERN ALASKA RANGE

The rocks of the Upper Chulitna district are interpreted in this report as recording progressive changes from oceanic crust through island-arc volcanism to a marine continental-platform environment and finally to a nonmarine basin. The record closely parallels that of the eastern Alaska Range described by Richter and Jones (1972). A summary of stratigraphy of the eastern Alaska Range, the corresponding assemblages from the Upper Chulitna district of the west-central Alaska Range, and the environments of deposition are shown in table 1.

The ophiolitic assemblage of the Upper Chulitna district is considered to be Permian(?) oceanic crust because of its resemblance to modern oceanic crust. The rocks of the overlying Permian and Triassic volcaniclastic unit indicate alternating volcanism and marine deposition. Although basalts are sparse in the unit, the clastic rock types are composed predominantly of volcanic material that imparts their characteristic red and green colors.

Because of the absence of material derived from a continental source and the proximity to the ophiolitic assemblage, the volcaniclastic rocks are thought to be derived from a volcanic island arc built directly on oceanic crust. The abundant fauna in limestones associated with the volcaniclastic rocks indicates quiet-water marine conditions at moderate to shallow depths. Recognition of the ophiolitic assemblage beneath the Permian and Triassic volcaniclastic unit in the Upper Chulitna district lends strong support to the concept of the development of a Permian island arc on oceanic crust in the eastern Alaska Range (Richter and Jones, 1972). The record of island-arc volcanism into Early Triassic time that is preserved in the west-central Alaska Range can be used to fill gaps in the record in the eastern Alaska Range.

In the Upper Triassic and Jurassic(?) limestone and basalt unit, the predominance of limestone in the lower part and absence of significant amounts of volcaniclastic rocks indicate

Table 1.—*Comparison of lithologic assemblages and depositional environments in the eastern and west-central Alaska Range*

Age	Lithologic assemblages		Depositional environment
	Upper Chulitna district of the west-central Alaska Range	Eastern Alaska Range (from Richter and Jones, 1972)	
Tertiary and Quaternary.	Arenaceous and carbonaceous sedimentary rocks, plutonic rocks.	Wrangell Lava.	Continental.
Late Cretaceous . . .	?	Nonmarine sedimentary deposits.	Continental.
Early Cretaceous . .	?	Andesitic volcanic, volcaniclastic, and minor marine sedimentary rocks.	Marine, associated volcanism in eastern Alaska Range.
Late Jurassic and Early Cretaceous.	Argillite, graywacke, and conglomerate.	Argillite and flyschlike clastic sedimentary rocks.	Marine foreland or successor basin.
Early and Middle Jurassic.	?	. . . . .	
Middle and Late Triassic.	Interlayered limestone and basalt. Limestone and calcareous siltstone.	Thin limestone beds interlayered with marine shale and cherty argillite. Massive micritic limestone. Subaerial flood basalts (submarine flows in Canada). Carbonaceous shale and limestone.	Alternating marine deposition on the continental platform with subaerial volcanism in the eastern Alaska Range and submarine volcanism in the Upper Chulitna district.
Early Triassic. . . . Permian	Volcaniclastic rocks and limestone with interlayered tuff, basalt, and locally quartz pebble conglomerate.	. . . . .	
		Black argillite and massive crinoidal limestone.	
		Marine volcanic and volcaniclastic rocks (may include rocks as old as Pennsylvanian).	Volcanic island arc, built directly on oceanic crust.
Late Paleozoic . . .	Ophiolitic assemblage; serpentinite, gabbro, basalt, and bedded chert.	Dunite locally; dunites and peridotites associated with pillow greenstone, and blueschists in the Kluane Range in Canada.	Oceanic crust.

a change in environment of deposition. The limestone and overlying clastic sequences are typical of marine continental-platform deposits. The sequence of pillow basalt and massive limestone in the upper part of the unit indicates periods of subaqueous volcanism alternating with carbonate accumulation. This sequence has its corollary in the eastern Alaska Range in a Triassic record of a general emergence of the continent and outpouring of a large volume of lava, followed by marine transgressions and the accumulation of limestones.

No definite record of Early or Middle Jurassic time has been identified in either the eastern or west-central Alaska Range. However, further south, this interval is recorded by Lower Jurassic volcanic and volcaniclastic rocks of the Talkeetna Formation and by Lower and Middle Jurassic marine sedimentary rocks in the southern Wrangell Mountains (MacKevett, 1969). In the central and southern Alaska Range, a major plutonic episode began in Early Jurassic time and continued for 25 million years (Reed and Lanphere, 1970).

The next record of sedimentation in both the eastern and west-central Alaska Range is the accumulation of marine graywackes, argillites, and conglomerates in Late Jurassic and Early Cretaceous time. These are foreland or successor-basin deposits on continental crust. Fossil *Buchia* are recorded in the marine sediments in both areas. Deposits equivalent to the Early and Late Cretaceous andesitic volcanic and nonmarine sedimentary rocks of the eastern Alaska Range (table 1) are not known in the Upper Chulitna district. The oldest nonmarine deposits in the district are of Tertiary age, but the sedimentary record of the Early and Late Cretaceous is absent, so that the environment during the time is not recorded.

REFERENCES

Bailey, E. H., Irwin, W. P., and Jones, D. L., 1970, On-land Mesozoic oceanic crust in California Coast Ranges, *in* Geological Survey Research 1970: U.S. Geol. Survey Prof. Paper 700-C, p. C70–C81.

Capps, S. R., 1919, Mineral resources of the Upper Chulitna region: U.S. Geol. Survey Bull. 692, p. 207–232.

Hawley, C. C., and Clark, A. L., 1968, Occurrences of gold and other metals in the Upper Chulitna district, Alaska: U.S. Geol. Survey Circ. 564, 21 p.

——1972a, Geology and mineral deposits of the Chulitna-Yentna mineral belt, Alaska: U.S. Geol. Survey Prof. Paper 758-A. [In press]

——1972b, Geology and mineral deposits of the Upper Chulitna district, Alaska: U.S. Geol. Survey Prof. Paper 758-B. [In press]

Hawley, C. C., Clark, A. L., Herdrick, M. H., and Clark, S. H. B., 1969, Results of geological and geochemical investigations in an area northwest of the Chulitna River, central Alaska Range: U.S. Geol. Survey Circ. 617, 19 p.

King, P. B., 1969, Tectonic map of North America: U.S. Geol. Survey, scale 1:5,000,000.

MacKevett, E. M., Jr., 1969, Three newly named Jurassic formations in the McCarthy C-5 quadrangle, Alaska, *in* Changes in stratigraphic nomenclature by the U.S. Geological Survey 1967: U.S. Geol. Survey Bull. 1274-A, p. A35–A49.

Moffit, F. H., 1915, The Broad Pass region, Alaska: U.S. Geol. Survey Bull. 608, 80 p.

Moxham, R. M., Eckhart, R. A., and Cobb, E. H., 1959, Geology and cement raw materials of the Windy Creek area, Alaska: U.S. Geol. Survey Bull. 1039-D, p. 67–100.

Reed, B. L., and Lanphere, M. A., 1970, Plutonic belts of the central and southern Alaska Range and Alaska Peninsula [abs.]: Am. Assoc. Petroleum Geologists Bull., v. 54, no. 12, p. 2502.

Richter, D. H., and Jones, D. L., 1972, The structure and stratigraphy of the eastern Alaska Range [Alaska] *in* 2d International Arctic Symposium Proc.: Am. Assoc. Petroleum Geologists Mem., v. 54, no. 12, p. 2502.

Ross, C. P., 1933, Mineral deposits near the West Fork of the Chulitna River, Alaska: U.S. Geol. Survey Bull. 849-E, p. 289–333.

Silberling, N. J., and Tozer, E. T., 1968, Biostratigraphic classification of the Marine Triassic in North America: Geol. Soc. America Spec. Paper 110, 63 p.

Wahrhaftig, Clyde, 1944, Coal deposits of the Costello Creek basin, Alaska: U.S. Geol. Survey open-file report, 7 p.

——1958, Quaternary geology of the Nenana River Valley and adjacent parts of the Alaska Range: U.S. Geol. Survey Prof. Paper 293-A, p. 1–68.

Wahrhaftig, Clyde, and Black, R. F., 1958, Engineering geology along part of the Alaska Railroad: U.S. Geol. Survey Prof. Paper 293-B, p. 69–118.

TERRANES OF THE WESTERN PALEOZOIC AND TRIASSIC BELT IN THE SOUTHERN KLAMATH MOUNTAINS, CALIFORNIA

By WILLIAM P. IRWIN, Menlo Park, Calif.

Abstract.—The western Paleozoic and Triassic belt of the Klamath Mountains is herein subdivided from west to east into the Rattlesnake Creek, Hayfork, and North Fork terranes, further emphasizing the previously known composite nature of the province. The Rattlesnake Creek terrane is dominantly ophiolitic, includes appreciable soda granite, is structurally incompetent, and contains many deposits of chromite and manganiferous chert. The Hayfork terrane is in large part andesitic, includes the syenodioritic Ironside Mountain batholith, is relatively competent, and contains lode-gold deposits. The North Fork terrane is also ophiolitic, but metalliferous deposits similar to those of the Rattlesnake Creek terrane seem nearly absent. All three terranes include lenses of Permian limestone, but the Rattlesnake Creek terrane also includes Triassic limestone. The lithologies of the terranes suggest that the Rattlesnake Creek and North Fork terranes are tectonic slices of oceanic crust and that the Hayfork terrane originated as an island arc.

The western Paleozoic and Triassic belt is the most extensive of several concentric lithic belts that constitute the Klamath Mountains of northwestern California and southwestern Oregon (fig. 1). It was defined during a reconnaissance of the northern Coast Ranges and Klamath Mountains of California in the 1950's (Irwin, 1960) and at that time was recognized as a catchall for a variety of formations that vary widely not only in lithology but also in probable age. Reexamination of some parts of the southern Klamath Mountains during the past decade has led to the presently proposed subdivision of the western Paleozoic and Triassic belt. This report is preliminary in the sense that its principal theme is based largely on geologic mapping still in progress.

The western Paleozoic and Triassic belt in the southern Klamath Mountains is herein subdivided into three concentric subbelts of rocks that are referred to, from west to east, as the Rattlesnake Creek, Hayfork, and North Fork terranes (fig. 2). The term "terrane" as used herein refers to an association of geologic features, such as stratigraphic formations, intrusive rocks, mineral deposits, and tectonic history, some or all of which lend a distinguishing character to a particular tract of rocks and which differ from those of an adjacent terrane.

The concentric distribution of the three terranes is parallel to that of other lithic belts of the Klamath Mountains

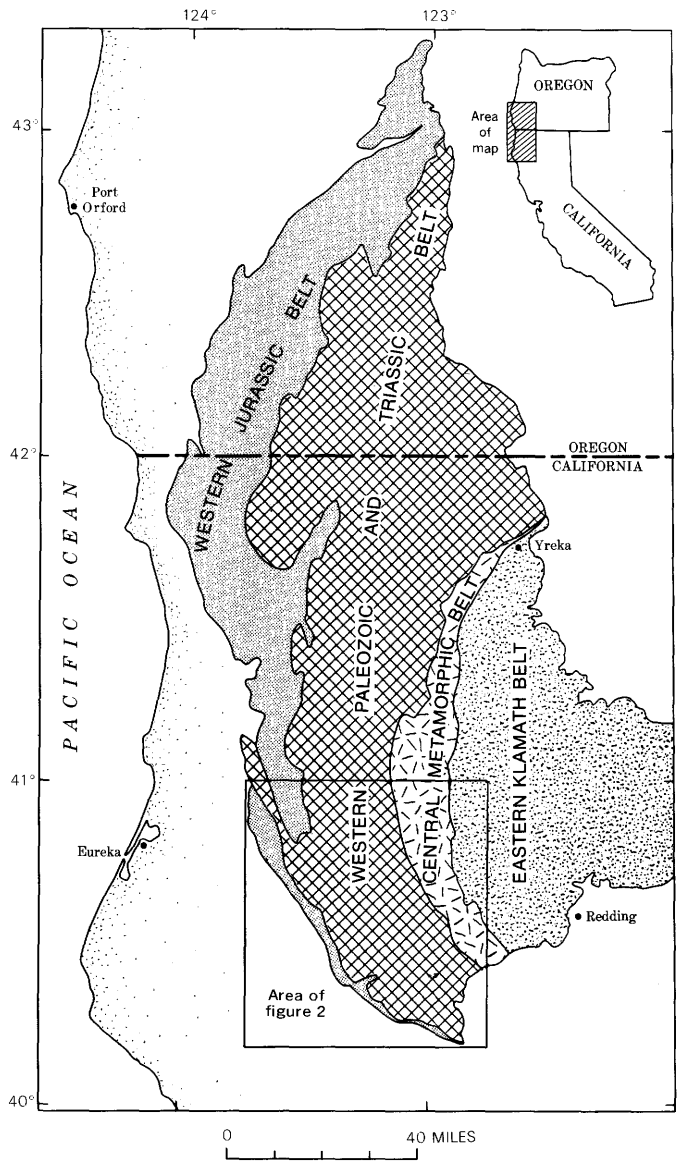

Figure 1.—Generalized map showing the lithic belts of the Klamath Mountains province of California and Oregon.

U.S. GEOL. SURVEY PROF. PAPER 800-C, PAGES C103-C111

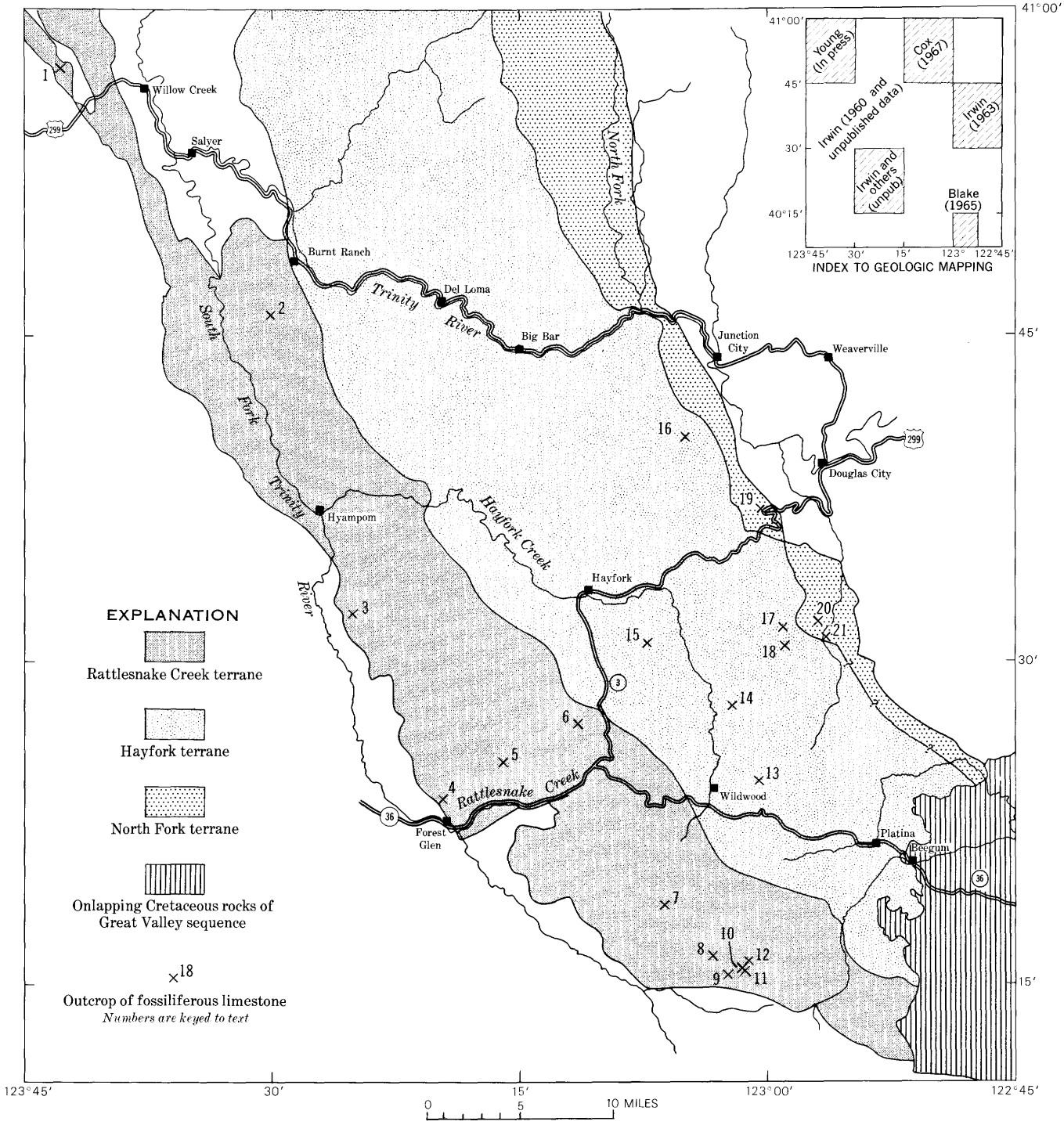

Figure 2.—Distribution of the Rattlesnake Creek, Hayfork, and North Fork terranes in the southern Klamath Mountains, Calif., showing fossiliferous limestone localities.

province, and in this respect the proposed subdivision of the western Paleozoic and Triassic belt further emphasizes the highly composite nature of the province as it is crossed from west to east. The Rattlesnake Creek terrane is bordered on the west for nearly its entire length by metasedimentary Galice Formation of the western Jurassic belt. In the northern part it is separated from the Hayfork terrane by the Galice Formation and terminates a few miles north of the area shown in figure 2 (see fig. 1). The North Fork terrane is bordered along its eastern side in the southern Klamath Mountains by the Salmon

Hornblende Schist (Devonian or older Paleozoic) of the central metamorphic belt. The southernmost extent of the North Fork terrane has not been mapped, and is inferred as shown on figure 2. The terranes of the western Paleozoic and Triassic belt are overlapped with great unconformity by Cretaceous strata of the Great Valley sequence at the south end of the Klamath Mountains province.

RATTLESNAKE CREEK TERRANE

The Rattlesnake Creek terrane is named after Rattlesnake Creek, which crosscuts much of that terrane in the Pickett Peak and Dubakella Mountain quadrangles. The terrane consists predominantly of serpentinized ultramafic rocks, gabbro, diabase, pillow lavas and other mafic volcanic rocks, phyllite, thin-bedded radiolarian chert, discontinuous lenses of limestone, and locally interbedded sandstone and pebble conglomerate. The rocks generally are metamorphosed to low greenschist facies, and the strata are considerably disarrayed by folding and faulting. The prevailing character of the terrane is that of a dismembered ophiolite suite. Leucocratic silicic igneous rocks are conspicuous in the eastern part of the terrane and probably include both soda granite and soda rhyolite; their structural and temporal relations to the rocks of more ophiolitic aspect are not clear. Plutons that range from hornblende diorite to biotite-hornblende-quartz diorite are sparsely scattered throughout the terrane. The Rattlesnake Creek terrane is one of structurally incompetent rocks, as indicated by an abundance of landslide features.

HAYFORK TERRANE

The Hayfork terrane is named after the town of Hayfork, which lies within the broad belt of that terrane in the Hayfork quadrangle. The terrane appears from reconnaissance to consist mainly of a layered structural sequence of three formations, and of syenodiorite of the Ironside Mountain batholith. The lowest formation of the sequence consists of distinctive augite-andesite metavolcanic rocks and locally attains a thickness of several thousand feet. It is succeeded upward by a formation consisting of slaty argillite, sandstone, pebble conglomerate, and thin-bedded chert, with sparse lenses of limestone and limestone breccia generally in the upper part of the formation. The third and uppermost formation consists of mafic volcanic rocks, thin-bedded chert, phyllite, quartzite, siliceous leucocratic volcanic rocks, and occasional lenses of limestone. Ultramafic rocks, so conspicuous in the Rattlesnake Creek terrane, occur at only a few places in the Hayfork terrane. The rocks of the Hayfork terrane generally are competent to sustain steep hillsides, and, in contrast to the Rattlesnake Creek terrane, landslides are a relatively minor feature of the landscape. In this regard, the syenodiorite and augite andesite are particularly outstanding, as they tend to form steep-walled canyons where cut by Hayfork Creek and the Trinity River.

NORTH FORK TERRANE

The North Fork terrane is named after the North Fork of the Trinity River, which flows through much of that terrane in the Helena quadrangle. It occupies a narrower belt in the southern Klamath Mountains than either the Rattlesnake Creek or Hayfork terranes. Serpentinite, gabbro, and diabase form a practically continuous selvage along the western side of the belt of the North Fork terrane, and these are succeeded to the east by pillow lavas, greenstone, mafic volcaniclastic rocks, thin-bedded radiolarian chert, limestone lenses, chert-limestone breccia, phyllite, and locally sandstone and pebble conglomerate. The lithic assemblage is dominantly that of an ophiolite suite, although an undisturbed normal lithostratigraphic ophiolite sequence has not been seen.

LIMESTONE AND FOSSILS

Limestone crops out sparsely in all three terranes of the western Paleozoic and Triassic belt. Traces of fossils are found in many of the limestone bodies, but fossils suitably preserved for precise age determination are found only in a few of them. The limestone occurs as deformed lenses and pods that commonly are 10 to 20 feet thick and are traceable for a few hundred feet. A few are as much as 200 feet thick and traceable for several hundred to several thousand feet. All are to some degree tectonically deformed and recrystallized. See table 1 for data on the fossiliferous limestone localities shown in figure 2.

The earliest significant search for fossils in limestone of the western Paleozoic and Triassic belt was carried out during a brief yet remarkably perceptive reconnaissance in 1902 by J. S. Diller in company with T. W. Stanton. On the basis of a meager collection of fossils, Diller (1903) concluded that the limestone bodies form a "southwestern Devonian belt" and a "southwestern Carboniferous belt." Limestone bodies of his "southwestern Devonian belt" are in the Rattlesnake Creek terrane; those of his "southwestern Carboniferous belt" are in the Hayfork and North Fork terranes.

The Devonian age for limestones of the Rattlesnake Creek terrane tends to be discounted by more recent study. Diller's designation of a Devonian age for these limestone lenses was based mainly on a collection of ammonites at one locality near White Rock, and on a coral-like fossil he found at localities 1, 3, 4, 6, and 7 (fig. 2) and which was referred to the genus *Chaetetes*. Reexamination of the original collection of ammonites, and additional collections from presumably the same locality (locality 10) near White Rock, show the ammonites to be Late Triassic (Karnian) rather than Devonian (Silberling and Irwin, 1962). In addition, the fossils that were referred to *Chaetetes* are not now considered determinable in age.

Limestone lenses in the Rattlesnake Creek terrane have been searched intensively for fossils during the past decade by the writer and others, but remarkably few have yielded diagnostic

Table 1.—*Fossiliferous limestone localities in the western Paleozoic and Triassic belt of the southern Klamath Mountains, Calif.*

Map No. (fig. 2)	Field No. or notation	Location[1]	Source data
		Rattlesnake Creek terrane	
1.....	Three Forks Creek.	T. 7 N., R. 4 E.	Diller (1903, p. 346).
2.....	WC.....	NW¼ sec. 34, T. 5 N., R. 6 E.	Young (unpub. data.), and this report.
3.....	D-711.....	NW¼ sec. 29(?), T. 2 N., R. 7 E.	Diller (1903).
4.....	D-709, 709a, 710, I-71-7.	W½ sec. 12, T. 29 N., R. 7 E.	Diller (1903), and this report.
5.....	P-1358.....	Center E. edge sec. 33, T. 30 N., R. 8 E.	This report.
6.....	D-707.....	1½ miles southwest of Peanut.	Diller (1903).
7.....	D-703, 706, I-68-30.	NE¼ sec. 4, T. 28 N., R. 11 W.	Do.
8.....	61-1.....	SW¼ sec. 13, T. 28 N., R. 11 W.	This report.
9.....	I-68-37.....	SW¼ sec. 19, T. 28 N., R. 10 W.	Do.
10.....	D-705.....	Center E½ sec. 19, T. 28 N., R. 10 W.	Diller (1903), and Silberling and Irwin (1962).
11.....	D-704.....	Center W½ sec. 20, T. 28 N., R. 10 W.	Diller (1903).
12.....	I-68-33.....	Center NW¼ sec. 20, T. 28 N., R. 10 W.	This report.
		Hayfork terrane	
13.....	D-702, 61-7, I-68-29.	SE¼ sec. 32, T. 30 N., R. 10 W.	Diller (1903), Irwin (1960), and this report.
14.....	D-701.....	Center W½ sec. 7, T. 30 N., R. 10 W.	Diller (1903).
15.....	I-68-32, I-70-18.	NW¼ of NW¼ sec. 28 (projected), T. 31 N., R. 11 W.	This report, and Merriam (1972).
16.....	I-70-32.....	NW¼ sec. 35 (projected), T. 33 N., R. 11 W.	This report.
17.....	W-318.....	SE¼ of NW¼ of NW¼ sec. 22, T. 31 N., R. 10 W.	Do.
18.....	T-63.....	SE¼ of NW¼ sec. 27, T. 31 N., R. 10 W.	Do.
		North Fork terrane	
19.....	W-57-28c	Center sec. 21, T. 32 N., R. 10 W.	Irwin (1960).
20.....	T-11.....	SW¼ of SW¼ sec. 13, T. 31 N., R. 10 W.	This report.
21.....	W-324, T-9...	Center S½ sec. 24, T. 31 N., R. 10 W.	Do.

[1]Land net is from Willow Creek (ed. 1952), Hyampom (ed. 1951), Pickett Peak (ed. 1954), Dubakella Mtn (ed. 1954), Hayfork (ed. 1951), and Weaverville (ed. 1950) 15-minute quadrangles.

fossils. Limestone collected by N. J. Silberling and the writer at locality 8 was examined by R. C. Douglass, who stated (written commun., 1963) that it contains the small fusulinid *Staffella* that elsewhere in the United States is found in deposits ranging from Middle Pennsylvanian into Permian. Limestone collected by the writer at locality 5 was examined by B. L. Mamet, who stated (written commun., 1970) that it contains good *Tetrataxis* and some apterinellid "ghosts," and that the possible age is early Carboniferous to Permian. Mamet also examined limestone collected by J. C. Young and R. H. Raschen at locality 2 and stated (written commun., 1970) that the limestone contains apterinellids, nodosariids, and *Pachyphloia* sp. and is undoubtedly Permian in age. The only suggestion of a Devonian age for limestone of the Rattlesnake Creek terrane is the presence of rugose corals at locality 12. The corals were examined by C. W. Merriam, who reported (written commun., 1968):

> ***[the] coral, although well preserved, is much deformed. It is a *Billingsastraea*-like thamnastraceoid colonial genus lacking outer wall, differing from *Billingsastraea* in possessing much thickened tapering septa. The nearest form structurally known to me is a specimen collected from the Kennett limestone***. For the present I would consider it to be of possible Devonian age. The dissepiments and character of septa would appear to eliminate the possibility of Mesozoic, in spite of the proximity of Triassic beds***.

In the Hayfork terrane, fossils of determinable age have been found in limestone at several widely spaced localities. The southernmost locality (loc. 13, fig. 2) is at Hall City Cave near Wildwood, where an ammonite collected by Diller was identified as Permian in age by J. P. Smith (Diller, 1903). On later examination the ammonite was considered to indicate a middle or Late Permian age (Miller and others, 1957). From the same locality, limestone collected by D. P. Cox was examined by L. G. Henbest, who identified foraminifers including *Staffella*, *Ozawainella*, or possibly *Eoverbeekina* (written commun., 1956). The foraminiferal assemblage was considered by Henbest to be neither older than Middle Pennsylvanian nor younger than middle Permian, and most likely Permian (see Irwin, 1960, p. 26). Additional material (61-7) from the Hall City Cave locality, collected by N. J. Silberling and the writer, is reported by R. C. Douglass (written commun., 1970) to contain broken and deformed specimens of a fusulinid probably referable to the genus *Cuniculinella*, as described by Skinner and Wilde (1965) in zone F of the Wolfcampian part of the McCloud Limestone.

The most prolific fauna of the Hayfork terrane has come from collections made by D. L. Jones and the writer at the Mueller mine area (loc. 15) about 10 miles northwest of Hall City Cave and 3 miles southeast of Hayfork. There the limestone occurs as abundant subrounded to subangular pebbles and cobbles in conglomerate. The stratigraphic position of the conglomerate is not precisely known but is at the approximate boundary between the argillite-chert formation and the overlying formation. The limestone fragments clearly are transported, as some are seen to contain fossils that are truncated at the boundary of the fragment, and as some adjacent fragments contain different faunas. One fragment (I-70-18A) examined by R. C. Douglass (written commun., 1970) contained ostracodes, bryozoans, gastropods, some small foraminifers including an undetermined textularid and *Tetrataxis* sp., *Pseudofusulinella* sp., and fragments of a

fusulinid with schwagerinid wall structure; this fragment is no older than Late Pennsylvanian and no younger than Early Permian. Another (I-70-18B) contained the smaller foraminifer *Climacammina* sp. and the fusulinids *Pseudofusulinella* sp. and *Schwagerina* sp., and is of Early Permian age (R. C. Douglass, written commun., 1970). Still another contained abundant specimens of *Staffella* sp., and although the range of the genus is from earliest Pennsylvanian into the Permian, the specimens suggest an Early Pennsylvanian age (R. C. Douglass, written commun., 1970). A collection of silicified gastropods (I-70-18), etched from a large fragment by C. W. Merriam, was examined by E. L. Yochelson, who stated (written commun., 1970) that the collection is similar though far superior to those from the McCloud Limestone and is almost certainly Wolfcampian (Early Permian) in age. A single fragment consisting mainly of a well-preserved rugose coral is the only evidence to suggest that limestone of widely different ages may be mixed in the Mueller mine area. The coral most nearly resembles but differs somewhat from *Shastaphyllum schucherti*, which is found in the Gazelle Formation (Silurian) of the eastern Klamath Mountains (Merriam, 1972).

Ten miles north-northeast of the Mueller mine, tectonically stretched fusulinids are abundant in one of several limestone lenses near the crest of a ridge that divides the upper reaches of Dutch and Soldier Creeks (loc. 16). The fossiliferous limestone is at an altitude of 4,050 feet just east of a gap in the ridge, about 1,900 feet east-northeast of hill 4688 (Hayfork 15 minute quadrangle). According to R. C. Douglass (written commun., 1970), the fusulinids have a schwagerinid wall and tight fluting, at least in the lower part of the chambers, and although they cannot be identified generically, an Early Permian age assignment is reasonable.

A conspicuous limestone mass caps the ridge between the upper fork of the East Fork of Hayfork Creek in southwestern Weaverville quadrangle (see Irwin, 1963) and is associated with mafic volcanic rocks and chert of the Hayfork terrane. A sample collected from the southern end of the limestone mass (loc. 18) was examined by B. L. Mamet, who stated (written commun., 1970) that it contains *Cribrogenerina* sp., dasyclad algae, *Macroporella?* sp., miliolids, and paleotextulariids, and that the age is undoubtedly Permian. A short distance north of the main limestone mass, float from small limestone lenses in the volcanic rock (loc. 17) also was examined by Mamet, who reported (written commun., 1970) that it contains *Tetrataxis*, *Pachyphloia*, apterinellids, cornuspirids, nodosariids, cf. *Protonodosaria* sp., and paleotextulariids, and that it is undoubtedly Permian in age.

In the North Fork terrane, fossils of determinable age have been found at three localities (loc. 19, 20, and 21, fig. 2). Limestone from locality 19 is reported by L. G. Henbest (see Irwin, 1960, p. 26) to contain fusulinids that indicate a Late Pennsylvanian or Early Permian age. Abundant microfossils occur in a small (2 by 6 foot) limestone lens (loc. 21) in volcanic rocks, exposed in Browns Creek about 200 feet upstream from the mouth of Maupin Gulch. According to R. C. Douglass (written commun., 1961), the microfossils include textularid foraminifers and *Schwagerina* spp. He stated that

> two species of *Schwagerina* are probably represented, one elongate form with axial filling, and the other more robust and without axial filling. The species are all distorted and are not easily compared with previously described species. Their general stage of evolution suggests Lower Permian age, McCloud equivalent. Neither of the forms present are considered to be as old as the fusulinids [from loc. 19].

A nearby limestone lens, about 30 feet upstream, is much more coarsely crystalline and contains unusually large crinoid stems. In Johnson Gulch, about a mile from its mouth, fossiliferous limestone float (loc. 20) was found in an area of dominantly volcanic rocks. According to B. L. Mamet (written commun., 1970), the limestone float contains endothyrid ghosts referrable to *Endothyra* of the group *E. prisca*, and is lower Carboniferous to Permian in age.

Although the data are sparse, the known distribution of fossils in the report area suggests that the chaetetids and fusulinids are almost mutually exclusive in occurrence (fig. 3). The limestone lenses that contain chaetetids (loc. 1, 3, 4, 6, and 7, fig. 2) were early recognized to closely follow the South Fork of the Trinity River (Diller, 1903). All the known

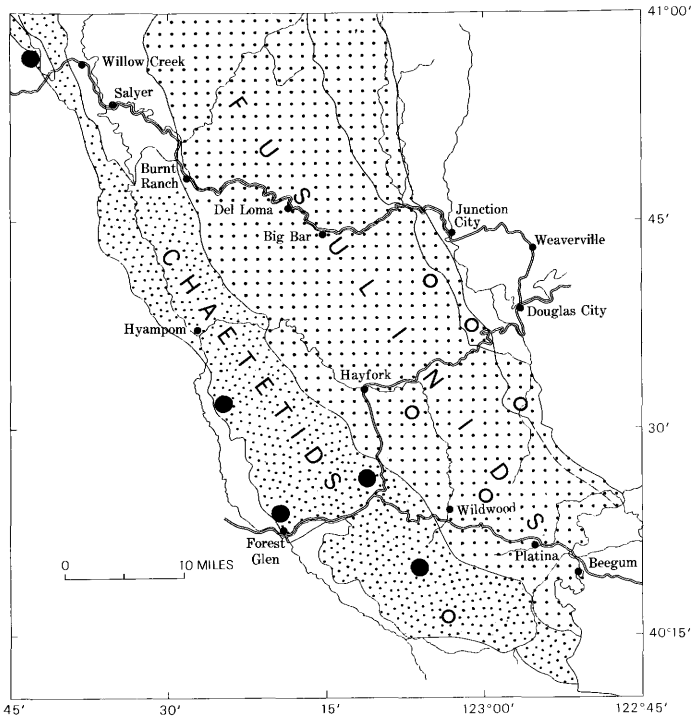

Figure 3.—Apparent distribution of chaetetids and fusulinids in the western Paleozoic and Triassic belt of the southern Klamath Mountains. Chaetetid localities indicated by solid circles, fusulinid localities by open circles.

chaetetid-bearing limestone lenses are in the Rattlesnake Creek terrane. Fusulinid localities (loc. 13, 15, 16, 19, and 21) are comparably abundant in the Hayfork and North Fork terranes, and only one (loc. 8) is known in the Rattlesnake Creek terrane. The virtual restriction of the chaetetid and fusulinid faunas to specific terranes enhances the subdivisions of the western Paleozoic and Triassic belt that are based primarily on lithologic differences. However, the significance of the faunal distribution cannot be assessed until the age of the chaetetid-bearing limestone is known.

METALLIFEROUS DEPOSITS

Deposits of chromite, manganese, and lode gold occur in the western Paleozoic and Triassic belt. Each of these mineral commodities tends to be restricted to a single terrane rather than being randomly distributed throughout all three. Most of the reported deposits of chromite and manganese in the report area are in the Rattlesnake Creek terrane. The lode-gold deposits are restricted to the Hayfork terrane.

The chromite deposits occur in the ultramafic rocks, generally as pods, segregation layers, and disseminated grains. In the area of this report, the locations of 51 chromite prospects (fig. 4) were reported by Wells and Hawkes (1965, pl. 19). Most are in the Rattlesnake Creek terrane, 10 are shown in the Hayfork terrane, and only one is in the North Fork terrane. Those shown in the Hayfork terrane are located with questionable accuracy, according to Wells and Hawkes, and it is likely that most if not all of those would be seen to lie in the Rattlesnake Creek terrane if accurately located. The preponderance of chromite prospects in the Rattlesnake Creek terrane is reasonable, as that terrane has the greatest area of outcrop of ultramafic rock. However, ultramafic rock also crops out over a considerable area in the North Fork terrane, and a disparity between the great number of chromite prospects located in the Rattlesnake Creek terrane and the single prospect located in the North Fork terrane is obvious. The ratio of area of ultramafic rock in the Rattlesnake Creek terrane to that in the North Fork terrane is perhaps 3 or 4 to 1, in contrast to a ratio of nearly 40 or 50 to 1 in number of prospects located. A similar disproportion in numbers of chromite prospects relative to area of outcrop of ultramafic rocks was noted by Wells and Hawkes (1965, p. 178) for the Trinity Alps area of the central Klamath Mountains. Present data are insufficient to determine whether a lack of chromite prospects indicates a difference in composition of the ultramafic magma, insufficient concentration of chromite to be of commercial interest, or failure of prospectors to locate such deposits—although Wells and Hawkes (1965) seemed to reject the last possibility.

The manganese deposits of the western Paleozoic and Triassic belt occur in lenses of thin-bedded radiolarian chert and are probably syngenetic with the chert. The primary ore minerals, rhodochrosite and bementite, are mostly metamorphosed to rhodonite and spessartite (Trask and others, 1943). Tephroite, an orthosilicate of manganese, probably also is widely present (Hewett and others, 1961). Most of the manganese deposits occur in lenses of chert that are reddish or purplish in color, rather than in those that are shades of gray. In the vicinity of ore bodies, fracture surfaces of surficially exposed chert commonly are stained black by manganese oxides. Of 38 deposits known in the report area (fig. 5), all are in the Rattlesnake Creek terrane except for three in the Hayfork terrane; surprisingly, none is reported in radiolarian chert of the North Fork terrane.

Gold-bearing quartz veins have been prospected and mined at various places along the length of the western Paleozoic and Triassic belt. Lode-gold mines and prospects in the report area (fig. 5) are restricted to the Hayfork terrane. Two additional prospects (Yellow Surprise and Watson) mentioned by Averill (1933) and O'Brien (1965) are not shown, as they are near terrane boundaries and as location data are insufficient to determine within which terrane they actually occur. The lode-gold deposits of the Hayfork terrane commonly occur in the chert-argillite unit that overlies the augite andesite. The distribution of placer gold reflects that of the lode deposits, although somewhat more disperse. Considerable placer gold has been mined from creeks that drain the Hayfork terrane, but little has been obtained where the drainage is confined to the Rattlesnake Creek terrane. Some creeks in the North Fork terrane have been productive, but most of that gold probably came from veins in the Devonian metamorphic rocks to the east.

CONCLUSIONS

As earlier subdivided (Irwin, 1960), the Klamath Mountains province was considered to consist of four concentric lithic belts separated by east-dipping thrust faults. Each of the presently proposed subdivisions (terranes) of the western Paleozoic and Triassic belt is considered to be as important a structural element as any of the original lithic belts, and thus the number of recognized major structural elements is increased to six. The name "western Paleozoic and Triassic belt" will be obsolete when the undivided part of the belt remaining in the central and northern Klamath Mountains is subdivided. It is noteworthy that although the total span in age represented by rocks of the three terranes is not known, evidence for a Permian age is found in all three terranes, but evidence for a Triassic age is found only in the Rattlesnake Creek terrane. This relationship follows the previously recognized pattern of the thrust plates of the Klamath Mountains tending to be successively younger to the west (oceanward).

Although the three terranes are at least in part the same age (Permian), they are markedly different in lithology and other parameters. The ophiolitic aspect of the Rattlesnake Creek and North Fork terranes may suggest that they formed as oceanic

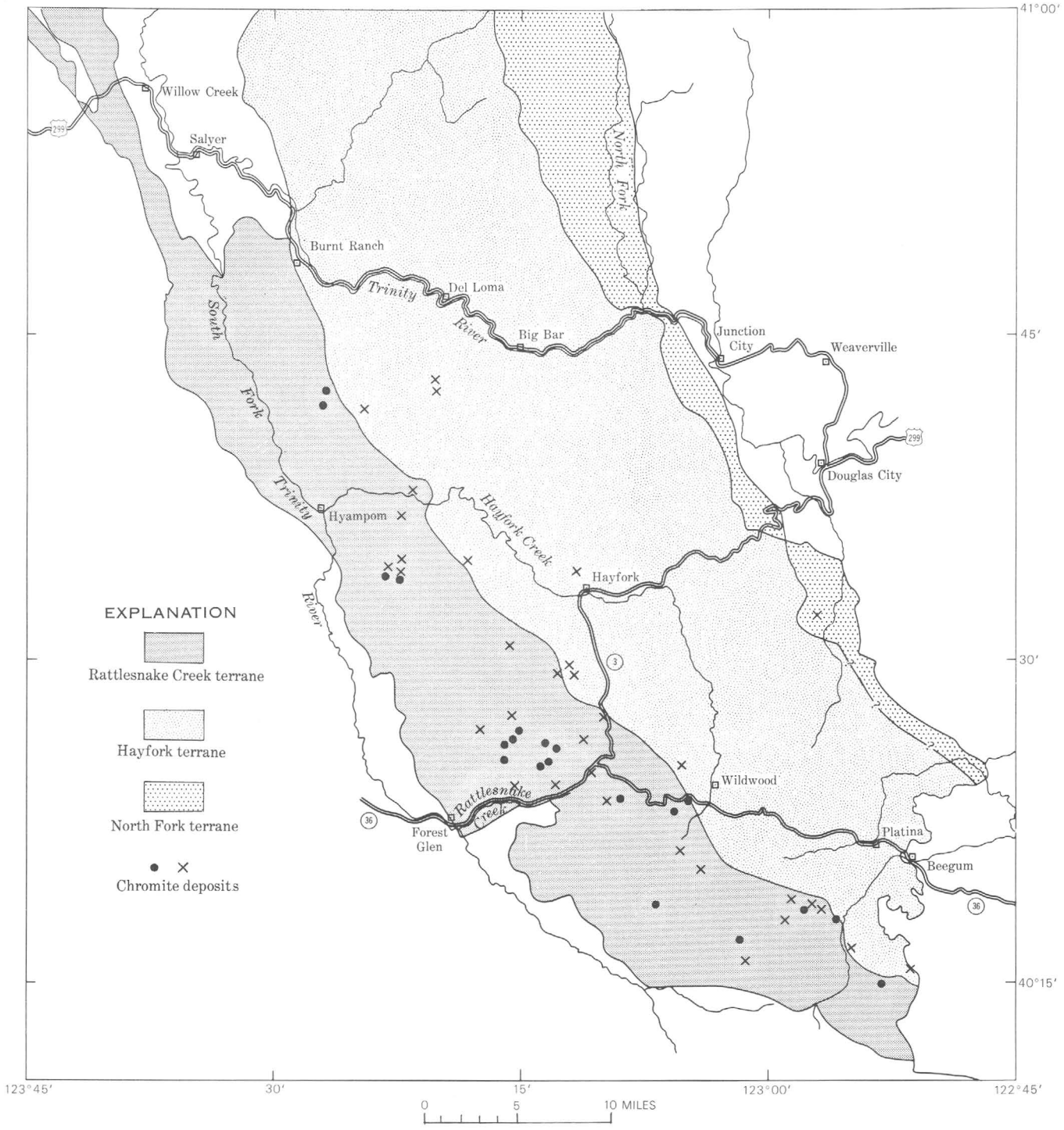

Figure 4.—Relation of chromite deposits to terranes of the western Paleozoic and Triassic belt in the southern Klamath Mountains. Distribution of chromite deposits is adapted from Wells and Hawkes (1965, pl. 19). Solid circles, deposits considered by Wells and Hawkes to be accurately located; crosses, deposits that may not be accurately located.

crust. The andesitic character of much of the Hayfork terrane suggests possible origin as an island arc. The apparent juxtaposition of the terranes is most readily explained by considering them to have been widely separated when formed, and subsequently to have been telescoped together along east-dipping thrust faults. In the context of the seafloor-spreading hypothesis, the various terranes may represent skimmed-off fragments of crust that successively have accreted to the western edge of North America along subduction zones, perhaps in the general style described by Hamilton (1969).

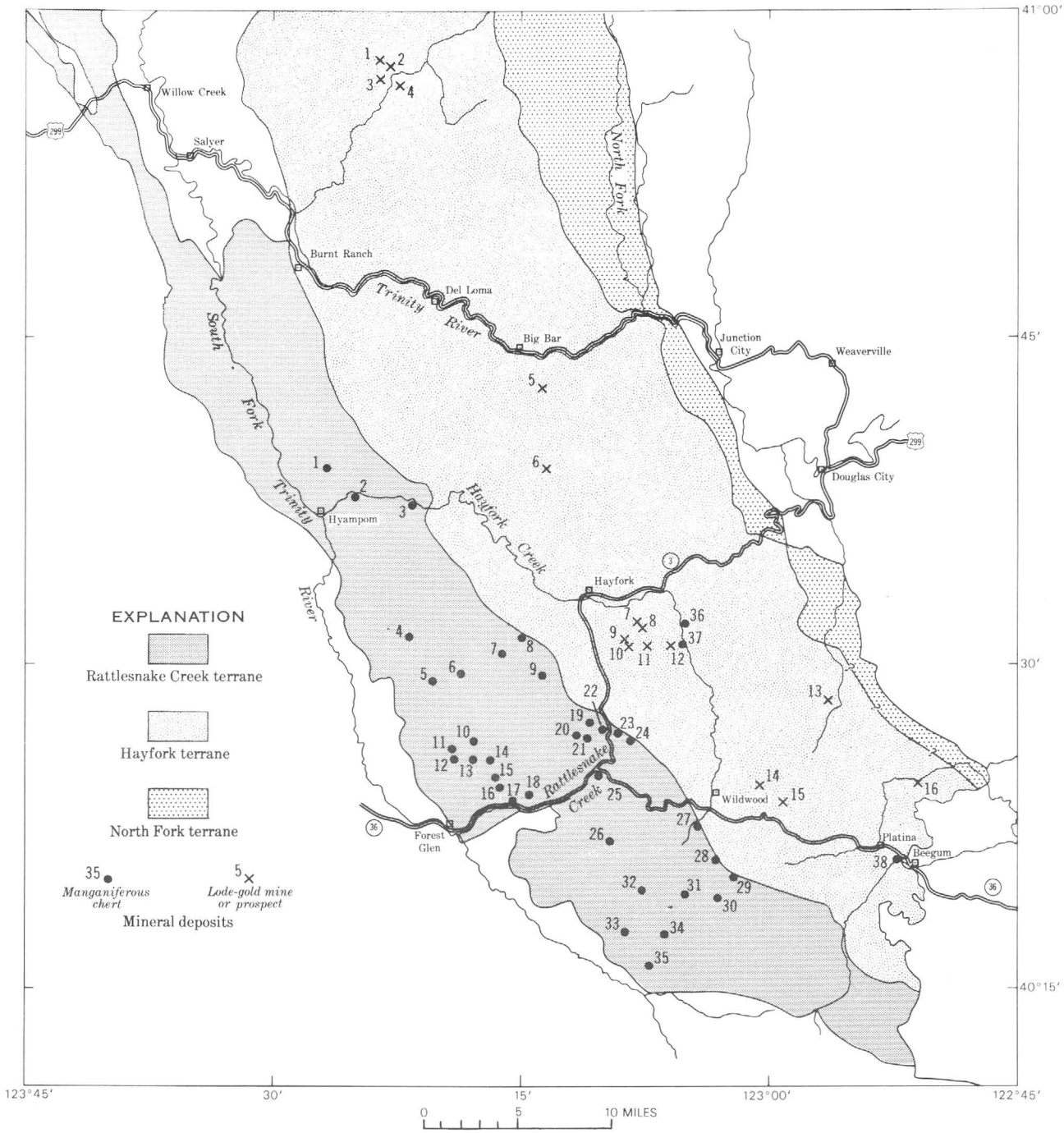

Figure 5.—Relation of manganiferous chert and lode-gold mines and prospects to the terranes of the western Paleozoic and Triassic belt in the southern Klamath Mountains. Data for manganiferous chert localities are from Trask and others (1950), with additions. Data for lode-gold mines and prospects are from Averill (1933, 1941) and O'Brien (1965), with additions. List of mines and prospects below: manganese, first 38; lode gold, sccond 16.

1—Big Rock
2—Name unknown
3—American Manganese No. 1 and No. 2
4—Snow Camp
5—No name
6—No name
7—Carr, Carrie, and Louella
8—Two Sugar Pines
9—Plummer Peak
10—Four Point
11—Arrowhead, Black Susan, Gool, and Whitman
12—Cedar Springs
13—Last Chance
14—Jaybird
15—Munson
16—Big Buck and The Manganese
17—Lucky Star
18—Rattlesnake
19—No name
20—No name
21—No name
22—Dry Lake
23—Salt Creek
24—Salt Creek No. 2 and No. 3
25—Manganese Queen
26—High Lead
27—Foss
28—Skaggs
29—Victor
30—Goat Camp
31—Sylvester-Wilson and Weed
32—Black Hawk and Jewett
33—Murphy-Bramlette
34—Lucky Bill
35—Spider
36—Reichert and Cliff
37—Last Hope and Woods
38—Nicol

1—Index
2—Slake Shack
3—Hazel D
4—Beartooth
5—Poor Boy
6—Kattmeier
7—Kelly
8—Layman
9—Kellogg
10—Farmer
11—Mueller
12—Scorpion
13—Chancelulla
14—Hall City
15—Midas
16—Bell Cow

REFERENCES

Averill, C. V., 1933, Gold deposits in the Redding and Weaverville quadrangles, *in* 29th report of the State Mineralogist: California Jour. Mines and Geology, v. 29, nos. 1 and 2, p. 2–73.

——1941, Mineral resources of Trinity County, *in* 37th report of the State Mineralogist: California Jour. Mines and Geology, v. 37, no. 1, p. 8–89.

Blake, M. C., Jr., 1965, Structure and petrology of low-grade metamorphic rocks, blueschist facies, Yolla Bolly area, northern California: Stanford Univ., unpub. Ph. D. thesis, 91 p.

Cox, D. P., 1967, Reconnaissance geology of the Helena quadrangle, Trinity County, California: California Div. Mines and Geology Spec. Rept. 92, p. 43–55.

Diller, J. S., 1903, Klamath Mountain section, California: Am. Jour. Sci., ser. 4, v. 15, p. 342–362.

Hamilton, Warren, 1969, Mesozoic California and the underflow of Pacific mantle: Geol. Soc. America Bull., v. 80, no. 12, p. 2409–2430.

Hewett, D. F., Chesterman, C. W., and Troxel, B. W., 1961, Tephroite in California manganese deposits: Econ. Geology, v. 56, no. 1, p. 39–58.

Irwin, W. P., 1960, Geologic reconnaissance of the northern Coast Ranges and Klamath Mountains, California: California Div. Mines and Geology Bull. 179, 80 p.

——1963, Preliminary geologic map of the Weaverville quadrangle, California: U.S. Geol. Survey Mineral Inv. Field Studies Map 275. [1964]

Merriam, C. W., 1972, Silurian rugose corals of the Klamath Mountains region, California: U.S. Geol. Survey Prof. Paper 738. [In press]

Miller, A. K., Furnish, W. M., Jr., and Clark, D. L., 1957, Permian ammonoids from western United States: Jour. Paleontology, v. 31, no. 6, p. 1057–1068.

O'Brien, J. C., 1965, Mines and mineral resources of Trinity County, California: California Div. Mines and Geology County Rept. 4, 125 p.

Silberling, N. J., and Irwin, W. P., 1962, Triassic fossils from the southern Klamath Mountains, California: Art. 23 *in* U.S. Geol. Survey Prof. Paper 450-B, p. B60–B61.

Skinner, J. W., and Wilde, G. L., 1965, Permian biostratigraphy and fusulinid faunas of the Shasta Lake area, northern California: Kansas Univ. Paleont. Contr., Protozoa, Art. 6, 98 p.

Trask, P. D., Wilson, I. F., and Simons, F. S., 1943, Manganese deposits of California, a summary report: California Div. Mines Bull. 125, p. 51–215.

Trask, P. D., and others, 1950, Geologic description of the manganese deposits of California: California Div. Mines Bull. 152, 378 p.

Wells, F. G., and Hawkes, H. E., 1965, Chromite deposits of Shasta, Tehema, Trinity, and Humboldt Counties, California, *in* Geological investigations of chromite in California: California Div. Mines and Geology Bull. 134, pt. 1, no. 3, p. 130–191.

Young, J. C., 1972, Geology of the Willow Creek quadrangle, California: California Div. Mines and Geology. [In press]

OFFSHORE EXTENSION OF THE ROSE CANYON FAULT, SAN DIEGO, CALIFORNIA

By GEORGE W. MOORE, La Jolla, Calif.

Abstract.—Northwest of San Diego, a possible offshore extension of the Rose Canyon fault has been recognized in a net of subbottom acoustic profiles spaced about 5 km apart. The fault zone, which appears to cut Holocene sediment on the sea floor, ranges from about 0.5 km wide along straight segments to as much as 2 km wide at curves. Projection of the zone farther north suggests that the Rose Canyon fault may be related to the Newport-Inglewood fault system; to the south, it may join the San Miguel fault in Baja California.

The Rose Canyon fault, which has been recognized since the reconnaissance mapping of Fairbanks (1893, p. 96), is a major geologic structure in the San Diego region. Its zone of faulting is locally more than 1 km wide, and it cuts Cretaceous and Tertiary sedimentary rocks that are generally nearly flat lying but dip moderately to steeply within and near the fault zone (Kennedy and Moore, 1971, fig. 5). On land in the city of San Diego, displacements associated with the Rose Canyon fault occur along a length of 16 km. To the southeast the fault is covered by San Diego Bay, and to the northwest it extends under the Pacific Ocean.

The Rose Canyon fault is subparallel with the San Andreas, Elsinore, and other well-known strike-slip faults to the east in California. In 1954, Corey extrapolated the Rose Canyon fault under the Pacific to the northwest on the basis of its onshore alinement and a paleogeographic reconstruction that explained known onshore sedimentary facies. This extrapolation has been accepted with slight modification by later investigators (Emery, 1960; Bayley and Muehlberger, 1968; King, 1969), but it has not previously been verified by subbottom profiling.

In 1969, several air-gun crossings of the inferred trace of the Rose Canyon fault were made using the research vessel *Oconostota* of Scripps Instititution of Oceanography. Faults were discovered, and the mapping was improved in 1970 by means of a sparker survey conducted from the RV *Polaris* of the U.S. Geological Survey. For the *Polaris* cruise, Hirex radionavigation provided horizontal positioning with an accuracy of about 10 m. Offshore geologic structures crossed by the *Polaris* and the *Oconostota* are plotted on figure 1, which shows a zone of faults and folds that extends at least 60 km northwest of the exposures on land.

The deformation of rock units along the zone commonly appears on the profiles as offsets of subbottom acoustic reflectors (fig. 2, profile B–B'). In places, rocks within the zone are compressed into folds (fig. 2, profile C–C'). Sedimentation is rapid in this coastal area, and displacement of nearshore surficial sediment seen at the sea floor on the profiles (fig. 2, profile C–C') suggests that the faulting is of Holocene age.

The recency of faulting indicated by the submarine evidence is compatible with known displacement of Pleistocene deposits on land (Peterson, 1970; Kennedy and Moore, 1971). Such deformation is especially well shown by warping and faulting of the Lindavista Formation, a reddish-brown marine-terrace deposit, 2–10 m thick, named by Hanna (1926) after Lindavista, a railroad junction at lat 32°53′ N., long 117°11′ W. This formation is herein considered to be lower Pleistocene, because it is less deformed than the underlying Pliocene San Diego Formation, and because its molluscan fauna, while lacking typical Pliocene species such as *Patinopecten healeyi*, contains *Pecten bellus*, an extinct species not known from late Pleistocene or younger deposits (G. L. Kennedy, written commun., 1971). The Lindavista Formation generally stands at an altitude of about 120 m in the San Diego area. Where cut by the Rose Canyon fault at La Jolla, however, the formation, which presumably was nearly planar originally, is now warped upward to 250 m. The greatest local uplift lies adjacent to an S-shaped bend in the Rose Canyon fault (fig. 3). This uplift is believed to have resulted from compression there as a consequence of right-lateral strike-slip movement along the fault.

No large earthquakes have been associated with the Rose Canyon fault during historic time. During 1964, however, three earthquakes in the magnitude range of 3.5–3.7 were felt along the fault in the vicinity of San Diego Bay (table 1).

Creep has not been recognized along the Rose Canyon fault, but Peterson (1970) has noted that the Bay Point Formation, named for Bay (Crown) Point in Mission Bay by Hertlein and Grant (1939), has been uplifted about 30 m near the fault in La Jolla. The Bay Point Formation, which is about 3 m thick, overlies the Lindavista Formation and is considered to be late

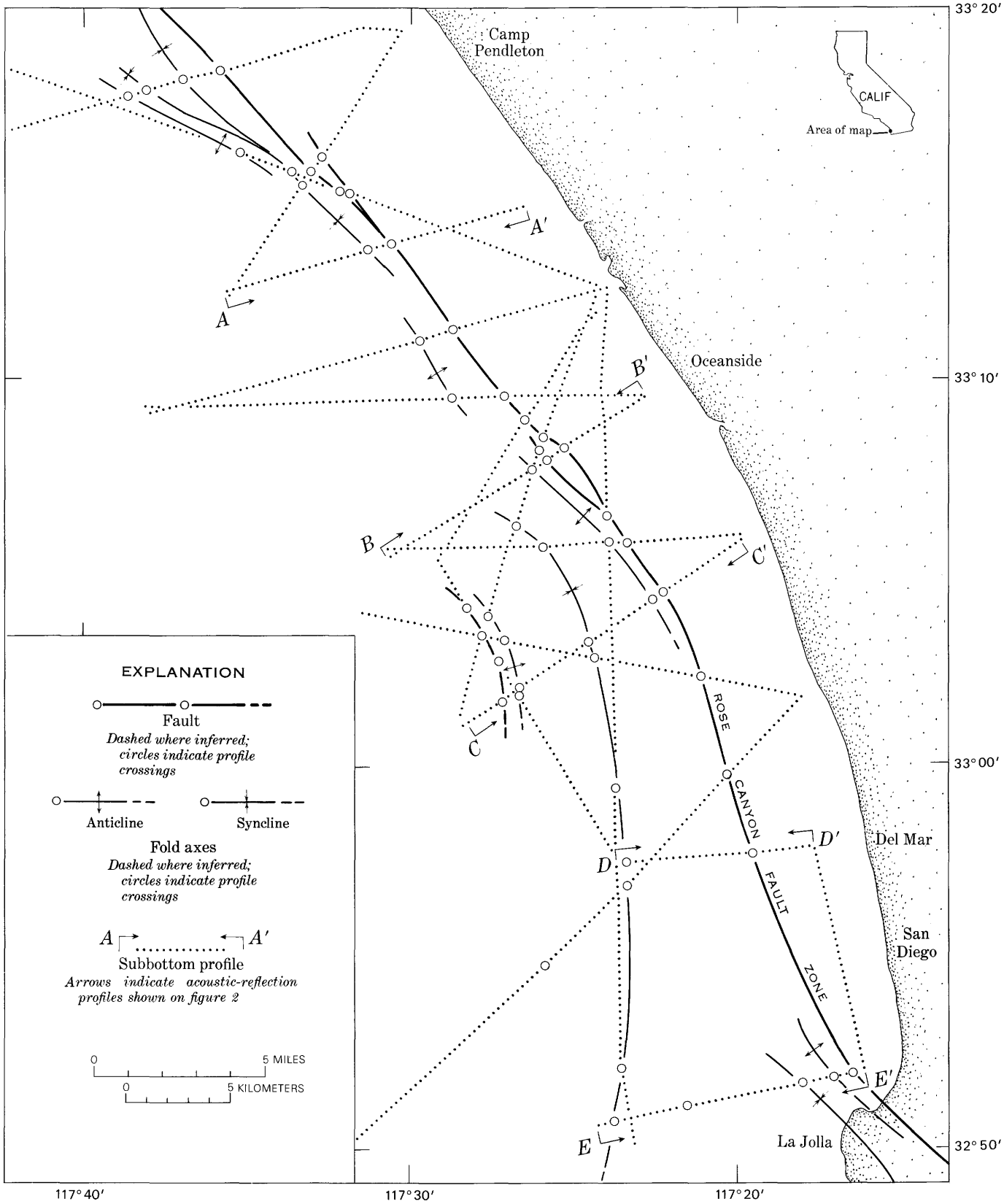

Figure 1.—Tectonic map of the sea floor northwest of San Diego, Calif.

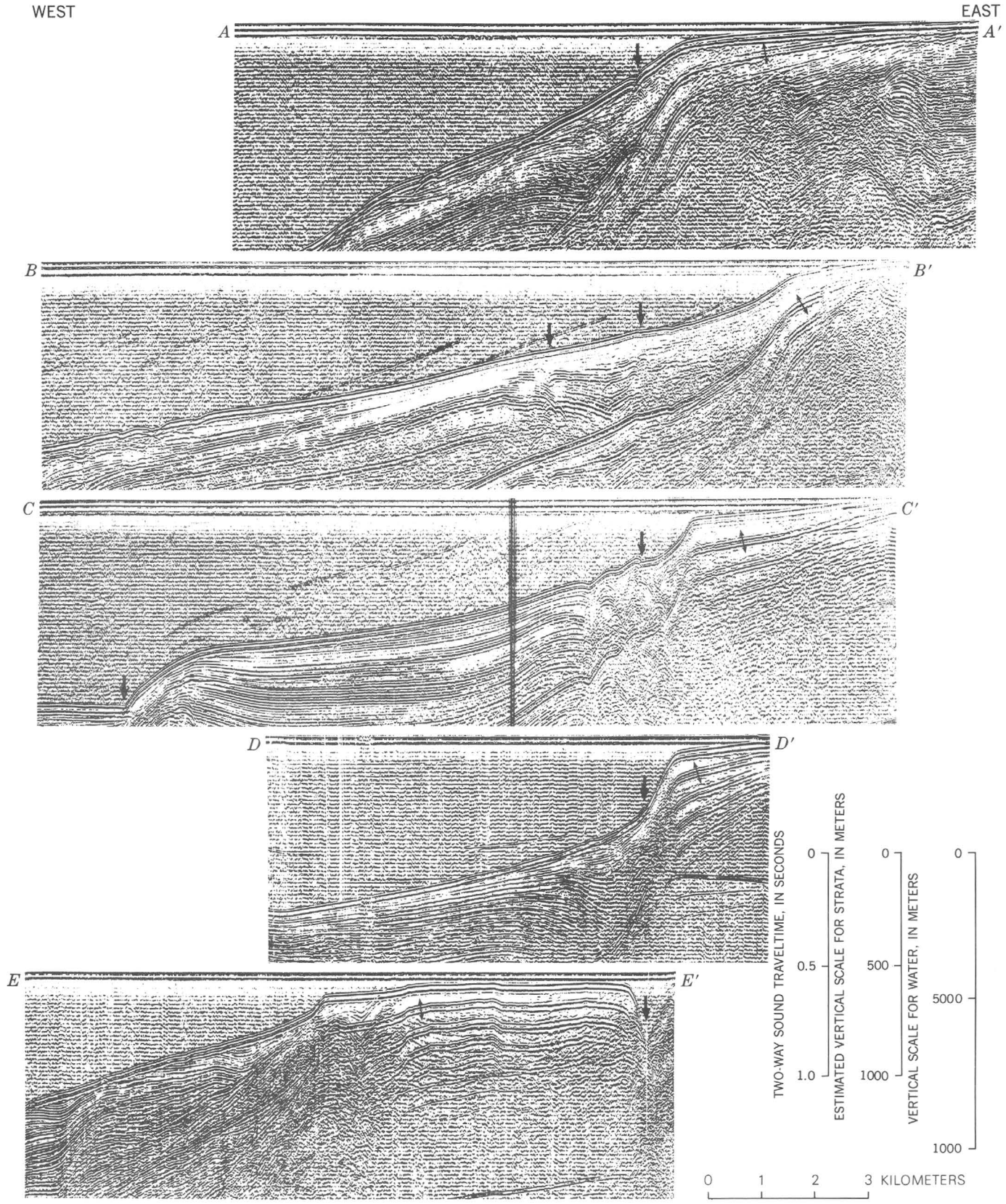

Figure 2.—Acoustic reflection profiles across the Rose Canyon fault zone. Single-ended arrows indicate the fault crossings shown on figure 1; double-ended arrows indicate multiple reflections. Owing to minor changes in ship speed along the tracks, the horizontal scale locally may be in error by as much as 10 percent.

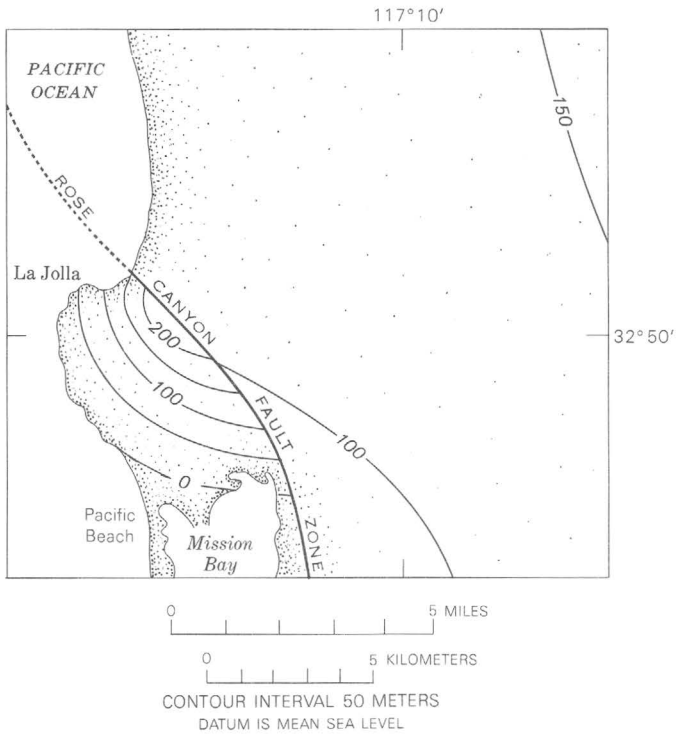

Figure 3.—Structure contours on the base of the Lindavista Formation of early Pleistocene age, showing uplift adjacent to an S-shaped bend in the Rose Canyon fault.

Table 1.—*Earthquakes of magnitude 3.5–3.7 near the trace of the Rose Canyon fault in 1964*

[After Richter and others (1967)]

Time (P.s.t.)	Date	Coordinates		Magnitude	Maximum intensity
		Lat N.	Long W.		
07:32:51.8	June 21	32°41.5′	117°09.7′	3.7	VI at Coronado and San Diego.
20:54:37.5	June 22	32°41.4′	117°07.4′	3.6	VI at Imperial Beach.
19:11:05.8	July 14	32°42.3′	117°06.8′	3.5	V at Chula Vista and San Diego.

Pleistocene (Sangamon), or about 100,000 years old, on the basis of its extensive molluscan fauna, which was most recently studied by Kern, Stump, and Dowlen (1971).

Corey (1954) and the other previously cited investigators that extrapolated the Rose Canyon fault to the northwest connected it with the Newport-Inglewood fault zone, near which the 1933 Long Beach earthquake of magnitude 6.3 occurred. The offshore evidence of the present study agrees with such a projection, at least as far north as Camp Pendleton. The location of the Rose Canyon fault is less certain to the southeast beyond San Diego Bay; it might follow the alluvial valley of the Río Tijuana in Baja California (Moore and Kennedy, 1970; Wiegand, 1970). If this is correct, the Rose Canyon fault could connect farther south with the San Miguel fault, on which an earthquake of magnitude 6.8 occurred in 1956.

REFERENCES

Bayley, R. W., and Muehlberger, W. R., 1968, Basement rock map of the United States: U.S. Geol. Survey, scale 1:2,500,000, two sheets.

Corey, W. H., 1954, Tertiary basins of southern California, [pt.] 8 *in* Chap. 3 *of* Jahns, R. H. ed., Geology of southern California: Calif. Dept. Nat. Resources Div. Mines Bull. 170, p. 73–83.

Emery, K. O., 1960, The sea floor off southern California: New York, John Wiley and Sons, 336 p.

Fairbanks, H. W., 1893, Geology of San Diego County: California State Mining Bur. Rept. 11, p. 76–120.

Hanna, M. A., 1926, Geology of the La Jolla quadrangle, California: California Univ., Dept. Geol. Sci. Bull., v. 16, p. 187–246.

Hertlein, L. G., and Grant, U. S., 4th, 1939, Geology and oil possibilities of southwestern San Diego county [Calif.]: California Jour. Mines and Geology, v. 35, p. 57–78.

Kennedy, M. P., and Moore, G. W., 1971, Stratigraphy and structure of the area between Oceanside and San Diego, California: California Univ. (Riverside) Mus. Contr., no. 1, p. 149–166.

Kern, J. P., Stump, T. E., and Dowlen, R. J., 1971, An upper Pleistocene marine fauna from Mission Bay, San Diego, California: San Diego Soc. Nat. Hist. Trans., v. 16, p. 329–338.

King, P. B., 1969, Tectonic map of North America: U.S. Geol. Survey, scale 1:5,000,000, two sheets.

Moore, G. W., and Kennedy, M. P., 1970, Coastal geology of the California–Baja California border area: Am. Assoc. Petroleum Geologists, Pacific Sec., Fall 1970 Guidebook, p. 4–9.

Peterson, G. L., 1970, Quaternary deformation patterns of the San Diego area, southwestern California: Am. Assoc. Petroleum Geologists, Pacific Sec., Fall 1970 Guidebook, p. 120–126.

Richter, C. F., Nordquist, J. M., Taylor, V., and Allen, C. R., 1967, Local bulletin of earthquakes in the southern California region, 1 January 1963 to 31 December 1966: Pasadena, California Inst. Technology Seismol. Lab., 34 p.

Wiegand, J. W., 1970, Evidence of a San Diego Bay–Tijuana fault: Assoc. Eng. Geologists Bull., v. 7, p. 107–121.

SEISMIC TRAVELTIMES AND NEAR-SURFACE CRUSTAL VELOCITY STRUCTURE BOUNDING THE SAN ANDREAS FAULT ZONE NEAR PARKFIELD, CALIFORNIA

By S. W. STEWART and M. E. O'NEILL, Menlo Park, Calif.

Abstract.—A detailed seismic-refraction study was conducted within the aftershock region of the magnitude-5.5 Parkfield, Calif., earthquake of June 28, 1966, primarily to provide local traveltime data and near-surface velocity models to further the precision in locating aftershocks associated with the main event. In the aftershock region, the northwest-trending San Andreas fault zone separates a crustal block of granitic basement southwest of the zone from a crustal block of intensely deformed Franciscan Formation northeast of the zone. Within these two crustal blocks, two reversed seismic profiles, each about 17 km long, were established parallel to, and a few kilometers from, the San Andreas fault zone. Seismic traveltimes within the southwestern (granitic) block are systematically delayed by 0.5 to 0.9 seconds with respect to traveltimes in the northeastern (Franciscan) block. The delay is accounted for by a Tertiary sedimentary cover about 1 to 2 km thick overlying the granitic basement. Pronounced near-surface lateral variations in seismic velocity exist on both sides of the fault zone. The near-surface crustal velocity models presented for the two crustal blocks are appropriate for use in computer-oriented earthquake location programs.

The Parkfield-Cholame region of central California has long been recognized as an active seismic region along the San Andreas fault zone. Earthquakes accompanied by surface fracture occurred in this region in 1857, 1901, 1922, and 1934 (Brown and Vedder, 1967). McEvilly, Bakun, and Casaday (1967) estimate that the earthquakes of 1901, 1922, and 1934 had Richter magnitudes near 6.

On June 28, 1966, at 0426 G.m.t. an earthquake of magnitude 5.5 occurred near Parkfield (fig. 1). This earthquake was accompanied by a zone of surface fracturing that propagated along the mapped expression of the San Andreas fault zone from Parkfield to the town of Cholame, approximately 23 km to the southeast. The instrumentally determined epicenter of the main shock (McEvilly and others, 1967) is near the northwest end of the fracture zone. Aftershock activity associated with the earthquake was quite large (Eaton and others, 1970). During the first hour, about 240 aftershocks could be identified on records from a seismograph station located within the aftershock region (fig. 1, station 11), and 10 days later identifiable aftershocks were occurring at a rate of approximately 2 or 3 per hour (Eaton, 1967).

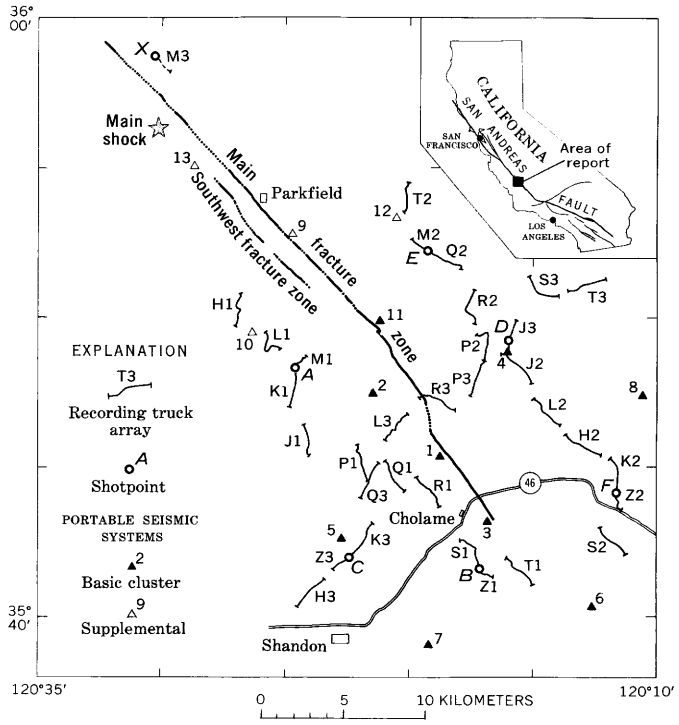

Figure 1.—Index map showing shotpoints and location of seismic instrumentation with respect to zones of ground fracture accompanying the Parkfield, Calif., earthquake of June 1966.

Within a few days of the main shock, the U.S. Geological Survey installed eight portable seismic recording systems southeast of the instrumentally determined epicenter, near the town of Cholame (fig. 1). Subsequently, the number of recording stations was increased to 13. It was expected that the vastly different geologic structures brought into contact by the San Andreas fault zone in this region might be expressed as systematic variation in seismic traveltimes, resulting in relatively poor determinations of locations for the many aftershocks being recorded. Preliminary locations determined for a few of the aftershocks recorded during the first month suggested that this was indeed the case. Further, it appeared

that aftershocks were occurring at relatively shallow depths, mainly from 1 to 6 km.

It became clear that a detailed seismic-refraction survey of the aftershock region would contribute greatly toward resolving many uncertainties in the velocity structure of the upper crust and most likely would lead to increased precision in locating aftershocks. The refraction survey would concentrate on determining the velocity structure to depths of only a few kilometers on both sides of the San Andreas fault zone.

This paper describes the methods and results of the refraction experiment designed to provide crustal velocity models appropriate to a computer-oriented earthquake location program. The aftershocks themselves have been described in another paper (Eaton and others, 1970).

GEOLOGIC SETTING

Within the central California Coast Ranges, right-lateral strike-slip movement along the San Andreas fault zone has brought together crustal blocks of remarkably dissimilar type. Southwest of the fault zone, the basement rocks consist of "*** Early(?) Cretaceous granitic intrusives and older metamorphic rocks"; northeast of the fault zone, of "*** a Jurassic-Cretaceous eugeosynclinal assemblage—the Franciscan rocks" (Page, 1966). These basement rocks may either crop out over large areas adjacent to the San Andreas fault zone or be covered by varying thicknesses of later Mesozoic or Cenozoic sedimentary or volcanic rocks.

The main geologic features of the area covered by the seismic-refraction survey have been summarized by Brown and Vedder (1967). In the Parkfield-Cholame area, the granitic basement of the crustal block southwest of the San Andreas fault zone is covered by marine and nonmarine sedimentary and volcanic rocks, chiefly of middle and late Miocene and of Pliocene age. Most of the surface exposures, however, consist of Pliocene or Quaternary alluvium and other poorly consolidated sedimentary rocks of continental origin. Although granitic rocks associated with this crustal block crop out about 7 km northwest of Parkfield and 13 km south of Cholame, drill-hole data indicate that basement is more than 1 km below sea level within the region of profile A–B of figure 1 (Smith, 1964). Structure and stratigraphy within the southwest block are relatively simple. The sedimentary rocks may be tightly folded close to the fault zone, but a few kilometers away the folds are open and have dips of approximately 10° to 20° (Brown and Vedder, 1967).

The crustal block northeast of the San Andreas fault zone is characterized by more complex structural and stratigraphic relations. Dickinson (1966) subdivides this block into four regions, progressively farther from the San Andreas fault zone, as follows:

> Four adjoining subparallel structural domains with common northwesterly trend can be recognized on the basis of geomorphology and style of deformation: (1) the San Andreas rift belt of fault scarps and related primary features along straight active fault traces and slightly bent dormant fault traces; (2) the San Andreas fault zone of intricately sliced bedrock, including exotic fault slivers and strongly flexed fault surfaces with varying dips; (3) a domain of superimposed folds and faults of different ages showing evidence of strike-slip offset roughly proportional to their ages; and (4) a domain of open folds beside the Great Valley.

Seismic profile E–D–F (fig. 1) is situated roughly along the northeast margin of zone 3 described above, within the Maxey fault belt (Dickinson, 1966). Within this region, highly folded and faulted Tertiary strata unconformably overlie the Franciscan Formation, which is intensely brecciated and deformed in this area. Northwest-trending anticlinal and synclinal structures constitute the main structural grain of the region. Closer to the San Andreas fault zone, the deformation is more intense, and slivers of crystalline rock of unknown origin crop out (Brown and Vedder, 1967). Depth to the Franciscan rocks in this region varies widely owing to intense deformation and complex structural relations. Within the vicinity of profile E–D–F, rocks assigned to the Franciscan Formation crop out at the surface, whereas a few kilometers northeast of Cholame, Franciscan rocks are buried by 300 to 1,000 m of material, as shown by drill-hole data (summarized by W. F. Hanna, written commun., 1970). Brown and Vedder (1967) suggest a depth to crystalline basement underlying the Franciscan Formation greater than 4,000 m in many places.

PLAN OF THE SEISMIC-REFRACTION SURVEY

The purpose of the seismic-refraction survey was primarily to define velocity structure in the upper few kilometers of crustal material for both sides of the San Andreas fault zone and only secondarily to study the fault zone itself or to provide "known" seismic traveltimes within the region to aid in precisely estimating epicentral locations. Accordingly, the two profiles A–B and E–D–F were established parallel to the fault zone, but a few kilometers from it. One profile, C–D, was established across the fault zone (fig. 1). Each profile was about 17 km long and was shot so as to obtain reversed subsurface coverage. In addition, a larger shot (X) was set off near the instrumental epicenter and recorded along the transverse profile, C–D (fig. 1). Data from the transverse profile are not discussed in this report.

Nine truck-mounted seismic-refraction recording units were used, each recording with an array of six vertical-component seismometers placed at intervals of one-half kilometer along a spread 2½ km long. The output of the seismometers was recorded on an FM magnetic tape system as well as on a conventional oscillographic recorder. Details of recording instrumentation and general field procedures may be found in Warrick and others (1961) and Jackson and others (1963).

The seismic-refraction survey was carried out approximately 2½ months after the main shock. By that time the possibility of an aftershock interfering with the explosion recording seemed remote. Shot sizes, times, and locations have been reported by Eaton (1967).

ANALYSIS OF THE DATA

Traveltime data for shots and recording points on each side of the fault zone are plotted in figure 2. Timing resolution is about ±0.01 second. The difference in seismic traveltimes on both sides of the fault zone is striking, confirming the value of obtaining these data to aid in earthquake location. A difference in seismic traveltimes of 0.5 second is not unusual. An extreme case is a traveltime difference of 0.9 second at a distance of only 6 km.

TRAVELTIMES SOUTHWEST OF THE SAN ANDREAS FAULT ZONE

From traveltime data for profile $A-B$ (as summarized by figure 3), it seems clear, despite considerable scatter, that velocities of 2.8 and 5.0 km/sec are indicated by recordings within the distance range 1 to 16 km. Reciprocity of traveltimes for the 5.0-km/sec phase is illustrated in the figure; the reciprocity principle is also used in constructing the traveltime relations for the 2.8-km/sec phase. The traveltime relations show that there is no consistent component of dip along profile $A-B$ on the interface separating the 2.8- and 5.0-km/sec refractors.

At distances of less than 1 km, the data indicate a near-surface layer with velocity less than 2.8 km/sec. The velocity of this material is lower at shotpoint A than at shotpoint B, illustrating the near-surface lateral inhomogeneity in the area. For purposes of interpretation, it is assumed that the surface layer has the same velocity along the entire profile. A velocity of 1.7 km/sec has been used, shown as a dashed line in the traveltime relations of figure 3*A*.

Traveltime data at the extreme ends of each profile suggest a velocity greater than 5.0 km/sec. Because the basement material in this region is known to be granitic, a P-wave velocity of 6.0 km/sec has been assumed. An intercept time of 1.60 seconds for this phase is consistent with the sparse data. By way of comparison, Healy (1963) reported a P-wave velocity of 6.1 km/sec and intercept times of 1.3 and 1.5 seconds for two crustal-refraction profiles extending northwest and southeast from a shotpoint near Camp Roberts, Calif. This shotpoint, approximately 40 km west of the region of this study, is similar in geologic setting to that described above for shotpoints A and B.

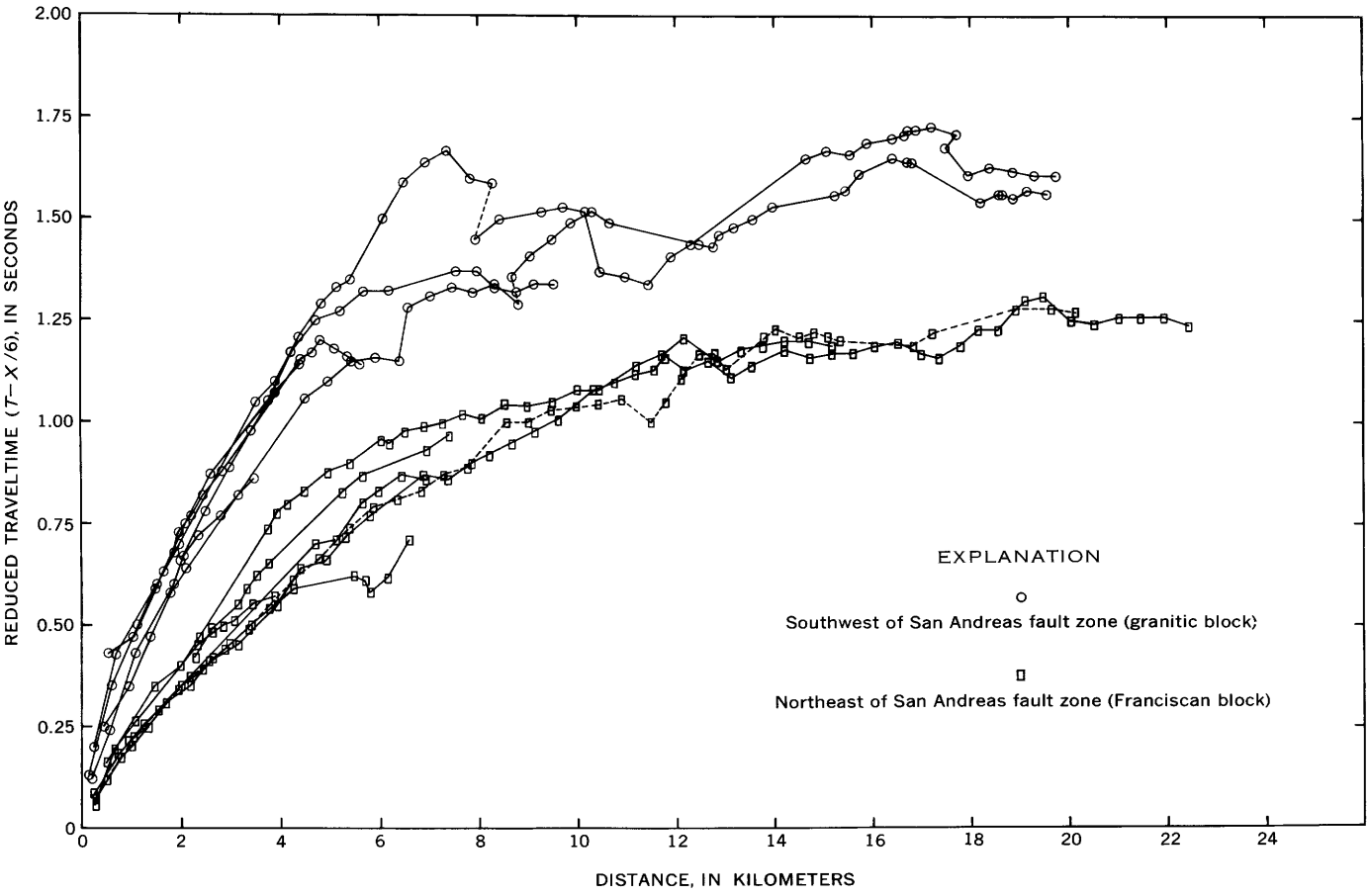

Figure 2.—Composite plot of reduced seismic traveltime data from the northeast and southwest sides of the San Andreas fault zone. Points connected by line segments correspond to observations for a particular profile.

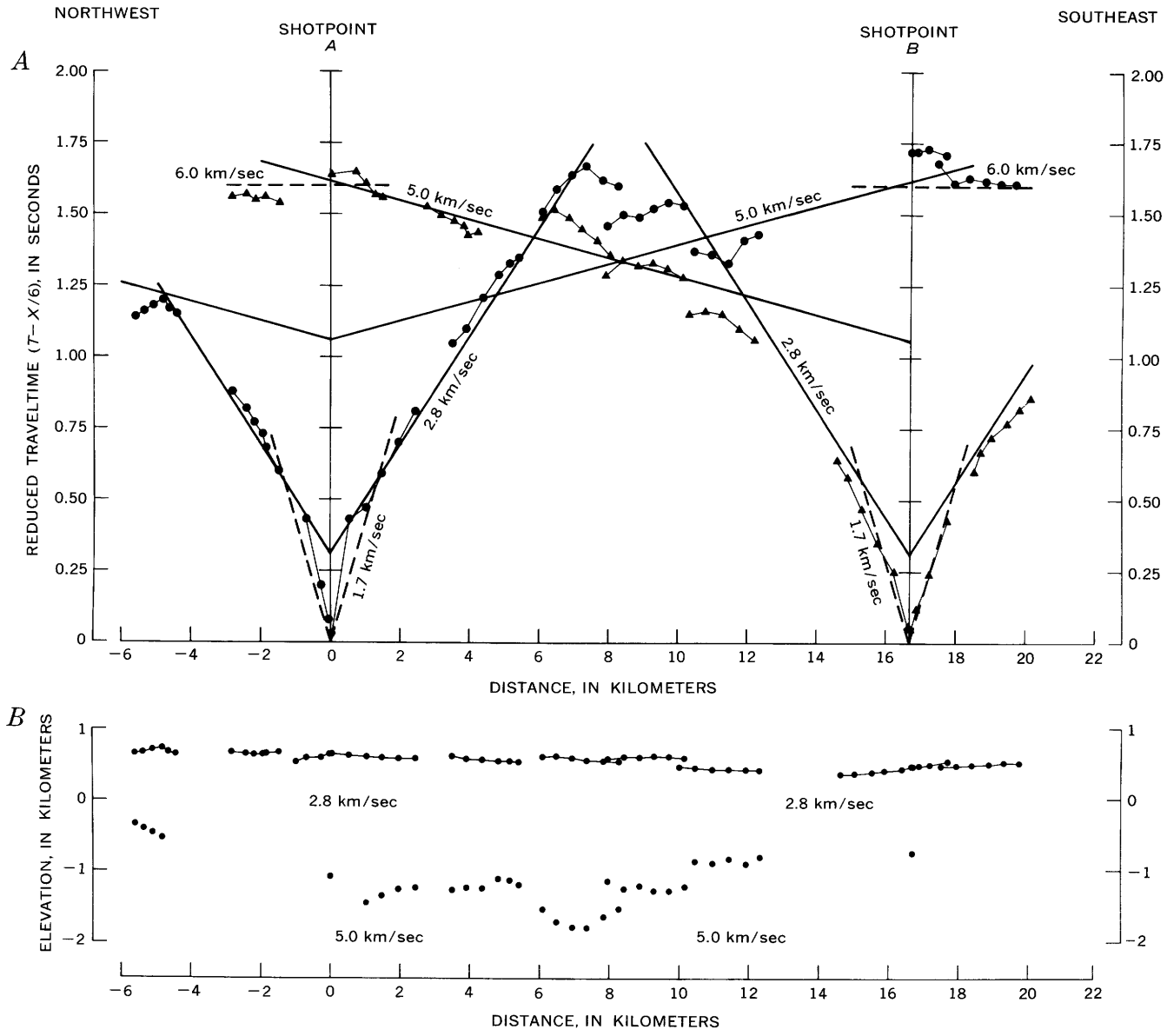

Figure 3.—Summary of data for profile *A*–*B*.

A, Reduced traveltime data for the area southwest of the San Andreas fault zone. Circles and triangles represent data from shotpoints *A* and *B*, respectively.

B, Elevations of shots and recording sites. Structural relief on the 5.0-km/sec refractor derived by the time-term method is shown below. Vertical exaggeration, × 2.

Table 1 summarizes traveltime relations and calculated layer depths for profile *A*–*B*.

The traveltimes for the 5.0-km/sec phase show considerable scatter (fig. 3*A*). Elevation corrections obtained by several different methods failed to reduce the scatter and have not been applied to the data used in the figure. The scatter suggests structural relief on the top of the 5.0-km/sec refractor and has been interpreted as such with the time-term method discussed by Berry and West (1966). The method permits departures from linear traveltime relations to be interpreted in terms of departures from planar velocity interfaces at constant depth. Because the topography is rough, several ways of converting time-terms to depths suggest themselves. The thickness of the uppermost, 1.7-km/sec material may vary directly, inversely, or not at all with elevation. Because the actual situation is unknown, it was assumed that the uppermost (weathered?) layer maintains constant thickness above the 2.8-km/sec material. A thickness of 0.33 km was calculated (see table 1). The depths to the 5.0-km/sec refractor computed from the time-terms are plotted directly below the appropriate sites in figure 3*B*. If all the scatter in the traveltime data for the 5.0-km/sec phase is caused by

Table 1.—*Summary of refraction data for Cholame-Parkfield region, California*

Layer No.	Apparent velocity (km/sec)	Intercept time (sec)	Depth to top of layer (km)	Apparent velocity (km/sec)	Intercept time (sec)	Depth to top of layer (km)	Layer velocity (km/sec)	Dip at top of layer (deg)
Profile *A*–*B*: Southwest of fault zone								
	Shotpoint *A*			Shotpoint *B*				
1	1.70	0.0	0.0	1.70	0.0	0.0	1.7	0.0
2	2.80	.31	.33	2.80	.31	.33	2.8	.0
3	5.00	1.06	1.50	5.00	1.06	1.50	5.0	.0
4	[1]6.00	1.60	3.70	[1]6.00	[1]1.60	3.70	6.0	.0
Profile *E*–*D*–*F*: Averaged model, northeast of fault zone								
1				2.36	0.00	0.0	2.36	0.0
2				3.34	.11	.18	3.34	.0
3				4.62	.57	1.24	4.62	.0
4				5.62	1.02	2.76	5.62	.0
5				[1]6.00	[1]1.30	4.44	6.0	.0
Profile *E*–*D*: Northeast of fault zone								
	Shotpoint *E*			Shotpoint *D*				
1	2.50	0.00	0.0	2.50	0.00	0.0	2.50	0.0
2	2.99	.08	.2	2.94	.04	.1	2.97	.6 NW.
3	4.89	.69	1.3	4.42	.53	1.0	4.64	2.2 NW.
Profile *D*–*F*: Northeast of fault zone								
	Shotpoint *D*			Shotpoint *F*				
1	2.50	0.00	0.0	2.50	0.00	0.0	2.50	0.0
2	3.54	.11	.2	3.54	.11	.2	3.54	.0
3	4.31	.39	1.0	4.36	.42	1.1	4.34	.4 SE.

[1] Assumed.

variations in depth to basement, the variations may be as large as 1.4 km along the profile.

The depth (D) in kilometers from the surface to the top of the 5.0-km/sec refractor was calculated from the appropriate time-term using the following expression:

$$t^* = \frac{h_1}{V_1}\cos i_{13} + \frac{(D-h_1)}{V_2}\cos i_{23},$$

where

t^* = time-term, in seconds,

h_1 = thickness of upper layer, in kilometers,

V_1, V_2, V_3 = velocities of various layers, in kilometers per second, and

$\sin i_{j3} = V_j/V_3, j = 1,2.$

For $h_1 = 0.33$, $V_1 = 1.7$, $V_2 = 2.8$, and $V_3 = 5.0$, D ranges from about 1 to 2.4 km, as shown in figure 3*B*.

Meager drill-hole data in the area of the survey indicate a depth to granitic basement varying from 1.4 km to perhaps as much as 2 km. This depth range corresponds closely to the top of the 5.0-km/sec refractor given in table 1 or shown in figure 3*B*. Although a velocity of 5.0 km/sec is not commonly associated with buried granitic material, it may represent the top of a fractured or decomposed granitic basement, the velocity within the basement increasing rather rapidly with depth to the more commonly reported velocity of 6 km/sec. Detailed seismic-refraction profiles within the outcropping granitic rock of the Gabilan Range of central California show near-surface velocities of 4.8 km/sec, increasing to more than 6 km/sec at approximately 2 to 3 km depth (Stewart, 1968). The granitic bedrock of the Gabilan Range is about 100 km northwest of Cholame and lies within the same crustal block southwest of the San Andreas fault zone as the profile *A*–*B*.

In light of the above interpretation, traveltimes were calculated for a number of velocity models. Each model is identical with that given in table 1 for the uppermost 1.5 km but has a linear increase in velocity below that depth. Those models that fit the observed data have velocities increasing from slightly less than 5.0 km/sec at a depth of 1.5 km to 6.0 km/sec or slightly greater at a depth of 5.0 km. Both the layered velocity model and the linearly increasing velocity model are consistent with the scattered traveltime data; the alternatives are shown in figure 4.

TRAVELTIMES NORTHEAST OF THE SAN ANDREAS FAULT ZONE

Detailed traveltime data from the northeast side of the San Andreas fault zone (profile *E*–*D*–*F*), summarized in figure 5,

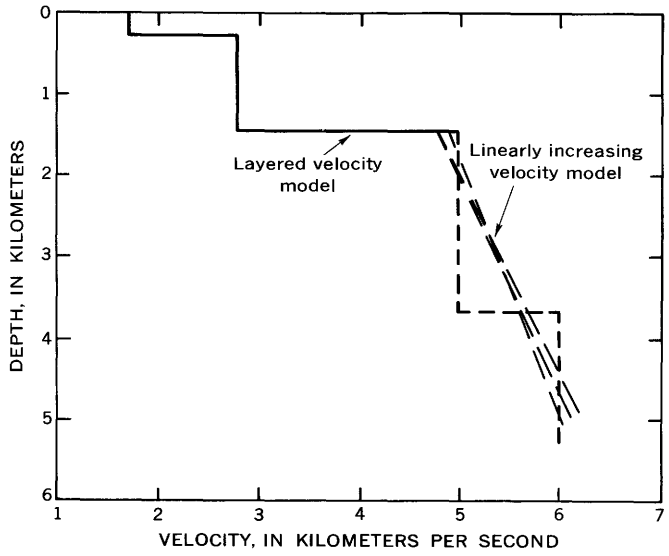

Figure 4.—Velocity-depth models for profile A–B, southwest of the San Andreas fault zone.

show a relatively abrupt change in apparent velocity at distances about 4 to 6 km from each shotpoint. Between shotpoints E and D, the apparent velocities change from about 2.9 km/sec to either 4.4 or 4.9 km/sec. Between shotpoints D and F, the apparent velocities change from 3.5 km/sec to slightly more than 4.3 km/sec. Standard methods of interpretation of the traveltime data indicate that a pronounced and laterally extensive velocity gradient exists at a depth of about 1 km in this region.

Variations in geologic structure at greater depths probably account for the scatter of the traveltime data at distances beyond 10 km, whereas the general increase of apparent velocity from 2.5 km/sec to approximately 6 km/sec is caused by a corresponding increase of velocity with depth in the upper few kilometers of the crust.

The crustal velocity section at the bottom of figure 5 represents an interpretation of the first-arrival data. It is unsuitable for use as a model for earthquake locations because (1) it actually represents two different models, (2) there is a

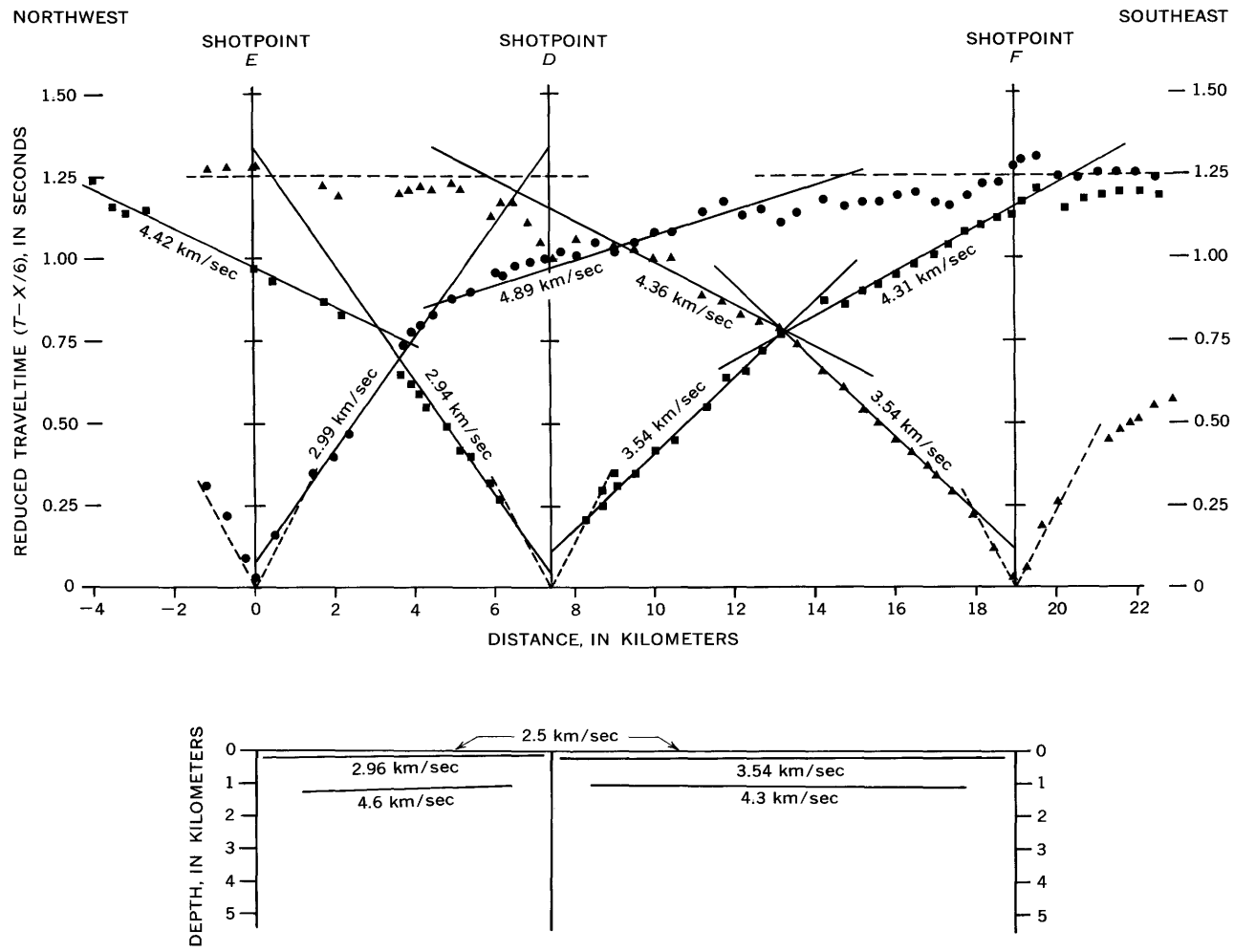

Figure 5.—Reduced traveltime data and structure sections for profile E–D–F, northeast of the San Andreas fault zone. Circles, squares, and triangles represent data from shotpoints E, D, and F, respectively.

slight amount of dip on the refractor at a depth of about 1 km, and (3) knowledge of the velocity structure to depths greater than 1 km is required for earthquake location methods.

In order to derive a single crustal model suitable for earthquake location purposes, the traveltime data in figure 5 were replotted in the form of a composite traveltime curve, figure 6. Linear traveltime relations with apparent velocities of 2.36 km/sec, 3.34 km/sec, and 4.62 km/sec were constructed on the basis of the detailed considerations leading to the interpretation in figure 5.

Although velocities greater than about 4.6 km/sec are indicated by the increasing slope of the traveltime data in figure 6, a clear change in slope at distances greater than about 6 km is not observed. Certain pieces of evidence helped in constructing the remaining lines. First, as mentioned previously, the shallow crustal material in this region is known to be largely Franciscan Formation. Earlier studies of crustal structure in the central California Coast Ranges region by Byerly (1939) and Tocher (1956) showed that much of the upper crust had a P-wave velocity less than 6 km/sec. Byerly suggested an upper crustal layer of velocity 5.61 km/sec and thickness about 9 km underlain by a layer with velocity 6.72 km/sec. Byerly's velocity of 5.61 km/sec for the upper crust is based upon data from recording stations, earthquakes, and blasts located within the Franciscan block northeast of the San Andreas fault zone. Tocher's simplest model is that of a layer of thickness 10 km and velocity 5.5 km/sec underlain by a layer of velocity 6.5 km/sec. It is reasonable in this refraction survey to expect first arrivals with velocity between 5.5 and 6.0 km/sec. In figure 6 a line with velocity 5.62 km/sec represents the remainder of the first-arrival traveltime data within the distance range 12 to 22 km.

More recent studies of seismic velocity distribution within the large outcrop of Franciscan Formation in the Diablo Range, about 150 km northwest of the region of this survey, have been reported by Stewart (1968). These studies confirm that at depths of 2–4 km, the Franciscan Formation has a compressional wave velocity of about 5.7 km/sec. At shallower depths, velocities of Franciscan rocks range from 3 to 5 km/sec.

In order to complete the traveltime relations appropriate for an earthquake location model, a line with apparent velocity 6.0 km/sec was constructed (fig. 6). With regard to crustal velocity structure, this line may be considered fictitious. At best, it places a minimum figure on the depth at which such a velocity might be expected, as greater depths would result in a larger intercept time for this phase. For purposes of earthquake location, however, such a structure is convenient, as it then gives a uniform velocity of 6.0 km/sec at depths greater than 4.5 km throughout the epicentral region.

Alternatively, the composite traveltime data of figure 6 may be interpreted assuming that seismic velocity increases continuously with depth rather than discontinuously. With this assumption, the Herglotz-Wiechert method of traveltime inversion (Slichter, 1933) was used to invert the traveltime data to the appropriate velocity-depth function.

Figure 7 summarizes the two interpretations, that for the discontinuous velocity-depth function and that for the con-

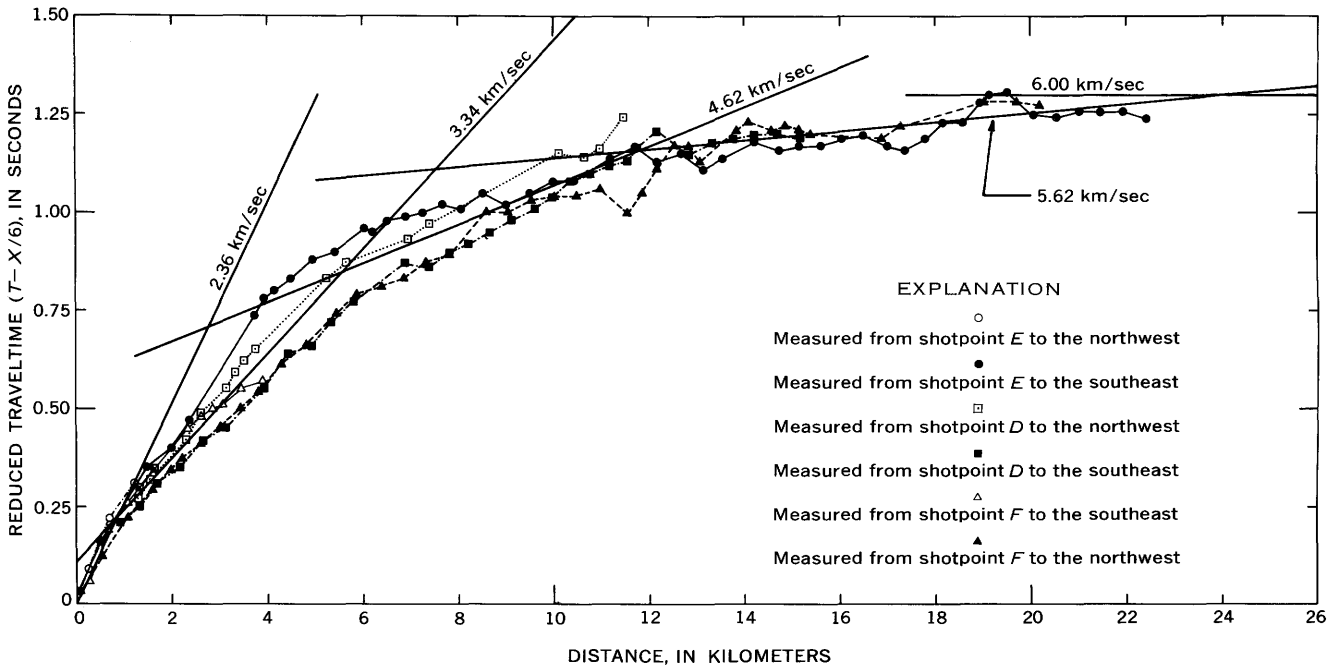

Figure 6.—Composite traveltime data and generalized traveltime relations for profile *E–D–F*. Circles, squares, and triangles represent data from shotpoints *E*, *D*, and *F*, respectively.

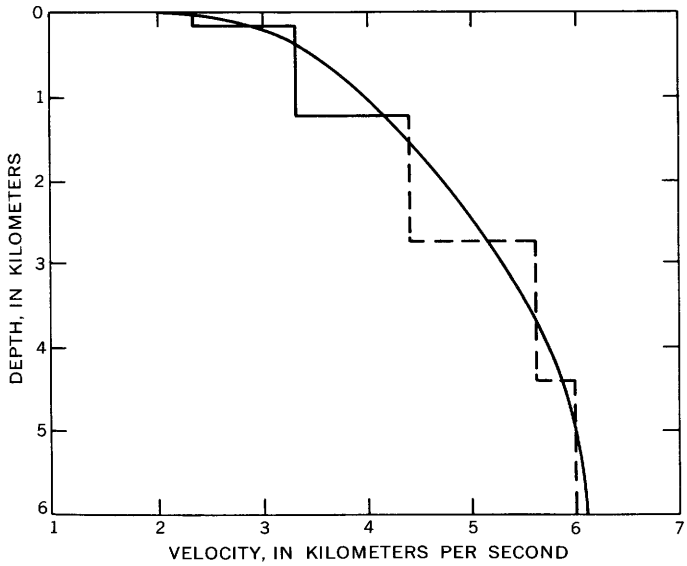

Figure 7.—Two interpretations of the generalized velocity structure for profile *E–D–F*, northeast of the San Andreas fault zone. Dashed where interpretation is less reliable.

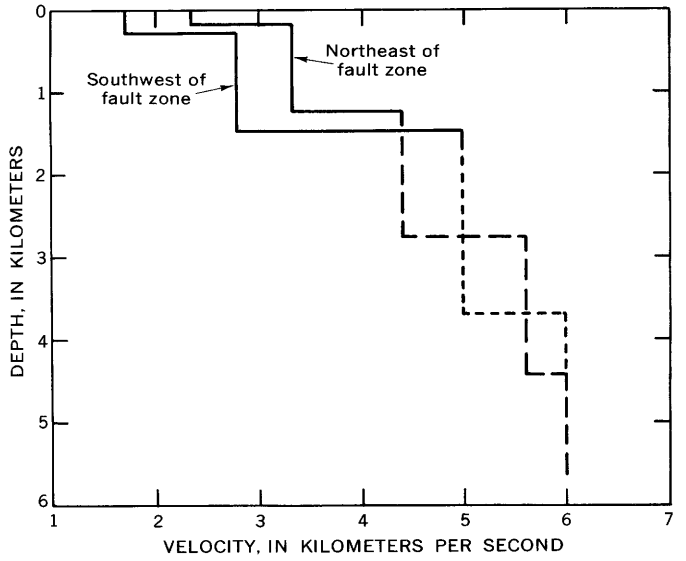

Figure 8.—Plane-layered velocity-depth models for the northeast and southwest sides of the San Andreas fault zone, Parkfield, Calif. Dashed where interpretation is less reliable.

tinuous. The seismic-refraction traveltime data in figure 5 suggest a pronounced velocity discontinuity (or zone of relatively large velocity gradient) at a depth of about 1.1 km. A more realistic velocity representation for this region might be a combination of the models summarized in figures 5 and 7. The composite model would be characterized by a relatively large vertical velocity gradient at a depth of approximately 1 km superposed on a complex system of continuously varying velocity gradients in the horizontal as well as vertical direction.

CONCLUSIONS

Simple velocity models for the upper 6 km of the crust near Parkfield, Calif., as summarized in figure 8, illustrate the velocity differences that exist between the two adjacent crustal blocks separated by the San Andreas fault zone. Sparse drill-hole data within the southwest crustal block suggest that the seismically determined depth of 1.5 km to the 5.0 km/sec refractor may represent the top of the granitic basement. Time-term analysis of the traveltime data suggest that structural relief on the granitic basement in this region may be as great as 1.4 km.

Lateral velocity variations within the complexly deformed crustal block northeast of the fault zone are illustrated by the traveltime data (fig. 5). Interpretation of these data suggests a pronounced increase in the vertical velocity gradient at a depth slightly greater than 1 km. At shallower depth, there is a clear lateral change in velocity from about 3.0 to 3.5 km/sec. Below 1 km, the data indicate a less pronounced lateral velocity change, 4.3 to 4.6 km/sec. These lateral changes in seismic velocity occur over distances of only a few kilometers and clearly represent a combination of locally complex structural relations and facies changes known to exist in this region.

The crustal velocity models derived are suitable for use in computer-oriented programs for locating earthquakes more precisely.

REFERENCES

Berry, M. J., and West, G. F., 1966, An interpretation of the first-arrival data of the Lake Superior experiment by the time-term method: Seismol. Soc. America Bull., v. 56, p. 141–171.

Brown, R. D., Jr., and Vedder, J. G., 1967, Surface tectonic fractures along the San Andreas fault, *in* The Parkfield-Cholame, California, earthquakes of June-August 1966: U.S. Geol. Survey Prof. Paper 579, p. 2–23.

Byerly, Perry, 1939, Near earthquakes in central California: Seismol. Soc. America Bull., v. 29, p. 427–462.

Dickinson, W. R., 1966, Structural relationships of San Andreas fault system, Cholame Valley and Castle Mountain Range, California: Geol. Soc. America Bull., v. 77, p. 707–726.

Eaton, J. P., 1967, Instrumental seismic studies, *in* The Parkfield-Cholame, California, earthquakes of June-August 1966: U.S. Geol. Survey Prof. Paper 579, p. 57–66.

Eaton, J. P., O'Neill, M. E., and Murdock, J. N., 1970, Aftershocks of the 1966 Parkfield-Cholame, California, earthquake—A detailed study: Seismol. Soc. America Bull., v. 60, p. 1151–1197.

Healy, J. H., 1963, Crustal structure along the coast of California from seismic-refraction measurements: Jour. Geophys. Research, v. 68, p. 5777–5787.

Jackson, W. H., Stewart, S. W., and Pakiser, L. C., 1963, Crustal structure in eastern Colorado from seismic-refraction measurements: Jour. Geophys. Research, v. 68, p. 5767–5776.

McEvilly, T. V., Bakun, W. M., and Casaday, K. B., 1967, The Parkfield, California, earthquakes of 1966: Seismol. Soc. America Bull., v. 57, p. 1221–1244.

Page, B. M., 1966, Geology of the Coast Ranges of California, *in* E. H. Bailey, ed., Geology of northern California: California Div. Mines and Geology Bull. 190, p. 255–276.

Slichter, L. B., 1933, Interpretation of seismic traveltime curves: Physics, v. 3, p. 273–295.

Smith, M. B., 1964, Map showing distribution and configuration of basement rocks in California: U.S. Geol. Survey Oil and Gas Inv. Map OM-215, scale 1:500,000.

Stewart, S. W., 1968, Preliminary comparison of seismic traveltimes and inferred crustal structure adjacent to the San Andreas fault in the Diablo and Gabilan Ranges of central California, *in* Dickinson, W. R., and Grantz, Arthur, eds., Proceedings of conference on geologic problems of San Andreas fault system: Stanford Univ. Pubs. Geol. Sci., v. 11, p. 218–230.

Tocher, Don, 1956, Seismic velocities and structure in northern California and Nevada: California Univ. (Berkeley), unpub. Ph.D. thesis, 120 p.

Warrick, R. E., Hoover, D. B., Jackson, W. H., Pakiser, L. C., and Roller, J. C., 1961, The specification and testing of a seismic-refraction system for crustal studies: Geophysics, v. 26, p. 820–824.

LISBURNE GROUP, FRANKLIN AND ROMANZOF MOUNTAINS, NORTHEASTERN ALASKA

By B. L. MAMET[1] and A. K. ARMSTRONG,
Montreal, Canada, Menlo Park, Calif.

Abstract.—Four sections of Lisburne Group, Carboniferous (Mississippian and Pennsylvanian), were measured on autochthonous but structurally complex terrane. The section on the west end of the Sadlerochit Mountains is 1,500 feet thick and consists of Viséan (Chester) and "Namurian" (Morrow and Atoka) age carbonates. The two sections in the Franklin Mountains are in excess of 2,400 feet thick and are of Viséan (Meramec and Chester) and "Namurian" (Morrow and Atoka) age. The Romanzof Mountains section is 2,800 feet thick and of similar age. Within these sections 10 foraminiferal assemblage zones are recognized and tied to the Cordilleran and Eurasian standards. A fauna of 14 taxa of lithostrotionoid corals is present in beds of Meramec through Atoka age equivalents.

Four sections of the Lisburne Group were measured and sampled by Armstrong in 1969 and 1970 from outcrops in the Brooks Range of northeastern Alaska (fig. 1). A foraminiferal zonation for the Lisburne Group in the central and eastern Brooks Range was established by Armstrong, Mamet, and Dutro (1970) and extended by them (1971) to the Lisburne Group of the Lisburne Hills and sea cliffs of northwestern Alaska. This report is a continuation of this microfossil zonation to the Lisburne Group of the Franklin and Romanzof Mountains of northeastern Alaska. The stratigraphic section of this paper extends in an east-west direction, from the north flank to the central part of the northeastern Brooks Range (figs. 2, 3). The carbonate classification used in this report is Dunham's (1962).

A detailed historical review of stratigraphic studies of the Lisburne Group can be found in Bowsher and Dutro (1957) and Armstrong, Mamet, and Dutro (1970).

Acknowledgments.—We wish to express our appreciation to Hillard N. Reiser, the party chief during the summers of 1969 and 1970, for his generosity in supporting the stratigraphic field studies and coral collecting. We thank the Naval Arctic Research Laboratory (Barrow), Office of Naval Research, for their logistical support of fieldwork in the summers of 1969 and 1970. We are grateful to our colleagues, J. Thomas Dutro, Jr., and William J. Sando, who helped in the preparation of the manuscript and provided critical review.

[1] Université de Montréal.

STRATIGRAPHY

Endicott Group

Kekiktuk Conglomerate.—Brosgé and others (1962) named the basal sandstone beneath the Kayak(?) Shale in northeastern Alaska the Kekiktuk Conglomerate. The type section is on Whistler Creek, near the Neruokpuk Lakes (fig. 2). Brosgé and others only found indeterminate plant fragments within the formation and assigned it a Late(?) Devonian or Mississippian age, but they believed that it may represent the basal conglomerate of the overlapping Mississippian sequence. We also believe from field evidence that the Kekiktuk Conglomerate underlies the Kayak(?) Shale. The base of the Kekiktuk Conglomerate is a pebble or cobble conglomerate grading upward to coarse-grained beach or near-shore deposits that in turn commonly grade upward into finer grained paralic sediments. The contact between the Kekiktuk Conglomerate and the overlying Kayak(?) Shale is generally gradational. Possibly owing to faulting at the base, the Kekiktuk Conglomerate is absent from the bottom of section 69A-1, west end of the Sadlerochit Mountains.

The Kekiktuk Conglomerate is well exposed at the base of section 70A-4, near the Canning River. Here the Kekiktuk rests with angular unconformity on metamorphic rocks of the Neruokpuk Formation and is some 30 feet thick. It consists of basal quartz-pebble conglomerate, black carbonaceous shales, and 17 feet of strongly crossbedded light-gray quartz sandstone, and is overlain by the dark-gray Kayak(?) Shale.

The Kekiktuk Conglomerate in section 70A-2, near the junction of Marsh Fork and the Canning River, is at least 200 feet thick. It unconformably overlies the greenish-gray slates and phyllites of the Neruokpuk Formation. The lower 125 feet of the Kekiktuk Conglomerate is medium- to massive-bedded pebble conglomerates and sandstones, with quartz and hematite cement, and it has been affected by low-grade thermal metamorphism, possibly from faulting. The upper 75 feet consists of medium- to thin-bedded quartz sandstone, dark-gray siltstones, dark-gray shales, thin (1 in. or less) coal

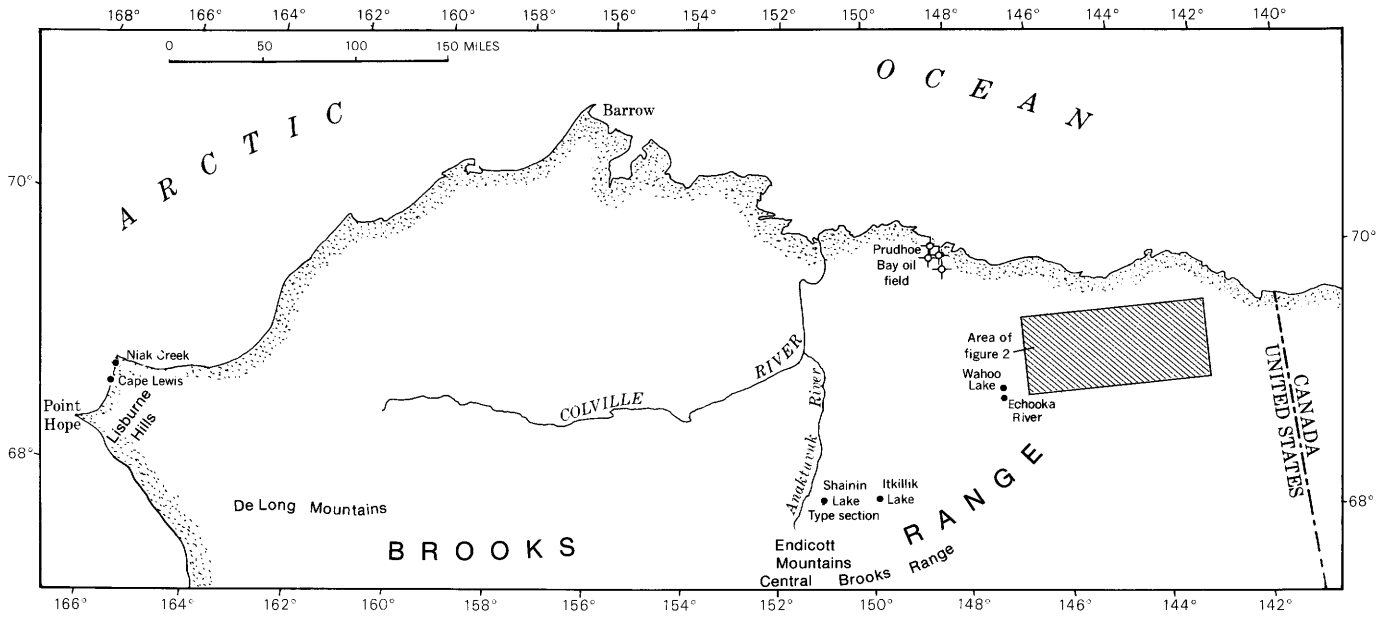

Figure 1.—Index map of arctic Alaska, showing location of the study area (fig. 2) containing the stratigraphic sections shown on figure 3.

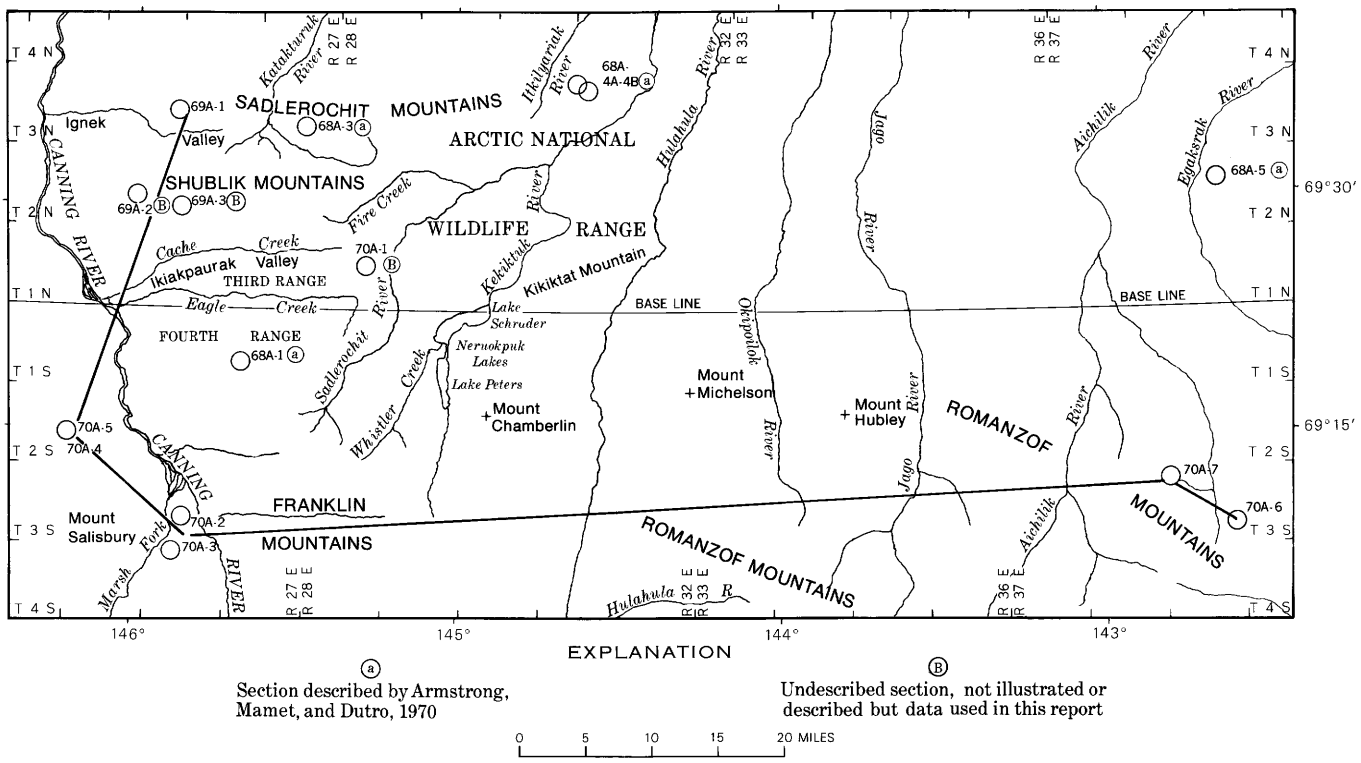

Figure 2.—Index map showing location of measured sections.

beds and abundant plant remains. The contact with the overlying Kayak(?) Shale is transitional, and the boundary between the two formations was arbitrarily picked.

The section 70A-7 on the north flank of the large synclinorium east of the Aichilik River contains about 100 feet of quartzite conglomerates, sandstones, and shales. The contact between the upper sandstones of the Kekiktuk Conglomerate and the Kayak(?) Shale is poorly exposed, but it appears to be a gradational zone about 50 feet thick.

Kayak(?) Shale.—Mississippian dark-gray to black shales lie beneath carbonate rocks of the Lisburne Group throughout the eastern and central Brooks Range. Bowsher and Dutro

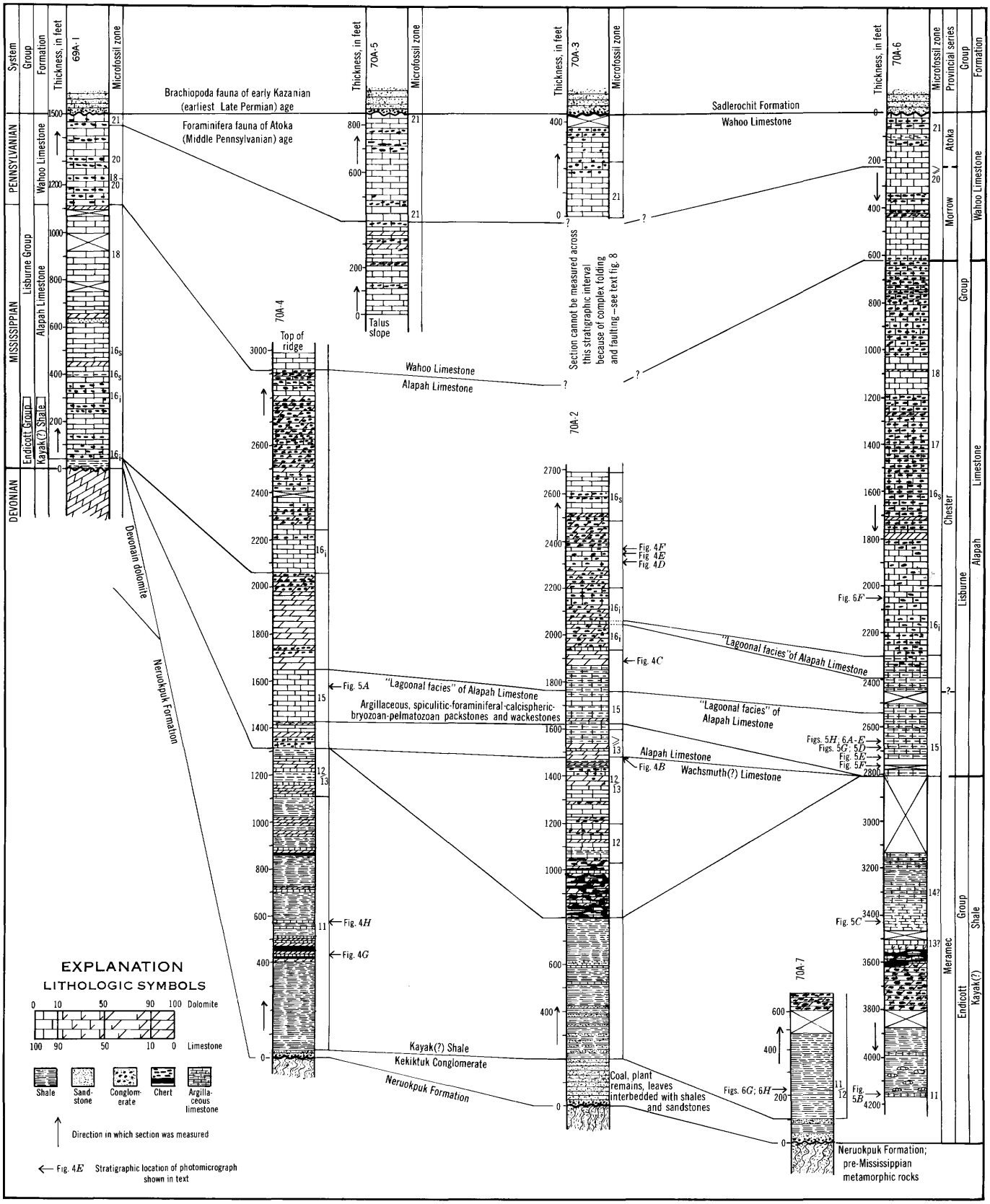

Figure 3.—Biostratigraphic correlation diagram of the Lisburne Group, northeastern, Alaska.

(1957, p. 6) in the Endicott Mountains named these the Kayak Shale, from the type section on the south side of Mount Wachsmuth, east of Shainin Lake. The Kayak Shale at its type locality and in the Endicott Mountains is Early Mississippian in age. Adjacent to and east of the Canning River, in the Arctic National Wildlife Range, a similar black shale occurs between the Kekiktuk Conglomerate and the Lisburne Group. Brosgé and others (1962) believed "this shale is at least in part of Late Mississippian age." They further stated, "Because of geologic structure, this shale can not be mapped continuously into the type Kayak. It might therefore be a discrete unit entirely younger than the Kayak and separated from the Kayak by a disconformity within the Mississippian rocks." Following Brosgé and others (1962), the shales in the area of this report are called Kayak(?) Shale.

The Kayak(?) Shale is thin, only about 50 feet thick in the western Sadlerochit Mountains. In section 69A-1 this brownish-gray calcareous unit rests unconformably on dolomites of Devonian age. The overlying basal beds of the Alapah Limestone are lower Chester in age, and probably the thin Kayak(?) Shale is of similar age. In section 70A-4, about 27 miles to the south (fig. 3), the unit thickens markedly and is older; it contains microfossils of Meramec, zone 11, age (fig. 3). Approximately 1,220 feet thick, it is a sequence of dark-gray shales, thin-bedded argillaceous lime mudstones, dolomites, and thin-bedded dark-gray to black cherts. The upper 100 to 200 feet of the unit becomes progressively more calcareous upward, and the contact with the Alapah Limestone is gradational.

The Kayak(?) Shale, 11 miles to the southeast in section 70A-2, is only about 600 feet thick (fig. 3). The predominant rock type is dark-gray shale, with only minor amounts of thin-bedded sandstones, siltstones, and yellow-weathering thin-bedded limestone (figs. 4*G*, 4*H*). The base of the unit is gradational with the Kekiktuk Conglomerate, which contains abundant plant remains. At the top of the Kayak(?) Shale there is an abrupt change from dark-gray shales to dark-gray bedded spiculitic cherts and dolomites.

The composite section 70A-6 and 70A-7 of the Kayak(?) Shale about 84 miles east of section 70A-2 is about 1,450 feet thick; the lower 450 feet is dark-gray shale with a few thin lime mudstone beds and nodules (fig. 5*B*, 5*C*). Above this segment is 300 feet of highly siliceous, argillaceous, cherty, gray and dark-gray dolomites and limestones. The upper 700 feet of the unit is calcareous dark-gray shale and thin-bedded argillaceous dark-gray coralliferous limestones. The contact with the basal Alapah Limestone is gradational.

Lisburne Group

In the Shainin Lake area, Endicott Mountains, Bowsher and Dutro (1957, p. 3, 4, 6) recognized two new formations within the Lisburne which they raised to group rank. The lower formation is the Wachsmuth Limestone, and the overlying one is the Alapah Limestone. Armstrong, Mamet, and Dutro's (1970, figs. 3, 4) study indicates that the age of the Wachsmuth based on microfossils is late Osage zone 8 through zone 12 and Meramec.

They found that the Alapah Limestone contains microfaunas of Meramec (transition of zones 12 and 13) through Chester (zone 19) ages.

Because the vast majority of the carbonate rocks of this study are younger than zone 12, the Wachsmuth carbonate facies is evidently very poorly represented. The interval 800 to 1,475 feet of section 70A-2 is considered to be a possible Wachsmuth equivalent.

Brosgé and others (1962, p. 2191–2192) described the type section of the Wahoo Limestone near Wahoo Lake as containing carbonates of both Pennsylvanian(?) and Permian age. In the area of this report, the Wahoo Limestone as mapped by Reiser and others (1970) may contain carbonates of Late Mississippian (very latest Chester) and Early and Middle Pennsylvanian age (Morrow and Atoka). The Pennsylvanian limestones overlie Mississippian carbonates without a recognizable hiatus. The boundary between the two systems and the zones within them are based on microfaunal assemblages. The beds of Atoka age are unconformably overlain by Late Permian arenaceous limestones, sandstones, and conglomerates in the lowest part of the Sadlerochit Formation.

Alapah Limestone.—As illustrated in figure 3, the base of the Lisburne Group is diachronous. The contact with the Kayak(?) Shale in section 70A-2 at the Junction of Marsh Fork and Canning River is Meramec, zone 12 in age, whereas 31 miles to the north the oldest beds of the Alapah Limestone are lower Chester, zone 16. The basal 100 feet of the Alapah Limestone at section 70A-2 is formed of black nodular and bedded chert and argillaceous dark-gray spiculite-lime mudstone. Bedded cherts are common at the base of many Lisburne exposures in the Franklin and Romanzof Mountains. Above the cherts are about 300 feet of bryozoan-pelmatozoan wackestones, and packstone and dolomite (fig. 4*B*), followed by a characteristic marker zone approximately 200 to 350 feet thick, the so-called "lagoonal facies" of the Alapah Limestone. In outcrop, these are gray medium-bedded argillaceous limestones, with little or no chert. The rock is typically argillaceous, may have birdseye structure, and is made up of spiculitic-foraminiferal-calcispheric-bryozoan-pelmatozoan-pelletoid packstones and wackestones. In sections 70A-4 and 70A-2 of the Franklin Mountains and section 70A-6 of Romanzof Mountains, the Chester-age beds of the Alapah Limestone are typically shallow-water lime mudstones and bryozoan-pelmatozoan-pelletoid wackestones and packstones (figs. 4*C*–4*F*; 5*A*, 5*D*–5*H*; 6*A*–6*G*). Dolomite is common and occurs in the limestones as scattered rhombs; it also forms thick units of bedded fine- to medium-grained dolomite rock. The Alapah Limestone in section 69A-1, on the west end of the Sadlerochit Mountains, is only 1,100 feet thick. The lower part of the section is pelmatozoan-bryozoan-ooid packstones

and grainstones that grade upwards into wackestones and pelletoid mudstones with a few beds of fine-grained dolomite.

The Alapah Limestone in the Franklin and Romanzof Mountains in outcrop shows little variation in lithology and bedding (figs. 7 and 8); it is typically medium to dark gray, has medium bedding, and shows few sedimentary structures. The upper third to half of the unit in sections 70A-4, 70A-2, and in particular 70A-6, contains abundant nodular, dark-gray to gray chert. (fig. 7).

Wahoo Limestone.—The Wahoo Limestone on the west end of the Sadlerochit Mountains is about 400 feet thick and consists primarily of pelmatozoan-bryozoan wackestone, packstones, and grainstones, and beds of ooid packstones and grainstones. The ooid facies of the units is generally absent in the sections studied in the Franklin and Romanzof Mountains. Here the unit is from 600 to 900 feet thick and consists of medium- to massive-bedded, gray to light-gray, slightly cross-bedded pelmatozoan-bryozoan wackestone and packstones, and minor amounts of grainstone. Occasional beds of thin dolomite and superficial ooid packstones may be present. Chert is typically nodular, light gray to brown and generally occurs in the lime-mud-rich beds. The contact (fig. 7) between the Wahoo and Alapah Limestones is generally sharp, marked by the darker gray, thinner bedded lime mudstones and wackestones of the Alapah Limestone overlain by the thicker bedded, lighter gray pelmatozoan wackestones and packstones of the Wahoo Limestone.

In the area of this study the Permian and Triassic Sadlerochit Formation unconformably overlies limestones of Atoka age. Detterman (1970) reports that the basal Echooka Member of the Sadlerochit Formation contains a brachiopod fauna of early Kazanian, earliest Late Permian age. The unconformity between the Wahoo Limestone and Sadlerochit Formation represents a hiatus of Des Moines through Leonard and, possibly, lower Guadalupe time.

Armstrong, Mamet, and Dutro (1970) have illustrated the westward thinning of the Atoka age carbonates in the Sadlerochit Mountains. This thinning and the northward thinning shown in figure 3 suggest uneven erosion, probably from differential uplift before deposition of the Sadlerochit Formation. At many localities the highest few feet of Atoka age carbonates beneath the Sadlerochit Formation shows evidence of vadose weathering in the form of enlarged vertical joints and vugs filled with a clay similar to terra rossa. The basal beds of the Echooka Member of the Sadlerochit Formation are conglomerates or conglomeratic sandstone formed partly of rounded chert and limestone pebbles and cobbles derived from the underlying Wahoo Limestone.

BIOSTRATIGRAPHY

Microfaunal assemblage zones

The microfaunal assemblage zones used in this study have been used by Mamet and Gabrielse (1969), Mamet and Mason (1968), and Mamet (1968) to correlate the Carboniferous of western Canada with the Carboniferous of the northern Cordillera of the United States (Sando and others, 1969). Armstrong, Mamet, and Dutro (1970, 1971) also used these zones to correlate the Lisburne Group of the eastern and central Brooks Range and the Lisburne Hills region of northwestern Alaska (fig. 9).

The microfacies of Alaska, as in most of the Taimyr-Alaska foraminiferal realm (Mamet, 1962; Mamet and Belford, 1968; Mamet and Skipp, 1970), are generally poor in foraminifers and algae. Within the sections of the Lisburne Group studied in this report of northeastern Alaska, 10 foraminiferal assemblages can be recognized and correlated with the Cordilleran and Eurasiatic Carboniferous zonations (Sando and others, 1969).

Late Tournaisian (middle and late Osage).—Microfaunas of this age or older have not been found in the stratigraphic sections of this report, but they were reported by Armstrong, Mamet, and Dutro (1970) from outcrops of the Lisburne Group in the Endicott Mountains, to the west. There the late Tournaisian Zones 8(?) and 9 have been found only in the basal part of the Shainin Lake and Itkillik Lake sections. These sections are characterized by the acme of the Tournayellidae, represented by *Glomospiranella, Septabrunsiina, Septatournayella,* and *Tournayella discoidae.* The spinose endothyrida, *Tuberendothyra* and *Spinoendothyra,* generally abundant at that level in the northern Cordillera of the United States and adjacent Canada are very scarce.

In the American cordillera, similar zones are known in the Shunda Formation of the Fort St. John region in southern Alberta. They also are observed in the Livingstone Formation of southwestern Alberta, in the lower part of the Mission Canyon Limestone of Montana and western Wyoming, and in the upper part of the Madison Limestone of central Wyoming (Sando and others, 1969). These zones are present in the Keokuk Limestone of the American midcontinent, in particular in its type section.

Early and early middle Viséan.—Armstrong, Mamet, and Dutro (1970) report that in the central Brooks Range (Endicott Mountains) no characteristic microfauna of the earliest Viséan zone 10 is known; the passage between the Tournaisian-Viséan is either barren or in a nondiagnostic *Earlandia* facies. In the sections described in this report, no microfossils of zone 10 are known, and strata that could be an equivalent stratigraphic level to zone 10 are black shales of the Kayak(?) Shale or are sandstone and siltstone. The late early Viséan zone 11 and early middle Viséan zone 12 are characterized by *Globoendothyra baileyi,* numerous species of *Stacheia-Stacheoides* and *Eoendothyranopsis,* and, in zone 12, *Koninckopora.* Similar faunas are known in the middle part of the Prophet Formation and in the lower part of the Debolt Formation in the Fort St. John region, in the middle part of the Flett Formation of the Northwest Territories, in the lower part of the Mount Head Formation in southwestern Alberta

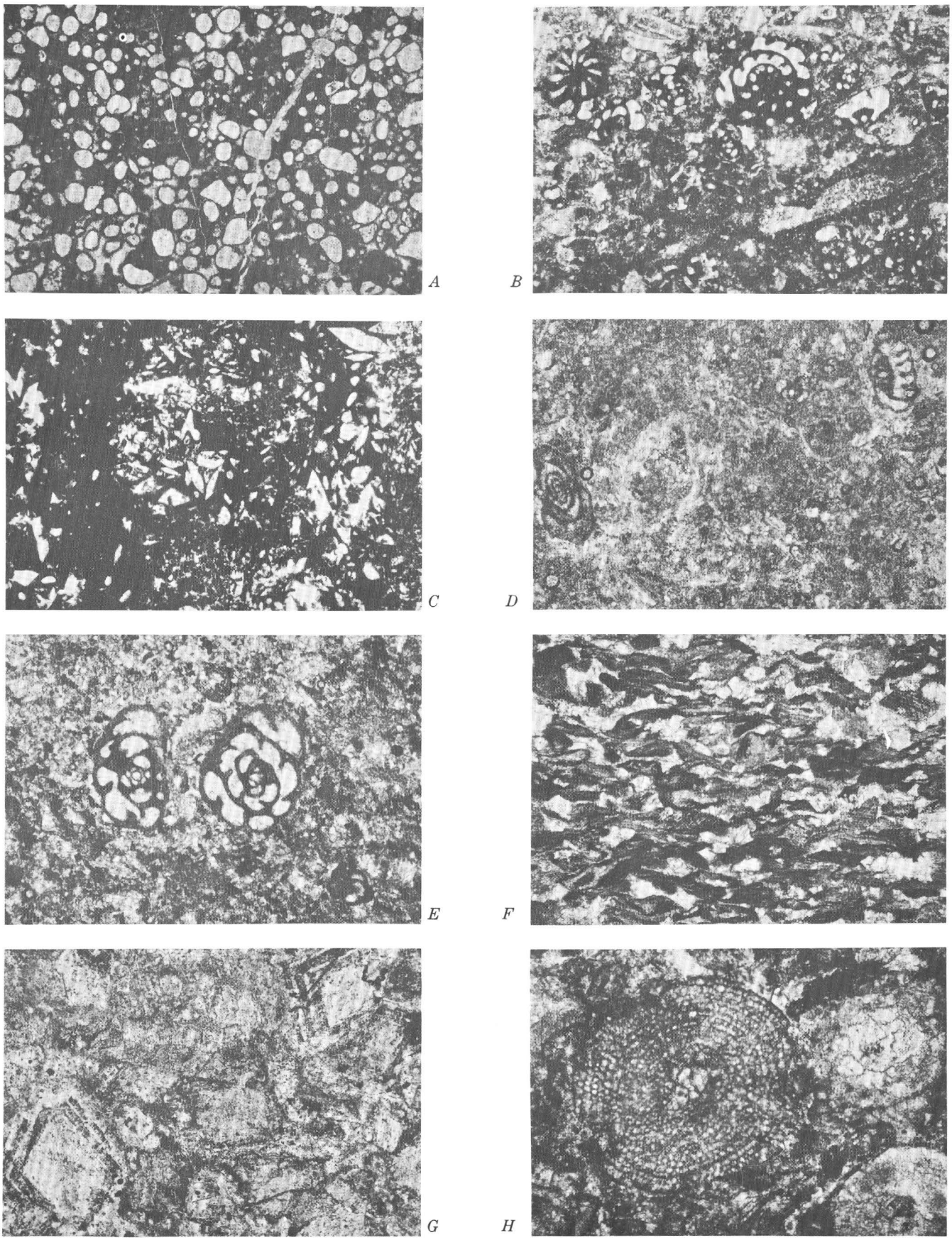

Figure 4.

Figure 4.—Photomicrographs of microfacies and microfossils of sections 70A-1, 70A-2, and 70A-4 of the Alapah Limestone and Kayak(?) Shale, northeastern Alaska.

A. Section 70A-1, 40 ft above base, × 25, Alapah Limestone, zone 13, late middle Viséan, St. Louis equivalent. Well sorted, rolled pelmatozoans and lumps of grainstone. Crinoids are usually resistant to abrasion; this is an unusual example of worn, reworked ossicles. Base of Alapah Limestone, east end of Third Range.

B. Section 70A-2, 1,475 ft above base, × 25, Alapah Limestone?, transition of zones 12 and 13, middle Viséan, Salem-St. Louis transition. Poorly sorted foraminiferal-algal packstone. *Eoendothyranopsis* of the group *E. spiroides* (Zeller), *Eoendothyranopsis hinduensis* (Skipp), *Eoendothyranopsis* sp., *Endothyra* sp., and *"Issinella"* sp. are conspicuous.

C. Section 70A-2, 1,890 ft above base, × 25, Alapah Limestone, undetermined zone 15 or 16_i?, late Viséan, uppermost Meramec or lowermost Chester equivalent. Calcite pseudomorphs after gypsum.

D. Section 70A-2, 2,310 ft above base, × 25, Alapah Limestone, undetermined zone 16_i or 16_s?, late Viséan, lower Chester equivalent. *Eostaffella* sp. and *Calcisphaera* sp. in a slightly recrystallized wackestone.

E. Section 70A-2, 2,340 ft above base, × 25, Alapah Limestone, undetermined zone 16_i or 16_s?, late Viséan, lower Chester equivalent. *Globoendothyra* sp. and *Globoendothyra paula* (Vissarionova) in a recrystallized, poorly sorted wackestone. Minute calcispheres and rare pellets are present.

F. Section 70A-2, 2,360 ft above base, × 25, Alapah Limestone, undetermined zone 16_i or 16_s?, late Viséan, lower Chester equivalent. Tectonically stressed limestone, deformed bryozoan fronds and brachiopod shells give a fluid appearance to the rock.

G. Section 70A-4, 435 ft above base, × 63, Kayak(?) Shale, zone 11, early Viséan, Salem equivalent. Dolomitized pelmatozoan-bryozoan packstone(?). Succession of calcite/dolomite carbonate generations is emphasized by silver nitrate staining.

H. Section 70A-4, 570 ft above base, × 30, Kayak(?) Shale, zone 11, early Viséan, Salem equivalent. Although recrystallization is fairly advanced, the wall structure of the red algae (*Stacheia* sp.) is still recognizable, and the regular subquadratic morphology of the cells is well displayed.

(Petryk and others, 1970), in the upper part of the Mission Canyon Limestone of Montana and western Wyoming, and in the uppermost part of the Madison Limestone of central Wyoming (Sando and others, 1969, zones 10 and 11 only). *Globoendothyra baileyi* and *Eoendothyranopsis spiroides* are common in the middle part of the Salem Limestone in its type region, and *Globoendothyra baileyi-Eoendothyranopsis spiroides* and *Koninckopora* are known in the upper part of the Salem Limestone.

Late middle and early late Viséan.—In Alaska, zone 13 is usually found in facies favorable to calcareous foraminifers (Armstrong, Mamet, and Dutro, 1970), such as pseudo-oolitic packstone, grainstone, or algal wackestone and packstone; hence, the assemblages of *Globoendothyra-Eoendothyranopsis, Endothyranopsis,* and *Archaediscus* of the group *A. krestovnikovi* are usually rich and diversified. *Eoendothyranopsis* of the group *E. pressa* (*E. scitula* Toomey) is present.

In contrast, zones 14 and 15 (St. Louis and Ste. Genevieve Limestones) are difficult to identify because the *"Brunsia* facies," which indicates abnormal salinity, eliminates most of the characteristic normal marine representatives of *Eoendothyranopsis* and *Endothyranopsis.* The *"Brunsia* facies" is found as far south as northeastern British Columbia and southeastern Yukon Territory.

The *Eoendothyranopsis pressa* fauna (zones 13–15) is known in the upper part of the Debolt Formation (Macauley, 1958, p. 298) of Fort St. John, in the upper part of the Mount Head Formation of southwestern Alberta (Lummus, Marston, Carnarvon, and Opal Members; Petryk and others, 1970), in the Middle Canyon Formation and in the basal part of the Scott Peak Formation of Huh (1967) in southwestern Idaho, and in the Little Flat Formation and lower part of the Monroe Canyon Limestone in the Idaho depositional province (Sando and others, 1969). This fauna is also a major one in the St. Louis and Ste. Genevieve Limestones of Missouri.

Late Viséan (early Chester).—Zones 16_i and 16_s are recognizable mainly from the presence of Archaediscidae and Endothyridae; Meramec fauna, such as *Eoendothyranopsis* or *Eoforschia,* are absent, and the *Neoarchaediscus-"Eostaffella" discoidea* fauna progressively becomes a major feature; the base of zone 16_s is drawn where *Neoarchaediscus incertus* and *Planospirodiscus* occur abundantly.

Both zones are known in the basal part of the Nizi Formation of British Columbia (Mamet and Gabrielse, 1969), in the lower Etherington Formation of southwestern Alberta (Mamet, 1968), in the upper part of the Scott Peak Formation and in the South Creek Formation in the Lost River Range, Idaho (Huh, 1967), and in the middle part of the Monroe Canyon Limestone in the Idaho depositional province (Sando and others, 1969). The zones are also present from the Aux Vases Sandstone to the Golconda Formation of the Chester type region.

Namurian (middle to upper Chester and Morrow).—The *Eumorphoceras* foraminiferal equivalents (zones 17 and 18) are recognized in the successive bursts of growth of *Asteroarchaediscus baschkiricus* and *Globivalvulina*(?) *parva.* These assemblages are known in an unnamed recessive interval succession of northern Yukon; in the Calico Bluff Formation, Yukon River, east-central Alaska; in the middle and upper part of the Nizi Formation in northern British Columbia; in Mississippian rocks on the Prince of Wales Island, southeastern Alaska; in the middle and upper parts of the Etherington Formation of southeastern British Columbia (Mamet, 1968); in the Surrett Canyon Formation of Huh (1967) in the Lost River Range, Idaho; in the upper part of the Monroe Canyon Limestone of the Idaho depositional province (Sando and others, 1969); and in the middle part of the Amsden Formation in Wyoming. In the midcontinent region, these zones are observed from the Glen Dean Limestone to the Kinkaid Limestone.

The microfauna of zone 19 was not found within the

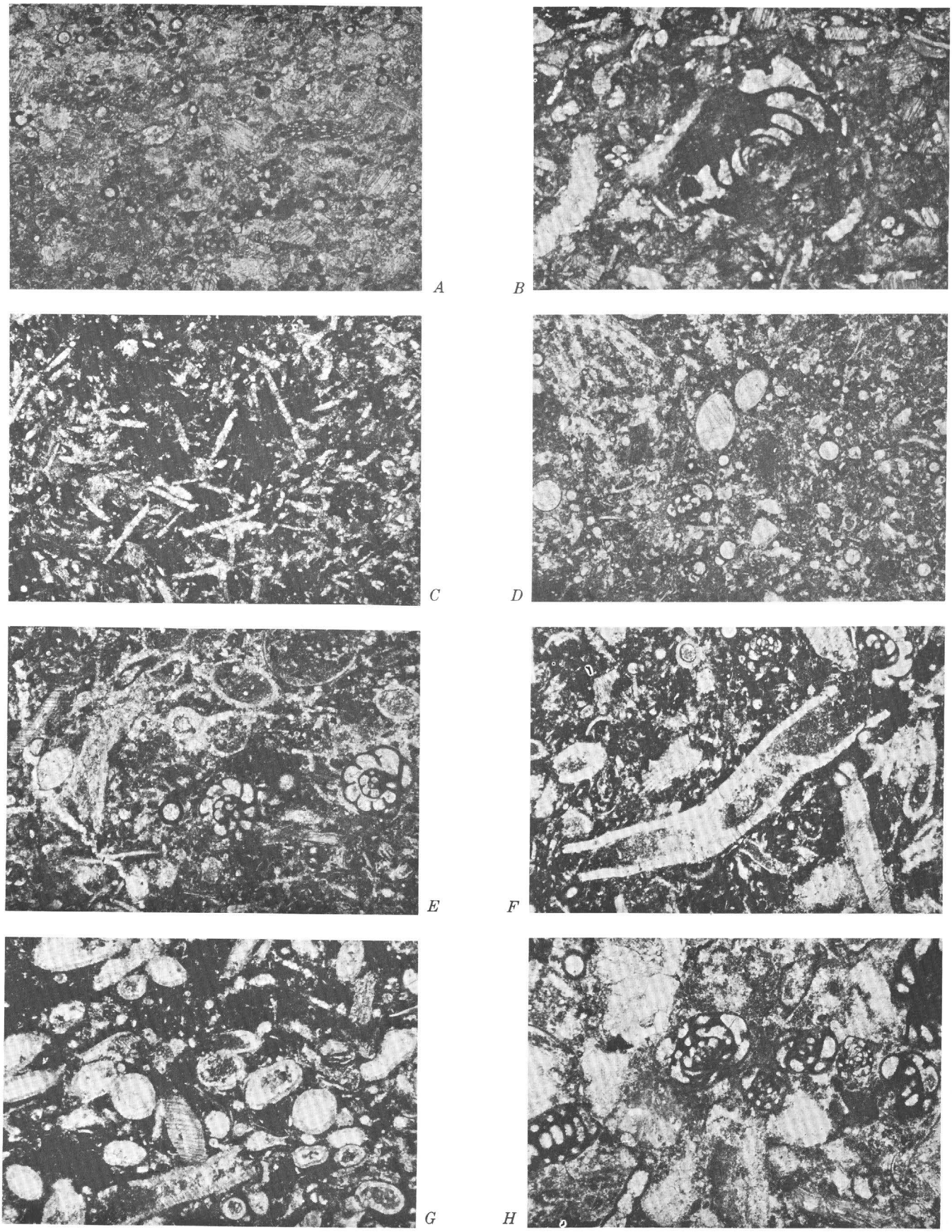

Figure 5.

Figure 5.—Photomicrographs of microfacies and microfossils of sections 70A-4 and 70A-6 of the Alapah Limestone and Kayak(?) Shale, northeastern Alaska.

A. Section 70A-4, 1,570 ft above base, × 25, Alapah Limestone, zone 15, late Viséan, Ste. Genevieve equivalent. Lagoonal, recrystallized grainstone and packstone. Abundant calcispheres (*Calcisphaera* sp.), *Parathurammina* sp., *Vicinesphaera* sp., and *Girvanella* sp. are conspicuous.

B. Section 70A-6, 4,165 ft from the top, × 25, Kayak(?) Shale, zone 11, early Viséan, Salem equivalent. Equatorial section of "*Septatournayella*" *henbesti* Skipp, Holcomb, and Gutschick in a dark, poorly sorted packstone.

C. Section 70A-6, 3,425 ft from the top, × 25, Kayak(?) Shale, zone 14? late Viséan, St. Louis equivalent? Sponge spiculite.

D. Section 70A-6, 2,690 ft from the top, × 25, Alapah Limestone, zone 15, late Viséan, Ste. Genevieve equivalent. Lagoonal, calcisphere-rich wackestone (*Calcisphaera laevis* Williamson, "*Radiosphaera*"). Ostracodes, and *Parathurammina* sp. and *Endothyra* sp. are also present.

E. Section 70A-6, 2,730 ft from the top, × 25, Alapah Limestone, zone 15, late Viséan, Ste. Genevieve equivalent. Poorly sorted packstone. *Endothyranopsis compressa* (Rauzer-Chernoussova and Reitlinger), *Calcisphaera pachysphaerica* (Pronina), *Earlandia* sp., *Kamaena* sp., and "*Issinella*" sp. are conspicuous.

F. Section 70A-6, 2,775 ft from the top, × 25, Alapah Limestone, zone 15, late Viséan, Ste. Genevieve equivalent. "*Issinella*" packstone. *Endothyranopsis* sp., *Calcisphaera* sp., and *Endothyra* sp. are also present.

G. Section 70A-6, 2,690 ft from the top, × 25, Alapah Limestone, zone 15, late Viséan, Ste. Genevieve equivalent. "*Issinella*" packstone.

H. Section 70A-6, 2,660 ft from the top, × 25, Alapah Limestone, zone 15, late Viséan, Ste. Genevieve equivalent. Foraminiferal-pelmatozoan packstone. *Eoendothyranopsis* of the group *E. pressa-E. rara* (*Eoendothyranopsis scitula* Toomey), *Eoendothyranopsis robusta* (McKay and Green), *Endothyra* sp., *Earlandia* sp., *Calcisphaera* sp., and *Earlandinella* sp. are conspicuous.

sections of this report. Zone 19, the *Homoceras* foraminiferal partial equivalent (*Eosigmoilina*?), is known in some of the Sadlerochit Mountains sections (Armstrong, Mamet, and Dutro, 1970) and is the probable equivalent of the basal Baschkirian of the Russian platform. *Homoceras* equivalents appear to be scarce in North America, although the *Eosigmoilina*? fauna has been identified in the upper part of the Surrett Canyon Formation of Huh (1967) in Idaho, in the upper part of the Indian Springs Formation of Rich (1963) in Nevada, and in scattered localities in the Great Basin. The zone is absent by hiatus in the American midcontinent.

Zone 20, characterized by the appearance of the *Lipinella-Millerella* sensu stricto assemblage, could be equivalent to part of the late Baschkirian of the Russian platform. If so, the zone would straddle the Namurian-Westphalian boundary (Gordon, 1964). However, the upper part of the late Baschkirian contains *Profusulinella*, whereas, in zone 22, this fusulinid is known only in the American cordillera. The zone-20 assemblage is known in the basal part of the Pennsylvanian System of Idaho and in the upper part of the Amsden Formation in central and western Wyoming. Zone 20 corresponds to the Morrow Series in the midcontinent.

Undetermined late Carboniferous.—The highest Carboniferous zone identified in this report is zone 21, recognized by the outburst of *Eoschubertella-Pseudostaffella*, associated with *Globivalvulina* sensu stricto. The zone is known in the basal part of the lower limestone unit in Yukon and in the upper part of the Amsden Formation of the Wyoming depositional province. It is present in the basal Atoka Series (Middle Pennsylvanian) of the midcontinent.

No post-Atoka microfaunas are reported here from the Wahoo Limestone.

Microfossils found in the Lisburne Group in the report area are given in the following tabulation:

Microfossils of the Lisburne Group, Franklin and Romanzof Mountains, northeastern Alaska

[Stratigraphic locations are shown on figure 3]

Section 70A-2
Interval: 1,090–1,195 feet
Calcisphaera laevis Williamson
Calcisphaera pachysphaerica (Pronina)
Dainella sp.
Earlandia of the group *E. vulgaris* (Rauzer-Chernoussova and Reitlinger)
Earlandinita sp.
"*Endothyra*" of the group *E.*? *prisca* Rauzer-Chernoussova and Reitlinger
Eoendothyranopsis sp.
Eoendothyranopsis hinduensis (Skipp)
Eoendothyranopsis of the group *E. spiroides* (Zeller)
"*Eoendothyranopsis*" *redwallensis* (Skipp)
Globoendothyra sp.
Globoendothyra of the group *G. baileyi* (Hall)
Globoendothyra of the group *G. tomiliensis* (Grozdilova)
Parathurammina sp.
Stacheia sp.
Stacheoides sp.
Age: zone 12

Interval: 1,390–1,475 feet
Calcisphaera sp.
Earlandia sp.
Endothyra sp.
Eoendothyranopsis sp.
Eoendothyranopsis hinduensis (Skipp)
Eoendothyranopsis of the group *E. pressa–E. rara* (Grozdilova in Lebedeva)
Eoendothyranopsis scitula (Toomey)
Eoendothyranopsis of the group *E. spiroides* (Zeller)
"*Issinella*" sp.
Globoendothyra sp.
Kamaena sp.
Tetrataxis sp.
Age: transition of zones 12 and 13

Interval: 1,495–1,600 feet
Archaediscus sp.
Archaediscus of the group *A. krestovnikovi* Rauzer-Chernoussova
Brunsia sp.
Calcisphaera sp.

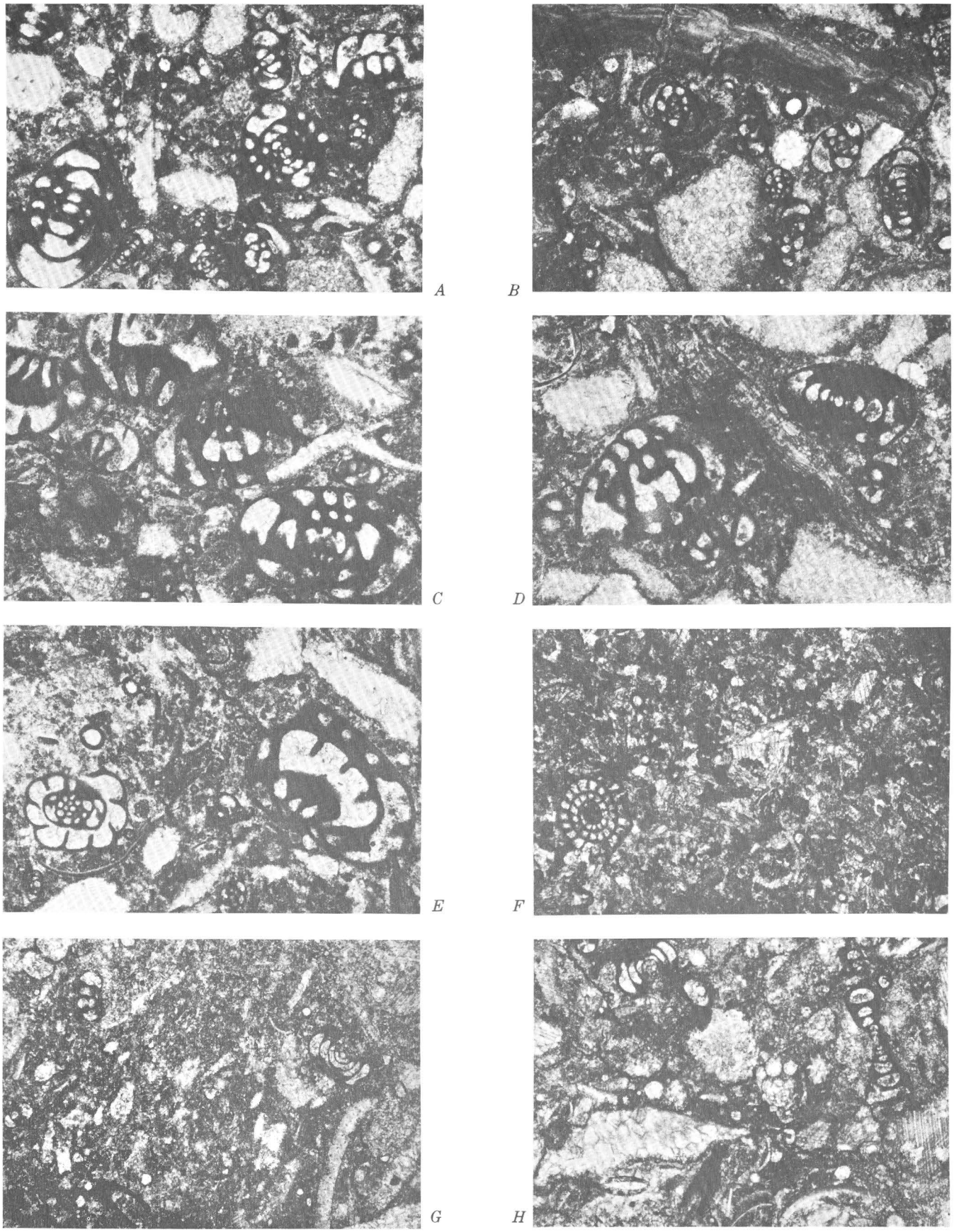

Figure 6.

Figure 6.—Photomicrographs of microfacies and microfossils of sections 70A-6 and 70A-7 of the Alapah Limestone and Kayak(?) Shale, northeastern Alaska.

A–E. Section 70A-6, 2,660 ft from the top, × 25, Alapah Limestone, zone 15, middle late Viséan, Ste. Genevieve equivalent. An exceptionally rich foraminiferal-pelmatozoan-brachiopodal wackestone. Foraminifers are abundant and represented mostly by Endothyranopsidae; *Eoendothyranopsis* of the group *E. ermakiensis* (Grozdilova *in* Lebedeva), *Eoendothyranopsis robusta* (McKay and Green), and *Endothyranopsis compressa* (Rauzer-Chernoussova and Reitlinger). *Calcisphaera pachysphaerica* (Pronina), *Calcisphaera* sp., *Globoendothyra* sp., and *Endothyra* sp. are also noticeable.

F. Section 70A-6, 2,055 ft from the top, × 25, Alapah Limestone, zone 16_i or 16_s undetermined, late Viséan, lower Chester equivalent. Equatorial section of *Eostaffella* sp. and scattered calcispheres in a recrystallized wackestone. Some cement present.

G and *H.* Section 70A-7, 230 feet from the base, × 25, Alapah Limestone, zone 11, early Viséan, Salem equivalent. Slightly recrystallized wackestone and packstone. *Earlandia* of the group *E. clavatula* (Howchin), *Earlandia* of the group *E. vulgaris* (Rauzer-Chernoussova and Reitlinger), *Parathurammina* sp., *Eoforschia* sp., and "*Septatournayella*" are present.

Figure 7.—Photograph of the contact between the Alapah and Wahoo Limestones in section 70A-6. Note the relatively uniform bedding within the Alapah Limestone.

Microfossils of the Lisburne Group, Franklin and Romanzof Mountains, northeastern Alaska—Continued

[Stratigraphic locations are shown on figure 3]

Section 70A-2—Continued
Interval: 1,495–1,600 feet—Continued
"*Cornuspira*" sp.
Dainella sp.
Earlandia sp.
Endothyra sp.
Endothyranopsis sp.
Eoendothyranopsis of the group *E. ermakiensis* (Grozdilova in Lebedeva)

Microfossils of the Lisburne Group, Franklin and Romanzof Mountains, northeastern Alaska—Continued

[Stratigraphic locations are shown on figure 3]

Section 70A-2—Continued
Interval: 1,495–1,600 feet—Continued
Eoendothyranopsis of the group *E. pressa–E. rara* (Grozdilova in Lebedeva)
"*Eoendothyranopsis*" *redwallensis* (Skipp)
Eoendothyranopsis scitula (Toomey)
Globoendothyra sp.
Kamaena sp.
Koninckopora inflata (de Koninck)
Parathurammina sp.
Planoarchaediscus? sp.
Stacheia sp.
Stacheoides sp.
Tetrataxis sp.
Age: zone 13

Interval: 1,650 feet
Archaediscus sp.
Archaediscus of the group *A. krestovnikovi* Rauzer-Chernoussova
Brunsia sp.
Calcisphaera laevis Williamson
Calcisphaera pachysphaerica (Pronina)
"*Cornuspira*" sp.
Earlandia of the group *E. clavatula* (Howchin)
Earlandia of the group *E. vulgaris* (Rauzer-Chernoussova and Reitlinger)
Earlandinella sp.
Endothyra sp.
"*Endothyra*" of the group *E.*? *prisca* Rauzer-Chernoussova and Reitlinger
Endothyranopsis compressa (Rauzer-Chernoussova and Reitlinger)
Endothyranopsis crassa (Brady)
Eoendothyranopsis of the group *E. ermakiensis* (Grozdilova in Lebedeva)
Eoendothyranopsis of the group *E. pressa–E. rara* (Grozdilova in Lebedeva)
Eoendothyranopsis robusta (McKay and Green)
Globoendothyra of the group *G. tomiliensis* (Grozdilova)
Globoendothyra of the group *G. globulus* (d'Eichwald)
Globoendothyra paula (Vissarionova)
"*Issinella*" sp.
Kamaena sp.
Koninckopora inflata (de Koninck)
Parathurammina sp.
Stacheia sp.
Stacheoides sp.
Yukonella sp.
Age: zone 15

Interval: 1,960–2,186 feet
Archaediscus sp.
Archaediscus of the group *A. krestovnikovi* Rauzer-Chernoussova
Calcisphaera sp.
"*Cornuspira*" sp.
Endothyra of the group *E. bowmani* Phillips in Brown emend Brady
Epistacheoides sp.
Globoendothyra of the group *G. globulus* (d'Eichwald)
Kamaena sp.
Parathurammina sp.
Pseudoglomospira sp.
Stacheia sp.
Stacheoides sp.
Zellerina sp.
Age: zone 16_i

Figure 8.—Photograph of sections 70A-2 and 70A-3 viewed to the west. The contact (dashed line) of the Neruokpuk Formation with the Kekiktuk Conglomerate is well exposed on the outcrop. The interval between sections 70A-2 and 70A-3 is marked by complex folding and faulting. The contact between the Wahoo Formation and the Sadlerochit Formation is indicated by solid line on the left side of the photograph.

Microfossils of the Lisburne Group, Franklin and Romanzof Mountains, northeastern Alaska—Continued

[Stratigraphic locations are shown on figure 3]

Section 70A-2—Continued
Interval: 2,490–2,696 feet
Archaediscus sp.
Archaediscus of the group *A. krestovnikovi* Rauzer-Chernoussova
Calcisphaera sp.
"Cornuspira" sp.
Endothyra sp.
Neoarchaediscus sp.
Neoarchaediscus of the group *N. incertus* (Grozdilova and Lebedeva)
Pseudoglomospira sp.
Age: zone 16_S

Section 70A-3
Interval: 0–240 feet
Archaediscus sp.
Asphaltina sp.
Asteroarchaediscus sp.
Asteroarchaediscus baschkiricus (Krestovnikov and Teodorovitch)
Biseriella sp.
Climacammina sp.
Endothyra sp.
Eoschubertella sp.
Eostaffella sp.
Globivalvulina of the group *G. bulloides* Brady
Globoendothyra sp.
Globoendothyra of the group *G. globulus* (d'Eichwald)
Lipinella sp.
Millerella sp.
Neoarchaediscus sp.

Microfossils of the Lisburne Group, Franklin and Romanzof Mountains, northeastern Alaska—Continued

[Stratigraphic locations are shown on figure 3]

Section 70A-3—Continued
Interval: 0–240 feet—Continued
Neoarchaediscus of the group *N. incertus* (Grozdilova and Lebedeva)
Orthovertella sp.
Planoendothyra sp.
Planospirodiscus sp.
Pseudoendothyra britishensis Ross
Pseudostaffella sp.
Tetrataxis sp.
Zellerina sp.
Age: zone 21

Section 70A-4
Interval: 435–690 feet
Calcisphaera sp.
Earlandia sp.
Endothyra sp.
Eoendothyranopsis sp.
Globoendothyra of the group *G. baileyi* (Hall)
Pa. athurammina sp.
Stacheia sp.
Stacheoides sp.
Tetrataxis sp.
Age: zone 11

Interval: 1, 160–1,210 feet
Calcisphaera sp.
Earlandia sp.
Endothyra sp.

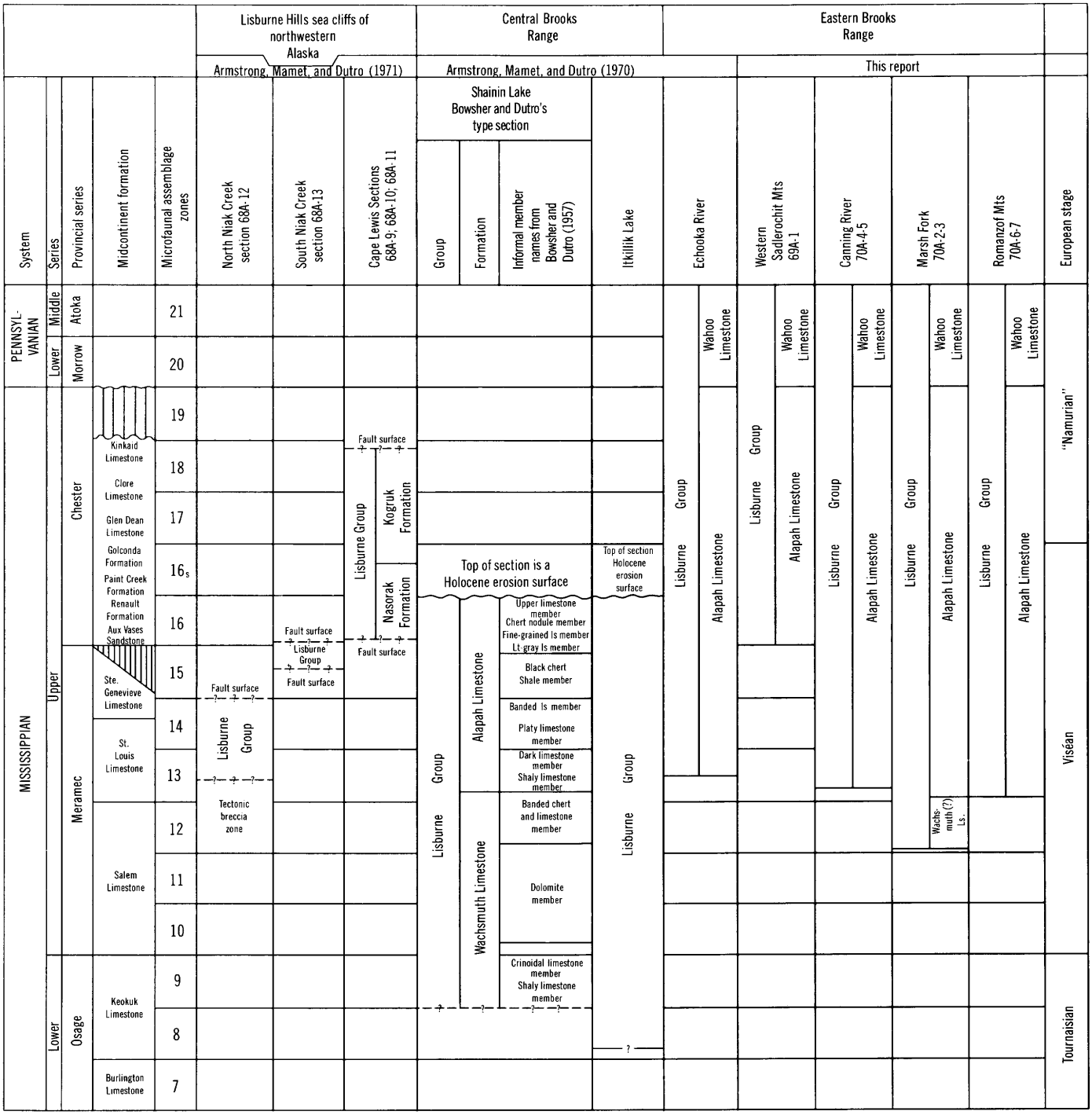

Figure 9.–Regional stratigraphic correlation chart for the Lisburne Group of the Brooks Range and Lisburne Hills of northwestern Alaska.

Microfossils of the Lisburne Group, Franklin and Romanzof Mountains, northeastern Alaska—Continued

[Stratigraphic locations are shown on figure 3]

Section 70A-4—Continued
Interval: 1,160–1,210 feet—Continued
"Endothyra" of the group *E.? prisca* Rauzer-Chernoussova and Reitlinger
Eoendothyranopsis of the group *E. pressa–E. rara* (Grozdilova in Lebedeva)
Eoendothyranopsis of the group *E. spiroides* (Zeller)
Eoendothyranopsis scitula (Toomey)
Globoendothyra paula (Vissarionova)
Stacheia sp.
Age: transition of zones 12 and 13

Interval: 1,310 feet
Archaediscus sp.
Calcisphaera sp.
Earlandia sp.
Endothyra sp.
Eoendothyranopsis of the group *E. pressa–E. rara* (Grozdilova in Lebedeva)
Eoendothyranopsis scitula (Toomey)
Stacheia sp.
Age: zone 13

Interval: 1,410–1,650 feet
Archaediscus of the group *A. krestovnikovi* Rauzer-Chernoussova
Brunsia sp.
Calcisphaera laevis Williamson
Calcisphaera pachysphaerica (Pronina)
Earlandia of the group *E. clavatula* (Howchin)
Earlandia of the group *E. vulgaris* (Rauzer-Chernoussova and Reitlinger)
Endothyra of the group *E. bowmani* Phillips in Brown emend Brady
"Endothyra" of the group *E.? prisca* Rauzer-Chernoussova and Reitlinger
Endothyranopsis compressa (Rauzer-Chernoussova and Reitlinger)
Endothyranopsis crassa (Brady)
Eoendothyranopsis of the group *E. ermakiensis* (Grozdilova in Lebedeva)
Eoendothyranopsis robusta (McKay and Green).
Girvanella sp.
Globoendothyra of the group *G. globulus* (d'Eichwald)
Globoendothyra paula (Vissarionova)
"Issinella" sp.
Kamaena sp.
Parathurammina sp.
Planoarchaediscus? sp.
Stacheia sp.
Stacheoides sp.
Vicinesphaera sp.
Yukonella sp.
Age: zone 15

Interval: 2,050–2,235 feet
Aoujgalia sp.
Archaediscus sp.
Archaediscus of the group *A. krestovnikovi* Rauzer-Chernoussova
Earlandia sp.
Endothyra sp.
"Endothyra" of the group *E.? prisca* Rauzer-Chernoussova and Reitlinger

Microfossils of the Lisburne Group, Franklin and Romanzof Mountains, northeastern Alaska—Continued

[Stratigraphic locations are shown on figure 3]

Section 70A-4—Continued
Interval: 2,050–2,235 feet—Continued
Eostaffella sp.
Globoendothyra sp.
Parathurammina sp.
Stacheia sp.
Stacheoides sp.
Zellerina sp.
Age: zone 16_i

Section 70A-5
Interval: 380–840 feet
Aoujgalia? sp.
Apterrinellids
Archaediscus sp.
Asphaltina sp.
Asteroarchaediscus sp.
Asteroarchaediscus baschkiricus (Krestovnikov and Teodorovitch)
Biseriella sp.
Climacammina sp.
Endothyra sp.
Eoschubertella sp.
Globivalvulina sp.
Globivalvulina of the group *G. bulloides* Brady
Globoendothyra sp.
"Issinella" sp.
Komia sp.
Neoarchaediscus sp.
Neoarchaediscus parvus (Rauzer-Chernoussova)
Palaeotextularia sp.
Planoendothyra sp.
Planospirodiscus sp.
Pseudoendothyra sp.
Pseudoendothyra britishensis Ross
Pseudoglomospira sp.
Pseudostaffella sp.
Stacheiinae
Tetrataxis sp.
Zellerina sp.
Age: zone 21

Section 70A-6
Interval: 4,150–4,165 feet
Calcisphaera laevis Williamson
Calcisphaera pachysphaerica (Pronina)
Earlandia of the group *E. vulgaris* (Rauzer-Chernoussova and Reitlinger)
Endothyra sp.
Eoforschia sp.
Globoendothyra of the group *G. baileyi* (Hall)
Latiendothyra sp.
Parathurammina sp.
"Septatournayella" henbesti Skipp, Holcomb, and Gutschick
Stacheia sp.
Stacheoides sp.
Age: zone 11

Interval. 3,510–3,515
Archaediscus krestovnikovi Rauzer-Chernoussova
Calcisphaera sp.

Microfossils of the Lisburne Group, Franklin and Romanzof Mountains, northeastern Alaska—Continued

[Stratigraphic locations are shown on figure 3]

Section 70A-6—Continued
Interval: 3,510–3,515—Continued

Earlandia sp.
Endothyra sp.
Eoendothyranopsis of the group *E. pressa–E. rara* (Grozdilova in Lebedeva)
Eoforschia sp.
Globoendothyra of the group *G. tomiliensis* (Grozdilova)
Stacheia sp.
Stacheoides sp.
Age: zone 13 or younger

Interval: 3,290–3,315 feet
Brunsia sp.
Brunsia lenensis Bogush and Yuferev
Brunsia irregularis (von Möller)
Earlandia sp.
Globoendothyra sp.
Age: probably zone 14?

Interval: 2,570–2,795 feet
Archaediscus sp.
Archaediscus of the group *A. krestovnikovi* Rauzer-Chernoussova
Calcisphaera sp.
Calcisphaera laevis Williamson
Calcisphaera pachysphaerica (Pronina)
Earlandia of the group *E. vulgaris* (Rauzer-Chernoussova and Reitlinger)
Earlandinella sp.
Endothyra sp.
Endothyranopsis sp.
Endothyranopsis compressa (Rauzer-Chernoussova and Reitlinger)
Eoendothyranopsis sp.
Eoendothyranopsis of the group *E. ermakiensis* (Grozdilova in Lebedeva)
Eoendothyranopsis of the group *E. pressa–E. rara* (Grozdilova in Lebedeva)
Eoendothyranopsis scitula (Toomey)
Eoendothyranopsis robusta (McKay and Green)
Girvanella sp.
Globoendothyra sp.
Globoendothyra of the group *G. globulus* (d'Eichwald)
Globoendothyra paula (Vissarionova)
"*Issinella*" sp.
Kamaena sp.
Parathurammina sp.
"*Radiosphaera*" sp.
Stacheia sp.
Stacheoides sp.
Vicinesphaera sp.
Age: zone 15

Interval: 1,970–2,360 feet
Archaediscus sp.
Archaediscus of the group *A. krestovnikovi* Rauzer-Chernoussova
Calcisphaera laevis Williamson
Calcisphaera pachysphaerica (Pronina)
"*Cornuspira*" sp.
Earlandia sp.
Earlandia of the group *E. clavatula* (Howchin)

Microfossils of the Lisburne Group, Franklin and Romanzof Mountains, northeastern Alaska—Continued

[Stratigraphic locations are shown on figure 3]

Section 70A-6—Continued
Interval: 1,970–2,360 feet—Continued

Earlandia of the group *E. vulgaris* (Rauzer-Chernoussova and Reitlinger)
Endothyra sp.
"*Endothyra*" of the group *E.? prisca* Rauzer-Chernoussova and Reitlinger
Eostaffella sp.
Globoendothyra sp.
Parathurammina sp.
Pseudoendothyra sp.
Pseudoglomospira sp.
cf. *Planoendothyra* sp.
Zellerina sp.
Age: zone 16_i

Interval: 1,600–1,630 feet
Archaediscus sp.
Archaediscus of the group *A. krestovnikovi* Rauzer-Chernoussova
Endothyra sp.
Eostaffella sp.
Globoendothyra sp.
Neoarchaediscus sp.
Planospirodiscus sp.
Pseudoendothyra sp.
Pseudoglomospira sp.
Tetrataxis sp.
"*Tetrataxis*" of the group *T.? eominima* Rauzer-Chernoussova
Age: zone 16_s

Interval: 1,420–1,400 feet
Archaediscus sp.
Asteroarchaediscus sp.
Asteroarchaediscus baschkiricus (Krestovnikov and Teodorovitch)
Endothyra sp.
Neoarchaediscus sp.
Planospirodiscus sp.
Age: zone 17

Interval: 1,160–1,180 feet
Archaediscus sp.
Asteroarchaediscus sp.
Biseriella parva (Chernysheva)
"*Cornuspira*" sp.
Endothyra sp.
Neoarchaediscus sp.
Age: zone 18

Interval: 310–380 feet
Asphaltina sp.
Biseriella sp.
Endothyra sp.
Globivalvulina sp.
Age: zone 20 or younger

Interval: 0–115 feet
Archaediscus sp.
Asphaltina sp.
Asteroarchaediscus sp.

Microfossils of the Lisburne Group, Franklin and Romanzof Mountains, northeastern Alaska—Continued

[Stratigraphic locations are shown on figure 3]

Section 70A-6—Continued
Interval: 0—115 feet—Continued
Asteroarchaediscus baschkiricus (Krestovnikov and Teodorovitch)
Biseriella sp.
Endothyra sp.
Eoschubertella sp.
Eostaffella sp.
Globivalvulina sp.
Globivalvulina bulloides Brady
Globoendothyra sp.
Lipinella sp.
Neoarchaediscus sp.
Orthovertella sp.
Planoendothyra sp.
Planospirodiscus sp.
Pseudoendothyra sp.
Pseudostaffella sp.
Tetrataxis sp.
Trepeilopsis sp.
Zellerina sp.
Age: zone 21

Section 70A-7
Interval: 230—250 feet
Calcisphaera sp.
Calcisphaera laevis Williamson
Earlandia sp.
Earlandia of the group *E. clavatula* (Howchin)
Earlandia of the group *E. vulgaris* (Rauzer-Chernoussova and Reitlinger)
Eotuberitina sp.
Endothyra sp.
Earlandinella? sp.
Eoforschia sp.
Globoendothyra of the group *G. baileyi* (Hall)
cf. *Latiendothyra* sp.
"Septatournayella" henbesti Skipp, Holcomb, and Gutschick
Stacheia sp.
Stacheoides sp.
Age: transition of zones 11 and 12

Lithostrotionoid coral zones

Lithostrotionoid corals are abundant in the Meramec-age parts of the Alapah Limestone and common in the Atoka-age beds of the Wahoo Limestone. They are rare in Chester-age beds (fig. 10).

The lithostrotionoid corals collected from northeastern Alaska belong to the same taxa that are prolific in the shallow-water shelf carbonates of the Lisburne Group in the central and western Brooks Range (Armstrong and Mamet, 1970; Armstrong, Mamet and Dutro, 1971; Armstrong, 1970, 1972a, 1972b).

Large stratigraphic coral collections were made from section 70A-2, from 855 to 2,200 feet above the base. The Wahoo Limestone from 15 to 100 feet above the base of section 70A-3 yielded several colonies of *Corwenia* sp. (figs, 3, 8). Smaller collections of Mississippian corals were made in the Alapah Limestone of section 70A-4. The Wahoo Limestone about 590 feet above the base of section 70A-5 has numerous tabulate corals belonging to the genus *Michelinia* sp. The Romanzof Mountains section 70A-6 contains a sparse coral fauna, relative to that in section 70A-2. No colonial corals were found in the Kayak(?) Shale in stratigraphic levels 3,200 feet below the top of the section. These beds are argillaceous limestone of zones 13? and 14? that was probably unfavorable for coral growth. Within all these sections corals are generally abundant in the cleaner, less argillaceous limestones of zones 12 through 15. In zones 16_s and 16_i above, *Lithostrotionella* aff. *L. mclareni* (Sutherland) is generally the only coral. The Alapah Limestone in the west Sadlerochit Mountains section, 69A-1, which is Chester in age and occurs 1,120 feet above the base, contains *Lithostrotion (Siphonodendron)* sp. in zone 18. The Wahoo Limestone at this section contains, in zone 21, numerous *Lithostrotionella* of Atoka age (Pennsylvanian).

The known stratigraphic distribution of lithostrotionoid corals in the Lisburne Group (Mississippian and Pennsylvanian) of northeastern Alaska is shown in figure 10. This figure, when compared with a similar illustration by Armstrong, Mamet, and Dutro (1970, fig. 9) for the lithostrotionoid corals of northwestern Alaska, reveals certain differences. In the Lisburne Hills sea cliffs and the De Long Mountains, the large and diversified Meramec coral fauna persists into the lower part of zone 16_i (lowest Chester), whereas, in the northeastern Brooks Range, stratigraphic evidence suggests that this coral fauna disappears at the end of zone 15. This late Meramec extinction conforms with Macqueen and Bamber's (1968) evidence from the Mount Head Formation of southwestern Alberta that shows the extinction of the *L. (S.) warreni* Nelson, *Thysanophyllum astraeiforme* (Warren), and *Lithostrotionella mclareni* (Sutherland) fauna at the end of Meramec (zone 15) time. Significant changes in the stratigraphic range of certain coral species are documented by the large coral collections from limestones in the Romanzof and Franklin Mountains. The stratigraphic range in the Lisburne Group of *Lithostrotion (Siphonodendron) sinuosum* (Kelly); *L. (S.) warreni* Nelson; *Sciophyllum alaskaensis* Armstrong; and *Thysanophyllum astraeiforme* (Warren) is extended into zone 12.

REFERENCES

Armstrong, A. K., 1970, Carbonate facies and lithostrotionid corals of the Mississippian Kogruk Formation, DeLong Mountains, northwestern Alaska: U.S. Geol. Survey Prof. Paper 664, 38 p.

—— 1972a, Biostratigraphy of Mississippian lithostrotionoid corals, Lisburne Group, arctic Alaska: U.S. Geol. Survey Prof. Paper 743-A. [In press]

—— 1972b, Pennsylvanian carbonates, paleoecology and colonial corals, north flank, eastern Brooks Range, arctic Alaska: U.S. Geol. Survey Prof. Paper 747. [In press]

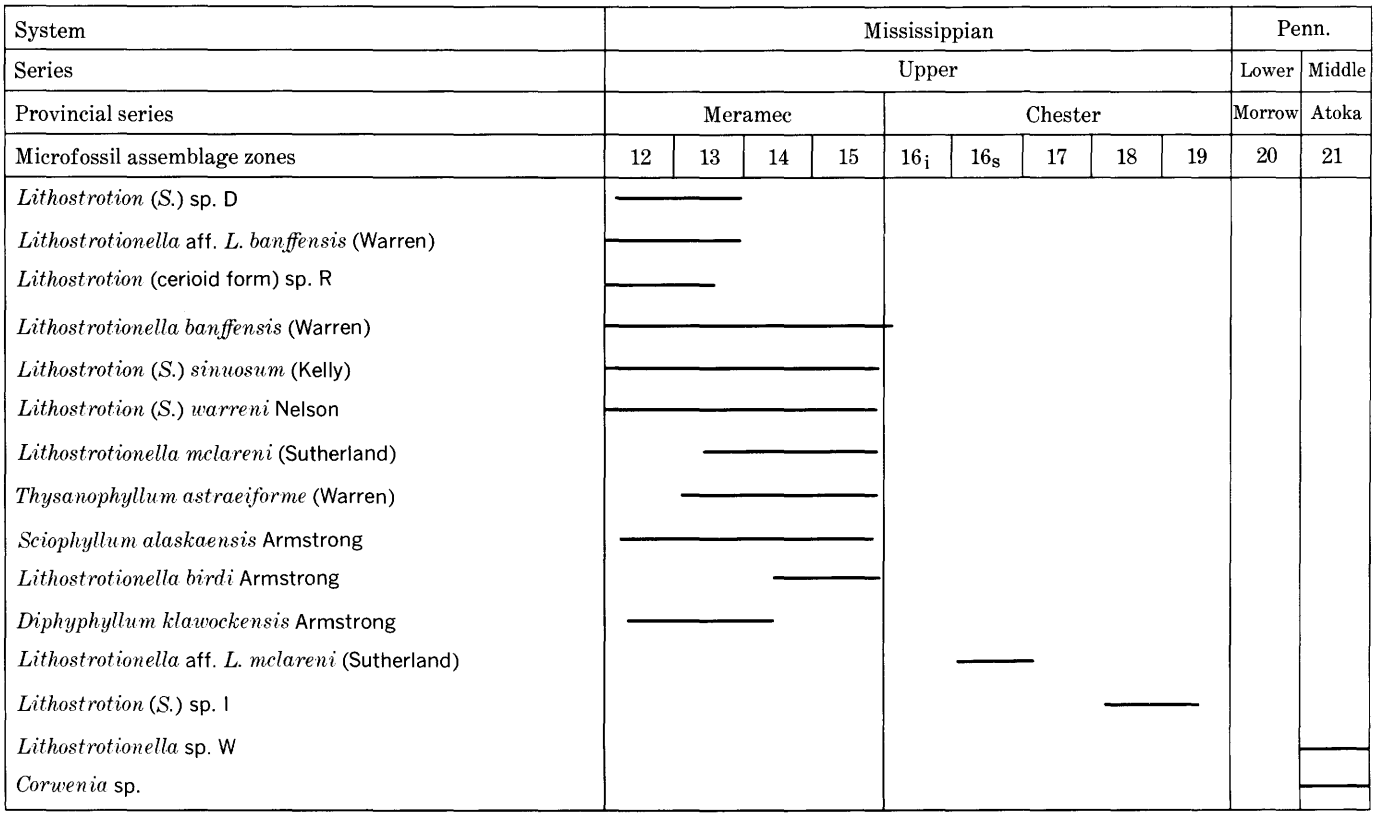

Figure 10.—Stratigraphic range chart of the lithostrotionoid corals in the Lisburne Group of northeastern Alaska.

Armstrong, A. K., and Mamet, B. L., 1970, Biostratigraphy and dolomite porosity trends of the Lisburne Group, *in* Adkison, W. L., and Brosgé, M. M., eds., Proceedings of the geological seminar on the North Slope of Alaska: Los Angeles, Pacific Sec. Am. Assoc. Petroleum Geologists, p. N1–N16, 12 figs.

Armstrong, A. K., Mamet, B. L., and Dutro, J. T., Jr., 1970, Foraminiferal zonation and carbonate facies of the Mississippian and Pennsylvanian Lisburne Group, central and eastern Brooks Range, Alaska: Am. Assoc. Petroleum Geologists Bull., v. 54, no. 5, p. 687–698, 4 figs.

—— 1971, Lisburne Group, Cape Lewis–Niak Creek, northwestern Alaska, *in* Geological Survey Research 1971: U.S. Geol. Survey Prof. Paper 750-B, p. B23–B34, 9 figs.

Bowsher, A. L., and Dutro, J. T., Jr., 1957, The Paleozoic section in the Shainin Lake area, central Brooks Range, Alaska: U.S. Geol. Survey Prof. Paper 303-A, 39 p., 6 pls., 4 figs.

Brosgé, W. P., Dutro, J. T., Jr., Mangus, M. D., and Reiser, H. N., 1962, Paleozoic sequence in eastern Brooks Range, Alaska: Am. Assoc. Petroleum Geologists Bull., v. 46, no. 12, p. 2174–2198.

Detterman, R. L., 1970, Sedimentary history of the Sadlerochit and Shublik Formations in northeastern Alaska, *in* Adkison, W. L., and Brosgé, M. M., eds., Proceedings of the geological seminar on the North Slope of Alaska: Los Angeles, Pacific Sec. Am. Assoc. Petroleum Geologists, p. O1–O13, 9 figs.

Dunham, R. J., 1962, Classification of carbonate rocks according to deposition texture, *in* Classification of carbonate rocks–A symposium: Am. Assoc. Petroleum Geologists Mem. 1, p. 108–121.

Gordon, Mackenzie, Jr., 1964, Carboniferous cephalopods of Arkansas: U.S. Geol. Survey Prof. Paper 460, 321 p.

Huh, O. K., 1967, The Mississippian System across the Wasatch line, east central Idaho, extreme southwestern Montana: Montana Geol. Soc. 18th Ann. Field Conf. Guidebook, p. 31–62.

Macauley, G., 1958, Late Paleozoic of Peace River area, Alberta, *in* Jurassic and Carboniferous of Western Canada: Am. Assoc. Petroleum Geologists Allen Memorial Vol., p. 289–308.

Macqueen, R. W., and Bamber, E. W., 1968, Stratigraphy and facies relationships of the Upper Mississippian Mount Head Formation, Rocky Mountains and foothills, southwestern Alberta: Canadian Petroleum Geology Bull., v. 16, no. 3, p. 225–287, 11 figs.

Mamet, B. L., 1962, Remarques sur la microfauna de Foraminiferes du Dinantien: Soc. Geol. Belgique Bull., v. 70, no. 2, p. 166–173.

—— 1968, Foraminifera, Etherington Formation (Carboniferous), Alberta, Canada: Canadian Petroleum Geology Bull., v. 16, no. 2, p. 167–179.

Mamet, B. L., and Belford, D., 1968, Carboniferous Foraminifera, Bonaparte Gulf basin, northwestern Australia: Micropaleontology, v. 14, no. 3, p. 339–347.

Mamet, B. L., and Gabrielse, H., 1969, Foraminiferal zonation and stratigraphy of the type section of the Nizi Formation (Carboniferous systems, Chesteran Stage), British Columbia: Canada Geol. Survey Paper 69-16, p. 1–21, 6 figs.

Mamet, B. L., and Mason, D., 1968, Foraminiferal zonation of the lower Carboniferous Connor Lake section, British Columbia: Canadian Assoc. Petroleum Geologists Bull., v. 16, no. 2, p. 147–166.

Mamet, B. L., and Skipp, B. A., 1970, Preliminary foraminiferal correlations of early Carboniferous strata in the North American Cordillera, *in* Colloque sur la stratigraphie du Carbonifère: Liège Univ. Cong. et Colloques, v. 55, p. 327–348.

Petryk, A. A., Mamet, B. L., and Macqueen, R. W., 1970, Preliminary foraminiferal zonation, lower Carboniferous Rundle Group, southwestern Alberta: Canadian Petroleum Geology Bull., v. 18, no. 1, p. 84–103.

Reiser, H. N., Dutro, J. T., Jr., Brosgé, W. P., Armstrong, A. K., and Detterman, R. L., 1970, Progress map, geology of the Sadlerochit and Shublik Mountains [Alaska]: U.S. Geol. Survey open-file map, scale 1:63,360.

Rich, Mark, 1963, Petrographic analysis of Bird Spring Group (Carboniferous-Permian) near Lee Canyon, Clark County, Nevada: Am. Assoc. Petroleum Geologists Bull., v. 47, no. 9, p. 1657–1681.

Sando, W. J., Mamet, B. L., and Dutro, J. T., Jr., 1969, Carboniferous megafaunal and microfaunal zonation in the northern Cordillera of the United States: U.S. Geol. Survey Prof. Paper 613-E, 29 p., 7 figs.

CORRELATION OF THE ORDOVICIAN SHELLY FACIES ORTHIDIELLA ZONE WITH ZONES OF THE GRAPTOLITIC FACIES, TOQUIMA RANGE, NEVADA, AND NORTH WHITE RIVER REGION, BRITISH COLUMBIA

By E. H. McKEE, B. S. NORFORD[1], and R. J. ROSS, JR.,
Menlo Park, Calif., Calgary, Alberta, Denver, Colo.

Abstract.—The *Orthidiella* zone of the carbonate facies is represented in the Antelope Valley Limestone of the Toquima Range where graptolites of the same strata allow correlation with the *Paraglossograptus etheridgei* zone. A thick development of the *Orthidiella* zone in the Glenogle and Outram Formations of the North White River region in British Columbia contains graptolites that indicate that much of the zone is equivalent to the *Isograptus caduceus* zone but that the upper part probably is equivalent to the *Paraglossograptus etheridgei* zone. Combination of the paleontologic and stratigraphic data from the two widely separated regions indicates that the *Orthidiella* zone spans the *Paraglossograptus etheridgei* zone and the underlying *Isograptus caduceus* zone, and that part of the *caduceus* zone is older and part of the *etheridgei* zone is younger than the *Orthidiella* zone. Presence of the *Paraglossograptus etheridgei* zone is established within the contrasting siliceous argillites of the Vinini Formation of the Toquima Range in a collection (USGS colln. D2130 C0) that includes *Trichograptus* aff. *T. immotus* Harris and Thomas and *Didymograptus spinosus* Ruedemann, associated with *Paraglossograptus etheridgei* Harris and species of *Diplograptus, Amplexograptus, Glossograptus,* and *Didymograptus.*

In the northern part of the Toquima Range in central Nevada (fig. 1) siliceous western and transitional facies rocks of the Vinini Formation are in fault contact (Roberts Mountains thrust) with carbonate rocks of about the same age, representative of the eastern assemblage recognized in Nevada (Roberts and others, 1958). The eastern assemblage rocks crop out in two windows; the southern window (fig. 2) near the upper reaches of Ikes Canyon exposes Antelope Valley Limestone from which graptolites as well as brachiopods and trilobites were collected (USGS collns. D2217 C0–D2220 C0).

The two facies (transitional and eastern) of lower Paleozoic rocks, telescoped together by the Roberts Mountains thrust, probably represent sites of sedimentation originally at least 60 miles apart.

Graptolites in the Vinini Formation and a shelly fauna associated with graptolites in the Antelope Valley Limestone offer a unique opportunity to correlate these units and to compare Middle Ordovician zonations based on graptolites and shelly fossils. The Glenogle and Outram Formations of the North White River region of southeastern British Columbia contain graptolites and other fossils that offer additional data

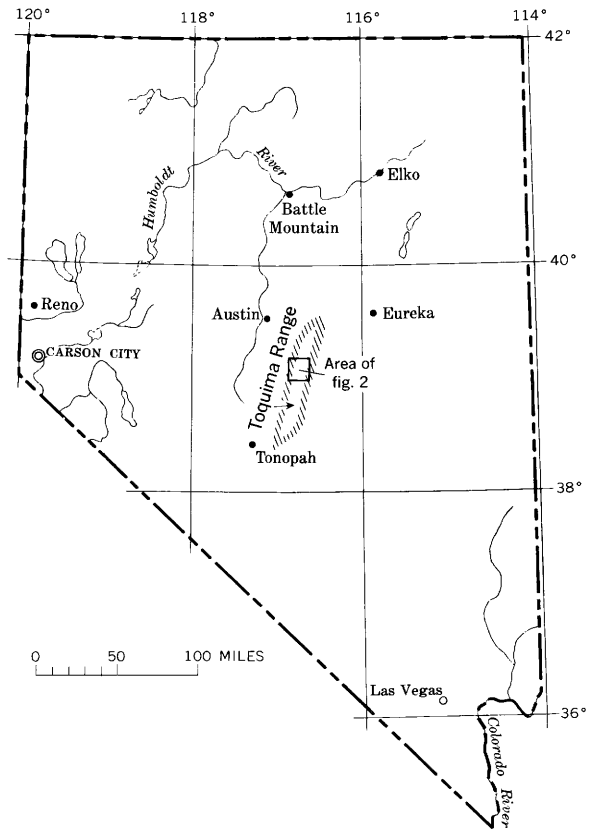

Figure 1.—Map of Nevada, showing area of the Toquima Range from which fossils described in this paper were collected.

[1]Geological Survey of Canada.

U.S. GEOL. SURVEY PROF. PAPER 800-C, PAGES C145-C156

on the zonations and extend the zonal relationships over a large part of the western Cordilleran belt.

Acknowledgments.—W. B. N. Berry of the University of California at Berkeley examined graptolites from the Toquima Range collections, verifying and correcting Ross's identifications. Our Canadian colleagues D. E. Jackson identified graptolites from sections in British Columbia, M. J. Copeland reported on ostracodes, and G. B. Leech collected from the Outram Formation important supporting evidence on the composition of the *Orthidiella* zone fossil assemblage in the Canadian section.

C. W. Merriam, F. J. Kleinhampl, W. B. N. Berry, and D. E. Jackson critically reviewed the manuscript.

STRATIGRAPHY IN NEVADA

Near Pete's Summit in the Toquima Range (fig. 2), unlike most of central and western Nevada, a stratigraphic succession of part of the Vinini Formation can be determined. Here about 1,000 feet of section can be pieced together from tectonic slices that are repeated by imbricate faults. The middle 400 to 600 feet of this composite section contains graptolites that span most of the Middle and the lower part of the Upper Ordovician (Arenig, Llanvirn, Llandeilo, Caradoc). This section of siliceous Ordovician rocks was first described by Kay (1960) and by Kay and Crawford (1964), who named it the Clipper Canyon Group consisting of four formations. The name Vinini Formation is used here in preference to Clipper Canyon because the rocks are similar to the Vinini from other parts of Nevada and because Kay and Kay and Crawford's formations are not recognizable map units elsewhere.

The graptolite-bearing part of the section is mostly siltstone (some shaly), fine-grained sandstone, and thin-bedded chert. Several thin limestone beds and at least two quartzite units as much as 60 feet thick are useful marker horizons. In general the rocks are shades of pastel purple, gray, and pink, although the chert and some of the shale are black. This lithology is typical of the western to transition facies of the Ordovician described by Roberts (1964, p. 22).

Vinini Formation

A composite section of the Vinini Formation in the Pete's Spring area and all graptolite horizons are shown in figure 3. Most of this section is unmeasured; thicknesses are estimated from one or more locations that usually contain less than 300 feet of unfaulted strata. The middle 400 to 600 feet, in which graptolites are found, can be measured more precisely because prominent quartzite beds as well as a variety of different lithologic types can be used as markers. Thickness and age of the remaining section are more speculative. Strata consist of uniform, unfossiliferous dark chert, siltstone, and, in a few places, pillow basalt. Estimated total thickness ranges from ours of about 2,000 feet to over 3,000 feet recorded by Kay and Crawford (1964, p. 434). All the Vinini in the region, not only that near Pete's Spring, may amount to as much as 5,000 or 6,000 feet of siliceous strata.

Graptolites from the Vinini Formation in the area studied include the following:

USGS colln. D2130 CO. Vinini Formation at the turquoise mine 0.6 mile south-southeast of Turquoise Spring. Nevada coordinates, central zone: E. 467,250 ft, N. 1,597,500 ft, Wildcat Peak quadrangle, Nevada.

Phyllograptus cf. *P. angustifolius* var. *magnificus* Ruedemann (Ruedemann, 1947, pl. 90, fig. 20) or *P. nobilis* Harris and Keble
Tetragraptus sp.
Didymograptus spinosus Ruedemann
Trichograptus aff. *T. immotus* Harris and Thomas
Cardiograptus crawfordi Harris
?Glossograptus acanthus Elles and Wood
Paraglossograptus etheridgei Harris
Diplograptus cf. *D. decoratus* var. *amplexograptoideus* Ross and Berry
Amplexograptus arctus Elles and Wood
Amplexograptus confertus (Lapworth)
Caryocaris sp. (phyllocarid crustacean)

This assemblage is considered to be equivalent to that of the *P. etheridgei* zone in Texas (zone 9 of Berry, 1960a, p. 22, and a few elements from zone 10 and zone 8) and accordingly would hold a similar position in the Middle Ordovician of Australia (Harris and Ghomas, 1938, p. 66).

Didymograptus spinosus Ruedemann has been reported in New York, Arkansas, and British Columbia by Ruedemann (1947, p. 348). Jackson and Lenz (1962, p. 35, 39) recorded this species in the Llanvirn of the Richardson Mountains, Yukon Territory, and noted that graptolite assemblages above this stage become less provincial. Jackson, Steen, and Sykes (1964, p. 147, 150) reported *D. spinosus* from northeastern British Columbia, and Larson and Jackson (1966, p. 496) record it in the Glenogle Formation.

Our specimens of the *D. spinosus* type show so much variation that it is almost impossible to distinguish some of them from *D. nodosus* Harris, a species of zonal value in the highest Darriwilian of Victoria (Harris and Thomas, 1935, p. 294–295) and there found with *Trichograptus immotus* and *Paraglossograptus etheridgei.* Berry (1960a, p. 41, 62) records *D. nodosus* in West Texas in his zone of *P. etheridgei.* It is probable that *D. spinosus* and *D. nodosus* are synonyms; certainly they seem to occur stratigraphically within the same zone. Neither species has been reported previously in central Nevada.

Another collection of about the same age is listed below:

USGS colln. D2131 CO. Vinini Formation at Pete's Summit. Nevada coord., central zone: E. 464,600 ft, N. 1,613,200 ft, Wildcat Peak quad., Nevada.

Didymograptus sp.
Phyllograptus nobilis Harris and Keble
Pterograptus sp. or *Pseudobryograptus* sp.
Glossograptus hincksi (Hopkinson)
Diplograptus decoratus Harris and Thomas
Amplexograptus cf. *A. confertus* (of Harris and Thomas)

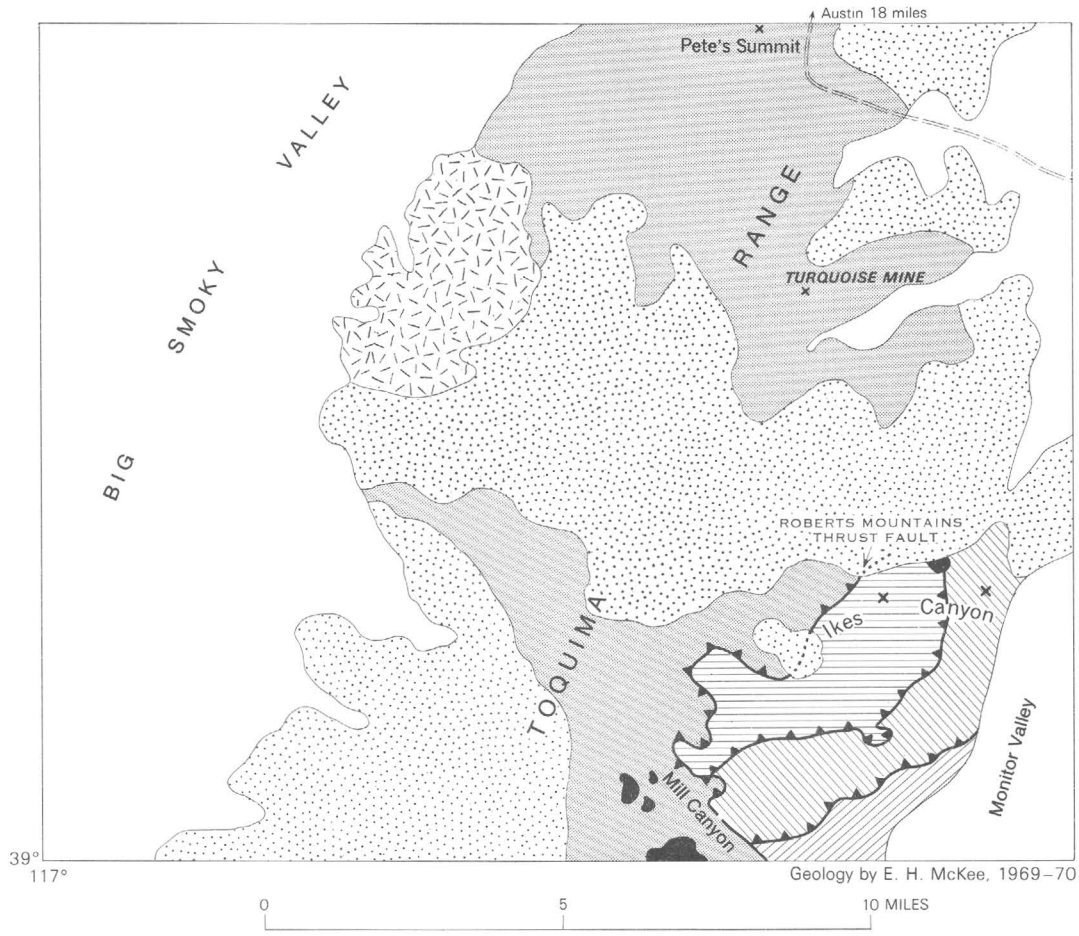

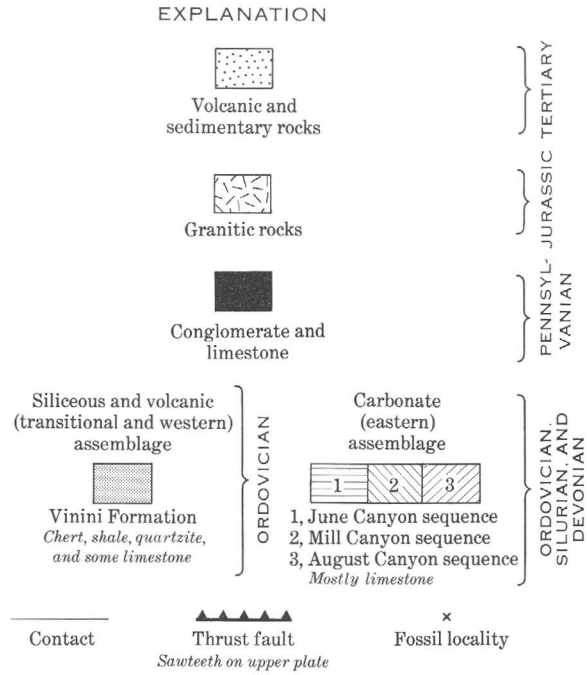

Figure 2.–Geologic map of part of the Toquima Range, Nev.

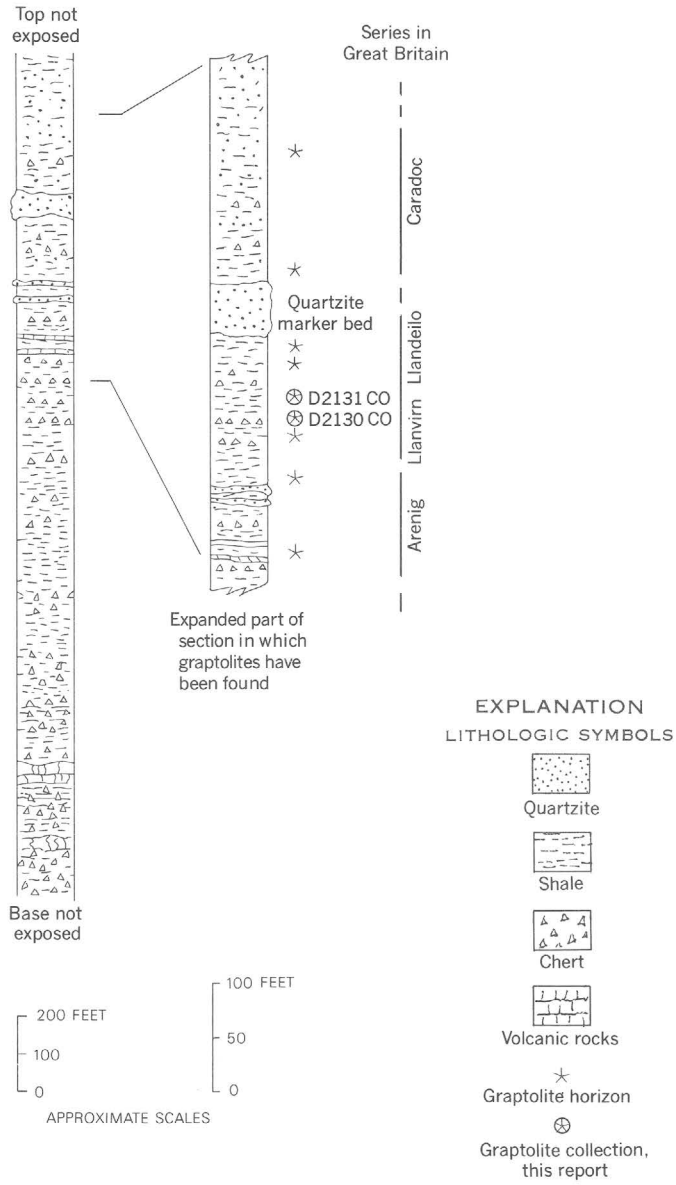

Figure 3.—Composite section of the Vinini Formation from the area near Pete's Summit (northern part of fig. 2). Thickness estimated.

The age of this collection is probably late in the zone of *P. etheridgei*; it includes some elements of the zone of *Glyptograptus teretiusculus* and, therefore, is probably slightly younger than collection D2130 C0.

We do not mean to imply that all the Vinini and Vinini-like strata of the Toquima Range are correlative with the zone of *P. etheridgei*. Kay and Crawford (1964, p. 433–436) have previously shown that these rocks have an extended stratigraphic range in the Ordovician.

Antelope Valley Limestone (June Canyon sequence)

The Antelope Valley Limestone occurs in three somewhat different sequences of Paleozoic rocks that have been thrust together and are now exposed in the Ikes Canyon window (fig. 2). The upper thrust slice, named the June Canyon sequence by Kay and Crawford (1964), contains about 600 to 700 feet of Antelope Valley Limestone between shaly beds of the Ninemile Formation (Ordovician) and massive limestone of the Tor Limestone (Silurian and Devonian) (fig. 4). A few feet of the monograptid-bearing Roberts Mountains Formation occurs below the Tor. About 10 feet of dark-gray calcarenite, probably referable to the Ordovician Caesar Canyon Limestone of Kay (1960), overlies the Antelope Valley limestones and underlies the Roberts Mountains Formation.

Collections made from the Antelope Valley Limestone in the north wall of the upper reaches of Ikes Canyon include

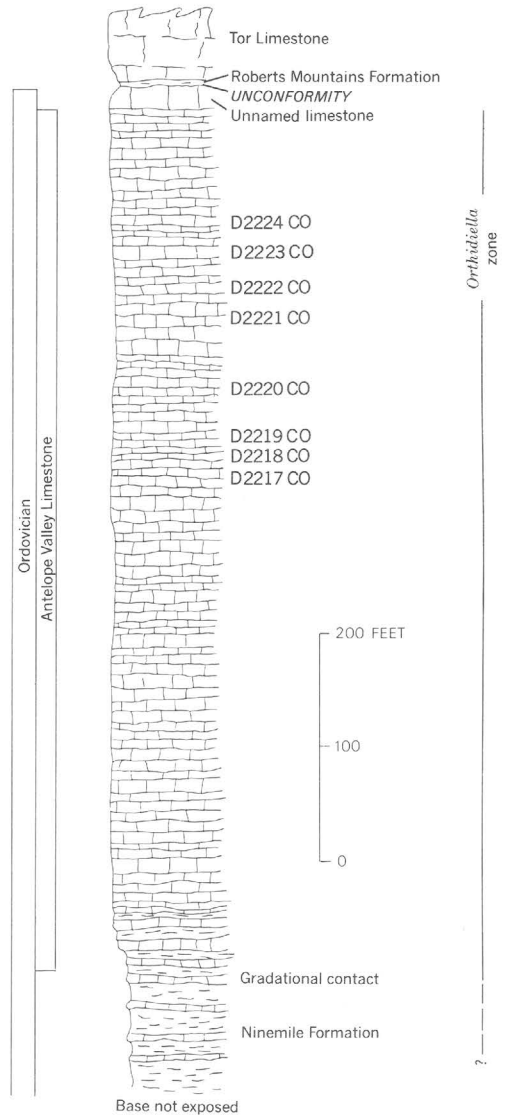

Figure 4.—Composite section of the Antelope Valley Limestone, June Canyon sequence, with approximate stratigraphic position of fossil collections discussed in this paper.

trilobites, brachiopods, and graptolites. In descending stratigraphic order these collections (Nevada coord., central zone: E. 473,150 ft, N. 1,567,750 ft) include:

USGS colln. D2224 C0. Antelope Valley Limestone 89 ft below highest exposure.
Brachiopods:
Taphrodonta? sp.
Orthambonites cf. *O. minusculus* (Phleger)
Trilobites:
Illaenus sp.
Pseudomera? sp.
Nileus sp.
Miracybele sp. 1 of Ross, 1967

Conodonts:

	Number of specimens
"*Oistodus*" sp.	3
Drepanodus suberectus (Branson and Mehl)	1
Drepanodus sp.	1
Scolopodus sp.	1
Drepanodus sp.	1

Conodonts identified by J. W. Huddle and S. M. Bergström (written commun., Apr. 22, 1971) who state, "An early Middle Ordovician age is reasonable but there is nothing diagnostic here."

Collection D2224 is correlated with USGS collection D1518 C0 (Ross, 1970, p. 26, pls. 20, 21).

USGS colln. D2223 C0. Antelope Valley Limestone, 153 ft below top of formation.
Brachiopods:
Orthambonites minusculus (Phleger)
Aporthophyla? sp.
Trilobite:
Nileus sp. (large species)

USGS colln. D2222 C0. Antelope Valley Limestone, 217 ft below top of formation.
Brachiopod:
Orthambonites minusculus (Phleger)
Trilobites:
Nileus sp.
Niobe cf. *N. morrisi* (Billings)
Peraspis sp.
Raymondaspis sp.
Telephina sp.
Miracybele sp.
Conodonts:
"*Acontiodus*" sp. cf. *A. cooperi* Sweet and Bergström
"*Drepanodus*" sp.
"*Oistodus*" sp. cf. *O. angulatus* Bradshaw
n. gen., n. sp. (platform conodont)
n. gen., n. sp. (prioniodiform element)
Conodonts identified by J. W. Huddle and S. M. Bergström (written commun., Apr. 22, 1971). "This list prepared by S. M. Bergström uses quotation marks on the simple cone genera because these genera are revised in a manuscript (by Lindström) in press [Geological Society of America Memoir 127]. These new genera will be difficult to use until large collections are available. The fauna of this slide is similar to the fauna on slide D1520-C0 and Bergström guesses that they are the same age. Until the ranges of the new forms are determined this remains uncertain." (J. W. Huddle.)

Collection D2222 is correlated with that part of the Mill Canyon sequence near the mouth of Ikes Canyon in the range of collections D1520 C0 to D1606 C0 (Ross, 1970, p. 25–26, pls. 20, 21).

USGS colln. D2221 C0. Antelope Valley Limestone about 25 ft below colln. D2222 C0.
Trilobites:
Nileus sp. (large species)
Pliomerid pygidium

USGS colln. D2220 C0. Antelope Valley Limestone, approx. 315 ft below top of formation.
Trilobites:
Trinodus sp. or *Geragnostus* sp. (pygidium)
Peraspis sp.
Graptolite:
?*Diplograptus decoratus* (questionable)

USGS colln. D2219 C0. Antelope Valley Limestone about 35 ft above colln. D2217 C0.
Trilobites:
Peraspis sp.
Remopleurid indet.
Olenid(?), n.gen., n. sp.
Calymenid
Graptolites:
Didymograptus sp. Berry (written commun., Nov. 4, 1970) states, "several fragments of didymograptids are present. One of them clearly is of the *D. nodosus* type and may be an abraded *D. spinosus*. Other fragments have slender stipes and low thecal overlap and hence are similar to *D. gracilis* and *D. compressus*. Fragments of *D. cuspidatus* may also be present."

USGS colln. D2218 C0. Antelope Valley Limestone about 20 ft above USGS colln. D2217 C0.
Trilobite:
Peraspis sp.
Graptolite:
Climacograptus riddelensis Harris
Age: *C. riddelensis* is considered a guide to the zones of *P. etheridgei* and *Glyptograptus teretiusculus*; it ranges as high as the zone of *Climacograptus bicornis*.

USGS colln. D2217 C0. Antelope Valley Limestone, about 30 ft above valley bottom.
Brachiopods:
Small, costellate orthids, indet.
Inarticulates, undet.
Ostracodes:
Undetermined to date, probably two or more genera
Trilobites:
Agnostids, undet.
New olenid genus and species
Peraspis sp.
Ectenonotus sp.
Blosyropsis sp., one cranidium, several free cheeks and thoracic segments found
Graptolites (W. B. N. Berry, written commun., Nov. 4, 1970):
Dictyonema sp.
Didymograptus sp.
Climacograptus cf. *C. riddelensis* Harris
Diplograptus decoratus
Glyptograptus? sp.

Age: Trilobites indicate equivalence to the slabby beds of the Antelope Valley Limestone, collections D1520 CO to D1606 CO (Ross, 1970, p. 25–26, pls. 20, 21), in the Mill Canyon sequence near the mouth of Ikes Canyon. Graptolites indicate correlation with the zones of *P. etheridgei* and *G. teretiusculus*.

In the June Canyon sequence section of Antelope Valley Limestone the graptolites of the *P. etheridgei* zone are interbedded and associated with a trilobite assemblage including *Miracybele*, *Telephina*, *Nileus*, *Raymondella*, and *Peraspis*. Brachiopods which occur a few feet higher in the section indicate correlation with the *Orthidiella* zone. The combined brachiopod and trilobite assemblage indicates correlation with strata below and in the lower part of the so-called sponge beds of the Antelope Valley Limestone, in the Mill Canyon sequence (Ross, 1970, p. 26–27, USGS colln. D1520 CO–D1602 CO). These strata below the sponge beds have been independently correlated with the *Orthidiella* zone by Ross.

The part of the Vinini Formation that includes USGS collections D2130 CO and D2131 CO is now believed to be equivalent to the lower Antelope Valley Limestone on the basis of graptolite correlations.

STRATIGRAPHY IN SOUTHEASTERN BRITISH COLUMBIA

Middle Ordovician Whiterock benthonic faunas are present in the Skoki Formation in the southern Rocky Mountains of southwestern Alberta (Norford, 1969, p. 37–38). The Skoki consists predominantly of dolomites deposited in relatively shallow and turbulent water, but the formation grades westward into limestones, shales, and siltstones assigned to the Outram Formation that accumulated in less agitated water (Aitken and Norford, 1967, p. 177–179). The lower half of the Skoki is equivalent to the Outram Formation near the British Columbia–Alberta border; the upper half persists farther west. Both formations are replaced by the Glenogle Shales of graptolitic facies in the Western Ranges of the Rocky Mountains near the Rocky Mountain trench.

A well-exposed stratigraphic section located about 20 miles west of the British Columbia–Alberta border is the only area of the southern Rocky Mountains of Canada in which the facies change between graptolitic and carbonate facies in the lower Middle Ordovician can be seen. Here, interbedded and intertonguing rocks with graptolitic and benthonic faunas have been measured by Norford in 1964 on a ridge (elevation 8,000–8,500 ft; 50°19′ N., 115°15′ W., Natl. Topog. Survey Sheet 82J, Kananaskis Lakes) near North White River at about 7 miles north of its confluence with White River. The base of the measured section is the top of the McKay Group, followed by a conformable sequence of Glenogle Shales (including a thick tongue of Tipperary Quartzite), a shaly development of Outram Formation, and ending within the Skoki Formation.

Graptolites identified by D. E. Jackson from the Glenogle Shales and the Outram Formation of the section indicate a sequence of *Didymograptus protobifidus* zone, *Isograptus caduceus* zone and possibly *Paraglossograptus etheridgei* zone. Elsewhere, the Glenogle Shales contain these three zones and the overlying *Glyptograptus* cf. *G. teretiusculus* zone and *Nemegraptus gracilis* zone (Jackson, 1964; Larson and Jackson, 1966; Norford, 1969, p. 35–36). Jackson (1966) has shown that the *Didymograptus bifidus* zone (expected above zone of *D. protobifidus*) is not developed in the western and northwestern Canadian Cordillera. Faunas of trilobites and brachiopods identified by Norford from the Glenogle Shales, Outram Formation, and Skoki Formation of the section reveal a very thick *Orthidiella* zone overlain by the *Anomalorthis* zone.

The stratigraphic relations within the North White River section show that much of the *Orthidiella* zone is equivalent to the *Isograptus caduceus* zone but that the upper part is probably equivalent to the *Paraglossograptus etheridgei* zone. No graptolites were collected within the *Anomalorthis* zone of the section, but this zone is assumed to be largely equivalent to the upper part of the *Paraglossograptus etheridgei* zone. The few known occurrences of graptolites within the Ordovician carbonate formations of adjacent southwestern Alberta (Norford, 1969, p. 35) help to compare benthonic with graptolitic zones (table 1). Similarly, the Tipperary Quartzite is dated as zone J (Norford, 1969, p. 16), and the presence of a tongue of this formation in the North White River section between the known *Didymograptus protobifidus* zone and the known *Isograptus caduceus* zone helps demonstrate the correspondence.

Table 1.—*Comparison of graptolitic and benthonic zones, southeastern British Columbia*

[Presence of zone 0 has not been demonstrated from the region]

<table>
<tr><th>Stages</th><th>Graptolitic zones</th><th>Benthonic zones</th></tr>
<tr><td>Llandeilo</td><td>Glyptograptus cf. G. teretiusculus (part)</td><td>Zone 0 ? (part)</td></tr>
<tr><td></td><td>?</td><td>?</td></tr>
<tr><td>Llanvirn</td><td rowspan="2">Paraglossograptus etheridgei</td><td rowspan="2">Anomalorthis</td></tr>
<tr><td rowspan="3">Arenig (part)</td></tr>
<tr><td>Isograptus caduceus</td><td rowspan="2">Orthidiella</td></tr>
<tr><td>Didymograptus protobifidus (part)</td><td rowspan="2">Zone J</td></tr>
</table>

Faunules noted in the North White River section are given in the following tabulation:

Faunules from the North White River section

[Geological Survey of Canada collections listed in descending stratigraphic order]

GSC colln. 64560. Skoki Formation, 222–232 ft above base; 2,150–2,160 ft above base of Glenogle Shales.
- Sponges

GSC colln. 64561. Skoki Formation, 156–164 ft above base; 2,084–2,092 ft above base of Glenogle Shales.
- Sponges
- Echinoderm fragments
- Gastropods:
  - Several undet. species
  - *Maclurites* sp.
- Brachiopods:
  - Indeterminate leptaenid
  - *Hesperomena* sp.
- Trilobite fragments
- Age: Late *Anomalorthis* zone, probably about equivalent to that of the upper Antelope Valley Limestone (USGS colln. D1508 CO) at Ikes Canyon (Ross, 1970, p. 23, pl. 21).

GSC colln. 64562. Skoki Formation, 45–50 ft above base; 1,973–1,978 ft above base of Glenogle Shales.
- Sponges

GSC colln. 64563. Outram Formation, float from 854–865 ft above base; 1,877–1,888 ft above base of Glenogle Shales.
- Gastropod
- Trilobite:
  - *Nileus* sp.

GSC colln. 64564. Outram Formation, 842–860 ft above base; 1,865–1,883 ft above base of Glenogle Shales.
- Gastropod:
  - *Maclurites* sp.
- Brachiopod:
  - ?*Desmorthis* sp.
- Trilobites:
  - Indeterminate cheirurinid
  - *Nileus* sp.
- Age: *Anomalorthis* zone.

GSC colln. 64565. Outram Formation, 840–842 ft above base; 1,863–1,865 ft above base of Glenogle Shales.
- Ostracode:
  - *Eoleperditia* sp. (identified by Copeland)

GSC colln. 64566. Outram Formation, 825–833 ft above base; 1,848–1,856 ft above base of Glenogle Shales.
- Cephalopod (orthocone)
- Gastropod
- Brachiopods:
  - Undetermined orthid
  - *Orthambonites* sp.
  - *Orthidiella* sp.
- Trilobites:
  - Undetermined asaphid
  - Undetermined cheirurinid
  - *Ectenonotus* sp.
- Ostracode
- Age: *Orthidiella* zone (or possibly early *Anomalorthis* zone).

GSC colln. 64567. Outram Formation, 632–644 ft above base; 1,655–1,667 ft above base of Glenogle Shales.
- Brachiopods:
  - Undetermined large lingullelid
  - Undetermined orthid
  - Indeterminate sowerbyellid
- Trilobites:
  - *Ectenonotus* sp.
  - *Peraspis* sp.
- Graptolite:
  - Indeterminate biserial form
- Age: *Orthidiella* zone; within span of *Isograptus caduceus* zone to *Paraglossograptus etheridgei* zone, probably the former (D. E. Jackson, written commun., 1970).

GSC colln. 64568. Outram Formation, 556–561 ft above base; 1,579–1,584 ft above base of Glenogle Shales.
- Echinoderm fragments
- Conulariid
- Brachiopods:
  - Undetermined inarticulate
  - Undetermined orthid
- Trilobites:
  - Undetermined form
  - *Kawina* sp.
  - *Peraspis* sp.
- Age: *Orthidiella* zone.

GSC colln. 64569. Outram Formation, 507–524 ft above base; 1,530–1,547 ft above base of Glenogle Shales.
- Trilobite:
  - *Peraspis* sp.
- Age: *Orthidiella* zone.

GSC colln. 64570. Outram Formation, float from 432–442 ft above base; 1,455–1,465 ft above base of Glenogle Shales.
- Conulariid

GSC colln. 64571. Outram Formation, 402–405 ft above base; 1,425–1,428 ft above base of Glenogle Shales.
- Echinoderm fragments
- Brachiopods:
  - Indeterminate inarticulate
  - ?*Orthambonites* sp.
- Trilobites:
  - Indeterminate agnostid
  - *Ectenonotus* sp.
  - ?*Miracybele* sp.
  - ?*Nileus* sp.
  - ?*Protocalymene* sp.
- Ostracode
- Graptolites:
  - Dichograptid fragment
  - *Glossograptus* sp.
  - *Loganograptus* sp.
- Age: *Orthidiella* zone; within span of *Isograptus caduceus* zone to *Paraglossograptus etheridgei* zone, probably the former (D. E. Jackson, written commun., 1970).

GSC colln. 64572. Outram Formation, 277–282 ft above base; 1,300–1,305 ft above base of Glenogle Shales.
- Echinoderm fragments
- Brachiopods:
  - Undetermined inarticulate
  - Undetermined orthid
- Trilobite:
  - ?*Protocalymene* sp.
- Graptolite:
  - *Glossograptus* cf. *G. hincksii* var. *fimbriatus* (Hopkinson)
- Age: Within span of *Isograptus caduceus* zone to *Paraglossograptus etheridgei* zone, probably the former (D. E. Jackson, written commun., 1970).

GSC colln. 64573. Outram Formation, 201–204 ft above base; 1,224–1,227 ft above base of Glenogle Shales.
- Trilobite:
  - Undetermined asaphid

GSC colln. 64574. Outram Formation, 53–57 ft above base; 1,076–1,080 ft above base of Glenogle Shales.
Graptolites:
Didymograptus sp. (pendent)
Glossograptus horridus Ruedemann
Isograptus caduceus var. *divergens* Harris
Isograptus caduceus mut. *nanus* Ruedemann
Age: Within span of *Isograptus caduceus* zone to *Paraglossograptus etheridgei* zone, probably the former (D. E. Jackson, written commun., 1970).

GSC colln. 64575. Outram Formation, 47–49 ft above base; 1,070–1,072 ft above base of Glenogle Shales.
Sponges

GSC colln. 64576. Glenogle Shales, 1,005–1,010 ft above base; 13–18 ft below base of Outram Formation.
Graptolites:
Glossograptus cf. *G. holmi* Bulman
Isograptus caduceus var. *divergens* Harris
Isograptus caduceus mut. *nanus* Ruedemann
Loganograptus logani mut. *pertenuis* Ruedemann
Paraglossograptus sp.
Age: Within span of *Isograptus caduceus* zone to *Paraglossograptus etheridgei* zone, probably the former (D. E. Jackson, written commun., 1970).

GSC colln. 64577. Glenogle Shales, 820–825 ft above base.
Graptolites:
?*Cryptograptus* sp.
Glossograptus cf. *G. horridus* Ruedemann
Isograptus caduceus var. *divergens* Harris
Tetragraptus sp. (extensiform)
Age: *Isograptus caduceus* zone (D. E. Jackson, written commun., 1970).

GSC colln. 64578. Glenogle Shales, 766–770 ft above base.
Graptolites:
Indeterminate biserial form
Didymograptus sp. (extensiform)
Isograptus caduceus var. *divergens* Harris
Isograptus cf. *I. caduceus* var. *imitata* Harris
Age: *Isograptus caduceus* zone (D. E. Jackson, written commun., 1970).

GSC colln. 64579. Glenogle Shales, 750–763 ft above base.
Cephalopod:
Undetermined orthocone
Brachiopod:
Undetermined inarticulate
Trilobites:
Indeterminate form
Ampyxina sp.
Nileus sp.
Ostracode:
cf. *Primitiella* sp. (identified by Copeland)
Graptolites:
Dichograptid fragments
Isograptus caduceus var. *divergens* Harris
Isograptus forcipiformis Ruedemann
Age: Probably *Orthidiella* zone; within span of *Isograptus caduceus* zone to *Paraglossograptus etheridgei* zone (D. E. Jackson, written commun., 1970) but from stratigraphic position, *Isograptus caduceus* zone.

GSC colln. 64580. Glenogle Shales, 643–644 ft above base.
Brachiopods:
Undetermined orthids

GSC colln. 64581. Glenogle Shales, 324–326 ft above base.
Graptolites:
Didymograptus sp.
Isograptus sp.
Age: *Isograptus caduceus* zone (D. E. Jackson, written commun., 1970).

GSC colln. 64582. Glenogle Shales, 220–230 ft above base.
Graptolites:
Didymograptus aff. *D. nitidus* (Hall)
Isograptus cf. *I. caduceus* var. *imitata* Harris
Isograptus caduceus var. *maximo-divergens* Harris
Age: *Isograptus caduceus* zone (D. E. Jackson, written commun., 1970).
(Note. A tongue of Tipperary Quartzite is present within the Glenogle Shales at 165–207 ft above the base of the Glenogle.)

GSC colln. 64583. Glenogle Shales, 28–35 ft above base.
Graptolites:
Indeterminate fragments
Didymograptus cf. *D. columbianus* Ruedemann
Age: *Didymograptus protobifidus* zone (D. E. Jackson, written commun., 1970).

In the same general region as the measured section, G. B. Leech has made several collections from spot localities within the Outram Formation. Three important collections are listed below; the faunules from all three indicate the *Orthidiella* zone and amplify the faunal knowledge of this zone in southeastern British Columbia. Raasch and Bruce (1966) reported an assemblage from the same region as an *Orthidiella-Ectenonotus* zone that probably represents the same stratigraphic interval.

GSC colln. 57482. Outram Formation at 50°13.75′ N., 115°10.35′ W., Elk Canyon (Sawmill Creek), NTS sheet 82J, Kananaskis Lakes.
Sponges
Echinoderm fragments
Gastropods:
Several undetermined species
Brachiopods:
Several undetermined species
Orthambonites marshalli (Wilson)
Orthidiella cf. *O. extensa* Ulrich and Cooper
Syntrophopsis sp.
Trilobites:
Several undetermined species
Ectenonotus sp.
Goniotelina sp.
Illaenus sp.
Pliomerops sp.
?*Raymondaspis* sp.
Arthropod:
Ribeiria sp. (identified by Copeland)
Ostracode:
Eoleperditia cf. *E. bivia* (White) (identified by Copeland)

GSC colln. 57559. Outram Formation at 50°23.85′ N., 115°14.9′ W., NTS Sheet 82J, Kananaskis Lakes.
Echinoderm fragments
Brachiopods:
Undetermined inarticulate
Undetermined orthids
Trilobites:
Carolinites sp.
Ectenonotus sp.
"Protopliomerops" subquadratus Kobayashi

GSC colln. 57561. Outram Formation at 50°40.5′ N., 115°23.8′ W., NTS Sheet 82J, Kananaskis Lakes
Sponges
Echinoderm fragments
Conularid

Bryozoan fragments
Brachiopods:
  Undetermined inarticulate
  Undetermined articulate
  Orthambonites sp.
  Orthidiella sp.
Trilobites:
  Undetermined agnostid
  Undetermined asaphid
  Undetermined isotelid
  Ectenonotus sp.
  Kawina sp.
  aff. *Lehua* sp.

ZONAL SIGNIFICANCE

The graptolite occurrences at Ikes Canyon, Toquima Range, central Nevada, supported by those in British Columbia, correct an often repeated but erroneous equation of the *Anomalorthis* zone in Utah and Oklahoma with the zone of *Didymograptus bifidus* in West Texas. This erroneous correlation has depressed "Whiterock" beds into too old a stratigraphic position. The zones as seen in Nevada, Utah, and British Columbia are shown in figure 5.

Collections made in 1971 in Ikes Canyon show that the zone of *Isograptus caduceus* is present in the Ninemile Formation below the Antelope Valley Limestone in the June Canyon sequence. Other 1971 collections from the Mill Canyon sequence establish that the lower slabby-bedded part of the Antelope Valley Limestone, equivalent to USGS colln. D1604 CO (Ross, 1970, p. 26; pls. 20, 21), contains *Diplograptus decoratus*, *Pseudoclimacograptus scharenbergi*, and *Tetragraptus* cf. *T. quadribrachiatus*; this assemblage indicates zone of *Paraglossograptus etheridgei*. A similar association has been noted by Erdtmann (1971, p. 1515, table 2) in the Table Head Formation at Black Cove, Port au Port, Newfoundland.

The Table Head Formation of western Newfoundland is correlative with much of the Antelope Valley Limestone in Ikes Canyon on the basis of both trilobites and graptolites (Whittington and Kindle, 1963; Morris and Kay, 1966; Whittington, 1968) and has been correlated with zones L, M, and N of the Utah sections. Ross (1970, p. 45–47) has shown that the fossil assemblages strongly suggest correlation of the lower part of the Ikes Canyon section (Mill Canyon sequence) with the *Orthidiella* zone, equivalent to zone L of the Utah sections. Based on our 1970 and 1971 graptolite collections,

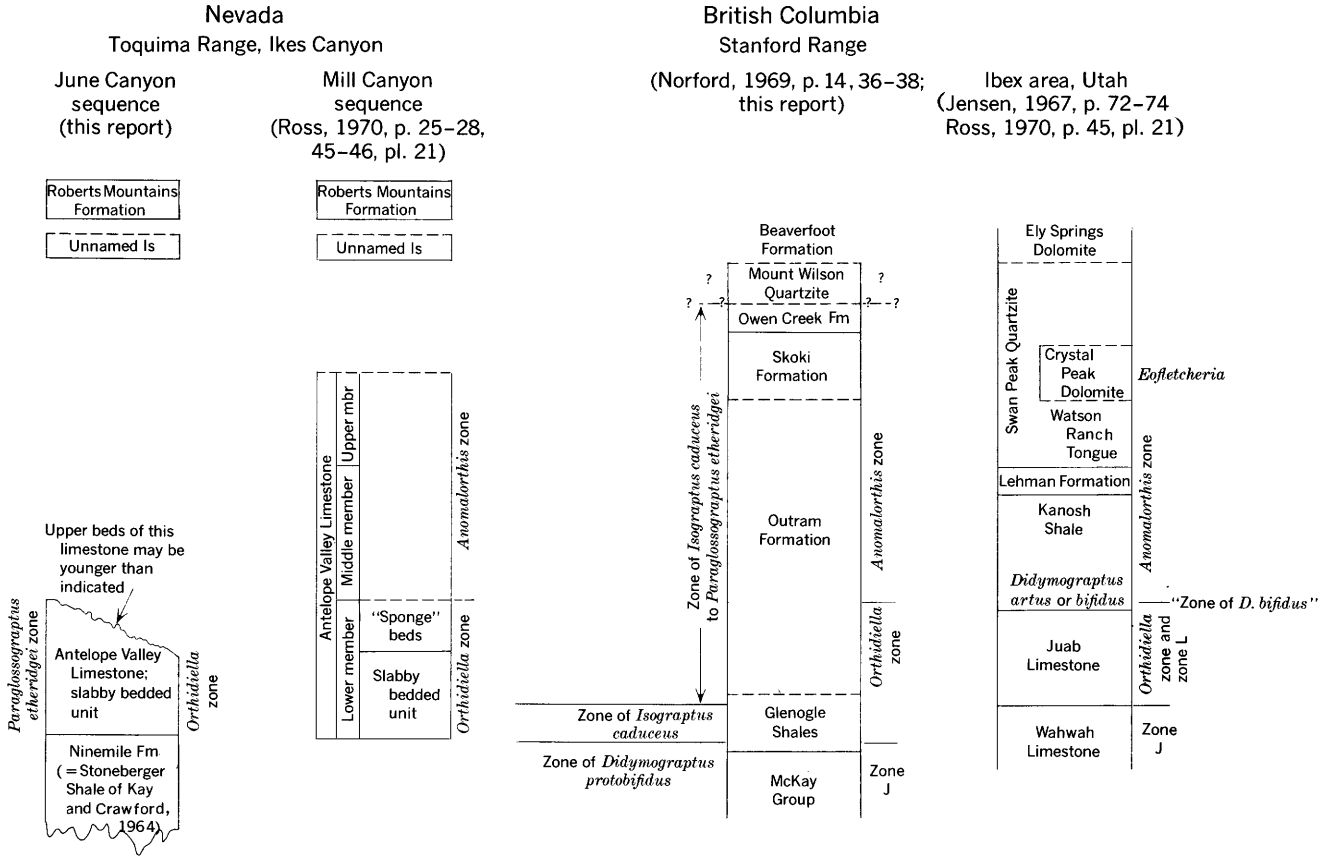

Figure 5.–Comparison of stratigraphic positions of fossil zones in Nevada, British Columbia, and Utah.
"Zone of *Didymograptus bifidus*" in Utah seems younger than zones of *Isograptus caduceus* and *Paraglossograptus etheridgei*.

the *Orthidiella* zone should, therefore, be equated with the zone of *Paraglossograptus etheridgei* and possibly also with the older zone of *Isograptus caduceus*. Thus the evidence from western Newfoundland, British Columbia, and central Nevada, all from the Toquima–Table Head faunal realm of Ross and Ingham (1970), is in agreement.

Graptolites from the Ordovician platform or shelf areas of Utah and Oklahoma seem to disprove this correlation. A single graptolite species, *Didymograptus artus* Elles and Wood, is found in the lower member of the Swan Peak Formation in northern Utah (Ross and Berry, 1963, p. 64, 69, 70, 85), where it is associated with trilobites and brachiopods of zone M (lower *Anomalorthis* zone). In the lower part of the Joins Formation of the Arbuckle Mountains, Okla., *D. artus* is again present in the same zone (Harris, 1957, p. 31, 32, 60, chart 1). *D. bifidus* is found in the lower Kanosh Shale (lower *Anomalorthis* zone and zone M) in western Utah (L. F. Braithwaite, oral commun., 1965).

Because *D. artus* is associated with *D. bifidus* in Great Britain, Ross and Berry (1963, table 1) assumed that the lower *Anomalorthis* zone (lower Swan Peak Formation and lower Kanosh Shale) was of the same age as the zone of *D. bifidus* and considerably older than the zone of *Paraglossograptus etheridgei*. However, the *Anomalorthis* zone indisputably overlies and is younger than the *Orthidiella* zone. In west-central Nevada and in southeastern British Columbia, the data indicate that the *Orthidiella* zone correlates in part with the zone of *P. etheridgei* and in part with the zone of *Isograptus caduceus*. In Utah the *Orthidiella* zone is below the *Anomalorthis* zone and, therefore, seems to lie beneath the zone of *D. bifidus*.

It becomes obvious that we must adjust our thinking on Early and Middle Ordovician zonation. The seeming inversion of graptolite zones relative to zones of shelly fossils indicates that this is no simple matter of miscorrelation that can be corrected by a slight vertical stratigraphic adjustment. The position of the *Didymograptus bifidus* zone as indicated by *D. bifidus* Hall and (or) *D. artus* Elles and Wood is the most discordant. Nor is this problem new or unique, for Harris and Thomas (1938, p. 65–66) noted the absence of *D. bifidus* in Australia from a succession similar to that in western Canada and Texas.

In the course of several discussions concerning intercontinental correlations, all including the zone of *D. bifidus*, Berry (1960b; 1964, p. 74–80; 1966, p. 1496–97; 1968), Skevington (1963, 1968), and Jackson (1964, 1969) have demonstrated that graptolite zonal assemblages older than that of *Nemagraptus gracilis* are provincial. This provincialism is based upon very large geographic areas of continental or circumoceanic extent. One wonders, however, if the provincialism of these early graptolite faunas differs greatly from those of the shelly faunas.

Ross and Berry (1963, table 1) showed the distribution of Ordovician graptolite-bearing collections in the Basin and Range province but failed to call particular attention to the absence of any representation for the zone of *D. bifidus* in the shaly western facies; only in the platform or shelf facies (Swan Peak Formation) was the zone presumed to occur, and there a single species, *D. artus* Elles and Wood in USGS colln. D204 CO (Ross and Berry, 1963, p. 64), was thought to indicate it.

Jackson and Lenz (1962, p. 35, 38–39, fig. 2; also Jackson, 1964, p. 525, 1969, p. 506) reported a succession of graptolite faunas from the Richardson Mountains, northern Yukon Territory, including the zones of *D. protobifidus*, *I. caduceus* and *P. etheridgei*. Similarly, in northeastern British Columbia, the same three zones can be recognized within the Kechika Group of northeastern British Columbia (Jackson and others, 1964, p. 142, 145, 150–152, fig. 2, table 3) and also within the Glenogle Shales of southeastern British Columbia (Larsen and Jackson, 1966, p. 492–497, fig. 3). No zone of *D. bifidus* could be recognized in any of these three regions, and in no case has it been suggested that the absence of the zone of *D. bifidus* is evidence of a hiatus in the stratigraphic record.

Jackson (1964) commented on the absence of *D. bifidus* and *D. artus* from western Canada and later (1969) explained this and other evidence of faunal provincialism by the existence of Pacific and European faunal provinces from mid-Arenig to late Llanvirn time. A similar explanation for graptolite distribution in Newfoundland has been suggested by Erdtmann (1971). The occurrences of the two species in Texas may represent incursions of forms from the European province into the Pacific province, but Jackson (1964, p. 526–527) thought that their Texas occurrences could be correlated with the upper part of the Arenig zone of *D. protobifidus* rather than with the Llanvirn zone of *D. bifidus*.

Ross (1964, p. C41) noted that *D. artus* seemed to occur as low as *D. protobifidus* in the northern Inyo Range, Calif. Berry (1962, p. 298) showed that graptolites assigned to *D. bifidus* have been reported over a wide stratigraphic range in Britain and Scandinavia.

Alternate explanations for zonal discrepancies between northern Utah and Oklahoma on the one hand and Nevada and British Columbia on the other are:

1. The graptolite zone, represented in western North America by *Didymograptus bifidus* and *D. artus* in the limestone-rich shelf or platform facies, is represented in the more extracratonic silty limestone and shale facies (Toquima Range, Nev.; Stanford Range, British Columbia; western Newfoundland) by an assemblage generally assigned to the *Isograptus caduceus* and *Paraglossograptus etheridgei* zones and possibly to the *Glyptograptus* cf. *teretiusculus* zone of North America.

2. The brachiopods, trilobites, pelmatozoans, and other shelly fauna that constitute the *Orthidiella* zone in the shelf facies of Utah and eastern Nevada migrated as a group into younger muddier beds closer to the eugeosynclinal facies.

Of the two possibilities the first seems the more likely, for it explains more of the apparent contradictions in zonal ranges

and provides greater accord among all groups of fossil evidence.

D. bifidus and *D. artus* occur only in limestone in the Marathon region of West Texas (Berry, 1960a, p. 59, 109, 118, 120–123). Their disappearance higher in the section might have resulted from the incursion of sediments represented now by the Alsate Shale and Fort Peña Formation and the invasion of a different graptolite assemblage.

Berry (1970) has described *Didymograptus bifidus* and *D. artus* from the Smithville Formation and the presumably correlative Black Rock Formation of late Early Ordovician age in Arkansas. This occurrence would seem to support Jackson's (1969, p. 507) belief that *D. bifidus* in North America is older than in Britain. Again it should be noted that the Arkansas occurrence is in the platform or shelf, not in the eugeosynclinal facies. Berry (1970, p. D64) concluded that the Lower Ordovician–Middle Ordovician boundary based on shelly fossils "may be within the *Didymograptus bifidus* graptolite zone." But Ross (1968, p. H2–H4) noted previously that the Smithville Formation might be early Middle Ordovician in age because of its shelly fossils and could be equivalent to the *Orthidiella* zone. This evidence indicates that *D. bifidus* and *D. artus* in the carbonate-rich platform facies may be equated with the *Orthidiella* zone as well as with the *Anomalorthis* zone and may range lower than both.

D. bifidus was originally described from the Levis Shale of Quebec and is reported from the Deepkill Shale (Berry, 1970) in New York. It is, therefore, present in the eugeosynclinal belt in eastern North America. Although similar pendent species are found, *D. bifidus* has not yet been reported in the western eugeosyncline.

We conclude that, in the platform facies of western North America, the zone represented primarily by one or very few species of *Didymograptus*, that is *D. bifidus*, *D. artus*, and close relatives, is the equivalent of the *Isograptus caduceus* and *Paraglossograptus etheridgei* zones of more extracratonic facies (Toquima–Table Head realm) on the east as well as the west. The environmental factors that may have controlled this graptolite distribution can be only conjectured at present.

REFERENCES

Aitken, J. D., and Norford, B. S., 1967, Lower Ordovician Survey Peak and Outram Formations, southern Rocky Mountains of Alberta: Canadian Petroleum Geology Bull., v. 15, no. 2, p. 150–207.

Berry, W. B. N., 1960a, Graptolite faunas of the Marathon region, West Texas: Texas Univ. Bur. Econ. Geology, Pub. 6005, 179 p.

——1960b, Correlation of Ordovician graptolite-bearing sequences: Internat. Geol. Cong., 21st, Copenhagen 1960, Rept., pt. VII, p. 97–108.

——1962, *Didymograptus bifidus* (J. Hall)–Its lectotype, description, and occurrence: Jour. Paleontology, v. 36, no. 2, p. 294–299.

——1964, Graptolites of the Ogygeocaris Series, the Middle Ordovician of the Oslo region, Norway: Norsk Geol. Tidsskr., v. 44, pt. 1, p. 61–170.

——1966, Zones and zones–With exemplification from the Ordovician: Am. Assoc. Petroleum Geologists Bull., v. 50, no. 7, p. 1487–1500.

——1968, Age of the Bogo shale and western Ireland graptolite faunas and their bearing on dating Early Ordovician deformation and metamorphism in Norway and Britain: Norsk Geol. Tidsskr., v. 48, no. 4, p. 217–230.

——1970, Pendant didymograptids from northern Arkansas, *in* Geological Survey Research, 1970: U.S. Geol. Survey Prof. Paper 700-D, p. D62–D70.

Erdtmann, Bernd-Deitrich, 1971, Ordovician graptolite zones of western Newfoundland in relation to paleogeography of the North Atlantic: Geol. Soc. America Bull., v. 82, no. 6, p. 1509–1528.

Harris, R. W., 1957, Ostracoda of the Simpson Group: Oklahoma Geol. Survey Bull. 75, 333 p.

Harris, W. J., and Thomas, D. E., 1935, Victorian graptolites (new series), Part III: Royal Soc. Victoria Proc. new ser., v. 47, pt. 2, p. 288–313.

——1938, A revised classification and correlation of the Ordovician graptolite beds of Victoria: Mines Dept. Victoria, Mining and Geology Jour., v. 1, no. 3, p. 62–72.

Jackson, D. E., 1964, Observations on the sequence and correlation of Lower and Middle Ordovician graptolite faunas of North America: Geol. Soc. America Bull., v. 75, p. 523–534.

——1966, Graptolitic facies of the Canadian Cordillera and Arctic Archipelago–A review: Canadian Petroleum Geology Bull., v. 14, no. 4, p. 469–485 [1967].

——1969, Ordovician graptolite faunas in lands bordering North Atlantic and Arctic Oceans: Am. Assoc. Petroleum Geologists Mem. 12, p. 504–512.

Jackson, D. E., and Lenz, A. C., 1962, Zonation of Ordovician and Silurian graptolites of northern Yukon, Canada: Am. Assoc. Petroleum Geol. Bull., v. 46, no. 1, p. 30–45.

Jackson, D. E., Steen, G., and Sykes, D., 1964, Stratigraphy and graptolite zonation of the Kechika and Sandpile Groups in northeastern British Columbia: Canadian Petroleum Geology Bull., v. 13, no. 1, p. 139–154.

Jensen, R. G., 1967, Ordovician brachiopods from the Pogonip Group of Millard County, western Utah: Brigham Young Univ. Geology Studies, v. 14, p. 67–100.

Kay, Marshall, 1960, Paleozoic continental margin in central Nevada, western United States: Internat. Geol. Congr. Rept., 21st sess., Copenhagen, Denmark, pt. 12, p. 93–103.

Kay, Marshall, and Crawford, J. P., 1964, Paleozoic facies from the miogeosynclinal to the eugeosynclinal belt in thrust slices, central Nevada: Geol. Soc. America Bull., v. 75, p. 425–454.

Larson, M. L., and Jackson, D. E., 1966, Biostratigraphy of the Glenogle Formation (Ordovician) near Glenogle, British Columbia: Canadian Petroleum Geology Bull., v. 14, no. 4, p. 486–503.

Morris, R. W., and Kay, Marshall, 1966, Ordovician graptolites from the Middle Table Head Formation at Black Cove, near Port au Port, Newfoundland: Jour. Paleontology, v. 40, no. 5, p. 1223–1229.

Norford, B. S., 1969, Ordovician and Silurian stratigraphy of the southern Rocky Mountains: Canada Geol. Survey Bull. 176, 90 p.

Raasch, G. O., and Bruce, C. J., 1966, Notes on Late Cambrian and Early Ordovician biostratigraphy of southeast British Columbia [abs.]: Canadian Petroleum Geology Bull., v. 14, no. 4, p. 600.

Roberts, R. J., 1964, Paleozoic rocks, *in* Mineral and water resources of Nevada: U.S. 88th Cong., 2d Sess., Senate Doc. 87, p. 22–26.

Roberts, R. J., Hotz, P. E., Gilluly, James, and Ferguson, H. G., 1958, Paleozoic rocks of north-central Nevada: Am. Assoc. Petroleum Geologists Bull., v. 42, p. 2813–2857.

Ross, R. J., Jr., 1964, Middle and Lower Ordovician Formations in southernmost Nevada and adjacent California: U.S. Geol. Survey Bull. 1180-C, 101 p.

——1967, Some Middle Ordovician brachiopods and trilobites from the Basin Ranges, Western United States, *with stratigraphic sections* A, north of Pyramid Peak, Calif., by R. J. Ross, Jr., *and* B, in

Specter Range, Nev., by Harley Barnes: U.S. Geol. Survey Prof. Paper 523-D, p. D1–D43, 11 pls.

——1968, Brachiopods from the upper part of the Garden City Formation (Ordovician), north-central Utah: U.S. Geol. Survey Prof. Paper 593-H, 11 p.

——1970, Ordovician brachiopods, trilobites, and stratigraphy in eastern and central Nevada: U.S. Geol. Survey Prof. Paper 639, 103 p.

Ross, R. J., Jr., and Berry, W. B. N., 1963, Ordovician graptolites of the Basin Ranges in California, Nevada, Utah, and Idaho: U.S. Geol. Survey Bull. 1134, 177 p.

Ross, R. J., Jr., and Ingham, J. K., 1970, Distribution of the Toquima-Table Head (Middle Ordovician Whiterock) faunal realm in the Northern Hemisphere: Geol. Soc. America Bull., v. 81, p. 393–408.

Ruedemann, Rudolf, 1947, Graptolites of North America: Geol. Soc. America Mem. 19, 652 p.

Skevington, David, 1963, A correlation of Ordovician graptolite-bearing sequences: Geol. Fören. Stockholm Förh., v. 85, pt. 3, no. 514, p. 298–319.

——1968, British and North American Lower Ordovician correlation–Discussion: Geol. Soc. America Bull., v. 79, p. 1259–1264.

Whittington, H. B., 1968, Zonation and correlation of Canadian and Early Mohawkian Series, *in* Zen, E-an, White, W. S., Hadley, J. B., and Thomason, J. B., Jr., eds., Studies of Appalachian geology –North and maritime: New York, John Wiley and Sons, Interscience Pub., p. 49–60.

Whittington, H. B., and Kindle, C. H., 1963, Middle Ordovician Table Head Formation, western Newfoundland: Geol. Soc. America Bull., v. 74, p. 745–758.

GEOCHEMISTRY AND DISTRIBUTION OF PLATINUM-GROUP METALS IN MAFIC TO ULTRAMAFIC COMPLEXES OF SOUTHERN AND SOUTHEASTERN ALASKA

By ALLEN L. CLARK and WILLIAM R. GREENWOOD,
Menlo Park, Calif., Jiddah, Saudi Arabia

Abstract.—Rock types and platinum-group metal concentrations were studied in seven mafic to ultramafic complexes in southern and southeastern Alaska. Anomalous concentrations of platinum-group metals correlate with rock types, oxide and sulfide phases, and major and trace elements. The correlations are consistent within an individual complex but differ for each complex. The occurrence of anomalous concentrations of platinum-group metals within the zoned ultramafic complexes shows that these bodies (particularly the complex at Union Bay) and the platiniferous zoned ultramafic bodies of the Ural Mountains, U.S.S.R., are even more similar than previously recognized.

Over 50 mafic to ultramafic complexes are known in southern and southeastern Alaska. The southeastern belt of zoned complexes (fig. 1) has been described by Taylor (1967, p. 99) as being almost identical with the platiniferous ultramafic complexes of the Ural Mountains, U.S.S.R. However, of all the mafic to ultramafic complexes in southern and southeastern Alaska, only the complex at Salt Chuck on Prince of Wales Island has produced appreciable amounts of platinum and palladium (Mertie, 1920), mainly as a byproduct of copper mining operations. To date, six complexes—at Union Bay, Duke Island, Blashke Islands, Eklutna, Salt Chuck, and Klukwan—have been studied by the authors. (See Clark and Greenwood, 1972, p. C21–C27, this chapter.) Data presented in this report on the complex at Mount Fairweather are from a report by Plafker and MacKevett (1970).

This paper presents preliminary data on the concentration of platinum-group metals in the mafic to ultramafic complexes studied and defines the elements and rock types most commonly associated with anomalous platinum metal concentrations in each.

Acknowledgments.—The five assay-spectrographic determinations of platinum-group metals were made by J. C. Negri, R. R. Carlson, and E. F. Cooley, and their services are gratefully acknowledged.

SETTING AND GENERAL GEOLOGY

The mafic to ultramafic complexes described in this report, with the exception of the complex at Mount Fairweather, occur within two distinct belts in southern and southeastern Alaska (fig. 1). The southeastern belt, described by Taylor and Noble (1960), is approximately 30 miles wide and 350 miles long. The southern Alaska belt, which includes the Eklutna ultramafic body, is less well known but probably extends from Kodiak Island on the southwest to beyond the Canadian border on the east. The complex at Mount Fairweather occurs approximately midway between the two belts.

The general characteristics of the ultramafic complexes in the southeastern Alaska belt have been discussed by Taylor and Noble (1960) and Taylor (1967). Reconnaissance and detailed geologic and petrographic studies have been made on all of the mafic to ultramafic complexes studied in this report (Mertie, 1920; Walton, 1951; H. P. Taylor, Jr., and R. H. Stebbins, unpub. data; Ruckmick and Noble, 1959; Irvine, 1963; Rose, 1966; and Plafker and MacKevett, 1970).

All the complexes studied are grossly similar in several aspects:

1. Olivine-bearing rocks occur near the center of the concentrically zoned complexes of the southeastern Alaska belt and near the base of the complexes in the southern Alaska belt (Sandra H. B. Clark, oral commun., 1970), indicating that both belts contain differentiated bodies.
2. Clinopyroxene, primarily diopsidic hedenbergite, occurs in all but the complex at Mount Fairweather, in which Plafker and McKevett (1970, p. B24) have reported both clinopyroxenes and orthopyroxenes in pyroxene gabbro samples.
3. Magnetite is commonly present and locally constitutes 15 to 20 percent of pyroxenite and hornblendite bodies. Ilmenite occurs as a major accessory mineral in all rock types and is normally associated with magnetite.
4. Chromite is commonly present, locally constituting up to 5 to 10 percent of dunite bodies. Chromite normally occurs as disseminations, isolated pods, and stringers and rarely (Eklutna) as discontinuous layers.

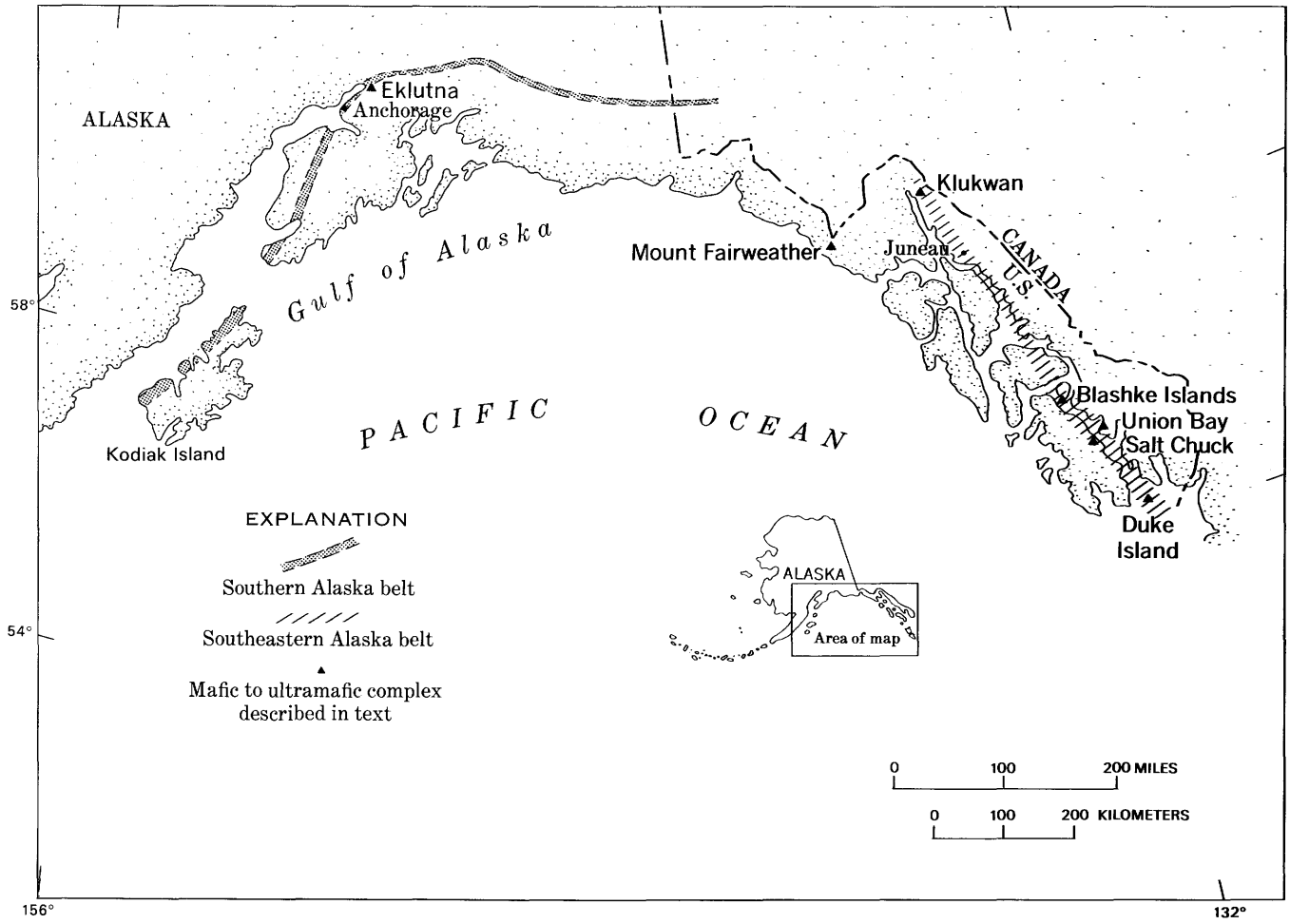

Figure 1.—Index map of southern and southeastern Alaska, showing location of mafic to ultramafic complexes studied.

SAMPLING AND ANALYTICAL METHOD

Sampling and analytical procedures for rocks collected by the authors closely follow those described by Plafker and MacKevett (1970, p. B25) for the complex at Mount Fairweather.

Rock samples of from 5 to 50 pounds were collected from surface outcrops as hand specimen samples. Sampling was directed toward selecting homogeneous rock types representative of the various phases of each complex. In areas where massive segregation of chromite and magnetite was observed, samples were selectively taken of each oxide phase. Samples were submitted as individual rock specimens weighing approximately 2 pounds or were crushed to minus 50 mesh and split, and a 2-pound fraction was sent to the analytical laboratories.

Platinum-group values were determined by the combination method of Haffty and Riley (1968).

Each sample underwent semiquantitative spectrographic analysis for the following 30 elements: Ag, As, Au, B, Ba, Be, Bi, Ca, Cd, Co, Cr, Cu, Fe, K, La, Mg, Mn, Mo, Nb, Ni, Pb, Sb, Sc, Sn, Sr, V, W, Y, Zn, and Zr. Samples that contained more than 5,000 ppm (parts per million) Cr or Ni were reanalyzed for chromium and nickel by quantitative chemical methods.

ANALYTICAL RESULTS

To date, 121 samples from the complexes have been quantitatively analyzed. The number of samples and the number of samples containing Pt, Pd, Rh, and Ir above their respective detection limits of 0.010, 0.004, 0.004, and 0.100 ppm from each complex are shown in table 1.

Table 2 lists the dominant rock types in each complex and the concentration of platinum-group metals in each type. Included are the average platinum and palladium values, the maximum values of platinum and palladium, and the maximum values of rhodium and iridium. Average values for rhodium and iridium were not calculated because too few samples contained the elements in detectable quantities.

Table 1.—*Distribution of samples from the mafic to ultramafic complexes*

Locality	Total No. samples	Platinum bearing	Palladium bearing	Rhodium bearing	Iridium bearing
Duke Island	22	10	16	6	0
Union Bay	50	21	22	6	2
Blashke Islands	10	8	10	0	0
Eklutna	16	12	12	0	0
Salt Chuck	6	6	6	0	0
Mount Fairweather	7	6	6	3	0
Klukwan	10	7	7	0	0

Table 2.—*Concentrations, in parts per million, of platinum, palladium, rhodium, and iridium*

Locality	Platinum		Palladium		Rhodium	Iridium
	Max	Avg	Max	Avg	Max	Max
Duke Island[1]	0.200	0.037	0.140	0.033	0.010	...
Union Bay[1]	1.600	.093	.200	.023	.062	0.215
Blashke Islands[1]	.020	.010	.020	.010	...	...
Eklutna[1]	.100	.042	.140	.060	...	...
Salt Chuck[2]	.160	.057	2.900	1.010	...	...
Mount Fairweather[2]	.170	.040	.184	.036	...	...
Klukwan[2]	.100	.046	.100	.040	...	...

[1]Dominant rock types: peridotite-dunite and hornblendite-pyroxenite.
[2]Dominant rock types: gabbro-hornblendite-pyroxenite-peridotite-dunite.

CORRELATION STUDIES

Petrographic studies of thin sections and polished sections were conducted on all chemically analyzed samples in order to correlate the highest platinum, palladium, and rhodium values with individual host-rock types and associated oxide or sulfide phases. The general rock types and mineral compositions were described by earlier workers. Correlation studies using scatter diagrams were made in order to compare platinum and palladium values within each complex with other trace and major elements. The results show a strong intercorrelation of platinum and palladium with Fe, Ni, Cr, Cu, and V, although the degree of correlation varies in different complexes. The results of these studies are listed in table 3.

CONCLUSIONS

Average platinum concentrations for the seven complexes range from 0.010 ppm (Blashke Islands) to 0.093 ppm (Union Bay—considerably below the "average" concentration of 0.20 ppm given by Vinogradov (1962). Either these Alaskan mafic to ultramafic complexes are anomalously low in platinum, or Vinogradov's figure is too high.

The same relation exists for palladium, which ranges from 0.010 ppm (Blashke Islands) to 0.060 ppm (Eklutna). Analytical values from the Salt Chuck platinum-palladium-copper mine are not considered in the preceding discussion of average values. Turekian and Wedepohl (1961) and Vinogradov (1962) estimate that "average" concentration of palladium in ultramafic rocks is 0.12 ppm, approximately four times higher than the average for the ultramafic rocks that we studied. The ultramafic complexes studied are anomalously low in palladium, as well as platinum, or the values given by Turekian and Wedepohl and by Vinogradov are high.

Table 3.—*Correlation of maximum platinum-palladium concentrations with host-rock type, oxide or sulfide phases, and other elements*

Locality	Associated rock type	Associated oxide or sulfide	Elements with positive correlation
Duke Island	Hornblendite	Magnetite, chalcopyrite	Fe, V
Union Bay	Dunite	Chromite, magnetite	Fe
Blashke Islands	Hornblendite	Magnetite, chalcopyrite	Fe, Ni
Eklutna	Peridotite	Chromite, native copper	Cu
Salt Chuck	Hornblendite	Bornite	Cu
Mount Fairweather	Dunite	Chromite	Ni, Cr
Klukwan	Pyroxenite	Magnetite, ilmenite	Fe, V

The similarity between the ultramafic rocks of the southeastern Alaska belt and the platiniferous complexes of the Ural Mountains, together with the anomalously high concentrations of platinum (1.60 ppm, Union Bay) and palladium (2.90 ppm, Salt Chuck), suggest that the complexes of the southeastern Alaska belt are not necessarily depleted in palladium. Therefore, the authors believe that the values given by Turekian and Wedepohl and by Vinogradov for platinum and palladium concentrations in "average" ultramafic rocks are high.

The petrographic studies and trace- and major-element correlations with platinum metals indicate that the platinum metals are closely associated with amounts of sulfide and oxide phases within the various rock types. This relation has been clearly demonstrated for the complex at Salt Chuck, where analyses of pure bornite and pure pyroxene showed 13 and 0.020 ppm Pd, respectively, and for the complex at Union Bay, where analyses of pure magnetite and pure olivine showed 30 and 0.040 ppm Pt, respectively. For each complex, the pure mineral separates were extracted from the same hand specimen.

In general, the concentration of platinum metals within each complex varies directly with olivine content. In order of decreasing platinum metal content, the rock types are dunite, peridotite, pyroxenite, and hornblendite. However, maximum values for platinum and palladium occur anomalously in hornblendites within the complexes at Duke Island, Blashke Islands, and Salt Chuck. Although the platinum-group metals are associated primarily with sulfide and oxide phases, their distribution seems to be controlled partly by the silicate phases, particularly olivine.

The platinum-group metals thus correlate with rock types, oxide and sulfide phases, and major and trace elements. However, the authors emphasize that, although the correlations are consistent within an individual complex, they differ between complexes.

Anomalous concentrations of platinum-group metals occur locally within each of the mafic to ultramafic complexes studied, but only the complexes at Union Bay and Salt Chuck are known to contain concentrations of possible economic significance.

The occurrence of anomalous concentrations of platinum-group metals within the ultramafic complexes studied, especially the one at Union Bay, shows that the Alaskan complexes resemble the platiniferous zoned ultramafic bodies of the Urals even more closely than previously recognized.

REFERENCES

Clark, A. L., and Greenwood, W. R., 1972, Petrographic evidence of volume increase related to serpentinization, Union Bay, Alaska, *in* Geological Survey Research 1972: U.S. Geol. Survey Prof. Paper 800-C, p. C21–C27.

Haffty, Joseph, and Riley, L. B., 1968, Determination of palladium, platinum and rhodium in geologic materials by fire assay and emission spectrography: Talanta, v. 15, p. 111–117.

Irvine, T. N., 1963, Origin of the ultramafic complex at Duke Island, southeastern Alaska: Mineralog. Soc. America Spec. Paper 1, p. 36–45.

Mertie, J. B., Jr., 1920, The Salt Chuck palladium-copper mine, Prince of Wales Island, Alaska: Eng. and Mining Jour., v. 110, p. 17–20.

Plafker, George, and MacKevett, E. M., Jr., 1970, Mafic and ultramafic rocks from a layered pluton at Mount Fairweather, Alaska, *in* Geological Survey Research 1970: U.S. Geol. Survey Prof. Paper 700-B, p. B21–B26.

Rose, A. W., 1966, Geology of chromite-bearing ultramafic rocks near Eklutna, Anchorage quadrangle, Alaska: Alaska Div. Mines and Minerals Geol. Rept. 18, 20 p.

Ruckmick, J. C., and Noble, J. A., 1959, Origin of the ultramafic complex at Union Bay, southeastern Alaska: Geol. Soc. America Bull., v. 70, p. 981–1018.

Taylor, H. P., Jr., 1967, The zoned ultramafic complexes of southeastern Alaska, *in* Wylie, P. J., ed., Ultramafics and related rocks: New York, John Wiley & Sons, p. 96–118.

Taylor, H. P., Jr., and Noble, J. A., 1960, Origin of the ultramafic complexes in southeastern Alaska: Internat. Geol. Cong., 21st, Copenhagen 1960, Rept., pt. 13, p. 175–187.

Turekian, K. K., and Wedepohl, K. H., 1961, Distribution of the elements in some major units of the Earth's crust: Geol. Soc. America Bull., v. 72, p. 175–192.

Vinogradov, A. P., 1962, Average contents of chemical elements in the principal types of igneous rocks of the Earth's crust: Geochemistry (translation of Geokhimiya), 1962, p. 641–664.

Walton, M. S., 1951, The Blashke Islands ultrabasic complex: Columbia Univ., New York, unpub. Ph. D. thesis, 266 p.

DISTILLATION TESTS OF OIL SHALE FROM THE PHOSPHORIA FORMATION OF SOUTHWESTERN MONTANA

By ANDREW F. BATEMAN, JR., Denver, Colo.

Abstract.—Recovery of oil from distillation tests of 45 samples of oil shale from the Phosphoria Formation of Permian age in southwestern Montana indicates that the shale beds are too lean to be of economic interest either now or in the foreseeable future. The kerogen once present may have been converted into the oil now present in some of the oil fields of Wyoming and Montana.

The mineral evaluation and appraisal of the Federal lands and the leasing of these lands requires immediately available information on the occurrence of the leasable minerals, one of which is oil shale. The tests herein described were made as part of the collection of data on the occurrence of oil shale in southwestern Montana.

The first published reference to oil shale in southwestern Montana was made by Bowen (1918, p. 315). Although oil shale is present in beds at eight or more stratigraphic levels ranging in age from Late Devonian to Tertiary, only the deposits in the Meade Peak and Retort Phosphatic Shale Members of the Phosphoria Formation of Permian age are discussed in this report. Detailed descriptions, measured geologic sections, the stratigraphy, and the petrology of the units of the Phosphoria are given by Cressman (1955), McKelvey and others (1959), and Cressman and Swanson (1964). Biostratigraphy is discussed by Yochelson (1968), and mineral resources are described by Swanson (1970).

DISTILLATION TESTS

Results from samples that yielded oil on distillation tests were published by Bowen (1918, p. 318), Condit (1919, p. 24–26), Winchester (1923, p. 85–87, 90, 91), and Cressman and Swanson (1964, p. 438, 439). On the basis of those results, Swanson (1970, p. 765) discussed the oil-shale resources in the Permian rocks of southwestern Montana.

During the investigation of the western phosphate field under the direction of V. E. McKelvey beginning in 1947, stratigraphic sections of Permian rocks were measured in considerable detail, and samples were taken for analyses. Logs of the measured sections and results of the sample analyses were published as U.S. Geological Survey Circulars 209, 260, 302, 303, 326, and 375. Most of the information was consolidated by Cressman and Swanson (1964).

In November 1968, after a study of the published stratigraphic sections, a selection was made of beds in the Retort and Meade Peak Phosphatic Shale Members whose characteristics indicated that they might yield oil. Because the individual beds are thin, they were assembled into 47 groups, each group of minable thickness. Samples from the individual beds were combined in the proper proportions to make a composite sample representative of each group. The resulting samples for two of the groups were too small to be tested, but for the remaining samples the yields of oil and water were determined using the modified Fischer assay method. The samples were taken from surface trenches and are believed to be unweathered in their oil content, but little is known concerning sampling techniques best suited to the Phosphoria oil shales. Localities of the measured sections from which the samples were taken are shown in figure 1 (p. C164). Results of the tests are given in table 1. Included in the table (locality 21) are selected combined results of distillation tests of samples from Sheep Creek (Cressman and Swanson, 1964, p. 438).

RESULTS

Table 1 shows that 27 of the 45 samples tested yielded less than 1 gallon of oil per ton and only three yielded more than 5 gallons per ton. At Sliderock Mountain (loc. 3) a section 16 feet thick had an average yield of 6.4 gallons per ton; at Big Sheep Canyon (loc. 19) 16.3 feet averaged 5.8 gallons per ton and the underlying 17.9 feet averaged 8.7 gallons per ton. The richest section, at Sheep Creek (loc. 21), yielded down the section as follows:

Thickness of unit (feet)	*Yield (gal per ton)*	*Thickness of unit (feet)*	*Yield (gal per ton)*
1.0	7.0	1.8	Barren
2.2	Barren	9.1	9.05
9.1	16.13	3.2	4.70

It is concluded that the possibility is remote that the beds in the Retort and Meade Peak Phosphatic Shale Members of the

U.S. GEOL. SURVEY PROF. PAPER 800-C, PAGES C161-C164

Table 1.—*Recovery of shale oil from samples of the Phosphoria Formation in southwestern Montana*

[Nos. 1–20, analyses by V. E. Shaw, U.S. Geological Survey; No. 21, analyses by U.S. Bureau Mines Petroleum and Oil-Shale Expt. Sta., Laramie, Wyo.]

No. on fig. 1	Locality	Lot No.	Reference: Author and year	Reference: Page No.	Member of Phosphoria Formation	Beds included in sample	Thickness of interval (feet)	Oil (gal per ton)	Water (gal per ton)
1.	Warm Springs Creek	1300	Cressman and Swanson (1964).	494	Retort Phosphatic Shale Tongue.	26–19	9.4	None	3.1
2.	Canyon Camp	1311	do	509	Retort Phosphatic Shale Member.	73–58	20.5	4.5	3.8
						56–50	10.7	(1)	(1)
3.	Sliderock Mountain	1301	do	496	do	63–49	16.0	6.4	5.4
4.	Hogback Mountain	1299	do	486	Retort Phosphatic Shale Tongue.	161–146	19.3	1.2	4.1
						145–131	22.8	<1.0	2.0
						130–109	21.9	1.2	4.9
						108–86	17.3	1.1	5.5
					Meade Peak Phosphatic Shale Tongue.	66–59	10.9	<1.0	2.0
5.	West Fork Madison River	1318	do	513	Retort Phosphatic Shale Tongue.	13–1	28.4	<1.0	2.5
6.	Sawtooth Mountain	1241	do	444	Retort Phosphatic Shale Member.	115–100	23.2	2.1	4.8
						96–92	25.0	<1.0	3.4
7.	West Fork Blacktail Creek	1302	do	500	do	86–74	26.6	None	7.2
						72–47	33.5	3.6	8.1
					Meade Peak Phosphatic Shale Member.	21–10	10.8	<1.0	4.1
8.	Wadhams Springs	1246, 1247	do	450	Retort Phosphatic Shale Member.	110–97	17.1	<1.0	6.1
						96–73	20.8	(1)	(1)
					Meade Peak Phosphatic Shale Member.	34–30	14.8	<1.0	2.4
9.	Crooked Creek	1296, 1297	do	481	Retort Phosphatic Shale Member.	105–94	31.3	1.9	7.7
						93–72	37.3	2.1	8.4
					Meade Peak Phosphatic Shale Member.	52–28	13.6	None	2.4
10.	Little Sheep Creek	1294, 1295	do	476	Retort Phosphatic Shale Member.	108–99	16.7	3.1	10.8
						97–81	10.9	None	4.8
					Meade Peak Phosphatic Shale Member.	59–45	14.0	None	4.8
11.	Upper French Creek	1248	Klepper and others (1953).	27	D member (Klepper and others [Retort Phosphatic Shale Member]).	10–1	14.5	<1.0	7.0
12.	Kelley Gulch	1249	Cressman and Swanson (1964).	457	Retort Phosphatic Shale Member.[2]	80–62	24.6	<1.0	5.0
						55–27	24.9	<1.0	5.0
13.	South Greenstone Gulch	1250	Klepper and others (1953).	14	D member (Klepper and others [Retort Phosphatic Shale Member]).	37–15	41.7	<1.0	7.2
						13–5	15.6	<1.0	6.8
14.	Cave Creek	1257	Cressman and Swanson (1964).	473	Retort Phosphatic Shale Member.	[3]45–35	14.2	<1.0	4.8
						34–2	20.5	<1.0	4.3
15.	North Big Hole Canyon	1358	do	537	Retort Phosphatic Shale Tongue.	62–42	22.7	<1.0	4.8
						36–26	9.9	<1.0	4.2
16.	South Big Hole Canyon No. 1.	1354-A	do	528	do	23–16	12.9	<1.0	3.6
17.	Dalys Spur	1222, 1223	do	408	Retort Phosphatic Shale Member.	85–69	20.6	1.9	17.4
						68–54	20.3	2.7	14.4
						52–35	12.8	<1.0	7.2
18.	Cedar Creek	1256	do	470	do	58–46	29.2	<1.0	3.1
						44–1	20.7	<1.0	4.2

Table 1.—*Recovery of shale oil from samples of the Phosphoria Formation in southwestern Montana*—Continued

[Nos. 1–20, analyses by V. E. Shaw, U.S. Geological Survey; No. 21, analyses by U.S. Bureau Mines Petroleum and Oil-Shale Expt. Sta., Laramie, Wyo.]

No. on fig. 1	Locality	Lot No.	Reference: Author and year	Reference: Page No.	Member of Phosphoria Formation	Beds included in sample	Thickness of interval (feet)	Oil (gal per ton)	Water (gal per ton)
19.	Big Sheep Canyon.....	1224, 1225	Cressman and Swanson (1964).	414	.....do.....	198–195	16.3	5.8	12.0
						193–176	17.9	8.7	7.7
						172–161	16.6	4.4	4.8
						159–133	26.1	4.6	7.2
					Meade Peak Phosphatic Shale Member.	76–70	9.2	2.6	3.6
20.	Little Water Canyon.....1341		.....do.....	519	Retort Phosphatic Shale Member.	71–63	14.3	<1.0	3.4
						61–44	17.1	1.2	5.4
					Meade Peak Phosphatic Shale Member.	16–2	15.4	<1.0	10.8
21.	Sheep Creek 1234		.....do.....	438	Retort Phosphatic Shale Member.	91–89	1.0	7.0	13.4
						88	2.2	None	16.8
						87–79	9.1	16.13	12.8
						78–77	1.8	None	15.0
						76–57	9.1	9.05	12.3
						56–54	3.2	4.70	12.1

[1]Insufficient sample for analysis.
[2]Bed 80 is in Tosi Chert Member but had to be included because there was one sample for beds To-80 and Rt-79.
[3]Volcanic rocks excluded from sample and thickness.

Phosphoria in southwestern Montana contain enough shale oil to be valuable economically either now or in the foreseeable future.

Such low yields of oil on distillation test are surprising inasmuch as the black shale, phosphorite, and chert facies of the Phosphoria Formation accumulated in an area of upwelling ocean waters, an environment extremely favorable for the production of organic matter and an excellent source for oil. It may be that, although there is enough organic carbon present, there is not enough available hydrogen to produce oil. On the other hand, many geologists have believed that the Phosphoria Formation was the source of oil found in many of the oil fields of Montana and Wyoming (Sheldon, 1967). Perhaps much of the kerogen once present in the black shale was converted into oil by the heat and pressure of tectonic movement and the weight of overburden, and the oil was thus released and made available for migration into the present reservoir rocks.

REFERENCES

Bowen, C. F., 1918, Phosphatic oil shales near Dell and Dillon, Beaverhead County, Montana: U.S. Geol. Survey Bull. 661-I, p. 315–320.

Condit, D. D., 1919, Oil shale in western Montana, southeastern Idaho, and adjacent parts of Wyoming and Utah: U.S. Geol. Survey Bull. 711-B, p. 15–40.

Cressman, E. R., 1955, Physical stratigraphy of the Phosphoria formation in part of southwestern Montana: U.S. Geol. Survey Bull. 1027-A, p. 1–31.

Cressman, E. R., and Swanson, R. W., 1964, Stratigraphy and petrology of the Permian rocks of southwestern Montana: U.S. Geol. Survey Prof. Paper 313-C, p. 275–569.

Klepper, M. R., Honkala, F. S., Payne, O. A., and Ruppel, E. T., 1953, Stratigraphic sections of the Phosphoria formation in Montana, 1948: U.S. Geol. Survey Circ. 260, 39 p.

McKelvey, V. E., and others, 1959, The Phosphoria, Park City, and Shedhorn Formations in the western phosphate field: U.S. Geol. Survey Prof. Paper 313-A, p. 1–47.

Sheldon, R. P., 1967, Long-distance migration of oil in Wyoming: Mtn. Geologist, v. 4, no. 2, p. 53–65.

Swanson, R. W., 1970, Mineral resources in Permian rocks of southwest Montana: U.S. Geol. Survey Prof. Paper 313-E, p. 661–777.

Winchester, D. E., 1923, Oil shale of the Rocky Mountain region: U.S. Geol. Survey Bull. 729, 204 p.

Yochelson, E. L., 1968, Biostratigraphy of the Phosphoria, Park City, and Shedhorn Formations: U.S. Geol. Survey Prof. Paper 313-D, p. 571–660.

[Figure 1 on next page]

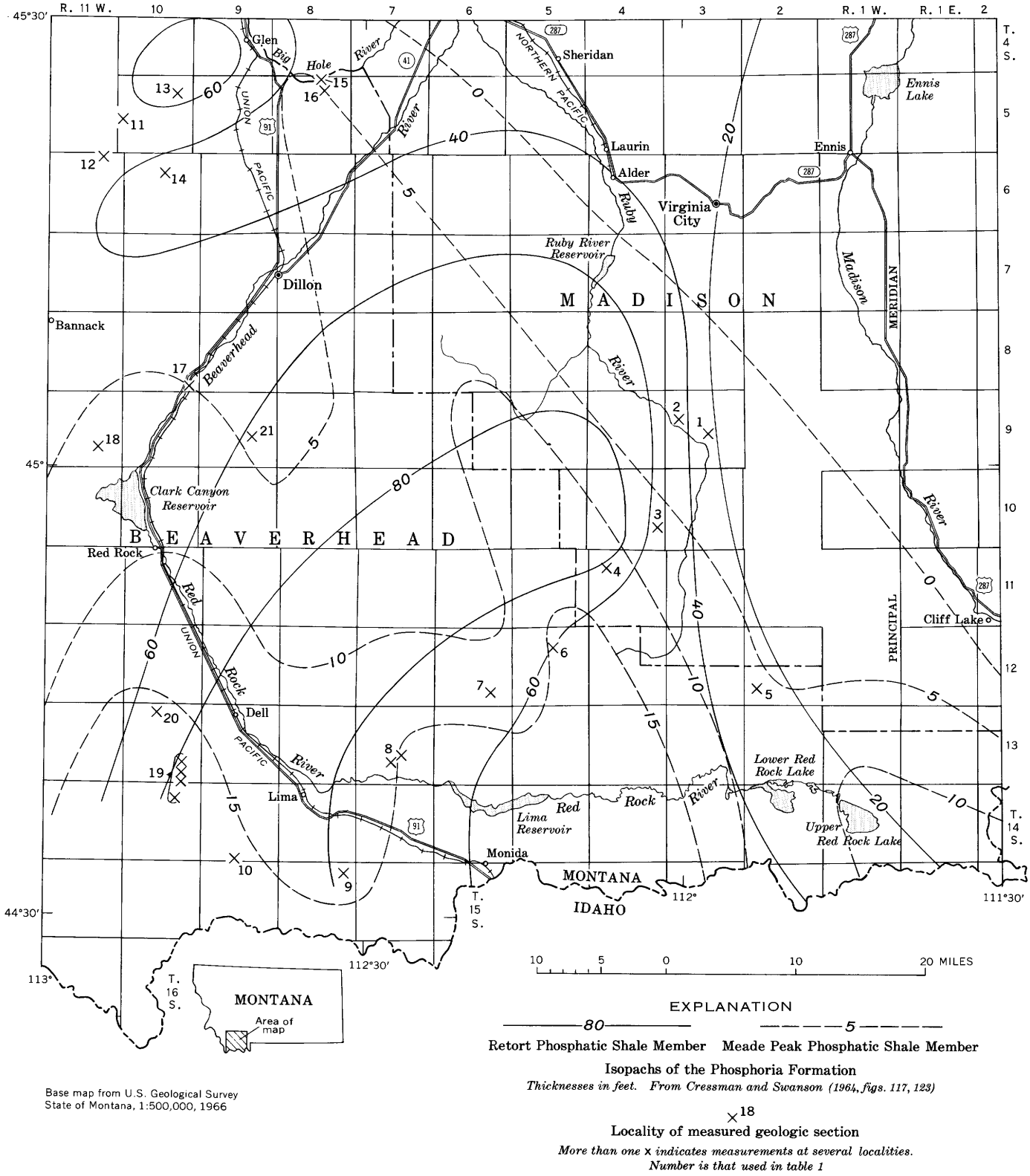

Figure 1.—Localities of measured geologic sections of the Phosphoria Formation in southwestern Montana from which samples were taken.

AGES OF PLUTONS AND TYPES OF MINERALIZATION, NORTHWESTERN ELKO COUNTY, NEVADA

By R. R. COATS and E. H. McKEE, Menlo Park, Calif.

Prepared in cooperation with the Nevada Bureau of Mines

Abstract.—In northwestern Elko County, Nev., K-Ar ages on several small and medium-sized plutons have confirmed the age distributions previously reported, which are centered around dates that fall in the Jurassic, Cretaceous, and Tertiary. The Mesozoic plutons can be grouped geographically into three belts, all having a roughly eastward trend in conformity with the predominant tectonic grain of the region. The rocks of the two more northerly belts range from granodiorite to granite; those of the more southerly belt are generally more mafic, locally dioritic. The known mineral deposits of the northern belts are few in number and negligible in size; those of the central belt include significant scheelite deposits and minor gold veins; those of the southern belt are vein deposits of silver, gold, and antimony. Two Tertiary plutons are spatially associated with silver, gold, tungsten, and base-metal deposits; not all of these metals are found in the vicinity of any one pluton.

In 1965, Coats, Marvin, and Stern (1965, p. D11) summarized existing views on the age of plutonism in northeasternmost Nevada and parts of neighboring states and reported new radiometric ages for nine plutons. At that time it was suggested that a pattern of distribution of the plutons with respect to age was discernible. In this report, we add six K-Ar ages that modify slightly these earlier views and discuss relation of type of mineralization to age and composition of the granitic body.

The plutons for which ages were previously reported (Coats and others, 1965; Bushnell, 1967) and those for which new ages are reported are mapped on figure 1; age data are given in table 1.

AGE DETERMINATIONS

The pluton ages reported here are K-Ar determinations on biotite mineral separates. Adularia was used to date vein material from one locality. The Ar analyses were carried out using standard isotope-dilution techniques in a Nier-type 6-inch-radius, 60°-sector mass spectrometer. The K analyses were done by flame photometer using a lithium internal standard. The plus-or-minus factor is assigned on the basis of experience with duplicate analyses and represents the additive effects of uncertainties in the Ar and K analyses, in the isotopic composition and concentration of the Ar^{38} tracer, and in the concentration of the flame photometer standards.

RELATION OF COMPOSITION TO LOCATION AND AGE

The Mesozoic plutons in northeastern Nevada can be grouped into three distinct belts, each oriented in an east-west direction (Coats and others, 1965, p. D11). Individual plutons of the northern and central belts are elongate east-west plutons; the plutons of the southern belt have nearly equidimensional outcrop patterns. The elongation of the northern plutons is thought to be related to intrusion into terrane having a strong east-west tectonic grain. As this grain dies out southward, the plutons become more equidimensional.

Northern belt

The northern belt includes the Skull Creek, McDonald Creek (Hicks Mountain), Cottonwood Creek, and Bearpaw Mountain (Deep Creek) plutons, and possibly the pluton north of the west end of the Bearpaw Mountain pluton. These plutons range in composition from hornblende-biotite granodiorite to muscovite-biotite granite (Coats, unpub. data; Bushnell, 1967, p. 19). K-Ar ages on four of these granitic bodies range from about 89 to 73 m.y. (table 1), suggesting that they are Cretaceous in age.

Central belt

The central belt includes the Sikikareh Mountain, Mountain City, and the Coffeepot (Bruneau River) plutons. These plutons range in composition (Coats, 1971, and unpub. data; Bushnell, 1967, p. 19) from hornblende-biotite granodiorite to biotite quartz monzonite. Alaskitic marginal phases are present locally. The Mountain City pluton has a K-Ar age of about 90 m.y. (table 1), and the Coffeepot body has been dated as 120±10 m.y. by lead-alpha (Coats and others, 1965; see also table 1), which suggests that they also are of Cretaceous age.

U.S. GEOL. SURVEY PROF. PAPER 800-C, PAGES C165-C168

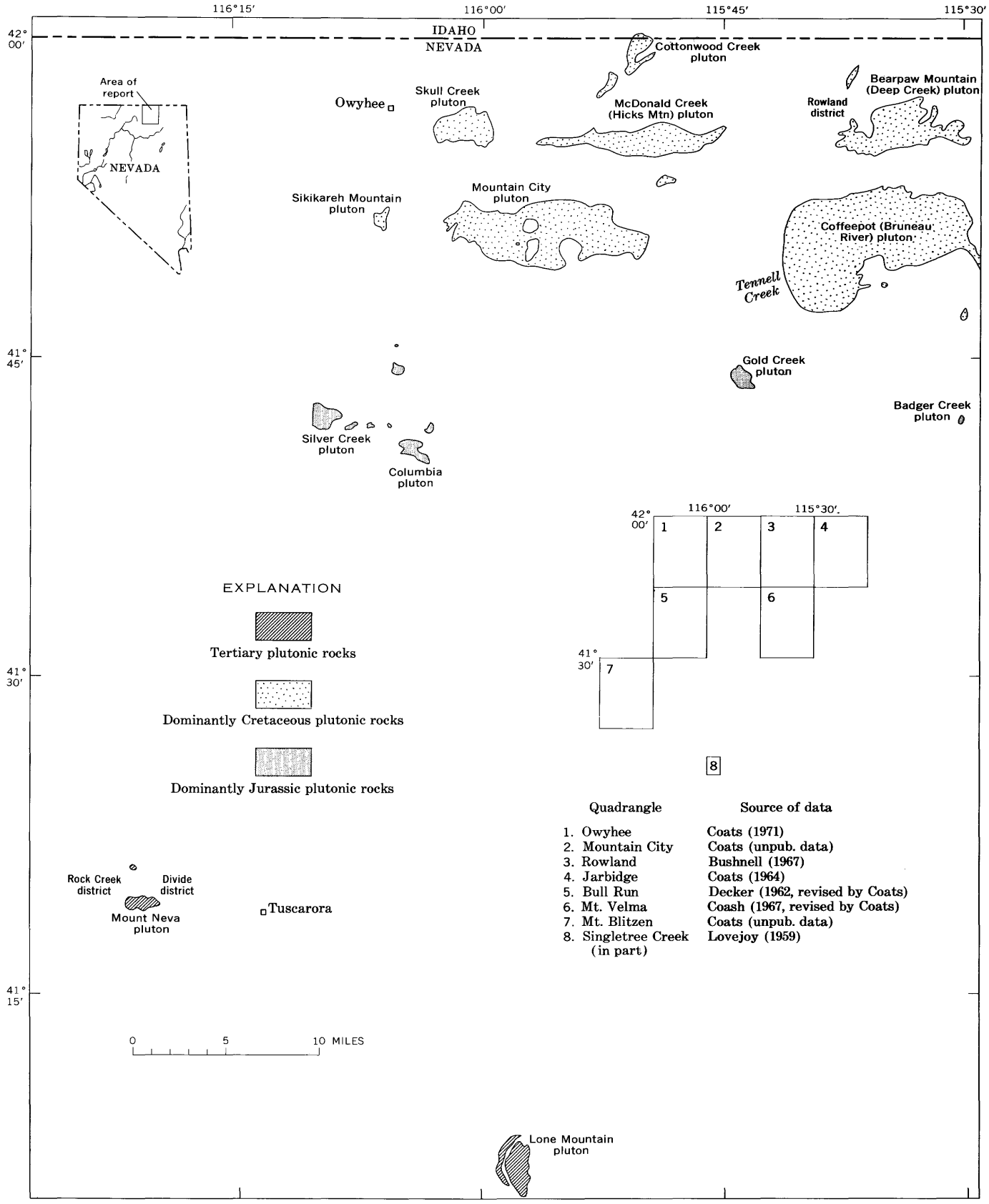

Figure 1.—Distribution of plutonic rocks in northwestern Elko County, Nev.

Table 1.—*Radiometric ages, analytical data from this report and published soruces, and location of plutonic rocks in northeastern Nevada*

Location		Field No.	Name of pluton	Mineral dated	^1K_2O (percent)	Radiogenic Ar^{40}		Apparent age (m.y.)
Lat (N.)	Long (W.)					10^{-10} mole/g	Percent	
				Northern belt				
42°00′05″	115°50′30″	66NC100	Cottonwood Creek	Biotite	9.43, 9.46	12.28	81.8	86.0±3
42°00′05″	115°50′30″	66NC100	... do....	.. do...	8.37, 8.38	11.30	73.9	89.2±3
41°55′25″	115°46′15″	[2]63NC40	McDonald Creek	.. do...	.....	.....	....	88±4.4
41°55′25″	116°01′05″	[2]60NC175	Skull Creek	.. do...	.....	.....	....	81±4.0
41°56′40″	115°33′30″	[2]63NC20	Bearpaw Mountain	.. do...	.....	.....	....	73±3.7
				Central belt				
41°48′25″	115°35′00″	[3]65NC80	Coffeepot	Zircon	Lead alpha	.....	....	120±10
41°51′30″	115°58′50″	[2]57NC89	Mountain City	Biotite	.....	.....	....	90±4.5
				Southern belt				
41°43′50″	115°44′10″	66NC24	Gold Creek	Biotite	8.32, 8.32	19.47	82.9	152.1±5
41°40′25″	116°04′05″	66NC35	Columbia	.. do...	8.58, 8.52	19.67	87.8	149.7±5
				Other plutonic rocks				
41°19′20″	115°51′40″	68NC126	Mount Neva	Biotite	8.40	4.81	59.6	38.4±1.5
41°18′55″	116°13′25″	67NC13	Mineralized vein	Adularia	14.77, 14.87	8.50	75.0	38.4±1.5

Constants used in K-Ar age determinations: $\lambda\epsilon = 0.585\times10^{-10}yr^{-1}$, $\lambda\beta = 4.72\times10^{-10}yr^{-1}$, and $K^{40}/K^{total} = 1.19\times10^{-4}$moles/mole.

[1]Potassium determinations by Lois Schlocker, U.S. Geological Survey. [2]Coats, Marvin, and Stern (1965, p. D13). [3]Bushnell (1967, p. 19).

Southern belt

The southern belt includes the Silver Creek, Columbia, Gold Creek, and Badger Creek plutons, and some other stocks. Most of these rocks differ from those in the northern and central belts in that they are characterized by higher color index and more mafic composition. The Columbia pluton is a hornblende-biotite quartz diorite and is part of an array of small east-west-trending intrusive bodies that range from hornblende diorite in the west to granodiorite in the east (Decker, 1962, p. 40–41). The Gold Creek pluton (Coash, 1967, p. 16) ranges from a hornblende-biotite diorite to a quartz monzonite.

The Gold Creek and Columbia plutons yield K-Ar ages of about 150 m.y. (table 1), which suggests a Middle Jurassic age for the time of cooling of these bodies.

South of the three belts of Mesozoic plutons are two isolated Tertiary plutons: the Mount Neva pluton, 7 miles west of Tuscarora, and the Lone Mountain pluton, 19 miles southeast of Tuscarora. The Mount Neva pluton, dated as 38.4 m.y., is an epizonal pluton that differs texturally from the mesozonal plutons of Mesozoic age. This pluton ranges from a hornblende-biotite granodiorite to a granodiorite porphyry with a granophyric groundmass to which most of the quartz and all potassium feldspars are confined. Much of the hornblende is uralitic, but no vestiges of the pyroxene have been found. Chloritization of hornblende is common, but the biotite is notably fresh.

The Lone Mountain pluton, a composite body almost identical in age (about 38 m.y., K. B. Ketner, written commun., 1970) and composition with the Mount Neva pluton, ranges from diorite through quartz monzonite to granite porphyry (Lovejoy, 1959, p. 553–554; T. S. Lovering and W. M. Stoll, in Granger and others, 1957, p. 110).

ORE DEPOSITION AND THE PLUTONS

In this discussion, we make the simplistic assumption that proximity of ore deposits to plutons connotes some kind of genetic relation, though we do not assume that the ore deposits have any necessary genetic relation to the immediately adjacent phase of the plutons. Nevertheless, there is practical value in outlining such relations as we have discerned, even though their ultimate cause is not clear.

Northern belt

Few mineral deposits of any kind have been reported in association with any of the northernmost belt of plutons. A possible exception is the minor gold production in the Rowland or Gold Basin district (secs. 22, 24, 27, 29, and 31, T. 47 N., R. 56 E., and sec. 17, T. 47 N., R. 57 E.) (Boswick, 1910; Bushnell, 1967, p. 34–35), but even here mining has been short lived and production very small.

Central belt

Mesothermal gold-quartz veins and scheelite-bearing tactites are closely associated with two of the Mesozoic plutons in the central belt, the Mountain City and Coffeepot (Bruneau River) bodies; some ore of each of these types of deposit has been mined and numerous scheelite prospects have been found around the Coffeepot pluton (Bushnell, 1967, p. 34). Bushnell (oral commun., 1955) noted the contrast between the Bear-paw Mountain (Deep Creek) and Coffeepot plutons with respect to the scheelite deposits, these being common around the Coffeepot and completely absent around the Deep Creek. This difference is not a function of wallrock, as both plutons intrude similar calcareous rocks, but rather of the difference in temperature of intrusion and fluid present, as suggested by Bushnell (1967, p. 19). The contact metamorphism around the Coffeepot pluton is of higher grade than that around the Deep Creek pluton, and there is some evidence that there was more fluid involved in the metamorphic reactions. We suggest that the Coffeepot intrusive body had a higher content of hyperfusible materials, and remained fluid for a longer time, thereby permitting the transfer of more heat and mobile elements to the wallrocks. Some scheelite has been found around the Mountain City pluton, but the wallrocks are mostly noncalcareous and not favorable for the formation of contact metasomatic deposits of scheelite. Some of the tactite deposits contain minor amounts of molybdenite, bismuthinite, and uraninite, for example, those at Tennell Creek, on the west margin of the Coffeepot pluton.

Southern belt

The mineral deposits associated with the southern belt of Mesozoic plutons, that which includes the Columbia and Gold Creek plutons, seem to be similar over the length of the belt. The mining districts (Aura, Edgemont, and Island Mountain) have been described by Emmons (1910, p. 71–80) and Decker (1962, p. 65) and have produced gold and silver with minor amounts of lead and antimony. Quartz veins in the Gold Creek pluton carry gold and silver with minor amounts of stibnite, sphalerite, and tetrahedrite, but the precious metal produced from these veins has been negligible.

The Mount Neva pluton, west of Tuscarora, has no mineral deposits in its immediate vicinity, but the distribution of rock alteration suggests that it may extend, in the subsurface, much closer to the Tuscarora district on the east than the outcrop pattern suggests. The coincidence of the age of the adularia associated with the Tuscarora deposits (about 38 m.y., Roberts and others, 1971, p. 29) and the age of the pluton suggests a genetic relation. The mineralogy of the silver deposits of the Tuscarora, Divide, and Rock Creek districts (Lawrence, 1963, p. 53–54; Emmons, 1910, p. 58–64; Nolan, 1936, p. 31) suggests epithermal mineralization; the texture of the granodiorite porphyry suggests that it may represent the upper part of a magma chamber from which the mineralized volcanic rocks of the district were erupted. It is noteworthy that the proportion of base metals in the ore was small, though larger than the production figures would suggest.

CONCLUSIONS

Dating of plutons reported in this paper confirms the earlier division by Coats, Marvin, and Stern (1965) of the plutons in this part of Nevada into three age groups: Jurassic, Cretaceous, and Tertiary. These groups correspond to the general age pattern for central and western Nevada pointed out by Silberman and McKee (1971) and by Smith, McKee, Tatlock, and Marvin (1971), indicating that the threefold age distribution is the significant plutonic age framework throughout most of the northern Great Basin. The factor that determines the dominant metal in the spatially associated ore deposits seems to be the geographic position of the plutons rather than age or gross composition.

REFERENCES

Boswick, F. E., 1910, Gold Basin district: The Mining Rev., Salt Lake City, May 15, 1910, p. 21–22.

Bushnell, Kent, 1967, Geology of the Rowland quadrangle, Elko County, Nevada: Nevada Bur. Mines Bull. 67, 38 p.

Coash, J. R., 1967, Geology of the Mount Velma quadrangle, Elko County, Nevada: Nevada Bur. Mines Bull. 68, 20 p.

Coats, R. R., 1964, Geology of the Jarbidge quadrangle, Nevada-Idaho: U.S. Geol. Survey Bull. 1141-M, p. M1–M24.

——1971, Geologic map of the Owyhee quadrangle, Nevada-Idaho: U.S. Geol. Survey Misc. Geol. Inv. Map I-665, scale 1:48,000.

Coats, R. R., Marvin, R. F., and Stern, T. W., 1965, Reconnaissance of mineral ages of plutons in Elko County, Nevada, and vicinity, *in* Geological Survey Research 1965: U.S. Geol. Survey Prof. Paper 525-D, p. D11–D15.

Decker, R. W., 1962, Geology of the Bull Run quadrangle, Elko County, Nevada: Nevada Bur. Mines Bull. 60, 65 p.

Emmons, W. H., 1910, A reconnaissance of some mining camps in Elko, Lander, and Eureka Counties, Nevada: U.S. Geol. Survey Bull. 408, 130 p.

Granger, A. C., Bell, M. M., Simmons, G. C., and Lee, Florence, 1957, Geology and mineral resources of Elko County, Nevada: Nevada Bur. Mines Bull. 54, 190 p.

Lawrence, E. F., 1963, Antimony deposits of Nevada: Nevada Bur. Mines Bull. 61, 248 p.

Lovejoy, D. W., 1959, Overthrust Ordovician and the Nannie's Peak intrusive, Lone Mountain, Elko County, Nevada: Geol. Soc. America Bull., v. 70, p. 539–564.

Nolan, T. B., 1936, The Tuscarora mining district, Elko County, Nevada: Nevada Univ. Bull., v. 30, no. 1, 36 p.

Roberts, R. J., Radtke, A. S., and Coats, R. R., 1971, Gold-bearing deposits in north-central Nevada and southwestern Idaho, *with a section on* Periods of plutonism in north-central Nevada, by M. L. Silberman and E. H. McKee: Econ. Geology, v. 66, p. 14–33.

Silberman, M. L., and McKee, E. H., 1971, K-Ar ages of granitic plutons in north-central Nevada: Isochron/West, no. 71-1, p. 15–31.

Smith, J. G., McKee, E. H., Tatlock, D. B., Marvin, R. F., 1971, Mesozoic granitic rocks in northwestern Nevada: a link between the Sierra Nevada and Idaho batholiths: Geol. Soc. America Bull., v. 82, p. 2933–2944.

A LEAD-ISOTOPE AGE AND U-Pb DISCORDANCE OF PRECAMBRIAN GNEISS FROM GRANITE MOUNTAINS, WYOMING

By I. T. NKOMO and J. N. ROSHOLT, Denver, Colo.

Abstract.—Lead isotopic composition and concentration in six paragneisses, a granitic gneiss, and two granites from the Granite Mountains area, Wyoming, were determined on whole-rock samples and seven associated feldspars. Uranium and thorium contents also were determined for the whole rocks and for three of the feldspar samples. The Pb^{207}/Pb^{204} versus Pb^{206}/Pb^{204} data from the whole rocks define a line with a slope equivalent to a 2,950±120-m.y. isochron. The age indicated by this isochron is similar to the 2,925±80-m.y. age obtained, by the Rb/Sr method, in another study on the same group of whole rocks and may indicate the time of major metamorphism of these rocks. Lead-uranium and lead-thorium relations show marked discordance and cannot be used to calculate ages. In the whole-rock samples, uranium loss seems to have predominated during the Cenozoic. The age of gneiss in this study indicates the preexistence of a solidified crust older than 2,950 m.y.

Relatively few studies have been reported which were carried out to determine concentration of uranium-thorium and isotopic composition and concentration of lead in granitic rock. The composition and distribution of these elements in Precambrian rock were first studied in 1955 (Tilton and others). Later, Moorbath and Welke (1969) determined Pb^{207}/Pb^{206} ages of igneous rocks from Scotland, and Rosholt and Bartel (1969) established the migration of uranium out of whole rocks from the Granite Mountains. Several authors, among them Doe, Tilton, and Hopson (1965) and Zartman (1965), have used feldspars to study geologic histories. More recently, associated minerals together with gneiss and granitic rocks have received greater attention in lead-age determinations. Rudnik and Sobotovich (1969a) have used lead isotopic composition in metamorphic rocks to date the oldest rocks of the Aldan complex in Siberia. Rudnik and Sobotovich (1969a, b), dealing with a sequence of tectonic events in the Iyengra, Timpton, and Dzheltula series of the Aldan shield in Siberia, revealed wide possible application of lead dating in whole-rock granites and accessory minerals, combined with Rb/Sr dating, to isolate geologic events. All these investigations show the importance of U-Th-Pb dating of rocks in geologic interpretation when the systems represent very old rocks that have accumulated a measurable radiogenic lead component. These techniques have been applied as well in the younger age ranges for rock and galena samples from Broken Hill, Australia, by Reynolds (1971).

An investigation of the U-Th-Pb systematics in the granites from Granite Mountains, Wyo., was made by Rosholt, Zartman, and Nkomo (1972), and the present work extends that investigation to metamorphic rock in the area.

Acknowledgments.—Z. E. Peterman provided the Rb/Sr age interpretation and supplied all the samples along with their geologic description. G. T. Cebula did the mineral separation work.

ANALYTICAL TECHNIQUES AND TREATMENT OF DATA

Methods applied in extracting, separating, and purifying lead, uranium, and thorium are virtually those of Doe, Tatsumoto, Delevaux, and Peterman (1967). Microclines were analyzed by use of methods of treating feldspar separates described by Zartman (1965). Concentrations of these elements were determined by using the techniques of isotope dilution; spikes used were those of purified isotopes of Pb^{206}, Th^{230}, and U^{235} obtained from Oak Ridge National Laboratory (Doe, 1970). The extracted and purified lead was loaded, as lead sulfide precipitate, onto a single rhenium filament and analyzed by surface ionization on a single-focusing 12-inch-radius-of-curvature mass spectrometer with a Faraday cup collector.

For purposes of establishing a basis for interlaboratory comparison of lead isotopic ratios obtained from the use of our mass spectrometer, we made several runs of the National Bureau of Standards (NBS) lead standards SRM-981 and SRM-982. We attempted to keep within narrow limits the variations in operational conditions for the standards as well as for all samples analyzed. Correction factors used were derived from analyses of these standards. All the raw data that were used in the present study, together with analyses of rock standards GSP-1 and G-2, are shown in table 1.

If conditions of a closed system for the history of whole rock are assumed, the time required to generate observed lead

U.S. GEOL. SURVEY PROF. PAPER 800-C, PAGES C169-C177

Table 1.—*Data on rock lead-isotope reference samples*

Sample	Method of analysis	Pb^{206}/Pb^{204}	Pb^{206}/Pb^{207}	Pb^{206}/Pb^{208}	Reference
SRM-981	$Pb(OH)_2$ triple filament.	16.937	1.093	0.4612	Catanzaro and others (1968).
SRM-982	do.	36.739	2.141	.9998	Do.
SRM-981	$PbS\text{-}NH_4NO_3$ single filament.	17.087	1.088	.4572	Present study.
SRM-982	do.	36.877	2.129	.9892	Do.
GSP-1	do.	18.077	1.154	.3819	Peterman and others (1967).
G-2	do.	18.518	1.175	.4706	Doe and others (1967).
GSP-1	do.	17.958	1.160	.3879	Present study.
G-2	do.	18.327	1.180	.4755	Do.

composition in the rock can be estimated by use of the following equation:

$$\frac{(Pb^{207}/Pb^{204})_{observed} - (Pb^{207}/Pb^{204})_{initial}}{(Pb^{206}/Pb^{204})_{observed} - (Pb^{206}/Pb^{204})_{initial}} = \frac{U^{235}}{U^{238}} \cdot \frac{(e^{\lambda' t} - 1)}{(e^{\lambda t} - 1)}, \quad (1)$$

where t is the unknown parameter, also referred to as "geologic age" (Doe, 1970), and λ and λ' are the decay constants of U^{238} and U^{235}, respectively. The values of these constants and U^{235}/U^{238} atom ratios are those used by Stieff, Stern, Oshiro, and Senftle (1959).

The time of lead mobilization in microclines can then be estimated from the following equation:

$$S = \frac{e^{\lambda' t} - e^{\lambda' t_m}}{137.8\,(e^{\lambda t} - e^{\lambda t_m})}, \quad (2)$$

where t is the age obtained from equation 1, t_m is the time lapsed since last lead mobilization took place, and S is the least-squares slope obtained from the linear array of feldspar data on the Pb^{207}/Pb^{204} versus Pb^{206}/Pb^{204} plot.

Descriptions and collection localities of samples used in the present study are given in table 2, and these localities are shown in figure 1. Lead isotopic ratios for whole rocks and feldspars are given in table 3 and concentrations of U-Th-Pb in the same systems are shown in table 4. In all samples, chemical digestion was carried out in a way to ensure complete dissolution and until no residue could be visually detected.

Table 2.—*Description and locality of Precambrian gneiss samples from Granite Mountains, Wyo.*

No. (fig. 1)	Field No.	Description and locality
	Paragneisses	
1	GM-35-68	Biotite-quartz-feldspar gneiss, ctr. sec. 11, T. 30 N., R. 93 W., Fremont County.
2	GM-76-68	Biotite augen gneiss, ctr. sec. 11, T. 30 N., R. 93 W., Fremont County.
3	GM-38-68	Biotite-quartz-feldspar gneiss, ctr. sec. 11, T. 30 N., R. 93 W., Fremont County.
4	W_2-CR-5	Medium-grained biotite gneiss and crudely banded biotite schlieren drill core, 153-ft depth, NW¼ sec. 7, T. 31 N., R. 89 W., Natrona County.
5	GM-77-68	Migmatitic biotite gneiss, SW¼ sec. 17, T. 30 N., R. 92 W., Fremont County.
6	GM-78-68	Biotite-quartz-feldspar gneiss, ctr. sec. 11, T. 30 N., R. 93 W., Fremont County.
	Granitic gneiss	
7	GM-98-68	Granitic gneiss, S½ sec. 29, T. 30 N., R. 95 W., Fremont County.
	Granite	
8	W_2-CR-1	Coarse-grained biotite granite, heavily iron stained along fractures, drill core, 99-ft depth, SE¼ sec. 35, T. 32 N., R. 88 W., Natrona County.
9	W_2-CR-1	Coarse-grained biotite granite, some intergranular iron stain, unfractured, drill core, 153-ft depth, SE¼ sec. 35, T. 32 N., R. 88 W., Natrona County.

RESULTS

Lead systematics in whole-rock and mineral samples

The six whole-rock paragneisses, one granitic gneiss, and two biotite granite samples that were analyzed for lead composition were found to contain various degrees of enrichment in radiogenic isotopes, ranging in Pb^{206}/Pb^{204} from 15.0 to 70.3. The least radiogenic sample (No. 1, fig. 2 and table 3) is a biotite-quartz-feldspar gneiss and is characterized by Pb^{206}/Pb^{204} of 15.02. In general, the Wyoming whole-rock paragneisses have an average Pb^{206}/Pb^{204} of 19.6 and Pb^{208}/Pb^{204} of 42.7. By application of equation 1, the age given by the paragneiss system, samples 1–6, and the granitic gneiss, sample 7, is found to be 2,950±120 m.y. Samples 8 and 9, however, which are orthogneisses or foliated granites, have Pb^{206}/Pb^{204} values of 56.5 and 70.3 (table 3), respectively, and may represent a rock that is different from the massive biotite granite that has been dated at 2,790 m.y. by lead

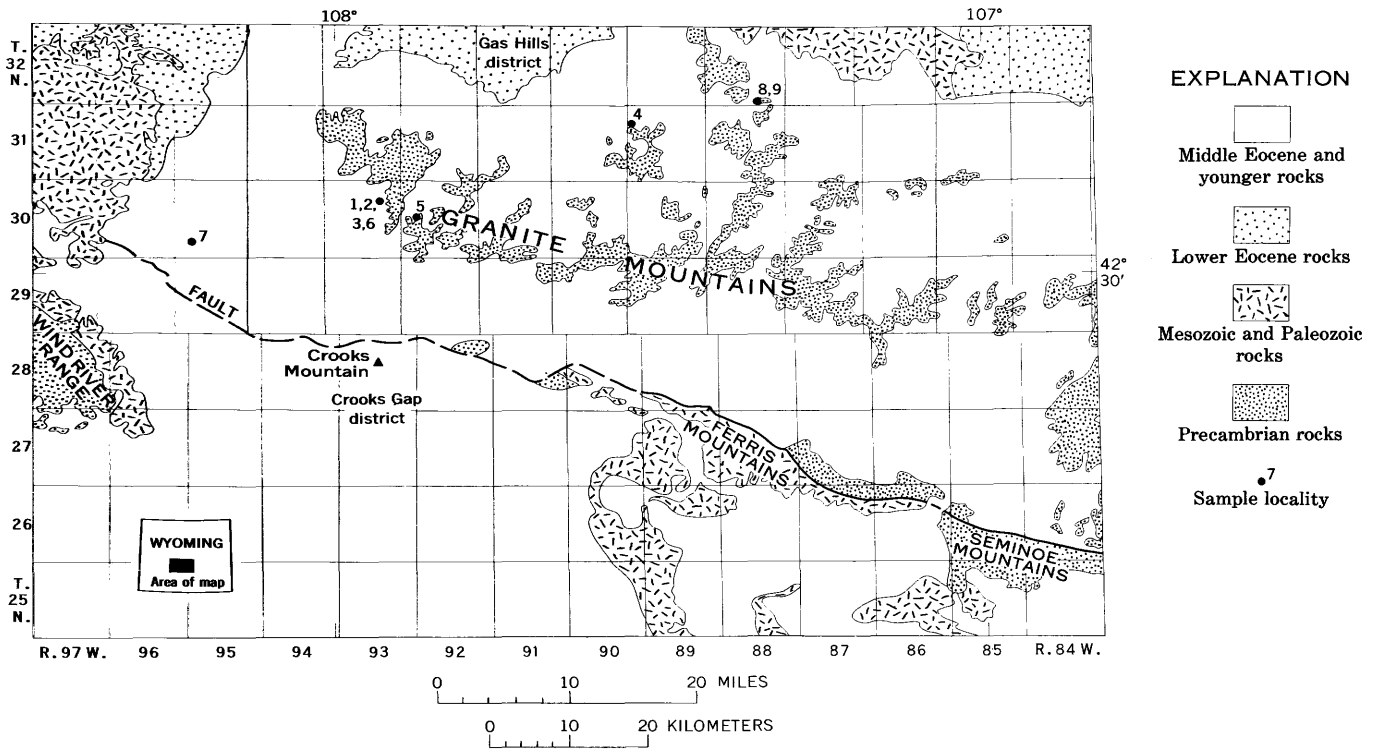

Figure 1.—Geologic map of the Granite Mountains area, Wyoming, showing sample localities (modified from Love and others, 1955).

methods (Rosholt and others, 1972). The 2,950-m.y isochron is of high quality and obviously was unaffected by the granite intrusion at 2,790 m.y., a thermal metamorphism at about 1,600 m.y. (discussed in next paragraph), or uranium redistribution in the relatively recent Cenozoic (discussed under "U-Th-Pb distribution in whole rocks and feldspars").

The feldspars range in Pb^{206}/Pb^{204} from 13.99 to 19.97, sample 1 being the least radiogenic and plotting slightly above the whole-rock isochron (fig. 3). All microclines define a definite trend above the whole-rock isochron but, contrary to the feldspars in the 2,790-m.y.-old granites, the feldspars in the older gneisses have a significant scatter on the

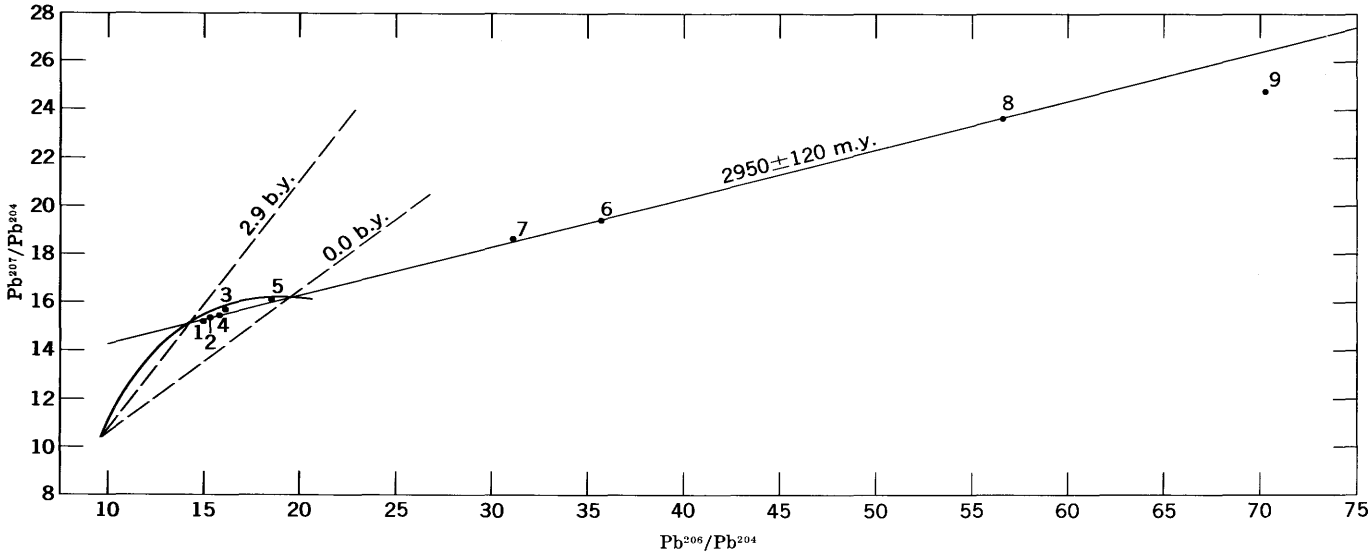

Figure 2.—A lead-lead age plot showing a whole-rock-gneiss isochron of 2,950 m.y. A growth curve with a μ value of approximately 9 intersects the whole-rock isochron at 2.9 and 0.0 b.y.

Table 3.—*Lead isotopic ratios for whole rocks and feldspars from Granite Mountains, Wyo.*

[All ratios are absolute values corrected using measurements of the lead standards NBS-981 and NBS-982]

No. (fig. 1)	Whole rock			Feldspar		
	Pb^{206}/Pb^{204}	Pb^{207}/Pb^{204}	Pb^{208}/Pb^{204}	Pb^{206}/Pb^{204}	Pb^{207}/Pb^{204}	Pb^{208}/Pb^{204}
1	15.019	15.189	37.622	13.986	15.085	34.038
2	15.592	15.313	43.529	...	...	...
3	16.363	15.648	42.993	15.207	15.112	33.494
4	16.322	15.586	40.261	...	...	...
5	18.614	16.044	47.184	15.252	15.738	35.932
6	35.544	19.235	44.313	18.498	16.406	34.452
7	31.276	18.648	47.453	19.965	16.555	36.621
8	56.472	23.525	54.806	18.171	16.116	35.609
9	70.265	24.803	65.320	18.485	16.074	37.208

Pb^{207}/Pb^{206} diagram; unique slope was not found from these data. A plagioclase, sample 3, is the only mineral separate that lies below the whole-rock isochron for the paragneisses. The poorer systematics on the feldspar gneisses likely are due to the effects of a combination of factors. Whereas Rosholt, Zartman, and Nkomo (1972) were able to retrieve a secondary age in a three-stage system, we were not able to do the same in a system complicated by at least four stages. This region appears to have been subjected to the impact of the following major geologic events: (1) formation of the gneisses at 2,950 m.y., (2) intrusion of the granite at 2,790 m.y., (3) thermal metamorphism at 1,600 m.y., and (4) uranium redistribution that was precipitated by tectonism during the later part of the Cenozoic. These four stages could account for the disruption of the feldspar systematics in these older gneisses.

In a study just completed (Rosholt and others, 1972), microclines, because of their unique ability to assimilate radiogenic lead almost to the total exclusion of parent nuclides, seemed to be ideally suited, in lead dating, for secondary age retrieval and pinpointing of major thermal

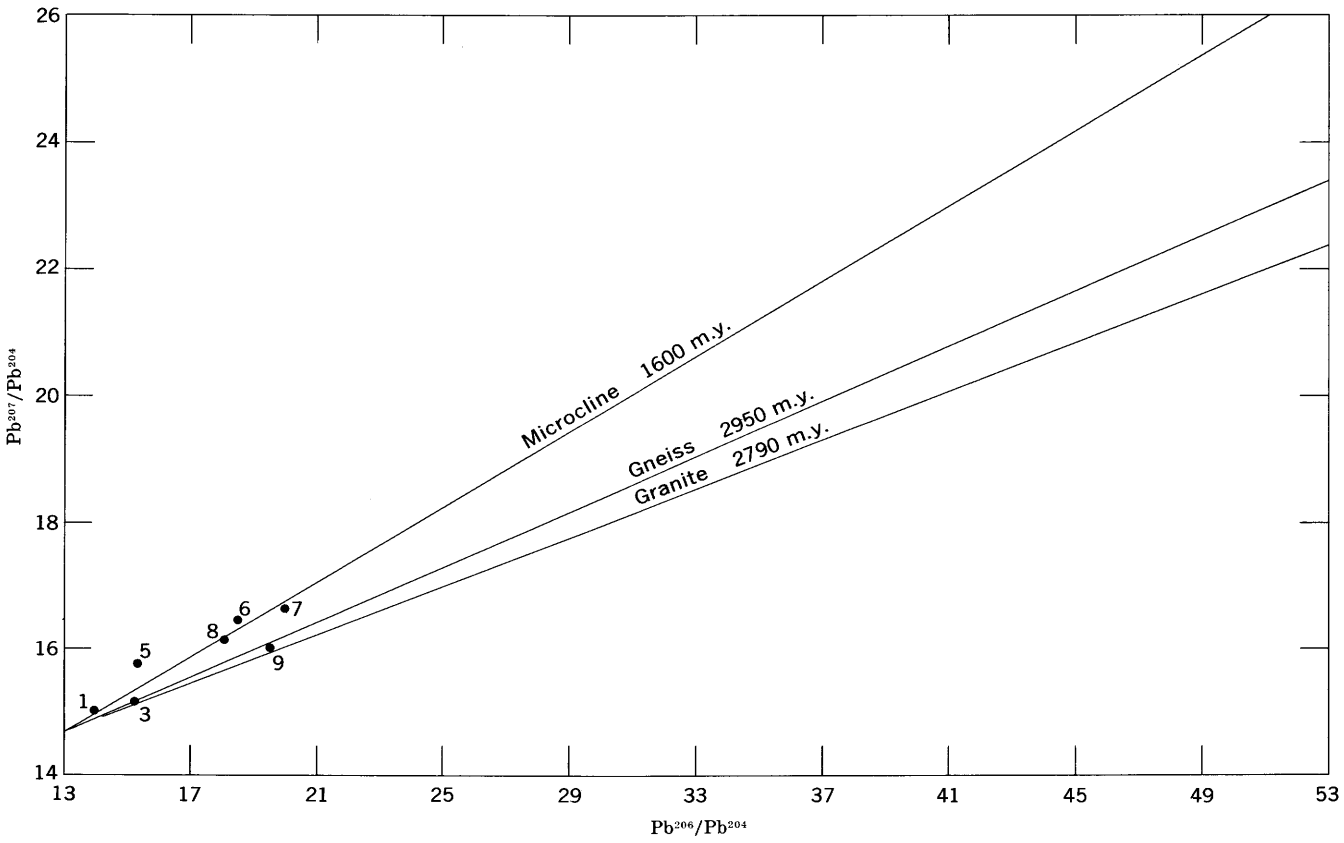

Figure 3.—Pb^{207}/Pb^{204} versus Pb^{206}/Pb^{204} plot showing the feldspar data and relative slopes of whole-rock gneiss, whole-rock granite, and granitic microcline age.

events in the history of a rock system. Given a whole-rock–feldspar system, one can characterize the history of crystallization and lead resetting in the feldspars as shown in figure 4 (where closed-system conditions prevail).

Under ideal conditions the slopes a'-a, b'-b, and c'-c are identical, and each slope independently dates the same event. Where feldspars have gained or lost lead during more than one thermal event they will show considerable spread on the Pb^{207}/Pb^{206} diagram, and their ability to single out any one episode is diminished or effaced. Significant losses of lead at some early time will tend to move the points horizontally toward greater Pb^{206} on the x-axis; a similar effect can be observed where lead gain results from the impact of relatively recent weathering.

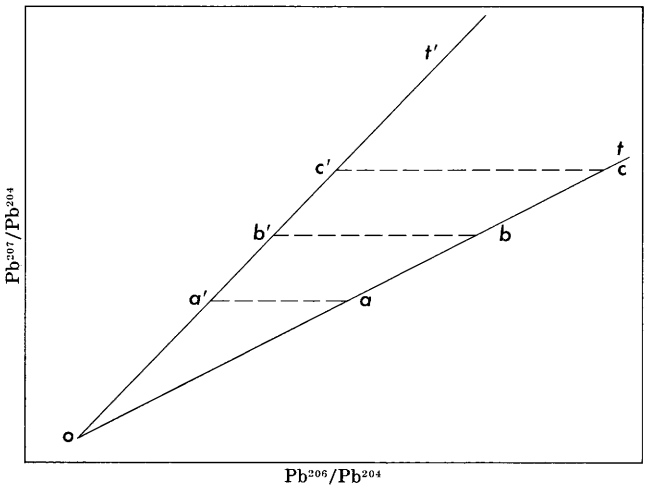

Figure 4.—Theoretical whole-rock (t) and microcline (t') slopes of an undisturbed system whose radiogenic lead component grew between times o and t, t'. Also shown are random intercepts specifying plot locations of microcline lead ratios relative to values of respective host rock. t' is the feldspar isochron with a slope greater than that defined by the whole-rock isochron, t.

These feldspars were reset by gaining radiogenic lead which was added to common lead (table 3). However, a plot of these feldspars on the Pb^{207}/Pb^{204} versus Pb^{206}/Pb^{204} diagram (fig. 3) clearly shows that a reliable slope cannot be obtained, owing to considerable scatter.

Radiogenic lead gain by these systems apparently was too slight to provide a reliable slope for the feldspar data and, for these rocks, the application of equation 2 to determine a secondary age is of little practical value.

U-Th-Pb distribution in whole rocks and feldspars

Uranium, thorium, and lead concentration in whole rocks and feldspars is shown in table 4. The isotopic abundance of U^{238} relative to Pb^{204} in whole rocks is shown in table 5, which presents the relative required and observed abundances

Table 4.—*Concentration of* U-Th-Pb, *in parts per million, in whole rocks and feldspars of Precambrian gneiss*

No. (fig. 1)	Whole rock			Feldspars		
	U	Th	Pb[1]	U	Th	Pb[1]
1.....	0.33	7.43	25.75	...	...	14.10
2.....	.86	13.89	14.26	...	...	...
3.....	.47	9.76	9.03	...	...	9.24
4.....	.74	9.47	19.93	...	...	...
5.....	1.12	20.26	17.15	...	...	...
6.....	3.71	25.04	38.19	0.78	1.49	50.05
7.....	2.22	19.09	19.21	1.06	.67	16.80
8.....	4.09	36.65	35.89	...	...	17.00
9.....	3.91	35.32	19.01	...	...	8.42

[1]Blank correction: 0.79μg.

of parent atom species based on observed daughter products in each sample (table 3 and 4). Most of the whole-rock gneisses and granites studied, as clearly shown in table 5, show a loss in uranium in amounts ranging from 14 to nearly 82 percent of the values required. In contrast, one sample (No. 2, table 5) shows an apparent gain in uranium or a loss in lead. Thorium

Table 5.—*Quantitative losses and gains of uranium and thorium in whole rocks from Granite Mountains, Wyo.*

No. (fig.1)	Uranium					Thorium				
	U^{238}/Pb^{204} *	U^{238}/Pb^{204} †	Apparent loss (percent)	Apparent gain (percent)	Variation (micrograms U per gram rock) ‡	Th^{232}/Pb^{204} *	Th^{232}/Pb^{204} †	Apparent loss (percent)	Apparent gain (percent)	Variation (micrograms Th per gram rock) ‡
1....	0.79	1.80	56.0	...	−0.42	6.64	26.03	74.5	...	−7.88
2....	4.07	2.80	...	45.4	+.27	68.01	63.27	...	7.0	+.97
3....	3.54	4.83	14.5	...	−.17	76.06	59.89	...	27.0	+2.08
4....	3.67	4.76	22.8	...	−.22	48.77	43.89	...	11.1	+.95
5....	4.83	8.07	40.2	...	−.75	90.23	86.32	...	4.5	+.88
6....	8.56	37.57	77.2	...	−12.48	59.72	68.22	12.5	...	−3.56
7....	10.09	30.13	66.5	...	−4.38	89.63	86.01	...	4.2	+.77
8....	13.66	74.06	81.6	...	−17.95	126.53	134.38	5.8	...	−2.27
9....	28.18	98.79	68.8	...	−9.73	263.09	194.91	...	35.0	+9.15

* Measured ratios.
† Required relative amounts for observed lead composition of the 2,950-m.y. gneiss.
‡ Plus sign (+) indicates that ratio measured is greater than required ratio; minus sign (−) indicates that ratio measured is smaller than required ratio.

movement apparently was about the same both into and out of the rock system. A few feldspars were analyzed for uranium-thorium and were found to contain about 1 ppm of these elements.

The variable distribution of lead-isotope ratios relative to abundance of parent nuclide in these whole-rock gneisses is shown in figure 5, which also shows that the paragneisses of the Granite Mountains, Wyo., are less radiogenic than the granite rocks in the area. The rather steep slope of these samples on a Pb^{208}/Pb^{204} versus Pb^{206}/Pb^{204} plot (fig. 6) suggests a high initial Th/U. Inasmuch as uranium migration occurred relatively late in the recent past, as shown by the present study and the accompanying work of Rosholt, Zartman, and Nkomo (1972), the probability of thorium gain is strongly suggested. Table 5 shows that of the six paragneisses, all except samples 1 and 6 have an excess thorium component ranging from 7 to 27 percent. However, whether the excess is indeed the effect of thorium gain is not certain, because in a system that remained closed until the Cenozoic, thorium infusion could only have occurred at that time. Some interesting questions are raised by these considerations. Figure 7 shows relatively minor scatter of the thorium-lead data about a 2,950-m.y. isochron for the gneisses.

DISCUSSION

U-Pb sequence in whole rocks and feldspars

A clear picture of the history of lead evolution in the Precambrian gneiss from Wyoming cannot be obtained from the lead data alone. Determinations made on the relative concentrations of parent species (tables 4 and 5) can shed more light on events that altered and affected these systems. The linearity of the total-rock data on the Pb^{207}/Pb^{206} diagram (fig. 3) suggests a reasonably stable geologic history that does not seem to have altered, to any significant degree, the lead evolutionary sequence in the whole rocks. The whole rocks that experienced a mobility of uranium and thorium apparently remained relatively unaltered with respect to lead isotopic composition. The fact that considerable amounts of uranium and thorium were shifted in the rocks studied indicates that such uranium migration would have had to occur in relatively recent times as also concluded by Rosholt, Zartman, and Nkomo (1972). In an earlier study, Rosholt and Bartel (1969) showed that much of the uranium contained in the granite from Granite Mountains, Wyo., was removed from the rock at a time that did not allow such uranium depletion to affect significantly the rate of lead evolution. In a

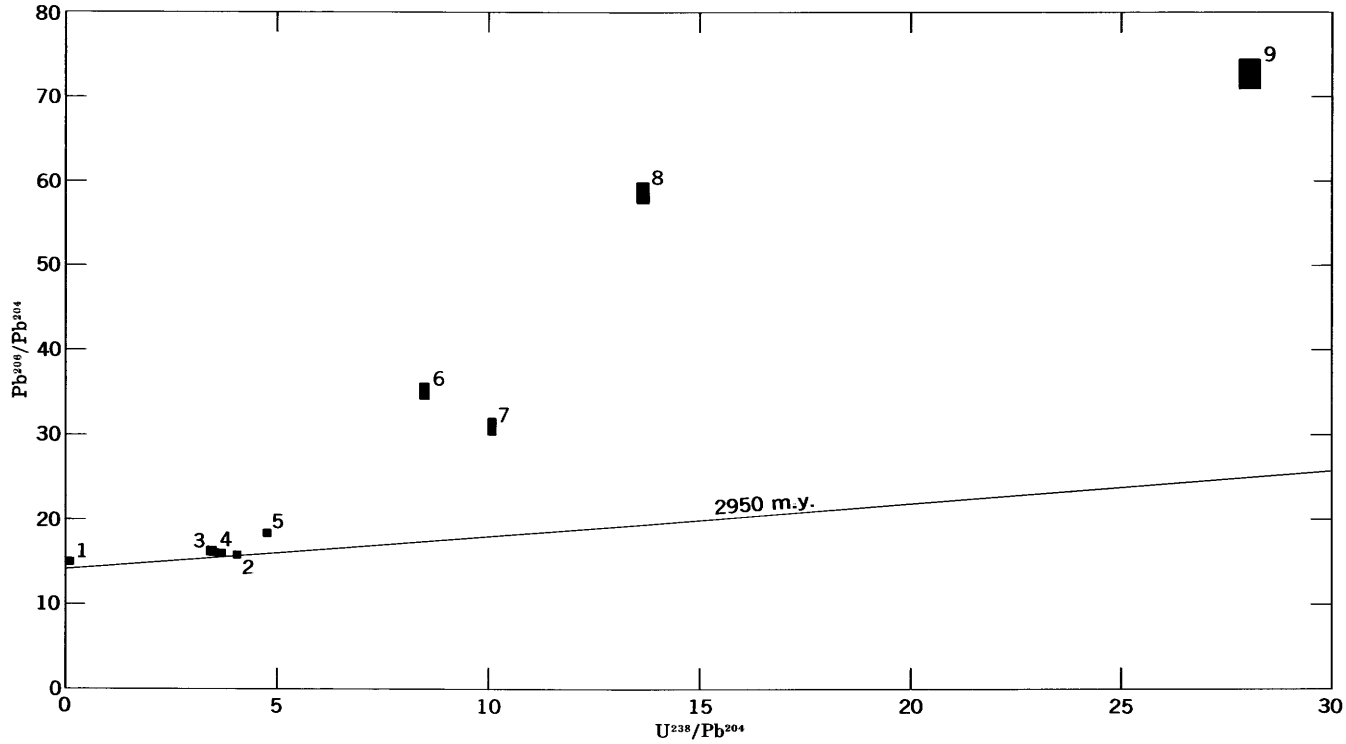

Figure 5.—Parent-daughter plot showing sample distribution relative to the 2,950-m.y. isochron. Four points lie decidedly above the isochron as a result of uranium loss in the Tertiary. Size of box is the approximate limit of uncertainty in location of individual points.

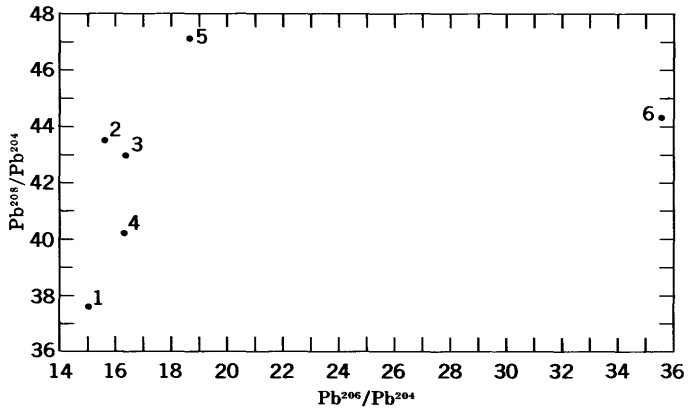

Figure 6.—Pb^{208}/Pb^{204} versus Pb^{206}/Pb^{204} for metamorphic paragneisses from Precambrian rock. Numbers refer to samples. Sample distribution on this plot indicates a very high thorite-lead in relation to abundance of Pb^{206} isotope.

continuation of that investigation, we were able to confirm these earlier observations and further establish that uranium migration probably occurred mainly in the Cenozoic Era.

Similar effects apparently influenced the history of the gneiss in the area studied. The fact that the data for these gneisses lie along a common isochron (fig. 2) suggests that the postmetamorphic history remained virtually the same for all samples analyzed. A possibility for uranium gain is suggested by sample 2, which shows an excess of observed amount of uranium relative to required amount. Because this sample is characterized by a small uranium concentration, the apparent uranium excess may be reflecting a relatively recent event that led to uranium assimilation. Also, this sample possibly was affected by lead movement as a result of weathering at later times when the relative isotopic abundances could no longer be effectively altered by the addition of radiogenic lead. Two other samples, Nos. 8 and 9, are included in this study although, because of their petrographic difference from the

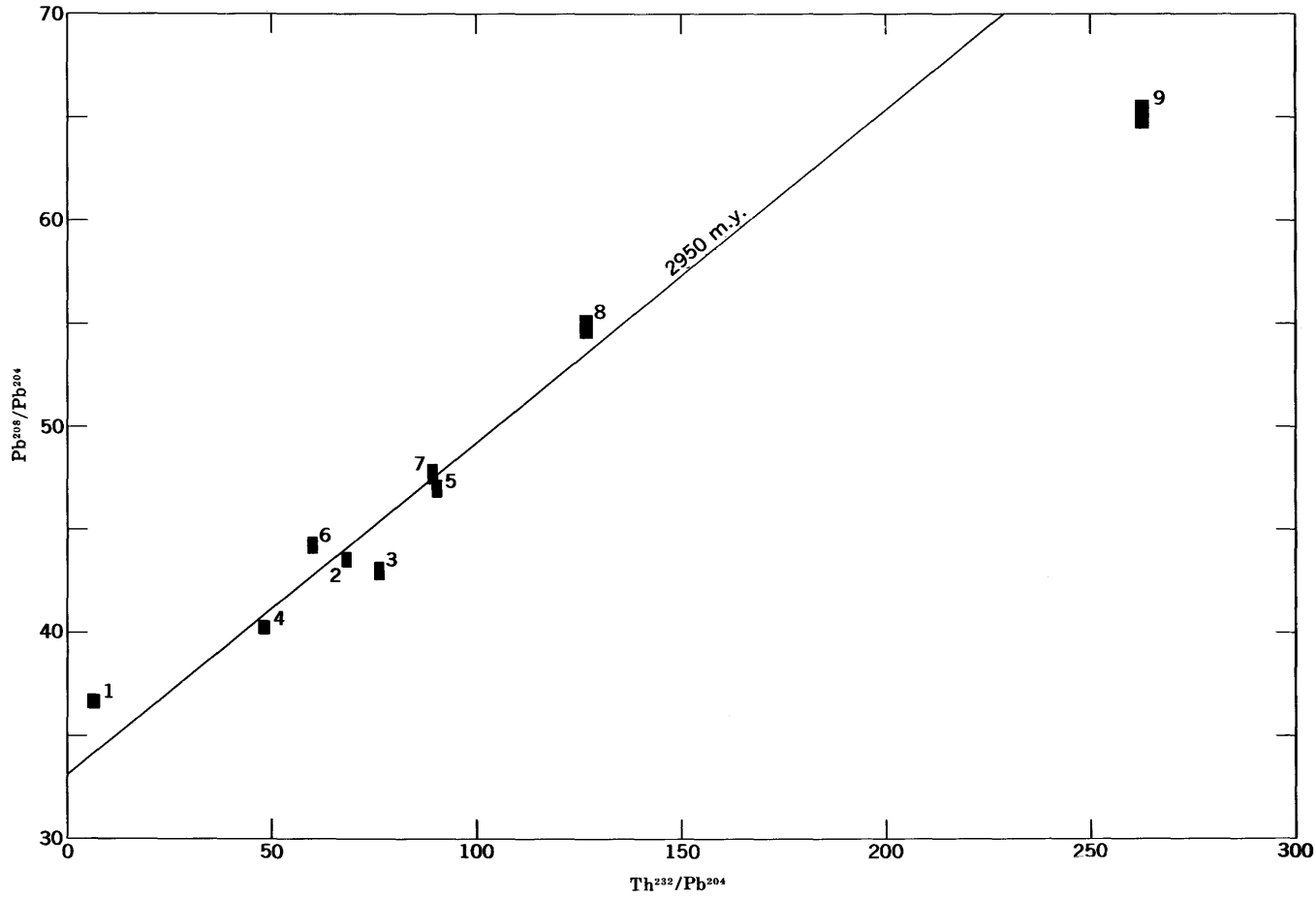

Figure 7.—Pb^{208}/Pb^{204} versus Th^{232}/Pb^{204} plot showing the position of 2,950-m.y. isochron. The spread of the points about this curve suggests minimal disturbance to the Pb-Th system. Size of box is the approximate limit of uncertainty in location of individual points.

main body gneiss, they were not used in the estimation of a best-fit slope for the data. These two samples are coarse-grained biotite granites and were obtained from depths in drill cores about 30 to 40 miles northeast of the primary sample collection area (fig. 1). They differ also petrographically from the massive biotitic granites that were dated at 2,790 m.y.

The Pb^{207}/Pb^{206} age of 2,950±120 m.y. compares favorably with a Rb/Sr age of 2,925±80 m.y. (Peterman and others, 1971). A source μ of 9.2 is indicated with an original lead composition characterized by Pb^{206}/Pb^{204} of 13.59, and Pb^{207}/Pb^{204} of 14.81. The fact that such a disparity exists between the expected and observed values of parent atom concentration explains why a discordance is obtained when Pb^{206}/Pb^{204} is plotted against U^{238}/Pb^{204} (fig. 5). Consideration of Pb^{208}/Pb^{204} and Th^{232}/Pb^{204} (fig. 7) indicates that thorium variations were not as great, in the same samples, as was uranium migration. If a material balance (of all samples except 8 and 9) between the apparent thorium gain and loss is taken into account (table 5), the average net thorium gain clearly does not exceed 1.0 μg per gram of rock. Similar considerations show that an average of 2.6 g U/g rock was removed from these samples in comparison with 20 g U/g rock that was removed from the Granite Mountains, Wyo., granites (Rosholt and others, 1972). The overall effect of uranium variations in the gneiss samples is presented in figure 8. A best-fitted slope through the points overshoots the calculated age of 2.95 b.y. by about 0.35×10^6 years, and the spread of the points is probably a consequence of the four-stage history mentioned previously.

The fact that no reliable slope can be obtained by plotting the feldspar data on the Pb^{207}/Pb^{206} diagram suggests that the feldspar minerals did not come under uniform influences of thermal event(s). As noted earlier, it is evident that in all these feldspars the amount of radiogenic lead component is small as compared to the amounts observed in whole rocks of comparable ages. All these considerations suggest three possibilities that the feldspars studied are displaying: (1) that incomplete homogenization occurred when redistribution of lead was initiated by granite intrusion and thermal metamorphism, (2) that the plagioclase may have been contaminated by lead from very young rocks during periodic multiple thermal events or episodes, or (3) that these feldspars may be reflecting in their isotopic composition the presence of relict feldspar component contributed during premetamorphic sedimentation cycle.

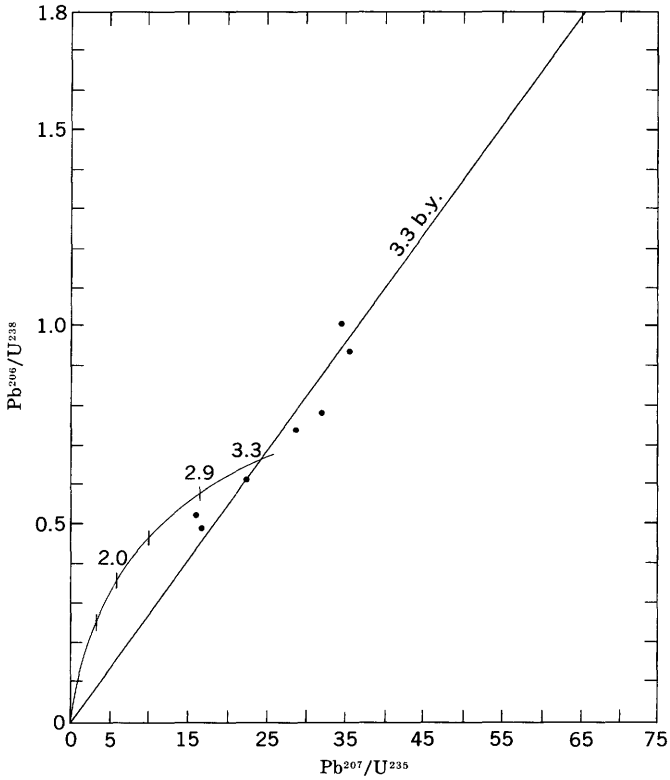

Figure 8.—A concordia diagram showing distribution of Wyoming metamorphic gneisses about 3.3-b.y. isochron.

SUMMARY

The date of 2,950±120 m.y. for the gneiss, based on the lead-lead method, is in excellent agreement with a Rb/Sr date of 2,950±80 m.y. obtained by Peterman, Hildreth, and Nkomo (1971). The fact that crystallization of massive biotite granite probably occurred some 2,790 m.y. ago indicates that most of the granitic Precambrian rocks belong to a series younger than a preexistent solidified crust of at least 2,950 m.y. This observation is compatible with the probability that the rocks of the Granite Mountains were formed from intrusive migmatized geosynclinal material which invaded a preformed crust.

The gneiss date of 2,950±120 m.y. suggests that metamorphism and uranium-thorium incorporation into the crustal system were probably of contemporaneous occurrence. Inasmuch as the age of the granite is 2,790 m.y., the gneiss cannot be regarded as cogenetic with the granite.

Feldspar age data will have to await further study necessary to determine if lead mobilization in these systems occurred in the premetamorphic period. Because only a single plagioclase was analyzed and included in this study (sample 3, feldspar) only further investigation may reveal if the behavior of these minerals is dissimilar to that of microclines.

REFERENCES

Catanzaro, E. J., Murphy, T. J., Shields, W. R., and Garner, E. L., 1968, Absolute isotopic abundance ratios of common, equal-atom, and radiogenic lead isotopic standards: U.S. Natl. Bur. Standards Jour. Research, v. 72A, no. 3, p. 261–267.

Doe, B. R., 1970, Lead isotopes—minerals, rocks, and inorganic materials: New York, Berlin, Springer-Verlag, v. 3, 137 p.

Doe, B. R., Tatsumoto, Mitsunobu, Delevaux, M. H., and Peterman, Z. E., 1967, Isotope-dilution determination of five elements in G-2 (granite) with a discussion of the analysis of lead, *in* Geological

Survey Research 1967: U.S. Geol. Survey Prof. Paper 575-B, p. B170–B177.

Doe, B. R., Tilton, G. R., and Hopson, C. A., 1965, Lead isotopes in feldspars from selected granitic rocks associated with regional metamorphism: Jour. Geophys. Research, v. 70, no. 8, p. 1947–1968.

Love, J. D., Weitz, J. L., and Hose, R. K., 1955, Geologic map of Wyoming: U.S. Geol. Survey, scale 1:500,000.

Moorbath, S., and Welke, H., 1969, Lead isotope studies on igneous rocks from the Isle of Skye, northwest Scotland: Earth and Planetary Sci. Letters, v. 5, p. 217–230.

Peterman, Z. E., Doe, B. R., and Bartel, Ardith, 1967, Data on the rock GSP-1 (granodiorite) and the isotope dilution method of analysis for Rb and Sr, *in* Geological Survey Research 1967: U.S. Geol. Survey Prof. Paper 575-B, p. B181–B186.

Peterman, Z. E., Hildreth, R. A., and Nkomo, I. T., 1971, Precambrian geology and geochronology of the Granite Mountains, central Wyoming [abs.]: Geol. Soc. America, Abs. with Programs, v. 3, no. 6, p. 403–404.

Reynolds, P. H., 1971, A U-Th-Pb lead isotope study of rocks and ores from Broken Hill, Australia: Earth and Planetary Sci. Letters, v. 12, p. 215–223.

Rosholt, J. N., and Bartel, A. J., 1969, Uranium, thorium, and lead systematics in Granite Mountains, Wyoming: Earth and Planetary Sci. Letters, v. 7, p. 141–147.

Rosholt, J. N., Zartman, R. E., and Nkomo, I. T., 1972, Lead isotope evolution and uranium loss in the Granite Mountains, Wyoming: Geol. Soc. America Bull. [In press]

Rudnik, V. A., and Sobotovich, E. V., 1969a, O vozraste porod timptonskoy i dzheltulinskoy seriy Aldanskogo shchita [Age of rocks of the Timpton and Dzheltula series of the Aldan Shield]: Akad. Nauk SSSR Doklady, v. 189, no. 3, p. 607–610; trans., Am. Geol. Inst., 1970, p. 67–70.

—— 1969b, O vozraste polimetamorficheskikh kompleksov iyengrskoy serii Aldanskogo shchita [Age of polymetamorphic complexes of the Iyengra series of the Aldan Shield]: Akad. Nauk SSSR Doklady, v. 189, no. 4, p. 834–837; trans., Am. Geol. Inst., 1970, p. 82–85.

Stieff, L. R., Stern, T. W., Oshiro, Seiki, and Senftle, F. E., 1959, Tables for the calculation of lead isotope ages: U.S. Geol. Survey Prof. Paper 334-A, p. 1–40.

Tilton, G. R., Patterson, Claire, Brown, Harrison, Inghram, Mark, Hayden, Richard, Hess, David, and Larsen, Esper, Jr., 1955, Isotopic composition and distribution of lead, uranium, and thorium in a Precambrian granite: Geol. Soc. America Bull., v. 66, p. 1131–1148.

Zartman, R. E., 1965, The isotopic composition of lead in microclines from the Llano Uplift, Texas: Jour. Geophys. Research, v. 70, no. 4, p. 965–975.

GLACIATION NEAR LASSEN PEAK, NORTHERN CALIFORNIA

By DWIGHT R. CRANDELL, Denver, Colo.

Abstract.—Lassen Volcanic National Park in northern California was mostly covered by icecap glaciers during the Tahoe and Tioga Glaciations, and at least once during pre-Tahoe time. Glacial deposits of various ages have been subdivided chiefly by weathering profiles in till, specifically by the relative amounts of clay formation, the presence and thickness of weathered rinds on volcanic stones at or near the ground surface, the depth of oxidation, and the color hues of the oxidized zone. During each glaciation the major ice-accumulation area in the western part of Lassen Volcanic National Park was on the slopes of the old Brokeoff Volcano, a Pleistocene andesitic stratovolcano which covered an area of more than 100 square miles. Lassen Peak is a dacite dome that evidently was erupted during late Tioga time, perhaps about 11,000 years ago. In latest Tioga time, small glaciers formed on the flanks of Lassen Peak and on adjacent mountains at altitudes above 8,000 feet, whereas during the Tioga icecap glaciation the regional snowline near Lassen Peak was probably at about 7,000 feet.

Surficial deposits near Lassen Peak in northern California record at least three major glacial episodes during which a sizable icecap glacier covered much of the area. The glacier that was formed during the last major glaciation was the largest ice mass between the Sierra Nevada icecap (see Wahrhaftig and Birman, 1965, fig. 3), 60 miles to the south, and an icecap that formed on the High Cascades of Oregon a little more than 100 miles north of Lassen Peak (see Crandell, 1965, fig. 3). I noted evidence of widespread glaciation in the western part of Lassen Volcanic National Park while making an appraisal, with Donal R. Mullineaux, of potential geologic hazards in the park. A review of pertinent literature indicated that little was known of the extent and sequence of glaciation in this region; consequently, 2 weeks were spent during July 1970 examining glacial deposits and preparing a reconnaissance map of glacier extents (fig. 1).

The region studied includes a glaciated area of about 100 square miles. It is the western part of an even larger glaciated area of at least 400 square miles which extends about 20 miles east of Lassen Peak. The glaciated area east of Lassen Peak, however, was not examined during this study.

High volcanic peaks in the western part of Lassen Volcanic National Park are bordered on the west by a volcanic plateau (Macdonald, 1966; Lydon and others, 1960). The most significant topographic feature of the area with respect to glaciation is the old Brokeoff Volcano, an andesitic stratovolcano of Pleistocene age (Williams, 1932). The base of the volcano has a diameter of at least 12 miles and perhaps as much as 15 miles. The top of the cone may once have reached an altitude of as much as 11,000 feet (Williams, 1932, p. 244), but the summit area collapsed or was removed by erosion some time before the last major glaciation. Brokeoff Mountain (alt 9,235 ft) and Mount Diller (alt 9,087 ft), the highest surviving remnants of the old volcano, lie just south and north, respectively, of the former summit area. Loomis Peak (8,658 ft), Reading Peak (8,701 ft), and the peak adjacent to Crescent Crater (8,645 ft) are dacite domes and flows which postdate Brokeoff Volcano but predate the last major glaciation. Lassen Peak (10,457 ft) is a dacite dome that was formed on the north flank of Brokeoff Volcano during a late phase of the last major glaciation. The Chaos Crags consist of several dacite domes that were erupted approximately 1,200 years ago (Crandell and others, 1970).

The distribution of glaciers during the last two glaciations shows a close relation to Brokeoff Volcano, rather than to Lassen Peak which is topographically the highest point in the region today. During each glaciation icefields on the slopes of Brokeoff fed glacier lobes that extended down each major valley from the volcano. A high area mostly underlain by post-Brokeoff dacite domes and lava flows, which trends northeastward from Brokeoff Mountain to the site of Lassen Peak, seems to have been an ice divide from which glaciers flowed to both the southeast and northwest (fig. 1). Ice that mantled these high areas in the western part of the park evidently merged with ice that covered a plateau to the east to form a single massive icecap.

There are no glaciers on Lassen Peak today, although snowbanks persist on north-facing slopes and on the summit throughout most summers. Existing glaciers on Mount Shasta (alt 14,162 ft), 70 miles north-northwest of Lassen, all originate at altitudes above 12,000 feet; thus, Lassen Peak is well below the present regional (climatic) snowline.

Most precipitation in the Lassen Peak area occurs during the period October through April, when the southward shift of the Pacific high-pressure area permits moisture-bearing storms to move southeasterly inland from the Aleutian low-pressure

U.S. GEOL. SURVEY PROF. PAPER 800-C, PAGES C179-C188

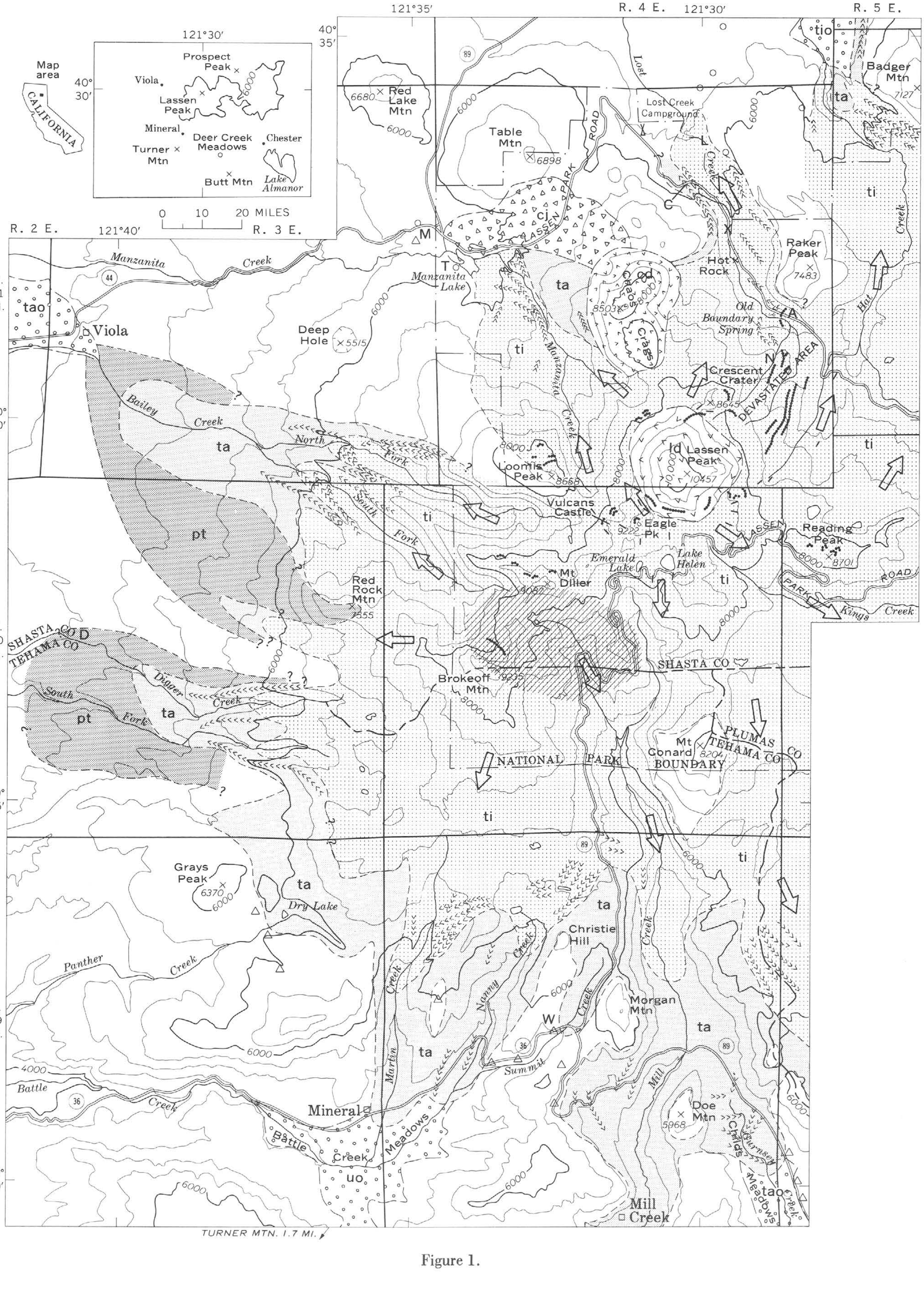

121°35′
R. 4 E.
121°30′
R. 5 E.
40° 35′
Map area
CALIFORNIA
Prospect Peak
Viola
Lassen Peak
Mineral
Deer Creek Meadows
Chester
Turner Mtn
Butt Mtn
Lake Almanor
0 10 20 MILES
R. 2 E.
121°40′
R. 3 E.
Red Lake Mtn
Table Mtn
Lost Creek Campground
LASSEN PARK ROAD
Badger Mtn
Raker Peak
Hot Rock
Chaos Crags
Old Boundary Spring
Crescent Crater
DEVASTATED AREA
Manzanita Creek
Manzanita Lake
Viola
Deep Hole
Bailey Creek
North Fork
South Fork
Loomis Peak
Lassen Peak
Vulcans Castle
Eagle Pk
Reading Peak
Lake Helen
Emerald Lake
Mt Diller
Red Rock Mtn
Kings Creek
SHASTA CO
TEHAMA CO
Digger Creek
Brokeoff Mtn
NATIONAL PARK BOUNDARY
Mt Conard
PLUMAS CO
Grays Peak
Dry Lake
Panther Creek
Christie Hill
Nanny Creek
Martin Creek
Morgan Mtn
Summit Creek
Battle Creek
Mineral
Battle Creek Meadows
Mill Creek
Doe Mtn
Childs Meadows
Gurnsey Creek
Mill Creek
TURNER MTN. 1.7 MI.

Figure 1.

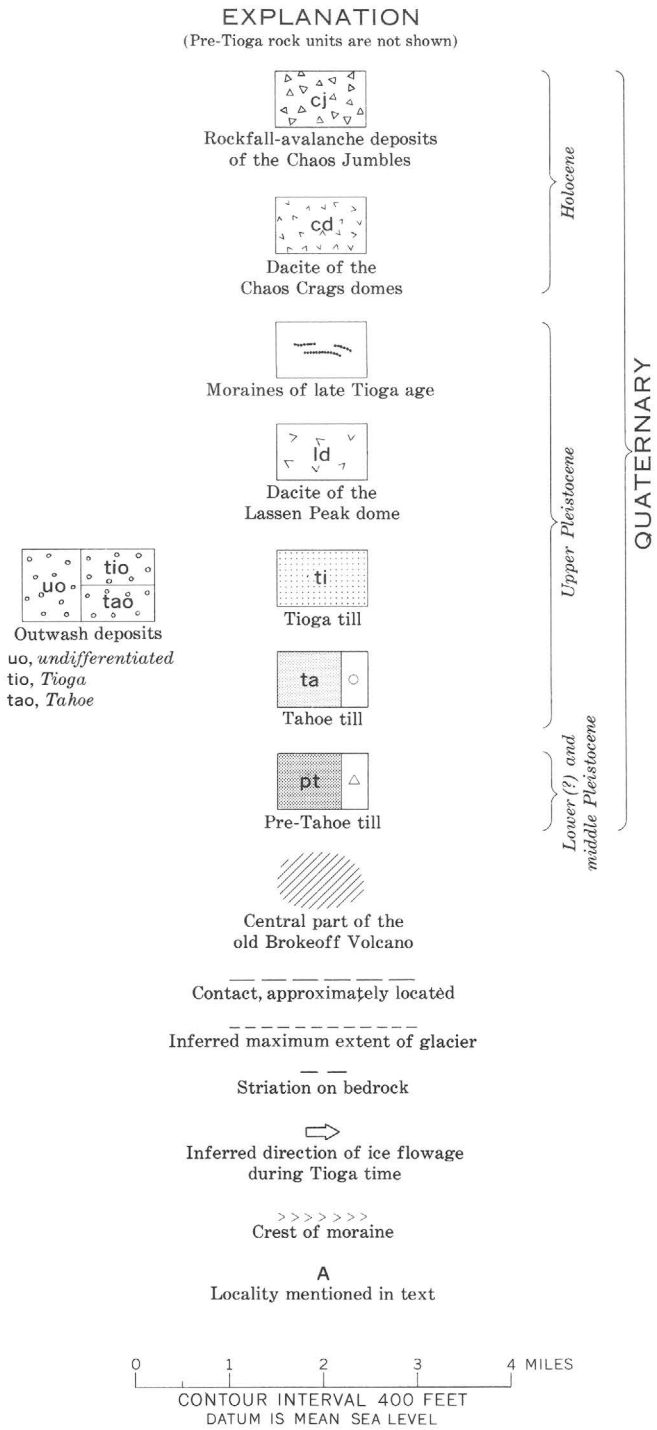

Figure 1.—Reconnaissance geologic map showing extent of Pleistocene glaciation in the western part of the Lassen Peak region.

area. Summers are cool and dry. The average annual precipitation at Mineral (alt about 4,900 ft) from 1950 to 1969 was 55.49 inches, and the average January and July temperatures were 30.8°F and 62.6°F. During the same period, Manzanita Lake (alt about 5,900 ft) had an average annual precipitation of 43.42 inches, and average January and July temperatures of 29.1°F and 63.0°F. According to an isohyetal map of northern California (U.S. Environmental Sci. Services Adm., 1959), Mineral and Manzanita Lake are in or near the zone of maximum precipitation in this part of the Cascade Range, and normal annual precipitation decreases in all directions from those localities except to the south.

The part of the Lassen Peak area that is below an altitude of about 8,000 feet is covered by a dense coniferous forest. The forest is dominated by red fir, Jeffrey pine, lodgepole pine, and mountain hemlock down to an altitude of about 6,000 feet, and by incense cedar, ponderosa pine, sugar pine, Douglas fir, and white fir at lower altitudes. Areas in which the forest has been destroyed by fire are thicketed by dense brush which includes manzanita, tobacco brush, and Sierra chinquapin (Gillett and others, 1961).

The part of the Lassen Peak area that lies west of the maximum extent of glaciation is characterized by reddish-brown lateritic soils. None of the soils on the glacial deposits, which probably are all noncalcic Brown Forest soils, are as red, thick, or clayey as the lateritic soils in the adjacent region.

GLACIAL SEQUENCE

Glacial drift in the area studied is subdivided into four units principally on the basis of weathering profiles and moraine morphology. From oldest to youngest these units are referred to as pre-Tahoe drift, Tahoe Drift, and Tioga Drift; in addition, moraines that were formed in late Tioga time are distinguished as a separate unit and are referred to as moraines of late Tioga age. The drift of the last major glaciation can be correlated with some confidence with the Tioga Drift of the Sierra Nevada, but drift called Tahoe in this report may include deposits that are correlative with the Mono Basin Drift of the Sierra Nevada, as well as Tahoe; thus, Tahoe is used in the sense of drift which is older than Tioga but which seems to be younger than the last major interglaciation. The pre-Tahoe drift of this report is thought to be older than the last major interglaciation.

Weathering profiles constitute the principal evidence of the last major interglaciation, on which part of this subdivision is based. The Tahoe and Tioga tills bear relatively immature soils that lack a well-defined and conspicuous zone of clay enrichment (B horizon). Weathered rinds on stones of intermediate and basic composition are no more than 2 mm thick in Tahoe till and are commonly absent in soils on till of both ages. By comparison with the glacial chronologies of other regions (see Birkeland and others, 1971, and references therein), the time represented by the development of the post-Tioga soil probably is between 10,000 and 15,000 years, and of the post-Tahoe soil between 30,000 and 40,000 years. The soil developed on the oldest part of the Tahoe till recognized in the Lassen Peak area is not greatly dissimilar to that on the youngest part of the Tahoe. In contrast, the extent of clay weathering, depth of oxidation, and oxidized colors all suggest that soils on pre-Tahoe till represent a weathering

interval of great duration. It seems likely that these pre-Tahoe soils were formed during one or more major interglaciations whose lengths were probably at least 100,000 years.

The relative age of a soil in the western part of Lassen Volcanic National Park can be approximated from the hue of the oxidized zone. None of the soils on glacial deposits are as red as the lateritic soils on volcanic rocks west of the park, in which hues of 10*R* or 2.5*YR* are typical (color notations are those of the Munsell system (Munsell Color Co., 1954)). Oxidized zones in glacial deposits of pre-Tahoe age have hues as red as 5*YR*, and the hues of soils on the Tahoe and Tioga tills are typically 7.5*YR* and 10*YR*, respectively. These color differences are thought to be due principally to weathering processes and not to lithologic differences in parent materials.

PRE-TIOGA GLACIATIONS

Pre-Tahoe drift

Glacial drift in which there has been extensive weathering and in which the original morphology of moraines has been very extensively modified is here called pre-Tahoe drift. Soils developed on pre-Tahoe till typically have a well-developed clayey B horizon, and stones in the till generally are extensively weathered to clay. The oxidized zone in pre-Tahoe till extends to depths of more than 15 feet. The moist color of the oxidized zone in till is commonly reddish brown (5*YR* 4/4) to yellowish red (5*YR* 4/6) or reddish yellow (7.5*YR* 6/8). Most small pebbles can be easily cut through with a pick mattock at depths of as much as 10 feet, and rock granules streak and smear out on the face of the cut. Unweathered till of pre-Tahoe age was not seen.

The most deeply weathered pre-Tahoe till that was recognized underlies a lava flow in a roadcut along State Highway 36 about 3 miles northeast of Mineral (loc. W, fig. 1). Most cobbles and boulders of andesite are weathered to clay throughout the exposed thickness of the till, which is about 8 feet. The lava flow is shown as part of the Brokeoff Andesite on Williams' (1932) geologic map of the Lassen Volcanic National Park area.

Pre-Tahoe till rarely displays any morainal topography, although broad smooth till ridges in some places probably are lateral moraines that have been greatly modified by erosional processes. Such a moraine lies on the north side of Digger Creek 6 miles west of Brokeoff Mountain (loc. D, fig. 1).

Pre-Tahoe till which has been buried by younger unconsolidated deposits crops out in the banks of Manzanita Creek 0.3 mile west of Lassen Volcanic National Park (loc. M, fig. 1). The dark-yellowish-brown clayey till contains cobbles and boulders of volcanic rock which have clayey weathering rinds as thick as 4 inches. The till is overlain by a compact, gray, unweathered, lithic sand that is as much as 4 feet thick. The sand is horizontally bedded and locally crossbedded, and it dips a few degrees westward. It may be the deposit of an ash cloud which accompanied a hot block-and-ash flow. The sand is overlain by a pumice-flow deposit containing charcoal which is more than 32,000 years old (radiocarbon sample W-2259, Meyer Rubin, written commun., 1969).

Pre-Tahoe outwash sand and gravel deposits which are partly weathered to clay were noted at several places, but are not shown on figure 1. The most widespread deposits recognized are in the area south of Bailey Creek and west of the outer limit of the pre-Tahoe till. Other deposits are present in the Mill Creek valley downstream from the community of Mill Creek, and on the east side of the Gurnsey Creek valley at Childs Meadows and at Deer Creek Meadows (index map, fig. 1).

A large pre-Tahoe glacier lobe derived from the Brokeoff icefields moved northwestward down the Bailey Creek valley. It is represented by drift near Viola, at a distance of about 8 miles from Brokeoff Mountain. Another glacier lobe, represented by the outcrop of till along Manzanita Creek west of the park, may have been of similar size; however, younger volcanic rocks have obscured the original extent of the drift there and in the area farther east.

Although scattered outcrops of pre-Tahoe drift were recognized southwest and south of the western part of the park, not enough were found to permit reconstruction of glacier lobes in those sectors. The valley of Mill Creek, which heads within the deeply eroded central part of old Brokeoff Volcano, contains pre-Tahoe drift between the community of Mill Creek and a point 4.5 miles farther downvalley. Some of this drift, however, may have been deposited by local glaciers that originated on Turner Mountain (alt 6,893 ft) and adjacent high ridges 1–2 miles west of the Mill Creek valley, rather than by ice from the Brokeoff Volcano. The valley of Gurnsey Creek contains scattered outcrops of pre-Tahoe till at least as far south as Deer Creek Meadows, which is 7 miles southeast of Childs Meadows (fig. 1). Although the till at Deer Creek Meadows probably was deposited by northward-moving glaciers that originated on the north flank of Butt Mountain and along the ridge to the west (index map fig. 1), till northwest of Deer Creek Meadows may have been formed by a glacier heading in the icecap to the north.

Tahoe Drift

Glacial drift which is substantially less weathered than pre-Tahoe drift but which is somewhat more weathered than Tioga Drift is here included in the Tahoe Drift. Some Tahoe till has a zone 1–2 feet below the ground surface which is slightly to moderately plastic and which is interpreted to be a slight textural B soil horizon, but the soil lacks the extensive alteration to clay that characterizes pre-Tahoe till. Stones of andesite or basalt in the upper foot of the soil may have weathered rinds as much as 2 mm thick. Oxidation extends to depths ranging from about 3 to 8 feet, but depths of 4 to 6 feet are most common. The oxidized till is generally strong brown (7.5*YR* 5/6) or dark brown (7.5*YR* 4/4), whereas the unoxidized till is gray.

The range in degree of weathering in the Tahoe till of the Lassen region suggests that it includes deposits of more than one age. For example, till in some moraines is oxidized to a depth of only 3–4 feet, and stones in the oxidized zone have weathered rinds no more than 1 mm thick. The till of adjacent moraines in the same general area, which are here included in the Tahoe Drift, may have oxidation depths of 7–8 feet, and stones near the ground surface may have rinds as much as 2 mm thick.

Tahoe till crops out beneath Tioga till in a streambank on the west side of Lost Creek 1 mile east of Lost Creek Campground (loc. L, fig. 1). The Tahoe till is more than 7 feet thick and is oxidized to a depth of about 6 feet; it is directly overlain by unoxidized Tioga till. This buried oxidized zone is thicker than that on some Tahoe till that has been exposed at the ground surface since it was deposited. The buried till presumably represents a relatively old part of the Tahoe Drift, and it may, in fact, be of Mono Basin age.

The only chronological control on the age of the Tahoe Drift in the Lassen Volcanic National Park area is from charcoal more than 32,000 years old which was obtained from the pumice-flow deposit described previously. The compact unweathered gray sand beneath the pumice-flow deposit overlies Tahoe till near the west edge of Manzanita Lake. Outcrops of the sand and till can be seen in a gully which was once an outlet for the lake and which is located just beyond the southwest edge of the lake (loc. T, fig. 1). Bouldery till exposed in the walls of this gully is oxidized to a depth of 4–6 feet. The till west of the lake forms a west-sloping ramp which probably is the front of a Tahoe end moraine. Just south of the southwest arm of the lake there is a low lateral moraine of Tahoe till whose upvalley end seems to be overlapped by a dacite lava flow. The flow was mapped as the "dacite flow of the Manzanita Lake area" by Macdonald (1963) and assigned an age of late Pleistocene. The flow is older than the Tioga Glaciation.

The oxidized zone on the Tahoe till exposed in the gully evidently was formed prior to 32,000 years ago, but it seems to be as thick as oxidized zones on some Tahoe till that has been exposed to weathering processes since it was deposited. The buried oxidized zone suggests that the till in the gully outcrop is of either early Tahoe or Mono Basin age and thus is at least 70,000 years old.

Moraines of Tahoe age are well preserved but have been substantially smoothed by erosional processes. Drainage on moraines is generally well integrated, and closed depressions are rare. The basin of Dry Lake, which is a marsh most of the year, is the only lake basin recognized on the Tahoe Drift.

Prominent lateral moraines of Tahoe age are present in the valleys of Bailey and Digger Creeks west of the park. Tahoe till, however, extends considerably farther west; thus, either the lateral moraines were formed during retreatal stands of the Tahoe glaciers or they represent a different part of the Tahoe Glaciation than does the till in front of them.

Glaciers of Tahoe age were somewhat smaller than some of the pre-Tahoe glaciers but were substantially larger than the Tioga glaciers. The approximate lowest altitudes, in feet, reached by glaciers in some valleys are shown for comparison as follows:

Valley	*Pre-Tahoe glaciers*	*Tahoe glaciers*	*Tioga glaciers*
North Fork Bailey Creek	4,400	4,600	5,700
South Fork Bailey Creek	.....	.....	5,600
Digger Creek	4,000(?)	4,700	5,500
South Fork Digger Creek	.....	.....	5,700
Martin Creek	.....	4,900	5,400(?)
Nanny Creek	.....	4,900	5,600(?)
Mill Creek–Childs Meadows	.....	4,850	.....
Mill Creek	.....	<4,400(?)	4,900
Lost Creek	.....	<5,500	5,600

The similarity in lowest altitudes reached by Tahoe glaciers in valleys on the west and south sides of the park suggests that a general scarcity of Tahoe Drift at comparable altitudes on the north side of the park is due, in part, to burial of once-extensive drift by younger lava flows. This suggestion is supported by the similarity in the lowest altitudes reached by Tioga ice north, west, and south of the park. Along Lost Creek, for example, Tahoe till is found downvalley to an altitude of about 5,500 feet, and it is bordered on the north by a pyroxene andesite lava flow that does not seem to have been glaciated, although the same flow is locally overlain by Tioga till at higher altitudes farther to the southeast. The lava flow was assigned an early Pleistocene age by Macdonald (1963, 1964). Its relations to glacial deposits suggest that the flow is of post-Tahoe age.

Tahoe outwash gravel can be recognized by a lack of the deeply weathered stones that characterize pre-Tahoe deposits and by the presence of thin rinds on stones, which are absent on stones in gravel of Tioga age. Tahoe outwash deposits were noted in the area north of Bailey Creek west of Viola, and beneath Battle Creek Meadows at Mineral. An outwash valley train of Tahoe age extends down the valley of Gurnsey Creek from the terminal moraine at Childs Meadows at least as far as Deer Creek Meadows, south of the area mapped.

TIOGA GLACIATION

The Tioga Glaciation is represented in Lassen Volcanic National Park by deposits of at least two distinct glacial episodes. During the earlier episode widespread Tioga Drift was deposited by ice originating in an icecap glacier. During the later episode small cirque glaciers developed at altitudes above 8,000 feet; the deposits that resulted are referred to here as moraines of late Tioga age. The Lassen Peak dome evidently was erupted between the two glacial episodes. The soils on till formed during each episode are similar; hence, both tills are assigned to the Tioga Glaciation.

Tioga Drift

Tioga Drift consists of deposits of till and outwash sand and gravel which were formed during the last major glaciation of the Lassen Peak region. A shallow zone of oxidation, which is rarely more than 2.5 feet deep, and a lack of weathered rinds on stones distinguish Tioga till from Tahoe till. Oxidized Tioga till is dark yellowish brown (10*YR* 4/4) to pale brown (10*YR* 6/3). Soils developed on the till do not have a zone of clay enrichment that is discernible in the field. Moraines are sharp crested and well defined and have constructional topography. Closed depressions are common on the Tioga till, and lakes and ponds are abundant in areas covered by Tioga glaciers. Many lakes are in basins excavated in rock by ice (for example, Lake Helen and Emerald Lake), but a few are dammed by moraines (for example, Summit Lake, which is about 2 miles northeast of Reading Peak).

Tioga till is especially well exposed in a cut through a lateral moraine along the Lassen Park Road 1 mile southeast of Lost Creek Campground (loc. C, fig. 1). The till is compact and gray and is oxidized to a depth of 2.5 feet. The moraine merges northward with a terminal moraine complex. Tioga recessional end moraines are present in the Lost Creek valley near the highway bridge across Lost Creek and a short distance south of Hot Rock.

The Hat Creek glacier of Tioga age split into two small lobes near its terminus. A massive outwash fan of very coarse gravel which lies north of the terminal moraines is probably chiefly of Tioga age, but it may include some deposits of Tahoe age.

A Tioga terminal moraine was not recognized in the Manzanita Creek valley, and if one is present it probably lies beneath the rockfall-avalanche deposits of the Chaos Jumbles, which are only a few centuries old. The most conspicuous lateral moraine in the valley is a long north-sloping ridge which holds Manzanita Creek along the east valley wall in a position several hundred feet higher than the central and lowest part of the valley. Inconspicuous recessional moraines curve out from this lateral moraine into the central part of the valley southeast of Manzanita Lake, and other recessional moraines are present farther south in the valley.

Although lobes extended several miles beyond the outer margin of the Tioga icecap glacier on the north, ice lobes were short on the south and west sides. Closely spaced recessional end moraines parallel the outer limit of Tioga ice on the plateaus adjacent to Mill Creek and on the upland just east of Martin Creek.

Tioga snowline

The regional (climatic) snowline during a glacial episode can be approximated from the average altitude of cirque floors formed during that episode. The floors of west- and northwest-facing cirques at Turner Mountain, about 11 miles south of the summit of Brokeoff Mountain, are at an altitude of about 6,200 feet. Although I did not visit that area, aerial photographs of the Turner Mountain area reveal several small lakes in the cirques as well as moraines whose morphology resembles that of Tioga moraines elsewere. Cirque floors near Lassen Peak indicate a snowline that probably was at an altitude of about 7,000 feet. Table Mountain, 7 miles north of the summit of Brokeoff, evidently has not been glaciated, despite a sizable summit area between altitudes of 6,500 and 6,900 feet. Badger Mountain, 10 miles northeast of Brokeoff, also seems to be unglaciated, although it has an extensive area at an altitude of nearly 7,000 feet. Prospect Peak, which has a summit altitude of about 8,300 feet, probably was not glaciated in Tioga time. Thus, the Tioga snowline in the Lassen Peak region evidently rose northeastward at a gradient of at least 70 feet per mile and probably was above 8,300 feet at a distance of 15 miles northeast of Brokeoff Volcano.

The eastward rise of the snowline near Lassen Peak is similar to that inferred for other areas in northern California which have a roughly similar climate today (table 1). On the east side of the Sierra Nevada near Truckee, 100 miles southeast of Lassen Volcanic National Park, Birkeland (1961) found that the climatic snowline was at an altitude of 8,200–8,400 feet during Tioga time. The snowline rose eastward from the Sierra Nevada to the Carson Range of western Nevada on a gradient of 72 feet per mile. Eighty miles west-northwest of the park the average altitude of cirque floors in the Trinity Alps is about 6,500 feet (Sharp, 1960, p. 338), and a map showing contours on climatic firn limits in northern California suggests that the snowline rose southeastward across the Trinity Alps on a gradient of 20–25 feet per mile (Wahrhaftig and Birman, 1965, p. 309).

Table 1.—*Climatological data from the Trinity Alps, Lassen Volcanic National Park, and Truckee area, California*
[Data from U.S. Environmental Science Services Administration (1959)]

Location	Normal annual precipitation (inches)	Mean temperatures (°F)			
		January		July	
		Max	Min	Max	Min
Trinity Alps	40–>44	44–48	24–28	>92–<96	>44–<48
Lassen Volcanic National Park (western part).	>48–<56	40–44	16–20	>80–<84	44
Truckee area	28–48	36–40	8–12	76–80	40

Eruption of Lassen Peak dome

The Lassen Peak dome was probably erupted during a late phase of the Tioga Glaciation, after the Brokeoff icecap had largely or wholly disappeared. The absence of extensive thick ice after the dome was erupted is demonstrated by the extensive taluses of the dome rock which bury the flanks of Lassen Peak; Williams (1932, p. 316) attributed these taluses to "fracturing of the dome during its actual emplacement." If Williams is correct, the presence of the voluminous taluses surely indicates that Lassen postdates the Brokeoff icecap of

Tioga age, because otherwise the loose rock would have been carried away by the glacier. In addition, the trends of some glacial striations on surfaces of pre-Lassen dacite around the base of Lassen also show that the dome postdates the Brokeoff icecap. Northwest-trending striations at the southwest base of Lassen Peak, just north of Eagle Peak, are especially significant, because if Lassen had been present when they were formed, glaciers descending the flank of the dome would have produced west- or southwest-trending striations at this locality. The flanks of the dome are, indeed, indented by shallow cirques, but I believe these to have been formed during the brief glacial episode which postdated the disappearance of the Tioga icecap.

Moraines of late Tioga age

Small moraines located in high cirques in the western part of Lassen Volcanic National Park represent an episode of glacier growth which followed the eruption of the Lassen Peak dome. Such a moraine on the north side of Brokeoff Mountain extends from an altitude of about 8,300 feet down to at least 7,800 feet. Others, on Vulcans Castle, Reading and Loomis Peaks, Mount Diller, and elsewhere (fig. 1), lie between 8,100 and 8,900 feet. Till in the moraines on the north side of Reading Peak (fig. 2) is oxidized to a depth of at least 2 feet and is overlain by pumice erupted from vents at the site of the Choas Crags about 1,200 years ago.

Similar high moraines lie at the downslope margins of shallow cirques on the southeast flank of Lassen Peak at about 8,900 feet (fig. 3), on the south flank at about 9,100 feet, and on the southwest flank at about 8,800 feet. Till in the moraines is oxidized yellowish brown (10*YR* 5/6) to a depth of 2–2.5 feet, and the moraines are overlain by the 1,200-year-old pumice.

The largest reentrant on the flanks of Lassen Peak dome lies on the northeast side (fig. 4). The reentrant is shallow and does not have the form of a typical cirque, but nevertheless I believe it to be primarily the result of glacial erosion and to have formed during the glacial episode represented by the high cirque moraines elsewhere in the area. Downslope from the reentrant, lateral moraines along Lost Creek (figs. 1 and 4) record a Lassen Peak glacier which, at its maximum extent, was about three-quarters of a mile wide and nearly 3 miles long. The lateral moraines lead down to an end moraine at an altitude of about 6,300 feet near Old Boundary Spring. Till in the end moraine at the west edge of the Devastated Area (loc. A, fig. 1) is oxidized to a depth of about 2 feet.

Alluvium and mudflows of late Tioga age

A thick sequence of mudflows interbedded with alluvial deposits fills a northeast-trending valley (loc. N, fig. 1)

Figure 2.—Moraines of late Tioga age at an altitude of about 8,200 feet on the north side of Reading Peak. View is to the north. Figure of man (circled) on moraine crest at left shows scale.

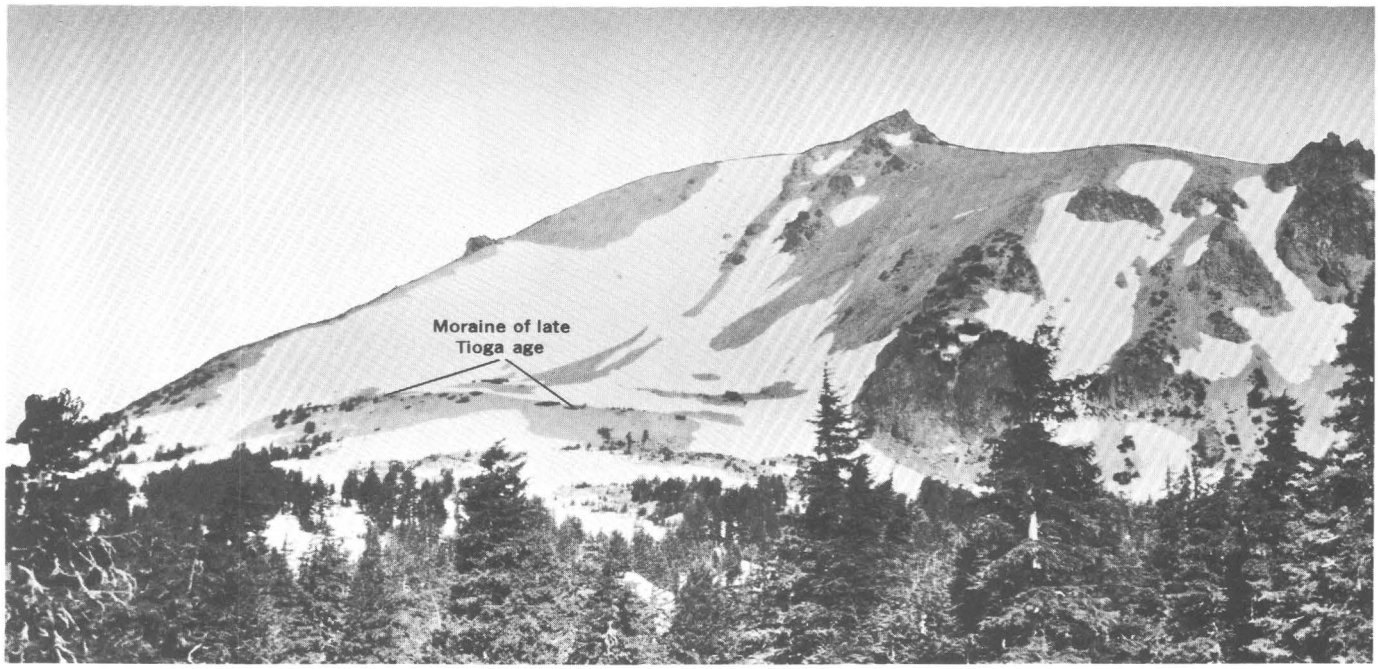

Figure 3.—End moraine of late Tioga age at an altitude of about 8,900 feet on the southeast side of Lassen Peak.

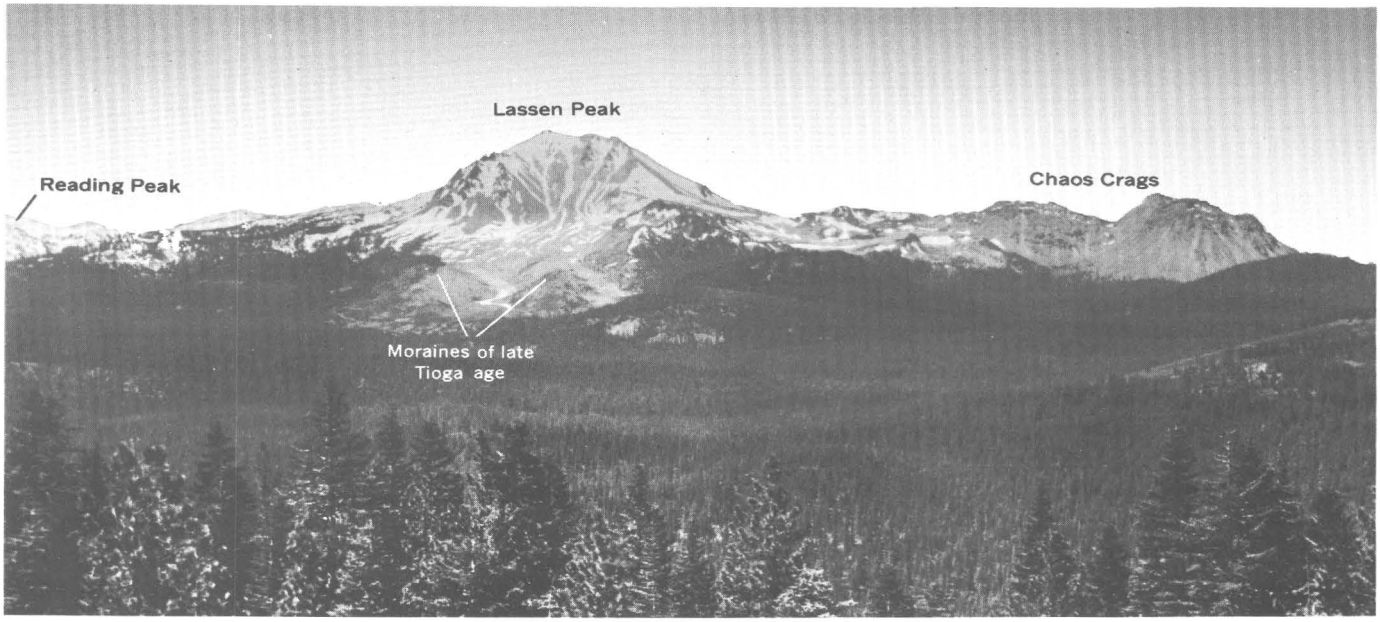

Figure 4.—Lateral moraines of late Tioga age flanking Lost Creek on the northeast side of Lassen Peak.

between lateral moraines of late Tioga age along Lost Creek. In places the fill deposits overlap and bury the moraines. The deposits are continuously exposed in gully walls 40–50 feet high, and their total thickness may be substantially greater than this amount. No other valley that heads on Lassen Peak contains a similar fill.

The fill deposits along Lost Creek consist mostly of coarse lenticular mudflows 5 feet thick or less, although a few are as much as 15 feet thick. The mudflow deposits contain angular to subround fragments of pink and gray dacite, some of which are as large as 6 feet in diameter, in a matrix of gray and reddish-gray sand and granule gravel. Beds of fluvial sand and gravel interbedded with the mudflows are a few inches to several feet thick. The interbedded mudflows and alluvium dip 5°–10° NE., parallel to the trend of Lost Creek in the Devastated Area. Oxidation at the top of the sequence extends

to an average depth of about 2 feet, and some beds of relatively high permeability within the sequence are also oxidized.

The interbedded mudflows and alluvium have not been radiometrically dated, but correlation with other deposits farther downvalley suggests an age limit. A sand and gravel deposit exposed in the west bank of Lost Creek (loc. X, fig. 1) may be correlative with the fill in the Devastated Area. The sand and gravel underlies, and is thus older than, a bed of peat, the base of which has been radiocarbon dated at about 5,400 years (sample W-2231, Meyer Rubin, written commun., 1969). The apparent absence of mudflow deposits downvalley from the Devastated Area may be the result of individual mudflows terminating within a mile or two of their source.

The depth of oxidation on the mudflows and alluvium is similar to that on the adjacent lateral moraines and on the high cirque moraines; all these deposits are therefore thought to be of about the same age. The mudflows and alluvium may have been formed when rock debris was moved downslope by glacial melt water during retreat of the late Tioga glacier that formed on the northeast flank of Lassen Peak.

CORRELATIONS

Recent detailed studies of glacial deposits in northern California include those of Sharp (1960) in the Trinity Alps and Birkeland (1964) in the Truckee area. Correlations with both areas can be suggested on the basis of soil development and moraine morphology. Some glacial drift in the Lassen Peak area may be correlative with deposits recognized so far only in the Bridgeport and Mono Lake areas of California, which are 195 and 220 miles southeast of Lassen Peak, respectively.

According to Sharp, the Pleistocene stratigraphic sequence in the Trinity Alps includes three drifts of Wisconsin age and one or more drifts of pre-Wisconsin age (table 2). Pre-Wisconsin (Swift Creek) till consisting of serpentine-rich rock debris has a deep-red, clay-rich soil, and the oldest serpentine-bearing till thought by Sharp to be of Wisconsin age (Alpine Lake) has a brownish-red clayey soil. Soils on the younger Wisconsin (Rush Creek and Morris Meadows) tills were not described by Sharp, and he stated that he did not find soils to be widely useful in differentiating the glacial deposits. The morphology of the Morris Meadows moraines described by Sharp suggests that they correlate with the Tioga moraines of the Lassen Peak area, as does also the fact that the Morris Meadows represents the last major glaciation of the Trinity Alps. The Rush Creek moraines represent the next older Trinity Alps glaciation, which suggests that they are of Tahoe age. Their subdued morainal morphology is consistent with this correlation. Sharp's Swift Creek glacial deposits are clearly of pre-Tahoe age, and the color and clayey nature of the Alpine Lake moraines suggest that they are at least as old as the oldest Tahoe till of the Lassen Peak area; possibly they are of Mono Basin age.

Table 2.—*Correlation chart*

Lassen Peak area (this report)	Trinity Alps (Sharp, 1960)	Truckee area (Birkeland, 1964)	Mono Lake area (Sharp and Birman, 1963)
Moraines of late Tioga age		Frog Lake Till	
Tioga Drift	Morris Meadow moraines	Tioga Till	Tioga moraines Tenaya moraines
Tahoe Drift	Rush Creek moraines	Tahoe Till	Tahoe moraines
	Alpine Lake moraines(?)		Mono Basin moraines
Pre-Tahoe drift	Swift Creek glacial deposits	Donner Lake Till	
		Hobart Till	Sherwin Till

The sequence near Truckee described by Birkeland (1964) includes the Tioga and Tahoe tills which are separated from the Donner Lake and Hobart tills by one or more major interglaciations. According to Birkeland the soil on the Donner Lake till is 6–7 feet thick, includes a well-developed B horizon, and is brown or strong brown. In contrast, soils on the Tahoe and Tioga tills are similar to one another in that textural B horizons are lacking and hues in the oxidized zones are more yellowish than in the older tills. According to Birkeland (1964) the Tahoe till seems to represent a single major glacial advance. An expansion or rebirth of glaciers in cirques during late Tioga time resulted in the formation of the Frog Lake till at altitudes between 7,400 and 7,900 feet. This till may be of the same age as the moraines of late Tioga age at Lassen.

The parts of the Tahoe Drift of the Lassen Peak area that are somewhat more deeply weathered than others may be correlative with the drift of the Mono Basin Glaciation which has been recognized at the east base of the Sierra Nevada 100 miles southeast of Truckee (Sharp and Birman, 1963). Sharp and Birman regarded the Mono Basin as a glaciation intermediate in age between the Sherwin and Tahoe and tentatively correlated it with the Illinoian Glaciation of the central United States. According to Smith (1968, p. 306–307), however, "* * * the deposits of the Mono Basin Glaciation of Sharp and Birman (1963) are correlated with the first half of the early Wisconsin deposits in Searles Lake, and the Tahoe Glaciation correlated with the second half of those deposits." Smith inferred that the Mono Basin Glaciation extended from about 130,000 to about 70,000 years ago. Birkeland and Janda (1971, table 1) have also suggested, from morphological and soils evidence, that the Mono Basin deposits are closer in age to the Tahoe till than to the Donner Lake till.

Several authors (Morrison, 1965, p. 272; Smith 1968, p. 307; Birkeland and Janda, 1971, p. 2498) suggest that the Tenaya (table 2) represents an early phase of the Tioga

Glaciation, rather than "a separate and distinct glacial phase" as indicated by Sharp and Birman (1963, p. 1080). If drift of Tenaya age is present in the Lassen Peak area, it probably has been included in the Tioga Drift on figure 1.

The pre-Tahoe drift of the Lassen Peak area cannot yet be correlated with assurance with any one of the old tills of other areas in northern California.

REFERENCES

Birkeland, P. W., 1961, Pleistocene history of the Truckee area, north Lake Tahoe, California: Stanford Univ., unpub. Ph. D. thesis, 126 p.

—— 1964, Pleistocene glaciation of the northern Sierra Nevada, north of Lake Tahoe, California: Jour. Geology, v. 72, no. 6, p. 810–825.

Birkeland, P. W., Crandell, D. R., and Richmond, G. M., 1971, Status of correlation of Quaternary stratigraphic units in the western conterminous United States: Quaternary Research, v. 1, no. 2, p. 208–227.

Birkeland, P. W., and Janda, R. J., 1971, Clay mineralogy of soils developed from Quaternary deposits of the eastern Sierra Nevada, California: Geol. Soc. America Bull., v. 82, p. 2495–2514.

Crandell, D. R., 1965, The glacial history of western Washington and Oregon, p. 341–353, *in* Wright, H. E., Jr., and Frey, D. G., eds., The Quaternary of the United States: Princeton, N.J., Princeton Univ. Press, 922 p.

Crandell, D. R., Mullineaux, D. R., and Bath, G. D., 1970, Late glacial and postglacial dacitic volcanism near Lassen Peak, California: Geol. Soc. America Abs. with Programs 1970, v. 2, no. 2, Cordilleran Sec., p. 83–84.

Gillett, G. W., Howell, J. T., and Leschke, Hans, 1961, A flora of Lassen Volcanic National Park, California: San Francisco State Univ., 185 p. [Repr. from The Wasmann Jour. Biology, v. 19, no. 1, 1961; copies may be purchased from California Acad. Sci.]

Lydon, P. A., Gay, T. E., Jr., and Jennings, C. W., Compilers, 1960, Geologic map of California, Westwood sheet, Olaf P. Jenkins edition: California Div. Mines.

Macdonald, G. A., 1963, Geology of the Manzanita Lake quadrangle, California: U.S. Geol. Survey Geol. Quad. Map GQ-248.

—— 1964, Geology of the Prospect Peak quadrangle, California: U.S. Geol. Survey Geol. Quad. Map GQ-345.

—— 1966, Geology of the Cascade Range and Modoc Plateau, *in* Geology of northern California: California Div. Mines and Geology Bull. 190, p. 65–96.

Morrison, R. B., 1965, Quaternary geology of the Great Basin, p. 265–285 *in* Wright, H. E., Jr., and Frey, D. G., eds., The Quaternary of the United States: Princeton, N.J., Princeton Univ. Press, 922 p.

Munsell Color Co., 1954, Munsell soil color charts: Baltimore, Md. Munsell Color Co., Inc.,

Sharp, R. P., 1960, Pleistocene glaciation in the Trinity Alps of northern California: Am. Jour. Sci., v. 258, no. 5, p. 305–340.

Sharp, R. P., and Birman, J. H., 1963, Additions to classical sequence of Pleistocene glaciations, Sierra Nevada, California: Geol. Soc. America Bull., v. 74, p. 1079–1086.

Smith, G. I., 1968, Late-Quaternary geologic and climatic history of Searles Lake, southeastern California, p. 293–310, *in* Morrison, R. B., and Wright, H. E., Jr., eds., Means of correlation of Quaternary successions–Internat. Assoc. Quaternary Research, 7th Cong., USA, 1965, Proc., v. 8: Utah Univ. Press, 631 p.

U.S. Environmental Science Services Administration, 1959, Climate of California: U.S. Weather Bur., Climatography of the United States, no. 60-4 *of the series* Climate of the States, 57 p. (rev. 1966, 1970).

Wahrhaftig, Clyde, and Birman, J. H., 1965, The Quaternary of the Pacific mountain system in California, p. 299–340, *in* Wright, H. E., Jr., and Frey, D. G., eds., The Quaternary of the United States: Princeton, N.J., Princeton Univ. Press, 922 p.

Williams, Howel, 1932, Geology of the Lassen Volcanic National Park, California: California Univ. Dept. Geol. Sci. Bull., v. 21, no. 8, p. 195–385.

PRELIMINARY STUDIES OF SOME APOLLO 14 LUNAR ROCKS

By FRANK CUTTITTA, H. J. ROSE, JR., C. S. ANNELL, M. K. CARRON, R. P. CHRISTIAN, E. J. DWORNIK, and D. T. LIGON, JR., Washington, D.C.

Abstract.—The major-, minor-, and trace-element compositions of two igneous rocks, seven breccias, four microbreccias, and two breccia clasts collected from the Fra Mauro Formation by the Apollo 14 mission were determined by combined semimicro chemical, X-ray fluorescence, and optical emission spectrographic techniques. Photographic and optical microscopic examinations indicate that most of the Apollo 14 returned lunar materials are breccias. Preliminary evaluation of these elemental, photographic, and optical microscopic studies indicate that the Fra Mauro highland materials have the same nonterrestrial compositional character exhibited by the lunar maria (lowland) materials. All the lunar samples have a higher refractory-element content, lower volatile-element content, and greater reducing capacity than comparable terrestrial rocks. Compared to the maria breccias, the Fra Mauro breccias are characterized by lower Fe/Ni, Cr/Ni, and Cr/V ratios and higher Ni/Co ratios. The Apollo 14 returned lunar samples are more complex mineralogically than the Apollo 11 and 12 materials, suggesting a different mode of formation.

The major-, minor-, and trace-element compositions of two igneous rocks, seven breccias, four microbreccias, and two breccia clasts, collected by the Apollo 14 mission from the Fra Mauro Formation (U.S. National Aeronautics and Space Administration, 1971), were determined by combined semimicro chemical, X-ray fluorescence, and optical emission spectrographic techniques previously described (Annell and Helz, 1970a, b; Cuttitta and others, 1971; and Rose and others, 1970a, b, c). Optical microscopic and photographic examination of the allocated lunar materials showed that the returned Apollo 14 lunar materials are breccias, supporting a previously reported finding (U.S. National Aeronautics and Space Administration, 1971). Compared to the Apollo 11 (Tranquility Base) and 12 (Ocean of Storms) igneous rocks, the Fra Mauro igneous rocks have similar mineral assemblages but different proportions of major components such as plagioclase, pyroxene, olivine, and ilmenite and of minor mineralogic constituents such as cristobalite, apatite, spinel, and troilite.

A related study of six lunar soils is reported in a companion paper (Annell and others, 1972) (p. C195–C198, this chapter).

BASALTS

Major- and minor-element analyses for the two igneous rocks are given in table 1, and results of trace-element analyses are presented in table 2. The two igneous rocks analyzed are very similar in chemical composition, showing only slight variations in some of their trace-element content (that is, Pb, Cu, and Mn).

Table 1.—*Major- and minor-element composition of some Apollo 14 basalts, in weight percent*

Constituent	14276,8	14310,114
SiO_2	47.60	47.81
Al_2O_3	21.34	21.54
Fe_2O_3	.00	.00
FeO	7.94	7.62
MgO	7.10	7.48
CaO	13.18	12.92
Na_2O	.72	.68
K_2O	.48	.48
TiO_2	1.20	1.11
P_2O_5	.40	.43
MnO	.12	.10
Cr_2O_3	.26	.25
Total	100.34	100.42
ΔRC	+.11	+.53

Note:
ΔRC = total reducing capacity (as FeO) measured for the lunar samples less the reducing capacity attributable to the FeO content of the lunar samples.

Comparisons of the elemental compositions of the lunar maria material returned by the Apollo 11 and Apollo 12 missions with the lunar highland material obtained by the Apollo 14 (Fra Mauro Formation) mission are given in tables 3 and 4. The elements Si, Al, Ca, Na, P, and Ni show an increasing trend—Apollo 11 < 12 < 14. In contrast, the Fe, Ti, Cr, and Sc contents decrease in the order of Apollo 11 > 12 > 14. Compared with the maria igneous rocks, the Fra Mauro highland rocks are characterized by greater concentrations of Ba, Be, K, La, Li, Nb, Pb, Rb, Sr, Y, and Zr, but lower

U.S. GEOL. SURVEY PROF. PAPER 800-C, PAGES C189-C193

Table 2.—*Trace-element abundance in some Apollo 14 basalts determined by optical emission spectroscopy, in parts per million*

Element	14276,8	14310,114
Pb	9.0	13.0
Ag	<.1	.32
Zn	<4	<4
Cu	42	9.0
Ga	4.2	3.2
Li	21	23
Rb	13	15
Co	9.0	17.0
Ni	113	120
Ba	700	780
Sr	165	175
V	37	38
Be	4.0	4.2
Nb	33	29
Sc	20	25
La	59	59
Y	200	185
Yb	16	16
Zr	620	610

Notes:
1. The following elements were looked for but not detected in the analyzed samples. If present, they would be in concentrations below those indicated in parentheses. Ag (0.2), As (4), Au (0.2), B (10), Bi (1), Cd (8), Ce (100), Cs (1), Ge (1), Hf (20), Hg (8), In (1), Mo (2), Nd (100), P (2,000), Pt (3), Re (30), Sb (100), Sn (10), Ta (100), Te (300), Th (100), Tl (1), U (500), and W (200).
2. Elements are listed in approximate order of decreasing volatility in the d-c arc.

Table 3.—*Comparison of average major- and minor-element composition of Apollo 11, 12, and 14 basalts, in weight percent*

Constituent	Apollo 11	Apollo 12	Apollo 14
SiO_2	40.10	47.10	47.70
Al_2O_3	8.60	12.80	21.44
Fe_2O_3	.00	.00	.00
FeO	18.90	17.40	7.78
MgO	7.74	6.80	7.29
CaO	10.70	11.40	13.05
Na_2O	.46	.64	.70
K_2O	.30	.07	.48
TiO_2	12.20	3.17	1.16
P_2O_5	<.2	.17	.42
MnO	.25	.24	.11
Cr_2O_3	.37	.31	.25
Total	99.82	100.10	100.38
ΔRC	+2.1	+.37	+.32

Notes:
1. ΔRC = total reducing capacity (as FeO) measured for the lunar samples less the reducing capacity attributable to the FeO content of the lunar samples.
2. Data for Apollo 11 from Rose and others (1970a, b, c).
3. Data for Apollo 12 from Levinson (1971, p. 1083–1122, 1169–1208, 1217–1236) and, in particular, Cuttitta and others (1971).

contents of Co, Ga, Mn, and V. A comparison of some elemental ratios of the Apollo 11, 12, and 14 basalts is given in table 5. Several critical elemental ratios also distinguish the Apollo 14 highland igneous rocks from those recovered from the Apollo 11 and 12 lunar maria. The element ratios Fe/Ni and Cr/Ni decrease markedly—Apollo 11 >> 12 > 14. In

Table 4.—*Comparison of average trace-element abundance of Apollo 11, 12, and 14 basalts, in parts per million*

Element	Apollo 11	Apollo 12	Apollo 14
Pb	<2	<2	11
Ag	<.2	<.2	.2
Zn	<4	<4	<4
Cu	8.8	10.5	9.0
Ga	4.8	4.9	3.7
Li	17.0	5.9	22.0
Rb	5.1	1.4	14.0
Co	30.8	64.0	13.0
Ni	6.6	70.0	116
Ba	440	63.0	740
Sr	135	64.0	170
V	72.8	160	37.5
Be	3.1	1.4	4.1
Nb	24.0	13.0	31.0
Sc	96.5	40.0	22.5
La	26.2	<20	59
Y	162	39	192
Yb	20.0	5.2	16.0
Zr	594	110	615

Notes:
1. Data for Apollo 11 from Annell and Helz (1970a, b).
2. Data for Apollo 12 from Levinson (1971, p. 1083–1122, 1169–1268, 1217–1236) and, in particular, Cuttitta and others (1971).

Table 5.—*Comparison of some significant elemental ratios of Apollo 11, 12, and 14 basalts*

Ratio	Apollo 11	Apollo 12	Apollo 14
Fe/Ni	21,000	2,520	504
Rb/Sr	.35	.008	.82
Ni/Co	.23	.98	8.92
Cr/V	34.3	13.5	46.4
Cr/Ni	357	39.0	15.0
Ba/V	6.04	.48	19.7
Ba/Sr	3.25	.95	4.35
Mg/Fe	.63	.39	.92

contrast, the Ni/Co ratio increases in the order of Apollo 11 < 12 < 14 and is an order of magnitude larger in the highland rocks. High Mg/Fe, Rb/Sr, Cr/V, Ba/V, and Ba/Sr ratios also characterize the Fra Mauro rocks when compared with the Apollo 11 and 12 maria rocks. The composition of Apollo 14 basalts can be interpreted as reflecting a high feldspar component as well as ferromagnesium silicates with a high MgO/FeO ratio (table 5).

BRECCIAS, MICROBRECCIAS, AND CLASTS

The lunar breccias are extremely complex, being composed of various types of mineral, glass, lithic, and microbreccia fragments, the latter belonging to earlier impact events. Major-, minor-, and trace-element data are given for seven breccias (tables 6 and 7), four microbreccias, and two breccia clasts (tables 8 and 9).

Breccia sample 14083 was received as two small separates of white and dark clasts isolated from the host rock. Three granular portions of microbreccia 14063 were also received for analysis. Breccia sample 14063 is a friable, nonregolith,

Table 6.—*Major- and minor-element composition of some Apollo 14 breccias, in weight percent*

Constituent	14047,27	14066,21 (203)	14066,31(4) (sawdust)	14301,62	14303,34	14318,27A	14318(M.F.)
SiO_2	47.45	47.59	46.31	48.26	47.49	47.97	47.94
Al_2O_3	17.75	14.61	14.80	16.52	16.05	17.80	17.95
Fe_2O_3	.00	.00	.00	.00	.00	.00	.00
FeO	10.36	10.82	9.59	10.29	10.96	9.62	9.43
MgO	9.35	13.67	10.78	9.98	10.99	9.79	9.63
CaO	11.19	9.07	9.32	10.29	10.03	11.16	11.13
Na_2O	.75	1.01	1.10	.84	.87	.79	.81
K_2O	.49	.45	.87	.75	.46	.60	.62
H_2O-	.00	.00	.06	.00	.00	.00	.00
TiO_2	1.71	1.68	1.49	2.06	1.98	1.48	1.44
P_2O_5	.39	.55	.58	.64	.56	.56	.55
MnO	.13	.13	.12	.14	.15	.13	.13
Cr_2O_3	.22	.26	.22	.21	.21	.19	.18
Cu	...	...	2.30	...	...	...	...
L.O.I.	...	...	2.94	...	...	...	...
Total	99.79	99.84	100.48	99.98	99.75	100.09	99.81
ΔRC	+3.97	+1.38	+8.29	+1.71	+1.64	+1.38	+1.32

Notes:
1. ΔRC = total reducing capacity (as FeO) measured for the lunar samples less the reducing capacity attributable to the FeO content of the lunar samples.
2. Sample 14318(M.F.) = composite of very small miscellaneous fragments from returned 14318 breccia.
3. L.O.I. = loss on ignition.

Table 7.—*Trace-element abundance in some Apollo 14 breccias determined by optical emission spectroscopy, in parts per million*

[N.D., looked for but not detected. See notes at bottom of table 2]

Element	14066,21 (203)	14066,31(4) (sawdust)	14301,62	14303,34	14318,27A	14318(M.F.)
Pb	12	6.4	15	8.5	18	18
Zn	N.D.	N.D.	39	N.D.	15	15
Cu	22	[1]	43	20	[2](170)	[2](150)
Ga	5.2	6.3	7.7	3.8	4.5	4.4
Li	28	28	28	26	24	24
Rb	12	26	17	10	14	16
Co	34	32	27	28	38	30
Ni	285	315	255	245	420	330
Ba	1,000	1,400	1,280	980	640	760
Sr	140	150	195	175	140	160
V	53	47	49	46	47	50
Be	5.4	12	10	8.0	7.6	8.0
B	15	27	24	24	16	17
Nb	44	51	64	53	52	48
Sc	20	22	26	26	22	24
La	87	97	92	88	66	75
Y	240	280	335	320	260	260
Yb	22	27	23	23	23	22
Zr	880	700	940	940	820	720

[1] Contaminated with copper fragments and wire.
[2] Data questionable—high results may be due to contamination during cutting of breccia.

unannealed, feldspathic microbreccia and represents the white materials seen in photographs of the large breccia boulders and blocks near Cone Crater. Because they could be considered breccia separates, the data for microbreccia 14063 and 14315 are included in tables 8 and 9 with those of the white and dark clasts separated from breccia 14083. The small size of our breccia sample 14047,27 permitted only the determination of the major and minor elements.

Lunar breccia sample 14066,31(4) (table 6) is a "sawdust" recovered from the sectioning of the original rocks at the Lunar Receiving Laboratory (LRL) into slabs suitable for further study by the scientific community. If insignificantly contaminated by the processing, it was thought at the LRL that this sawdust material could reflect the bulk composition of the 14066 breccia and serve as bulk material for further investigations. Optical microscopic and photographic examinations by us revealed significant amounts of copper chips and fine wires, fragments that appear to be stainless steel, diamond chips, and a large number (≈ 1–3 percent v/v) of organic fibers. On the basis of the foregoing and the comparison of the

Table 8.—*Major- and minor-element composition of some Apollo 14 microbreccias and breccia clasts, in weight percent*

Constitutent	14063,46	14063, 37A-11-2	14063, 37B-11-2	14083,2d (dark clasts)	14083,2w (white clasts)	14315,4
SiO_2	44.79	45.02	45.22	46.19	44.20	47.76
Al_2O_3	22.60	21.53	21.02	17.16	22.06	21.31
Fe_2O_3	.00	.00	.00	.00	.00	.00
FeO	6.71	7.00	6.94	9.66	7.16	7.82
MgO	10.80	10.79	10.40	11.55	11.48	8.28
CaO	12.70	12.40	12.76	10.76	12.66	12.77
Na_2O	.77	.93	.93	1.01	.65	.76
K_2O	.15	.20	.16	.40	.23	.35
TiO_2	1.48	1.58	1.87	2.21	.80	.80
P_2O_5	.22	.29	.23	.63	.45	.23
MnO	.08	.09	.09	.11	.06	.11
Cr_2O_3	...	.19	.17	.21	.14	.23
Total	100.30	100.02	99.79	99.89	99.89	100.42
ΔRC	.0	.0	.0	.0	.0	+3.93

Note:
ΔRC = total reducing capacity (as FeO) measured for the lunar samples less the reducing capacity attributable to the FeO content of the lunar samples.

Table 9.—*Trace-element abundance in some Apollo 14 microbreccias and breccia clasts determined by optical emission spectroscopy, in parts per million*

[N.D., looked for but not detected. See notes at bottom of table 2]

Element	14063,46	14063, 37A-11-2	14063, 37B-11-2	14083,2d (dark clasts)	14083,2w (white clasts)	14315,4
Pb	2.9	4.2	3.0	6.0	11.0	15
Zn	<4	4.0	<4	4.0	4.0	34
Cu	2.3	3.3	5.0	6.0	11.0	10
Ga	4.8	6.0	5.5	4.6	4.4	5.2
Li	24	23	21	18	26	16
Rb	5.0	6.0	4.0	5.2	8.8	10
Co	16	17	16	17	25	30
Ni	110	110	110	73	180	355
Ba	250	380	315	500	940	410
Sr	205	220	200	160	140	165
V	33	38	36	31	44	50
Be	2.2	3.7	3.7	3.3	6.7	3.0
B	20	16	15	N.D.	N.D.	18
Nb	16	20	16	27	56	30
Sc	13	15	18	12	23	18
La	27	30	26	61	97	41
Y	94	130	110	190	300	155
Yb	6.8	9.5	8.2	16	31	11
Zr	260	300	340	380	800	400

chemical analyses shown for samples 14066,31(4) and 14066,21(203) in tables 6 and 7, it is strongly recommended that the breccia 14066,31(4) sawdust not be used for any scientific lunar studies.

Breccia sample 14318(M. F.) is composed of miscellaneous fragments in contrast to breccia sample 14318,27A, which is a single chip from the parent breccia undergoing various studies by a number of lunar sample investigators (consortium principal investigator—Mitsunobu Tatsumoto, U.S. Geol. Survey, Denver, Colo.).

Tables 10 and 11 give a comparison of the average elemental composition of the Apollo 14 breccias with those of Apollo 11 and 12. Si, Al, Mg, Na, K, Ba, and Zr show an increasing concentration trend in progressing across the lunar surface from the Apollo 11 and 12 lowlands to the Fra Mauro highlands—Apollo 11 < 12 < 14. The elements Fe, Ca, Ti, Sc, and Mn have a decreasing trend—Apollo 11 > 12 > 14. The V content is lowest in Apollo 14 breccias, whereas the Cu, Ni, Zr, and Y contents are greater in the Apollo 14 impact rocks. Some significant elemental ratios of the Apollo 11, 12, and 14 breccias are compared in Table 12. The data show that Mg/Fe, Rb/Sr, Ba/V, and Ba/Sr ratios increase in the order Apollo 11 < 12 < 14. Compared to the maria breccias, the Fra Mauro highland breccias are characterized by lower Fe/Ni, Cr/Ni, and Cr/V ratios and higher Ni/Co ratios.

CONCLUSIONS

Preliminary evaluation of these and unpublished elemental, photographic, and mineralogic data suggests:

1. Our work coupled with studies of Lunar Receiving Laboratory photographs and data indicate that most of the Apollo 14 returned lunar materials are breccias. These studies also strongly support a previous suggestion (U.S. National Aeronautics and Space Administration, 1971) that the breccias that characterize the Fra Mauro Formation are a gigantic ejecta blanket generated by the catastrophic impact event which formed the largest of the lunar seas—the Mare Imbrium.

2. The Fra Mauro highland materials have the same nonterrestrial compositional character shown by the lunar lowland samples returned from the Sea of Tranquility and the Ocean of Storms sites by the Apollo 11 and 12 missions, respectively. All of the lunar samples have a higher refractory-element content, lower volatile-element content, and greater reducing capacity than comparable terrestrial rocks.

3. Optical microscopic and photographic examinations show that the Fra Mauro highland material is more complex mineralogically than the Apollo 11 and 12 lowland material, implying a different mode of formation or a different history from rocks returned from lunar mare regions.

Table 10.—*Comparison of average major- and minor-element composition of Apollo 11, 12, and 14 breccias, in weight percent*

[n.d., not determined. See notes at bottom of table 3]

Constituent	Apollo 11	Apollo 12	Apollo 14
SiO_2	41.80	46.52	47.78
Al_2O_3	13.10	14.64	16.76
Fe_2O_3	.00	.00	.00
FeO	15.90	13.85	10.24
MgO	7.70	9.06	10.57
CaO	11.80	11.15	10.48
Na_2O	.46	.61	.83
K_2O	.16	.40	.56
TiO_2	8.49	2.17	1.68
P_2O_5	<.2	n.d.	.54
MnO	.22	.19	.13
Cr_2O_3	.32	.33	.21
Total	99.95	98.92	99.78

Table 11.—*Comparison of average trace-element abundance of Apollo 11, 12, and 14 breccias, in parts per million*

[N.D., looked for but not detected. See notes at bottom of tables 2 and 4]

Element	Apollo 11	Apollo 12	Apollo 14
Zn	24	6.9	23
Cu	15	5.7	28
Ga	5.0	4.6	5.0
Li	12	22	26
Rb	3.0	10.3	14
Co	32	36	32
Ni	202	165	313
Ba	250	500	910
Sr	131	177	160
V	60	87	49
Sc	68	35	23
Nb	23	N.D.	51
La	19	54	81
Y	102	107	278
Yb	14	19	22
Zr	401	583	840

Table 12.—*Comparison of some significant elemental ratios of Apollo 11, 12, and 14 breccias*

Ratio	Apollo 11	Apollo 12	Apollo 14
Fe/Ni	612	640	254
Rb/Sr	.023	.058	.088
Ni/Co	6.31	4.59	9.78
Cr/V	53.3	37.9	28.6
Cr/Ni	16.3	20.3	4.47
Ba/V	4.17	5.75	19.0
Ba/Sr	1.91	2.82	5.69
Mg/Fe	.42	.65	.80

ACKNOWLEDGMENTS

This research was undertaken on behalf of the National Aeronautics and Space Administration under requisition No. 0-365-036, Order No. T-2360-A.

We are deeply grateful to our colleague E. C. T. Chao for providing portions of five breccias.

REFERENCES

Annell, C. S., Carron, M. K., Christian, R. P., Cuttitta, Frank, Dwornik, E. J., Ligon, D. T., Jr., and Rose, H. J., Jr., 1972, Preliminary studies of six Apollo 14 lunar soils, *in* Geological Survey Research 1972: U.S. Geol. Survey Prof. Paper 800-C, p. C195–C198.

Annell, C. S., and Helz, A. W., 1970a, Emission spectrographic determination of trace elements in lunar samples: Science, v. 167, no. 3918, p. 521–523.

—— 1970b, Emission spectrographic determination of trace elements in lunar samples from Apollo 11, *in* Levinson, A. A., ed., Proceedings of the Apollo 11 Lunar Science Conference, Houston, Tex., January 5–8, 1970, v. 2, Chemical and isotope analyses: New York, Pergamon Press, p. 991–994.

Cuttitta, Frank, Rose, H. J., Jr., Annell, C. S., Carron, M. K., Christian, R. P., Dwornik, E. J., Greenland, L. P., Helz, A. W., and Ligon, D. T., Jr., 1971, Elemental composition of some Apollo 12 lunar rocks and soils, *in* Levinson, A. A., ed., Proceedings of the Second Lunar Science Conference, Houston, Tex., January 11–14, 1971, v. 2, Chemical and isotope analyses: Cambridge, Mass., MIT Press, p. 1217–1229.

Levinson, A. A., ed., 1971, Proceedings of the Second Lunar Science Conference, Houston, Tex., January 11–14, 1971, v. 2, Chemical and isotope analyses: Cambridge, Mass., MIT Press, p. 987–1952.

Rose, H. J., Jr., Cuttitta, Frank, Dwornik, E. J., Carron, M. K., Christian, R. P., Lindsay, J. R., Ligon, D. T., Jr., and Larson, R. R., 1970a, Semimicro chemical and X-ray fluorescence analysis of lunar samples: Science, v. 167, no. 3918, p. 520–521.

—— 1970b, Semimicro X-ray fluorescence analysis of lunar samples, *in* Levinson, A. A., ed., Proceedings of the Apollo 11 Lunar Science Conference, Houston, Tex., January 5–8, 1970, v. 2, Chemical and isotope analyses: New York, Pergamon Press, p. 1493–1497.

—— 1970c, Errata and addenda: Geochim. et Cosmochim. Acta, v. 34, p. 1367.

U.S. National Aeronautics and Space Administration, 1971, Apollo 14 preliminary science report: U.S. Natl. Aeronautics and Space Adm. Spec. Pub. SP-272, 309 p.

PRELIMINARY STUDIES OF SIX APOLLO 14 LUNAR SOILS

By C. S. ANNELL, M. K. CARRON, R. P. CHRISTIAN, FRANK CUTTITTA, E. J. DWORNIK, D. T. LIGON, JR., and H. J. ROSE, JR., Washington, D.C.

Abstract.—Major-, minor-, and trace-element analyses made by combined semimicro chemical, X-ray fluorescence, and optical emission spectrographic techniques are presented for six samples of lunar highland soil from the Fra Mauro Formation returned by the Apollo 14 mission. The analyzed soil samples are very similar in major-element chemical composition but show a possible bimodal distribution for Ni ($\approx$300 and $>$400 ppm), B($<$10 and $\approx$18 ppm), and Nb ($\approx$40 and $\approx$70 ppm). Compared to the Apollo 11 and 12 lunar maria soils, the Apollo 14 soil is characterized by higher content of Al_2O_3, Na_2O, and K_2O, and by lower FeO and TiO_2. This distribution is correlated with a higher observed percentage of feldspar in the Apollo 14 soil. The Apollo 14 soil has more Fe and Ni than the Apollo 14 basalts, which we interpret as indicating a meteorite component.

Six soil samples, collected on the Fra Mauro Formation highlands by the Apollo 14 mission, were analyzed by semimicro chemical, X-ray fluorescence, and optical emission spectrographic methods. The samples were collected in an area approximately 500 km south of the southern rim crest of the Imbrium Basin. The formation is believed to be in part the ejecta blanket that resulted from the catastrophic excavation of that basin (U.S. National Aeronautics and Space Administration, 1971). Our photographic and optical microscopic examinations show that the physical nature of these samples differs from that of the maria materials of the Apollo 11 and 12 missions both in the generally lighter color of the samples from Fra Mauro and in their greater range in particle size. This concurs with the findings reported in the previously cited reference.

The methods used in our laboratories have been described previously for the Apollo 11 and 12 samples (Annell and Helz, 1970a, b; Cuttitta and others, 1971; and Rose and others, 1970a, b, c). Results of the soil analyses are shown in tables 1 and 2, along with notes briefly describing the samples as reported by the Lunar Receiving Laboratory, National Aeronautics and Space Administration, Houston, Tex.

A related study of 15 lunar basalts and breccias is reported in a companion paper (Cuttitta and others, 1972) (p. C189–C193, this chapter).

DISCUSSION AND CONCLUSIONS

The different mineralogical character of the Apollo 14 highland soil, when compared with the character of the Apollo 11 and 12 soils reported earlier (Annell and Helz, 1970a, b; Annell and others, 1971; Cuttitta and others, 1971; Rose and others, 1970a, b, c; Rose and others, 1971), is apparent in the higher Al and lower Fe and Ti concentrations in the Apollo 14 soil. A wide variation in mineral and glass spherule distribution has been reported at the different sampling stations (U.S. National Aeronautics and Space Administration, 1971) and has been substantiated by our photographic and mineralogic findings. This variation can be attributed to the numerous cratering events that contributed to the ejecta blanket at Fra Mauro. Despite the mineralogical heterogeneity, the major-element composition of the six different soil samples is remarkably uniform (table 1). The trace-element data (table 2) are more variable and suggest a bimodal distribution for Ni ($\approx$ 300 and $>$ 400 ppm), B ($<$ 10 and $\approx$ 18 ppm), and Nb ($\approx$ 40 and $\approx$ 70 ppm).

The differences between the average composition of Apollo 14 highland soil and the Apollo 11 and 12 maria soils (tables 3 and 4) are correlated with a greater amount of feldspathic components in the Fra Mauro soil. The differences are as follows:

1. Concentrations of K_2O and Na_2O, as well as Al_2O_3, are higher in the Apollo 14 soil.
2. FeO and TiO_2 concentrations are noticeably lower in the Fra Mauro highland soil.
3. Zn, Cu, Rb, Li, Ni, Ba, Sr, Nb, La, Y, Yb, and Zr concentrations are significantly higher in Apollo 14 soil.
4. Higher Pb concentrations are present in the Fra Mauro highland soils than in the maria soils. This is compatible with higher U and Th concentrations for the Apollo 14 soils (U.S. National Aeronautics and Space Administration, 1971).

Table 4 lists the minor and trace elements in the order of decreasing ionic radii, assuming sixfold coordination (Rankama and Sahama, 1950). This table shows an increase in concentration of the largest cations when going from a maria

U.S. GEOL. SURVEY PROF. PAPER 800-C, PAGES C195-C198

Table 1.—*Major- and minor-element compositions of Fra Mauro Formation soil returned by the Apollo 14 mission, in weight percent*

Constituent	14003,30	14049,37	14163,54	14240,9	14259,12	14421,23
SiO_2	48.08	47.81	47.97	47.77	48.16	47.80
Al_2O_3	17.59	17.44	17.57	17.99	17.60	17.40
Fe_2O_3	.00	.00	.00	.00	.00	.00
FeO	10.45	10.44	10.41	10.02	10.41	10.48
MgO	9.27	9.08	9.18	9.47	9.26	9.36
CaO	11.12	11.13	11.15	11.25	11.25	11.26
Na_2O	.65	.75	.68	.70	.61	.68
K_2O	.54	.56	.58	.54	.51	.49
TiO_2	1.77	1.79	1.77	1.67	1.73	1.74
P_2O_5	.58	.56	.52	.55	.53	.44
MnO	.14	.14	.14	.14	.14	.14
Cr_2O_3	.26	.22	.26	.24	.26	.27
Total	100.45	99.92	100.23	100.34	100.46	100.06
ΔRC	+ 2.70	+ 3.40	+ 2.37	+ 2.50	+ 2.94	+ 3.20

Notes:
1. ΔRC = total reducing capacity (as FeO) measured for the lunar samples less the reducing capacity attributable to the FeO content of the lunar samples.
2. Lunar Receiving Laboratory classification of allocated Apollo 14 soils:
   14003,30—Collected during extravehicular activity-1 (EVA-1) near lunar module (LM). Contingency sample.
   14049,37—Obtained several hundred meters east of LM along with friable, clastic rock, on EVA-2. Grab sample.
   14163,54—Collected near LM on EVA-1. Soil generally medium grain size (≈0.065 mm) consisting of 40–75 percent glass.
   14240,9—Sample collected at bottom of trench about 300 m east of LM, using lunar trenching tool. Sampled from light-colored stratum.
   14259,12—Soil skimmed from upper 1 cm of surface as part of comprehensive sample, from area about 100 m west of LM. Medium grain size (0.050 mm) and lighter color than Apollo 11 and 12 soils.
   14421,23—Part of bulk sample obtained near LM.

Table 2.—*Trace-element abundances in Fra Mauro Formation soil returned by the Apollo 14 mission, in parts per million*

Element	14003,30	14049,37	14163,54	14240,9	14259,12	14421,23
Pb	10	11	11	12	8	8
Zn	28	23	28	23	24	23
Cu	16	18	17	16	19	21
Ga	5.0	4.4	5.5	7.5	4.4	6.2
Li	24	25	24	23	22	19
Rb	13	14	13	13	12	13
Co	38	28	36	33	38	38
Ni	430	295	400	320	440	335
Ba	1,000	990	1,100	1,170	1,100	920
Sr	135	150	140	390	150	170
V	58	42	57	52	62	62
Be	6.0	5.1	7.0	7.2	6.0	8.0
B	18	N.D.	17	N.D.	17	N.D.
Nb	70	44	70	42	67	39
Sc	27	22	25	28	28	30
La	75	70	79	67	77	75
Y	300	240	290	250	285	290
Yb	27	19	28	23	30	21
Zr	740	900	820	930	800	640

Notes:
1. The following elements were looked for but not detected (N.D.) in the analyzed samples: If present, they would be in concentrations below the amount (in parts per million) indicated in the parentheses: Ag (0.2), As (4), Au (0.2), B (10), Bi (1), Cd (8), Ce (100), Cs (1), Ge (1), Hf (20), Hg (8), In (1), Mo (2), Nd (100), P (2,000), Pt (3), Re (30), Sb (100), Sn (10), Ta (100), Te (300), Th (100), Tl (1), U (500), and W (200).
2. The arrangement of elements is in order of decreasing volatility in the d-c arc (Ahrens and Taylor, 1961).

basaltic region to a highland area where more potassium feldspars exist in the soils (Taylor and others, 1971).

A comparison between the composition of the fragmented or brecciated rocks (Cuttitta and others, 1972) and the soils shows similarities in composition. However, the greater uniformity in composition among the soils than among the breccias may be attributed to some mixing or turnover of the soil particles by micrometeoritic impact. The basaltic rocks also have a large diversity in chemical composition (U.S. National Aeronautics and Space Administration, 1971). We

Table 3.—*Comparison of average major- and minor-element compositions of the Apollo 14 Fra Mauro highland soil with those of the Apollo 11 and 12 maria soils, in weight percent*

Constituent	Apollo 11[1]	Apollo 12[2]	Apollo 14
SiO_2	42.04	46.40	47.93
Al_2O_3	13.92	13.50	17.60
Fe_2O_3	.00	.00	.00
FeO	15.74	15.50	10.37
MgO	7.90	9.73	9.24
CaO	12.01	10.50	11.19
Na_2O	.44	.59	.68
K_2O	.14	.32	.55
TiO_2	7.48	2.66	1.74
P_2O_5	.12	.40	.53
MnO	.21	.21	.14
Cr_2O_3	.30	.40	.25
Total	100.30	100.21	100.22
ΔRC	+4.1	+1.3	+2.8

[1]Rose and others (1970b).
[2]Cuttitta and others (1971).

offer the following preliminary conclusions regarding the Apollo 14 Fra Mauro materials:

1. Greater Fe and Ni concentrations in soils and breccias compared to concentrations in basalts are probable indicators of meteoritic contribution.

2. As in Apollo 11 and 12 soils and breccias, the Zn, Co, Ni, Ba, La, Y, and Zr concentrations in Apollo 14 soil and breccias are higher than in the highland basalts. These differences further support the concept that the lunar soil contains a significant meteoritic component.

3. Differences in composition of the Fra Mauro highland soil compared to maria soils, including the marked enrichment of Be (Apollo 14/Apollo 11 Be ratio = 4.1), reflect greater amounts of feldspathic components in the highland soils.

4. Greater concentrations of K, Na, Al, and P are concordant with the lighter colored soil and the higher concentrations of large or highly charged cations (table 4).

Table 4.—*Relationship of ionic radii to the average minor- and trace-element composition, in parts per million, of Apollo 11, 12, and 14 soils*

[See notes at end of table 2 for list of elemental detectabilities]

Ionic radii[1]	Ion	Apollo 11[2]	Apollo 12[3]	Apollo 14	14/11[4]
1.49	Rb^{+}	2.7	6.2	13	4.8
1.43	Ba^{+2}	210	423	1,030	4.9
1.33	K^{+}	1,200	2,700	4,600	3.8
1.32	Pb^{+2}	[5]1.39	[6]3.16	10	7.0
1.14	La^{+3}	16	40	74	4.6
1.12	Sr^{+2}	130	123	189	1.5
.96	Cu^{+}	10	12	18	1.8
.92	Y^{+3}	81	145	276	3.4
.91	Mn^{+2}	1,617	1,617	1,078	.66
.86	Yb^{+3}	10	14	25	2.5
.81	Sc^{+3}	56	42	27	.5
.79	Zr^{+4}	273	498	813	3.0
.74	Zn^{+2}	19	8	25	1.3
.74	V^{+3}	50	121	56	1.1
.72	Co^{+2}	24	52	35	1.5
.69	Ni^{+2}	185	222	370	2.0
.69	Nb^{+3}	18	29	55	3.1
.68	Li^{+}	11	17	23	2.1
.64	Cr^{+3}	2,050	2,740	1,771	.86
.62	Ga^{+3}	3.8	4.9	5.5	1.4
.35	Be^{+2}	1.6	3.3	6.6	4.1
.20	B^{+3}	([7])	([7])	([7])	...

[1]Ionic radii in angstroms (sixfold coordination) from Rankama and Sahama (1950, p. 794–795).
[2]Rose and others (1970b).
[3]Cuttitta and others (1971).
[4]Ratio of element in Apollo 14 soil to that in Apollo 11 soil.
[5]Data from Tatsumoto (1970).
[6]Data from Tatsumoto and others (1971).
[7]Boron was not detected in the Apollo 11 and 12 soils, indicating that if present, its concentration would be below 10 ppm. For the Apollo 14 soils, the trace-element data suggest a bimodal distribution for B (that is, <10 ppm for soil samples 14049, 14240, and 14421 and ≈ 18 ppm for soils 14003, 14163, and 14421).

ACKNOWLEDGMENT

This research was undertaken on behalf of the National Aeronautics and Space Administration under requisition No. 0-365-036, Order No. T-2360-A.

REFERENCES

Ahrens, L. H., and Taylor, S. R., 1961, Spectrochemical analysis, 2d ed.: Reading, Mass., Addison-Wesley Publishing Co., Inc., 454 p.

Annell, C. S., Carron, M. K., Christian, R. P., Cuttitta, Frank, Dwornik, E. J., Helz, A. W., Ligon, D. T., Jr., and Rose, H. J., Jr., 1971, Chemical and spectrographic analyses of lunar samples from Apollo 12 mission, *in* Geological Survey Research 1971: U.S. Geol. Survey Prof. Paper 750-C, p. C179–C181.

Annell, C. S., and Helz, A. W., 1970a, Emission spectrographic determination of trace elements in lunar samples: Science, v. 167, no. 3918, p. 521–523.

——1970b, Emission spectrographic determination of trace elements in lunar samples from Apollo 11, *in* Levinson, A. A., ed., Proceedings of the Apollo 11 Lunar Science Conference, Houston, Tex., January 5–8, 1970, v. 2, Chemical and isotope analyses: New York, Pergamon Press, p. 991–994.

Cuttitta, Frank, Rose, H. J., Jr., Annell, C. S., Carron, M. K., Christian, R. P., Dwornik, E. J., Greenland, L. P., Helz, A. W., and Ligon, D. T., Jr., 1971, Elemental composition of some Apollo 12 lunar rocks and soils, *in* Levinson, A. A., ed., Proceedings of the Second Lunar Science Conference, Houston, Tex., January 11–14, 1971, v. 2, Chemical and isotope analyses: Cambridge, Mass., MIT Press, p. 1217–1229.

Cuttitta, Frank, Rose, H. J., Jr., Annell, C. S., Carron, M. K., Christian, R. P., Dwornik, E. J., and Ligon, D. T., Jr., 1972, Preliminary studies of some Apollo 14 lunar rocks, *in* Geological Survey Research 1972: U.S. Geol. Survey Prof. Paper 800-C, p. C189–C193.

Rankama, Kalervo, and Sahama, Th. G., 1950, Geochemistry: Chicago, Univ. of Chicago Press, 912 p.

Rose, H. J., Jr., Cuttitta, Frank, Dwornik, E. J., Carron, M. K., Christian, R. P., Lindsay, J. R., Ligon, D. T. Jr., and Larson, R. R.,

1970a, Semimicro chemical and X-ray fluorescence analyses of lunar samples: Science, v. 167, no. 3918, p. 520–521.

——1970b, Semimicro X-ray fluorescence analysis of lunar samples, *in* Levinson, A. A., ed., Proceedings of the Apollo 11 Lunar Science Conference, Houston, Tex., January 5–8, 1970, v. 2, Chemical and isotope analyses: New York, Pergamon Press, p. 1493–1497.

——1970c, Errata and addenda: Geochim. et Cosmochim. Acta, v. 34, p. 1367.

Rose, H. J., Jr., Cuttitta, Frank, Annell, C. S., Carron, M. K., Christian, R. P., Dwornik, E. J., Helz, A. W. and Ligon, D. T., Jr., 1971, Semimicro analysis of Apollo 12 lunar samples, *in* Geological Survey Research 1971: U.S. Geol. Survey Prof. Paper 750-C, p. C182–C184.

Tatsumoto, Mitsunobu, 1970, Age of the moon: An isotopic study of U-Th-Pb systematics of Apollo 11 lunar samples–II, *in* Levinson, A. A., ed., Proceedings of the Apollo 11 Lunar Science Conference, Houston, Tex., January 5–8, 1970, v. 2, Chemical and isotope analyses: New York, Pergamon Press, p. 1595–1612.

Tatsumoto, Mitsunobu, Knight, R. J., and Doe, B. R., 1971, U-Th-Pb systematics of Apollo 12 lunar samples, *in* Levinson, A. A., ed., Proceedings of the Second Lunar Science Conference, Houston, Tex., January 11–14, 1971, v. 2, Chemical and isotope analyses: Cambridge, Mass., MIT Press, p. 1521–1546.

Taylor, S. R., Rudowski, R., Muir, Patricia, and Graham, A., 1971: Trace element chemistry of lunar samples from the Ocean of Storms, *in* Levinson, A. A., ed., Proceedings of the Second Lunar Science Conference, Houston, Tex., Jan. 11–14, 1971, v. 2, Chemical and isotope analyses: Cambridge, Mass., MIT Press, p. 1083–1099.

U.S. National Aeronautics and Space Administration, 1971, Apollo 14 preliminary science report: U.S. Natl. Aeronautics and Space Adm. Spec. Pub. SP-272, 309 p.

URANIUM-SERIES SYSTEMATICS IN NATURAL MATERIALS FROM THE NEWPORT AREA, OREGON

By B. J. SZABO, Denver, Colo.

Abstract.—Analyses of uranium, thorium, and protactinium isotopes in recent and fossil wood and kelp samples from the Newport area, Oregon, indicate that migration of these radioelements has been extensive. Thus, this type of material at this location is unsuitable for uranium-series dating. The analytical data from a shell sample from the same area showed evidence of recent uranium assimilation, which contributed to a minimum age estimate only.

Marine-terrace deposits occur at various localities along the west coast of the United States. They commonly contain assemblages of fossil molluscan shells and other fossil marine fauna and flora. Shell samples from several of these deposits have been dated by the uranium-series method (Thurber, 1965; Richards and Thurber, 1966; Rosholt, 1967; Veeh and Valentine, 1967; Bradley and Addicott, 1968; Szabo and Rosholt, 1969; Szabo and Vedder, 1971). However, no application has been made of the uranium-series method to dating the fossil wood that is rather abundant in Quaternary sediments in Oregon. The primary objective of this report is to evaluate the reliability of uranium-series dating of fossil wood.

Dating of wood, peat, and various organic soils has been attempted before (Cherdyntsev and others, 1964, 1965; Titayeva, 1966). Some of the ^{230}Th dates that were obtained seemed to be reliable, but in many samples migration of uranium and thorium was evident. Andreyev, Komarov, Lopatkina, and Sergeyev (1969) reported rapid uranium accumulation in bog soils of east Siberia without indication of secondary migration of radioelements; the calculated dates from the $^{230}Th/^{234}U$ activity ratios were in agreement with radiocarbon dates.

All samples for this study (table 1) were collected near Newport, Oreg.; the assistance of P. D. Snavely and J. N. Rosholt in collecting the wood samples is gratefully acknowledged. Sample AB-1 is wood collected at site of growth, roots standing in water. Samples JOJ-1, JOJ-2, and SRB-1 are fossil wood from marine deposits older than 38,000 years (P. D. Snavely, oral commun., 1970). A fresh sample of kelp (Kelp-1) was gathered on the beach. The shell sample (0-S-1) was collected by P. D. Snavely from a shell bed that underlies marine sediments dated by radiocarbon as older than 38,000 years.

Table 1.—*Sample descriptions and uranium, thorium, and ash contents of natural materials collected near Newport, Oreg.*

Sample	Material	U (μg/g ash)	Th (μg/g ash)	Th/U	Percent ash
AB-1	Wood[1]	19.4±0.3	5.6±0.1	0.29	1.8
JOJ-1	do.[2]	121±2	47±1	.39	.8
JOJ-2	do.[3]	13.3±0.2	19.0±0.4	1.4	1.2
SRB-1	do.[4]	2.81±0.04	10.2±0.2	3.6	22
Kelp-1	Kelp[5]	.93±0.01	1.08±0.02	1.2	18.5
0-S-1	Shells[6]	[7].394±0.006	[7].122±0.006	.31	...

[1]Wood collected at site of growth, roots standing in water; at mouth of Big Creek on Agate Beach.

[2]Hardwood; 7.5 m below top of terrace at Jump Off Joe, Newport, Oreg.

[3]Mixed hardwood and softwood, partially carbonized; 15 m below top of terrace at Jump Off Joe, Newport, Oreg.

[4]Strongly carbonized wood; Seal Rock Beach at Seal Rock State Park; collected near asphalt path, 9 m below top and 4.5 m above base of terrace.

[5]From beach at Otter Rock, Oreg.

[6]Collected by P. D. Snavely, U.S. Geol. Survey, from shell bed outcrop on south side of Yaquina Bay; identified by W. O. Addicott, U.S. Geol. Survey, as *Saxidomus giganteus*; >97 percent aragonite.

[7]μg/g dry material.

The samples of wood were oven dried and ground to small fragments. They were then cleaned by sieving and flotation over water to remove adhering sediment. They were charred and then were ignited at 800°C for about 14 hours. The kelp was rinsed with distilled water and dried and then was ignited at 800°C for about 14 hours. The fossil shells were scraped and cleaned ultrasonically, and crushed to a fine powder.

The $^{235}U/^{238}U$ ratios and the abundances of uranium and thorium, using enriched ^{230}Th and ^{235}U spikes, were determined on a solid-source mass spectrometer. The ^{230}Th content, using a ^{228}Th spike, and the activity ratios of $^{234}U/^{238}U$ were measured by alpha spectrometery, as described by Szabo and Rosholt (1969). The $^{231}Pa/^{235}U$ activity ratios were determined by thermal neutron activation and alpha spectrometry (method of Rosholt and Szabo, 1969).

U.S. GEOL. SURVEY PROF. PAPER 800-C, PAGES C199-C201

The results of uranium and thorium analyses, together with other sample data, are shown in table 1. The thorium contents of all samples are high; the Th/U concentration ratios range from 0.29 to 3.6. The Th/U ratio of 3.6 for the strongly carbonized sample SRB-1 is as high as the ratios reported for soils and rocks by Rosholt, Doe, and Tatsumoto (1966). The high Th/U ratios and high ash contents may indicate that these samples were not adequately cleaned and that they still contained adherent sediment.

The measured isotopic-activity ratios and independent date estimates for the samples are given in table 2. The $^{235}U/^{238}U$ ratios relative to the Republic of Congo Pitchblende reference material are unity within limits of experimental error. This accords with the results of previous measurements of various terrestrial samples (Hamer and Robbins, 1960; Rosholt and others, 1964, 1966). In fact, this ratio was found to be constant in Apollo 11 moon samples and the same as that reported previously for terrestrial uranium (Rosholt and Tatsumoto, 1970).

Recent wood sample AB-1 has a $^{230}Th/^{234}U$ activity ratio of 0.061±0.006 and has a resulting apparent ^{230}Th date of 6,800±700 years. This value indicates that the sample contains initial ^{230}Th which was probably assimilated, together with common thorium (^{232}Th), from the surrounding environment. The $^{231}Pa/^{235}U$ activity ratio of 0.13±0.01 indicates initial ^{231}Pa contamination, and the resulting apparent ^{231}Pa date for the recent wood is 6,500±1,000 years.

The initial ^{230}Th content is high in the recent kelp sample, resulting in an anomalous apparent ^{230}Th date of 24,000±2,800 years.

The apparent ^{230}Th dates for the samples JOJ-1, JOJ-2, and SRB-1 are calculated to be 13,900, 65,000, and >220,000 years, respectively. However, the activity ratios of $^{232}Th/^{234}U$ and $^{230}Th/^{232}Th$ reveal that ^{230}Th was not produced by ^{234}U decay within the samples; thus the samples are not suitable for uranium-series dating. The apparent ^{231}Pa dates for samples JOJ-1 and JOJ-2 are 6,000 and 34,000 years, respectively.

The ^{231}Pa date of the shell sample 0-S-1 is younger ($92{,}000^{+21{,}000}_{-14{,}000}$ years) than that of the ^{230}Th date (164,000±25,000 years); thus, this sample did not remain closed through time with respect to uranium isotopes and their daughter elements thorium and protactinium. A similar discrepancy recently found for fossil shells from Pleistocene deposits of southern California (Szabo and Vedder, 1971) is attributed to recent assimilation of uranium by the samples, which resulted in lowering of both $^{230}Th/^{234}U$ and $^{231}Pa/^{235}U$ ratios. On the assumption of recent uranium uptake, a minimum date for sample 0-S-1 is estimated as 90,000 years. This estimate is not contradicted by geological evidence (P. D. Snavely, oral commun., 1970), but additional shell materials need to be collected and dated from similar Pleistocene units along the coast before definite conclusions concerning the true age of these deposits can be made.

REFERENCES

Andreyev, A. G., Komarov, V. S., Lopatkina, A. P., and Sergeyev, A. N., 1969, Evaluation of the ages of uranium-bearing hydromorphic soils from the accumulation of thorium^{230}: Geochemistry Internat., v. 6, no. 3, p. 580–584.

Bradley, W. C., and Addicott, W. O., 1968, Age of first marine terrace near Santa Cruz, California: Geol. Soc. America Bull., v. 79, no. 9, p. 1203–1209.

Cherdyntsev, V. V., Kazachevskiy, I. V., and Kuz'mina, Ye. A., 1965, Dating of Pleistocene carbonate formations by the thorium and uranium isotopes: Geochemistry Internat., v. 2, no. 5, p. 794–801.

Cherdyntsev, V. V., Malyshev, V. I., Sokolova, Z. A., Kazachevskiy, I. V., and Borisov, I. V., 1964, Isotopic composition of uranium and thorium in the supergene zone: Geochemistry Internat., v. 1, no. 3, p. 398–401.

Hamer, A. N., and Robbins, E. J., 1960, A search for variations in the natural abundance of uranium-235: Geochim. et Cosmochim. Acta, v. 19, no. 2, p. 143–145.

Richards, H. G., and Thurber, D. L., 1966, Pleistocene age determinations from California and Oregon: Science, v. 152, no. 3725, p. 1091–1092.

Rosholt, J. N., 1967, Open system model for uranium-series dating of Pleistocene samples, p. 299–311 *in* Radioactive dating and methods of low-level counting–Symposium, Monaco, 1967, Proc.: Vienna, Internat. Atomic Energy Agency, 744 p.

Rosholt, J. N., Doe, B. R., and Tatsumoto, Mitsunobu, 1966, Evolution of the isotopic composition of uranium and thorium in soil profiles: Geol. Soc. America Bull., v. 77, no. 9, p. 987–1003.

Rosholt, J. N., Garner, E. L., and Shields, W. R., 1964, Fractionation of uranium isotopes and daughter products in weathered granite and uranium-bearing sandstone, Wind River basin region, Wyoming, *in*

Table 2.–*Isotopic-activity ratios and independent age estimates for samples collected near Newport, Oreg.*

Sample	$^{1}235U/^{238}U$	$^{234}U/^{238}U$	$^{230}Th/^{234}U$	$^{232}Th/^{234}U$	$^{230}Th/^{232}Th$	$^{231}Pa/^{235}U$	^{14}C or estimated age (years)
AB-1.....	0.996±0.005	1.16±0.02	0.061±0.006	0.082	0.74	0.13±0.01	[2] <500
JOJ-1.....	.994±0.005	1.12±0.02	.12±0.01	.12	1	.124±0.007	[3] >38,000
JOJ-2.....	.999±0.005	1.09±0.02	.45±0.05	.44	1	.51±0.03	[2] >38,000
SRB-1.....	.997±0.005	1.04±0.02	.94±0.06	1.16	.81	...	[2] >38,000
Kelp-1.....	...	1.15±0.02	.20±0.02	.34	.60	...	Recent
0-S-1	...	1.24±0.02	.81±0.05	.08	10	.86±0.05	[3] >38,000

[1] Uranium equivalent units. [2] Dates estimated from stratigraphic correlation. [3] Dates based on ^{14}C determinations.

Geological Survey Research 1964: U.S. Geol. Survey Prof. Paper 501-B, p. B84–B87.

Rosholt, J. N., and Szabo, B. J., 1969, Determination of protactinium by neutron activation and alpha spectrometry, p. 327–333 *in* DeVoe, J. R., ed., Modern trends in activation analysis: U.S. Natl. Bur. Standards Spec. Pub. 312, v. 1, 691 p.

Rosholt, J. N., and Tatsumoto, M., 1970, Isotopic composition of uranium and thorium in Apollo 11 samples, p. 1499–1502 *in* Levinson, A. A., ed., Proceedings of the Apollo 11 lunar science conference, Houston, Texas, January 5–8, 1970: New York, Pergamon Press, v. 2, 2,492 p.

Szabo, B. J., and Rosholt, J. N., 1969, Uranium-series dating of Pleistocene molluscan shells from southern California–An open system model: Jour. Geophys. Research, v. 74, no. 12, p. 3253–3260.

Szabo, B. J., and Vedder, J. G., 1971, Uranium-series dating of some Pleistocene marine deposits in southern California: Earth and Planetary Sci. Letters, v. 11, no. 4, p. 283–290.

Thurber, D. L., 1965, The dating of molluscs from raised marine terraces by the Th^{230}/U^{234} method, *in* Symposium on marine geochemistry, 1964, Proc.: Rhode Island Univ. Narragansett Marine Lab. Occasional Pub. 3, p. 1–27.

Titayeva, N. A., 1966, Possibility of absolute dating of organic sediments by the ionium method: Geochemistry Internat., v. 3, no. 5, p. 941–950.

Veeh, H. H., and Valentine J. W., 1967, Radiometric ages of Pleistocene fossils from Cayucos, California: Geol. Soc. America Bull., v. 78, no. 4, p. 547–549.

DETERMINATION OF MERCURY IN GEOLOGIC MATERIALS BY FLAMELESS ATOMIC ABSORPTION SPECTROMETRY

By CLAUDE HUFFMAN, JR., RAMONA L. RAHILL, VAN E. SHAW, and DANIEL R. NORTON, Denver, Colo.

Abstract.—A flameless atomic absorption spectrometric method is used for determining submicrogram quantities of mercury in rocks and in other geologic materials such as soil, shale, and coal that are high in organic matter. Samples are taken into solution under oxidizing conditions. Mercury is then reduced to the elemental state and aerated from solution onto a silver screen where it is amalgamated. The silver screen is subsequently heated and the released mercury vapor swept through an absorption cell where its concentration is measured.

Instrumental methods that have been used to determine mercury in a variety of materials are emission spectrography, mass spectroscopy, X-ray fluorescence spectrometry, flameless atomic absorption spectrometry, atomic fluorescence flame spectrometry, neutron activation (destructive and nondestructive), and polarography. Of these methods, two seem to be preferred at present—flameless atomic absorption spectrometry and neutron activation.

Flameless atomic absorption methods for determining mercury in a variety of materials are numerous and have been summarized in a review by Manning (1970). These methods may be classified into two general types: (1) reduction of mercury in a sample solution to the elemental state and then aeration into an absorption cell where its concentration is measured, and (2) amalgamation or deposition of mercury from the sample onto a metal (generally gold or silver) and subsequent thermal release of the mercury into an absorption cell.

Methods of the first type have been described by Hatch and Ott (1968) and by the Dow Chemical Co. (1970). In these procedures, the sample is digested under oxidizing conditions. Mercury in solution is reduced to its elemental state with stannous chloride or stannous sulfate solution and then aerated from solution into an absorption cell using air as a carrier gas. The Dow Chemical Co. method uses the open system, which allows the mercury to pass through the absorption cell only once, whereas Hatch and Ott prefer the closed system in which the air containing the mercury vapor is continuously recirculated through the absorption cell until a constant reading is obtained.

Methods of the second type (amalgamation or deposition of mercury onto a metal) have been described by Vaughn and McCarthy (1964) and Marinenko, May, and Dinnin (1972). In these procedures, mercury is generally vaporized by heating a solid powdered sample and it is trapped or collected by condensing and amalgamating onto a metal. This metal is subsequently heated by a resistance or induction furnace. The mercury is vaporized and carried by an air stream into the absorption cell. In the method of Marinenko, May, and Dinnin, the samples are heated with a calcium oxide–cupric oxide flux in a quartz combustion tube packed with lime and elemental copper. The evolved mercury vapor is collected onto gilded silica. This modification of the decomposition technique allows for the decomposition of rocks and minerals with the evolution of mercury while retaining other volatile constituents that may be present, such as sulfur, selenium, and the halogens. At the same time organic matter is oxidized to carbon dioxide and water.

The deposition of mercury from solution onto a silver screen has been described by Hinkle and Learned (1969) using chemical deposition and by Brandenberger and Bader (1967) using electrolysis.

The method described here is applicable to the determination of parts per billion and higher levels of mercury in geologic materials. Sample decomposition procedures are described here for rocks and for other geologic materials, such as soils, shales, and coal, that are high in organic matter. In these procedures, the powdered sample is digested under oxidizing conditions. The stannous chloride reduction-aeration technique is combined with a silver amalgamation technique to collect the mercury. The silver screen is subsequently heated, and the mercury vapor carried by an air stream to an absorption cell. The absorption cell is provided with an inlet and outlet for the air and is placed between the light source and the detector. The outlet of the cell (open system, single pass) is vented into a hood. The method is free from interferences by organic matter or other volatile constituents in the sample. However, elements that are easily reduced to the elemental state by stannous chloride, such as tellurium or

U.S. GEOL. SURVEY PROF. PAPER 800-C, PAGES C203-C207

gold, will interfere and will cause low results in the determination of mercury. The probable reason for such interference is the binding of mercury as a telluride or amalgam formation with gold, thereby hindering the release of mercury during the aeration step. However, these elements are not usually present in sufficient quantity to cause interference.

REAGENTS

Mercury standard stock solution: Dissolve 17.10 g of mercuric nitrate, $Hg(NO_3)_2 \cdot H_2O$, in 100 ml of 2 percent v/v nitric acid, and dilute to 1 liter. This solution contains 10,000 μg/ml of mercury.

Mercury standard solution, 200 μg/ml of mercury: Pipet 5 ml of the mercury stock solution into a 250-ml volumetric flask, acidify with 5 ml of 1:4 H_2SO_4, and dilute to volume with distilled water. This solution is diluted to obtain working standards with the same concentration of sulfuric acid. Mercury solutions more dilute than 1 ppm are prepared daily as needed.

Stannous chloride solution, 10 percent w/v: Dissolve 10 g of reagent grade $SnCl_2 \cdot 2H_2O$ in 10 ml of warm concentrated hydrochloric acid, and dilute to 100-ml volume with distilled water. Prepare fresh once a week.

Hydroxylamine hydrochloride solution, 10 percent w/v: Dissolve 50 g of reagent grade $NH_2OH \cdot HCl$ in 500 ml of distilled water.

Potassium permanganate solution, 5 percent w/v: Weigh 50 g of reagent grade $KMnO_4$ into a 250-ml beaker. Add approximately 60 ml of distilled water, and stir for about 20 seconds. Allow the potassium permanganate crystals to settle. Decant the supernatant liquid into a 1-liter volumetric flask. Repeat the operations of dissolving and decanting until all the potassium permanganate has dissolved. Dilute to 1 liter, mix, and store in a bottle. Allow the solution to age for 3 days and decant into another bottle before use.

Hydrochloric acid, reagent grade, concentrated.

Nitric acid, reagent grade, concentrated.

APPARATUS

Atomic absorption spectrophotometer: A Perkin-Elmer Model 303 instrument equipped with a Perkin-Elmer Model 165 recorder. Other atomic absorption instruments having an open sample presentation area to mount the absorption cell could be used.

Mercury hollow cathode lamp: Westinghouse, type W122847, argon filled.

Absorption cell: The absorption cell was constructed from borosilicate glass tubing with quartz windows cemented at each end with epoxy. The cell is 200 mm long and 19 mm OD.

Induction furnace: A Ther-Monic Induction Heating Corp. induction furnace, Model 50, equipped with a copper water-cooled heating coil. The coil, made in our own workshop, is 30 mm long and 10 mm ID.

Silver-screen amalgamator: The amalgamator is made by rolling a suitable length of fine silver screen, 12 mm in width, so that it fits into 10-mm ID pyrex tubing. The silver screen was obtained from a Perkin-Elmer Model 240-0092 silver gauze kit.

Aeration train: A schematic diagram of the aeration apparatus is shown in figure 1. All gas connections are made with Tygon tubing. The aeration flask is a tall form, gas washing bottle of 125-ml capacity with a 29/42 standard taper stopper and a coarse porosity fritted glass aerator.

DIGESTION PROCEDURES

Soil and rock samples of low organic content (less than 5 percent organic carbon).—Samples are digested with aqua regia. Transfer 0.5 g of sample to a 150-ml beaker. Moisten sample with water and add 3 ml HNO_3 and 8 ml HCl. Cover beaker with watchglass, heat on hotplate, and boil for 8 minutes. Cool. Transfer the solution and undissolved solids to the aeration flask, and proceed as detailed under "Aeration Procedure."

Soil and rock samples of high organic content.—Samples are digested with sulfuric and nitric acids and potassium permanganate. Transfer 0.5 g of sample to a 150-ml beaker. Add 5 ml H_2SO_4 to the beaker, cover, and digest on a steam bath for 5 minutes. Cool. Add 5 ml HNO_3, cover, and digest an additional 15 minutes on the steam bath. Place the beaker in a pan containing cold water. Add slowly 5 ml of 5-percent $KMnO_4$ solution. Allow the permanganate to react with the organic matter about 30 minutes. The solution should be purple at this point; if not, add additional permanganate solution. Decant the solution to the aeration flask. Add 10 ml of 10-percent hydroxylamine hydrochloride solution to the beaker, and swirl to dissolve the manganese dioxide. Transfer this solution to the aeration flask, and rinse with about 10 ml of water. Swirl the aeration flask to reduce the excess permanganate, and proceed as directed under "Aeration Procedure."

Coal samples.—Samples are digested with sulfuric acid–potassium permanganate solution. Experience has shown that 60 ml of 5-percent $KMnO_4$ is sufficient to oxidize the organic matter in most 0.2-g samples of coal. Transfer the 0.2-g sample to a 150-ml beaker. Add 5 ml H_2SO_4 to the beaker, cover with watchglass, and let stand for 15 minutes at room temperature. Add the permanganate solution in 5-ml increments from a pipet or buret while swirling the contents of the beaker. The first two increments (10 ml) are added dropwise into the beaker after placing it in a cold water bath. The next five 5-ml increments are added rapidly at room temperature. The remaining increments are added rapidly to the beaker contents which have been heated on a steam bath to a gradually increasing temperature. After the final 5-ml increment is added the solution is heated on the steam bath for 2 hours. The sides of the beaker are rinsed with distilled water to wash down any unreacted sample, and the contents are frequently stirred by swirling the beaker. The permanganate color should persist during the 2-hour digestion period; if not, add additional permanganate solution. A set of 15 samples may be conveniently processed together to give adequate reaction time for each sample. Allow the sample solution to cool. Add directly from a pipet 10 ml of 10-percent hydroxylamine sulfate solution while swirling the contents of the beaker. Decant the solution into the aeration flask, and add 4 ml of hydroxylamine hydrochloride solution directing the flow to rinse down the sides of the beaker. Allow 1 minute for the unreacted manganese dioxide to react with the hydroxylamine solution. Transfer the contents quantitatively to the aeration flask. At this point all the excess permanganate and precipitated manganese dioxide should be reduced; if not,

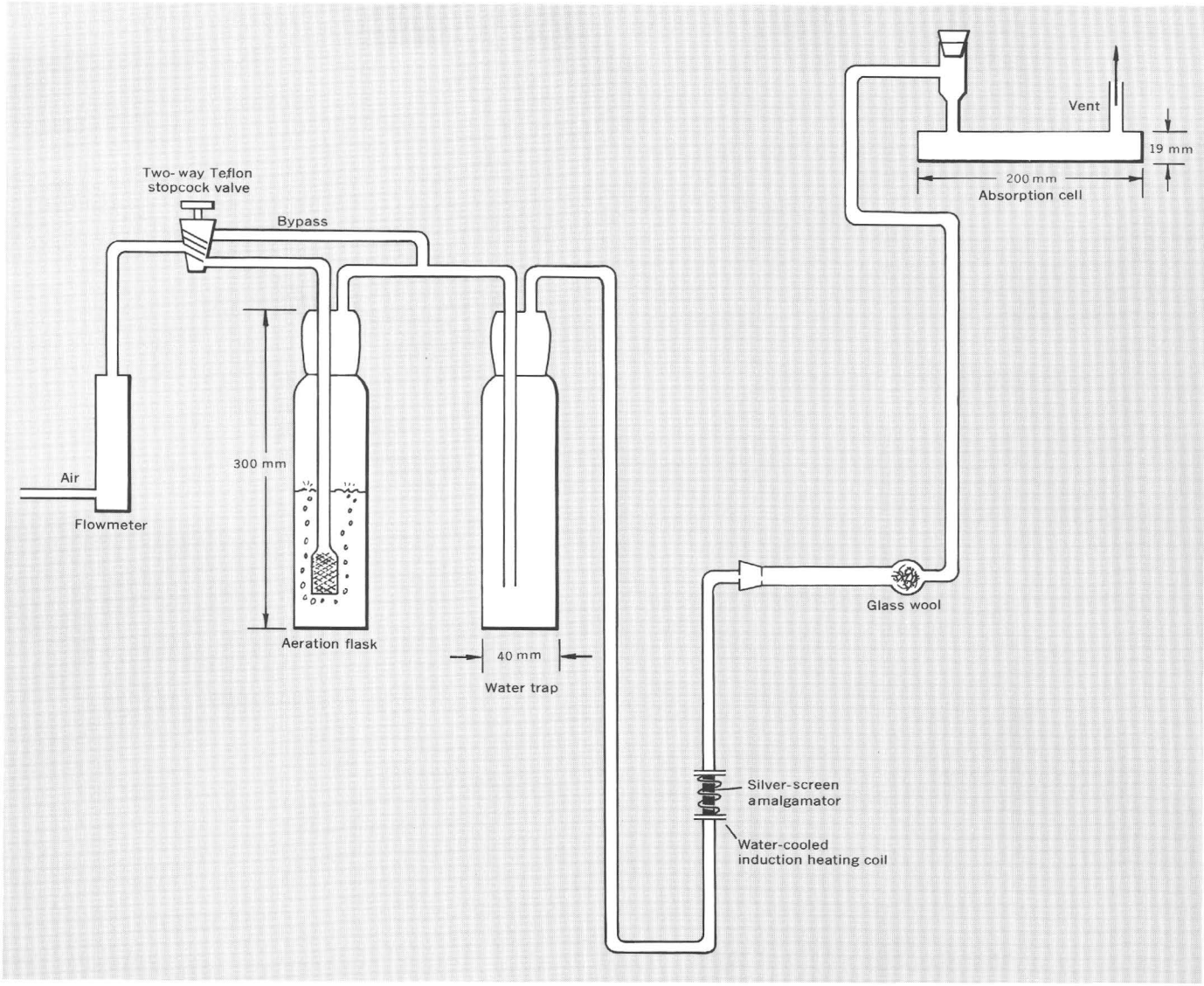

Figure 1.—Schematic diagram of aeration apparatus.

add additional hydroxylamine solution. Rinse down the sides of the aeration flask with water, and proceed as detailed under "Aeration Procedure."

Shale samples.—Samples are digested in aqua regia using the procedure described for rock and soil samples of low organic content. This digestion procedure seems to work well on shales, and no frothing problem occurred during the aeration step. The success with this procedure is attributed to the type of organic matter present in the shales. In the event some shale samples present a frothing problem, use the digestion procedure described for coals.

AERATION PROCEDURE

Adjust the volume of the sample solution in the aeration flask with water to about 100 ml, and add 2 ml of 10-percent stannous chloride solution. Turn the stopcock valve in the aeration train to the bypass position, and immediately connect the aeration flask to the train. Adjust the flow rate of compressed air through the absorption cell (train apparatus) to 0.82 liter per minute. Swirl the contents of the aeration flask. Turn the stopcock valve from the bypass position and aerate the solution for 2 minutes, collecting the mercury vapor on the silver screen. Return the stopcock valve to the bypass position, and adjust the baseline of the recorder. Heat the silver screen for 25 seconds (induction furnace preset to 130 milliamperes) to volatilize the mercury into the absorption cell. Measure the peak height on the recorder, and compare against known mercury standards processed through the aeration procedure. The 2,537-A mercury resonance line is used.

STANDARDIZATION

The working range for the recorder set on the 1X scale is 0.02 to 0.2 μg Hg. For the 3X scale expansion the range is 0.01 to 0.07 μg. Standards are processed through the aeration step in the following manner: Transfer a known amount of a mercury standard solution to the aeration flask, add 3 ml HNO_3, adjust the volume to 100 ml with water, and proceed with the aeration procedure, starting with the addition of the stannous chloride solution. Process reagent blanks through the entire method including the sample digestion procedure. Standards should be occasionally processed through the entire procedure.

RESULTS AND DISCUSSION

Reagent blanks can be minimized by determining the mercury content of the various reagents used in the method, selecting the bottle of reagent with the lowest blank. For example, the mercury content of various lots of reagent-grade hydroxylamine hydrochloride varied widely (ranging from 0.002 to 0.04 ppm). Hydroxylamine sulfate was recently substituted for hydroxylamine hydrochloride because its mercury content was found to be low for several lots tested. The average blank for all reagents used in the aqua regia digestion procedure and the sulfuric acid-permanganate digestion procedure gives an absorbance of 0.0057, corresponding to about 0.0025 μg Hg.

The parameters that must be adjusted for high sensitivity are the air-flow rate through the aeration train and the temperature and rate of heating of the silver-screen amalgamator. The optimum parameters for our aeration apparatus were determined to be: (1) air-flow rate of 0.82 liter per minute; (2) induction coil controls set to heat the silver-screen amalgamator for 25 seconds at 130 milliamperes. During the heating period, the silver screen reaches approximately 450°C. Under these conditions, the peak mercury absorbance is obtained after approximately 20 seconds.

Recovery tests were made by processing two weighed portions of each sample (soil, coal, and so forth) through the entire method after spiking one portion with a known amount of mercury. These tests showed recoveries of 90 to 105 percent at submicrogram levels.

Hatch and Ott (1968) stated that the solution must not contain large amounts of easily reducible elements inasmuch as such elements will cause interferences. To quantitatively determine the effects of known amounts of gold, tellurium, silver, and copper the following studies were made: Test solutions made to obtain 0, 2, 4, 6, 8, 10, and 12 μg Au were each spiked with 0.2 μg Hg and then processed through the method. The results indicate that as much as 4 μg Au can be tolerated. At the 6-μg Au level, 83 percent of the mercury was recovered. Higher levels of gold gave both low and erratic recoveries of mercury. Test solutions with 10, 20, and 50 μg Ag showed no interference. Test solutions with 0.1, 0.2, and 0.3 μg Te each gave low and erratic recoveries of mercury. Test solutions with 5, 10, 20, 30, and 50 mg Cu showed no interference. Many geologic samples contain little or no tellurium or gold; however, anyone applying this procedure to geologic samples should be aware of their possible interference. Although selenium may interfere, preliminary tests show that 10 μg Se can be tolerated. The procedure is free from interference by organic matter or other volatile constituents in the sample.

The method described here has been applied to determine the mercury content in four U.S. Geological Survey standard rock samples, in six soil and six shale samples, and in 14 coal samples. These values together with values determined by other methods are shown in tables 1, 2, and 3. Four of the soil samples (Hg-1, Hg-2, Hg-3, Hg-4) had been previously collected and analyzed by Dr. K. W. Edwards, Colorado School of Mines. Eleven of the coal samples were collected by Schlesinger and Schultz (1972) and were distributed by them to several laboratories in an evaluation of methods for the determination of mercury in coals.

Table 1.—*Mercury content of U.S. Geological Survey standard rocks as determined by method of present report and by other methods*

Sample type and No.	Mercury (ppm)							
	Method of present report		Other methods					
			A	B		C		D
	Run 1	Run 2		Run 1	Run 2	Run 1	Run 2	
Granite, G-1	0.075	0.080	0.087	0.11	0.08	0.07	0.095	...
Diabase, W-1	.20	.21	.18	.18	.18	.17	.16	...
Granite, G-2	.040	.045	.040	...	...	...	...	0.039
Granodiorite, GSP-1	.024	.020	.015	...	...	...	...	.021

A. Marinenko, May, and Dinnin (1972), by combined combustion-amalgamation flameless atomic absorption method.
B. Hatch and Ott (1968), by flameless atomic absorption method.
C. Hatch and Ott (1968), by dithizone-spectrophotometric method.
D. Ehmann and Lovering (1967), by neutron activation method.

Table 2.—*Mercury content of six soil samples and six shale samples as determined by method of present report and by other methods*

Sample No.	Mercury (ppm)					
	Method of present report		Other methods			
			A		B	C
	Run 1	Run 2	Run 1	Run 2		
Soil samples						
Hg-1	1.29	1.20	0.92	1.07	...	1.35
Hg-2	.26	.31	.32	.30	...	.31
Hg-3	13.8	13.9	14.2	14.2	...	14.5
Hg-4	5.5	5.3	5.17	...	...	5.7
D145126	.08	.09	.080	.089	0.11	...
D145160	.07	.08	.094	...	.094	...
Shale samples						
D120656	0.50	...	0.53	0.52	...	...
D120658	.47	...	.51	.48	...	...
D120667	3.1	...	2.92	2.85	...	...
D120753	.22	...	.18	.20	...	...
D120756	.31	...	.33	...	...	...
D120764	.61	...	.76	...	...	...

A. Analyses by Marinenko, May, and Dinnin (1972), by combined combustion-amalgamation flameless atomic absorption method.
B. Analyses by P. J. Aruscavage, U.S. Geol. Survey, by neutron activation method.
C. Analyses by Dr. K. W. Edwards, Colorado School of Mines, by flameless atomic absorption following acid digestion with HNO_3 and $HClO_4$.

Table 3.—*Mercury content of 14 coal samples as determined by method of present report and by other methods*

Sample No.	Mercury (ppm)			
	Method of present report		Other methods	
	Run 1	Run 2	A	B
D137672	0.13	0.15	...	0.16
D153928	.47	.50	...	.67
D153934	.90	.95	...	1.19
DRB-A	.15	.12	0.15 (32)	...
DRB-B	.37	.37	.41 (28)	...
DRB-C	.21	.22	.24 (30)	...
DRB-D	.07	.05	.07 (27)	...
DRB-E	.09	.07	.12 (29)	...
G-1	.07	.08	.07 (23)	...
P-1	.18	.17	.19 (30)	...
P-2	.07	.05	.06 (22)	...
P-3	.13	.16	.16 (37)	...
P-4	.02	.04	.05 (29)	...
P-5	.05	.06	.06 (26)	...

A. Schlesinger and Schultz (1972). Average based on statistical analysis for the number of values shown in parentheses.
B. Analyses by John Marinenko, U.S. Geol. Survey, by a combined combustion amalgamation flameless atomic absorption method.

REFERENCES

Brandenberger, H., and Bader, H., 1967, The determination of nanogram levels of mercury in solution by a flameless atomic absorption technique: Atomic Absorption Newsletter, v. 6, no. 5, p. 101–103.

Dow Chemical Co., 1970, Determination of mercury in fish flesh: Midland, Mich., Dow Chemical Co. Method No. CAS-AM-70.10.

Ehmann, W. D., and Lovering, J. F., 1967, The abundance of mercury in meteorites and rocks by neutron activation analysis: Geochim. et Cosmochim. Acta, v. 31, no. 3, p. 357–376.

Hatch, W. R., and Ott, W. L., 1968, Determination of submicrogram quantities of mercury by atomic absorption spectrophotometry: Anal. Chemistry, v. 40, no. 14, p. 2085–2087.

Hinkle, M. E., and Learned, R. E., 1969, Determination of mercury in natural waters by collection on silver screens, *in* Geological Survey Research 1969: U.S. Geol. Survey Prof. Paper 650-D, p. D251–D254.

Manning, D. C., 1970, Non-flame methods for mercury determination by atomic absorption, a review: Atomic Absorption Newsletter, v. 9, no. 5, p. 97–99.

Marinenko, John, May, Irving, and Dinnin, J. I., 1972, Determination of mercury in geologic materials by flameless atomic absorption spectrometry, *in* Geological Survey Research 1972: U.S. Geol. Survey Prof. Paper 800-B, p. B151–B155.

Schlesinger, M. D., and Schultz, Hyman, 1972, An evaluation of methods for detecting mercury in some U.S. coals: U.S. Bur. Mines Rept. Inv. 7609, 11 p.

Vaughn, W. W., and McCarthy, J. H., Jr., 1964, An instrumental technique for the determination of submicrogram concentrations of mercury in soils, rocks, and gas, *in* Geological Survey Research 1964: U.S. Geol. Survey Prof. Paper 501-D, p. D123–D127.

A NEUTRON ACTIVATION ANALYSIS PROCEDURE FOR THE DETERMINATION OF MERCURY IN SOIL AND ROCK SAMPLES

By PHILIP J. ARUSCAVAGE, Denver, Colo.

Abstract.—A radiochemical procedure was developed for the determination of mercury in soil and rock samples. After irradiation in a thermal neutron flux of 2×10^{12} n/cm^2 sec^{-1} for 4–16 hours, the sample is decomposed by fusion with Na_2O_2 in the presence of carrier mercury. A distillation of elemental mercury and a precipitation as mercury (II) sulfide leaves mercury in a radiochemically pure form suitable for counting. The chemical yield is determined by reirradiation. Mercury was determined in a series of samples, first by instrumental neutron activation analysis and then by the radiochemical procedure, to verify that the radioactive mercury in the sample equilibrates with the carrier mercury before fractionation can occur. The coefficient of variation for replicate determinations on the U.S. Geological Survey standard rock W-1 (0.12 ppm) was 7.9 percent and for the Colorado School of Mines mercury standard No. 3 (12 ppm) was 3.6 percent. The results for mercury in the eight U.S. Geological Survey standard rocks and the Colorado School of Mines mercury standard compared favorably with literature values. The three-sigma detection limit for a 16-hour irradiation in a thermal neutron flux of 2×10^{12} n/cm^2 sec^{-1} is 0.3 ppb.

The increased concern about trace-element pollution of our environment emphasizes the need for the accurate determination of mercury at background levels (0.005–0.5 ppm). This need has led to the examination of many older methods with a view to improving the sensitivity, accuracy, precision, and speed with which determinations can be made. For example, the sensitivity and precision for determining mercury by atomic absorption spectrometry have been improved recently by the use of flameless techniques (Manning, 1970). However, the problems of reagent blanks and losses of mercury still remain for solution methods. These problems are greatly reduced by use of the dry fusion technique (Marinenko and others, 1972).

Neutron activation analysis (NAA) is well suited for the determination of mercury. The nuclear properties of the mercury isotopes are given in table 1. The high thermal neutron cross section for the reaction Hg^{196} $(n,\gamma)Hg^{197}$ results in an activity for Hg^{197} ($t_{1/2}$, half-life, = 65 hours) equal to 8.2×10^4 disintegrations per minute/μg for a 16-hour irradiation in a thermal neutron flux of 2×10^{12} n/cm^2 sec^{-1}, as calculated from the data presented by Girardi, Guzzi, and Pauly (1965). This high sensitivity permits an easy, interference-free determination once the mercury is separated from most of the matrix activity. Other advantages of NAA with radiochemical separations are: (1) contamination from apparatus and reagents is not significant, and (2) losses during chemical separations are controlled by determination of carrier yield.

Table 1.—*Nuclear properties of mercury isotopes of interest in activation analysis*

Reaction	Half-life of product (days)	Principal decay mode	Principal gamma energies (Kev)	Saturation activity[1] (counts per minute/μg)
$Hg^{196}(n,\gamma)Hg^{197m}$	1.0	IT (97 percent)	133.9 279 Hg X-rays	1.19×10^5
$Hg^{196}(n,\gamma)Hg^{197}$	2.7	EC	77.6 191.4 Au X-rays	3.24×10^5
$Hg^{202}(n,\gamma)Hg^{203}$	46.9	β^- (100 percent)	279	2.78×10^5

[1] From Girardi, Guzzi, and Pauly (1965); calculated at a thermal neutron flux of 1×10^{13} n/cm^2 sec^{-1} using a 3- by 3-inch NaI detector.

NAA procedures for the determination of mercury in rocks have previously been described (Alian and Shabana, 1967; Ehmann and others, 1967; Ishida and others, 1970; Laul and others, 1970; Morris and Killick, 1964). In all these procedures a lengthy acid digestion is used which must be done carefully owing to the volatility of many of the mercury compounds. This care requires more time for analysis and cleanup. In the method presented here, a Na_2O_2 fusion is used because of the relative ease of decomposition of most rock samples and the speed with which most elements equilibrate with their carrier during fusion.

Acknowledgments.—The author is grateful to Prof. Kenneth Edwards, of the Colorado School of Mines, and Arthur S. Radtke, of the U.S. Geological Survey, for samples used in this work.

EXPERIMENTAL METHOD

Reagents and apparatus

Mercury standard solution: Dissolve a weighed quantity of triple-distilled polarographic-grade mercury metal in 8*N* HNO_3 and dilute with water to give a solution of 50 μg of Hg/ml in 2*N* HNO_3.

Mercury carrier solution: Dissolve a weighed quantity of triple-distilled polarographic-grade mercury metal in 8*N* HNO_3 and dilute with water to give a solution of 50 mg of Hg/ml in 2*N* HNO_3.

γ-counting systems:

Planar Ge(Li): 1-cm diameter by 4.6-mm sensitive depth Ge(Li) planar detector coupled to a 512-channel analyzer. System resolution = 600 ev FWHM (electron volts, full width half maximum) at 122 Kev. Gain = 0.3 Kev/channel.

Coaxial Ge(Li): 30-cc Ge(Li) coaxial detector coupled to a 4,096-channel analyzer. System resolution = 3.0 Kev FWHM at 1,333 Kev. Gain = 1.0 Kev/channel.

NaI (Tl): A 3- by 3-inch NaI (Tl) well detector coupled to a 512-channel analyzer. System resolution = 7.7 percent FWHM at 662 Kev. Gain = 10 Kev/channel.

Irradiation and radiochemical separation

Weigh and seal 0.1- to 0.5-g portions of powdered rock samples into $^2/_5$-dram polyethylene vials or quartz ampoules. Pipet 50 μl of the mercury standard solution (2.5 μg of Hg) for use as a monitor into a quartz ampoule. Seal with a torch while cooling the bottom of the ampoule in water. Irradiate the samples and monitors in a thermal neutron flux of about 2×10^{12} n/cm^2 sec^{-1} for a period of 4–16 hours and allow the samples to decay 2–3 days before processing. Pipet 0.2 ml of the mercury carrier solution (10 mg of Hg) into a zirconium crucible containing four pellets of NaOH and dry overnight at the lowest possible temperature. Add a layer of Na_2O_2 (≈ 5 g). Open the sample vial, pour the contents into the crucible, and add an additional 10 g of Na_2O_2 (total Na_2O_2 about 15 g). Completely cover the crucible with an inverted top from a 50-ml Vycor crucible. Keep the top filled with water during the fusion. Use a Transite board with a hole cut in the middle to hold the crucible and to shield the top from the flame. Fuse the contents for 3–5 minutes. Cool the crucible and its contents quickly in water and place in a 250-ml plastic beaker. Leach the melt with 40 ml of water. If any material has condensed on the Vycor lid, wash it into the beaker with a few drops of 8*N* HNO_3. Add 2 ml of 1-percent w/v hydrazine sulfate solution; stir and centrifuge the contents. Discard the supernatant, add 40 ml of water, stir and centrifuge. Discard the supernatant and repeat the washing with 20 ml of methanol. Dry the residue, which contains the hydroxides of the reduced basic elements, under a heat lamp. Add 5 g of Fe powder and mix thoroughly with the residue. Transfer the dried contents to an 18- by 150-mm combustion tube by means of a long-stem filter funnel. Heat the sample to redness at a 45° angle over a Meker burner and condense the mercury vapors on the sidewall of the combustion tube using a cold cloth as in the Penfield method for water determination (Hillebrand and others, 1953, p. 827) and as extended to mercury by Dinnin and Worthing (1966). Allow to cool and redistill the mercury onto a cold finger (see fig. 1) by heating the combustion tube for 10 minutes in an aluminum tube wrapped with electrical heating tape. Wash the mercury metal off the cold finger with a few drops of aqua regia into a 10-ml

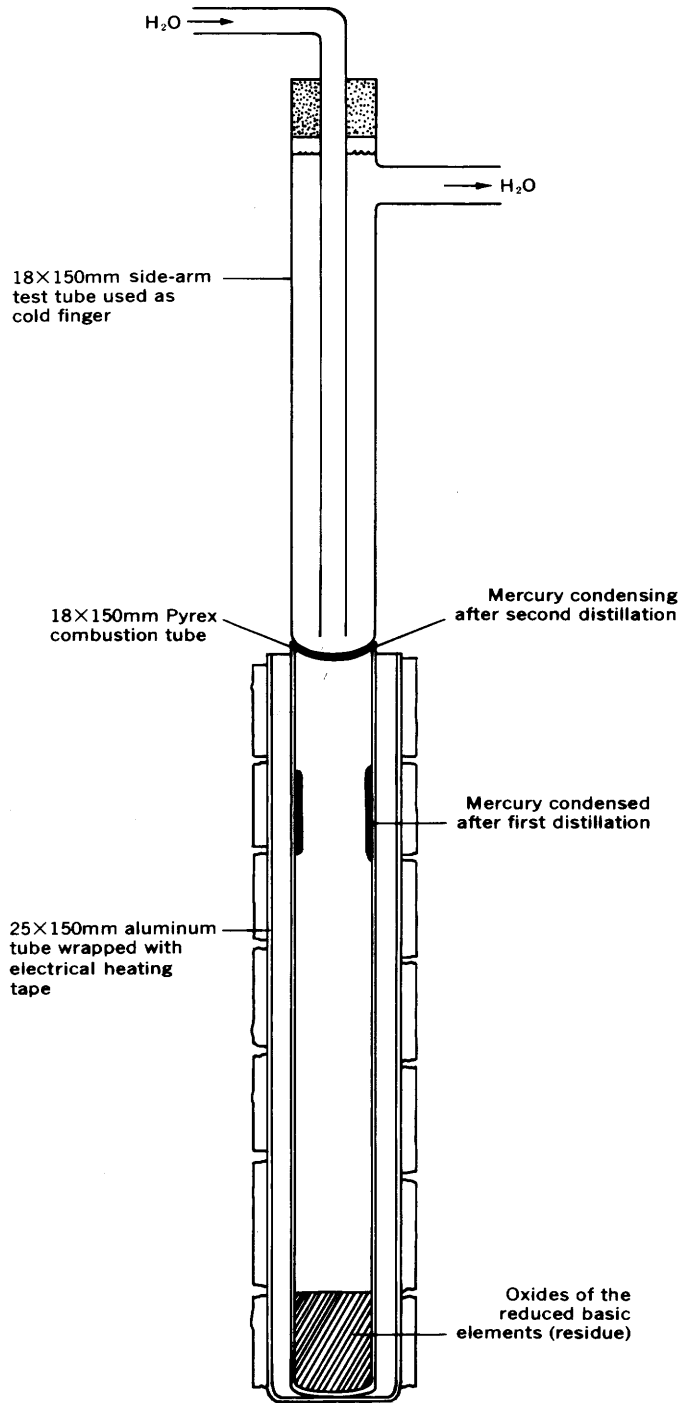

Figure 1.—Mercury redistillation apparatus.

beaker. Cover the beaker with a watchglass and heat on a hotplate to dissolve the mercury. Transfer the solution to a 250-ml beaker and adjust the volume to 200 ml with water. Pass H_2S gas into the solution to precipitate HgS. Filter the solution onto a 2.5-cm 5μ Millipore filter disk and mount the precipitate on an aluminum planchet using transparent tape.

After the samples have been processed, open the quartz ampoule containing the monitor and transfer the monitor to a beaker containing 5 mg of Hg carrier solution. Add 1 ml of conc HNO_3 and adjust the volume to 200 ml with water. Allow to equilibrate for 15 minutes, precipitate HgS, filter, and mount the same way as the samples.

Counting procedure and determination of chemical yield

The samples and monitors are counted on any of the systems described under "Reagents and apparatus." Counting times range from 10 minutes to 1,000 minutes, depending on the length of irradiation and the amount of mercury in the samples. Total peak areas were determined by integrating under the peak and subtracting the background under the baseline between the minima on either side of the peak.

Allow the Hg^{197} to decay ($\approx$ 10 days for 1 μg of Hg) and remove the samples and monitors by cutting around the filter. Add another layer of transparent tape to the back of the filter, fold, and seal into 2/5-dram polyethylene vials. A reirradiation monitor is prepared by pipetting 50 μl of the carrier solution (2.5 mg of Hg) onto a filter-paper disk, drying in air, sealing in transparent tape, and encapsulating in a 2/5-dram polyethylene vial. The yield of mercury is then determined after reirradiation for 30 minutes in a thermal neutron flux of 1×10^{11} n/cm^2 sec^{-1}. The samples are removed from their vials and mounted on an aluminum planchet by means of transparent tape. The 77.6-Kev γ-photopeak of Hg^{197} is counted and the reirradiation-monitor activity compared to sample and monitor activities.

DISCUSSION AND RESULTS

Mercury presents special problems to the analyst who uses NAA. Mercury is lost through the walls of the container when monitors consisting of the solutions or solutions dried on quartz powder are irradiated in polyethylene vials (Bate, 1971). Thus quartz vials must be used. However, no loss occurs from the soil or rock samples encapsulated in polyethylene vials, as established by the data in table 4. Care must also be taken to ensure that no mercury is lost during the decomposition of the sample before equilibration with the carrier. It has been stated that mercury can be lost during fusion with Na_2O_2 (Dolezal and others, 1968, p. 111–120). However, no data are available to indicate the degree to which radioactive mercury in a rock sample equilibrates with carrier mercury before any loss occurs. In the present work, the degree of equilibration was established by determining mercury concentrations in selected mercury samples by instrumental neutron activation analysis (INAA) (that is, without radiochemical separation) and then determining mercury in these same samples by means of the radiochemical separation procedure outlined above. The results of the two determinations are shown in table 2. Inasmuch as there is good agreement within the stated statistics between the two methods for the same sample, the conclusion is that the

Table 2.—*Comparison of mercury concentration, in parts per million, determined by different counting arrangements*

[Irradiation time = 16 hours = 2×10^{12} n/cm^2 sec^{-1}. Error indicated is the standard deviation based on counting statistics. Samples on planchet from radiochemical procedure counted on top of detector. Samples from INAA counted in quartz vials at a source-detector distance of 4.0 cm]

Sample	Radiochemical			INAA
	Planar Ge(Li) Hg^{197}, 77.6 Kev	Coaxial Ge(Li) Hg^{203}, 279 Kev	NaI Hg^{203}, 279 Kev	Coaxial Ge(Li) Hg^{203}, 279 Kev
Org-1	.....	42 ± 1	....	40 ± 5
2	.....	26 ± 1	27 ± 1	26 ± 2
3	.....	80 ± 1	79 ± 2	79 ± 3
4	.....	65 ± 1	65 ± 1	52 ± 2
RK-1	.....	.12 ± .02	.....	.16 ± .21
2	.....	7.2 ± .2	8.0 ± .4	7.9 ± .4
3	.....	13.7 ± .3	13.7 ± .4	12.5 ± .8
4	.....	8.8 ± .2	8.8 ± .4	8.7 ± .9
CSM-3 1	.....	12.4 ± .3	13.6 ± .7	12.2 ± 1.4
2	.....	12.3 ± .2	13.6 ± .7	13.3 ± 1.2
3	.....	11.6 ± .2	11.9 ± .6	11.7 ± 1.1
4	.....	12.9 ± .2	13.6 ± .7	12.3 ± 1.1
AGV-1	0.007 ± 0.002	.....	.....	.....
BCR-1	.017 ± .002	.02 ± .01	.....	.....
W-1	.103 ± .006	.09 ± .02	.....	.....
G-1	.050 ± .005	.06 ± .02	.....	.....
2	.025 ± .005	.03 ± .01	.....	.....
PCC-1	.016 ± .002	.02 ± .01	.....	.....
DTS-1	.005 ± .001	.018 ± .007	.....	.....
Sensitivity (counts per minute/μg of Hg)	4,000	126	985	29

mercury in these samples was equilibrated with carrier mercury before any loss occurred. Agreement with literature values (table 4) is further evidence for the completeness of this equilibration down to the low concentrations found in the U.S. Geological Survey standard rocks.

Because of the high degree of radiochemical purity of the separated mercury, a choice of counting arrangements is available. The 77.6-Kev γ-photopeak of Hg^{197} ($t_{1/2}$ = 65 hours), when counted with the planar Ge(Li) detector, is the most sensitive method. The 279-Kev γ-photopeak of Hg^{203} ($t_{1/2}$ = 46.9 days), when counted with coaxial Ge(Li) or NaI, can also be used for determination with lower sensitivity.

The results obtained by counting on the three different systems are given in table 2. Good agreement was obtained. Figures 2 and 3 show typical spectra obtained with the planar-detector and coaxial-detector systems. The high degree of radioactive purity of the mercury separated from the CSM-3 soil standard is evident when its spectrum is compared with that for the mercury monitor.

An experiment to determine the degree of neutron self-shielding within the HgS precipitates during reirradiation, as well as the effect of absorption of the 77.6-Kev γ-ray, was performed by irradiating various amounts of HgS and measuring the specific activity of each (fig. 4, p. C214). This curve shows that there is no appreciable reduction in the specific activity up to about 5 mg of HgS. Inasmuch as the chemical yield through the radiochemical steps is no more than 50 percent, no corrections due to neutron absorption or self-shielding are required for this procedure. Determination of the chemical yield by counting the 134-Kev γ-photopeak of Hg^{197m} ($t_{1/2}$ = 24 hours) is also possible. This method may be better than counting of the 77.6-Kev γ-photopeak of Hg^{197} because of the shorter decay time required before reirradiation (7 days for 10 μg of Hg) and the higher energy of its γ-ray.

The precision of the method was established by replicate determinations of mercury in the U.S. Geological Survey standard rocks AGV-1 and W-1 and the Colorado School of Mines standard No. 3. The results are shown in table 3. The coefficient of variation for the method does not exceed 8 percent at the 0.1-ppm concentration level, if the samples are assumed to be homogeneous. The coefficient of variation rises to 64.3 percent near the detection limit for an 8-hour irradiation.

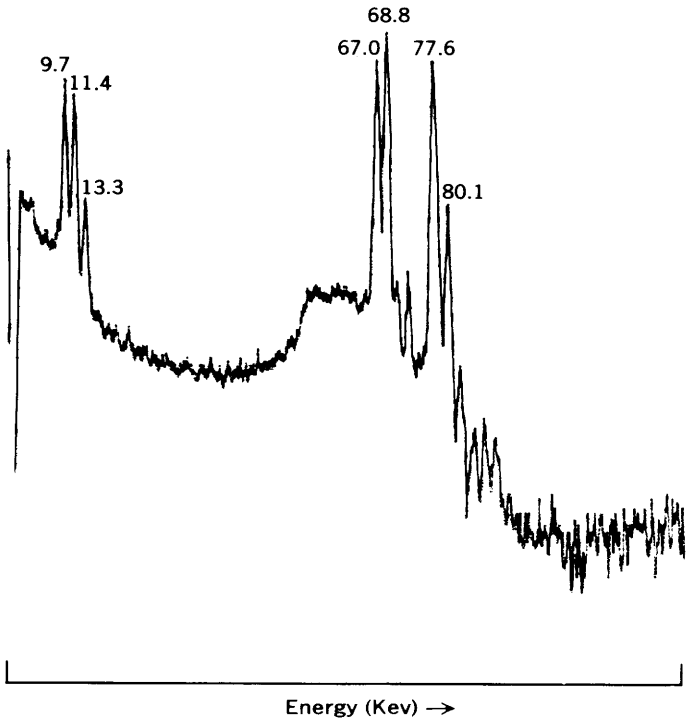

Figure 2.—Low-energy spectrum of CSM-3 obtained using the planar Ge(Li) detector. The $L\alpha$, $L\beta$, $L\gamma$, $K\alpha_2$, $K\alpha_1$, and $K\beta_1$ Au X-rays at 9.7, 11.4, 13.3, 67.0, 68.8, and 80.1 Kev, respectively, as well as the 77.6-Kev γ-ray of Hg^{197} are resolved. Decay time = 8 days.

Table 3.—*Precision of the NAA method on the basis of replicate analysis on the U.S. Geological Survey standard rocks AGV-1 and W-1, and the Colorado School of Mines mercury standard No. 3*

Sample	NAA (ppm)	Mean (ppm)	Coefficient of variation of the mean (percent)
CSM-3	[1]12.4, [1]12.3, [1]11.6, [1]12.9	12.2 ± 0.4	3.6
W-1.....	0.123, 0.107, 0.126, 0.117, 0.111, [1]0.103	.115 ± .009	7.9
AGV-1	[1]0.007, 0.015, 0.005, 0.006, 0.021	.011 ± .007	64.3

[1]Irradiation in quartz ampoules.

Table 4 is a list of the results for mercury obtained by the NAA procedure of eight U.S. Geological Survey standard rocks, the Colorado School of Mines mercury standard No. 3, and two Missouri soil samples, and a comparison with literature values. From the agreement with literature values, it is concluded that the method is accurate and useful for the routine determination of mercury in rock and soil.

The detection limit for a 16-hour irradiation in a neutron flux of 2×10^{12} n/cm^2 sec^{-1}, based upon a three-sigma variation in the counter background and assuming a typical yield of 50 percent on a 0.5-g sample, is 0.3 ppb Hg using the Hg^{197} 77.6-Kev γ-photopeak (planar Ge(Li) detector) and 3 ppb using the Hg^{203} 279-Kev γ-photopeak (coaxial Ge(Li) detector). The practical detection limit is probably several times higher, as indicated by the data for AGV-1 (table 4). However, this limit can be extended by using a longer irradiation time.

REFERENCES

Alian, A., and Shabana, R., 1967, Neutron activation analysis by standard addition and solvent extraction. Determination of some trace elements in granite and diabase rocks: Microchem. Jour., v. 12, p. 427–433.

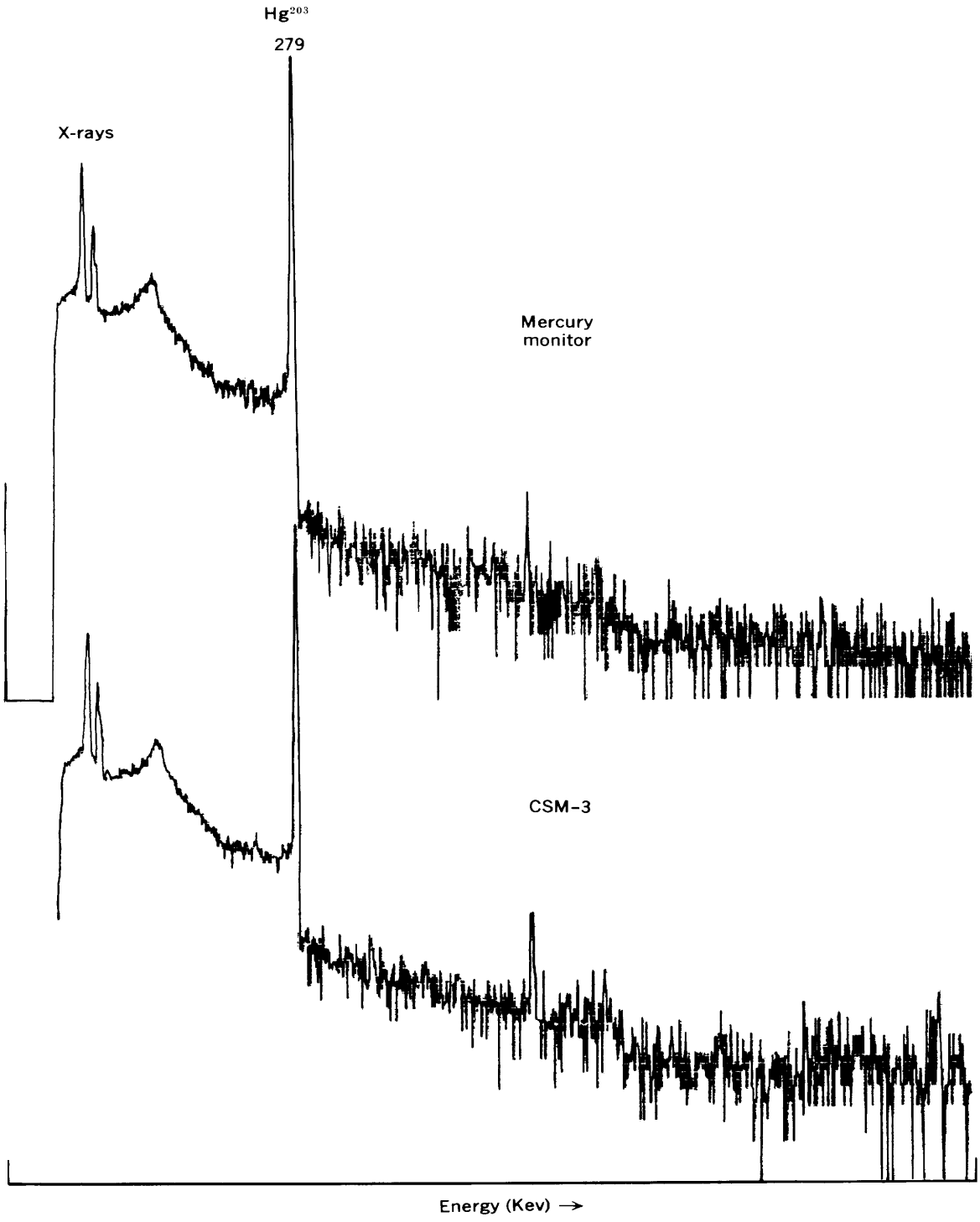

Figure 3.—Energy spectra of CSM-3 and a mercury monitor obtained with the coaxial Ge(Li) detector. Decay time = 50 days.

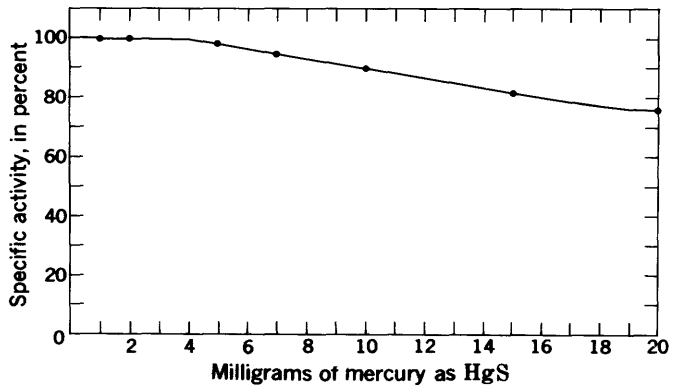

Figure 4.—Effects of neutron self-shielding during reirradiation and self-absorption of the 77.6-Kev γ-photopeak by the HgS precipitate.

Table 4.—*Comparison with literature values for the mercury concentrations in eight U.S. Geological Survey standard rocks, the Colorado School of Mines standard No. 3, and two Missouri soil samples*

[Error indicated for W-1, AGV-1, and CSM-3 is standard deviation of the mean; all others are standard deviations based on counting statistics]

Standard rock	NAA by this method (ppm)	Literature values (ppm)
Diabase, W-1	0.115±0.009 (mean of 6)	[1]0.18, [2]0.20, [3]0.094
Granite, G-1	.050±.005	[1].087, [2].075, [3].070
Granite, G-2	.025±.005	[1].040, [4].039, [2].040, [3].029
Basalt, BCR-1	.017±.002	[1].018, [4].007, [3].004
Andesite, AGV-1	.011±.007 (mean of 5)	[1].009, [4].004, [3].016
Peridotite, PCC-1	.016±.002	[1].020, [4].004, [3].0036
Dunite, DTS-1	.005±.001	[1].007, [4].004, [3].006
Granodiorite, GSP-1	.034±.005	[1].015, [4].021, [2].024, [3].041
Missouri soil 1	.094±.003	[1].094, [2].08
Missouri soil 2	.110±.003	[1].085, [2].09
CSM-3 soil standard	12.2±.4 (mean of 4)	[5]10–14.8

[1]Marinenko and others (1972); flameless atomic absorption (dry-decomposition technique).
[2]Claude Huffman (written commun., 1979); flameless atomic absorption (acid-digestion technique).
[3]Laul and others (1970); NAA.
[4]Ehmann and others (1967); NAA.
[5]Kenneth Edwards (written commun., 1971); atomic absorption, colorimetric, and NAA methods.

Bate, L. C., 1971, Loss of mercury from containers in neutron activation analysis: Radiochem. Radioanal. Letters, v. 6, p. 139–144.

Dinnin, J. I., and Worthing, H. W., 1966, Determination of microquantities of mercury in sulfide ores by Penfield tube–dithizone and semiquantitative spectrographic methods, *in* Geological Survey Research 1966: U.S. Geol. Survey Prof. Paper 550-C, p. C220–C223.

Dolezal, J., Povondra, P., and Sulcek, Z., 1968, Decomposition techniques in inorganic analysis: London, Iliffe Books Ltd., 1st ed., 224 p. [Translated from Czech]

Ehmann, W. D., and Lovering, J. F., 1967, The abundance of mercury in meteorites and rocks by neutron activation analysis: Geochim. et Cosmochim. Acta, v. 31, p. 357–376.

Girardi, F., Guzzi, G., and Pauly, J., 1965, Data handbook for sensitivity calculations in neutron activation analysis, Eur 1898.e: Joint Nuclear Research Center, Ispra Establishment, Italy.

Hillebrand, W. F., Lundell, G. E. F., Bright, H. A., and Hoffman, J. I., 1953, Applied inorganic analysis with special reference to the analysis of metals, minerals, and rocks: New York, John Wiley & Sons, Inc., 2d ed., 1,034 p.

Ishida, K., Kawamura, S., and Izawa, M., 1970, Neutron activation analysis for mercury: Anal. Chim. Acta, v. 50, no. 2, p. 351–353.

Laul, J. C., Case, D. R., Wechter, M., Schmidt-Bleek, F., and Lipschutz, M. E., 1970, An activation analysis technique for determining groups of trace elements in rocks and chondrites: Jour. Radioanal. Chemistry, v. 4, no. 2, p. 241–264.

Manning, D. C., 1970, Non-flame methods for mercury determination by atomic absorption, a review: Atomic Absorption Newsletter, v. 9, no. 5, p. 97–99.

Marinenko, John, May, Irving, and Dinnin, J. I., 1972, Determination of mercury in geologic materials by flameless atomic absorption spectrometry, *in* Geological Survey Research 1972: U.S. Geol. Survey Prof. Paper 800-B, p. B151–B155.

Morris, D. F. C., and Killick, R. A., 1964, The determination of mercury in rocks by neutron-activation analysis: Talanta, v. 11, p. 781–788.

CONTAMINATION CORRECTION FOR THE DOUBLE-SPIKE LEAD METHOD

By R. J. KNIGHT and MITSUNOBU TATSUMOTO,
Denver, Colo.

Abstract.—A refinement of the double-spike method for isotopic analyses for low-level lead has been developed. This is a mathematical analysis that can correct for experimental contamination, as well as for variable mass fractionation. This refinement can mathematically establish when the blank is significant.

Significant progress has recently been made in the isotopic analyses for lead. Methods have been developed (Akishin and others, 1947 ; Cameron and others, 1969; Tatsumoto, 1970) that make possible mass-spectrometer determinations of very small amounts of lead ($\approx$ 0.1 μg). A technique has been described by Catanzaro (1967) that eliminates variable mass discrimination for large samples ($\approx$500 μg). Compston and Oversby (1969) described a technique that uses a double spike to correct for variable mass discrimination for intermediate "ideal" samples (10–20 μg) in which the "discrimination is the sole source of experimental error" (p. 4339).

All analyses of lead have an inherent experimental error resulting from laboratory contamination. In order to analyze very small amounts of lead, this contamination must be precisely evaluated and not just qualitatively estimated as neglible. Using the method presented in this paper, one can mathematically establish if the contamination is significant and correct for it while correcting for variable mass discrimination. Both corrections are necessary for low-level analysis for lead. Unfortunately, the effect of contamination is a function of the specific sample and of the specific contamination as well as the relative amounts of sample and contamination, thus requiring a calculation for each sample. This calculation is reiterative inasmuch as a nonreiterative method similar to the methods introduced by Dallwitz (1970), Gale (1970), and Russell (1971), but correcting for contamination, has not been devised. Because a calculation is required for each sample and the calculation is reiterative, a computer is recommended even though the calculation can be done by desk calculator.

Acknowledgments.—We are grateful to V. M. Oversby, Australian National University, for detailed explanation of her computer program and to J. R. Richards, Australian National University, for reviewing the manuscript.

PRINCIPLES

This method is an extension of the double-spike method (Dietz and others, 1962) for strontium isotopic analysis (Dodson, 1963) and of the method presented by Compston and Oversby for lead (1969). Thus, any contamination error during low-level, double-spike analysis of strontium, lead, and other elements can be evaluated and eliminated by minor changes in this computer program.[1]

Let i and n represent different isotopes. Let $rinu$, $rinx$, $rinsp$ respectively represent the ratios of i/n in the unspiked sample, the mixture, and the tracer before fractionation has taken place.

When a sample is analyzed, the unspiked ratios have a contribution from the blank. Thus, the ratios $rinu$ are defined as

$$rinu = (Z_i^{sa} + Z_i^b)/(Z_n^{sa} + Z_n^b),$$

where Z^{sa} and Z^b are the moles or atoms of the noted isotope in the sample and in the laboratory contamination (or blank), respectively. Similarly, the ratios of the spiked run are defined as

$$rinx = (Z_i^{sa} + Z_i^{sp} + Z_i^c)/(Z_n^{sa} + Z_n^{sp} + Z_n^c),$$

where Z^{sp} is the atoms from the spike and Z^c the atoms from the contamination during the spiked run which may be different from the contamination (or blank) during the unspiked run, Z^b. Exclusion of the b and c terms introduces an error that can invalidate the double tracer results (Gale, 1970). The corrected equations and definitions for lead isotopes are listed in the section on equations for convenience

[1] Detailed documentation is in the following reference: Bowen, R. W., 1970, True composition (lead), Program C530, U.S. Geol. Survey Computer Program Documentation (unpub.).

U.S. GEOL. SURVEY PROF. PAPER 800-C, PAGES C215-C219

of use; therefore, only their derivation and usage shall be discussed here.

Most of the corrected equations can be derived from rearrangements of the above definitions. The mixture fractionation factor is defined similarly to the one by Compston and Oversby (1969), which is equivalent to the definitions of Dallwitz (1970) and Gale (1970). However, the unspiked fractionation factor cannot be similarly defined because the corrected ratios, *Cin*sa, which are from the mixture, do not contain a blank contribution, but the observed fractionated ratios, R*in*u, do contain a blank contribution. Therefore, the unspiked fractionation factor is derived by considering the experimental error measured by the fractional difference between the corrected ratios (*Cin*sa) and the measured fractionated ratios (R*in*u) to be the sum of the blank contribution, δ, and the true fractionation factor, FST,

$$\frac{\text{R}in\text{u} - \text{C}in\text{sa}}{\text{C}in\text{sa}} = \delta + \text{FST},$$

then using the definition of *rin*u to evaluate δ when FST = 0. Specifically, when FST = 0,

$$\frac{\text{R}in\text{u} - \text{C}in\text{sa}}{\text{C}in\text{sa}} = \frac{\text{QUE}n\ (rin\text{b} - \text{R}in\text{u})}{\text{C}in\text{sa}} = \delta\ ,$$

where $\text{QUE}n = Z_n^b / Z_n^{sa}$. Thus, when FST $\neq$ 0,

$$\text{FST} = \frac{\text{R}in\text{u} - \text{C}in\text{sa}}{\text{C}in\text{sa}} - \frac{\text{QUE}n\ (rin\text{b} - \text{R}in\text{u})}{\text{C}in\text{sa}}$$

The exact use of the program requires homogeneity of sample, uniformity of blank, and an assumption concerning loss of sample.

As in all lead isotope studies, the sample must be sufficiently homogeneous to make two aliquots, one spiked and one unspiked. A complete solution of the sample must be made and then divided into two portions if the sample cannot be assumed to be homogeneous.

A uniform blank is required. The number of moles or atoms of the blank, Z_i^c and Z_i^b, is determined independently but under the same conditions as the sample dissolution and subsequent chemical separations. The measured ratios from the reagent blanks can be used with slight modifications of the equations in the listing in this report or with the Compston and Oversby (1969) equations to determine the Z_i^c, Z_i^b, and the respective nonfractionated ratios.

One must assume that if a large part of the unspiked sample is lost, it is lost only after all the contamination has occurred. This assumption is necessary if one is to establish the ratio of blank to sample in the unspiked determination, that is, QUE6. If there is a large preferential loss of sample, then there is no way to correct precisely for the blank, and the only solution is to analyze absolute standards under exactly the same conditions. Small errors due to small losses of unspiked sample will be reduced.

In the use of this computer program, one question arises: What happens if the unspiked ratios of the blanks cannot be or were not determined? It is better to estimate the necessary ratios than to ignore the blank, because the blank can introduce unexpected errors (see "Discussion", this report; also Gale, 1970). A unique feature of estimating the blank ratios is that if the high and low values of the probable range in the ratios are used, then the difference in the answers will be the associated error due to contamination.

Another advantageous feature of this program is that it can establish when the blank is mathematically significant. The reagent blanks are significant when the reiterated ratios for zero blank and the ratios calculated by this program are >0.1 percent different. Again the percentage difference between the two methods is a mathematical measure of the contamination error. One can find the point when the blank becomes significant by calculating, by both methods, a test or hypothetical sample that is near the composition of the real samples and that has been increasingly contaminated.

EQUATIONS

Let R*in*u and R*in*x represent the fractionated ratios of *i*/*n* in the unspiked sample and mixture, respectively. Let *rin*sp be the true ratios of the spike. Because this method is reiterative, let *Cin*sa and *Cin*x represent the corrected approximations or the successive reiterations of the ratios in the sample and mixture. These notations are adapted from Compston and Oversby (1969).

$$Q_{7C} \equiv Z_7^c / Z_7^{sp}\ , \qquad (1)$$

where Z_7^c is the atoms or moles of Pb^{207} determined from a reagent blank, and Z_7^{sp} is the atoms or moles of Pb^{207} known from the amount of spike added.

$$Q_7 = \frac{\text{R67x} - \text{r67sp} + [\text{R67x} - \text{r67c}]\ Q_{7C}}{\text{R67u} - \text{R67x}} = \frac{Z_7^{sa}}{Z_7^{sp}}\ , \qquad (2)$$

where *rin*c is the nonfractionated composition ratio of the contamination.

$$\text{C47x} = \frac{\text{r47sp} + Q_7\ (\text{R47u}) + Q_{7C}\ (\text{r47c})}{1 + Q_7 + Q_{7C}}\ , \qquad (3)$$

$$F^n = \frac{\text{R47x} - \text{C47x}}{\text{C47x}}\ , \qquad (4)$$

$$\text{C86x} = \text{R86x}/(1 - 2/3\ F^n)\ , \text{and} \qquad (5)$$

$$\text{C67x} = \text{R67x}/(1 + 1/3\ F^n). \qquad (6)$$

The numbers "2/3" and "1/3" in equations 5 and 6 refer to the fractional difference in mass. (See Compston and Oversby, 1969, p. 4339.) For nonideal fractionation, the numbers "2/3" and "1/3" may not be exact, but calibrations can be made to obtain exact numbers (Ozard and Russell, 1970; Doe and others, 1967).

$$Q_6 \equiv Z_6^{sa}/Z_6^{sp} = Q_7(R67u)/r67sp, \quad (7)$$

$$Q_{6c} \equiv Z_6^{c}/Z_6^{sp} = Q_{7c}(r67c)/r67sp, \text{ and} \quad (8)$$

$$C86sa = (1 + 1/Q_6)C86x - (1/Q_6)(r86sp) + (Q_{6c}/Q_6)[C86x - r86c], \quad (9)$$

where C*in*sa is the ratio corrected for blank and fractionation.

$$QUE6 \equiv \frac{Z_6^b}{Z_6^{sa}} = \frac{Z_6^b}{Q_6} \times \frac{1}{Z_6^{sp}} \times \frac{1}{\frac{\text{wt sap}}{\text{wt sax}}}, \quad (10)$$

where wt sap and wt sax are the weights of the sample in the unspiked or composition run and in the mixture, respectively; and where Z_6^b is determined from a reagent blank.

$$FST = \frac{R86u - C86sa}{C86sa} - \left(\frac{r86b - R86u}{C86sa}\right)(QUE6), \quad (11)$$

where r86b is the composition ratio of the blank which can be different from r86c.

$$C67sa = \left[\frac{R67u}{1 + QUE6 - (R67u)(r76b)(QUE6)}\right]\left[\frac{1}{1 - 1/2\ FST}\right]. \quad (12)$$

Note that r76b would be 207/206 of the blank.

$$QUE7 = QUE6\ (C67sa)/r67b, \text{ and} \quad (13)$$

$$C47sa = \frac{[R47u(1 + QUE7) - (r47b)(QUE7)}{1 - 3/2\ FST}. \quad (14)$$

Again, the numbers "1/2" and "3/2" in equations 12 and 14 refer to the fractional difference in mass. (See Compston and Oversby, 1969, p. 4339).

At this point, reiterations should be made to equation 2 until successive values of C*in*sa change insignificantly, that is, <0.1 percent. However, QUE6 must be set to zero for each following reiteration so that correction for the blank is not made twice in the ratios C67sa and C47sa.

DISCUSSION

The error due to calculations that do not consider contamination depends on the specific sample, the particular contamination, and the relative amounts of sample and contamination. Nevertheless, to help visualize the error we have necessarily chosen an arbitrary test sample (208/206 = 2.2182; 206/207 = 1.0488; and 204/207 = 0.064910) and two blanks, L and M, whose ratios are 208/206 = 2.088, 1.941; 206/207 = 1.16, 1.29; and 204/207 = 0.0641, 0.0633, respectively. The sample was contaminated by each blank at varying levels, then fractionated proportionally to the difference in mass to simulate actual data. All the samples were 1 μg to emphasize any differences between the calculated ratios and the known answer that would occur for low-level analysis; however, the same results would be generated for other size samples and the same percentage contamination. These test data are then treated by this program and also by a program that disregards contamination.

The results of the treatments are given in table 1 and figures 1 and 2. For all analyses our program yields data to within 0.1 percent Δ, where percent Δ is the value calculated minus the true value divided by the true value in percent. The data from the other program are outside the 0.1-percent error for all contamination levels greater than 0.01 μg or 1 percent. The arrows in the figures show where the indicated points would move if the blank from the composition run were subtracted

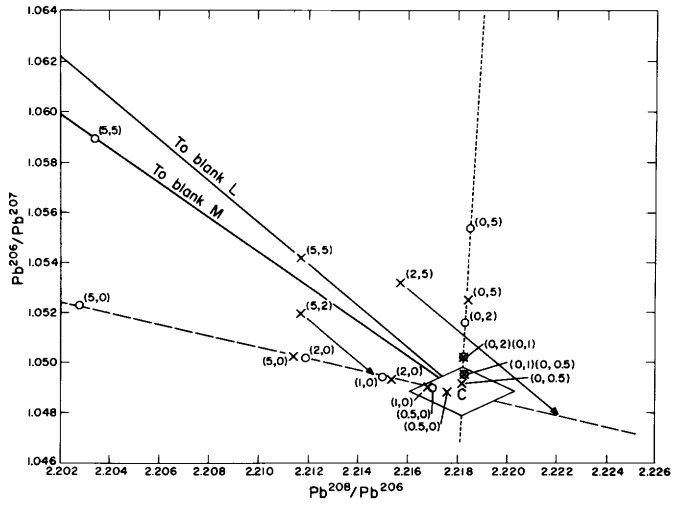

Figure 1.—Reiterated lead ratios of Pb^{206}/Pb^{207} versus Pb^{208}/Pb^{206} produced by neglecting contamination. The long-dashed line indicates the trend of ratios if contamination is in the mixture analyses only. The short-dashed line indicates the trend of analyses if contamination is in the unspiked analyses only. The solid lines with arrows show where the indicated ratios would move if the blanks were subtracted after reiteration. The plain solid lines connect the test sample with the blanks, L and M, which are not shown. C, test sample (common lead-composition); diamond indicates 0.1-percent limits of test sample; X indicates contamination by L lead; open circle indicates contamination by M lead. Pairs of numbers in parentheses indicate percent contamination in mixture and in sample, respectively. For the overlapping points, the first set of parentheses indicates the percent contamination by L lead; the second set indicates the percent by M lead.

Table 1.—*Errors, in percent, produced without contamination correction*

[L, lead whose ratios are 208/206=2.088; 206/207=1.16; 204/207=0.0641. M, lead whose ratios are 208/206=1.941; 206/207=1.29; 204/207=0.0633. Percent Δ, value calculated minus the true value, divided by the true value in percent]

Percent contamination By L lead	By M lead	208/206	Percent Δ	206/207	Percent Δ	204/207	Percent Δ	206/204	Percent Δ	207/204	Percent Δ	208/204	Percent Δ
COMMON LEAD													
0	0	2.2182	.....	1.0488	.....	0.064910	.....	16.158	.....	15.406	.....	35.841	.....
Contamination in mixture only													
0.5	0	2.2176	<0.1	1.0488	<0.1	0.064921	<0.1	16.155	<0.1	15.403	<0.1	35.825	<0.1
0	.5	2.2169	<.1	1.0489	<.1	.064953	<.1	16.149	<.1	15.396	<.1	35.800	-.11
1	0	2.2168	<.1	1.0490	<.1	.064954	<.1	16.150	<.1	15.396	<.1	35.801	-.11
0	1	2.2150	-.14	1.0494	<.1	.065033	+.19	16.136	-.14	15.377	-.19	35.742	-.28
2	0	2.2154	-.13	1.0493	<.1	.065016	+.16	16.139	-.12	15.381	-.16	35.755	-.24
0	2	2.2119	-.28	1.0502	+.13	.065171	+.40	16.115	-.27	15.344	-.40	35.644	-.55
5	0	2.2114	-.31	1.0503	+.14	.065193	+.44	16.110	-.30	15.339	-.43	35.627	-.60
0	5	2.2028	-.69	1.0523	+.33	.065577	+1.03	16.047	-.69	15.249	-1.02	35.348	-1.38
Contamination in composition only													
0.5	0	2.2182	<0.1	1.0492	<0.1	0.064874	<0.1	16.173	<0.1	15.414	<0.1	35.875	<0.1
0	.5	2.2183	<.1	1.0495	<.1	.064838	-.11	16.186	+.17	15.423	+.11	35.907	+.18
1	0	2.2183	<.1	1.0495	<.1	.064838	-.11	16.186	+.17	15.423	+.11	35.907	+.18
0	1	2.2183	<.1	1.0503	+.14	.064770	-.22	16.216	+.36	15.439	+.21	35.971	+.36
2	0	2.2183	<.1	1.0503	+.14	.064770	-.22	16.216	+.36	15.439	+.21	35.971	+.36
0	2	2.2183	<.1	1.0516	+.26	.064602	-.47	16.278	+.74	15.479	+.47	36.113	+.75
5	0	2.2185	<.1	1.0525	+.35	.064571	-.52	16.300	+.88	15.487	+.53	36.161	+.89
0	5	2.2188	<.1	1.0554	+.63	.064169	-1.56	16.518	+2.23	15.651	+1.59	36.657	+2.28
Contamination in both composition and mixture													
5	0	2.2117	-0.29	1.0542	+0.51	0.064869	<0.1	16.251	+0.58	15.416	<0.1	35.943	-0.28
0	5	2.2035	-.66	1.0592	+.99	.064840	-1.10	16.336	+1.10	15.422	+.10	35.995	+.43
*5_x, 2_u	.....	2.2116	-.30	1.0519	+.30	.065070	+.25	16.166	<.1	15.368	-.25	35.752	-.25
(†)	.....	2.2142	-.18	1.0497	<.1	.065089	+.28	16.127	-.19	15.364	-.28	35.709	-.37
*2_x, 5_u	.....	2.2157	-.11	1.0532	+.42	.064694	-.38	16.280	+.76	15.457	+.33	36.071	+.64
(†)	.....	2.2223	+.19	1.0479	+.1	.064730	-.28	16.189	+.19	15.449	+.28	35.976	+.38
RADIOGENIC LEAD													
0	0	1.0106	.....	1.96232	.....	0.010488	.....	187.10	.....	95.347	.....	189.08	.....
Contamination in mixture only													
0.5	0	1.0141	+0.3	1.9589	-0.17	0.010441	-0.45	187.63	+0.28	95.781	+0.46	190.27	+0.63
Contamination in composition only													
0.5	0	1.0104	<0.1	1.9616	<0.1	0.010828	+3.24	181.16	-3.17	92.352	+3.14	183.04	-3.19

*Numbers represent the percentage contamination in the mixture x and in the unspiked run u.
†Ratios obtained by subtracting the blank after reiteration.

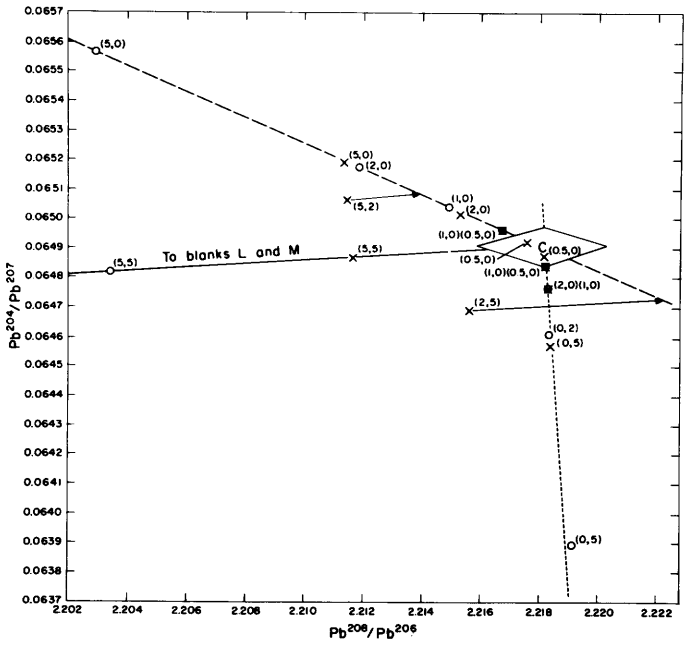

Figure 2.—Reiterated lead ratios of Pb^{204}/Pb^{207} versus Pb^{208}/Pb^{206} produced by neglecting contamination. Refer to figure 1 for explanation of lines and symbols. The plain solid lines which connect the test sample with blanks L and M are coincident in this figure.

after reiteration. Only for the special circumstance when the levels of contamination in the mixture and in the unspiked sample runs are the same is it valid to subtract contamination after reiteration, because only then are the three points of the contamination, the calculated value, and the sample on a straight line.

To emphasize that the blank error is a function of the specific sample, two extremes can be taken. If the contaminant and sample have the same composition, no amount of contamination can change the ratios. If the sample is radiogenic material, 206/207 = 1.96232, 204/207 = 0.010488, and 208/206 = 1.0106, and the contaminant is the L lead, then 0.5 percent contamination will introduce an error of 3 percent in the calculations, which upon subtracting the blank after reiteration reduces only to 0.5 percent. (See table 1.) Lunar samples, being very radiogenic, require the use of this program to eliminate contamination error.

In order to evaluate the maximum amount of blank for which this program can correct, the test sample was contaminated with L and M lead at 10-percent intervals up to 50 percent of the sample. At 50 percent in both mixture and composition, an error of 0.25 percent in the 204/207 ratio was detected, whereas the other ratios were within 0.1 percent. At 50 percent, the contaminant is becoming the sample and the sample is contaminating it.

SUMMARY

We have presented a program that can eliminate contamination errors and mass fractionation using modified double-spike equations. The program can also precisely evaluate when the blanks are significant and what percentage of error is due to contamination. We have shown this program to be essential to the analysis of small amounts of lead isotopes.

REFERENCES

Akishin, P. A., Nikitin, O. T., and Panchenkov, G. M., 1947, A new effective ionic emitter for the isotopic analyses of lead: Geokhimiya, v. 5, p. 429.

Cameron, A. E., Smith, D. H., and Walker, R. L., 1969, Mass spectrometry of nanogram-size samples of lead: Anal. Chemistry, v. 41, no. 3, p. 525–526.

Catanzaro, E. J., 1967, Triple-filament method for solid-sample lead isotope analysis: Jour. Geophys. Research, v. 72, no. 4, p. 1325–1327.

Compston, W., and Oversby, V. M., 1969, Lead isotopic analysis using a double spike: Jour. Geophys. Research, v. 74, no. 17, p. 4338–4348.

Dallwitz, M. J., 1970, Fractionation corrections in lead isotopic analysis: Chem. Geology, v. 6, no. 3, p. 311–314.

Dietz, L. A., Pachucki, C. F., and Land, G. A., 1962, Internal standard technique for precise isotopic abundance measurements in thermal-ionization mass spectrometry: Anal. Chemistry, v. 34, no. 6, p. 709–710.

Dodson, M., 1963, A theoretical study of the use of internal standards for precise isotopic analysis by the surface ionization technique: Jour. Sci. Instruments, v. 40, p. 289–295.

Doe, B. R., Tatsumoto, Mitsunobu, Delevaux, M. H., and Peterman, Z. E., 1967, Isotope-dilution determination of five elements in G-2 (granite), with a discussion of the analysis of lead, *in* Geological Survey Research 1967: U.S. Geol. Survey Prof. Paper 575-B, p. B170–B177.

Gale, N. H., 1970, A solution in closed form for lead isotopic analysis using a double spike: Chem. Geology, v. 6, no. 3, p. 305–310.

Ozard, J. M., and Russell, R. D., 1970, Discrimination in solid source lead isotope measurement: Earth and Planetary Sci. Letters, v. 8, no. 5, p. 331–336.

Russell, R. D., 1971, The systematics of double spiking: Jour. Geophys. Research, v. 76, no. 20, p. 4949–4955.

Tatsumoto, Mitsunobu, 1970, U-Th-Pb age of Apollo 12 rock 12012: Earth and Planetary Sci. Letters, v. 9, no. 2, p. 193–200.

AN EVALUATION OF THE USE OF HERBICIDES TO CONTROL AQUATIC WEEDS IN SIX PENNSYLVANIA RECREATION LAKES

By JAMES L. BARKER, Harrisburg, Pa.

Prepared in cooperation with the Pennsylvania Department of Environmental Resources, Bureau of State Parks

Abstract.—The application of the herbicides diquat, Kuron, and Aquathol Plus to one-third or less of the surface areas of six Pennsylvania recreation lakes was found to have no serious or persistent effects upon the environments of the lakes. However, reductions in dissolved oxygen of up to 44 percent of saturation and reductions in phytoplankton of up to 95 percent were measured after treatment. Diquat applied at a rate of 0.3 to 1.25 gallons per acre was highly successful in providing seasonal control of *Potamogeton crispus, P. natans,* and *P. epihydrus.* Kuron applied at a rate of 0.64 to 1.3 gallons per acre to species of *Nuphar, Nymphaea,* and *Brasenia* required a minimum of two successive treatments, 3 months apart, to achieve 90-percent control. The use of Aquathol Plus at a rate of 2.9 gallons per acre was successful in giving two seasons' control of *Myriophyllum humile, Utricularia purpurea, Nuphar variegatum,* and *Brasenia schreberi* in a soft-water lake. The effectiveness of the Aquathol Plus appears to have been greater on the same plant species than that of the diquat-Kuron applications in waters of similar physicochemical characteristics.

In the long-term cycle of change in the aquatic environment, there is a natural tendency for every lake to become dry land. The aquatic transformation from lake to marsh to dry land is likely to be accelerated or delayed by man through his varied alteration of environmental forces, but inevitably the geological sequence is fulfilled.

The increase in abundance of aquatic vascular plants is the phase of the geologic transformation that is most easily recognized by those who habitually visit a lake. When the plants become so abundant that they interfere with man's recreational, commercial, or esthetic uses, there is generally sufficient justification to initiate control measures. In 1969, chemical control was the only practical and economical method available for the large-scale eradication of unwanted weeds.

The degree of plant eradication that can be tolerated without disrupting the ecosystem has not been determined, and, no doubt, it is different for all lakes. However, the dependence of higher forms of life upon plants is unquestioned and is probably just as great in water as it is on land, perhaps even greater. The importance of plantlife to fish and wildlife and to cycles of nutrients and respiratory gases has been discussed at length by Burdick (1961), Reid (1961), and others.

In cooperation with the Pennsylvania Department of Environmental Resources, Bureau of State Parks, the U.S. Geological Survey conducted a study to map and identify the distribution and abundance of hydrophytes at six State-owned recreation lakes; measure the effectiveness of the 1969 aquatic-herbicide program of the Bureau of State Parks upon the target species of plants; document any reestablishment or plant succession within the areas of eradication; measure selected physical and chemical parameters, including nutrient levels before and after treatment; and measure the effect of the treatment upon the plankton community.

The purpose of this report is to present the data gathered during the investigation and evaluate the use of herbicides in controlling aquatic weeds in the treated lakes.

DESCRIPTION OF STUDY

The lakes selected for study were Conewago Lake (Gifford Pinchot State Park) in the Triassic Lowland of south-central Pennsylvania; four lakes in the Pocono Plateaus section—Promised Land Lake and Lower Lake (Promised Land State Park), Tobyhanna Lake (Tobyhanna State Park), and Gouldsboro Lake (Gouldsboro State Park); and two lakes in the Allegheny High Plateaus section—Lake Jean (Ricketts Glen State Park) and Black Moshannon Lake (Black Moshannon State Park). Gouldsboro Lake was selected as the untreated or ecological control because of its chemical similarity and proximity to the other Pocono lakes and because it had never received aquatic-herbicide treatment.

The surface areas of the lakes range from 170 to 422 acres. All seven lakes are used for swimming, fishing, and boating. Conewago Lake is also used as a source of potable water for the park facilities.

U.S. GEOL. SURVEY PROF. PAPER 800-C, PAGES C221-C232

The lakes are located within State-park boundaries in the northeastern, central, and south-central counties. All the lake basins are predominantly or solely within forested areas, and they receive no appreciable fertilization other than that contained in natural runoff.

Promised Land, Lower, Gouldsboro, and Tobyhanna Lakes are situated on infertile shale and sandstone of the glaciated Catskill Formation. Lake Jean and Black Moshannon Lake are located on infertile sandstone, shale, and conglomerate of the Pocono Group. Conewago Lake is located on moderately fertile sandstone and shale of the Gettysburg Shale and on diabase (Pennsylvania Geol. Survey, 1960). Figure 1 shows the location of the lakes.

All the lakes, with the exception of Conewago, have many characteristics of dystrophic, or infertile, bog lakes. Productivity, both qualitative and quantitative, is limited by the small amount of inorganic nutritive substances. Their waters range from weakly to strongly brown, are typically soft, and are generally acidic. Conewago Lake is characterized as mesotrophic, or moderately fertile, owing primarily to the greater fertility of the basin soils (Ott and others, 1971).

Previous control measures

Conewago Lake has received applications of copper sulfate for both weed and algae control since 1964. In 1965, a mechanical harvesting machine was also used in an attempt to control the growth of rooted plants. In June 1968, 29 percent of the lake surface was treated with Ortho Diquat at the rate of 2 gallons per acre to control a heavy infestation of curly-leaf pondweed (*Potamogeton crispus*). The treatment had spectacular but temporary success, as the plants grew back heavier than ever by May 1969. None of the other lakes evaluated had ever received herbicide treatment.[1]

Investigational methods

During April 1969, immediately after removal of the ice cover, each lake was visited for the collection of water and lake-sediment samples for chemical analysis. The lakes were visited again just prior to herbicide treatment to obtain physical and chemical data, map the distribution of aquatic vascular plants, and obtain a sample of the plankton for quantitative analysis.

Posttreatment samples collected for physical and chemcial data coincide approximately with the 7th, 14th, 28th, and 90th days after treatment. Each lake was revisited the following spring and summer for the primary purpose of

[1] Harmon, William, 1969, Aquatic weed project report: Pennsylvania Dept. of Environmental Resources, Bureau of State Parks, duplicated, 46 p.

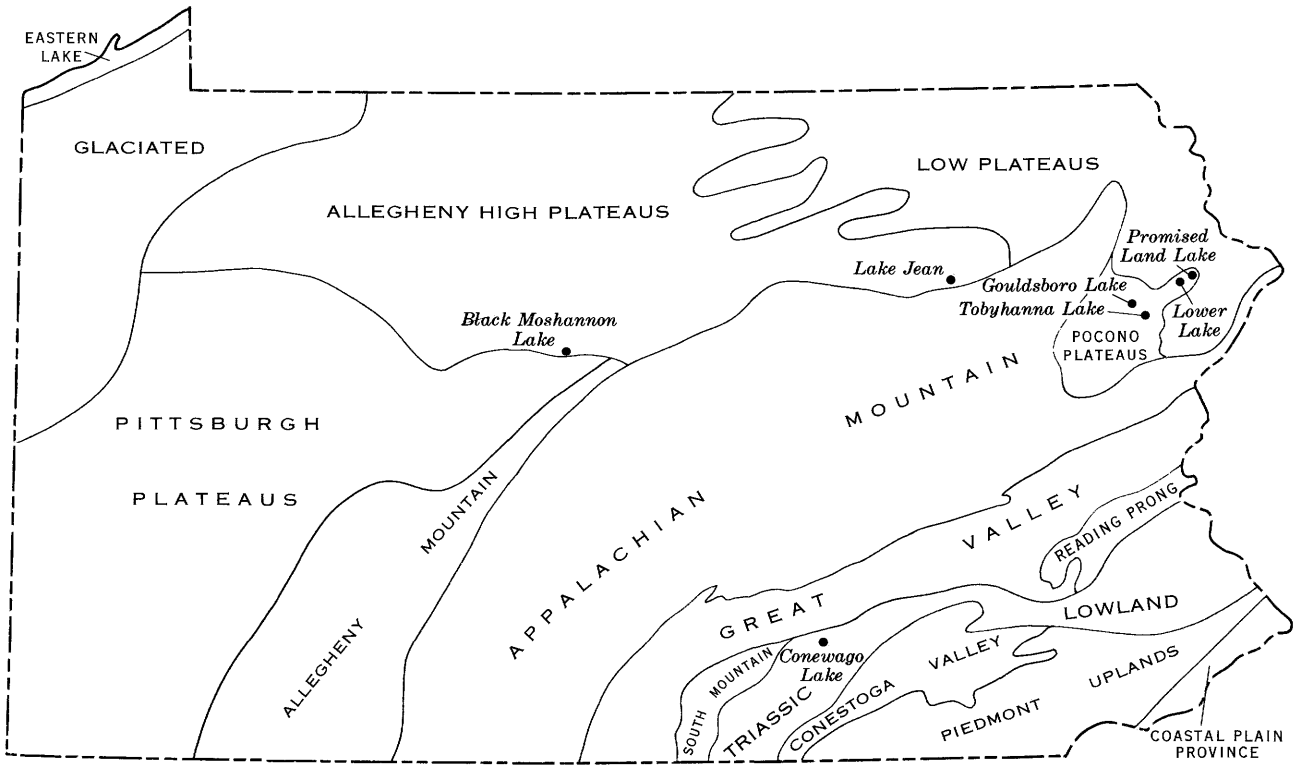

Figure 1.—Location of lakes and the physiographic sections of Pennsylvania. (Section names are those of the Pennsylvania Topographic and Geologic Survey.)

determining nutrient concentrations and documenting reinfestation.

Physical, chemical, and biological data were collected at a point believed to be representative of the lake water. Sample collection and analytical methods used were in accord with the methodology described by Rainwater and Thatcher (1960) and the American Public Health Association and others (1965). Hydrophytes and plankton were identified with the keys prepared by Muenscher (1964), Prescott (1964), and Needham and Needham (1962).

PRESENTATION OF DATA

Distribution of aquatic plants

Occurrence of the major species of submersed and floating-leaved aquatic plants is presented in table 1 for each of the lakes studied. There is a distinct difference in the species composition of the plant communities between Conewago Lake and the other lakes. This difference is attributed to the dissimilarity in water chemistry and substrate characteristics.

Table 1.—*Occurrence of major submersed and floating-leaved aquatic plants at lakes studied*

Common name	Scientific name	Lake						
		Conewago	Promised Land	Lower	Tobyhanna	Jean	Black Moshannon	Gouldsboro
Curly-leaf pondweed	*Potamogeton crispus*	X	..	..	..	..	..	..
	spirillus	X	..	..	..	..	..	..
	nodosus	X	..	..	..	..	..	..
	epihydrus	..	X	..	..	..	X	X
	natans	..	..	..	..	..	X	..
Bushy pondweed	*Najas flexilis*	X	..	..	..	..	..	..
	minor	X	..	..	..	..	..	..
Northern water milfoil.	*Myriophyllum exalbescens.*	X	..	..	..	..	..	..
Lowly water milfoil.	*Myriophyllum humile*	..	X	X	X	X	X	X
Coontail	*Ceratophyllum demersum.*	X	..	..	..	..	..	..
Waterweed	*Anacharis canadensis*	X	..	..	..	..	..	X
Water celery	*Vallisneria americana*	X	X	X	..	..	..	X
Bladderwort	*Utricularia purpurea*	..	X	X	X	X	..	X
	geminiscapa	..	..	..	..	..	X	..
	gibba	..	..	..	..	..	X	..
Spatterdock	*Nuphar variegatum*	..	X	X	X	X	..	X
	advena	..	..	..	..	..	X	..
White water lily	*Nymphaea odorata*	..	X	X	..	X	..	..
	tuberosa	..	..	..	..	..	X	..
Watershield	*Brasenia schreberi*	..	X	X	X	X	X	X
Water starwort	*Callitriche heterophylla.*	..	..	..	X	..	..	..
Stonewort	*Chara* sp.	X	..	..	..	..	..	..
	Nitella sp.	..	X	X	..	..	..	..
Bog moss	*Sphagnum* sp.	..	X	X	X	..	..	..
Total		10	9	8	6	5	8	7

Lake sediments

Chemical properties of lake sediment were determined from samples collected during April 1969. A summary of the sediment data is presented in table 2.

The most outstanding of the lake-sediment characteristics is the high percentage of organic matter in the sediment of all the lakes except Conewago. This high percentage reflects the bog- or mountain-type lake habitat characteristic of the Allegheny High Plateaus and Pocono Plateaus physiographic sections.

The lakes containing a highly organic substrate lacked high colonization by rooted submersed species. Evidently the substrate is somewhat inhospitable to many species for mechanical and (or) chemical reasons.

Herbicide treatment

The initial 1969 herbicide applications to the six lakes were begun June 3 and completed by June 9. Three lakes were re-treated between September 5 and 12. Most herbicides were injected beneath the lake surface to protect the applicator and eliminate problems of drift onto terrestrial plants bordering the lake. The only exception to the underwater application was at Lower Lake, where Kuron was applied to the surface. All material was applied from an airboat and distributed by the turbulence produced by the craft.

Ortho Diquat is used for controlling all types of aquatic vegetation but is most often used on submersed species of weeds. The manufacturer recommends that it be applied at the rate of 1 to 2 gallons per surface acre. Lipinot (1968) recommends concentrations of 0.25 to 1.0 mg/l (milligram per liter) for the common submersed species.

Kuron is used on submersed, emersed, and floating-leaved plants. The manufacturer recommends that it be applied at the rate of 1.36 gallons per acre-foot (2.0 mg/l).

Aquathol Plus is a combined contact and systemic action herbicide recommended for submersed, emersed, and floating-leaved plants. The manufacturer recommends an application rate of 1 to 4 mg/l or ½ to 2 ⅛ gallons per acre-foot of water. (See table 3 for chemical formulations of the three herbicides.)

Because of the potential hazard to man from the treatment of water with herbicides, all treated lakes were closed for 3 to 14 days after application as prescribed on the manufacturer's label.

A complete summary of the treatment areas, herbicide(s) applied, application rate, date(s) of treatment, and target species is presented in table 4. Maps of the treated lakes describing the sampling site, treatment area(s), and distribution of submersed and floating plant species prior to treatment are illustrated in figures 2–7.

Table 2.—*Chemical properties of lake sediments, April 1969*

Lake	pH	Total nitrogen (percent)	Organic matter (percent)	Carbon-nitrogen ratio	Total phosphorus as P_2O_5 (percent)	Available phosphorus (lb per acre)	Cation exchange capacity (me per 100 g)	Exchangeable cations (me per 100 g)					Unsaturation (percent)
								Na	K	Ca	Mg	H	
Conewago	5.4	0.194	6.6	18.3	0.014	0	24.70	0.10	0.23	11.25	9.37	3.75	14.9
Promised Land ...	4.9	1.780	56.4	17.2	.354	13	80.80	.13	.46	67.50	7.76	4.95	6.1
Lower	5.1	1.800	55.4	16.6	.212	0	125.46	.10	.16	23.50	6.25	95.45	76.8
Tobyhanna	4.6	1.230	78.9	35.4	.130	0	104.70	.10	.18	24.00	6.25	74.17	70.7
Jean	4.7	1.411	46.1	17.6	.212	10	54.48	.52	.33	7.00	2.08	44.55	81.7
Black Moshannon .	4.6	.567	17.7	16.8	.159	10	38.60	.16	.23	7.00	2.08	28.13	72.9
Gouldsboro	4.9	1.495	75.3	27.1	.190	0	139.61	.13	.20	75.00	8.75	55.33	32.5

Table 3.—*Names and formulations of herbicides used*

Chemical	Trade name (manufacturer)	Chemical formulation and amount of active ingredient
Diquat dibromide	Ortho Diquat (Chevron Chemical Co.)	[6, 7 dihydrodipyrido (1, 2-a: 2′, 1′-c) pyrazinediium dibromide.] Active ingredient 35.3 percent by weight or 2 pounds of cation per gallon.
Potassium endothal–silvex combination.	Aquathol Plus (Pennwalt Chemical Corp.)	1, 2-dicarboxy- 3,6-endoxcyclohexane plus potassium salt of 2 (2, 4, 5-trichloro-phenoxy) propionic acid. Contains 1.7 pounds of endothal acid equivalent and 2.4 pounds of silvex acid equivalent per gallon.
Liquid silvex ester ...	Kuron (Dow Chemical Co.)	[2- (2, 4, 5-trichloro-phenoxy) propionic acid] propylene, glycol butyl ether esters. Silvex acid equivalent 4.0 pounds per gallon.

EFFECTIVENESS OF HERBICIDES

Ortho Diquat

The use of Ortho Diquat to control the submersed species at five of the lakes met with varying degrees of success. The relative success of the treatments, based upon the percentage of treated area cleared, is summarized in table 4.

Diquat, applied for the second consecutive year, achieved spectacular results in killing *Potamogeton crispus* at Conewago Lake at the applied rate of 1.25 gallons per acre (0.25 mg/l). Within 4 days of treatment, the stems and leaves of plants within the treatment area had become flaccid and chlorotic and had separated from the root system. By the 14th day after treatment, the plants had turned brown and had sunk to the bottom. *P. crispus* was killed throughout the remainder of the lake by the diquat treatment within 12 days after its application.

Extensive sprouting of *P. crispus* winterbuds within the treated area was observed by the 90th day after treatment. Many of the sprouts were found free-floating with 12 inches or more of new growth and a developing root system.

Northern water milfoil, *Myriophyllum exalbescens*, was only partly controlled at Conewago Lake by the diquat, and it too was found to be regrowing in the treatment area within 90 days after treatment.

The other species at Conewago Lake, namely *Anacharis canadensis, Najas flexilis, N. minor, Ceratophyllum demersum, Potamogeton nodosus, P. spirillus,* and *Chara* sp., were not controlled by the diquat at the 1.25-gallons-per-acre rate. The use of diquat at lakes Jean, Promised Land, Lower, and Black Moshannon to control growths of pondweed (*Potamogeton natans*), lowly water milfoil (*Myriophyllum humile*), and bladderwort (*Utricularia* sp.) had variable results.

An estimated 85 percent of the *Potamogeton natans* was controlled at Black Moshannon Lake. Disintegration of *P. natans* tissue was observed by the 16th day after treatment. No regrowth was observed by the 90th day after treatment.

Hiltibran (1965) reported similar results with diquat in central Illinois ponds. His studies indicated that *P. crispus* and *M. exalbescens* could be controlled by applying diquat at the rate of 1.0 gallon per acre, whereas *N. flexilis* required 1.5 gallons per acre, and *A. canadensis* and *C. demersum* required 2.0 gallons per acre.

Yeo (1967), conducting weed toxicity studies with diquat at Davis, Calif., found similar results. While curly-leaf pondweed and elodea were controlled 6 and 8 weeks, respectively, by a concentration of 0.25 mg/l, coontail and milfoil required 0.50 mg/l and *Chara* tolerated 1.0 mg/l. Underlying shoots of curly-leaf pondweed also were resistant to 1.0 mg/l.

At Lake Jean, Lower Lake, and Promised Land Lake, lowly water milfoil was killed within 14 days after treatment, but some regrowth of plant fragments was observed by the 90th day. Bladderwort, on the other hand, was only partly controlled with diquat applied at the rate of 0.3 to 0.9 gallon per acre.

Kuron

The first application of Kuron at concentrations of 1.0 to 2.0 mg/l to control spatterdock (*Nuphar* sp.), white water lily

Table 4.—*Summary of 1969 aquatic-weed control program*

Lake	Total acres	Total acres treated	Percent treated	Herbicide and rate applied: Submersed species	Herbicide and rate applied: Floating species	Date applied	Target species (F, floating; S, submersed)	Effective control (percent)
Conewago...	340	125	37	Diquat 157 gal per 125 acres (0.25 mg/l)	.....	6-9-69	*Potamogeton crispus* (S)	99
							Myriophyllum exalbescens (S)	40
							Ceratophyllum demersum (S)	20
							P. spirillus (S)	0
							P. nodosus (S)	0
Promised Land	422	30	7	Diquat 10 gal per 30 acres (0.25 mg/l)	Kuron 20 gal per 30 acres (1.0 mg/l)	6-3-69	*Nuphar variegatum* (F)	70
							Nymphaea odorata (F)	60
							Brasenia schreberi (F)	85
							Utricularia purpurea (S)	30
Lower	173	68	39	Diquat 35 gal per 68 acres (0.25 mg/l)	Kuron 16 gal per 25 acres (1.0 mg/l)	6-3-69	*Nuphar variegatum* (F)	80
							Brasenia schreberi (F)	90
							Utricularia purpurea (S)	20
							Myriophyllum humile (S)	25
		25	14	.....	Kuron 25 gal per 25 acres (1.5 mg/l)	9-5-69		
Tobyhanna..	170	52	31	Aquathol Plus 150 gal per 52 acres (1.0 mg/l)		6-6-69	*Nuphar variegatum* (F)	90
							Brasenia schreberi (F)	90
							Utricularia purpurea (S)	50
							Myriophyllum humile (S)	70
Jean	254	90	35	Diquat 80 gal per 90 acres (0.25 mg/l)	Kuron 15 gal per 15 acres (1.5 mg/l)	6-4-69	*Nuphar variegatum* (F)	80
							Nymphaea odorata (F)	75
							Brasenia schreberi (F)	80
							Utricularia purpurea (S)	70
							Myriophyllum humile (S)	85
		15	6	.....	Kuron 16 gal per 15 acres (1.5 mg/l)	9-11-69		
Black Moshannon.	250	49	20	Diquat 45 gal per 45 acres (0.25 mg/l)	Kuron 44 gal per 35 acres (2.0 mg/l)	6-4-69	*Nuphar advena* (F)	60
							Nymphaea sp. (F)	50
							Brasenia schreberi (F)	75
							Potamogeton natans (S)	85
							P. epihydrus (S)	85
		25	10	.....	Kuron 33 gal per 25 acres (2.0 mg/l)	9-12-69		

(*Nymphaea* sp.), and watershield (*Brasenia* sp.) had little effect, except on *Brasenia.* A second application during early September achieved control of 50 to 90 percent of the floating-leaved plants in the treated areas at all lakes. Regrowth of floating-leaved species during the spring of 1970 was heavy only at Black Moshannon Lake.

It was observed that in most of the treated areas the spatterdock and white water lily were curled and appeared to be dying within 2 weeks after the first treatment. Subsequent inspections found the plants to be in apparent good health and vigorously sprouting new leaves. On the other hand, watershield was controlled to a high degree, and only limited regrowth was observed through the remainder of the growing season. White water lily appeared to have made the greatest regrowth and, in some lakes, became the dominant species where spatterdock foliage was removed.

No appreciable drift of Kuron out of the treatment areas at any of the lakes was detected. Some curling of spatterdock stems up to 200 yards from the treatment area was noticed at Promised Land Lake, but the plants recovered and appeared healthy for the remainder of the summer.

Aquathol Plus

The use of Aquathol Plus at Tobyhanna Lake at the rate of 1.0 mg/l for the control of water milfoil, bladderwort, spatterdock, and watershield was highly successful. The plants within the treatment area showed effects of the herbicide when the lake was sampled 6 days after treatment. Aquatic vegetation throughout the remainder of the lake also showed signs of being affected, indicating considerable drift of the liquid herbicide.

The stems of the spatterdock and watershield were corkscrewed and flaccid 6 days after treatment. Water milfoil and bladderwort had turned black and flaccid and had sunk to the bottom. Nearly all the spatterdock throughout the lake was dead 27 days after treatment, and the watershield leaves were turning shades of red, yellow, and brown.

Approximately 90 days after treatment the lake was nearly clear of weeds, and little regrowth was observed. Some water milfoil, bladderwort, and spatterdock near the inflow were not killed.

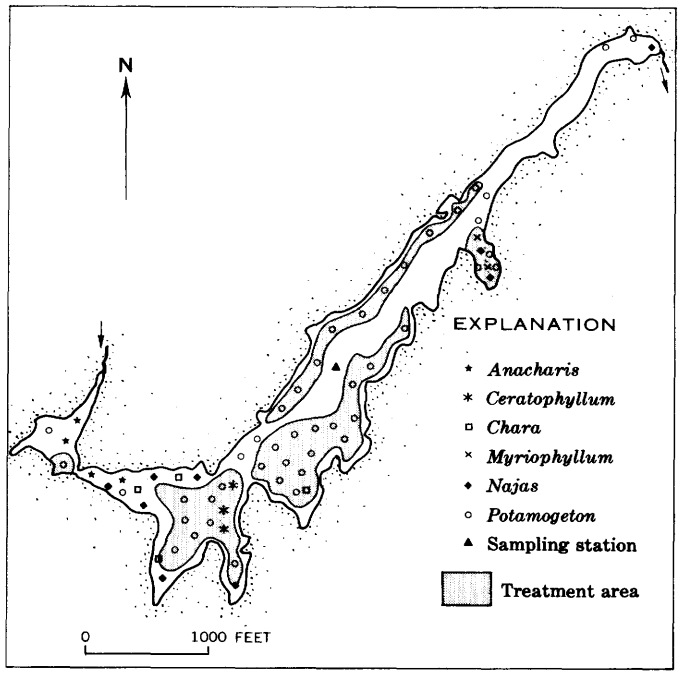

Figure 2.—Map showing location of weed beds, treatment areas, and sampling station in Conewago Lake, June 1969.

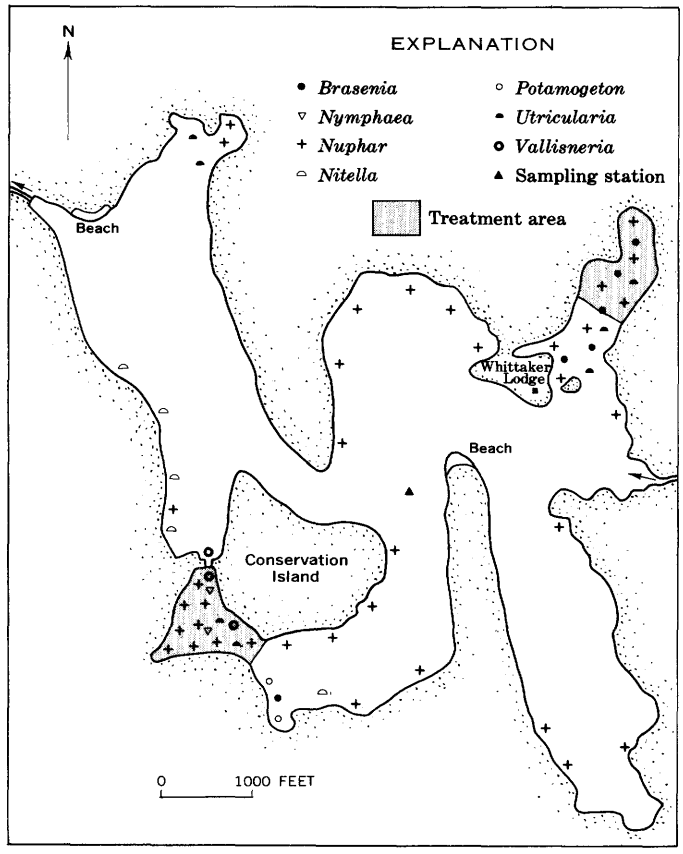

Figure 3.—Map showing location of weed beds, treatment areas, and sampling station in Promised Land Lake, June 1969.

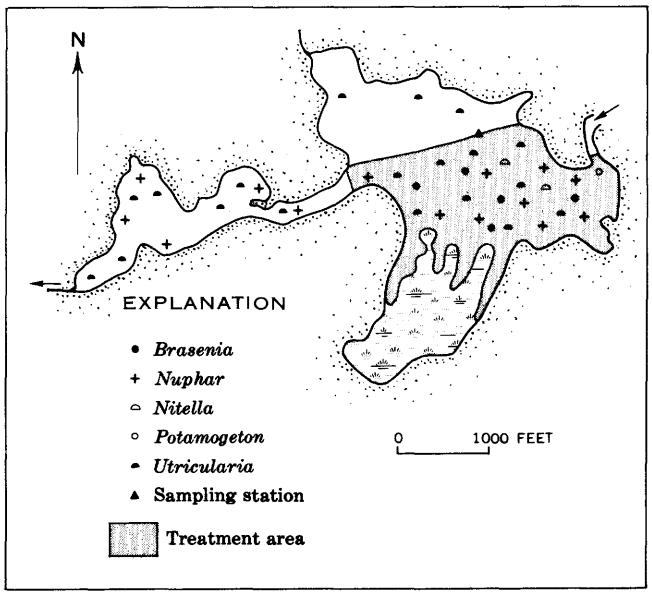

Figure 4.—Map showing location of weed beds, treatment area, and sampling station in Lower Lake, June 1969.

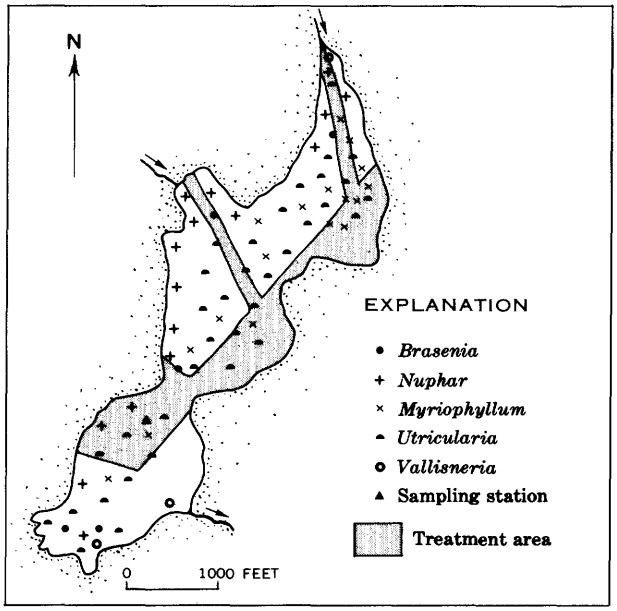

Figure 5.—Map showing location of weed beds, treatment area, and sampling station in Tobyhanna Lake, June 1969.

EFFECT OF TREATMENT ON ECOSYSTEM

Dissolved oxygen

Limiting the area of treatment at the six lakes to a maximum of 39 percent of the lake surface prevented any fish kills due to loss of oxygen. Minor temporary imbalance of dissolved oxygen was noted at most of the lakes.

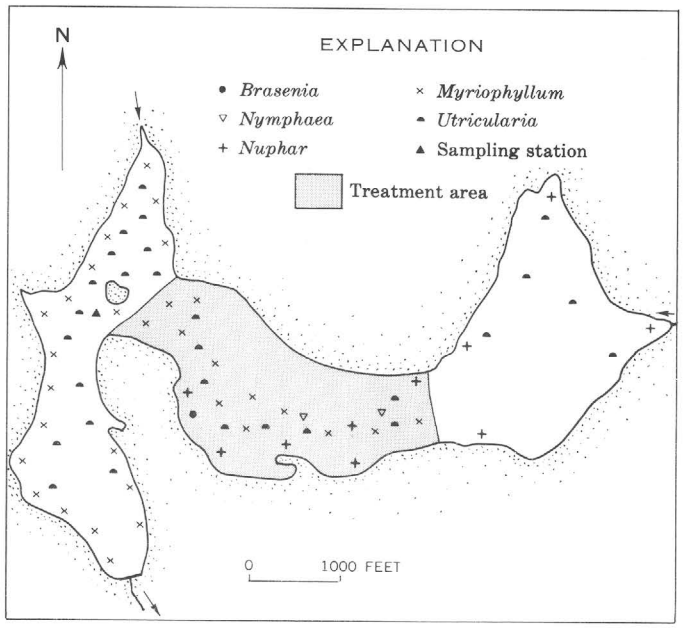

Figure 6.—Map showing location of weed beds, treatment area, and sampling station in Lake Jean, June 1969.

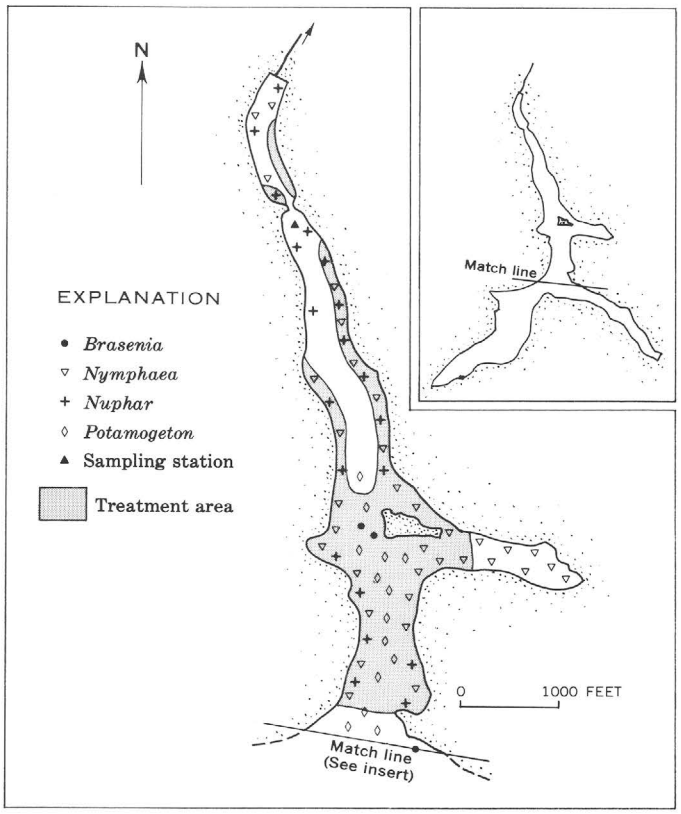

Figure 7.—Map showing location of weed beds, treatment areas, and sampling station in Black Moshannon Lake, June 1969.

Dissolved-oxygen percentage saturation was reduced 2–44 percent at the treated lakes within 7–83 days after the initial herbicide applications. The period of lowered dissolved oxygen corresponds to the period of observed rapid decomposition of plant material and reduced photosynthetic activity. In general, dissolved oxygen remained depressed through the summer of treatment. None of the lakes experienced dissolved-oxygen depletion critical to the biota.

The greatest initial decrease in dissolved oxygen occurred at Tobyhanna and Conewago Lakes where, because of dispersion of herbicide, the largest amount of plant material was killed. A summary of the field measurements at each of the lakes is presented in table 5.

Nutrients

As indicated in table 6, nutrient (nitrate and phosphate) levels at each of the lakes showed a small increase between spring 1969 and 1970. Samples collected throughout the summer of treatment failed to reveal any overall significant increase. The lack of significant increases suggests that the nutrients contained in the dead vegetation are not released rapidly but are released over a period of time.

Although a temporary imbalance or increase in nutrient content is to be expected after the death and decomposition of tons of plant matter, an explanation of the significance of the observed increase in the treated lakes is complicated by an increase of 0.2 mg/l nitrate and 0.11 mg/l total phosphate in the untreated control lake (Gouldsboro Lake) for the same period. The measured increase in nutrients between 1969 and 1970 could, in fact, be due to a normal fluctuation in the biota-nutrient balance and not to the herbicide-killed vegetation.

See table 7 for a summary of surface-water analyses before treatment.

Plankton

Analyses of the plankton community at each of the treated lakes before and as long as 90 days after herbicide application enabled a cursory evaluation of the plankton response. The data presented in table 8 and figure 8 suggest that phytoplankton populations were adversely affected by the herbicide, particularly at Conewago Lake, where a reduction of 95 percent was measured 7 days after treatment.

A significant decline in the percentage and numbers of phytoplankton was noted in four of the six lakes treated. An increase in phytoplankton was noted at Lower Lake despite the herbicide treatment. The degree and time of response was variable and no doubt was partly dependent upon the percentage of water area treated, the herbicide used, and the species of plankton inhabiting each of the lakes. No overall increase in plankton population was noted during the course of the study. A list of plankton observed in the six study lakes is included in table 9.

Table 5.—*Summary of field measurements*

[Collected at sampling point indicated in figures 2–7]

Date	Time	Depth (meters)	Temperature (°C)	Dissolved oxygen		pH	Specific conductance (micromhos)	Color	Depth of visibility (meters)	Weather
				Mg/l	Percent saturation					
Conewago Lake										
4-16-69	1500	0.3	14.0	10.4	100	7.6	165	Gray-brown	0.8	Rain.
6-6-69	1500	.3	24.5	9.0	106	8.0	177	Clear	2.4	Clear.
6-16-69	0935	.3	24.0	6.7	77	7.4	178	Gray-brown	1.0	Overcast.
		3.0		5.1	60					
6-23-69	1100	.3	24.0	8.0	93	7.1	180	Gray	1.4	Do.
		3.0		8.0	93					
7-7-69	1115	.3	25.0	7.0	82	7.5	185	Gray-green	.8	Rain.
		3.0		6.5	75					
8-29-69	1300	.3	26.0	8.8	110	8.4	158	Gray	1.5	Clear.
		1.5		8.8	108					
		3.0		8.0	97					
4-28-70	1400	.3	16.0	12.4	124	7.6	125	... do ...	1.0	Do.
		4.3	13.5	9.8	93	7.6	125			
Promised Land Lake										
4-22-69	1130	0.3	12.0	10.8	100	5.6	34	Clear	[1]2.1	Rain, cold.
5-28-69	1800	.3	19.0	9.2	98	5.7	38	... do ...	2.6	Clear.
6-3-69	....	.3	21.0	....	....	....	....	... do ...	....	Do.
6-11-69	1440	.3	21.0	8.6	95	5.9	37	... do ...	2.7	Do.
		2.4		8.0	88					
6-17-69	1410	.3	22.0	7.6	85	5.8	36	... do ...	[1]2.7	Do.
6-30-69	1400	.3	24.0	7.4	86	6.5	36	... do ...	[1]2.4	Do.
8-25-69	1400	.3	23.0	7.0	80	6.1	37	... do ...	2.3	Do.
5-5-70	1200	.3	15.0	10.4	102	7.1	31	... do ...	2.5	Do.
Lower Lake										
4-22-69	1400	0.3	10.0	11.3	100	6.0	47	Clear	1.26	Rain.
5-29-69	1230	.3	23.0	9.2	104	5.8	38	... do ...	2.0	Clear.
6-12-69	1010	.3	22.5	8.2	92	5.9	38	Brown	[1]1.2	Overcast.
6-17-69	1440	.3	22.0	9.0	100	5.6	38	Clear	1.7	Clear.
6-30-69	1530	.3	27.0	7.2	89	6.7	38	... do ...	[1].6	Do.
8-25-69	1500	.3	23.0	7.6	87	6.6	35	... do ...	[1]1.2	Do.
5-5-70	1400	.3	17.0	11.4	117	6.5	32	... do ...	[1]1.2	Do.
Tobyhanna Lake										
4-21-69	1200	0.3	11.0	11.1	100	4.9	32	Brown	[1]1.5	Clear.
6-2-69	1430	.3	23.5	9.4	108	5.1	29	... do ...	[1]1.5	Do.
6-12-69	1230	.3	22.0	8.2	94	5.8	27	... do ...	[1]1.5	Do.
6-18-69	1400	.3	20.0	7.6	82	5.5	26	... do ...	1.5	Overcast.
7-1-69	1100	.3	25.0	6.1	72	5.2	28	... do ...	1.5	Clear.
8-26-69	1100	.3	22.5	5.8	64	5.5	28	... do ...	1.0	Do.
		1.5		5.8						
5-6-70	1000	.3	12.0	9.3	85	5.1	30	... do ...	1.5	Do.
		1.5	13.0	8.7	82					
Lake Jean										
4-18-69	1200	0.3	12.0	10.8	100	4.8	33	Clear	[1]1.8	Overcast.
6-3-69	1230	.3	21.0	8.6	97	4.9	32	... do ...	[1]3.0	Clear.
6-13-69	1000	.3	22.0	8.6	97	5.0	33	... do ...	[1]2.7	Overcast.
6-19-69	1130	.3	19.0	8.4	89	5.2	34	... do ...	2.4	Do.
7-1-69	1300	.3	25.0	7.9	95	6.1	33	... do ...	2.1	Clear.
8-27-69	1030	.3	20.0	6.6	70	6.5	31	... do ...	1.9	Do.
		2.7		6.5						
5-7-70	1010	.3	10.0	9.3	82	5.5	36	Light brown	2.4	Do.
		3.0	10.5	8.9	79		34			
Black Moshannon Lake										
4-17-69	1130	0.3	15.0	10.2	100	6.5	29	Brown	1.8	Clear.
6-4-69	1100	.3	18.5	7.6	80	5.0	29	... do ...	1.5	Overcast.
6-20-69	1330	.3	20.0	6.6	70	5.2	24	... do ...	1.1	Clear.
		1.4		4.6	49					
7-8-69	1145	.3	22.0	6.0	67	6.3	27	... do ...	1.2	Do.
8-28-69	1200	.3	21.5	6.2	68	6.4	25	... do ...	1.0	Do.
		2.1		1.4	14					
4-29-70	1145	.3	17.0	10.1	104	5.7	30	... do ...	1.8	Do.
		3.0	11.0	9.4	99		34			

[1] Visibility to bottom.

Table 6.—*Summary of nutrient analyses, in milligrams per liter*

Date	Nitrate (NO_3)	Ammonia (NH_4)	Total organic nitrogen	Total phosphate (PO_4)	Total organic carbon
Conewago Lake					
4-16-69	0.5	0.64	0.84	0.08	5.5
6-6-69	.0	.0	....	.00	....
6-16-69	.1	....	....	.05	....
6-23-69	.0	.36	.78	.06	....
7-7-69	.1	....	....	.19	....
8-29-69	.1	.21	.69	.13	5.0
4-28-70	1.2	.28	.40	.06	7.0
Promised Land Lake					
4-22-69	0.0	0.28	0.36	0.02	5.0
5-28-69	.1	....	....	.00	....
6-11-69	.0	....	....	.00	....
6-17-69	.1	....	....	.00	....
6-30-69	.0	....	....	.31	....
8-25-69	.4	.15	.39	.22	7.0
5-5-70	.2	.00	.19	.05	5.0
Lower Lake					
4-22-69	0.0	0.19	0.45	0.03	5.5
4-29-69	.1	....	....	.00	....
6-12-69	.0	....	....	.00	....
6-17-69	.0	....	....	.14	....
6-30-69	.0	....	....	.00	....
8-25-69	.3	.17	.45	.20	5.0
5-5-70	.2	.00	1.1	.11	4.0
Tobyhanna Lake					
4-21-69	0.1	0.50	0.42	0.02	8.0
6-2-69	.1	....	....	.18	....
6-12-69	.1	....	....	.05	....
6-18-69	.1	....	....	.00	....
7-1-69	.3	....	....	.05	....
8-26-69	.4	.22	.54	2.5	9.0
5-6-70	.3	.69	.54	.12	8.0
Lake Jean					
4-18-69	0.8	0.23	0.37	0.01	4.0
6-3-69	.6	....	....	.00	....
6-13-69	.4	....	....	.06	....
6-19-69	.4	....	....	.17	....
7-1-69	.2	....	....	.00	....
8-27-69	.3	.28	.48	.12	2.0
5-7-70	2.0	1.4	.56	.14	4.0
Black Moshannon Lake					
4-17-69	0.1	0.50	0.24	0.03	5.0
6-4-69	.1	....	....	.12	....
6-20-69	.0	.39	.60	.07	....
7-8-69	.4	....	....	.24	....
8-28-69	.3	.17	.48	.09	5.0
4-29-70	.3	.23	.05	.03	....
Gouldsboro Lake					
4-21-69	0.0	0.19	0.36	0.02	4.5
5-6-70	.2	.08	.28	.13	6.0

Plant succession

Plant succession was difficult to define or document in the short period of time that the lakes were observed. Nearly all reinfestation was by indigenous species. Re-treatment during September 1969 and the spring of 1970 at five of the six lakes made the succession or regrowth of plants nearly impossible to evaluate.

The only lake not re-treated in 1970 was Tobyhanna. Regrowth of submersed species was dominated by *Utricularia purpurea*, when the lake was checked during May 1970. *Myriophyllum humile* was also found to be regrowing throughout the lake. Light regrowth of watershield and spatterdock was found along the margins of the lake in areas they formerly occupied.

Although Conewago Lake was treated in 1968, 1969, and 1970, abundance of *Myriophyllum*, *Ceratophyllum*, and *Najas* increased in areas formerly occupied by *Potamogeton crispus*. *Chara*, a branched, bottom-dwelling alga, also proliferated throughout the littoral.

The problem of plant succession is further complicated by the fact that plant-species density is affected by seasonal

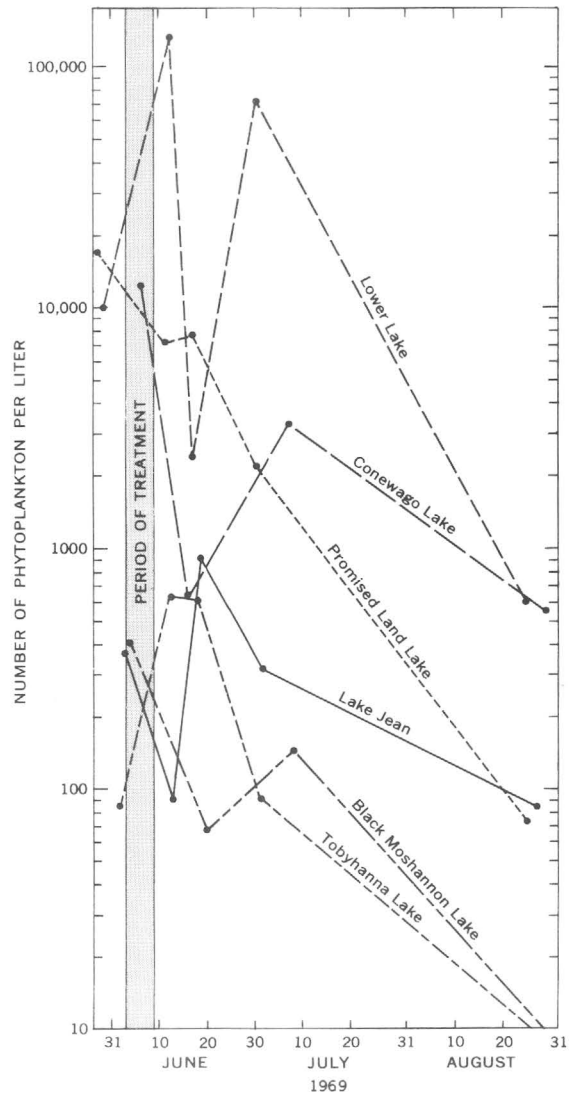

Figure 8.—Number of phytoplankton in the plankton population before and after herbicide application.

Table 7.—*Summary of surface-water analyses of selected Pennsylvania recreation lakes, April 1969*

[Results in milligrams per liter, except as indicated]

Lake	Date	Silica (SiO_2)	Iron (Fe)	Manganese (Mn)	Calcium (Ca)	Magnesium (Mg)	Sodium (Na)	Potassium (K)	Bi-carbonate (HCO_3)	Sulfate (SO_4)	Chloride (Cl)	Fluoride (F)
Conewago ...	4-16-69...	12.0	0.06	0.06	17	6.6	6.0	1.6	50.0	32	9.0	0.1
Promised Land	4-22-69...	.9	.03	.02	3.6	.6	.6	.4	5.0	10.0	2.9	.1
Lower	4-22-69...	.0	.01	.00	3.8	.7	1.0	.4	5.0	11.0	3.0	.1
Tobyhanna ..	4-21-69 ...	1.1	.12	.03	2.8	.5	.8	.6	3.0	9.2	3.0	.2
Gouldsboro ..	4-21-69...	.3	.09	.00	3.7	.6	1.5	.6	6.0	9.9	4.0	.2
Jean	4-21-69...	.0	.04	.15	2.4	.4	1.1	.6	2.0	7.2	4.0	.1
Black Moshannon.	4-17-69...	1.0	.10	.00	2.8	.5	.8	1.1	6.0	6.8	2.7	.1

Lake	Date	Nitrate (NO_3)	Total phospate (PO_4)	Dissolved solids (ROE)	Hardness as $CaCO_3$		Color	Field measurements			
					Calcium, magnesium	Non-carbonate		Temper-ature (°C)	pH	Specific conductance (micromhos)	Dissolved oxygen
Conewago ...	4-16-69...	0.5	0.08	120	70	29	0	14.0	7.6	165	10.4
Promised Land	4-22-69...	.0	.02	23	12	8	0	12.0	5.6	34	10.8
Lower	4-22-69...	.0	.03	24	13	9	0	10.0	6.0	47	11.3
Tobyhanna ..	4-21-69...	.1	.02	27	9	7	30	11.0	4.9	32	11.1
Gouldsboro ..	4-21-69...	.0	.02	21	12	7	3	13.0	6.7	41	....
Jean	4-21-69...	.8	.01	19	8	6	0	12.0	4.8	33	10.8
Black Moshannon.	4-17-69...	.1	.03	26	9	4	6	15.0	6.5	29	10.2

variation. As stated by Sculthorpe (1967, p. 426), "* * * the specific composition of a [plant] community and the status of its various constituents are still likely to show seasonal variation: there is no reason to suppose that growth is finely synchronized throughout the population."

Seasonal changes in species density were observed in both treated and untreated lakes. For example, the pondweed *Potamogeton epihydrus* was only sparsely distributed in August 1969 at Gouldsboro Lake. The following spring there were scattered but dense stands of *P. epihydrus* in the same areas. At Conewago Lake it was observed that both *Najas minor* and *N. flexilis* become obviously more dense in August than earlier in the growing season and that *Potamogeton crispus* begins to die back early in August.

Observed seasonal changes in species density indicate that more than one growing season is necessary to establish a discernible succession of plant species.

SUMMARY AND CONCLUSIONS

Diquat applied at the rate of 0.3 to 1.25 gallons per acre to achieve a concentration of 0.25 mg/l active ingredient was highly successful in controlling the pondweeds *Potamogeton crispus* at Conewago Lake and *P. natans* and *P. epihydrus* at Black Moshannon Lake. It was less effective upon other species of pondweed and species of *Myriophyllum*, *Utricularia*, *Najas*, *Ceratophyllum*, and *Anacharis* found in the same and different bodies of water. Good seasonal control was achieved, but regrowth of pondweeds from sprouting of winterbuds and root systems was observed within 90 days of treatment. Successive treatments may give longer lasting control.

On the basis of studies by Hiltibran (1965), Yeo (1967), and others, it is not surprising that the dosage of 0.25 mg/l did not achieve the desired degree of control on many of the other target species. Concentrations of 0.50 to 1.0 mg/l are suggested by Lipinot (1968) as minimum for partial treatments.

The use of diquat to control lowly water milfoil (*Myriophyllum humile*) was reasonably successful at Lake Jean and Lower Lake. Initial control was satisfactory, but regrowth was prolific by the end of the summer. Bladderwort (*Utricularia* sp.), a common coinhabitant with lowly water milfoil in the soft-water lakes of northern Pennsylvania, was not appreciably affected by diquat at the 0.25 mg/l dosage rate.

The use of Kuron at 0.64 to 1.3 gallons per acre required a second application to achieve the desired degree of control of floating-leaved plants. The initial application in June resulted in removal of 10 to 60 percent of the exposed vegetation. However, regrowth of plants within the treatment area necessitated a second application. It was not possible to evaluate the second application, but field reports indicate up to 90-percent control of all target species. White water lily assumed a dominant role in most areas where spatterdock was removed. Watershield, like spadderdock, was more susceptible to Kuron at the applied rate than was white water lily.

The use of Aquathol Plus at a concentration of 1.0 mg/l was highly successful in controlling the target species in Tobyhanna Lake. The effectiveness of the combined potassium endothol-silvex formulation (see table 3) appears to have been greater on the same plant species than that of the Ortho Diquat-Kuron applications in waters of similar physicochemical characteristics.

Table 8.—*Summary of plankton analyses*

Date	Total cells per liter	Percent phyto-plankton	Total phyto-plankton per liter	Chlorophyta	Chrysophyta	Cyanophyta	Protozoans	Crustaceans
Conewago Lake								
6-6-69	14,000	85	12,000	7	78	0	14	1
6-9-69			Herbicide applied					
6-16-69	2,800	22	620	6	16	0	72	7
7-7-69	5,600	63	3,500	22	19	22	27	10
8-29-69	550	97.5	540	.5	4	93	.5	2
Promised Land Lake								
5-28-69	20,000	86	17,000	10	68	8	14	0
6-3-69			Herbicide applied					
6-11-69	12,000	60	7,200	<1	57	2	37	4
6-17-69	13,000	60	7,800	4	55	<1	41	<1
6-30-69	16,000	15	2,400	2	6	7	84	1
8-25-69	280	27	75	0	24	3	65	8
Lower Lake								
5-29-69	13,500	75	10,000	33	40	2	22	3
6-3-69			Herbicide applied					
6-12-69	213,500	64	140,000	5	47	12	35	1
6-17-69	31,200	9	2,800	2	6	1	91	<1
6-30-69	117,700	62	73,000	12	2	48	35	3
8-25-69	1,300	46	600	31	15	0	54	0
Tobyhanna Lake								
6-2-69	860	10	86	4	6	<1	85	5
6-6-69			Herbicide applied					
6-12-69	1,800	35	630	3	30	2	64	1
6-18-69	2,300	27	620	1	26	0	71	1
7-1-69	4,600	2	92	1	<1	<1	98	<1
8-26-69	1,500	1	2	0	1	0	96	3
Lake Jean								
6-3-69	4,600	8	370	4	4	0	89	3
6-4-69			Herbicide applied					
6-13-69	1,300	7	91	2	5	0	77	15
6-19-69	22,000	4	880	1	3	0	94	2
7-1-69	11,000	3	330	2	1	0	97	0
8-27-69	1,400	6	84	3	3	0	92	2
Black Moshannon Lake								
6-4-69	1,000	40	400	17	19	4	52	8
6-4-69			Herbicide applied					
6-20-69	980	7	68	0	7	0	93	0
7-8-69	780	24	190	9	13	2	71	5
8-28-69	140	0	0	0	0	0	97	3

Table 9.—*Plankton observed in the six lakes studied from April through August 1969*

Organism	Lake: Conewago	Promised Land	Lower	Tobyhanna	Jean	Black Moshannon
Chlorophyta:						
Spirogyra	...	...	X	...	...	...
Chroococcus	...	...	X	...	...	...
Gonium	...	...	X	...	...	...
Eudorina	...	...	...	...	X	...
Cyanophyta:						
Anabaena	X	X	X	...	...	X
Microcystis	X	X	X	X	...	X
Coelosphaerium	...	...	X	...	...	...
Chrysophyta:						
Diatoma	...	...	...	X	X	...
Asterionella	...	X	X	...	...	X
Tabellaria	...	X	X	X	...	X
Fragilaria	X	X	...	X	...	...
Dinobryon	...	X	X	...	X	X
Synura	...	X	X	X	...	...
Pyrrophyta:						
Ceratium	X	...	...	...	...	...
Desmids:						
Cosmarium	...	...	X	...	...	...
Micrasterias	...	...	X	...	...	...
Staurastrum	...	...	X	...	...	...
Rotatoria:						
Keratella	...	X	X	...	...	...
Polyarthra	...	X	X	...	...	...
Rotaria	...	X	X	...	...	...
Killicottia	X	...	...	X	X	X
Crustacea:						
Cladocera	...	X	...	X	...	...
Copepoda	X	X	X	X	X	X
Ostracoda	X	...	...	...	...	...

Considerable drift of Aquathol Plus resulted in a near-complete kill of hydrophytes throughout the lake. Regrowth of bladderwort and water milfoil was of little consequence until the spring of 1971. No appreciable regrowth of other species was observed through the same period.

Plant succession was difficult to document because of subsequent interim treatment(s) and the necessity of additional growing seasons for significant recolonization. Successive treatments with Ortho Diquat in 1968 and 1969 have resulted in Conewago Lake indicating signs of a diminishing stand of *P. crispus* and invasion by species of *Myriophyllum*, *Ceratophyllum*, *Najas*, and *Chara*.

In general, the herbicide treatments and the subsequent microbiological activity had negligible effects upo the chemical and physical characteristics of the six lakes studied. No significant increases in nitrate or phosphate levels were measured at any of the treated lakes during the summer following treatment. Increases noted 1 year after treatment were difficult to evaluate because of increases in the control lake.

Dissolved-oxygen and percentage-saturation values decreased an average of 2.2 mg/l and 22 percent, respectively, in the six lakes during the period of rapid decomposition of the plant material, but no oxygen deficiency critical to the biota occurred in any of the lakes.

Effects of the treatment program on the biology of the lakes investigated were also negligible. A decrease in the phytoplankton population was measured, but, again, it is not known how much of the decrease was due to the herbicide and how much to a "normal" population fluctuation.

There are two primary reasons contributing to the lack of readily discernible environmental alterations as a result of the herbicide applications: (1) The lakes, except for Conewago Lake, are all relatively infertile bodies of water having meager

populations of organisms; (2) the herbicide(s) were applied to approximately one-third or less of the surface area of each lake involved, thereby minimizing the total effect of the treatment on the lake and its inhabitants.

More definitive studies of this nature would include the collection of comparable data one or two growing seasons before treatment and two or three growing seasons after treatment. Unfortunately, that was not possible in this study.

REFERENCES

American Public Health Association, American Water Works Association, Water Pollution Control Federation, 1965, Standard methods for the the examination of water and wastewater, including bottom sediment and sludges [12th ed.]: New York, Am. Public Health Assoc., Inc., 769 p.

Burdick, G. E., 1961, Chemical control of aquatic vegetation in relation to the conservation of fish and wildlife: Northeastern Weed Science Society Proc., New York, Jan. 1961, v. 15, p. 485–492.

Hiltibran, R. C., 1965, The effect of diquat on aquatic plants in central Illinois: Weeds, v. 13, p. 71–72.

Lipinot, A. C., 1968, Aquatic weeds–their identification and methods of control: Illinois Dept. Conserv., Div. Fisheries, Fishery Bull. 4, 53 p.

Muenscher, W. C., 1964, Aquatic plants of the United States: Ithaca, N.Y., Cornell University Press, 374 p.

Needham, J. G., and Needham, P. R., 1962, A guide to the study of fresh-water biology [5th ed.]: San Francisco, Holden-Day, Inc., 107 p.

Ott, A. N., Barker, J. L., and Growitz, D. J., 1971, Physical, chemical, and biological characteristics of Conewago Lake drainage basin, York County, Pennsylvania: U.S. Geol. Survey open-file report, 229 p.

Pennsylvania Geological Survey, 1960, Geologic map of Pennsylvania: Pennsylvania Geol. Survey, 4th ser., scale 1:250,000.

Prescott, G. W., 1964, How to know the fresh-water algae: Dubuque, Iowa, Wm. C. Brown Co., 272 p.

Rainwater, F. H., and Thatcher, L. L., 1960, Methods for collection and analysis of water samples: U.S. Geol. Survey Water-Supply Paper 1454, 301 p.

Reid, G. K., 1961, Ecology of inland waters and estuaries: New York, Reinhold Publishing Corp., 375 p.

Sculthorpe, C. D., 1967, The biology of aquatic vascular plants: London, Edward Arnold, Ltd., 610 p.

Yeo, R. R., 1967, Dissipation of diquat and paraquat, and effects on aquatic weeds and fish: Weeds, v. 15, no. 1, p. 42–46.

NATURAL BACKGROUND CONCENTRATION OF MERCURY IN SURFACE WATER OF THE ADIRONDACK REGION, NEW YORK

By WILLIAM BULLER, Albany, N.Y.

Work done in cooperation with the New York State Department of Health and the New York State Department of Environmental Conservation

Abstract.—The danger of mercury contamination in water supplies is well known, but natural background concentrations of mercury in water supplies are not well known. Establishment of these natural background concentrations requires the study of areas relatively free of man's influence on the environment. The Adirondack region of New York State is such an area. Determinations of mercury concentration of samples collected from streams and lakes of the Adirondack region in fall, winter, and spring 1970–71 indicate that the natural background concentration of mercury is less than 0.5 μg/l (microgram per liter), which is less than one-tenth the 5-μg/l limit recommended for drinking water in New York.

The danger of mercury contamination of water supplies is well known. The occurrence of mercury in some water supplies can be attributed directly to natural phenomena rather than to man-caused pollution. Knowledge of the natural background concentration of a material is needed before water can be described as either "contaminated by" or "free of contamination from" that material. Thus, to protect water supplies from contamination by mercury, the natural background concentration of mercury in lakes and streams must be known. As a step in acquiring such knowledge, the Adirondack region of New York State was chosen as the site of an investigation into the natural background concentration of mercury. This site was chosen because, relative to most areas in the State, it is free of man's influence on the environment. As an aid to understanding the mode of occurrence of mercury in surface water, the distribution and the occurrence of mercury in other phases of the environment and properties of mercury are discussed in this paper.

DISTRIBUTION AND OCCURRENCE OF MERCURY

Mercury is a rare element that ranks eighth from the bottom of the list of elements in abundance in the earth's crust (Vinogradov, 1962). It occurs naturally in more than trace amounts in only a few places in the earth. The only mineral containing mercury in amounts sufficient for commercial extraction is cinnabar (mercuric sulfide). A small number of mines scattered around the globe account for most of the world's production; the richest ore deposits of mercury are in Spain and Italy (Lange and Forker, 1967, p. 82).

In addition to its trace occurrence in rocks and soils, mercury also occurs in trace amounts in the hydrosphere, the atmosphere, and the biosphere. Concentrations in rocks and soils other than ore deposits range from 10 to 20,000 μg/kg (micrograms per kilogram). In the hydrosphere, mercury generally occurs in concentrations less than 1 μg/l (microgram per liter). In the atmosphere, where mercury occurs both in vapor and particulate forms, concentrations are usually less than 0.1 $\mu g/m^3$ (microgram per cubic meter) (U.S. Geological Survey, 1970, table 15, p. 59). Concentrations as high as 20 $\mu g/m^3$ (U.S. Geological Survey, 1970, table 28, p. 67) have been found over ore deposits and over areas of volcanic activity. Plants concentrate mercury in their tissues under certain conditions, but the concentration of mercury in plants probably seldom exceeds 500 μg/kg (Shacklette, 1970).

A simplified diagram of the mercury cycle is shown in figure 1. Note that mercury is dispersed through the lithosphere, the hydrosphere, and the atmosphere, as well as the biosphere, which interpenetrates the other three. Biological activity within the mercury cycle is of particular interest to man because the aquatic food chain is a mechanism in which mercury is concentrated. According to Goldwater (1971, p. 16), less mercury is excreted than ingested at each trophic level. Algae proportionately contain more mercury than the water in which they live, and fish that feed on the algae have even a greater proportion of mercury.

CHEMICAL PROPERTIES OF MERCURY

Known to ancient Chinese and Hindus and found in Egyptian tombs of 1500 B.C., mercury is the only common metal that is liquid at ordinary temperatures. The silvery liquid metal, commonly called quicksilver, is about 13.5 times as

U.S. GEOL. SURVEY PROF. PAPER 800-C, PAGES C233-C238

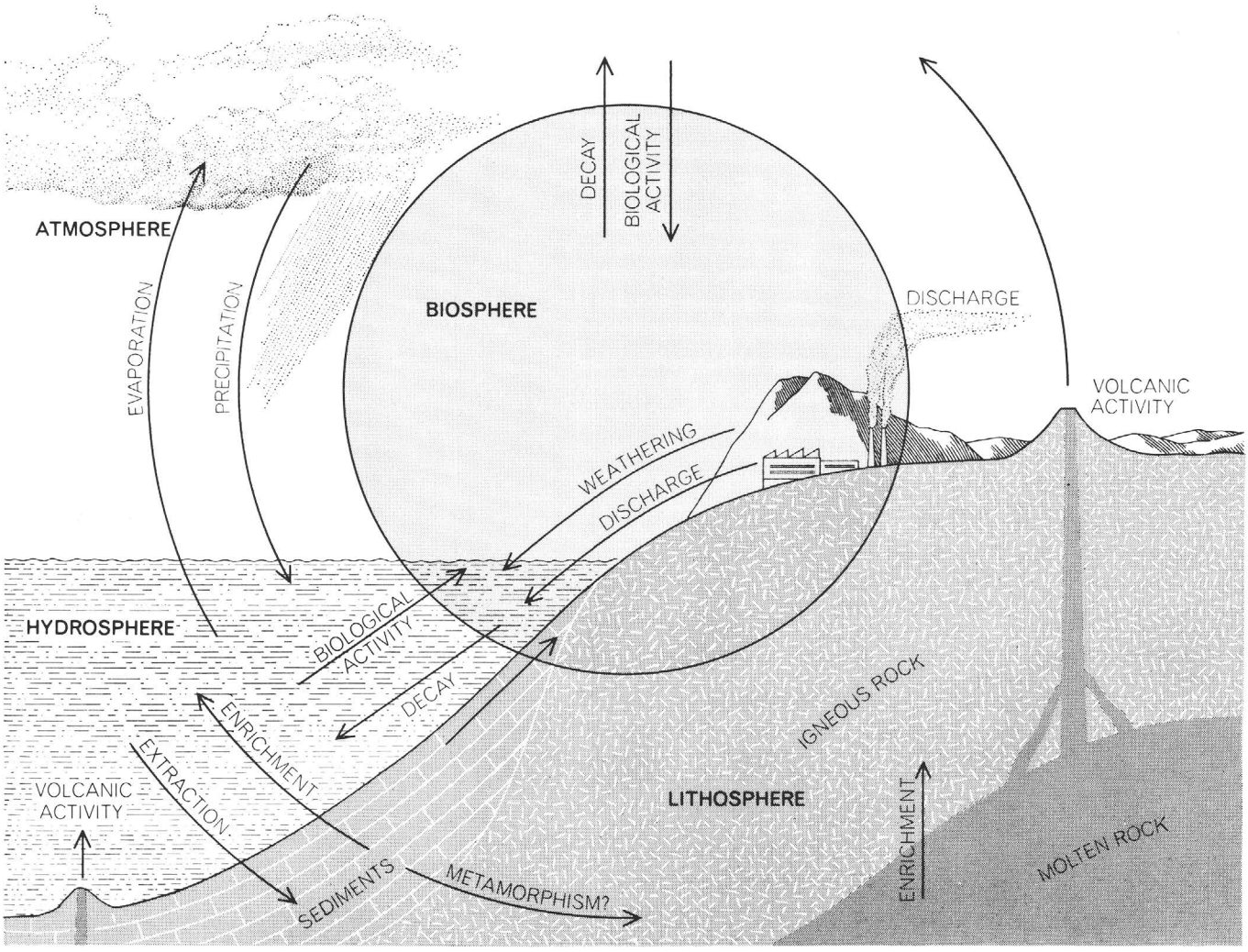

Figure 1.—Mercury cycle. (From "Mercury in the Environment," by Leonard J. Goldwater. Copyright 1971 by Scientific American, Inc. All rights reserved.)

heavy as water. As do other liquids, it vaporizes and condenses in a pattern determined by its own vapor pressure and by the atmospheric temperature and pressure of its environment.

The chemical behavior of mercury in water is complex and not entirely understood. In natural waters and sediments, mercury can occur in as many as three oxidation states: (1) the most reduced form, or metallic state Hg°; (2) the mercurous ion Hg_2^{+2}; and (3) the stable form in oxidizing conditions, the mercuric ion Hg^{+2}.

Hem (1970) presented stability diagrams that indicated the main features of the aqueous inorganic chemistry of mercury under equilibrium conditions. The predominant species of mercury in solution under moderately oxidizing conditions above a pH of 5 is undissociated metallic mercury. This form has a nearly constant solubility of about 25 μg/l under such conditions. In oxygenated aqueous solutions having a chloride concentration of as much as 30 mg/l (milligrams per liter), the solubility of mercury may be greatly increased by the formation of the uncharged mercuric chloride $HgCl_2$ complex or of anionic complexes such as $HgCl_4^{-2}$. Under conditions common in many lake and streambed sediments, mercury may also be precipitated as the sulfide, cinnabar, a compound of extremely low solubility (Hem, 1970).

Much of the mercury in natural water occurs in complexes of the organic form. The organic complexes can be the result of transformation of inorganic forms to organic forms. According to Jensen and Jernelov (1969), much of the inorganic and the organic mercury wastes from industrial effluent is converted by anaerobes to methylmercury, CH_3Hg^{+}, or dimethylmercury, $(CH_3)_2Hg$.

Evidence indicates that concentrations of mercury may be higher in water and sediment mixtures than in water free of sediments. In fact, Hinkle and Learned (1969) found from 5 to 25 times as much mercury in the suspended sediment as in the filtered water. Soluble mercury introduced into streams may be quickly transformed to the particulate form in several

ways—reduction to metallic mercury, adsorption onto sediments, complexing with other materials, or ingestion by living organisms. Evidence (Heide and others, 1957, Dall'Aglio, 1968) showed that stream sediment and related fine-grained materials remove a high percentage of mercury introduced into streams. When mercury is eliminated by adsorption onto sediments or by other means, the mercury may be slowly released from bed sediments to the stream through complexing by soluble organic and inorganic compounds (Jenne, 1970.)

DISCUSSION OF PROJECT

Present (1971) knowledge of mercury and its environmental effects makes it desirable to estimate the natural background concentration of mercury in the lakes and the streams of New York State. To do this, lakes and streams in an area generally free of manmade sources of pollution should be sampled for determination of mercury. The Adirondack region of New York was chosen as the study area because it is virtually free of major industrial sites. The location of the study area is shown in figure 2 (p. C238). Industry consists of only a few paper mills and mines (Thomas Lang, oral commun., Sept. 15, 1971).

Because of the geologic origin of mercury, a brief discussion of the general geology of the Adirondack region is presented here. Nearly all the bedrock in the region is of Precambrian age (Fisher and others, 1962). Felsic metamorphic rocks such as granite gneiss, charnockite, anorthosite, and anorthositic gneiss predominate. Marble, calcium silicate rocks, and gneisses of sedimentary origin are present in lesser amounts. Except for marble, these rocks tend to resist erosion and chemical weathering; thus their ability to release chemical constituents to the hydrologic cycle is less than that of other rock types. The average content of mercury in felsic igneous rocks similar to the metamorphic rocks of the study area is probably less than 100 μg/kg, according to data quoted by Rankama and Sahama (1950, p. 716).

The Adirondack area was subjected to extensive glaciation by both alpine glaciers and continental ice sheets. Alpine glaciers moved rock materials only locally; but the ice sheets moved minor amounts of rock material into the area from the north, possibly from as far away as Canada (Buddington and Leonard, 1962, p. 16). All valleys in the Adirondacks are partly mantled with glacial deposits. The glacial deposits may have more effect than bedrock on chemical content of surface water because much of the water has had direct contact with glacial drift without contacting bedrock.

In the northwestern periphery of the Adirondacks, zinc ores, traces of which may be incorporated in the glacial drift, contain minor amounts of mercury. No separate mercury minerals are reported to occur in the study area (P. R. Whitney, oral commun., 1971).

The two major drainage basins in the region are those of the St. Lawrence and Hudson Rivers. The St. Lawrence River drains the northern and the western parts of the region; the Hudson River drains the southern and the eastern parts. Sampling sites were selected according to drainage patterns so that most of the area would be represented. Most major lakes and streams were included in the study. Surface water was sampled at a total of 39 sites (fig. 2), all but five of which are within the boundaries of Adirondack Forest Preserve. These five sites are site 21, near Edwards; site 22, near Fowler; site 23, at Fullerville; site 24, at Fowler, and site 25, near Balmat. Water samples were taken at streamside or from highway bridges; all samples were taken near major highways. A few snow and sediment samples were also taken. Sediment samples, taken from stream bottoms, consisted mainly of fine to coarse sand and fine gravel.

As discussed previously, water with high sediment concentrations may carry higher mercury loads than water with lower concentrations. Because sediment concentration varies with streamflow, higher streamflows generally have higher sediment concentrations. Therefore, sampling was done in fall, winter, and spring to obtain samples representing a wide range of hydrologic conditions. Water samples were taken during two low-flow periods, November 9 and 10, 1970, and February 16–19, 1971. During these two periods, streamflows were near base flow. Water samples were also taken during a high-flow period, April 21–23, 1971. At this time, streams were receiving runoff from snowmelt as well as water from rainfall; streamflow was near peak flow.

Only unfiltered water samples were taken in November 1970. In February and April 1971, both filtered and unfiltered samples were taken. Filtered samples were passed through a 0.45μ membrane filter. All samples were acidified in the field with nitric acid. Total and dissolved mercury concentrations of the samples were determined in the Albany laboratory of the U.S. Geological Survey. Total mercury includes mercury dissolved in the water as well as mercury adsorbed on the sediment suspended in the water. Total mercury in the unfiltered sample was determined by the flameless atomic absorption method (Hatch and Ott, 1968). Dissolved mercury in the filtered sample was determined by the silver-wire method (Brandenberger and Bader, 1967; Hinkle and Learned, 1969). Snow samples were treated the same as surface-water samples. Sediment samples were air dried and weighed before distilled water was added; then mercury content of each sample was determined by the method of Hatch and Ott.

RESULTS

Results indicate that total mercury concentrations of all water and snow samples (table 1) except one were less than the detectable limit of 0.5 μg/l. That sample was taken in February at site 24, which is near the zinc-mining area at Balmat. Total mercury concentration of that sample was 0.9 μg/l. The dissolved mercury concentration of most samples was less than the detectable limit of 0.1 μg/l. All samples had concentrations of total and dissolved mercury well below the

Table 1.—*Concentrations of mercury in selected streams, lakes, and snow samples of the Adirondack region, New York*

Sampling site	Location	Collection date	Total mercury (μg/l)	Dissolved mercury (μg/l)
	Water samples			
1	Hudson River, 1 mile southeast of The Glen, next to State Highway 28.	Nov. 9, 1970	<0.5	...
		Feb. 16, 1971	<.5	0.2
		Apr. 21, 1971	<.5	<.1
2	Hudson River at North Creek, at bridge on State Highway 28N.	Nov. 9, 1970	<.5	...
		Feb. 16, 1971	<.5	...
		Apr. 21, 1971	<.5	<.1
3	Balfour Lake, 4 miles north of Minerva, next to State Highway 28N.	Nov. 9, 1970	<.5	...
4	Boreas River, 1 mile north of Aiden Lair, at bridge on State Highway 28N.	Nov. 9, 1970	<.5	...
		Feb. 16, 1971	<.5	.3
		Apr. 21, 1971	<.5	<.1
5	Hudson River, 2 miles east of Newcomb, at bridge on State Highway 28N.	Nov. 9, 1970	<.5	...
		Feb. 16, 1971	<.5	<.1
		Apr. 21, 1971	<.5	<.1
6	Bog, 5 miles west of Newcomb, next to highway markers 1202 and 1030 on State Highway 28N.	Nov. 9, 1970	<.5	...
7	Stream, ½ mile east of the village of Long Lake, next to State Highway 28N.	Nov. 9, 1970	<.5	...
		Feb. 16, 1971	<.5	.2
		Apr. 21, 1971	<.5	<.1
8	Long Lake at the village of Long Lake, next to State Highway 30.	Nov. 9, 1970	<.5	...
		Feb. 17, 1971	<.5	<.1
		Apr. 21, 1971	<.5	<.1
9	Tupper Lake at the village of Tupper Lake, 5 miles north of junction of State Highways 421 and 30, next to Highway 30 at water-supply building.	Nov. 9, 1970	<.5	...
		Feb. 17, 1971	<.5	.2
		Apr. 21, 1971	<.5	<.1
10	Raquette River at the village of Tupper Lake, 1½ miles south of junction of State Highways 3 and 30, next to Highway 30.	Nov. 9, 1970	<.5	...
11	Raquette River, 3 miles east of the village of Tupper Lake, next to State Highways 30 and 3.	Nov. 9, 1970	<.5	...
		Feb. 17, 1971	<.5	.2
		Apr. 21, 1971	<.5	<.1
12	Upper Saranac Lake at Wawbeek, next to State Highway 30.	Nov. 9, 1970	<.5	...
		Feb. 17, 1971	<.5	.4
		Apr. 21, 1971	<.5	<.1
13	Lake, 4½ miles north of Wawbeek, next to State Highway 30.	Nov. 9, 1970	<.5	...
		Feb. 17, 1971	<.5	.1
		Apr. 21, 1971	<.5	.1
14	Bog, 4½ miles southwest of the village of Lake Clear, next to State Highway 30.	Nov. 9, 1970	<.5	...
15	Lake Clear at the village of Lake Clear, next to State Highway 30.	Nov. 9, 1970	<.5	...
		Feb. 17, 1971	<.5	.2
		Apr. 21, 1971	<.5	<.1
16	Drainage across State Highway 3, 2 miles northwest of Piercefield.	Nov. 9, 1970	<.5	...
		Feb. 17, 1971	<.5	<.1
		Apr. 22, 1971	<.5	<.1
17	South Branch Grass River, 3 miles northeast of the village of Cranberry Lake, at bridge on State Highway 3.	Nov. 9, 1970	<.5	...
		Feb. 18, 1971	<.5	<.1
		Apr. 22, 1971	<.5	<.1
18	Cranberry Lake at the village of Cranberry Lake, next to State Highway 3.	Nov. 9, 1970	<.5	...
19	Oswegatchie River at the village of Cranberry Lake, at bridge just below dam.	Nov. 9, 1970	<.5	...
		Feb. 17, 1971	<.5	.2
		Apr. 22, 1971	<.5	.2
20	Oswegatchie River at Fine at bridge on State Highway 58.	Apr. 22, 1971	<.5	<.1
21	Drainage across State Highway 58, 3 miles southwest of Edwards.	Feb. 17, 1971	<.5	<.1
22	West Branch Oswegatchie River, 2 miles east of Fowler at bridge on State Highway 58.	Feb. 18, 1971	<.5	...
		Apr. 22, 1971	<.5	<.1
23	West Branch Oswegatchie River at Fullerville, at bridge.	Feb. 18, 1971	<.5	<.1
24	Drainage across State Highway 58 at Fowler.	Feb. 18, 1971	.9	<.1
		Apr. 22, 1971	<.5	<.1
25	Lake Sylvia, 1 mile west of Balmat.	Apr. 22, 1971	<.5	<.1
26	Raquette Lake, 2 miles east of the village of Raquette Lake, next to State Highway 28.	Nov. 10, 1970	<.5	...
		Feb. 18, 1971	<.5	...
		Apr. 22, 1971	<.5	.2
27	Bog, 1 mile southwest of the village of Raquette Lake, next to State Highway 28.	Nov. 10, 1970	<.5	...
28	Fulton Chain of Lakes, 3 miles west of Eagle Bay, next to State Highway 28.	Nov. 10, 1970	<.5	...
		Apr. 23, 1971	<.5	<.1
29	North Branch Moose River, 3 miles north of McKeever, next to State Highway 28.	Nov. 10, 1970	<.5	...
		Feb. 18, 1971	<.5	<.1
		Apr. 23, 1971	<.5	<.1
30	Moose River at McKeever, at bridge on State Highway 28.	Nov. 10, 1970	<.5	...
		Feb. 18, 1971	<.5	...
		Apr. 23, 1971	<.5	<.1
31	Rock River, 3 miles east of the village of Blue Mountain Lake, at bridge on State Highways 28 and 30.	Nov. 10, 1970	<.5	...
		Apr. 23, 1971	<.5	<.1

Table 1.—*Concentrations of mercury in selected streams, lakes, and snow samples of the Adirondack region, New York*—Continued

Sampling site	Location	Collection date	Total mercury (μg/l)	Dissolved mercury (μg/l)
32	Cedar River, 2 miles west of the village of Indian Lake, at bridge on State Highway 30-28.	Nov. 10, 1970	<.5	...
		Feb. 19, 1971	<.5	<.1
		Apr. 23, 1971	<.5	<.1
33	Indian River, 1 mile east of the village of Indian Lake, at bridge on State Highway 28.	Nov. 10, 1970	<.5	...
		Feb. 19, 1971	<.5	...
		Apr. 23, 1971	<.5	<.1
34	Indian Lake, 8 miles south of Sabael, at drainage line between Lewey Lake and Indian Lake, next to State Highway 30.	Nov. 10, 1970	<.5	...
		Feb. 19, 1971	<.5	...
		Apr. 23, 1971	<.5	<.1
35	Lake Pleasant at Speculator, at bridge on State Highway 30.	Nov. 10, 1970	<.5	...
		Feb. 19, 1971	<.5	...
		Apr. 23, 1971	<.5	<.1
36	Sacandaga River, 6 miles east of Speculator, next to State Highway 30, at bridge on side road.	Nov. 10, 1970	<.5	...
		Feb. 19, 1971	<.5	...
		Apr. 23, 1971	<.5	<.1
37	East Branch Sacandaga River, 1½ miles northeast of Griffin, next to State Highway 8.	Nov. 10, 1970	<.5	...
		Feb. 19, 1971	<.5	...
		Apr. 23, 1971	<.5	<.1
38	Algonquin Lake at Wells, near bridge on State Highway 30.	Nov. 10, 1970	<.5	...
		Feb. 19, 1971	<.5	...
		Apr. 23, 1971	<.5	<.1
39	Sacandaga River, 5 miles northwest of Northville, at bridge on State Highway 30.	Nov. 10, 1970	<.5	...
		Feb. 19, 1971	<.5	...
		Apr. 23, 1971	<.5	<.1
	Snow samples			
4	1 mile north of Aiden Lair, near State Highway 28N bridge over Boreas River.	Feb. 16, 1971	<.5	<.1
19	At the village of Cranberry Lake, near dam.	Feb. 18, 1971	<.5	.3
		Apr. 22, 1971	...	<.1

recommended limit (5 μg/l) for drinking water in New York (New York State Department of Health, 1971). The concentration of mercury in four of five snow samples was also less than the detectable limits; however, one sample had a concentration of dissolved mercury of 0.3 μg/l. The two sediment samples (table 2) had mercury concentrations of <0.1 and 0.2 μg/kg, respectively.

Limits of detection for concentrations of total and dissolved mercury were based on the precision of the analytical methods used; concentrations of mercury below these values could not be determined.

Table 2.—*Mercury on sediment in two streams of the Adirondack region, New York*

Sampling site	Location	Collection date	Mercury adsorbed by sediment (μg/kg)
7	Stream, ½ mile east of the village of Long Lake, next to State Highway 28N.	Apr. 21, 1971	<0.1
19	Oswegatchie River at the village of Cranberry Lake, at bridge just below dam.	Apr. 22, 1971	.2

SUMMARY AND CONCLUSIONS

Total mercury concentration includes mercury dissolved in water as well as mercury adsorbed on suspended sediment carried by a stream or lake. Because both forms of mercury could be available to organisms, the total value should be used to establish a natural background concentration. Data from this study indicate that the natural background concentration of mercury in lakes and streams of the Adirondack region of New York State is less than 0.5 μg/l. Concentrations higher than 0.5 μg/l could be considered an indication of pollution. A similar natural background concentration of mercury might be assumed for other areas having similar geologic and hydrologic conditions.

REFERENCES

Brandenberger, H., and Bader, H., 1967, The determination of nanogram levels of mercury in solution by a flameless atomic absorption technique: Atomic Absorption Newsletter, v. 6, no. 5, p. 101–103.

Buddington, A. F., and Leonard, B. F., 1962, Regional geology of the St. Lawrence County magnetite district, northwest Adirondacks, New York: U.S. Geol. Survey Prof. Paper 376, 145 p.

Dall'Aglio, M., 1968, The abundance of mercury in 300 natural water samples from Tuscany and Latium (central Italy), *in* Ahrens, L. H., ed., Origin and distribution of the elements: New York, Pergamon Press, p. 1065–1081.

Fisher, D. W., Isachsen, Y. W., Rickard, L. W., and Broughton, J. G., 1962, Geologic map of New York, 1961: New York State Mus. and Sci. Service Map and Chart Ser., no. 5.

Goldwater, L. J., 1971, Mercury in the environment: Sci. American, v. 224, no. 5, p. 15–22.

Hatch, W. R., and Ott, W. R., 1968, Determination of submicrogram quantities of mercury by atomic absorption spectrophotometry: Anal. Chemistry, v. 40, no. 14, p. 2085–2089.

Heide, Fritz, Lerz, H., and Bohn, G., 1957, Lead and mercury content of waters from Saale River: Naturwissenschaften, v. 44, no. 16, p. 441–442. [In German]

Hem, J. D., 1970, Chemical behavior of mercury in aqueous media, *in* Mercury in the environment: U.S. Geol. Survey Prof. Paper 713, p. 19–22.

Hinkle, M. E., and Learned, R. E., 1969, Determination of mercury in natural waters by collection on silver screens, *in* Geological Survey Research 1969: U.S. Geol. Survey Prof. Paper 650-D, p. D251–D254.

Jenne, E. A., 1970, Atmospheric and fluvial transport of mercury, *in* Mercury in the environment: U.S. Geol. Survey Prof. Paper 713, p. 40–45.

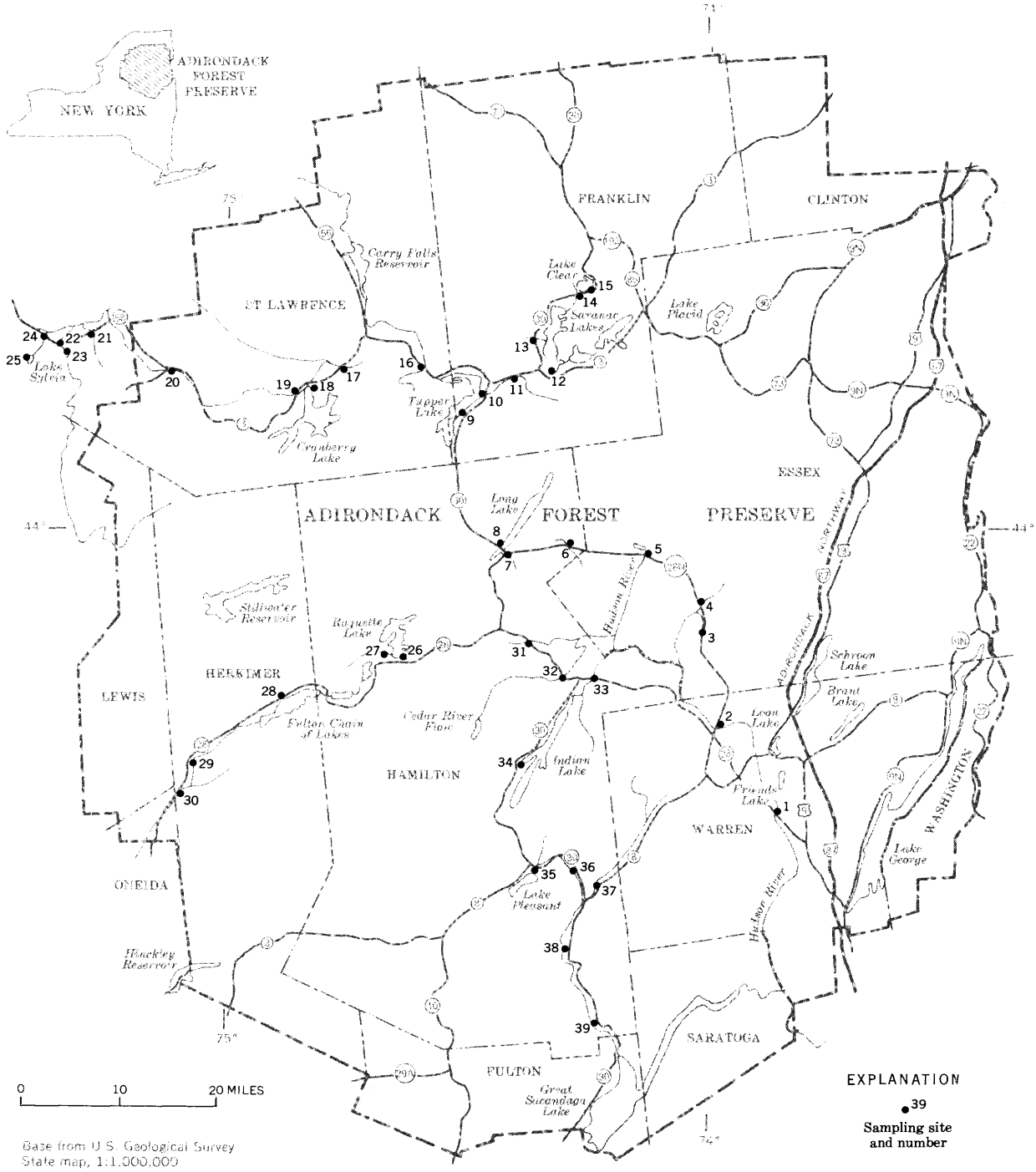

Figure 2.—Location of study area and sampling sites in the Adirondack region, New York.

Jensen, S. R., and Jernelov, A., 1969, Biological methylation of mercury in aquatic organisms: Nature, v. 223, no. 5207, p. 753–754.

Lange, A. D., and Forker, G. M., eds., 1967, Handbook of chemistry, revised 10th ed.: New York, McGraw-Hill Book Company, 2000 p.

New York State Department of Health, 1971, Part 170, Subchapter C—Water supply sources of chapter III, title 10 (health): Official Compilation of Codes, Rules, and Regulations of the State of New York.

Rankama, Kalervo, and Sahama, Th. G., 1950, Geochemistry: Chicago, Univ. Chicago Press, 912 p.

Shacklette, H. T., 1970, Mercury content of plants, *in* Mercury in the environment: U.S. Geol. Survey Prof. Paper 713, p. 36.

U.S. Geological Survey, 1970, Mercury in the environment: U.S. Geol. Survey Prof. Paper 713, 67 p.

Vinogradov, A. P., 1962, Average contents of chemical elements in the principal types of igneous rocks of the earth's crust: Geokhimiya 1962, no. 7, p. 555–571 [In Russian]; translation in Geochemistry, 1962, no. 7, p. 641–664.

SPECIFIC-CONDUCTANCE SURVEY OF THE MALAD RIVER, UTAH AND IDAHO

By L. J. McGREEVY, Logan, Utah

Work done in cooperation with the Utah Department of Natural Resources, Division of Water Rights

Abstract.—A specific-conductance survey of the Malad River, August 12–13, 1971, indicates that Woodruff Warm Springs and Udy Hot Springs are sources of large amounts of dissolved solids in the river, and that flow derived from other sources contains a relatively low average concentration of dissolved solids. Conditions at the time of the survey generally represent average June-September conditions.

Field measurements of specific conductance of water from the Malad River and some of its tributaries were made August 12 and 13, 1971. Samples were collected at 30 sites between the headwaters of the river at Big Malad Spring in Idaho and the mouth at the Bear River in Utah. The purpose of the specific-conductance survey was to estimate the salinity of the Malad River, as defined by the specific conductance,[1] and to identify the principal sources of the dissolved solids.

The U.S. Geological Survey operates gaging stations at four of the sampling sites:

10125500 Malad River at Woodruff, Idaho;
10125600 Malad River near Plymouth, Utah;
10125700 Bear River Duck Club Canal near Bear River City, Utah; and
10125800 Malad River below Bear River Duck Club Canal, near Bear River City, Utah.

(Station names are abbreviated in the discussions that follow.) The discharge of the Malad River at the Bear River Duck Club Canal diversion is the sum of the discharges measured at two stations, 10125700 and 10125800. Discharge at most ungaged sampling sites was estimated from measurements of surface velocity and cross-section area. Field estimates of discharge were adjusted on the basis of discharge at the gaging stations. Because some of the discharge at Woodruff Warm Springs and Udy Hot Springs is directly into the river, estimates of total spring discharge are approximate.

Results of the specific-conductance survey, discharge values, and locations of gaging stations and springs are shown in figure 1. The relative salt load at the sampling sites is indicated by the areas of the shaded rectangles. At the time of the survey, most of the water in the drainage system upstream from Woodruff Warm Springs was diverted for irrigation. Most of the water and most of the salt load that passed the Woodruff station and entered Utah was contributed by Woodruff Warm Springs. Udy Hot Springs is a large source of salt, and more than 90 percent of the salt load in the river at the Plymouth station was from Woodruff and Udy Springs. Minor gains and losses in flow and in salt load between the Woodruff and Plymouth stations are overshadowed by the large salt contribution of Udy Hot Springs.

Discharge of the Malad River increased substantially in the reach from the Plymouth station to Tremonton, Utah, and in the reach below the Bear River Duck Club Canal diversion. Part of the increase was irrigation "wastewater," but most of the increase was ground water from springs, seeps, and drains. Between the Plymouth station and the Bear River Duck Club Canal diversion, the river gained 33 cfs (cubic feet per second) of water with a calculated specific conductance of 1,800 μmhos/cm (micromhos per centimeter). The total flow of 57 cfs at the diversion had a specific conductance of about 4,000 μmhos/cm. Without the discharge and salt load contributed by Woodruff Warm Springs and Udy Hot Springs, the net discharge at the diversion would have been 40 cfs and the calculated specific conductance 1,600 μmhos/cm. Between the diversion and a sampling site near the mouth of the Malad River, the river gained an estimated 27 cfs of water with a calculated specific conductance of 2,500 μmhos/cm.

Evapotranspiration in an area between Malad City, Idaho, and Woodruff Warm Springs causes salt to accumulate in soils

[1]Specific conductance is a measure of the ability of water to conduct electricity and is expressed in micromhos per centimeter at 25°C. The specific conductance can be used to estimate the concentration of dissolved solids in the water. For the water discussed in this report, the concentration of dissolved solids (in milligrams per liter) is generally near 60 percent of the specific conductance (in micromhos per centimeter).

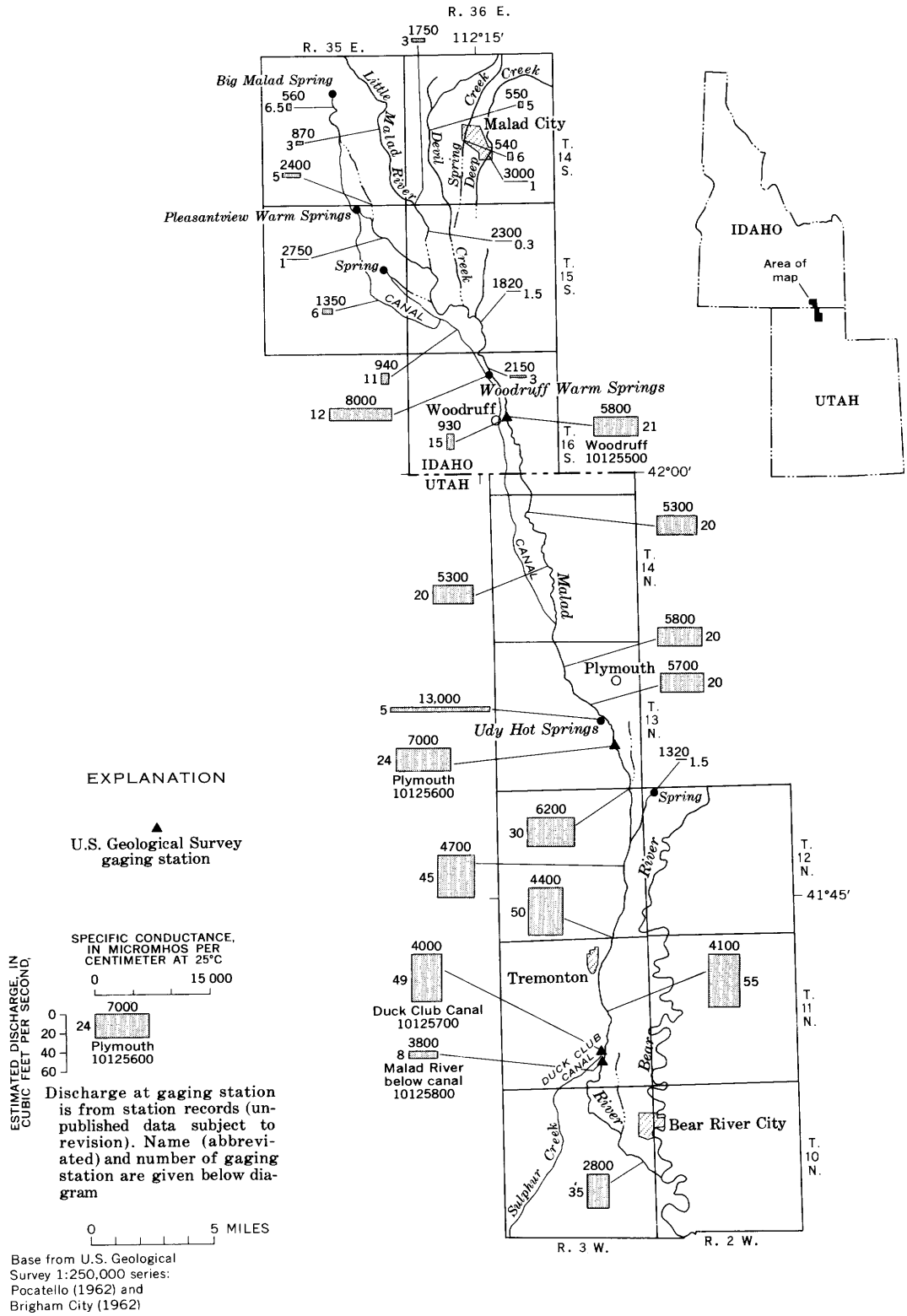

Figure 1.—Specific conductance and discharge at selected sites on the Malad River, Utah-Idaho, August 12–13, 1971.

and locally produces salt crusts. During times of high runoff, some of the salt may be dissolved and carried to the Malad River. Such solution may be a significant source of dissolved solids in the river at times during the year, but it was a negligible source at the time of the specific-conductance survey.

Comparison of data from the specific-conductance survey with published records (Waddell, 1970, p. 48–55; U.S. Geological Survey, 1965–69a, b) indicates that conditions at the time of the survey generally represent average June-September conditions. During June-September 1965–69, mean discharge and estimated specific conductance of the water were 21 cfs and 5,900 μmhos/cm at the Woodruff station, 27 cfs and 6,600 μmhos/cm at the Plymouth station, and 56 cfs and 4,100 μmhos/cm at the Bear River Duck Club Canal diversion. (Specific conductance of the mean discharge was estimated from fig. 2.) These figures are generally similar to data collected for the specific-conductance survey (fig. 1).

Monthly mean discharge at the gaging stations for the 1969 water year, the most recent year with complete published records, is shown by bars in figure 3. Specific conductance of the mean discharge, which is shown by the numbers above the bars, was estimated from figure 2. During June-September 1969, mean discharge and specific conductance were generally similar to data collected at the time of the survey; during the rest of the year, mean discharge was generally higher and specific conductance was lower.

Estimated discharge and specific conductance of water in the Malad River from sources other than Woodruff Warm Springs and Udy Hot Springs are shown in figure 3 for the 1969 water year. Bars showing mean discharge at the gaging stations are subdivided to show the source of water; the calculated specific conductance of the water from sources other than the springs is shown by the numbers beside the bars. The discharge and specific conductance of the springs were those determined during the specific-conductance survey. Discharge from sources other than Woodruff Warm Springs and Udy Hot Springs ranged from about 4 to 213 cfs, and specific conductance ranged from about 1,600 to 2,600 μmhos/cm.

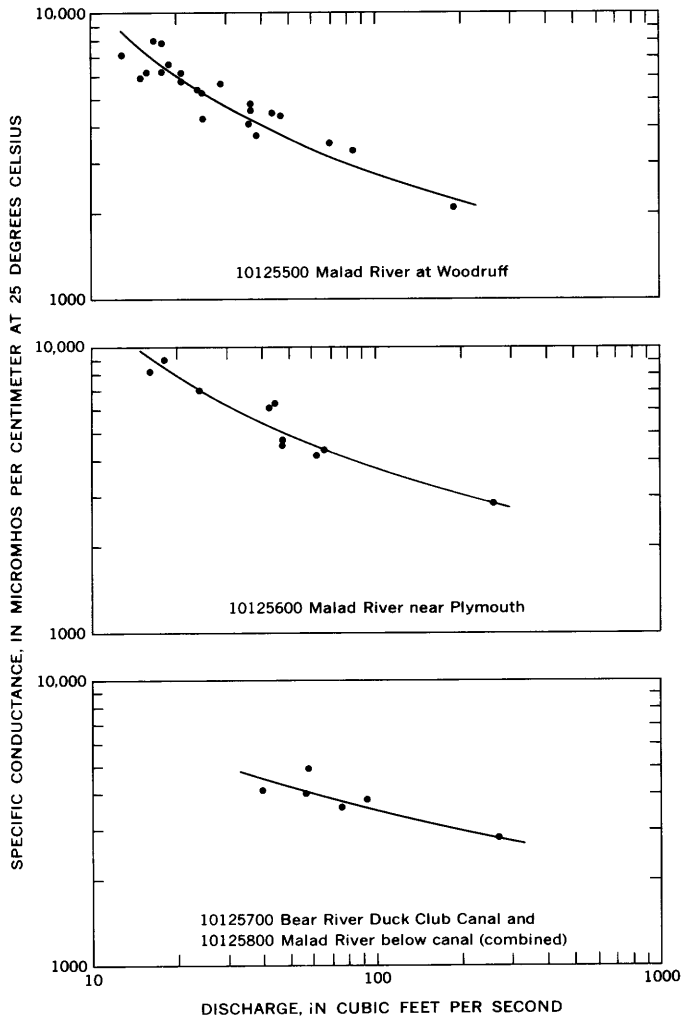

Figure 2.–Relation of specific conductance to discharge at gaging stations on the Malad River. Data from miscellaneous measurements, 1959–71.

REFERENCES

U.S. Geological Survey, 1965–69a, Water resources data for Utah, Pt. 1, Surface water records; Pt. 2, Water quality records: Salt Lake City, Utah, U.S. Geol. Survey.

——1965–69b, Water resources data for Idaho, Pt. 1, Surface water records; Pt. 2, Water quality records: Boise, Idaho, U.S. Geol. Survey.

Waddell, K. M., 1970, Quality of surface water in the Bear River basin, Utah, Wyoming, and Idaho: U.S. Geol. Survey open-file rept.; Utah basic-data release 18, 65 p.

[Figure 3 on next page]

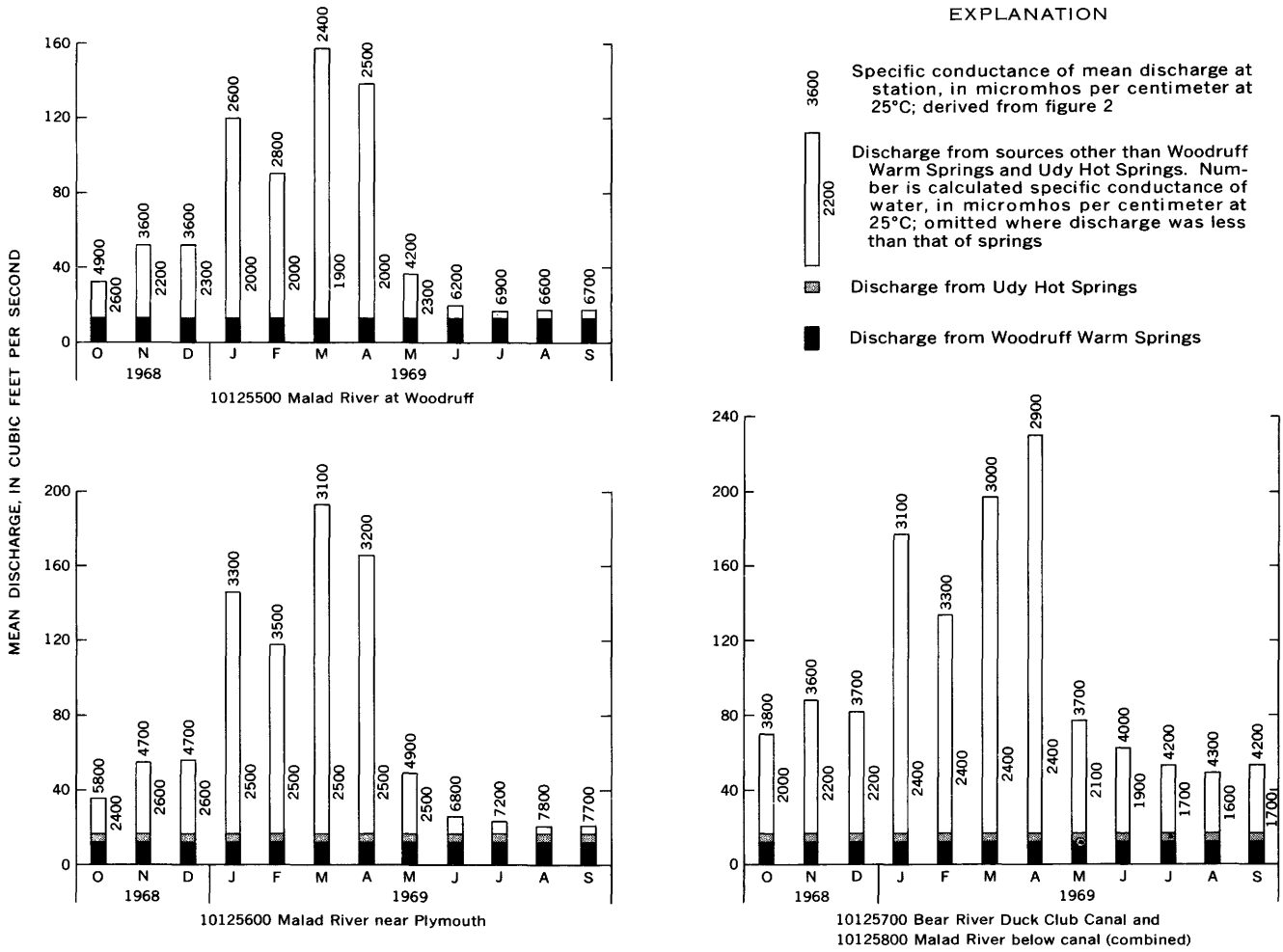

Figure 3.—Monthly mean discharge and estimated specific conductance of the Malad River and estimated discharge and specific conductance of water in the river from sources other than Woodruff Warm Springs and Udy Hot Springs, 1969 water year.

REMOTE SENSING OF NEW YORK LAKES

By JANICE M. WHIPPLE, Albany, N.Y.

Work done in cooperation with the National Aeronautics and Space Administration and the New York State Department of Environmental Conservation

Abstract.—Reverse flow through the outlet of Onondaga Lake and thermal activity associated with the spring mixing of Cayuga Lake were discerned on thermal-infrared imagery. Thermal radiances of natural and artificial discharges into Lake Ontario were measured, delineating the thermally pulsating nature of discharges into the open lake and thermal relationships between water masses. Quantitative imagery (radiometry) will become most useful in defining energy exchanges at the air-water interface.

This report is part of a 2-year investigation of the application of remote sensing for acquisition and communication of information about lake processes.

Three different New York lake environments were studied:

1. Lake Ontario (shoreline): very large, one of the Great Lakes, rural and urban areas, nearshore ice cover.
2. Cayuga Lake: moderate size, deep, one of the Finger Lakes, predominantly rural, little ice cover.
3. Onondaga Lake: small, relatively shallow, in an urban setting, subject to major ice cover.

For each lake, aerial visible photography and thermal-infrared imagery were provided by the U.S. Air Force Rome Air Development Center, and calibrated thermal-infrared imagery was contracted commercially as part of a Geological Survey cooperative program with the New York State Department of Environmental Conservation. Imagery was correlated with available water and weather data.

For guidelines to remote sensing in hydrology, see Robinove and Anderson (1969), and for information on infrared photography and imagery, see Robinove (1965).

LAKE ONTARIO

Figure 1 is a reduced-scale print of infrared imagery of Lake Ontario, N.Y., at Oswego Harbor on the night of June 9, 1971. Quantitative imagery is shown as the bottom data strip of three on original 9-inch film; lighter tones represent greater thermal radiances corresponding to higher temperatures. In quantitative imagery, gray shades are related to radiance in a constant, linear fashion through controllable d-c amplifying circuits and are referenced to scanner blackbody radiators with calibrated radiances. In this image, the radiators are set at temperatures 4°C apart, and the corresponding gray shades are shown along the edges of the image (bottom) strip. Qualitative imagery is printed in the top data strip for locating the line of sight of the separate radiometer. This imagery has no blackbody references, uses an a-c amplifier, and is sometimes subjected to automatic gain control. It is printed here in negative format.

The radiometer and scanner blackbody reference temperatures are available but are not shown here. The radiometer trace is printed so that radiance values increase upward. The imagery is not corrected for geometric scanner distortion; therefore, the transverse scale decreases from center to edge, as shown in the bottom strip (fig. 1), where h = flying height above ground level. General information on line scanners and infrared systems is given by Lowe (1968) and Parker (1968). For a description of data-collection equipment and operation, see Whipple (1971).

Imagery of the Lake Ontario shoreline, acquired at several times throughout the year, showed thermal contrasts between natural discharges of the tributary streams, artificial discharges, and the lake proper. In July 1970 and June 1971 the apparent thermal radiance of the Oswego River at Oswego Harbor was greater than that of the adjacent discharge of heated water from a generating plant at the west end of the harbor enclosure; both discharges were warmer than the ambient nearshore lake surface (fig. 1). The fact that streams respond more quickly than large lakes to rising air temperatures in spring contributes to this situation. During November and April, however, the river is cooler than the plant discharge, and in November the river appears to be cooler than the lake.

Conditions similar to those at Oswego also occurred near Rochester on the night of June 9, 1971 (fig. 2). Nearshore water (bottom of image) of Lake Ontario is generally warmer

U.S. GEOL. SURVEY PROF. PAPER 800-C, PAGES C243-C247

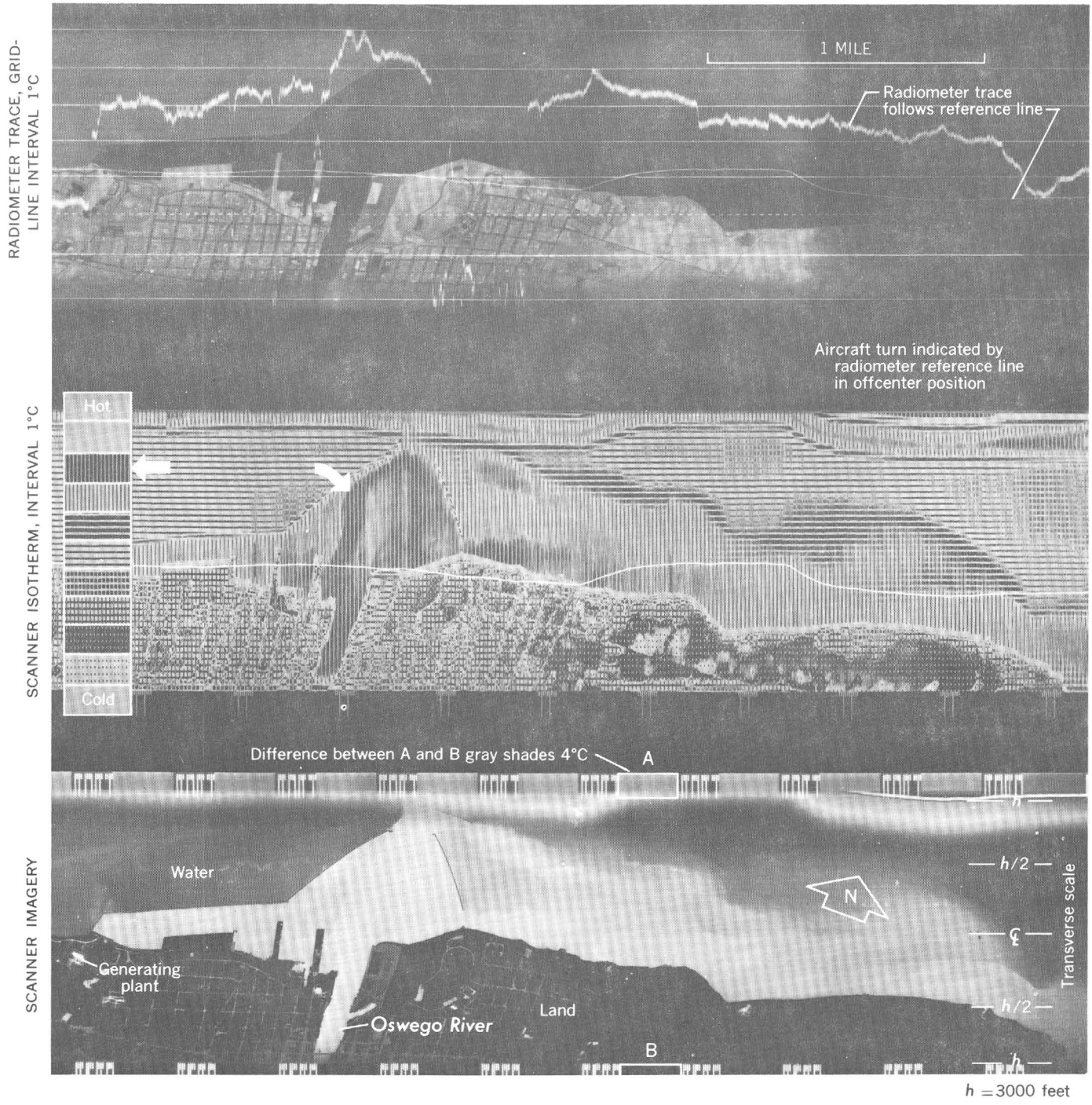

Figure 1.—Infrared imagery of Lake Ontario, N.Y., at Oswego Harbor, June 9, 1971, 2340 hours e.s.t. (Data by HRB-Singer, Inc., for U.S. Geological Survey.)

than the land (top of image), except for streets. The Genesee River (left) flows through breakwaters extending some 2,000 feet offshore, and a generating plant discharges cooling water into the lake about 7,000 feet west (right) of the river. The isothermal printout (center strip) points out that at this particular time the surface of the river is warmer than all but a small part of the generating-plant plume. The imagery (bottom strip) shows that the discharges also have a thermally pulsating appearance, a phenomenon noted elsewhere and at other seasons.

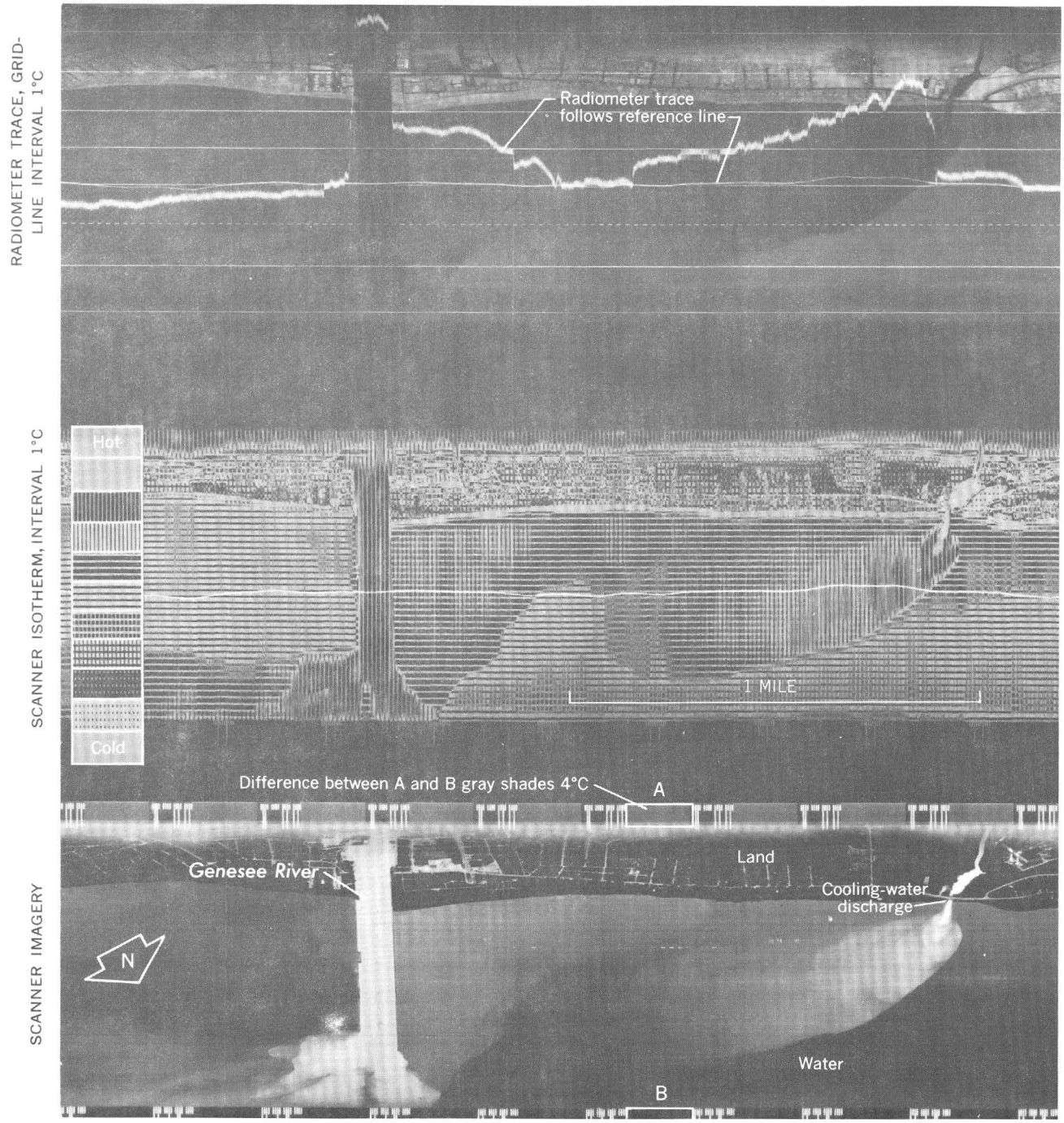

Figure 2.—Infrared imagery of Lake Ontario, N.Y., near Rochester, June 9, 1971, night. (Data by HRB-Singer, Inc., for U.S. Geological Survey.)

CAYUGA LAKE

Figure 3 is a reduced-scale print of thermal-infrared imagery showing about 4 miles of Cayuga Lake's eastern shoreline north of Aurora, N.Y., flown on the night of April 15, 1971. The zone of warmer water out from Ellis Point is about 700 feet wide. The radiometer trace (where legible on the print) shows that the thermal contrast with the cooler water offshore is about 3°–4°C. By reference to the flight log showing the radiometer blackbody setting, the radiance (emitted radiant energy or radiant temperature) of offshore water is about 0°C.

Similar features had been observed on qualitative imagery of the lake March 19, 1970, but no measurements of radiant energy were available. The thermal range measured in 1971 suggests that these features are part of the spring mixing of Cayuga Lake. If these thermal-infrared data could be collected

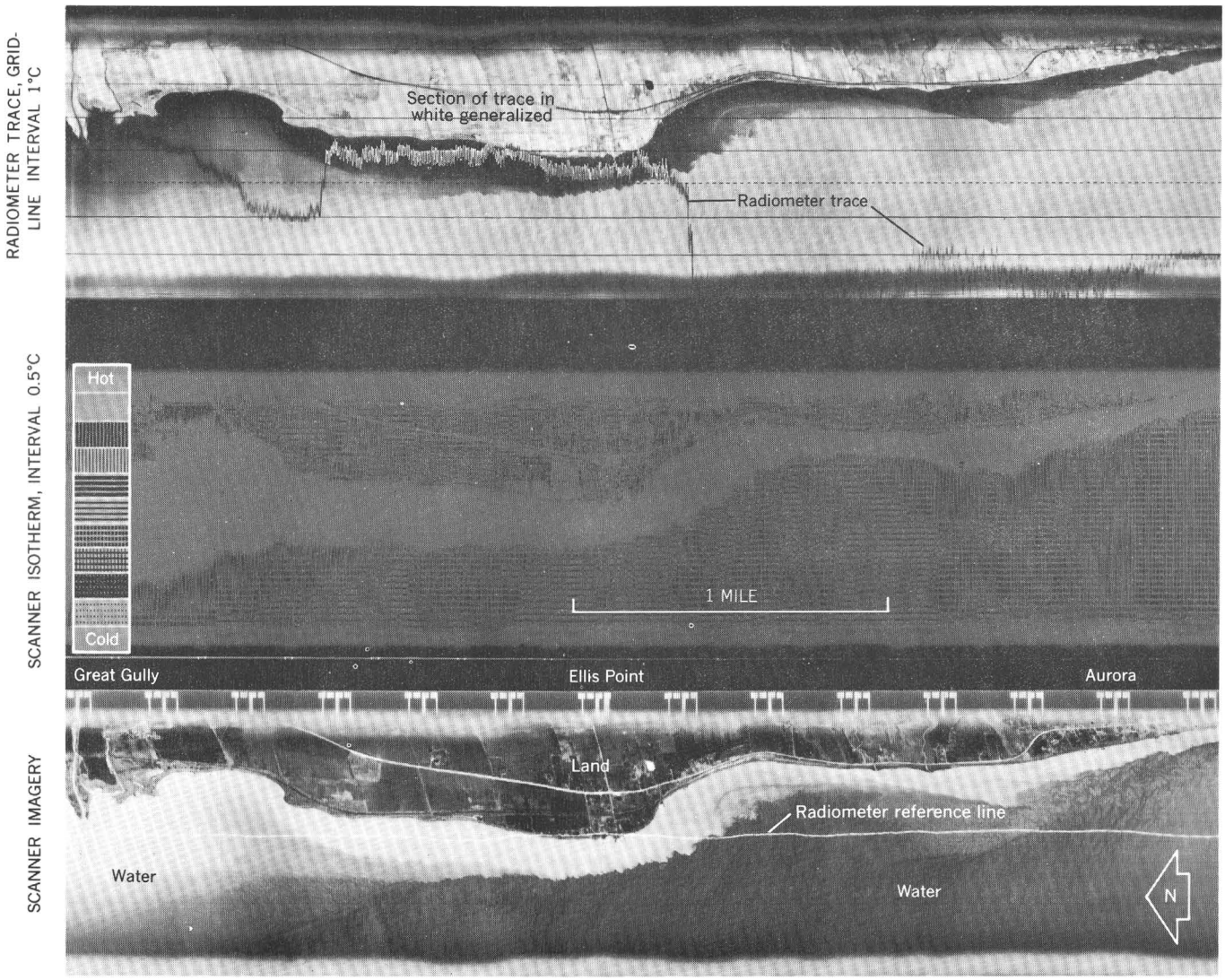

Figure 3.—Infrared imagery of Cayuga Lake, N.Y., near Aurora, April 15, 1971, night. (Data by HRB-Singer, Inc., for U.S. Geological Survey.)

systematically, insight into the lake-mixing processes could be gained.

ONONDAGA LAKE

On several occasions, imagery revealed cool water from the Onondaga Lake outlet protruding into the warmer lake. This phenomenon, illustrated in another report (Whipple and Haynes, 1971, p. 52–9), indicates that there is a reversal in direction of flow in the outlet. Flow was of varying intensity and occurred against the wind in at least one instance. The occurrence of this reverse flow had been previously suggested, but the outlet has been difficult to gage because of the small elevation gradient and the difficulty of separating wind and flow effects at low water velocities (Whipple, 1971). Subsequent field measurements showed that a reverse flow occurred in the upper 4.5 feet of a 15-foot deep channel. Water-level regulation in other parts of the basin probably causes the reverse flow, and lake salinity influences its specific behavior.

CONCLUSIONS

These lake studies have shown that thermal radiance variations displayed on qualitative imagery are effective natural indicators of water circulation patterns. However, quantitative imagery (radiometry) is necessary to help assess the proportions of natural and manmade heat inputs, espe-

cially to better define the term "thermal pollution." Quantitative imagery also reduces the fieldwork necessary for limnological ground truth. Analysis of such imagery has pointed out the need for calibrating individual in-place temperature sensors and locating them at sites suitable for collecting the water information required.

Ultimately thermal-infrared radiometry will be used to define energy exchanges at the air-water interface. Activity at this surface is difficult to measure by traditional methods and is an important part of the energy cycle for all water bodies.

REFERENCES

Lowe, D. S., 1968, Line scan devices and why use them, *in* Symposium on remote sensing of environment, 5th, 1968, Ann Arbor, Mich., Univ. Michigan, Willow Run Labs., Proc.: p. 77–101.

Parker, D. C., 1968, Remote sensing for engineering investigations of terrain–infrared systems, *in* Symposium on remote sensing of environment, 5th, 1968, Ann Arbor, Mich., Univ. Michigan, Willow Run Labs., Proc.: p. 701–707.

Robinove, C. J., 1965, Infrared photography and imagery in water resources research: Am. Water Works Assoc. Jour., v. 57, no. 7, p. 834–840.

Robinove, C. J., and Anderson, D. G., 1969, Some guidelines for remote sensing in hydrology: Water Resources Bull., v. 5, no. 2, p. 10–19.

Whipple, J. M., 1971, Airplanes and hydrologists–a beneficial alliance: Conservationist, Oct.–Nov. 1971, p. 17–21.

Whipple, J. M., and Haynes, R. B., 1971, Management applications for thermal infrared imagery of lake processes, *in* Annual earth resources program review, 3d, Houston, 1970: Houston, Tex., Natl. Aeronautics and Space Adm., Manned Space Center, v. 3, sec. 52, p. 1–13.

A LOSING DRAINAGE BASIN IN THE MISSOURI OZARKS IDENTIFIED ON SIDE-LOOKING RADAR IMAGERY

By G. L. FEDER and J. H. BARKS, Rolla, Mo.

Work done in cooperation with the Missouri Geological Survey and Water Resources

Abstract.—Logan Creek basin, a losing drainage basin in the Missouri Ozarks, is identified on side-looking radar imagery. Owing to the rapid infiltration of precipitation in the Logan Creek basin, erosion and dissection are greatly reduced in comparison with rates of these processes in the surrounding normal or gaining basins. Thus the Logan Creek basin has a more uniform tone and a smoother texture on the side-looking radar imagery than the highly dissected surrounding basins. This distinctive tonal and textural contrast may be useful in identifying other losing drainage basins in carbonate terranes.

The purpose of this report is to show the potential usefulness of SLAR (side-looking airborne radar) imagery in identifying losing parts of basins in the Missouri Ozarks. A losing basin is a drainage area which loses water to another basin; a gaining basin gains water from another basin. Ordinarily a basin neither loses water to nor gains water from another basin to any appreciable extent. It is hoped that the principles of recognition developed in this study will be applicable elsewhere as more radar imagery becomes available.

STUDY AREA

The study area includes the Logan Creek drainage basin and springs and streams in surrounding areas (fig. 1). Logan Creek basin contains a surface area of approximately 200 square miles and has an overall length of about 50 miles from its beginning to its confluence with the Black River in Clearwater Lake.

Rocks cropping out in the basin are dolomites of Cambrian and Ordovician age. The losing part of the basin is mostly covered by a thick, permeable, cherty residuum, and very few bedrock exposures exist. The Ellington fault (fig. 1) is the most conspicuous structural feature of the area.

Floods

During floods the losing part of Logan Creek generally remains well within its banks while other nearby streams inundate their flood plains. Local residents report that flow is seldom continuous throughout the length of the creek, and that the flood of 1915 was the last time Logan Creek inundated a large part of its flood plain. Because of the low flood potential many buildings are located on the flood plain, some immediately adjacent to the stream.

In January 1969, an estimated 200 cfs (cubic feet per second) of water was observed to disappear from the stream in the 2-mile reach downstream from the Ellington fault. A dye-tracing study was made in order to determine the path of this water.

Dye study

During a low-flow period in October 1969, 5 pounds of Rhodamine WT dye was injected into Logan Creek at point A (fig. 1). The elevation above sea level at this point is 880 feet. The flow was 3.2 cfs, but all surface flow disappeared within 1 mile downstream from the point of dye injection. Wire-mesh packets containing activated charcoal granules were placed at all sampling points (see fig. 1), including Logan Creek (B) 17 miles below the point of dye injection, where the stream started flowing again, and 5 miles farther downstream (point C) just below several springs. The dye was recovered between 3 and 10 days later at point C (elevation 590 feet), where the stream is once again north of the Ellington fault. At point B, just north of the fault, no dye was recovered even though the stream starts flowing again in this vicinity. The water flowing to Logan Creek at point B probably comes from the residuum overlying the hills in this vicinity. Apparently the bedrock is not as permeable in this area as it is farther upstream, and ground water is perched at the residuum-bedrock interface and then flows to Logan Creek.

The dye was adsorbed by charcoal packets between 3 and 10 days later at Blue Spring (point H), which confirms a hypothesis by Bridge (1930, p. 40) that water lost from Logan Creek resurges in Blue Spring. However, as noted above, some water does resurge within the downstream part of Logan

U.S. GEOL. SURVEY PROF. PAPER 800-C, PAGES C249-C252

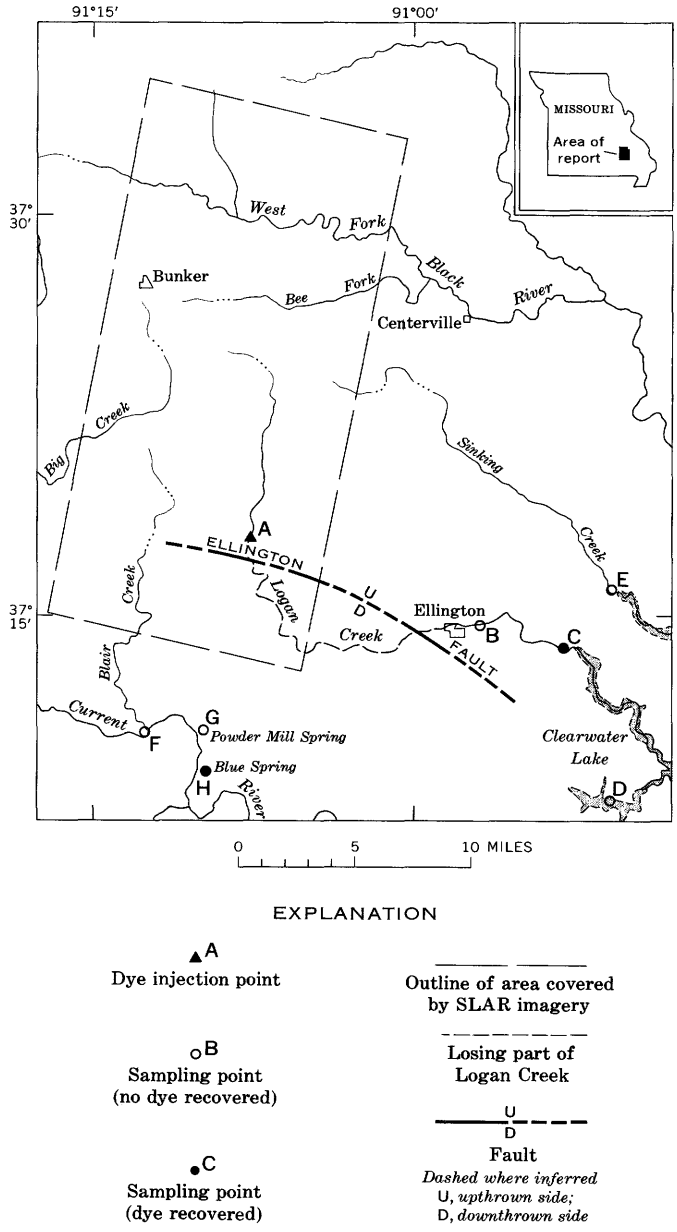

Figure 1.—Map of study area in the Missouri Ozarks, showing dye injection point, sampling points, and area covered by SLAR imagery.

Creek. Blue Spring is located in the Current River basin south of the Ellington fault and has an elevation of 550 feet. It has an average discharge of 140 cfs and appears to be one of the main outlets for water from the Logan Creek basin.

SIDE-LOOKING RADAR IMAGERY

The SLAR imagery available for the study area shows the upper part of Logan Creek basin and some of the surrounding basins (fig. 2). It was acquired on National Aeronautics and Space Administration flight 128, July 28, 1966. The plane was flying in a southerly direction, and the radar was looking westerly.

In the SLAR imagery the Logan Creek basin has a more uniform tone and a smoother texture than do the surrounding "normal" basins. The surrounding highly dissected basins produce stronger tonal and textural differences on the imagery. According to Rydstrom (1966, p. 193), "Radar can only illuminate those surfaces which are directly on a line-of-sight from the antenna. Surfaces not in this line receive no energy and are recorded by the system as a shadow no-return." The shadowing appears on the imagery as dark areas. As shown in the schematic cross section of figure 3, deeply dissected basins will produce radar shadows on the imagery. In the deeply dissected basins surrounding Logan Creek basin radar shadowing is one of the major factors producing the distinctive imagery pattern.

In the Logan Creek basin the thick residuum and solutionally enlarged fracture openings drain the ground water to Blue Spring and other lower openings with sufficient rapidity that the potentiometric surface rarely builds up to a level high enough to cause surface runoff within the losing part of the basin. Because of the high infiltration rate in the losing part of the Logan Creek basin, surface runoff and the accompanying erosion and dissection of the basin are greatly reduced. Even though the upper part of Logan Creek is gaining, this part of the stream cannot cut below the level established downstream. The thick cherty residuum on the upstream part of the basin acts to retard surface runoff, thereby further reducing erosion and dissection.

MacDonald and others (1969, p. 639) stated that look direction has an important influence on analysis of radar imagery. This influence is most pronounced in distinguishing linear topographic features. In the study area, look direction probably would only have minor effect because the low relief of a losing basin would produce the same fairly uniform tonal and textural image from any look direction, while the more dissected surrounding gaining basins would still produce strong tonal and textural differences owing to the variety of directions that the deeply dissected stream valleys follow. Look direction may be important in distinguishing losing basins in areas of low relief where topographic differences between losing and gaining basins would be more subtle.

Radar imagery has a unique character which makes it preferable to topographic maps, geologic maps, or airphotographs for this type of interpretation. The small scale enables the observer to compare large areas easily. Cultural features such as buildings and roads are indistinct or not visible and therefore do not distract the eye. Topography is emphasized, and textural and tonal contrasts are visible. None of the other types of maps or photographs provide tonal or textural contrasts or emphasize topography by shading. Thus, radar imagery can be scanned for shallow, relatively undissected basins much faster than the other maps and photographs.

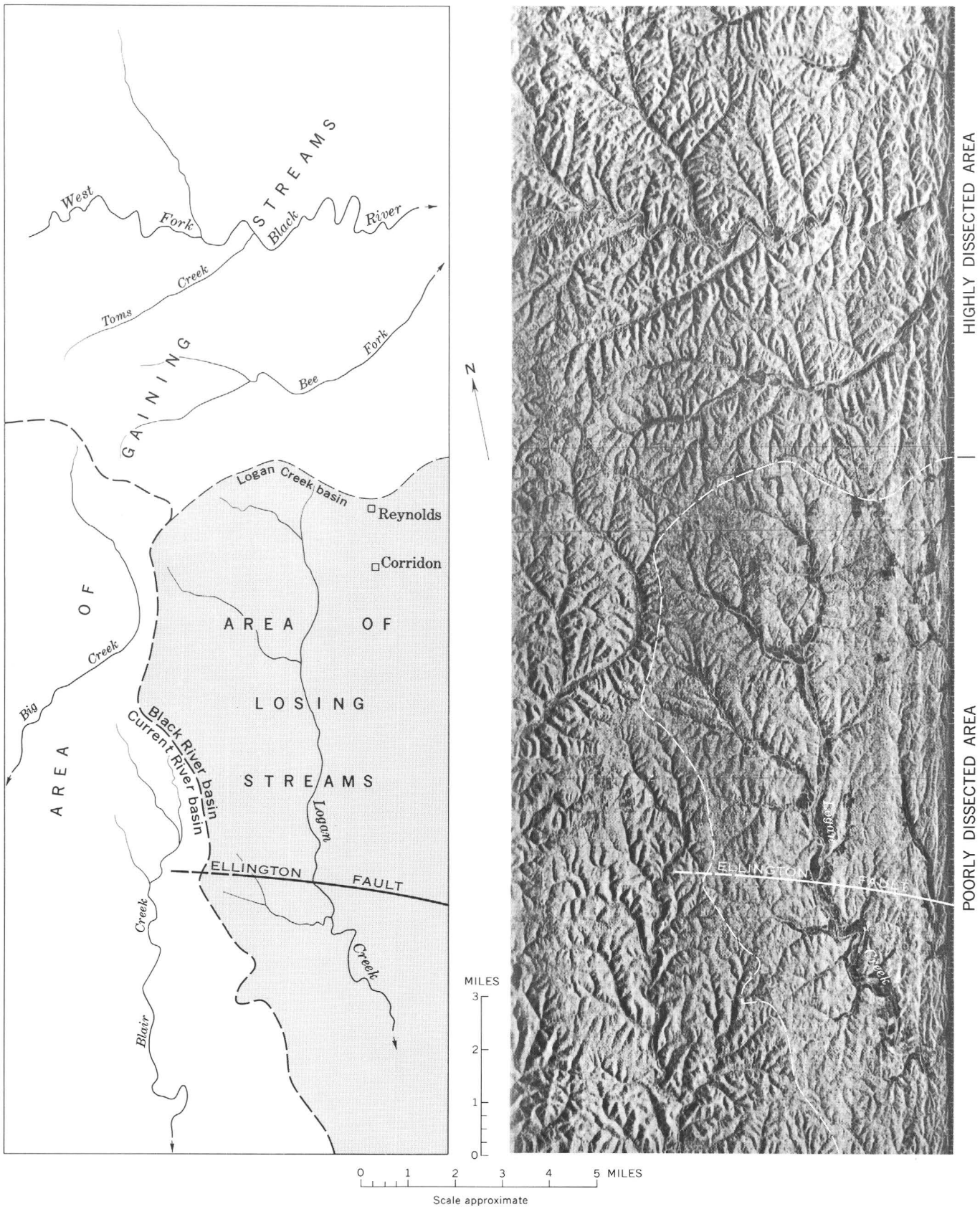

Figure 2.—Side-looking airborne radar imagery and reference map of a part of Logan Creek and surrounding basins, showing the contrast due to dissection.

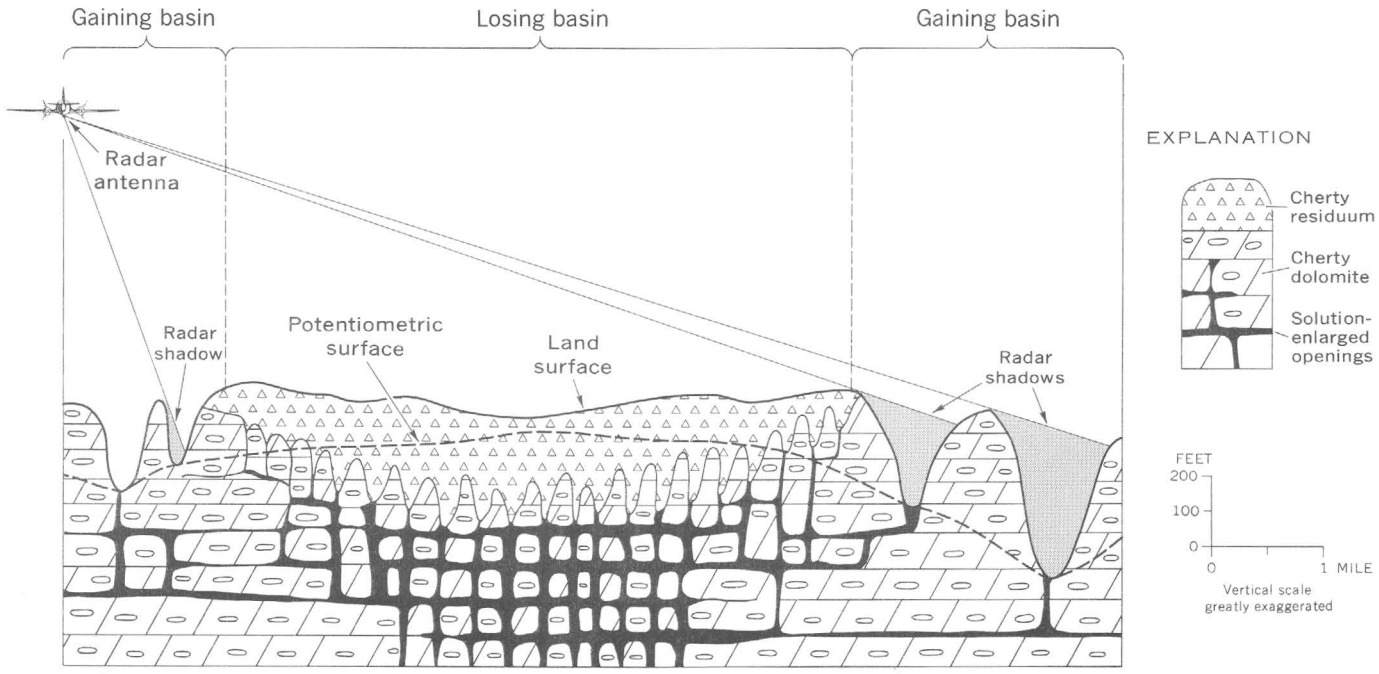

Figure 3.—An idealized cross section of a losing basin surrounded by gaining basins, showing the relationship of the potentiometric surface to the losing and gaining basins. The radar shadowing effect of deeply dissected basins is also shown.

CONCLUSIONS

Highly dissected and poorly dissected carbonate terranes can be identified on SLAR imagery by tonal and textural contrasts. As difference in dissection is caused by variations in overland runoff characteristics, interpretations from SLAR imagery are useful in identifying losing and gaining basins.

REFERENCES

Bridge, Josiah, 1930, Geology of the Eminence and Cardareva quadrangles: Missouri Bur. Geology and Mines, ser. 2, v. 24, 228 p.

MacDonald, H. S., Kirk, J. N., Dellwig, L. F., and Lewis, A. J., 1969, The influence of radar look-direction on the detection of selected geological features, *in* Symposium on remote sensing of environment, 6th, Ann Arbor, Mich., 1969, Proc.: v. 1, p. 637–650.

Rydstrom, H. O., 1966, Interpreting local geology from radar imagery, *in* Symposium on remote sensing of environment, 4th, Ann Arbor, Mich., 1966, Proc.: p. 193–201.

DEGRADATION OF THE EARTHQUAKE LAKE OUTFLOW CHANNEL, SOUTHWESTERN MONTANA

By M. V. JOHNSON and R. J. OMANG, Helena, Mont.

Work done in cooperation with the U.S. Forest Service

Abstract.—The Madison River is downcutting through the Madison Slide, which was caused by the Hebgen Lake earthquake of August 17, 1959. Since July 15, 1960, the crest of the outlet channel of Earthquake Lake, on the slide, has been lowered about 4 feet by degradation. The outlet channel has been degraded as much as 19 feet in one short reach. Degradation of the channel was as much as 8.5 feet during the 1971 spring and summer runoff. Vertical and horizontal changes in the channel have been accompanied by sloughing of the banks. Degradation is expected to continue until the slope of the channel is adjusted to provide only the velocities necessary to transport the available sediment. Future adjustments in the reach of the channel through the landslide may endanger some works of man and cause environmental changes to the river downstream from the landslide.

The Hebgen Lake earthquake of August 17, 1959, caused the Madison Slide, which in turn dammed the Madison River and formed Earthquake Lake, about 20 miles northwest of West Yellowstone, Mont. (fig. 1). The slide partly filled about a mile of the river canyon to a maximum depth of about 430 feet. The crest of the low point in the slide was at an altitude of about 6,480 feet. The U.S. Army Corps of Engineers immediately started excavating a relief spillway channel through the landslide area. By September 10, 1959, excavation had lowered the crest of the outlet to an altitude of 6,450 feet and permitted outflow from Earthquake Lake. The stream continued to downcut this channel. By October 1959, in order to help control erosion, the crest of the spillway channel was further lowered to an altitude of about 6,390 feet.

Degradation of the outflow channel since the last excavation has been accompanied by sloughing of its banks. This study was made by the U.S. Geological Survey in cooperation with the U.S. Forest Service to determine the amount of degradation in the slide area.

METHODS AND OBSERVATIONS

Data for a water-surface profile for July 15, 1960 (fig. 2), were furnished by the U.S. Army Corps of Engineers, who

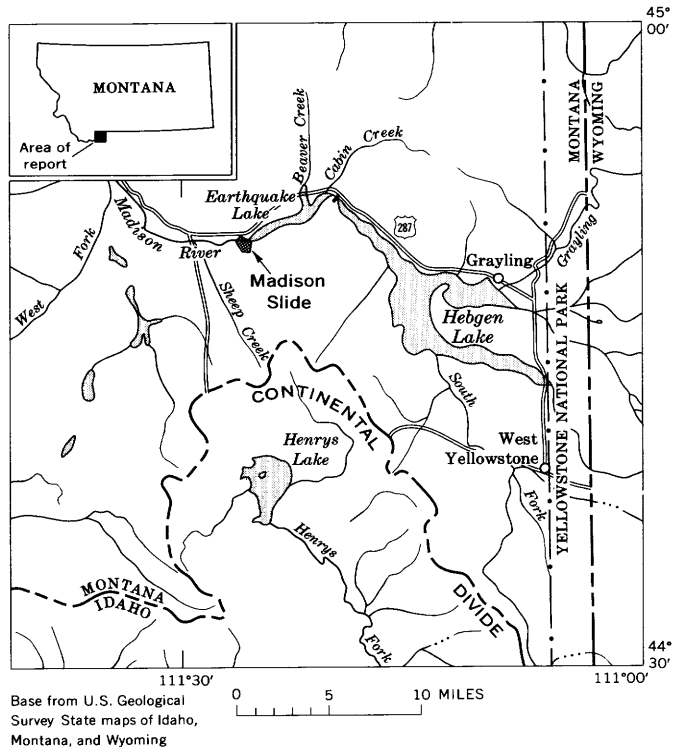

Figure 1.—Location of Earthquake Lake, Madison Slide, and the Madison River in southwestern Montana.

drilled and cased a series of test holes along the edge of the excavation. Water levels measured in the test holes on July 15, 1960, are assumed to be equal to the level of the adjacent water surface in the outflow channel. Outflow on July 15, 1960, was about 690 cfs (cubic feet per second). Since August 28, 1961, the Geological Survey has occasionally determined the lake altitude and has maintained rating curves showing the approximate stage-discharge relation at the lake outlet (fig. 3). On September 1, 1965, three reference marks were established near the lake outlet, and water-surface altitudes were measured from the lake outlet to a point 400 feet downstream. Outflow

U.S. GEOL. SURVEY PROF. PAPER 800-C, PAGES C253-C256

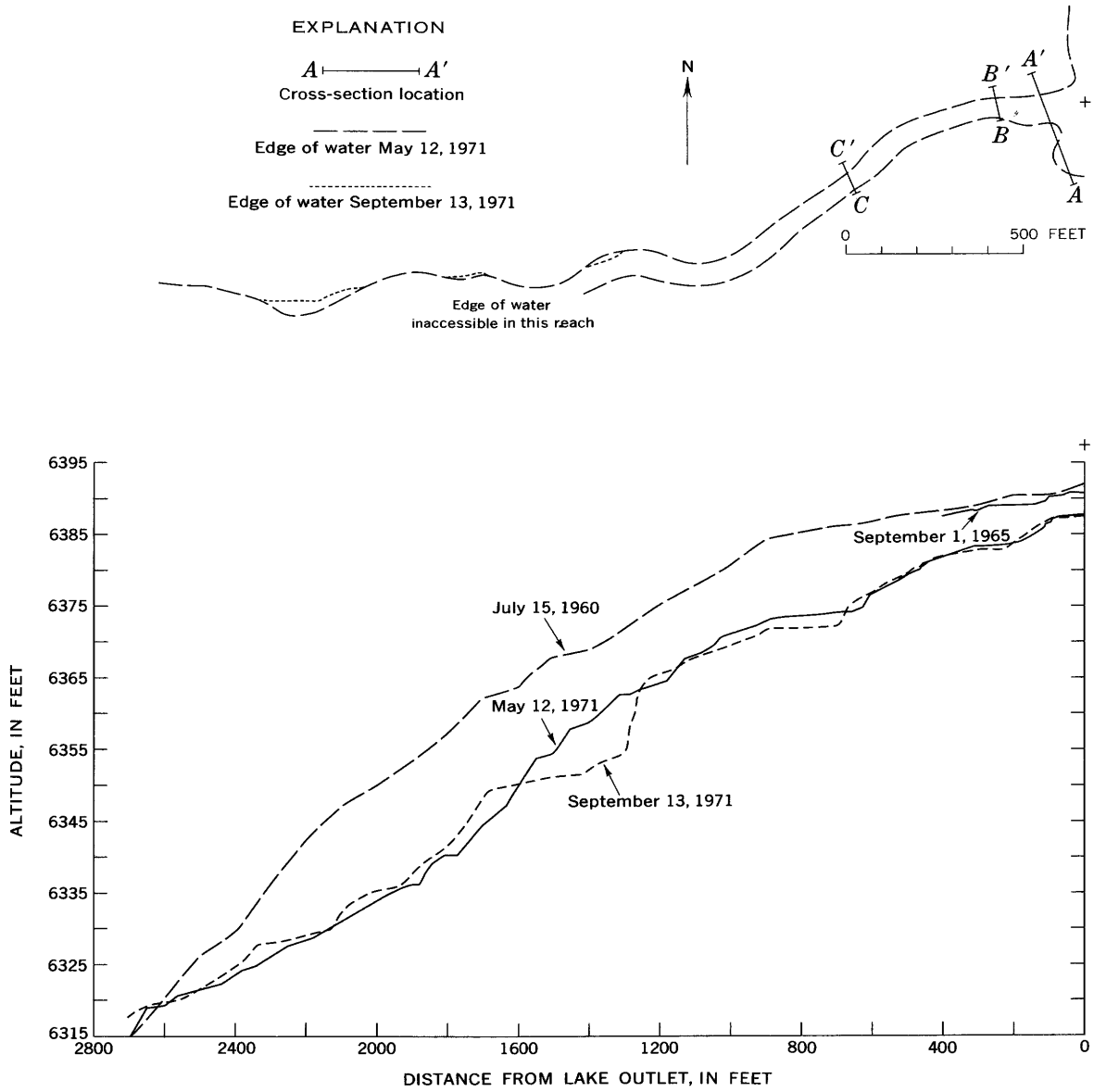

Figure 2.—Plan view and water-surface profiles of the Madison River through the landslide area.

on this date was 550 cfs. On May 12, 1971, and again on September 13, 1971, water-surface altitudes were measured from the lake outlet to a point 2,700 feet downstream. Outflow was 700 cfs on May 12 and 400 cfs on September 13. Channel cross sections were surveyed near the spillway crest and at several locations downstream from the outlet. Since May 12, 1971, the U.S. Forest Service has been making stage measurements at Earthquake Lake and has obtained inflow data from Cabin and Beaver Creeks.

The greatest lateral movement of the channel that took place between May 12 and September 13 was located about 2,200 feet downstream from the lake outlet as shown in figure 2. Lateral movement of the channel is generally caused by (1) sloughing of high steep banks (fig. 4, left), which forces the flow to shift toward the opposite bank, and by (2) alluvium deposited in the channel (fig. 4, right), which causes the stream to shift and cut a new channel.

Water-surface profiles (fig. 2) show changes since July 15, 1960. The profile of September 1, 1965, shows that the altitude of the lake outlet had not yet been changed by channel degradation. However, the outlet was lowered about 4 feet between September 1965 and September 1971. The profiles of May 12, 1971, and September 13, 1971, show the reaches of scour and fill. As much as 8.5 feet of degradation occurred during the 1971 spring and summer runoff. Streamflow across the slide from Earthquake Lake is largely provided by controlled releases from Hebgen Lake. The maximum release from May to September 1971 was 3,250 cfs. Since 1940 the annual maximum outflow from Hebgen Lake has exceeded 3,000 cfs in 11 different years. Thus streamflow was

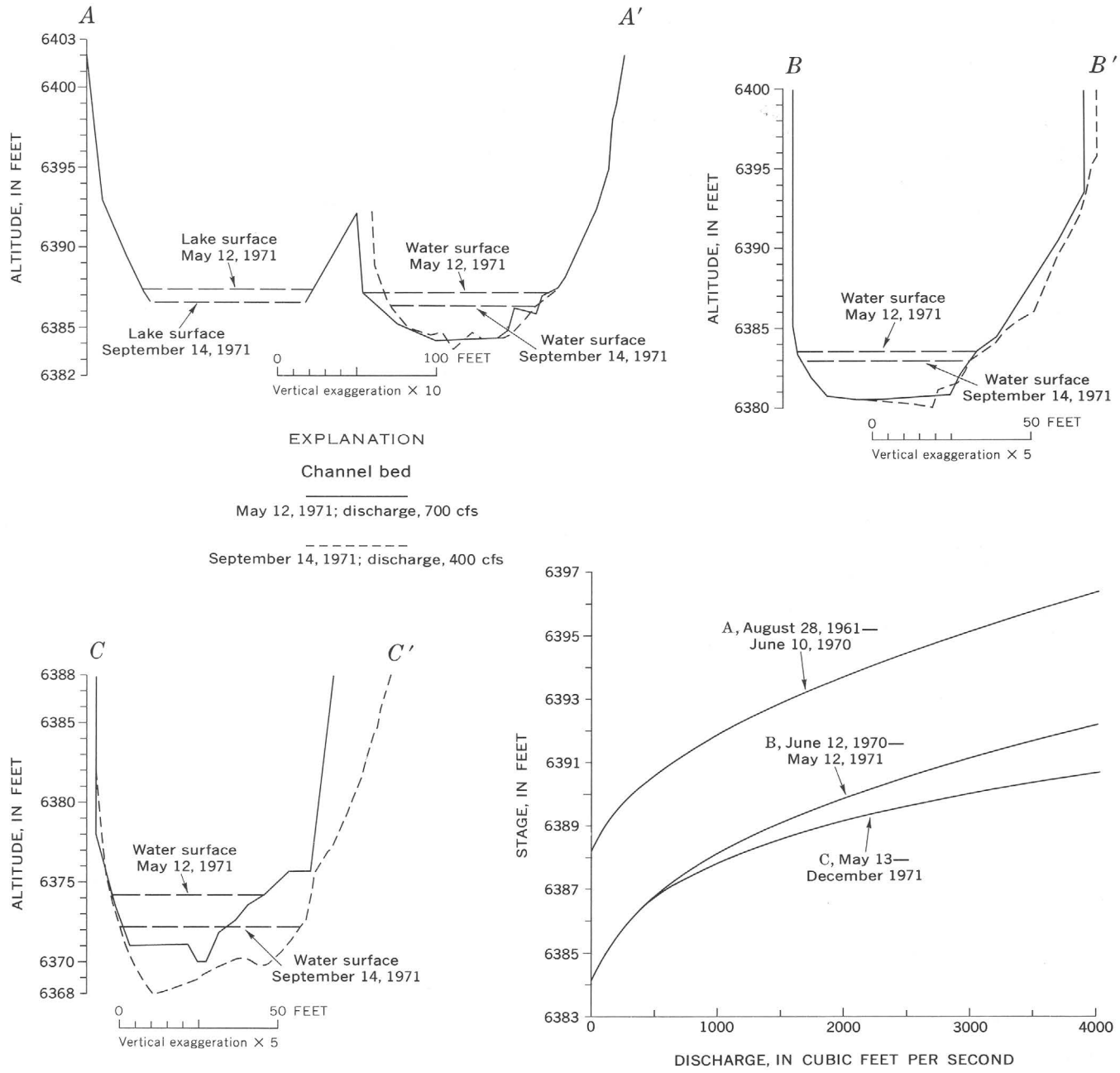

Figure 3.—Cross sections of the Madison River channel and stage-discharge relations at Earthquake Lake outlet. The left (south) half of section *A*–*A′* defines a loop in the shoreline of the lake, and no flow will occur in this area under present conditions. Location of cross sections is shown on figure 2.

not unusually large during the period between the May and September profiles—yet degradation was significant.

The profiles show that extensive channel degradation is occurring throughout most of the reach. Maximum degradation of the channel between July 15, 1960, and September 13, 1971, about 19 feet, occurred 1,770 feet downstream from the lake outlet. The channel bed, however, appears to have changed little in altitude 2,600 feet downstream from the outlet.

The profiles appear to indicate that scour occurs in a step pattern. For example, compare the May 12 and September 13 profiles in the reach from 1,200 feet to 1,800 feet downstream from the outlet. The step pattern is possibly the result of erosion of finer material from around large boulders in the channel, which causes the boulders to move downstream a short distance. Apparently, the rate of erosion becomes rapid in certain reaches as the boulders are removed and as the geometry of the channel changes; thus, certain reaches develop an oversteepened slope. Further erosion causes the oversteepened slope to progress upstream and to flatten as material

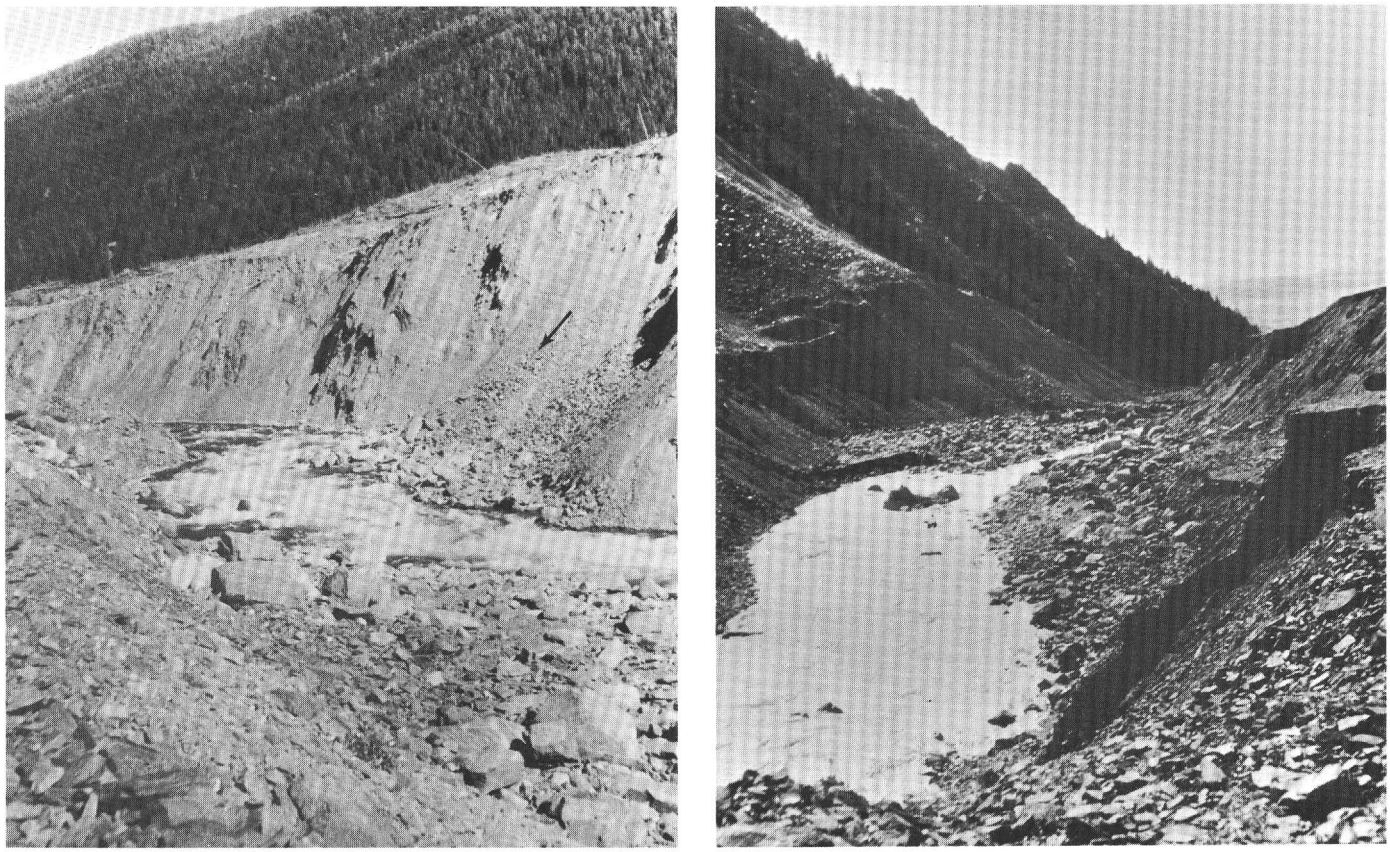

Figure 4.—Madison River channel. Left, sloughing of the banks (arrow), causing the flow to shift and cut a new channel; right, shifting of the channel caused by alluvial fill.

is deposited at its toe. It appears, therefore, that although the erosion of large boulders in part causes oversteepened slopes, the material deposited at the slope toe resists extremely rapid erosion, thus producing a step pattern in the profile.

Because the size of material in the slide appears to be one of the controls of the rate of degradation, the subsurface composition of the slide needs to be determined. If the slide contains large pockets of relatively fine-grained material below the present level of the stream, rapid degradation through this finer grained material could be expected. Rapid degradation of the outlet could release enough water to cause damage to downstream areas.

Changes in the altitude of the crest of the spillway can be determined from changes in the stage-discharge relation at the lake outlet. Curves showing the approximate stage-discharge relation at the lake outlet from August 1961 to September 1971 are shown in figure 3. Curve A was effective from August 28, 1961, to June 10, 1970. The stage-discharge relation was not determined for June 11, 1970, because at that time there was rapid scour of the spillway crest. Curve B was effective from June 12, 1970, to May 12, 1971, and curve C from May 13, 1971, to the present (December 1971). Although the altitude of the spillway crest is the same for curves B and C, curve C extends to the right of B because the control section of channel at the lake outlet widened. The material forming the left bank at the outlet is relatively fine grained and unconsolidated and thus is susceptible to erosion; therefore, the spillway will probably continue to widen toward the left bank. This may in turn subject the right bank near cross section B–B' to additional erosion; such erosion may endanger a road and a building.

CONCLUSIONS

Data presented here show that the Madison River has degraded its channel across the landslide as much as 19 feet since July 15, 1960. It is reasonable to assume that degradation will continue until the slope and shape of the channel are adjusted to provide only the velocities necessary to transport the available sediment. The time required for the adjustment is unknown; however, the rate of adjustment will be affected by the size of the materials deposited by the slide.

Obviously, large volumes of water could be released from storage in Earthquake Lake if degradation of the spillway were rapid and uncontrolled. Even if degradation were slow, material eroded from the landslide and deposited downstream might cause deterioration of fish and game habitats, make bridges unusable, and decrease the value of land along the river. Continued uncontrolled degradation might require changes in the operation of upstream reservoirs (Hebgen Lake) to impound storage when high streamflow is likely to cause rapid degradation.

CLEAR-CUTTING AND ITS EFFECT ON THE WATER TEMPERATURE OF A SMALL STREAM IN NORTHERN VIRGINIA

By E. J. PLUHOWSKI, Arlington, Va.

Abstract.—Tree and shrub removal from an 1,100-foot reach at the lower end of Colvin Run near Reston, Va., has altered stream-temperature patterns. Owing to increased solar radiation, especially in summer, maximum water temperature at the lower end of the reach is frequently 1° to 3.5°C (Celsius) higher than that observed at the upper end. An energy budget, prepared for the period 1415–1500 hours, July 15, 1969, quantifies the principal energy sources controlling stream temperature in the reach.

The Colvin Run basin in northern Virginia is undergoing rapid urbanization. The proliferation of houses and newly paved streets and an expanding sewer system have altered the hydrologic regimen of Colvin Run. Silt carried by sharply increased storm runoff from the new town of Reston, near Washington, D.C., is diminishing the recreational value of Lake Fairfax (fig. 1) and, to a lesser extent, of Lake Anne. Not only have man's activities increased sediment production and storm runoff, but also by the creation of impoundments, sewer outfalls, and clear-cutting of vegetation he has changed water-temperature patterns of the stream. The purpose of this paper is to assess the impact on water temperature of the removal of bank vegetation associated with a channel alinement project.

Despite urban encroachment, bank vegetation along most reaches of Colvin Run is nearly intact. Under natural conditions, the bank vegetation consists of deciduous trees associated with a dense brush understory. Shading provided by the dense vegetal cover is very effective in preventing solar energy from reaching the stream, especially during the growing season. Noteworthy exceptions occur at Lake Anne and Lake Fairfax, where the size of the impoundments limits the effectiveness of bank vegetation in providing shade. Additionally, bank-cover shading has been sharply reduced in an 1,100-foot reach immediately above the confluence of Colvin Run with Difficult Run. This reach (fig. 2) is characterized by the complete absence of trees, although considerable low-profile brush covers both banks. The cleared reach, located between sites 5A and 5B (fig. 1), is practically straight. It parallels Leesburg Pike (Virginia Route 7), whose south shoulder forms the stream's left bank.

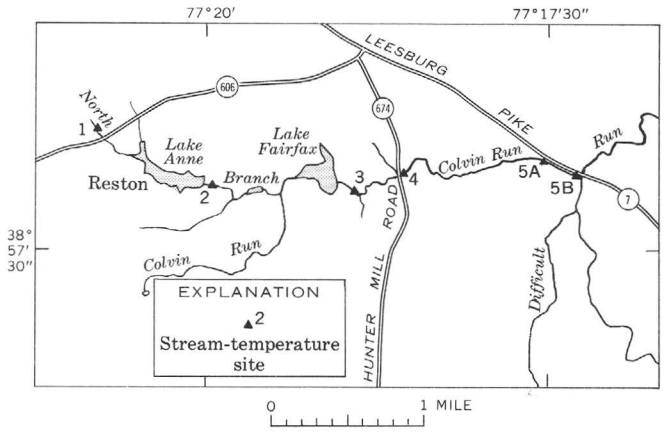

Figure 1.—Map of Colvin Run near Reston, Va., showing the location of six stream-temperature sites.

COLVIN RUN TEMPERATURE PATTERNS

Thermograph records indicate substantial concurrent water-temperature differences between sites 5A and 5B during the afternoon hours of days with intense solar radiation. For example, on July 15, 1969, under clear skies, a maximum stream-temperature reading of 24.4°C (Celsius) was recorded at site 5A, whereas the highest temperature at site 5B was 27.8°C (fig. 3). Minimum temperatures measured shortly after daybreak differed only slightly at the two sites, 20.3°C at site 5A and 20.6°C at site 5B. Stream-temperature patterns at site 4, 4,300 feet above site 5A, are very similar to those at 5A. Maximum water temperatures at both sites are nearly identical, whereas minimum temperatures at site 4 are about 1°C cooler than at site 5A. Unlike along the cleared study reach, a dense deciduous tree stand flanks both banks of Colvin Run between sites 4 and 5A. The trees limit the amount of solar energy reaching the stream, thereby maintaining fairly uniform stream-temperature patterns throughout the reach. Upon entering the cleared reach, streamflow is exposed to a flood of solar energy, which is converted into heat. Thus, the 3.4°C differential in the maximum stream temperatures between the

U.S. GEOL. SURVEY PROF. PAPER 800-C, PAGES C257-C262

Figure 2.—View of Colvin Run (looking upstream from site 5B), showing its realined cleared lower reach.

upper and lower ends of the 1,100-foot study reach on July 15, 1969, is the result of clear-cutting, which altered the heat budget of the reach. Under overcast skies, concurrent water temperatures of sites 5A and 5B are generally within 0.5°C of each other.

Temperature patterns at site 1 in a heavily wooded area near the source of the North Branch of Colvin Run are generally very similar to those at sites 4 and 5A. By way of contrast, temperatures at sites 2 and 3 immediately below Lake Anne and Lake Fairfax, respectively, are highly dependent upon whether or not the lakes are spilling. For example, on the date of this survey (July 15, 1969), Lake Anne was not spilling, so that the water flowing below its outlet was a mixture of cold ground water and leakage, primarily from the lowest levels of the lake. Because of thermal stratification in the lake, water temperatures in its lowest levels were cold (10°–12°C). Accordingly, temperatures at site 2 were 5° to 7°C colder than anticipated. Similarly, all streamflow below Lake Fairfax originated as leakage from the lowest levels of that lake. However, Lake Fairfax is relatively shallow, so that thermal stratification there is not as pronounced as it is in Lake Anne. Stream temperatures at site 3 were about 2°C higher than at site 2. Owing principally to the uniformity of ground-water temperatures, diurnal temperature fluctuations in the streamflow below both lakes are greatly reduced relative to those measured elsewhere in the basin.

The reaches immediately below both Lake Anne and Lake Fairfax are also subject to short-term temperature anomalies. For example, the time of arrival of street runoff below Lake Anne often is detectable from thermograph traces obtained at site 2. This situation occurs whenever the incoming street-runoff flow rate is at least 10 percent of the ambient stream discharge and when its temperature is at least 2°–3°C higher or lower. A unique disruption in expected stream-temperature patterns occurred below Lake Fairfax on February 11, 1970. Ice floes on the lake were driven past its outlet by high winds, resulting in an anomalous drop in temperature of 4°C at site 3 (Pluhowski, 1972).

ENERGY BUDGET

Theory

To assess the factors controlling water temperatures in the cleared reach, an energy budget was prepared for July 15, 1969, covering the period 1415–1500 hours e.s.t. The study period was selected to coincide with the time when stream temperatures were at their highest levels for the day. Moreover, the 45-minute span of the study period is equal to the time required for water to move through the cleared reach on the day of the survey. The principal factors affecting the heat balance of streams are illustrated schematically in figure 4, where

Q_s = incoming short-wave solar radiation (direct and diffuse),
Q_r = reflected solar radiation,
Q_a = atmospheric radiation (long wave),
Q_{ar} = reflected atmospheric radiation,
Q_f = forest radiation (long wave),
Q_{fr} = reflected forest radiation,
Q_{bw} = back radiation from the water surface (long wave),
Q_e = energy used by evaporation,
Q_h = energy gained or lost by convection,
Q_{hb} = heat conducted to or from the streambed or banks,
Q_{gw} = heat advected into the reach by ground water,
Q_{in} = heat content of streamflow entering the reach, and
Q_{out} = heat content of streamflow leaving the reach.

Missing from the above are energy contributions from friction generated by moving water and from biological and chemical processes. The amount of heat added to the stream from these sources is assumed to be minor, so it was disregarded. Forest radiation from vegetation overhanging the stream is an important heat source along most reaches of Colvin Run; however, clear-cutting of all trees and high-profile shrubs along the study reach eliminates this factor from the heat balance. Discharge measurements indicate no pickup (increase) in streamflow in the reach, so that heat advected into the reach by ground water is assumed to be negligible.

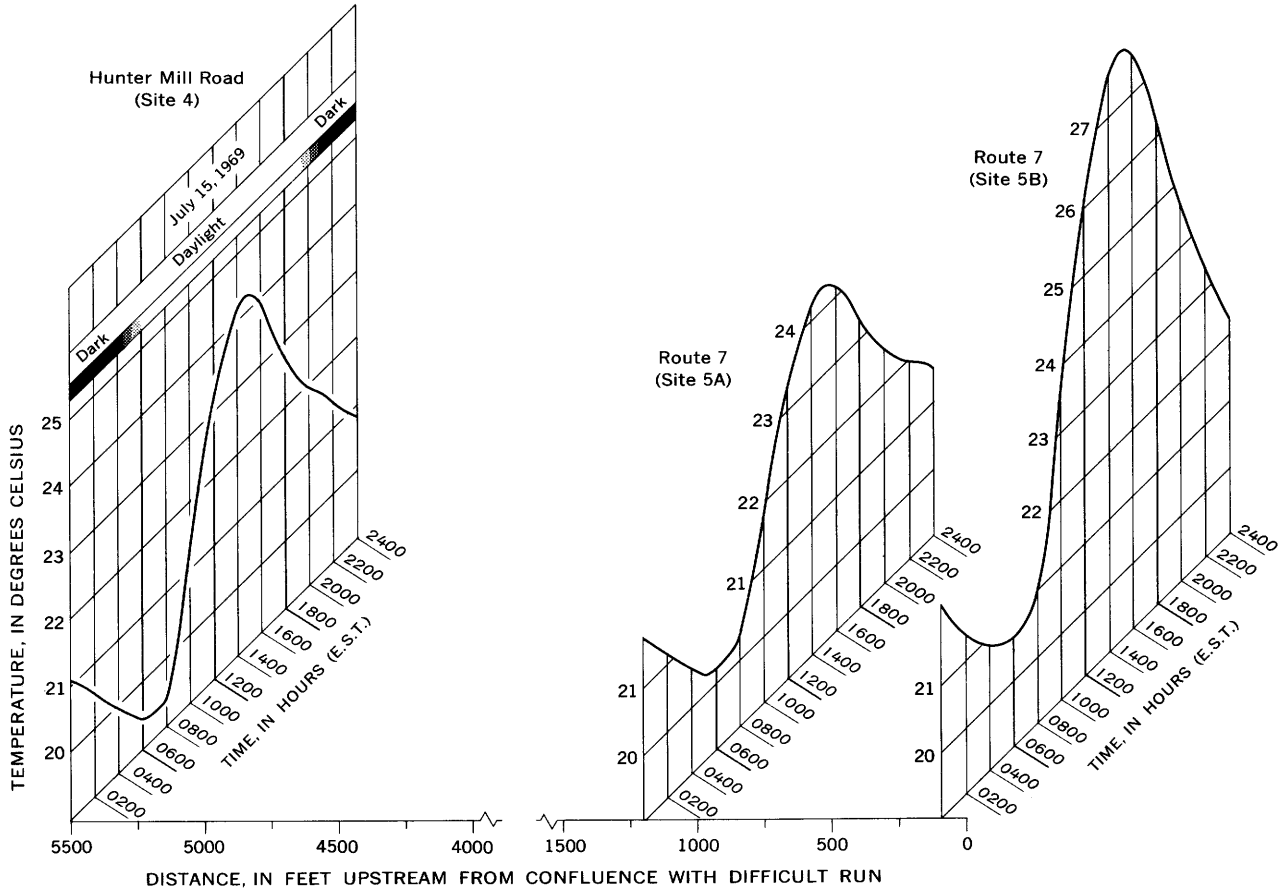

Figure 3.—Stream temperatures at selected study sites on Colvin Run, July 15, 1969.

As indicated in figure 4, Q_h, convective heat flux at the air-water interface, and Q_{hb}, heat exchanged through the bed of the watercourse, can be directed either to or away from the stream. On the date of the survey, air temperatures were significantly higher than stream temperatures during most of the day, whereas the stream was warmer than the underlying bed material. Thus, heat was added to the watercourse through the air-water interface and lost through the streambed.

To calculate the impact of the various heat fluxes on water temperatures in the cleared reach, a heat budget was prepared for an elemental volume of water as it moves through the reach. The length of the elemental volume was selected as 1 cm, and its width and depth were made equal to the average values of these parameters as measured in the cleared reach on July 15, 1969.

Energy enters the reach from the following sources:

$$\text{Inflow} = Q_s + Q_a + Q_h. \quad (1)$$

Energy leaves the elemental volume as follows:

$$\text{Outflow} = Q_r + Q_{ar} + Q_{bw} + Q_e + Q_{hb}. \quad (2)$$

The net quantity of heat added (ΔQ) is:

$$\Delta Q = \text{inflow} - \text{outflow}, \quad (3)$$

or

$$\Delta Q = (Q_s - Q_r) + (Q_a - Q_{ar}) + Q_h - Q_{bw} - Q_e - Q_{hb}, \quad (4)$$

where the terms in parentheses have been grouped for convenience.

From equation 4 it is possible to predict the temperature at the downstream end of the reach at the end of whatever time period is used in the analysis. The predictive capability and accuracy of the various factors in equation 4 may be ascertained by comparing the predicted temperature with observed temperature at the outlet section.

Solar radiation, sky cover, and estimated wind velocities were based on weather records from the National Weather Service at Dulles International Airport 7 miles west of the site. Relative humidity, air and water temperatures, streambed temperature profiles, streamflow, and net radiation data were obtained with onsite instrumentation.

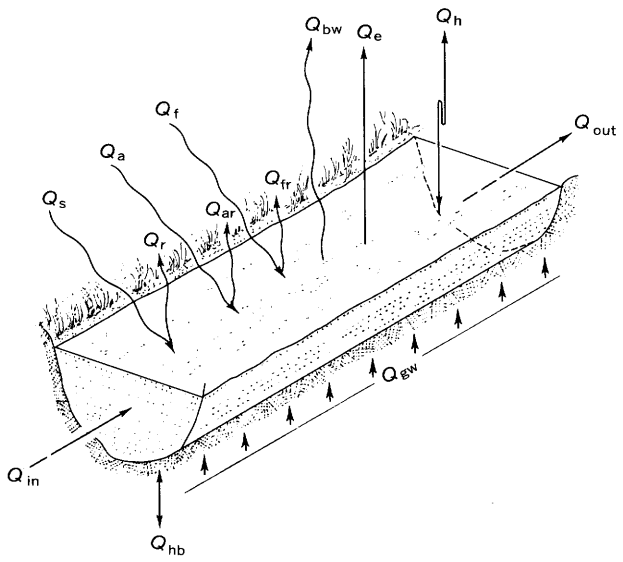

Figure 4.—Principal energy components in the heat balance of small streams. See text for explanation of symbols.

Atmospheric radiation

Atmospheric radiation, accurate within 10 percent, is obtained by use of the Brunt (1932) equation:

$$Q_{ao} = \epsilon\sigma T^4 (a+b\sqrt{e}), \quad (5)$$

where

Q_{ao} = clear-sky atmospheric radiation,
ϵ = emissivity of the atmosphere,
σ = Stephan-Boltzman constant,
T = absolute temperature of the air near the ground,
e = vapor pressure of the air near the ground, and
a and b = empirical coefficients.

Values of the empirical coefficients are estimated to be a = 0.61, and b = 0.05, close to the median values of 22 evaluations as computed by Sellers (1965).

Long-wave incoming radiation calculated from equation 5 is clear-sky radiation. As water vapor is the most important source of long-wave radiation in the atmosphere, it is obvious that a greater flux of atmospheric radiation may be expected under cloudy skies than under clear skies. Geiger (1965) suggested the following equation to evaluate atmospheric radiation under cloudy skies:

$$Q_a = Q_{ao} (1+kn^2), \quad (6)$$

where

Q_{ao} = clear-sky atmospheric radiation,
n = cloud cover expressed in tenths (complete cloud cover = 1.0), and
k = a function of cloud type.

Countering the downward fluxes of energy from the sun and atmosphere is long-wave radiation (wavelengths greater than 2 μm) emitted by the stream itself. Stream back radiation (Q_{bw}) was computed according to the Stephan-Boltzman law for black-body radiation, with an emissivity factor of 0.97 for water (Anderson, 1954) as follows:

$$Q_{bw} = \epsilon\sigma T^4, \quad (7)$$

where

ϵ = emissivity of water,
σ = Stephan-Boltzman constant, and
T = absolute temperature of the water.

Evaporation

Evaporation was computed by using a formula suggested by Delay and Seaders (1963) for use in streams, which, when expressed to yield energy flux in langleys per unit time, becomes

$$Q_e = 0.18U(e_w - e_a)t, \quad (8)$$

where

Q_e = evaporation energy flux (langleys per unit time),
U = wind speed (knots),
e_w = saturation vapor pressure at water-surface temperature (millibars),
e_a = vapor pressure of the air (mb), and
t = unit of time.

Convection

Bowen (1926) related the convective heat flux to evaporative heat loss as follows:

$$R = \frac{Q_h}{Q_e}, \quad (9)$$

where

R = The Bowen ratio,
Q_e = evaporation heat flux (cal/cm^2 unit time^{-1}), and
Q_h = convective heat flux (cal/cm^2 unit time^{-1}).

The Bowen ratio, expressed algebraically, is:

$$R = C_b \frac{(T_w - T_a)}{(e_w - e_a)} \frac{P}{1{,}000}, \quad (10)$$

where

C_b = 0.61,
T_w = water-surface temperature (°C),
T_a = air temperature (°C),
e_w = saturation vapor pressure at water-surface temperature (mb),
e_a = vapor pressure of the air (mb), and
P = atmospheric pressure (mb).

Conduction

Heat is gained or lost through the streambed—depending on the direction of the heat flux in the material underlying the stream, the intensity of the thermal gradient, and the thermal conductivity of the bed material. This relation may be written as

$$Q_{hb} = K \frac{dT}{dz}, \quad (11)$$

where

Q_{hb} = conduction (cal/cm^2 unit time^{-1}) to or from the streambed,

$\frac{dT}{dz}$ = temperature gradient in the bed material (°C/cm), and

K = thermal conductivity of the bed material (cal/cm sec^{-1} °C^{-1}).

Application to Colvin Run

The energy-evaluation techniques described above were used during the study of the 1,100-foot reach between sites 5A and 5B from 1415 to 1500 hours e.s.t. on July 15, 1969 (table 1). The average width and depth of the reach (item 1) were computed from cross sections made at 50-foot intervals. Estimates of the amount of shade provided by the banks were obtained at each cross section. The average of these estimates (12.5 percent) was used to calculate reduction of the total amount of incoming solar radiation (item 5). After an additional reduction for albedo losses, the absorbed solar radiation was computed to be 37.8 ly (langleys)—largest of all energy sources. Other high-energy components include atmospheric radiation, 23.0 ly, and back radiation from the stream, -29.2 ly.

Much lower in magnitude were the evaporation, conductive, and convective heat fluxes (items 8–10). Conduction (item 9) was computed by using a K value (equation 11) of 3.94×10^{-3} cal cm^{-1} sec^{-1} °C^{-1} for water-saturated sand (Clark, 1966, p. 477). The algebraic sum of all heat sources entering the elemental volume used in the computations was +27.9 ly (item 11). The increase in temperature of the elemental volume of water in its passage through the study reach may now be computed. The predicted temperature change (item 12) of +3.7°C indicates the expected rise in stream temperature between sites 5A and 5B based on the energy budget for the elemental volume of water. The predicted 1500-hours temperature at site 5B of 28.1°C compares favorably with the observed temperature of 27.8°C, thereby confirming the validity of the overall heat budget. Failure to include an estimate for bank shading in the computations would have resulted in a predicted heat rise of nearly twice that computed in the analysis. Because of the small heat capacity and consequent low thermal inertia of Colvin Run, consideration of factors affecting the principal heat sources is important to the success of temperature-prediction methods based on energy-budget techniques.

Table 1.—*Energy-budget computations for Colvin Run near Reston Va., for the period 1415–1500 hours (e.s.t.), July 15, 1969*

[1 ly (langley)=1 gram-calorie cm^{-2}]

Stream reach (1):		
Beginning at site 5A	feet above mouth	1,190
Ending at site 5B	feet above mouth	90
Length of reach	feet	1,100
Average width	feet	9.0
Average depth	foot	.25
Discharge (2):		
At site 5A	cfs	1.3
At site 5B	cfs	1.3
Time of travel (3):		
From site 5A to site 5B	minutes	45
Measured stream temperatures (4):		
Initial (site 5A at 1445 hr)	°C	24.4
Final (site 5B at 1500 hr)	°C	27.8
Solar radiation (5):		
Q_{so}, total incoming solar radiation	ly	44.6
Reduced 12.5 percent for bank shading	ly	-5.6
Q_s, solar radiation reaching stream	ly	39.0
Q_r, reflected solar radiation (3 percent)	ly	-1.2
Q_i, absorbed solar radiation (insolation)	ly	37.8
Atmospheric radiation (6):		
ϵ, emissivity		.87
Q_a, atmospheric radiation (reduced 3 percent to include albedo losses)	ly	23.0
Outgoing long-wave radiation (from stream to atmosphere) (7):		
ϵ, emissivity		.97
Q_{bw}, back radiation	ly	-29.2
Evaporation (8):		
Q_e, evaporation heat flux	ly	-3.6
Conduction (at streambed) (9):		
T_{gw}, ground-water temperature below stream	°C	16.7
Q_{hb}, conductive heat flux	ly	-1.1
Convection (at air-water interface) (10):		
Q_h, convective heat flux	ly	1.0
Heat-flux summary (11):		
Net heat flux to stream	ly	+27.9
Predicted temperature at site 5B, 1500 hr (12):		
Temperature change caused by heat gain	°C	+3.7
Final temperature	°C	28.1
Remarks (13):		
A positive heat flux indicates incoming energy to the reach, whereas a negative heat flux denotes loss of energy.		

The importance of shade, especially that provided by overhanging trees, in attenuating the impact of solar radiation on the heat balance of small streams is illustrated in figure 5. Net radiation—the residual of insolation, atmospheric radiation, and back radiation—is plotted for sites 4 and 5B. Site 5B, at the downstream end of the study reach, is clear of trees, whereas site 4 is in a predominantly wooded park area. Net radiation at both sites is negative in the early morning hours and again at night, indicating a net loss of heat from the stream and a decline in stream temperature during both periods. During the daylight hours, under a sky devoid of opaque cloudiness, the net radiation at site 5B soared to a peak value of nearly 1.2 ly/min. This is about 6 times the maximum net radiation recorded at site 4, where trees effectively shielded the stream from the sun. Clearly, the anomalous discrepancy of 3.4°C in maximum stream temperature recorded on July 15, 1969, between the upper and lower ends of the 1,100-foot reach of Colvin Run resulted from clearcutting.

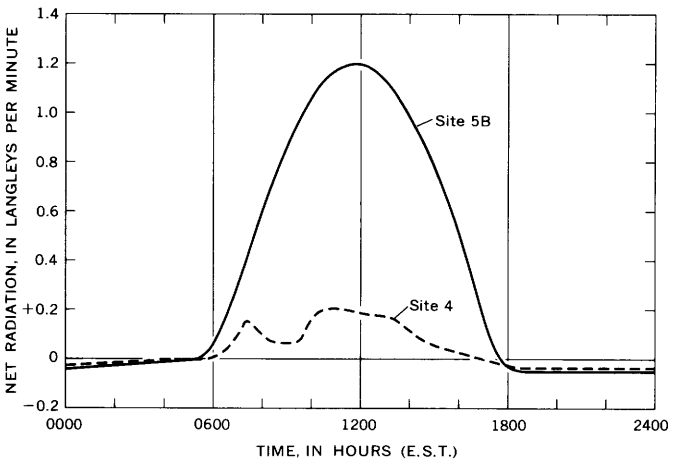

Figure 5.—Net radiation at sites 4 and 5B on Colvin Run, July 15, 1969.

Owing to the relatively low heat-carrying capacity of small streams, their water-temperature patterns are predisposed to wide change, particularly if the amount of insolation received by the streams is sharply altered. By maintaining trees and shrubs along the banks of small streams, possible deleterious effects on aquatic life of high summer water temperatures resulting from energy-budget changes may be avoided.

REFERENCES

Anderson, E. R., 1954, Energy-budget studies, *in* Water-loss investigations—Lake Hefner studies, technical report: U.S. Geol. Survey Prof. Paper 269, p. 71–119.

Bowen, I. S., 1926, The ratio of heat losses by conduction and by evaporation from any water surface: Phys. Rev., v. 27, p. 779–787.

Brunt, D., 1932, Notes on radiation in the atmosphere: Royal Meteorol. Soc. Quart. Jour., v. 58, p. 389–420.

Clark, S. P., Jr., 1966, Thermal conductivity, sec. 21 *in* Handbook of physical constants (revised edition): Geol. Soc. America Mem. 97, p. 459–482.

Delay, W. H., and Seaders, John, 1963, Temperature studies on the Umpqua River, Oregon, *in* Symposium on water temperature—influences, effects, and control: Pacific Northwest meeting, 12th, Corvallis, Oreg., 1963, Proc., p. 57–75.

Geiger, Rudolf, 1965, The climate near the ground: Cambridge, Mass., Harvard Univ. Press, 611 p.

Pluhowski, E. J., 1972, Unusual temperature variations in two small streams in northern Virginia, *in* Geological Survey Research 1972: U.S. Geol. Survey Prof. Paper 800-B, p. B255–B258.

Sellers, W. D., 1965, Physical climatology: Chicago, Ill., Chicago Univ. Press, 272 p.

PRELIMINARY STUDIES OF COLLOIDAL SUBSTANCES IN THE WATER AND SEDIMENTS OF THE CHESAPEAKE BAY

By IRVING A. BREGER, PETER ZUBOVIC, and JOHN C. CHANDLER,
Washington, D.C.

Abstract.—Colloidal substances passing through a 1.2-μm filter but retained by a 0.0024-μm membrane have been isolated from both water and sediment of the Chesapeake Bay. The colloidal fraction obtained from the water had a high content of magnesium, whereas the colloidal fraction from the sediment had a high content of manganese. Further study of the colloidal substances isolated from the sediment may provide an explanation for the formation of manganese nodules.

Colloidal properties are rarely considered during geochemical studies of sediments. This is particularly unfortunate inasmuch as phenomena such as adsorption, protection, coprecipitation, syneresis, and coacervation may have played major roles in the origin of coals, crude oil, and carbonaceous shales. As an example, it has occasionally been noted that certain carbonaceous shales must initially have been composed of particulate mineral matter dispersed in a matrix of gel-like colloidal organic substances. Theoretical aspects of the geochemical significance of colloidal phenomena have been discussed in detail by Breger (1970); more recently, Perhac (1971) reported the results of studies of suspended substances in streams of Tennessee. The studies reported in this paper reflect our particular interest in the origin of carbonaceous shales and in the colloidal phenomena that accompany the formation of these shales in relation to the concentration of such elements as copper and vanadium. They also reflect our interest in shales as source beds for crude oil.

Our studies have been conducted with samples of sediment and water taken from an unpolluted area of the Chesapeake Bay south of Annapolis, Md. Sampling was done under the guidance of Dr. Jerry Schubel, of the Chesapeake Bay Institute of The Johns Hopkins University.

The initial objectives of this work were to develop techniques for the collection and storage of samples, to find satisfactory methods for the isolation and characterization of the colloidal substances, and to determine the organic and inorganic composition of the substances isolated.

STORAGE OF SAMPLES

Fresh specimens containing organic substances are generally subject to attack by microorganisms unless carefully stored prior to and during study. Addition of preservatives to prevent microbial attack is, however, not desirable because of possible interaction with the organic substances; in the current studies they may even lead to destruction of the colloidal systems. For these reasons, such common additives as ethyl or butyl alcohol or chloroform could not be safely used.

Although samples are frequently frozen to preserve them, this method also was rejected for fear that it might lead to destruction of the colloidal system. After much consideration, samples of both water and sediment were preserved by chilling them in ice as soon as they were collected and then maintaining them just above the freezing point by refrigeration until they were used.

ANALYTICAL METHODS

Attempts to effect separations and identifications of colloidal substances present in the water and sediment were made by techniques normally used by biochemists. Neither electrophoresis nor ultracentrifugation has proved useful in our studies to date. Use of ultrafiltration and dialysis, however, have together provided a means for isolation and classification of the colloidal particles based on their size. Infrared absorption analysis has proved useful in attempts to characterize the colloids, and initial work points to likely success in the use of gel permeation chromatography for additional or parallel classifications of colloidal substances based on their molecular weights.

BAY WATER

Water samples were obtained by lowering a stoppered, weighted, 5-liter glass bottle to the desired depth, pulling the stopper, and raising the full bottle. Repetition of this procedure at the same site led to the collection of 74 liters of

U.S. GEOL. SURVEY PROF. PAPER 800-C, PAGES C263-C265

water at a depth of 2 m below the surface, the water at this point being approximately 16 m deep. The 2-m depth was chosen to avoid contamination from possible surficial oil films or from particulate matter associated with the bottom sediments. Each sample so taken was cooled in ice until it could be transported to the laboratory (approximately 2 hours), at which time it was immediately passed through 1.2-μm Millipore filters. The procedure, which required about 2 hours, removed coarse particulate matter, bacteria, and plankton, all of which was discarded inasmuch as equivalent samples have been studied in detail by biologists of the Chesapeake Bay Institute. The filtered water was reduced to 1 liter by distillation under vacuum at temperatures not exceeding 35°C, the final product being a pale-yellow solution saturated with and containing considerable precipitated salt.

The salt-saturated water was decanted from the precipitated salt and dialyzed against distilled water through a 0.0024-μm cellophane membrane. The contents of the dialysis sleeve were stirred continuously, and the water outside the sleeve was tested from time to time with a 1*N* solution of silver nitrate to follow progress in the diffusion of the chloride ion through the membrane. It was calculated that 1 ppb of chloride ion could be detected in this way. The distilled water outside the sleeve was replaced twice each day until, at the end of about 10 days, the test for chloride was negative and it was concluded that all the salt had diffused out of the sample. All the water outside the sleeve was saved, combined, and reduced, by distillation under vacuum at temperatures below 35°C, to a volume of 141 ml. Subsequent evaporation under a stream of helium led to a product that was primarily salt but which contained tan material indicating that some organic substances in the water sample were of sufficiently small size and low molecular weight to have diffused through the cellophane membrane.

The water remaining in the dialysis sleeve at this point contained only colloidal substances; this suspension was evaporated at temperatures only slightly above room temperature and under a stream of helium to yield several milligrams of a dark-brown residue. It is estimated from this work that the concentration of colloidal substances in the water was less than 10 ppm. An analysis of this material is shown in tables 1 and 2. An infrared absorption curve of the colloidal isolate (fig. 1) was obtained using a Perkin-Elmer Model 621 infrared spectrophotometer. The sample for this analysis was prepared as a 13-mm disk consisting of 300 mg of KBr and 0.735 mg of sample.

Table 1.—*Analysis of colloidal isolate, in percent, from Chesapeake Bay water*

	As is[1]	Ash-free
C	15.5	27.0
H	4.6	8.0
N	1.8	3.1
O (by difference)	35.6	61.9
Ash	42.5	...

[1] All analyses were conducted in duplicate.

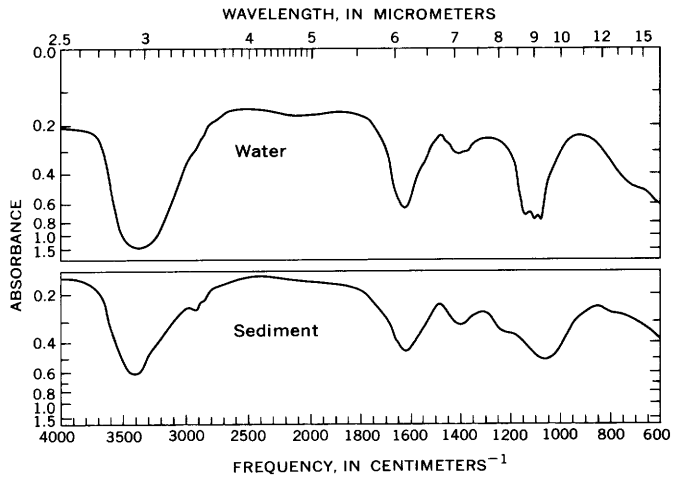

Figure 1.—Infrared absorption curves of colloidal substances isolated from water and sediment of the Chesapeake Bay.

Table 2.—*Semiquantitative spectrographic analysis, in percent, of ash from colloidal isolate from Chesapeake Bay water*

[Analysis of 1-mg sample by Norma Rait. Looked for but not found: Ti, Al, P, Mn,[1] Ag, As, Au, B, Ba, Be, Bi, Cd, Co, La, Mo, Nb, Pb, Pd, Pt, Sb, Sc, Sn, Sr, Te, U, V, W, Y, Zn, Zr, Ce, Ga, Ge, Hf, In, Re, Ta, Th, Tl, Yb, Ir, Os, Rh, Ru, Cs, Rb, Hg]

Mg	>30	Cu	0.1
Ca	.3	Fe	.03
Si	1	Cr	.03
Na	> 8	Ni	.03
K	3	Li	.001

[1] Detection limit, 0.002 percent.

BAY SEDIMENTS

Bottom surficial sediment was collected from a site close to that where the water was sampled. A Petersen grab sampler was used to collect a number of samples from which one, amounting to 465 g, was arbitrarily chosen for study.

The initial problem centered on separation of the coarse inorganic sediment from the desired colloidal constituents. To do this as effectively as possible, the entire sample was shaken with 2 liters of distilled water containing 1.5 percent by weight of NaCl. This concentration was chosen to approximate the salinity of the bay at the sampling point; the saline solution was used to prevent changes in the properties of the organic and inorganic colloids in the sediment.

After settling, the supernatant solution, in which the colloidal material was suspended, was decanted and saved. This procedure was repeated 10 times.

The combined, decanted, cloudy, amber liquid (20 liters) was filtered through 1.2-μm Millipore filters, as was the water sample, to remove particulate matter. After concentration to 500 ml in a rotary evaporator, as in the case of the

water, the clear filtrate was dialyzed in the manner already described. A portion of the dialyzed sample, after drying, had the analysis shown in tables 3 and 4. It is estimated that the colloidal substances isolated from the sediment accounted for approximately 20 ppm of the sample. It must be kept in mind, however, that the procedure used may not have led to the recovery of all the colloidal substances present. An infrared spectrum of this colloidal isolate is shown in figure 1.

Table 3.—*Analysis of colloidal isolate, in percent, from Chesapeake Bay sediment*

	As is	Ash-free
C	24.0	38.5
H	3.8	6.1
N	2.3	3.7
O (by difference)	32.4	51.7
Ash	37.5	...

Table 4.—*Semiquantitative spectrographic analysis, in percent, of ash from colloidal isolate from Chesapeake Bay sediment*

[Analysis of 1-mg sample by Norma Rait. Looked for but not found: Ti, As, Au, Be, Bi, Cd, La, Mo, Nd, Pd, Pt, Sb, Sc, Sn, Te, U, V, W, Y, Zn, Zr, Ce, Ga, Ge, Hf, In, Re, Ta, Th, Tl, Yb, Ir, Os, Rh, Ru, Cs, Rb, Hg]

Mn	>10	Co	0.3
Si	10	Ni	.3
P	10	Ba	.3
Mg	3	Sr	.3
Ca	3	B	.1
Al	3	Cr	.03
Na	3	Ag	.01
K	3	Pb	.01
Cu	3	Li	.001
Fe	.3		

DISCUSSION

Ultrafiltration followed by dialysis of the filtrates has led to isolation of colloidal substances from both the water and sediment that can pass through a 1.2-μm filter but are retained by a 0.0024-μm membrane. Inasmuch as dialysis also effectively removed all soluble ionic species, it must be concluded that analyses of the ash obtained from the colloids (tables 2 and 4) must reflect either inorganic colloids, organometallic complexes or compounds, organic-inorganic protective colloids, or mixtures. High oxygen and hydrogen values and low carbon contents of the isolated colloids, however, make the analyses of tables 1 and 3 suspect. In particular, the hygroscopic character of the isolates may have resulted in the absorption of atmospheric moisture prior to analysis in spite of attempts to prevent this from occurring. Analyses of isolates from future studies will be conducted under more stringent conditions to eliminate this possibility.

Both colloidal isolates clearly have high ash contents, averaging approximately 40 percent. The high content of magnesium (> 30 percent) in the colloids from the water may be associated with mineral matter, such as dolomite, chlorite, or serpentine. On the other hand, the magnesium could, in part at least, also be associated with colloidal chlorophyll residues. As a third possibility, the magnesium could also be accounted for in terms of demineralized porphyrin residues which could, under the proper conditions, attract and complex vanadium or nickel. The high sodium and potassium contents of these colloids give us reason to suspect the presence of salts of organic acids. Such a conclusion is also suggested by the infrared curves (fig. 1), which show little evidence of carbonyl groups at about 1,725 cm^{-1}, indicating either chelated carbonyl groups, the carboxylate ion, or both. The low values for silicon, calcium, and aluminum point to the absence of significant quantities of silicates or of apatite in the isolate.

Examination of the composition of the ash derived from the colloidal isolate from the sediment points to an entirely different picture. Here the major element is manganese, but silicon and phosphorus are also present in high concentrations. The presence of colloidal silica or silicates is suggested, and apatite may also be present. Inasmuch as there appears to be an excess of phosphorus over calcium, however, some organically bound phosphorus or ionic phosphates may also be present. The high concentration of manganese in the colloidal isolate from the sediment suggests, as one possible explanation, the presence of a colloidal organic complex which could possibly undergo syneresis to form a manganese nodule. However, the manganese may alternatively be precipitating from the water in the form of an inorganic colloid, or in an ionic form that becomes associated directly with the colloids in the sediment.

It is premature to try to characterize the organic isolates. Infrared curves for both isolates are very similar and, in turn, are similar to humic acid isolates from low-rank coals. This similarity would seem to indicate that the material was derived from terrestrial sources.

Although the results presented in this paper are preliminary, the distribution of magnesium and manganese between the colloidal fractions recovered from the water and sediment is, we feel, of sufficient interest to warrant description. Extended studies of the colloidal substances are continuing.

REFERENCES

Breger, I. A., 1970, What you don't know can hurt you: Organic colloids and natural waters, *in* Symposium on Organic Matter in Natural Waters, Univ. Alaska, Sept. 2–4, 1968, Proc.: Alaska Univ. Inst. Marine Sci. Occasional Pub. 1, p. 563–574.

Perhac, R. M., 1971, Distribution of heavy metals among dissolved and suspended solids in stream waters [abs.]: Geol. Soc. America Abs. with Programs, v. 3, no. 5, p. 337–338.

DISTORTION OF THE GEOTHERMAL FIELD IN AQUIFERS BY PUMPING

By ROBERT SCHNEIDER, Washington, D.C.

Abstract.—The extent and nature of distortion of geothermal fields in aquifers by pumping was assessed by comparing observed geothermal profiles with reconstructed natural profiles for three areas of contrasting geohydrologic conditions in three Tertiary aquifers. In the Sparta Sand at Fordyce, Ark., a negative departure of about 0.8°C, believed to result from induced downward flow of cool water, was measured near the level of the bottom of a municipal well. A positive departure of about 1.9°C in a shallow zone of the heavily pumped artesian carbonate-rock aquifer in Brunswick, Ga., near the center of an extensive potentiometric depression, is believed to result from horizontal flow of warm water possibly derived in part from a distant region where water moves upward. A more complex condition was found in the intensively developed "500-foot" sand (Claiborne Group) in Memphis, Tenn. A positive departure of about 0.8°C near the lower part of the screened interval of a municipal well and a negative departure of about 0.4°C near the upper part suggest simultaneous movement of warm water from below and cool water from above. In the confining beds above the artesian aquifer downward infiltration of warm water from a shallow water-table aquifer is suggested by the positive >1.2°C departure.

The geothermal field in broad regions of the earth's crust is controlled primarily by the heat flow from the interior of the earth and by the thermal conductivity of the rocks. Locally, the temperature distribution may be affected by tectonic or volcanic activity, by the associated circulation of hot water, or by exothermic chemical reactions.

In view of the fact that heat is transported by the mass movement of water, the circulation of water in aquifer systems affects the geothermal field. The extent to which the temperature distribution is affected is in part a function of the rate and direction of fluid flow. Owing to the high heat capacity of water and the relatively fast rates of ground-water flow near areas of pumping, as compared to natural flow rates, the geothermal field should be measurably distorted by pumping. For this reason, in studying the natural geothermal characteristics of aquifers in Arkansas, Georgia, and Tennessee, temperature logging was usually done at sites remote from pumped wells. However, for the purpose of determining the extent, nature, and hydrologic significance of the distortion under selected conditions, temperature studies were made in three areas near pumped wells.

The temperature measurements were made in the cased parts of unused wells by means of a thermistor in circuit with a three-conductor rubber-coated cable. Resistances of the thermistor were measured at selected depths with a five-dial wheatstone bridge and an external galvanometer. The thermistor was calibrated against a platinum resistance thermometer, and precision of the measurements is near 0.01°C.

GEOHYDROLOGIC AND GEOTHERMAL CONDITIONS

Temperature measurements were made in three areas of contrasting geohydrologic conditions: a small municipal well field tapping a sand aquifer in the coastal plain of Arkansas; the heavily pumped principal artesian aquifer in southeastern Georgia, consisting of fissured and cavernous carbonate rocks; and one of the intensively developed municipal well fields in Memphis, Tenn., tapping a coastal-plain sand aquifer.

Coastal-plain sand aquifer at Fordyce, Ark.

The municipal wells at Fordyce, Dallas County, south-central Arkansas, obtain water from the Tertiary Sparta Sand. The lithologic sequence shown graphically in figure 1 is the log of one of the municipal wells (No. 10S-13W-34 aca2, NE¼SW¼NE¼ sec. 34, T. 10 S., R. 13 W.), about 20 to 30 feet from the observation well in which the geothermal profile was made. At the time the temperature measurements were made the supply well was pumping about 560 gallons per minute. Reportedly this rate of pumping had been prevalent for some years on an intermittent regimen governed by the daily or hourly water requirements of the municipal supply system.

The most obvious feature of the geothermal profile is that in the vicinity of the upper half of the sand aquifer tapped by the pumped well the entire profile is shifted toward the "cold" side. The maximum departure from the reconstructed profile is about 0.8°C about 10 to 20 feet above the level of the top of the screen. The reconstructed profile was drawn on the basis of profiles measured in three other wells in southeastern Arkansas. All these wells penetrated the same aquifer but were

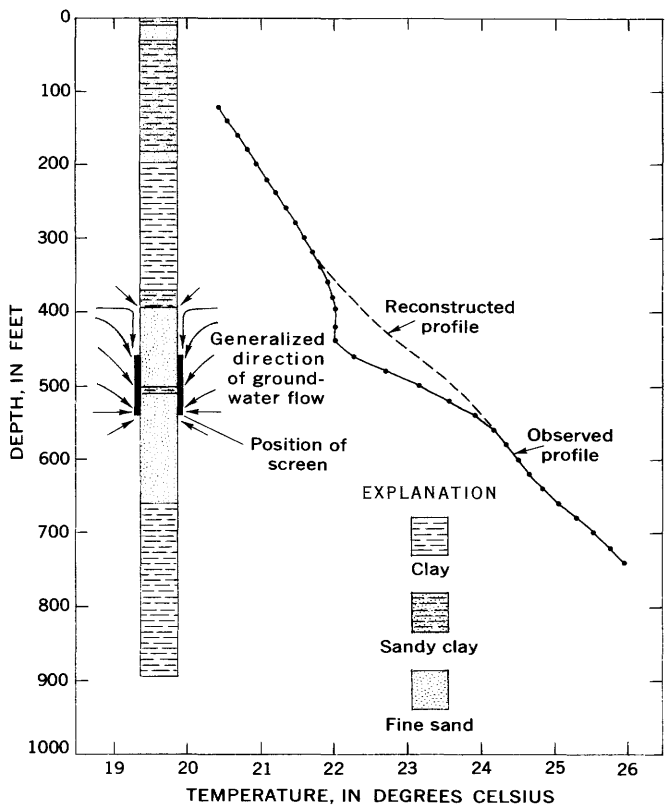

Figure 1.—Lithologic well log and geothermal profile at Fordyce, Ark. The observed geothermal profile was made in an observation well 20 to 30 feet from the supply well.

not near pumped wells, and the thermal gradients measured in them were closely similar.

Of the three most pronounced inflections in the geothermal profile, two coincide with the levels of the top and bottom of the screen and the geothermal field appears to be relatively undisturbed below the screen. In view of the fact that there is no basis for interpreting large permeability changes near the top and bottom of the well screen, it must be inferred that the inflections in the geothermal profile at these levels are related to the hydraulic influence of the well. In most of the 65-foot-sand section above the screen the geothermal gradient is near zero, suggesting that the dominant flow direction is vertically downward. The shift of the profile toward the "cold" side suggests that most of the water in the vicinity of the pumped well is moving horizontally or downward toward the screen, that is, from regions where the water is of the same or of lower temperature. The inflection at the contact between the sand and the upper confining clay strata is believed to reflect the change in permeability, and the small shift of the thermal profile in the clay is probably caused by induced downward leakage of water from the clay to the sand.

Carbonate-rock aquifer at Brunswick, Ga.

At Brunswick, Ga., the well studied penetrates early Miocene, Oligocene(?), and Eocene carbonate rocks known collectively as the principal artesian aquifer in southeastern Georgia. The aquifer includes porous fossiliferous limestone, cavernous dolomitic limestone, cherty limestone, and chert (Wait, 1965, p. E25). The geothermal profile (fig. 2) was made in a completely cased well (No. 33H 127, or test well 3) that is near the center of an extensive cone of depression in the piezometric surface although not very close to a pumping well. Pumpage from the Brunswick area was estimated to be more than 100 million gallons a day in 1961, and the piezometric levels near the center of pumping had declined about 60 to 70 feet between 1880 and 1965 (Warren, 1944; and D. O Gregg, written commun., Jan. 31, 1967).

The most obvious feature of the geothermal profile is the pronounced bulge in the "hot" direction in the vicinity of the water-bearing zone. The reconstructed geothermal profile is an extension of the similar and nearly linear profiles above and below the apparently distorted section of the profile. Judging from geothermal profiles in the same aquifer in northern Florida where there is no pumping, the reconstructed profile probably is not exactly correct. Under natural conditions it is likely that there were inflections in the profile near the top and bottom of the water-bearing zone and the gradient in the zone probably was somewhat smaller than that immediately above and below (Schneider, 1967).

The maximum departure from the reconstructed profile is about 1.9°C at a depth of 520 feet, near the top of the

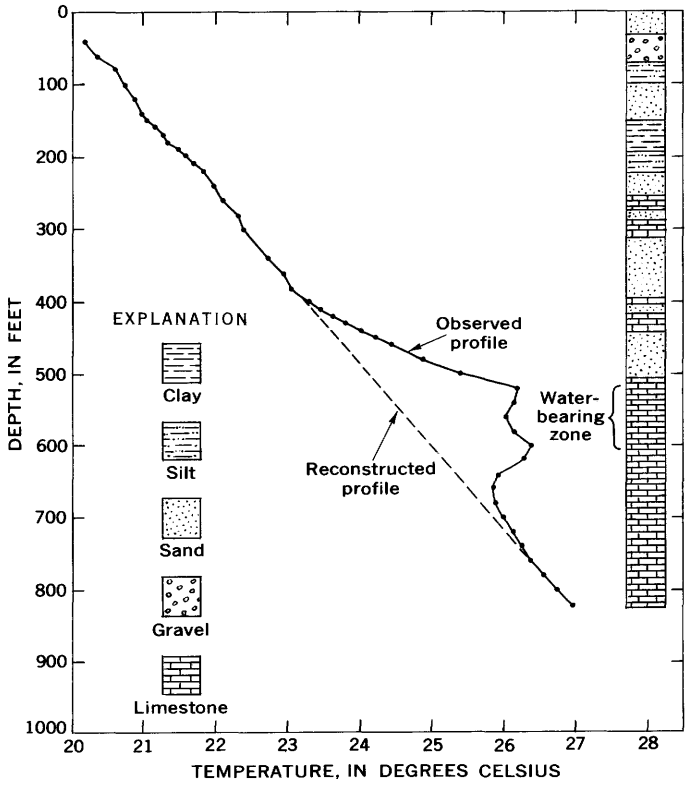

Figure 2.—Lithologic well log and geothermal profile at Brunswick, Ga.

water-bearing zone. The distinct inflections in the profile at 400 feet and between 600 and 700 feet suggest abrupt changes in permeability above and below the water-bearing zone. This zone, which is cased off in the observation well, is the uppermost of four distinct zones in which the potentiometric head is successively higher with depth. From about 1,040 to 1,400 feet there is a zone containing brackish water (Wait, 1965, p. E48). Most of the flow at this site is believed to be horizontal, but hydrologic studies by Wait (1965) and Hanshaw and others (1965) have shown that about 1½ miles to the southeast there is a region in which the aquifer is contaminated by brackish water which appears to be leaking upward from the deeper water-bearing zones. The water in this contaminated region was found to contain up to about 1,600 mg/l chloride as compared to an average chloride content of about 25 mg/l for native fresh water from the aquifer (Wait, 1962, p. 23). For comparison, the chloride content from the water-bearing zone at the site of the thermal study is about 100 mg/l (D. O. Gregg, written commun., Jan. 31, 1967).

On the basis of the available hydrologic information and the characteristics of the geothermal profile, it is believed that the distortion of the geothermal field at this site is caused by the horizontal flow of relatively warm water, part of which probably is derived from a region some distance away where water moves upward into the shallow water-bearing zone.

Coastal-plain sand aquifer at Memphis, Tenn.

The primary source of the municipal water supply at Memphis, Tenn., is the Tertiary Claiborne Group, about 500 to 800 feet of mostly sand interbedded with some clay. The more permeable sandy layers are known locally as the "500-foot" sand. The transmissivity of the aquifer ranges between 13,400 and 54,800 ft^2 day^{-1} (100,000 and 410,000 gpd per ft) and, since the first well was installed in 1886, the piezometric surface has been drawn down into an extensive cone on which are superimposed several smaller cones (Criner and others, 1964, p. O30; Wells, 1931, p. 2–5). By 1964, the water level in the deepest part of the cone had dropped about 85 feet from the original level (Bell and Nyman, 1968, p. 9). The average rate of withdrawal from 1935 to 1960 was about 100 mgd (Criner and others, 1964, p. O18–O19).

The well studied (No. SH: K-45) is an observation well in one of the municipal well fields in the southeastern part of the city that has been producing since 1931. The well screen shown on the graphic log (fig. 3) represents the position of the screen in a pumped well (No. SH: K-43) about 30 feet from the observation well. At the time of the temperature measurements the nearby pumped well had been producing about 580 gpm for 30 days.

The reconstructed geothermal profile is believed to represent natural conditions very closely because it was drawn on the basis of two profiles about 8 miles north of the center of heavy pumping, and another about 30 miles northeast.

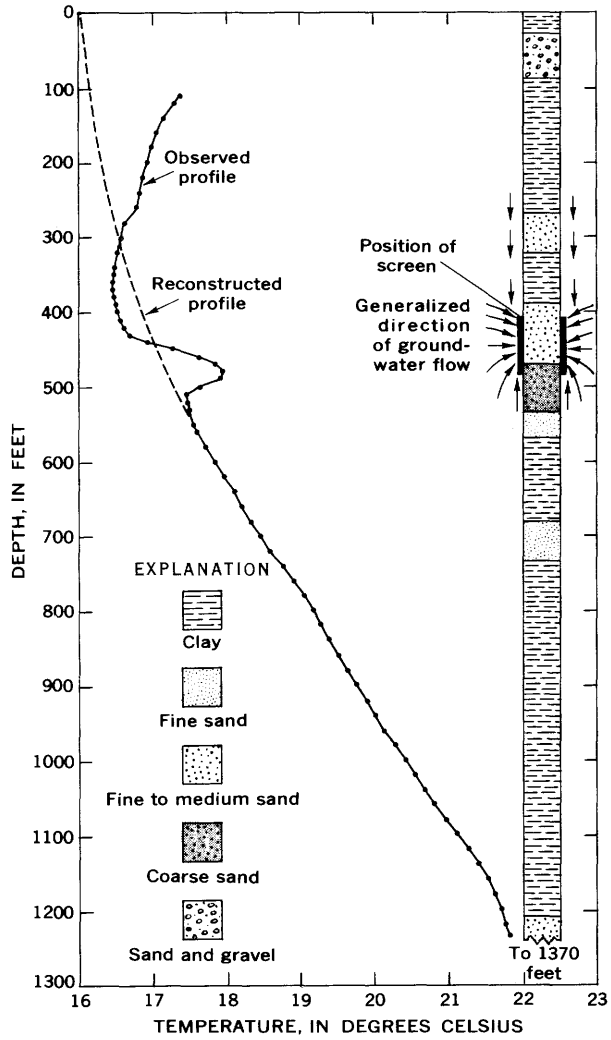

Figure 3.—Lithologic well log and geothermal profile at Memphis, Tenn. The observed geothermal profile was made in an observation well 30 feet from the supply well.

In places the observed profile departs to the right of the reconstructed profile, and in places to the left; below a depth of about 530 to 540 feet the observed profile appears to be unaffected by pumping. Near the bottom of the apparently distorted segment of the profile there is a pronounced departure of 0.75°C from the reconstructed curve in the "hot" direction. The point of maximum positive departure coincides with the contact of a unit of coarse sand below and a unit of fine-to-medium sand above. The bottom of the well screen is near the same level; only the top 15 feet of the 65-foot layer of coarse sand is screened. The deflection of the profile to the right is believed to be caused by relatively warm water moving upward toward the screen. It should be noted that even though there is a unit of fine sand below the coarse one, the geothermal profile does not appear to be distorted in this fine

sand. This is interpreted as indicating that little or no water from the fine sand is moving upward toward the screen. Opposite the top half of the screen and for nearly 100 feet above it the geothermal profile apparently departs to the left of the reconstructed profile. The point of maximum departure, 0.35°C, coincides with the level of the top of the screen. The shift toward the "cold" direction is believed to be caused by relatively cold water moving downward toward the screen from the region about 100 feet above. Above a depth of about 300 feet the observed profile departs to the right of the reconstructed profile and the departure becomes progressively greater at successively shallower depths. The maximum observed departure, about 1.2°C, is at the upper end of the observed profile which terminates at the water level in the well. However, a geothermal profile measured under similar conditions elsewhere in Memphis indicated that the trend of this profile continues upward into the lower part of the shallow sand and gravel strata, referred to as terrace deposits by Criner, Sun, and Nyman (1964, p. O12). This part of the geothermal profile indicates that heat and water are moving downward. In view of the fact that the head in the artesian aquifer is lower than the water table in the terrace deposits, the departure of the observed geothermal profile from the reconstructed profile above a depth of 300 feet is interpreted as being caused by downward leakage of relatively warm water from the terrace deposits. From analyses of pumping tests, Criner and Armstrong (1958, p. 17) have stated that a logical source for apparent recharge to the "500-foot" sand is leakage from the upper confining layers. In one pumping test they observed a drawdown in the shallow water-table aquifer which could be attributed to pumping from the artesian aquifer. It is not within the scope of this study to determine why ground water moving downward from the shallow sand and gravel strata at this site appears to be warmer than the water at a depth of several hundred feet. However, it may be mentioned that in a study of shallow ground-water temperatures (to a depth of about 80 feet), on Long Island, N.Y., Pluhowski and Kantrowitz (1963, p. B187) found that the mean annual temperature of ground water under a cleared urbanized area was about 0.8°C higher than that under a heavily wooded undeveloped area. The site of the well studied in Memphis is cleared and urbanized.

CONCLUSIONS

The induced movement of water in aquifers in the vicinity of areas of pumping distorts the geothermal field measurably. The magnitude and direction of departure of the resultant geothermal profile from the reconstructed natural profile depend on the spatial distribution of permeability (and particularly the vertical permeability of the rocks above and below the levels of withdrawal), the magnitude of pumpage, and the hydraulics and geometry of the intake openings of the well. Generally, these departures are believed to result from the induced upward flow of warm water and (or) the induced downward flow of cool water.

REFERENCES

Bell, E. A., and Nyman, D. J., 1968, Flow pattern and related chemical quality of ground water in the "500-foot" sand in the Memphis area, Tennessee: U.S. Geol. Survey Water-Supply Paper 1853, 27 p.

Criner, J. H., and Armstrong, C. A., 1958, Ground-water supply of the Memphis area: U.S. Geol. Survey Circ. 408, 20 p.

Criner, J. H., Sun, P-C. P., and Nyman, D. J., 1964, Hydrology of aquifer systems in the Memphis area, Tennessee: U.S. Geol. Survey Water-Supply Paper 1779-O, 54 p.

Hanshaw, B. B., Back, William, Rubin, Meyer, and Wait, R. L., 1965, Relation of carbon-14 concentrations to saline water contamination of coastal aquifers: Water Resources Research, v. 1, no. 1, p. 109–114.

Pluhowski, E. J., and Kantrowitz, I. H., 1963, Influence of land-surface conditions on ground-water temperatures in southwestern Suffolk County, Long Island, New York: Art. 51 *in* U.S. Geol. Survey Prof. Paper 475-B, p. B186–B188.

Schneider, Robert, 1967, An interpretation of the geothermal field associated with the carbonate-rock aquifer system of Florida [abs.]: Geol. Soc. America Spec. Paper 101, Abstracts for 1966, p. 191–192.

Wait, R. L., 1962, Interim report on test drilling and water sampling in the Brunswick area, Glynn County, Georgia: Georgia Geol. Survey Inf. Circ. 23, 46 p.

—— 1965, Geology and occurrence of fresh and brackish ground water in Glynn County, Georgia: U.S. Geol. Survey Water-Supply Paper 1613-E, 94 p.

Warren, M. A., 1944, Artesian water in southeastern Georgia with special reference to the coastal area: Georgia Geol. Survey Bull. 49, 140 p.

Wells, F. G., 1931, A preliminary report on the artesian water supply of Memphis, Tennessee: U.S. Geol. Survey Water-Supply Paper 638-A, 34 p.

REGIONAL RATES OF GROUND-WATER MOVEMENT ON LONG ISLAND, NEW YORK

By O. L. FRANKE and PHILIP COHEN, Mineola, N.Y.

Work done in cooperation with Nassau County Department of Public Works, the New York State Department of Environmental Conservation, the Suffolk County Department of Environmental Control, and the Suffolk County Water Authority

Abstract.—Regional rates of ground-water movement on Long Island, N.Y., computed with the aid of a steady-state electrical analog model, indicate that near the boundary between Nassau and Suffolk Counties the length of time required for ground-water recharge to move seaward of the barrier beaches is about 800 years for water entering the Magothy aquifer and 3,000 years for water entering the Lloyd aquifer. These computations are based upon an assumed rate of natural recharge of 21 inches per year and upon the configuration of the natural ground-water flow net associated with that rate of recharge. About 25–30 years is the maximum time required for water to drain from one of the shallow ground-water subsystems into East Meadow Brook. If the dissolved substances are assumed to move at the same rate as the water, then these lengths of time indicate the orders of magnitude of the times required for ground water containing substances of sewage origin (largely derived from cesspools and septic tanks) to be flushed from the ground-water system after completion of planned wide-scale sanitary sewering systems in Nassau and Suffolk Counties.

Rates of ground-water movement on Long Island, N.Y., are of considerable concern to individuals and agencies responsible for developing and managing the water resources on the island. In recent years, much of the concern has been directed toward time of travel and disposition of waste water from hundreds of thousands of cesspools and septic tanks. This report provides preliminary information on the rates of ground-water movement on Long Island and on the implications of those rates deduced from information developed largely from ongoing cooperative water-resources studies by the U.S. Geological Survey and several local and State agencies.

HYDROGEOLOGIC SETTING

Long Island is underlain by a wedge-shaped mass of unconsolidated deposits that attain a maximum thickness of about 2,000 feet in south-central Suffolk County. Pertinent characteristics of these deposits are listed in table 1.

Under natural, predevelopment conditions, precipitation on Long Island was the source of all the fresh ground water

Table 1.—*Major hydrogeologic units on Long Island, N.Y.*

Hydrogeologic unit[1]	Approximate maximum thickness (feet)	Description	Estimated average hydraulic conductivity[2] (feet per day)	
			Horizontal	Vertical
Upper glacial aquifer.	400	Mainly sand and gravel; some thin beds of clayey material.	270	27
Gardiners Clay.	150	Clay, silty clay, and a little fine sand.	.01	.001
Jameco aquifer.	200	Mainly medium to coarse sand. Not found along section $A-A'$ (figs. 1, 2, and 3).	...	...
Magothy aquifer.	1,000	Mainly very fine sand, silt, and clay; some coarse to fine sand; locally contains gravel.	50	1.4
Raritan clay.	300	Clay; some silt and fine sand.	.01	.001
Lloyd aquifer.	300	Sand and gravel; some clayey material.	40	7
Bedrock	...	Crystalline rock of very low interstitial hydraulic conductivity.	...	...

[1] Nomenclature after Cohen, Franke, and Foxworthy (1968).
[2] Data mainly from McClymonds and Franke (1970), and G. D. Bennett (written commun., 1968).

U.S. GEOL. SURVEY PROF. PAPER 800-C, PAGES C271-C277

beneath the island. Ground water was discharged naturally by (1) seepage to streams that flowed into the bordering bodies of salty surface water; (2) subsurface outflow to the bays, the Atlantic Ocean, and Long Island Sound; and (3) to a small extent, evapotranspiration near the shorelines.

At present (1971), ground-water recharge on Long Island results mainly from (1) infiltration of precipitation through unpaved areas, (2) infiltration of storm runoff through about 2,100 recharge basins, (3) injection of water used for industrial purposes into roughly 1,000 recharge wells, and (4) discharge of domestic and industrial waste water into cesspools, septic tanks, and disposal basins. All the natural mechanisms of ground-water discharge are still operative on Long Island, but, in addition, on the order of 100 mgd (million gallons per day) of ground water in Nassau and Suffolk Counties is artificially discharged by pumping from wells and subsequent disposal of the pumped water to the sea by way of sewage-treatment plants.

The overall ground-water system of Long Island can be considered to include an islandwide regional flow system and a series of shallow subsystems associated with the island's streams. According to Franke and McClymonds (1970, p. 94), flow paths in the regional systems range in length from 1 to several miles; and the flow is generally two dimensional (in roughly vertical planes perpendicular to the length of the island). Flow paths in the shallow subsystems range in length from a few to several thousand feet, and the flow is generally three dimensional.

In general, the regional flow system on Long Island may be visualized as separated into two major subsystems by an approximately east-trending, roughly vertical imaginary surface, which is termed "the regional ground-water divide" (fig. 1). North of this divide the regional direction of ground-water movement is generally toward Long Island Sound; south of this divide the regional direction of ground-water movement is generally toward the southshore bays and the ocean.

Ground water in the shallow subsystems discharges mainly into Long Island's streams, which flow to tidewater. "Local interstream ground-water divides" (figs. 4 and 5) separate the shallow ground-water subsystems from one another. These divides are roughly vertical imaginary plane surfaces, most of whose traces trend northward. The shallow ground-water subsystems are separated from the underlying regional ground-water system by nearly horizontal, undulating, imaginary surfaces termed "stream subsystem ground-water divides." Traces of these surfaces (figs. 4 and 5), most of which commonly trend eastward (roughly perpendicular to the streams), are found near the headwaters of the streams.

RATES OF GROUND-WATER MOVEMENT

Rates of ground-water movement on Long Island were studied for both the regional ground-water system and for the shallow subsystems associated with Long Island's streams.

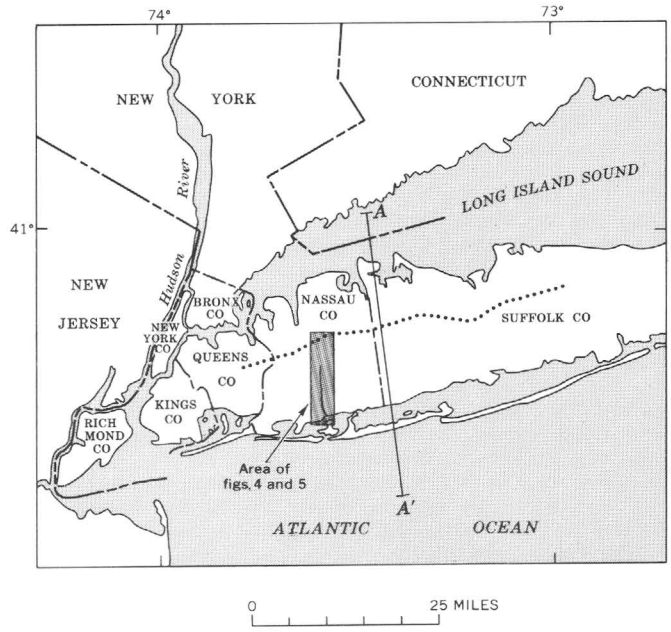

Figure 1.—Index map of Long Island, N.Y., showing the regional ground-water divide (dotted line) and location of section A–A'.

Because of the characteristics described in the previous paragraphs, many aspects of the regional ground-water system on Long Island can conveniently be described and studied by the use of north-trending geologic and hydrologic cross sections. (For example, see Franke and McClymonds, 1970, fig. 17.) Accordingly, a steady-state electrical analog model, of the type described by Walton and Prickett (1963), was constructed to simulate hydrologic conditions along a north-trending section near the boundary between Nassau and Suffolk Counties (section A–A', fig. 1). This section was chosen partly because of its general interest to the water managers of Long Island and partly because the section nearly coincides with the one that Collins and Gelhar (1970) studied with the aid of a Hele-Shaw viscous-fluid model.

Electrical properties of the model, which contains about 5,000 nodes, were chosen and scaled to be analogous to the pertinent hydrologic parameters (horizontal and vertical hydraulic conductivity) of the hydrogeologic units. Values of average horizontal and vertical hydraulic conductivities for the major hydrogeologic units on Long Island are listed in table 1. These values largely reflect the values listed in a report by McClymonds and Franke (1970) and in the references listed in that report. Also, the values reflect the results of unpublished analog-model studies on Long Island made by G. D. Bennett (written commun., 1968).

Regional rates of ground-water movement along section A–A' were determined as follows:

1. The assumed rate of ground-water recharge under natural conditions was 1 mgd per square mile (about 21 inches per year). This value is in general agreement with assumptions

or calculations of most previous writers. (For example, see Isbister, 1966, p. 43.)

2. By imposing the assumed rate of ground-water recharge under natural conditions on the analog model, a potential distribution that reasonably simulates the potential distribution inferred for natural conditions along the section was measured. A flow net was then constructed from the measured potential distribution (fig. 2).

3. Hydraulic gradients and flow lines were determined from the flow net.

4. The porosity of all the saturated material was assumed to be 30 percent.

5. Selected flow lines were divided into discrete segments along which hydraulic conductivities and hydraulic gradients could be estimated with a moderate degree of confidence. Rates of ground-water movement were then computed for successive segments of flow lines using the following modified form of the Darcy equation,

$$V_s = \frac{K_s i}{n},$$

where

V_s = the velocity along a segment of the flow line s,
K_s = the hydraulic conductivity of the aquifer along the segment of the flow line s,
i = the hydraulic gradient along the segment of the flow line, and
n = the porosity of the aquifer.

Appropriate values of K_s were calculated using a formula describing the so-called "ellipse of direction" (Harr, 1962, p. 28). The major axes of the ellipse correspond to directions of

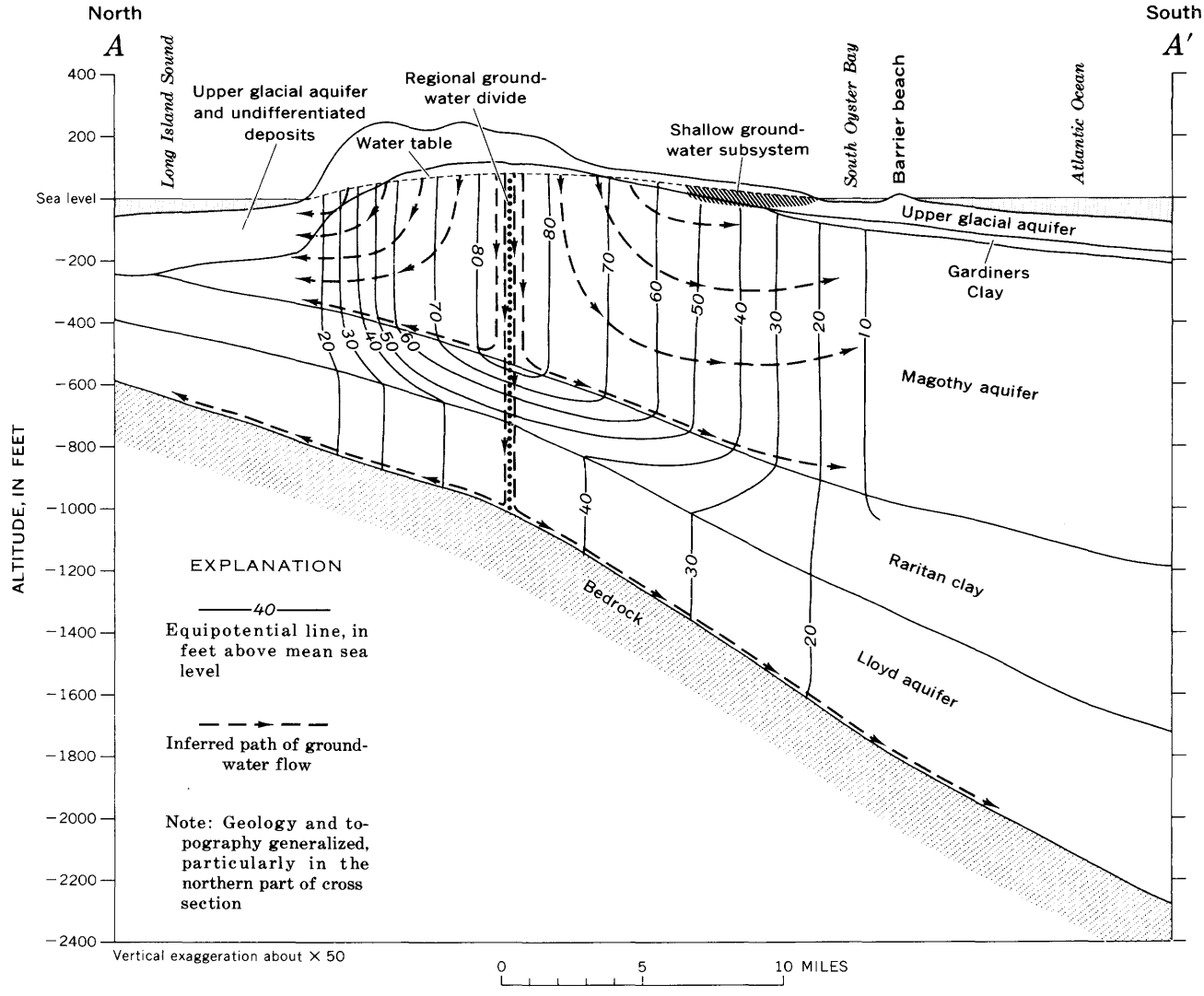

Figure 2.—Generalized equipotential and flow lines along section A–A' in the ground-water system of Long Island, N.Y., under natural conditions.

maximum and minimum hydraulic conductivities in the aquifer, which were assumed to be horizontal and vertical, respectively.

Flow lines shown in figure 2 are not everywhere perpendicular to the equipotential lines because (1) there is marked vertical exaggeration of the scale and (2) the hydrogeologic units are moderately anisotropic to the flow of water (table 1).

The time required for water to travel from the water table to various positions within the regional ground-water system, as computed by the procedure outlined in the previous paragraphs, is shown in figure 3. For example, disregarding the time required for water to move through the zone of aeration, which on Long Island may range from several hours (Seaburn, 1970, p. B196) to several months (Isbister, 1966, p. 49), the computed time required for water to move from the water table to the bottom of the Magothy aquifer beneath the ground-water divide, or the estimated "age" of the water at that point, is about 100 years. Likewise, the estimated age of water at the base of the Magothy beneath the barrier beach is about 800 years, and the computed age of water at the base of the Lloyd aquifer beneath the barrier beach is nearly 3,000 years.

The very low horizontal and vertical hydraulic conductivities of the Raritan clay result in computed ages of water in that unit that locally are more than 50,000 years. Moreover, equal-age lines are not shown in the Raritan clay because the configuration of such lines within and immediately below the unit is too complex.

A rough check on the internal consistency of the data and some of the major assumptions can be made as follows: Where the direction of ground-water flow is vertical or nearly so, as along the regional ground-water divide, the time, T, (in years)

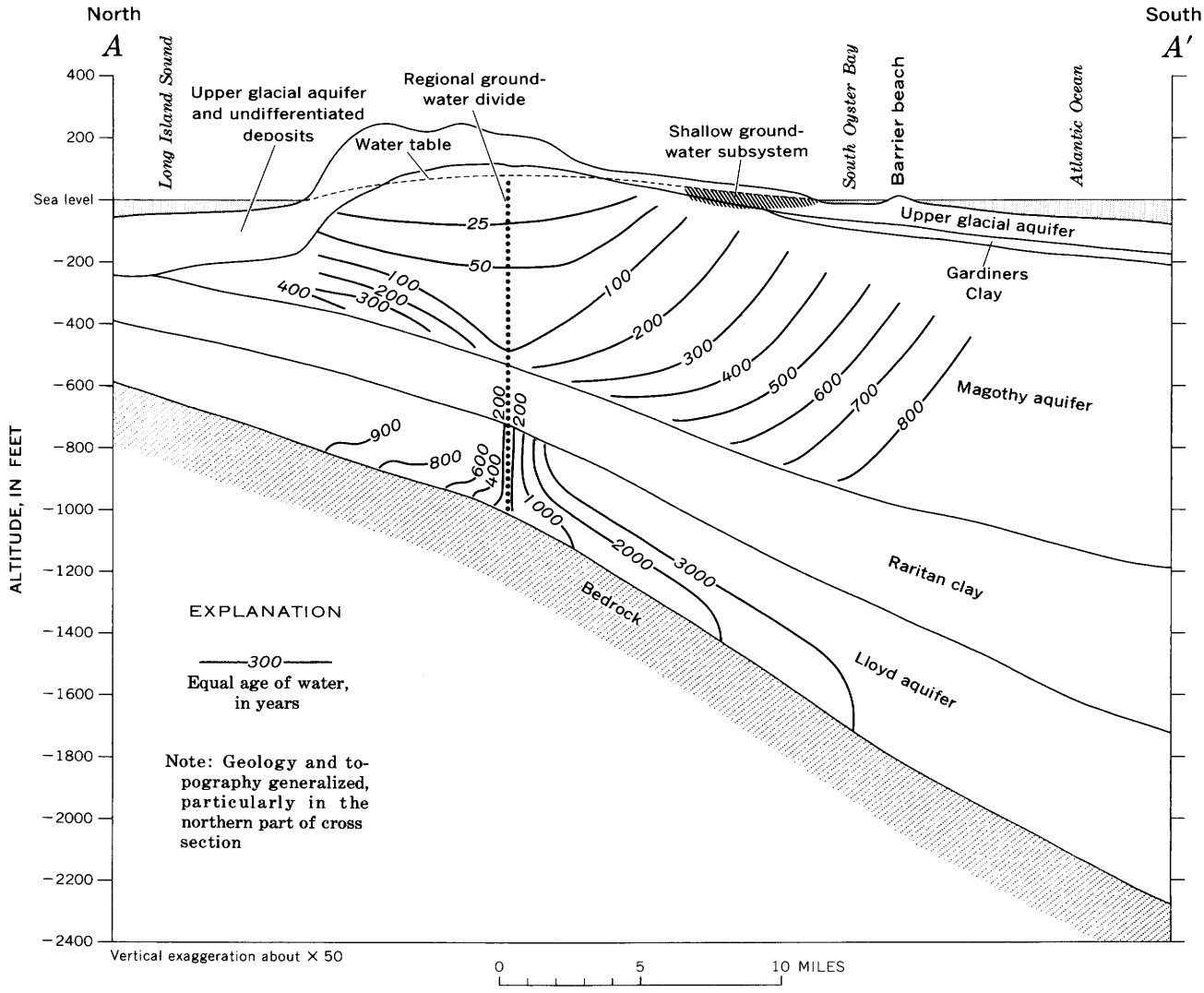

Figure 3.—Approximate time required for water along section A–A' to move from the water table to points within the regional ground-water system of Long Island, N.Y.

required for water to reach a given depth, Z, (in feet) can be calculated from the recharge rate, R, (in feet per year) and the following continuity relationship:

$$T = \frac{Zn}{R},$$

where n is the average porosity of the medium. The estimated recharge of 1 mgd is equivalent to about 21 inches or about 1.75 feet per year. Assuming that the average porosity is 30 percent, ground water moves downward about 5.8 feet per year in the vicinity of the regional ground-water divide. Accordingly, the time required for water to move downward 600 feet from the water table to the base of the Magothy in the vicinity of section $A-A'$ (fig. 3) is about 100 years. This value is virtually identical with the age determined from the analog model.

Rates of ground-water movement were computed for the shallow subsystem associated with East Meadow Brook in south-central Nassau County (fig. 1). Both the procedure used and the method of expressing the results were somewhat different from those for the regional flow system.

A flow net depicting water-level contours and flow lines associated with the shallow subsystem of East Meadow Brook in 1961 is shown in figure 4. The water-level contours reflect field data obtained in 1961. That year was chosen because of the availability of adequate data and because the hydrologic conditions were probably closer to natural conditions than in any subsequent year.

The shallow subsystem associated with East Meadow Brook is bounded on the north by a stream subsystem ground-water divide; on the south by the shoreline of Merrick Bay; and on the east and the west by local interstream ground-water divides. Depths and positions of the divides bordering the subsystem change as ground-water levels fluctuate. Partly because of these facts, the depth of the shallow subsystem in 1961 is uncertain. However, its average depth in 1961 was probably not more than 50–75 feet.

Under natural conditions, all the ground-water recharge within the ground-water divides bounding the shallow subsystem associated with East Meadow Brook that was not subsequently discharged by evapotranspiration ultimately discharged into either East Meadow Brook or Merrick Bay. Ground-water recharge in the area bounded by the stream subsystem divide on the south, the regional ground-water divide on the north, and the local interstream divides on the east and the west, was incorporated into the regional ground-water system. This water flowed southward beneath the shallow subsystem and ultimately probably discharged partly into Merrick Bay and partly into the ocean.

Although ground-water flow in the shallow subsystem is three dimensional, flow for computing rates of ground-water movement was assumed to be horizontal. This is not a serious departure from the actual field situation. Rates of ground-water movement were computed by using the value for the

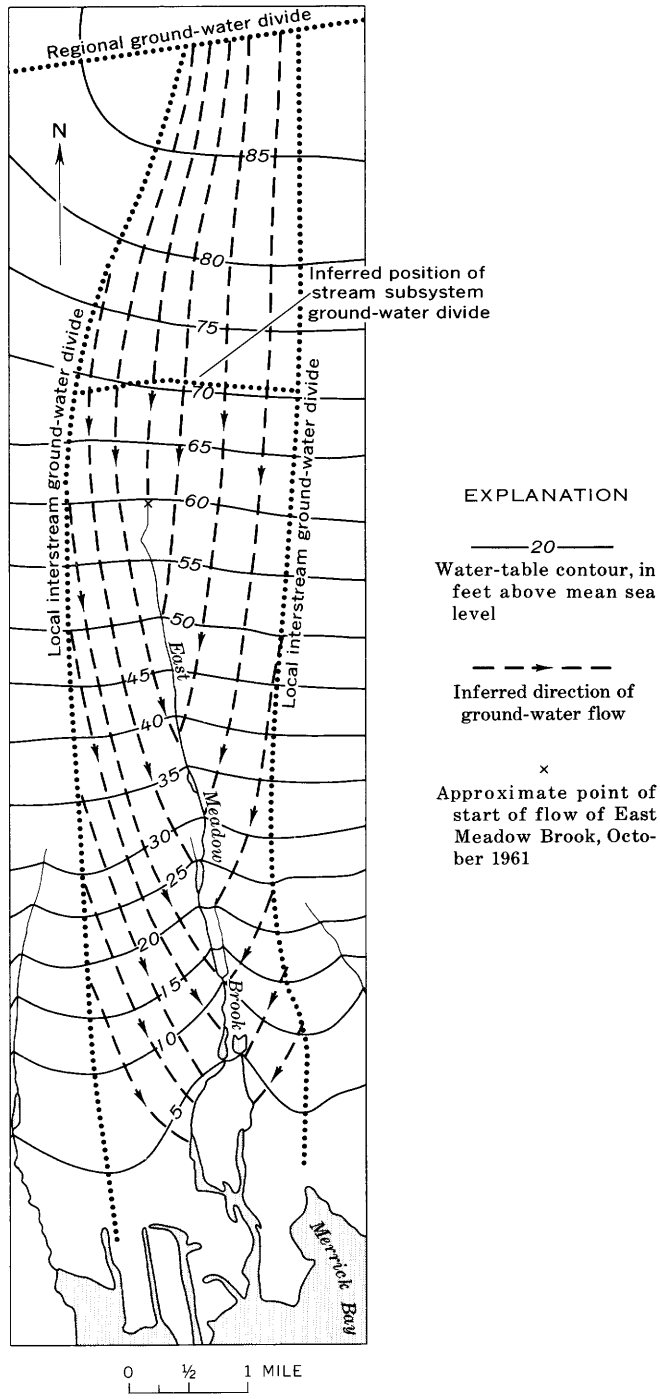

Figure 4.—Ground-water flow net in the vicinity of East Meadow Brook in October 1961.

horizontal hydraulic conductivity of the upper glacial aquifer listed in table 1; hydraulic gradients were determined from figure 4, and a value of 30 percent was used for the porosity of the material. These computed values were then used to develop lines showing the approximate time required for a particle of water entering the shallow subsystem to discharge into East Meadow Brook (fig. 5). For example, a particle of

water recharging the shallow aquifer at point A in figure 5 would take about 7 years to discharge into the stream, and a particle of water recharging the aquifer at point B would take about 20 years to discharge into the stream. These estimates are for the hydraulic gradients that existed in 1961. If the gradients steepen or flatten in the future, the time of travel will decrease or increase proportionately.

IMPLICATIONS OF COMPUTED RATES OF GROUND-WATER MOVEMENT

If hydraulic gradients remain unchanged or virtually so, and if dissolved constituents are assumed to move at the same velocity as water, then the information in figures 2–5 can assist in predicting paths and rates of movement of any dissolved substance introduced into Long Island's ground water. At present (1971) this information is especially pertinent for dissolved nitrate.

Smith and Baier (1969) and Perlmutter and Koch (1972) have shown that the nitrate nitrogen content (nitrate reported as nitrogen) of water from numerous wells in Nassau County has increased more than 5 mg/l (milligrams per liter) during the past decade or so. Perlmutter and Koch showed that much of the nitrate nitrogen is derived from cesspool and septic-tank effluent and that the direction of flow of the body of water having a high nitrate nitrogen content roughly follows the regional hydraulic gradient. Beneath the regional ground-water divide in parts of Nassau County, water having a high nitrate nitrogen content (locally as much as 20 mg/l) has moved down to the base of the Magothy aquifer and from there has moved southward 5–7 miles toward the bays and the ocean. Perlmutter and Koch (1972) estimated that the age of the water having a high nitrate nitrogen content at the base of the Magothy aquifer beneath the regional ground-water divide in the western and central parts of Nassau County is about 50 years.

Water having a high nitrate nitrogen content has not yet reached the base of the Magothy aquifer in western Suffolk County in the vicinity of section A–A' (figs. 1–3). However, such water has been noted in shallow wells in that area (Harr, 1971). The Magothy aquifer is thicker along section A–A' than it is in most of Nassau County. Moreover, widespread use of cesspools and septic tanks began more recently in western Suffolk County, about 10–20 years ago. In addition, wells screened at or near the base of the Magothy aquifer in western Suffolk County have been pumped sparingly, as compared with similar wells in Nassau County. As a result of the greater pumping in Nassau County, downward gradients there have steepened, and associated rates of downward movement have increased.

Ninety to ninety-five percent of the streamflow on Long Island is derived from shallow ground-water subsystems (Pluhowski and Kantrowitz, 1964, p. 35). Much of the shallow ground water and most of the streamflow contains dissolved

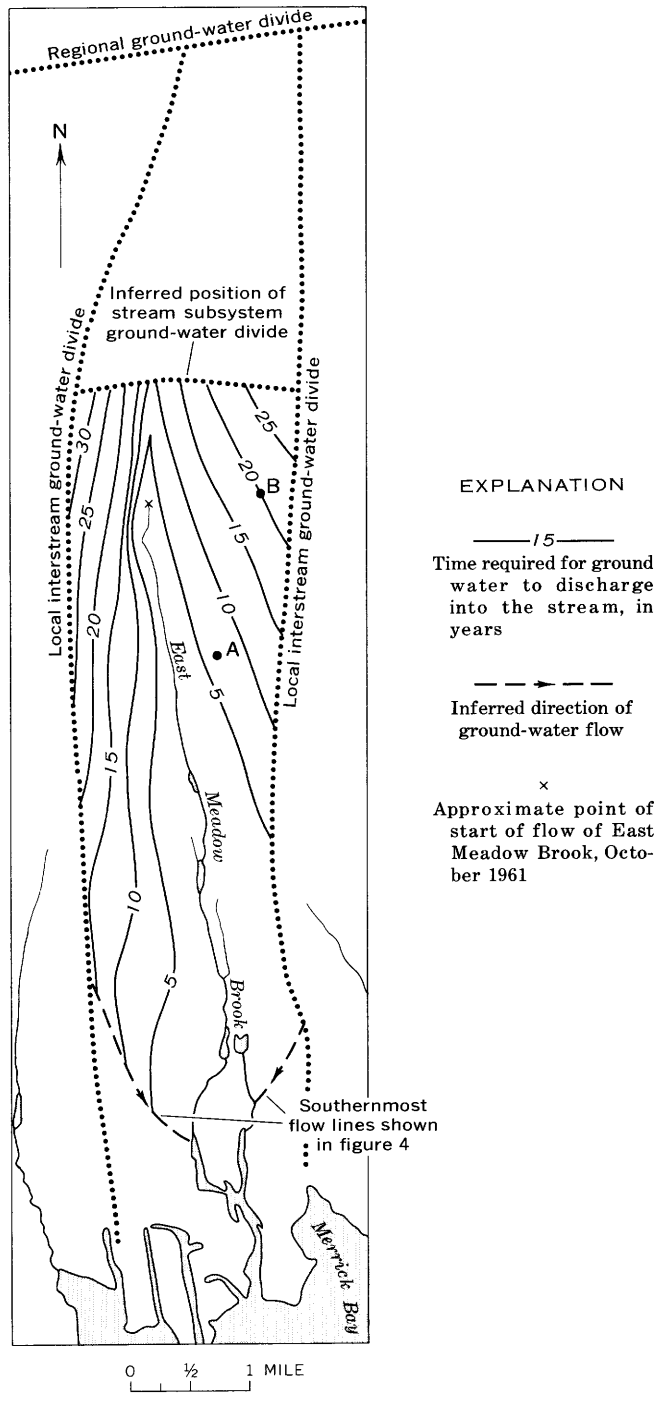

Figure 5.—Approximate time required for a particle of water in the shallow ground-water subsystem to discharge into East Meadow Brook under conditions similar to those in October 1961. Points A and B are discussed in text.

substances derived from cesspools and septic tanks (Cohen and others, 1971; and Perlmutter and Koch, 1971, 1972). Widespread sanitary-sewering systems are presently (1971) either under construction or in various stages of planning. Data shown in figure 5 suggest that the length of time required for

water containing substances of sewage origin to be fully flushed from the shallow subsystems to the streams after the sewer construction is completed is 25–30 years. However, such water in the Magothy and the Lloyd aquifers will probably take 500 and 3,000 years, respectively, to move seaward of the barrier beaches.

As previously noted, the preceding time estimates are based on several simplifying assumptions. Moreover, the time lines associated with section $A-A'$ (fig. 3) and with the area near East Meadow Brook (fig. 5) are not necessarily representative of all Long Island. However, these time lines do indicate the probable order of magnitude involved in the flow of ground water in most of Nassau and Suffolk Counties. If ground-water levels and associated hydraulic gradients locally change markedly as a result of future development, then, as previously noted, the rate of ground-water movement will change in proportion to the changes in hydraulic gradients. Moreover, the stream subsystem divides will shift seaward as ground-water levels decline. As a result of this shift, some ground water that formerly would have discharged into a stream within several decades or less will become part of the regional flow system, and a significantly longer period of time will elapse before that water discharges through the subsurface into salty water.

Hydraulic gradients steepen markedly in the vicinity of large-capacity pumping wells. In such areas, local rates of movement of ground water and associated dissolved constituents may differ markedly (in places by orders of magnitude) from natural rates of movement in the regional system and the shallow subsystems.

REFERENCES

Cohen, Philip, Franke, O. L., and Foxworthy, B. L., 1968, An atlas of Long Island's water resources: New York State Water Resources Comm. Bull. 62, 117 p.

Cohen, Philip, Vaupel, D. E., and McClymonds, N. E., 1971, Detergents in the streamflow of Suffolk County, Long Island, New York, *in* Geological Survey Research 1971: U.S. Geol. Survey Prof. Paper 750-C, p. C210–C214.

Collins, M. A., and Gelhar, L. W., 1970, Ground-water hydrology of the Long Island aquifer system: Massachusetts Inst. Technology, Hydrodynamics Lab. Rept. 122, 185 p.

Franke, O. L., and McClymonds, N. E., 1970, Summary of the hydrologic situation on Long Island, N.Y., as a guide to water-management alternatives: U.S. Geol. Survey open-file report, 220 p., 39 figs.

Harr, C. A., 1971, Partial chemical analyses of water from selected sources in Nassau and Suffolk Counties, Long Island, New York: U.S. Geol. Survey open-file report, 21 p.

Harr, M. E., 1962, Groundwater and seepage: New York, McGraw-Hill Book Co., 315 p.

Isbister, John, 1966, Geology and hydrology of northeastern Nassau County, Long Island, New York: U.S. Geol. Survey Water-Supply Paper 1825, 89 p.

McClymonds, N. E., and Franke, O. L., 1970, Water-transmitting properties of aquifers on Long Island, N.Y.: U.S. Geol. Survey open-file report, 78 p., 31 figs.

Perlmutter, N. M., and Koch, Ellis, 1971, Preliminary findings on the detergent and phosphate contents of water of southern Nassau County, New York, *in* Geological Survey Research 1971: U.S. Geol. Survey Prof. Paper 750-D, p. D171–D177.

——1972, Preliminary hydrogeologic appraisal of nitrate in ground water and streams, southern Nassau County, Long Island, New York, *in* Geological Survey Research 1972: U.S. Geol. Survey Prof. Paper 800-B, p. B225–B235.

Pluhowski, E. J., and Kantrowitz, I. H., 1964, Hydrology of the Babylon-Islip area, Suffolk County, Long Island, N.Y.: U.S. Geol. Survey Water-Supply Paper 1768, 119 p.

Seaburn, G. E., 1970, Preliminary analysis of rate of movement of storm runoff through the zone of aeration beneath a recharge basin on Long Island, New York, *in* Geological Survey Research 1970: U.S. Geol. Survey Prof. Paper 700-B, p. B196–B198.

Smith, S. O., and Baier, J. H., 1969, Report on nitrate pollution of ground water, Nassau County, Long Island: Nassau County Dept. Health, 32 p.

Walton, W. C., and Prickett, T. A., 1963, Hydrogeologic electric analog computers: Am. Soc. Civil Engineers Proc., Jour. Hydraulics Div., v. 89, p. 67–91.

SUBJECT INDEX

[For major headings such as "Economic geology," "Geochronology," "Ground water," see under State names or refer to table of contents]

AUTHOR INDEX

☆ U.S. GOVERNMENT PRINTING OFFICE: 1972 O—471-169